UNIVERSITA' DELLA CALABRIA
Dipartimento di Chimica e Tecnologie Chimiche

Scuola di Dottorato
Scienza e Tecnica "Bernardino Telesio"

Indirizzo
Mesofasi e Materiali Molecolari

in co-tutela di tesi con

UNIVERSITE PARIS-SUD
Institut de Chimie Moléculaire et des Matériaux d'Orsay

Scuola di Dottorato
Ecole Doctorale de Chimie de Paris-Sud, n°470

Con il contributo di (Ente finanziatore)
Fondo Sociale Europeo

CICLO XXVI

NMR IN DIFFERENT PARTIALLY ORDERED MEDIA:
A ROUTE FOR STRUCTURE, ORDER AND CONFORMATION
OF SMALL ORGANIC COMPOUNDS

Settore Scientifico Disciplinare CHIM/02 – CHIMICA FISICA

Direttore: Prof. Roberto Bartolino

Firma _____

Supervisori: Prof. Giuseppina De Luca   Prof. Denis Merlet

Firma _____   Firma _____

Dottorando: Dott.ssa Maria Enrica Di Pietro

Firma _____

UNIVERSITE PARIS-SUD

ÉCOLE DOCTORALE: 470 - Chimie de Paris-Sud
Laboratoire de RMN en Milieu Orienté, ICMMO, UMR 8182

DISCIPLINE chimie

en co-tutelle avec

UNIVERSITA' DELLA CALABRIA

ÉCOLE DOCTORALE: Scienza e Tecnica "Bernardino Telesio"
Dipartimento di Chimica e Tecnologie Chimiche

DISCIPLINE CHIM/02 – chimie physique

THÈSE DE DOCTORAT

soutenue le 14/12/2013

par

Maria Enrica DI PIETRO

RMN dans différents solvants partiellement orientés: pour la détermination de la structure, l'ordre et la conformation de molécules organiques

---

| Directeurs de thèse: | Giuseppina DE LUCA | Prof. (Università della Calabria) |
| | Denis MERLET | Prof. (Université Paris-Sud) |

Composition du jury:

Président du jury:	Arnold MALINIAK	Prof. (Stockholm University)
Rapporteurs:	Alberta FERRARINI	Prof. (Università di Padova)
	Burkhard LUY	Prof. (Karlsruhe Institute of Technology)
Examinateurs:	Giuseppina DE LUCA	Prof. (Università della Calabria)
	Denis MERLET	Prof. (Université Paris-Sud)
	Christie AROULANDA	Dr. (Université Paris-Sud)

to those who support me,

without saying a word

Contents

NMR spectroscopy in weakly and highly orienting media is used as a route for dealing with orientational, positional, structural and conformational problems of a variety of small rigid and flexible organic molecules in solution.

First, the very weak orientational order of a *quasi*-spherical molecule dissolved in a nematic phase is exploited for exploring the role of the different contributions to the observed dipolar coupling. In such a limit condition, a predominant effect of the non-rigid reorientation-vibration coupling term emerges. Then, NMR data obtained from small rigid probes dissolved in smectic solvents are combined with a statistical thermodynamic density functional theory, in order to measure the positional order parameters of both solutes and solvent. The methodology gives good results when applied to a conventional smectic A liquid crystal and to the more delicate case of an interdigitated smectic A_d phase.

The strategy is subsequently extended to the investigation of structure, order and conformational equilibrium of flexible bioactive or biomimetic molecules dissolved in various partially ordered NMR solvents. A first experimental and theoretical study is presented on the symmetric single-rotor molecule of biphenyl dissolved in a thermotropic liquid crystal. This test-case indicates molecular dynamics simulations are a promising tool for estimating a set of dipolar couplings of a solute in a thermotropic solvent, to be used as starting set of parameters in a standard operator-mediated NMR spectral analysis. Then, we report the conformational study of some single- and two-rotor nonsteroidal anti-inflammatory drugs, belonging to the families of salicylates and profens, dissolved in weakly orienting chiral nematic PBLG phases. A new pulse sequence, the Gradient Encoded heTeronuclear ^{1}H-^{19}F SElective ReFocusing NMR experiment (GET-SERF), is proposed here for the trivial edition of all ^{1}H-^{19}F couplings in one single NMR experiment, for a given fluorine atom. Starting from homo- and heteronuclear dipolar couplings, difficult to extract in thermotropic solvents because of a too complex spectral analysis, the torsional distributions of such molecules can be satisfactory described by the Additive Potential model combined with the Direct Probability Description of the torsional distribution in terms of Gaussian functions (AP-DPD approach). Finally, the conformational and orientational study of two stilbenoids displaying cooperative torsions is discussed in both a highly and weakly ordering liquid crystal phase. This comparative study allows to draw some conclusions on reliability, accuracy and accessibility of desired data in the two phases.

Overall, this work proves NMR in liquid crystals is a flexible and meaningful tool for studying order, structure and conformation and it can greatly benefit from the availability of several aligning media inducing a different degree of order.

GENERAL INTRODUCTION

The investigation of molecular properties, namely structure, order and, for flexible compounds, conformational equilibrium, is a crucial goal chemists, physicists and biologists pursue. Among the different techniques available for this purpose, NMR spectroscopy proved, since its first observation in 1945 by Bloch and Purcell, to be "an analytic method of the highest value in the hands of scientists" [1]. Over the decades, the technique gained a leading role for yielding detailed information on the topology, dynamics and three-dimensional structure of molecules, both in solution and in solid state, in a large variety of disciplines of natural science, from solid state physics to chemistry, biochemistry, biology, pharmaceutics, medicine and food science [2-3]. Its potentiality is further risen when it is combined with the use of partially ordered media, where molecules take up a preferred orientation with respect to the magnetic field [4-5]. Thanks to the peculiar dualism "flow-anisotropy" of these media, anisotropic interactions can be observed, even if partially averaged by molecular motions, with a quite high resolution. Indeed, these second-rank tensor quantities, averaged to zero in isotropic liquids by brownian motions, are the observables that, in anisotropic phases, do allow to extract the desired information. We have, in other words, a gateway giving direct access to molecular properties in solution. Out of the four anisotropic observables - chemical shift anisotropy, anisotropy of indirect coupling, direct dipolar coupling and quadrupolar splitting, - mainly dipolar couplings have been recognised to contain a unique wealth of structural, orientational and conformational data, thanks to their dependence on the spin-spin distances and on the orientations of the internuclear vectors with respect to the external magnetic field [4-5]. In the last 50 years, the NMR technique in partially ordered media has been largely applied both to investigate structure, order and dynamics of mesogenic molecules and to study solutes dissolved therein, with the aim of directly exploring their molecular properties or of using them as indirect probes of solute-solvent interactions and/or phase properties. At the beginning the anisotropic observables were essentially used for the determination of very accurate structural and orientational parameters in small rigid molecules dissolved in highly ordering liquid crystals. The technique was later extended to the study of small symmetric flexible compounds, where the description of conformational equilibrium, more than structural and orientational information, was the main target. The current interest moves towards more and more complex, large and asymmetrically substituted flexible molecules and this trend is particularly marked for biomolecular systems. However, if intramolecular dipolar couplings represent the "door" towards all these molecular properties, we need a "key", that is a tool able to translate the experimental data enclosed in NMR spectra into the desired physical information. Indeed, orientational order and conformational distribution are inextricably linked together. As a result of this interdependence, theoretical models are

needed in order to relate the experimental set of dipolar couplings to structure, order and conformational equilibrium of the molecule of interest [6]. A series of theoretical approaches have been proposed in the past for solving this problem and among them one of the most useful is a combination of the Additive Potential model [7] with the Direct Probability Description of the torsional distribution [8].

The orienting media used almost exclusively up to the mid-1990s include thermotropic liquid crystals, mainly nematic ones, which induce a rather high degree of alignment to the solute. Spectra of organic molecules dissolved therein consist of thousand of lines evenly dispersed in the kHz range, due to intramolecular dipolar interactions among all magnetically active nuclei in the molecule, carrying highly precise information. Despite the extremely informative content, spectral analysis is not trivial and requires graphical iterative procedures, where the availability of a good set of starting parameters represents the crucial step. With the increase in the size of the spin network and the decrease in molecular symmetry, the determination of the dipolar coupling set becomes problematic and this is the reason why the technique was traditionally limited to highly symmetric molecules with no more than 8-10 spins [4-6]. An appealing alternative came with the advent of orienting media that induce a lower degree of order compared to thermotropic mesophases. In weakly ordering phases, anisotropic interactions are averaged significantly but not entirely, so that the dipolar couplings can be scaled down from many kHz to a few Hz and the spectral quality of high-resolution NMR spectra is retained. Hence, these so-called residual dipolar couplings (RDCs) make it possible to access structural and conformational information even for large compounds with low symmetry. During the years several aligning media with a low-order parameter for molecules soluble in polar or non-polar media have been reported and successfully applied to the structural study and enantiomeric discrimination of a variety of compounds [9-12]. Among them, the chiral liquid crystalline phases made of poly-γ-benzyl-L-glutamate (PBLG) dissolved in helicogenic organic solvents are probably the most popular [13]. Despite the spreading success obtained by weakly orienting media, it should be remembered they may have some drawbacks, too. First, although the information accessibility seems to be easier than in highly ordering liquid crystals, the extraction of a large set of couplings often requires performing several multidimensional experiments and in some cases developing *ad hoc* pulse sequences. Additionally, since the size of couplings is tremendously reduced compared to strongly orienting systems, only the largest dipolar couplings between the nearest nuclei can be practically measured and the percentage error in the extracted data is supposed to be higher than in thermotropics. Generally speaking, two main philosophies have been individuated [9]. One is the "physicists' approach": the central idea is to learn as many

details as possible about a molecule in solution, in order to disclose fundamental accurate understanding of molecular arrangements and motions. In this case, thus, the molecule should be aligned as strongly as possible to give valuable long-range dipolar couplings. The second one is the "chemists' approach": the goal here is to get limited information of more complex molecules for solving specific constitutional and configurational questions. In this case, one works with very weakly aligning samples, where relatively small RDCs are available, but with sufficiently resolved spectra also to look at complex organic molecules as spin networks. The two approaches should not be considered antithetical, but rather complementary. Indeed, the possibility of following one philosophy rather than the other, *i.e.* of choosing between highly and weakly aligning media, makes NMR spectroscopy a flexible and versatile tool able to face multiple issues and to obtain molecular information in various systems, while taking into account each time the balance between difficulty in spectral analysis *versus* extent and precision of the data set.

The basic idea of this Ph.D. thesis will be then the use of NMR spectroscopy of a variety of small organic molecules dissolved in different partially ordered media as a route for (*i*) treating orientational and positional problems in systems composed of rigid compounds in uniaxial highly orienting nematic and smectic phases, and (*ii*) exploring 3D structure and conformational equilibrium of flexible bioactive molecules as solutes in highly and/or weakly aligning media. The discussion will be organized into three chapters.

An overview on the basic tools of NMR spectroscopy in partially ordered media will be given in the first chapter, with a recall of all NMR interactions and their relationship with structure, order and conformational equilibrium, along with a survey of the main theoretical models required to unlock such an extremely valuable information content. Moreover, the main classes of aligning media will be described, giving more emphasis to thermotropic LCs and PBLG phases that are used in this thesis. We will end with a discussion of the peculiar NMR methodologies necessary for recording and analysing NMR spectra of solutes dissolved in these two classes of solvents.

The second chapter will focus on the ordering behavior in highly orienting thermotropic phases. In the first part, we will study the highly symmetric molecule of tetramethylallene dissolved in the I52 nematic phase, with the aim of exploiting such a limit condition of very small orientational order to explore the role of reorientation-vibration coupling on the observed dipolar coupling. In the second part, NMR data obtained from small rigid probes dissolved in smectic solvents will be combined with a statistical thermodynamic density functional theory (ST-DFT) in order to measure the positional order parameters of both

solutes and solvent. The methodology will be applied to the conventional smectic A liquid crystal HAB and to the more delicate case of the interdigitated smectic A_d liquid crystal 8OCB.

In the third chapter the attention will be moved to flexible molecules, whose structure and conformational equilibrium will be investigated when dissolved in various liquid crystalline phases. The elucidation of the spatial arrangement of flexible organic chemicals in solution is a common target for the scientific community and this is especially true in life science and medicinal chemistry. Indeed, bioactivity and 3D structure are often intimately related. NMR in oriented phases reveals in this context particularly useful when classical NMR structural determination by short-range ^3J-coupling constants or nOe measurements fails in refining the spatial distribution of molecular sites that are far apart. In this last chapter a clearer picture will emerge about the different problems one has to face and the quality of the results one can get in the conformational analysis of a solute dissolved in a highly or weakly ordering phase. First, we will present a comparative study - NMR experiments *versus* molecular dynamics (MD) simulations - of the symmetric single-rotor molecule of biphenyl dissolved in the thermotropic 8CB liquid crystal. This well-studied molecule is chosen as test for evaluating the predictivity of MD in simulating dipolar couplings of solutes in highly ordering media, to be used as starting set of parameters for the iterative operator-mediated spectral analysis. Second, we will address the conformational investigation of some more complex anti-inflammatory molecules. Due to the asymmetry and large spin system of these drugs, PBLG-based mesophases will be used as solvent for all studies. Thanks to the small magnitude of dipolar couplings, a broad array of ^1H, ^{13}C, ^{19}F and ^2H 1D and 2D experiments are performed - or even designed - for samples of diflunisal (and its non fluorinated analogue) and naproxen, in order to collect an experimental data set as large as possible. The torsional distribution of these single- and two-independent rotor molecules will be described by the AP-DPD approach. Finally, the conformational and orientational study of two stilbenoids, *trans*-stilbene and *trans*-4,4'-dichlorostilbene, displaying two cooperative torsions, will be discussed in both a thermotropic and a lyotropic phase. From this final comparison it will be possible to draw some interesting conclusions on reliability, accuracy and accessibility of conformational information in highly and weakly ordering phases.

References

[1] *Les Prix Nobel en 1952*, G. Liljestrand ed., Nobel Foundation, Stockholm, **1953**

[2] *Modern Magnetic Resonance*, G. A. Webb ed., Springer, Dordrecht, The Netherlands, **2006**, ISBN: 9781402038945

[3] R. R. Ernst, Recent development in NMR methodology for the study of molecular structure and dynamics, *Pure Appl. Chem.*, 66, **1994**, 1583-1588

[4] *NMR of Ordered Liquids*, E. E. Burnell, C. A. de Lange eds., Kluwer Academic, Dordrecht, **2003**, ISBN: 1402013434

[5] *Nuclear Magnetic Resonance of Liquid Crystals*, J. W. Emsley ed., Reidel, Dordrecht, **1985**, ISBN: 9027718784

[6] J. W. Emsley, Liquid crystalline samples: structure of nonrigid molecules, in *Encyclopedia of Magnetic Resonance*, John Wiley & Sons, Ltd, **2007**

[7] J. W. Emsley, G. R. Luckhurst, C. P. Stockley, A theory of orientational ordering in uniaxial liquid crystals composed of molecules with alkyl chains, *Proc. R. Soc. Lond. A*, 381, **1982**, 117-138

[8] G. Celebre, G. De Luca, J. W. Emsley, E. K. Foord, M. Longeri, F. Lucchesini, G. Pileio, The conformational distribution in diphenylmethane determined by nuclear magnetic resonance spectroscopy of a sample dissolved in a nematic liquid crystalline solvent, *J. Chem. Phys.*, 118, **2003**, 6417-6426

[9] G. Kummerlöwe, B. Luy, Residual dipolar couplings as a tool in determining the structure of organic molecules, *Trends Anal. Chem.*, 28, **2009**, 483-493

[10] C. M. Thiele, Residual dipolar couplings (RDCs) in organic structure determination, *Eur. J. Org. Chem.* **2008**, 5673-5685

[11] J. Yan, E. R. Zartler, Application of residual dipolar couplings in organic compounds, *Magn. Reson. Chem.*, 43, **2005**, 53-64

[12] J. Courtieu, P. Lesot, A. Meddour, D. Merlet, C. Aroulanda, Chiral liquid crystal NMR: a tool for enantiomeric analysis, in *Encyclopedia of Nuclear Magnetic Resonance, vol. 9: Advances in NMR*, D. M. Grant, R. K. Harris eds., John Wiley & Sons, Ltd, Chichester, UK, **2002**

[13] E. T. Samulski, A. V. Tobolski, Some unusual properties of poly(γ-benzyl L-glutamate) films cast in strong magnetic fields, *Macromolecules*, 1, **1968**, 555-557

Chapter 1

NMR IN PARTIALLY ORDERED MEDIA

1.1.   Introduction

NMR spectroscopy is currently recognised as an extremely powerful technique to obtain detailed information on the topology, dynamics and three-dimensional structure of molecules both in solution and solid state as well as on the solute-solvent interaction nature. In isotropic liquids, the brownian motions average all anisotropic spin interactions to zero, yielding quite simple and well resolved spectra. On the other hand, in solids, that are "fully oriented", intra- and intermolecular interactions are present, and this results in broad and featureless spectra, which contain yet plenty of information. Only in 1963, when Saupe and Englert reported the first highly resolved spectrum in a liquid crystalline solvent [1], a smart compromise could be achieved and the potential usefulness of a study of solute molecules in liquid-crystalline phases became evident [2]. Since then, many different alignment media have been published for various applications. The uniqueness of this approach is that in partially ordered media molecules still rotate and diffuse as in normal liquids, but, owing to their anisotropic interactions, they are partially oriented [3-4]. The diffusion and rotation are responsible for the averaging out of intermolecular direct dipolar coupling so that we observe the "isolated" spins system of one molecule. Since the motion of the molecules does not deviate appreciably from that of normal liquids, linewidths of the order of few Hertz can be obtained. Therefore, anisotropic interactions can be measured with considerable accuracy. Among them, residual dipolar couplings (RDCs) have come to occupy a leading position since they provide access to incomparable information about molecular structure, orientation and conformation [3, 5-6]**.**

The aim of this chapter is to present a rapid overview on the basic tools of NMR spectroscopy in partially ordered media. In section 1.2 we will briefly describe the main classes of aligning media, focusing principally on those used in this thesis. A recall of the theoretical principles of NMR spectroscopy, including the description of all the NMR interactions, will be given in section 1.3. The relationship existing between such anisotropic observables and the structure, order and conformational equilibrium will be described in section 1.4, where the theoretical models required to unlock such an extremely valuable information content will be also presented. Finally section 1.5 will display the NMR methodology necessary for recording and analysing NMR spectra of solutes dissolved in partially ordered media.

1.2.   Partially ordered media for NMR studies

What makes partially ordered media exceptional materials for NMR studies is that they provide a unique balance between the order of solids and the flow of liquids [7-9]. Indeed, molecules in partially ordered media diffuse about much like the molecules of a liquid but concomitantly they maintain some degree of orientational order and sometimes some positional order too [10]. The amount of ordering is quite small relative to a crystal: there is only a slight tendency for the molecules to point more in one direction than others. This preferred direction is called director and is denoted by $\hat{d}$. In the absence of aligning forces the director is not constant over large volumes but varies smoothly throughout a sample without discrete changes, hence one often speaks of the director field $\hat{d}(r)$, where r is the space coordinate [9]. Broadly speaking, when a partially ordered phase is put into the magnetic field $\vec{B}_0$, the latter will induce a uniform order in the mesophase so that the preferred orientation, the director $\hat{d}$, is the same for the whole sample [11]. The orientation dependent free energy of the interaction, G, between the magnetic field and the mesophase can be expressed as [12]:

$$G = -\Delta\chi B_0{}^2 (3cos^2\theta - 1)/6 \qquad (1.1)$$

where $\Delta\chi = \chi_\parallel - \chi_\perp$ is the difference between the magnetic susceptibility parallel and perpendicular to the director (that is the anisotropy in the bulk diamagnetic susceptibility) and θ is the angle between the director and the magnetic field. The direction of minimal G, that is the preferred alignment, will depend on the quantity $\Delta\chi$ [11]: if $\Delta\chi$ is positive $\hat{d}$ will align along $\vec{B}_0$ (θ is zero to give a minimum free energy), if $\Delta\chi$ is negative the perpendicular orientation is preferred (θ = π/2 to give a minimum free energy). Fluctuations in the alignment are always present so that a more or less peaked distribution around the direction of the preferred alignment is obtained depending also on the strength of $\vec{B}_0$.

There are in principle many different possible ways to classify ordered media. For the purpose of this thesis the degree of alignment they induce on a solute dissolved therein rather than their structural properties will be underlined. For this reason, we distinguish between highly ordering and weakly ordering media. Whereas only thermotropic liquid crystals are known to induce a strong alignment, a broad array of phases inducing weak alignment of the solute molecule has been published. Among them we will give a concise description for the main classes, namely lyotropic liquid crystals and strained gels.

From the above, the needful features for a medium to be used as solvent in NMR studies are: (*i*) ability to be ordered in a magnetic field and (*ii*) ability to induce order to solutes dissolved therein. Looking at materials available in literature, many examples of anisotropic

phases that order homogenously in a magnetic field can be found among synthetic liquid crystal polymers [13-14], carbon nanotubes [15-18], ionic liquid crystals (such as ammonium, phosphonium, imidazolium, pyridinium, vinamidinium, and dithiolium salts) [19-24] or chromonic liquid crystals [25-27]. It may be interesting in the future to evaluate whether such ordered phases are also able to induce a detectable order to a solute dissolved therein and if, eventually, they could offer some advantages with respect to the already available NMR ordered phases.

1.2.1.   Highly ordering media: thermotropic liquid crystals

Two main classes of liquid crystal (LC) exist, thermotropics and lyotropics. The former induces a high degree of orientational order for a solute dissolved inside the mesophase, while the latter will be considered in the next section, among the weakly ordered media.

Thermotropic liquid crystals are built up by individual molecules and no further molecular species (specifically solvent molecules) are required for the liquid crystal phase formation. Temperature is the fundamental thermodynamic control parameter determining the phase, the two key temperature values being those defining the beginning and the end of liquid crystalline order, the melting point T_m from the crystalline solid and the clearing point T_c into an isotropic liquid [28]. Typical thermotropic liquid crystalline molecules have either a rod-like (or calamitic) or disk-like (or discotic) shape (Figure 1.1), but many exceptions on this basic motif have been described, such as sanidic (or lath-like or board-like) liquid crystals [29-30], bent-core (or banana-shaped) liquid crystals [31-35] and LC dendrimers [36-38].

Depending on the arrangement of molecules and the degree of order, thermotropic liquid crystals can show different supramolecular assemblies. The nematic phase (abbreviated N or N_D, for rod-shaped and disc-shaped molecules, respectively) is the least ordered mesophase that generally precedes the isotropic transition temperature. In this phase long-range order is of purely orientational type: the anisometric building blocks (rods or discs) are roughly oriented along one and the same direction, the director $\hat{d}$ (Figure 1.2). At the microscopic level, these molecules are mobile and their centers of mass are distributed at random throughout the volume. In other words, these molecules do not have any positional order [4, 9].
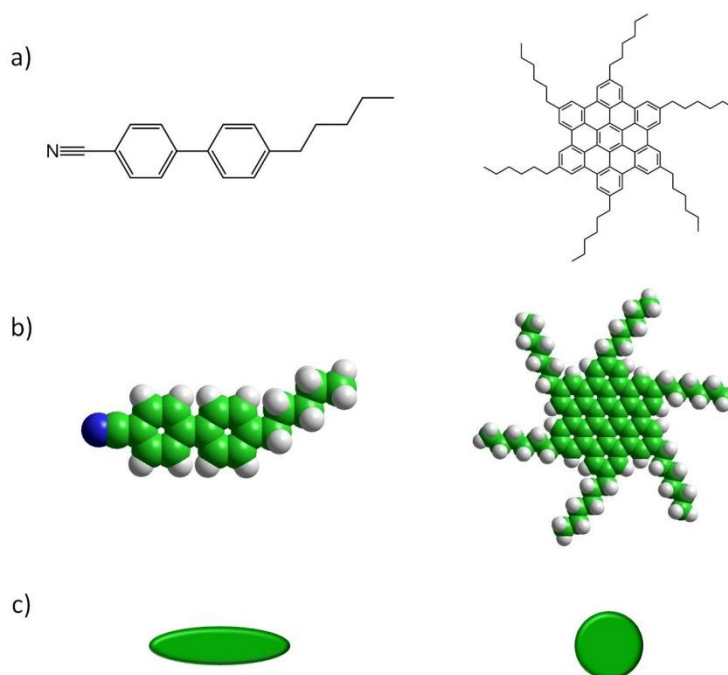
Figure 1.1. Representations of typical rod-like (4-pentyl-4'-cyanobiphenyl, 5CB, on the left) and disk-like (hexa-peri hexabenzocoronene, HBC-C6, on the right) mesogen molecules at different levels of precision: (a) topological structure, (b) "balls" representation and (c) classical schematic picture.

When both orientational long-range and positional order are observed, the phase is called smectic for rod-shaped molecules and columnar for disk-shaped ones.

In smectic phases, rod-shaped molecules are arranged parallel to each other and are separated into layers such that their long axes preferentially point in the same direction. The degree of positional order is still not very high and molecules frequently move from one layer to the next [9, 28]. Smectics are further classified depending on the molecular arrangement within and between the layers (smectic A, B, C etc) (Figure 1.3).
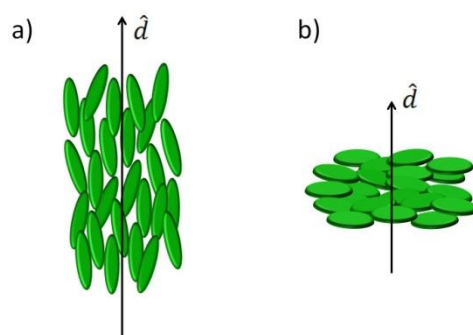
Figure 1.2. Molecular organization in a nematic phase composed of (a) rod-like and (b) disk-like molecules. The order degree is strongly exaggerated.
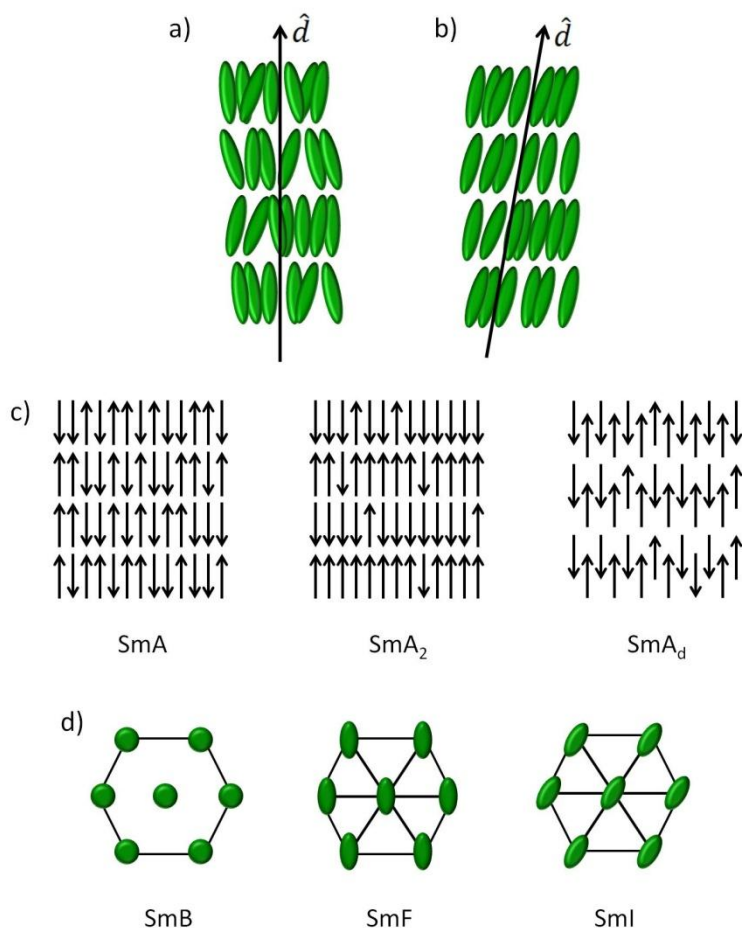
Figure 1.3. Molecular organization in the (a) smectic A and (b) smectic C phases. (c) Molecular arrangement of apolar or polar constituents of smectic layers in a monolayer SmA, bilayer SmA_2 and interdigitated bilayer SmA_d phase. (d) Schematic representation of the short-range ordering organization within the hexagon layers of a smectic B, smectic F and smectic I phase. In SmB phase, molecules are perpendicular to the smectic plane and are indicated by circles, while in SmF and SmI phases mesogens are tilted, with the major axis of the ellipse indicating the molecular tilt direction with respect to the hexagon axes. In all figures the order degree is strongly exaggerated.

For the smectic A (SmA) phase, the least ordered smectic phase, the director points along the smectic layer normal. The molecules are arranged randomly within each layer, and they have a considerable freedom for rotation around their long axis and even for translation in the smectic layer. Two modified forms of the conventional non-polar monolayer smectic A phase are generated when the constituent molecules contain strong dipole moments [39-41]: the bilayer smectic A_2 phase, where the molecules are arranged up to down within each layer producing a periodicity equal to twice the molecular length; the interdigitated bilayer smectic A_d phase, with molecules tending to pair up in a slipped-parallel configuration. The smectic C phase (SmC) is very similar to the smectic A phase but with the difference that the director makes an angle, the so-called tilt angle, with the smectic layer normal [10]. In the smectic B

phase (SmB or hexatic B phase) the symmetry within the layers is higher than A or C [9-10]: there is a 6-fold bond orientational order, which means that the lattice orientation is retained in the layers, but the translational order is lost within a few intermolecular distances. The hexagonal nature of the SmB phase generates two tilted analogues called the smectic I (SmI) phase and the smectic F (SmF) phase, where the molecules are tilted such that the hexagonal lattice tilts toward the apex and the side, respectively [10].

The columnar phase (N_{col}) is typically formed by discotic mesogens, stacked in order to form columns as in piles of coins. The columns themselves can be arranged in different two-dimensional lattices (Figure 1.4). In the hexagonal columnar phase (D_h) the molecules are stacked into columns that are further arranged into a hexagonal lattice [10]. The lattice distance from a molecule to its nearest neighbour is identical whatever the direction. Another types of columnar phases is the rectangular columnar phase (D_r), characterized by a rectangular unit cell. The lattice distance from a molecule to its nearest neighbour is directional [10].

N_{col} D_h D_r
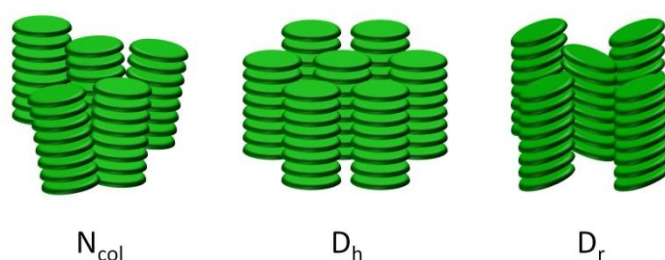
Figure 1.4. Molecular organization in a nematic columnar, hexagonal columnar and rectangular columnar phase. The order degrees (orientational and positional) are strongly exaggerated.

When optically active mesogens are used or chiral non-mesogenic dopants are added to a liquid crystal phase, the macroscopic liquid crystal phase is also chiral (this is generally indicated by adding a star to the shorthand of the corresponding achiral phase). The best studied chiral liquid crystal is the chiral calamitic nematic phase, N*, often referred to as the cholesteric phase, since many of the first compounds that possessed this phase were derivatives of cholesterol [10]. In such phases the director rotates in helical fashion about an axis perpendicular to the director (Figure 1.5). The pitch of the N* phase is the distance along the helix over which the director rotates by 360° [10]. Note however that the structure repeats itself every half pitch due to the equivalency of $\hat{d}$ and $-\hat{d}$.

The chiral discotic nematic phase (N_D*) has an analogous structure to the calamitic chiral nematic phase with a gradual rotation of the molecular director through the phase

which describes a helix [10]. In smectic A phases, a helical director modulation perpendicular to $\hat{d}$ would break the layers and is thus not normally admitted (an exception is the rare class of twist-grain boundary phases) [28]. The SmA* phase therefore has the same structure as an achiral SmA phase, but it shows interesting paraelectric properties unlike its achiral analog [28]. In contrast to SmA*, the chiral SmC* phase does allow a helical superstructure, but it applies to the direction along which the molecules tilt away from the layer normal. In other words, $\hat{d}$ in SmC* does not twist as in N*, but rotates around the cone generated by the tilt angle as the position along the normal to the layers is varied [10, 28, 42]. The SmC* phase exhibits a spontaneous polarization and can thus shows ferroelectric and antiferroelectric switching properties [43]. More recently, chiral discotic materials that exhibit tilted columnar mesophases have attracted attention too [10].
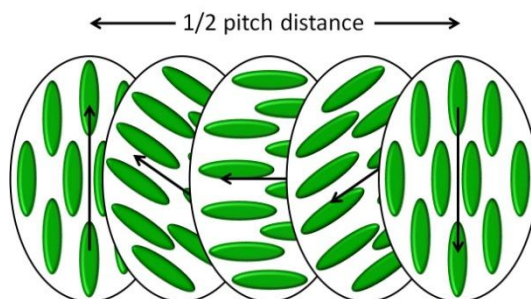
Figure 1.5. Calamitic nematic (or cholesteric) phase.

Out of the different types of thermotropic liquid crystals, nematics are the most commonly used as solvents in high resolution NMR studies since they are the least ordered and enjoy low viscosity and high mobility [4, 9]. Since nematic phases have densities and viscosities of the same order of the most common isotropic liquids, solutes in such anisotropic phases are usually considered to share the same behavior in terms of structure and conformation as in ordinary liquid phases. This issue is quite important and different opinions about the point can be found in literature [44]. Smectic and columnar phases are rarely used as NMR solvents, mainly because of their very high viscosity path [4]. Cholesterics also are not routinely used as solvents in NMR studies, probably owing to difficulty in their alignment [4], although their use may be an advantage in studying the optically active solutes [45]. In the choice of the most suitable thermotropic liquid crystal for NMR studies, attention should be paid on the two key temperature values T_m and T_c. In fact, in order to easily handle the sample, *i.e.* to obtain homogeneous samples and consequently resolved spectra, the liquid crystalline range should occur around room temperature. Additionally, it is easily understandable that the

choice of the liquid crystal for a particular NMR study strongly depends on the solubility of the solute. In Table 1.1 are listed some of the most commonly used thermotropic mesophases, together with their transition temperatures.

Table 1.1. Examples of thermotropic nematic liquid crystals used as NMR solvents.

Type	Formulae	Approximate nematic range (°C)	Approximate smectic range (°C)
Azoxybenzenes	$RO-C_6H_4-NNO-C_6H_4-OR'$	$R=R'=C_4H_9$ 18-27 $R=R'=C_6H_{13}$ 20-48 $R=R'=C_7H_{15}$ (HAB) 53-70	- - 29-53
Azobenzenes	$RO-C_6H_4-NN-C_6H_4-OR'$	$R=C_2H_5$; $R'=COC_{11}H_{23}$ 64-107	-
Schiff's bases	$R-C_6H_4-CHN-C_6H_4-R'$	$R=OCH_3$; $R'=C_4H_9$ (MBBA) 21-46 $R=OC_2H_5$; $R'=C_4H_9$ (EBBA) 35-79	- -
Cianobiphenyls	$R-C_6H_4-C_6H_4-CN$	$R=C_5H_{11}$ (5CB) 24-35 $R=C_6H_{13}O$ (6OCB) 58-76 $R=C_8H_{17}O$ (8OCB) 67-80	- - 55-67
Benzoic acid derivatives	$R-C_6H_4-COOR'$	$R=C_8H_{17}O$; $R'=H$ 107-147 $R=C_4H_9OCOO$; $R'=OC_2H_5$ 56-87	101-107 -
Cinnamic acid derivatives	$R-C_6H_4-CH-CH-COOR'$	$R=CH_3O$; $R'=H$ 171-189	-

1.2.2.   Weakly ordering media

A wide array of aligning media inducing a low degree of order does exist. In the following, only the main families will be described, even if many other methods for the weak alignment of solutes are actually employed, such as purple membrane fragments [46-48], the use of thermotropic liquid crystals close to their clearing point [49], methods of orientation of macromolecules *via* paramagnetic ions and tags [50-53] and the alignment of biomolecules as

a result of their own magnetic susceptibility anisotropy [54-56]. For a brief summary of some selected weakly ordered solvents see Table 1.2.

1.2.2.1. Lyotropic liquid crystals

The most widely used weakly ordered media are lyotropic liquid crystalline phases, which are composed, in contrast to thermotropic mesophases, of at least two components: a "liquid crystal builder", which is responsible for the anisotropic behaviour, and a solvent, that is generally polar (mainly water) but can also be apolar. For these compounds, the concentration is as important, if not more important, than the temperature in determining whether a liquid crystal phase is stable [10].

The standard constituent molecules of the liquid crystal builder are typically amphiphilic but lyotropic liquid crystals can form also by anisometric non-amphiphilic macromolecules or particles such as viruses or inorganic rods or disks in colloidal suspension. At extreme dilution, the constituent compounds are distributed randomly throughout the solution and interact only transiently with each other [57]. As their concentration is increased, molecules start aggregating and at a concentration known as critical micellar concentration, aggregates of the molecules begin to form stable semispherical entities known as direct or reversed micelles [10] (Figure 1.6).
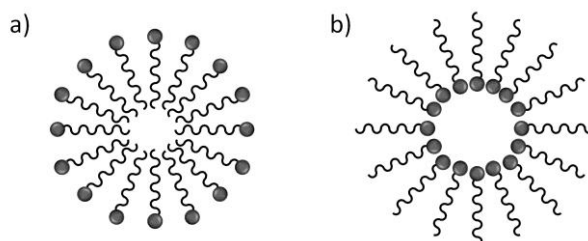
Figure 1.6. Cross sections of (a) direct and (b) reversed spherical micelles.

With a continued increase in the concentration of the constituent compound, a variety of differently shaped aggregates forms, so that several lyotropic liquid crystal phases (hexagonal, lamellar, cubic) are observed. Their description is out of the scope of this work and the reader is referred to references for more information [10, 57-60].

Compared to thermotropic systems, a remarkable advantage of lyotropic LCs is that the order induced can be manipulated within certain borders since it varies with the

concentration of the liquid crystal builder. Nevertheless, it has to be noted that the existence of a critical concentration imposes a lower concentration limit below which the liquid crystalline phase is disrupted.

i. Water-based lyotropic LCs

A large amount of lyotropic phases are known for water soluble compounds and this explains why RDCs have been extensively used in biomolecular NMR spectroscopy [56, 61-67]. Among them we just recall:

- *Lipid bicelles,* formed by planar phospholipid particles, like mixtures of dimyristoyl phosphatidylcholine (DMPC) and dihexanoyl phosphatidylcholine (DHPC), in aqueous buffer [68-71]. Their use has greatly improved the accuracy in the structural determination of biologically interesting macromolecules and in the study of intermolecular interactions [72-74].

- *Surfactant/n-alkyl alcohol mixtures,* namely aqueous solutions of cetylpyridinium chloride (CPCl) or cetylpyridinium bromide (CPBr) and *n*-hexanol [75-76] or mixtures of *n*-alkyl poly(ethylene glycol)/glucopone and *n*-alkyl alcohol (the so-called Otting phase) [77].

- *Rod-shaped* negatively charged *virus*, like the filamentous bacteriophage *Pf1* [78-80], the bacteriophage *fd* [81-82] and the tobacco mosaic virus [82].

- *DNA nanotubes* [83] *and crystalline phase G-tetrad DNA* [84]. Unlike previous lyotropic phases, they show the advantage of being compatible with the solvents typically used to solubilise membrane proteins for structural study.

- *Cellulose crystallites* in aqueous suspensions [85-87].

- *Mineral lyotropic liquid crystals*, such as V_2O_5 (vanadium pentoxide) [88-89] or $H_3Sb_3P_2O_{14}$ [90]. Important to note is that they might change the conformational equilibrium in flexible domains of the molecule studied. Although this result is not causing a problem for the structure determination of large structured biomolecules, the alignment tensor of small molecules might change.

ii. Organic solvents-based lyotropic LCs

Although widely used to align biomolecules, lyotropic LCs were not as extensively exploited at the beginning for the analysis of small organic molecules [5, 91-92], principally because the traditional aligning media were only applicable to water-soluble compounds. In order to be able to partially align small molecules that are typically insoluble in water, it is necessary to have access to orienting media compatible with organic solvents.

The first available lyotropic media based on organic solvents were the chiral liquid crystalline phases made of homopolypeptides, namely poly-γ-benzyl-L-glutamate (PBLG), poly-γ-ethyl-L-glutamate (PELG), or poly-ε-carbobenzyloxy-L-lysin (PCBLL), dissolved in helicogenic organic solvents, introduced as NMR solvents first in the mid 1990s [93-102]. In helicogenic cosolvents the main chain of the synthetic polypeptide adopts a rigid chiral α-helical conformation, while the substituted aminoacid (glutamate or lysin) side chains, which branch from the main helix, may also form a secondary molecular helix [103-104]. Spontaneously, the chiral fibers orientate to form a macroscopic, supramolecular helical structure of directors in the mesophase, typical of that exhibited by cholesteric liquid crystals. When submitted to a routine NMR magnetic field, the supramolecular helix unwinds, and the system behaves like a chiral nematic phase with positive anisotropy of the molecular diamagnetic susceptibility, with the director homogeneously aligned parallel to the static magnetic field [96, 105-106]. It can then be considered as parallel rods (formed by the α-helices of the main chain, pointing in the direction of the magnetic field) with glutamate/lysin side chains pointing out into the interstices between the rods [107] (Figure 1.7). The solute molecules are oriented in these interstices.

First advantages of homopolypeptides are their chemical inertness and ready commercial availability with high degree of polymerisation (DP) which ensures the existence of a large liquid-crystalline phase range. An additional benefit is that both the organic molecule of interest and polypeptide are readily soluble in common low viscosity organic solvents [96, 108-109]. This allows orientational information to be accessible for small organic molecules that have little or no solubility in aqueous based alignment systems. Note that the organic co-solvent employed has to homogeneously dissolve the polypeptide and preserve the α-helical structure of the polymer [96]. Therefore, trifluoroacetic acid and DMSO, for instance, are not suitable co-solvents since they form strong intermolecular hydrogen bonds with the polypeptide chain, giving rise to a random coil conformation for the polymer, and consequently, the liquid crystalline properties of the solvent disappear [96, 109].
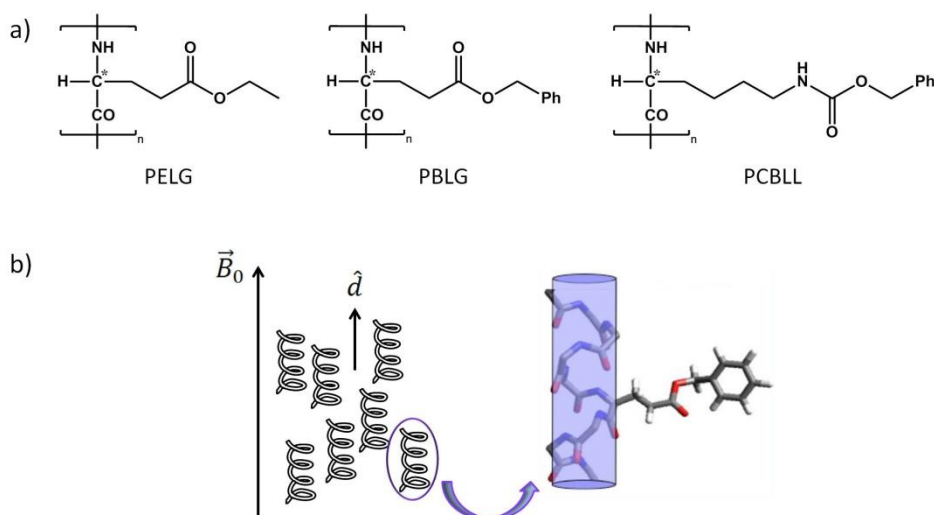
Figure 1.7. (a) Structural formulae of the chiral homopolypeptides poly-γ-benzyl-L-glutamate (PBLG), poly-γ-ethyl-L-glutamate (PELG), and poly-ε-carbobenzyloxy-L-lysin (PCBLL), and (b) the uniaxial nematic chiral liquid crystalline phase they create when dissolved in helicogenic organic solvents.

Probably the most exploited advantage of the LC phases made of homopolypeptides is their chirality, which formed the basis for the impressive work on enantiodiscrimination done first by the precursor group of Courtieu [110-120]. This property arises because the difference in the enantioselective interactions between the *S* and *R* isomers and the chiral liquid crystal generally generates a differential ordering effect (DOE) large enough to discriminate between them using order-sensitive NMR observables [97, 100, 121]. This method is found to be useful not only for systems that possess a chiral center but also for those that exhibit enantiomerism due to the presence of either a chiral axis or a chiral plane [122] and also for atropisomers [123]. Besides enantiodiscrimination, the chirality of the LC phase would, in principle, allow the determination of the absolute configuration without any derivatisation [124]. However, this is possible only if supplementary data, as the interaction of liquid crystal and single enantiomers, are known precisely in addition to NMR observables [125].

As seen above, the main disadvantage of lyotropic liquid crystalline systems is their limitation to certain concentration ranges. Indeed, this is especially true for polypeptidic lyotropic LCs since most of them align very strongly for medium-sized organic molecules even at the lower concentration limit. However, RDC amplitudes can be monitored by means of the so-called Variable Angle Sample Spinning (VASS) [126-128], which consists in spinning the sample close to the magic angle, thus reducing the magnitude of RDCs.

Recently, in the wake of the success gained by homopolypeptides, a new class of one-handed helically chiral non-racemic polymers suitable for the orientation of organic

compounds and the discrimination of enantiomers, have been proposed, including polyisocyanates [129-131], polyacetylenes [132-134], polyisocyanides [135-137], and polyguanidines [138-140]. The major drawback of these new compounds is that signals from solvents may hide those from solutes unless deuterated polymers are synthesized.

1.2.2.2. Strained gels

A conceptually different approach of inducing order is the SAG method, Strain induced Alignment in a Gel [141-143]. A common preparation scheme consists in introducing a dry polymer cylinder into an NMR tube which is then swollen by adding a solvent. Initially, the gel has pores that can be considered spherical. Homogeneous mechanical stress of the gel distorts the pores and induces partial orientation of dissolved molecules. Two main procedures can be applied to induce strain into the gel:

a) vertical stress, compression: by pushing the plunger of a Shigemi tube onto the gel which has a slightly smaller diameter (0.5 mm) than the inner diameter of the NMR tube, at the end of the reswelling process. As a consequence, the cavities in the gel will be oblate with their normal axis in the direction of the tube.

b) radial stress, stretching: by squeezing into a regular NMR tube a gel originally polymerized in a tube of larger diameter than the sample tube. In this case, the gel in the swollen state has an equilibrium diameter larger than the inner diameter of the NMR tube, so that the swelling is confined by the glass walls of the NMR tube (Figure 1.8). This results in prolate shaped pores. Radial compression can be also obtained via a commercially available device [144].

A series of different gels is currently available for the measurement of RDCs in compounds soluble both in aqueous solutions (stretched poly(acrylamide) (PAA) [143, 145-146], charged poly(acrylamide) derivatives [147-149], collagen-based gelatin [150-153] and collagen itself [154-155]) and in organic solvents (poly(vinylacetate) (PVAc) [156], polystyrene (PS) [142, 157], poly(dimethylsiloxane) (PDMS) [158], poly(methylmethacrylate) (PMMA) [159], poly(acrylonitrile) (PAN) [160], PH-poly(dimethylacrylamide) (PH-PDMAA) [161] and polyurethane (PU) [162]). Very recently, poly(ethyleneoxide) (PEO) cross-linked with γ-irradiation (γ-PEO) and chemically cross-linked (PEO-methylmethacrylate, PEOMMA) has been proposed as alignment medium possessing exceptional compatibility with both polar and nonpolar solvents [163].

The main advantage of SAG media in comparison to liquid crystalline solvents is that the order induced is independent of the strength of the magnetic field and there is no critical concentration below which phase anisotropy is lost. Therefore, RDCs can be modulated at will by varying the degree of cross linking of the gel [156-160] and by mechanically compressing or stretching the gel within the NMR sample tube, both in highly polar [151-152, 164-165] and apolar solvents [160, 166]. Other advantageous features of SAG include its effectiveness over wide ranges of temperature, pH, and ionic strength. One major drawback, however, is that, although a chiral gelatin-based SAG medium for water soluble molecules has been reported [150, 152, 167], there is, to the best of our knowledge, no chiral SAG medium based on organic solvents. Another remarkable disadvantage of stretched gels is the long time that is sometimes required for equilibration of the stretched polymer gel and for diffusion of the solute molecule into the gel (typically several days) [168].
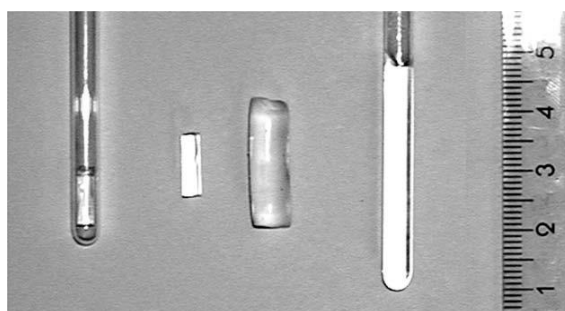
Figure 1.8. Cross-linked polystyrene in different swelling states as an example of the SAG method. From left to righ: unswollen polymer stick in a standard NMR tube, polymer stick directly after polymerization; fully swollen polymer stick; polymer stick swollen in an NMR tube with effective stretching along the tube axis [142].

Table 1.2. Selected solvent and alignment media combinations.

Description	Compatible solvents	Remarks	Ref.
Liquid crystals			
Pf1 phage	H_2O	Charged	[79]
Bicelles	H_2O		[67]
Otting phases	H_2O		[77]
Poly-γ-benzyl-L-glutamate (PBLG)	$CHCl_3$, CH_2Cl_2, DMF, dioxane, THF	Chiral	[105, 109]
Poly-γ-ethyl-L-glutamate (PELG)	$CHCl_3$, CH_2Cl_2, DMF, dioxane, THF	Chiral	[93]
Poly-ε-carbobenzyloxy-L-lysin (PCBLL)	$CHCl_3$, CH_2Cl_2, DMF, dioxane, THF	Chiral	[116]
Polyguanidines	$CHCl_3$	Chiral	[138]
Polyisocyanides	$CHCl_3$, CH_2Cl_2, THF	Chiral	[135]
Polyacetylenes	$CHCl_3$, CH_2Cl_2, C_6H_6, pyridine, THF, toluene	Chiral	[132]
Stretched gels			
Gelatin	H_2O	Chiral	[153]
Poly(acrylamide) (PAA)	H_2O		[143, 145]
Poly(dimethylacrylamide) copolymers (PH-PDMAA)	H_2O, DMF, DMSO	Charged	[161]
Poly(acrylonitrile) (PAN)	DMF, DMSO		[160]
Poly(vinylacetate) (PVAc)	acetone, $CHCl_3$, CH_2Cl_2, CH_3CN, CH_3OH, C_6H_6, DMSO, dioxane, DMF, EtOAc, THF		[156]
Poly(methylmethacrylate) (PMMA)	acetone, CH_3CN, C_6H_6, $CHCl_3$, CH_2Cl_2, EtOAc		[159]
Polystyrene (PS)	$CHCl_3$, CH_2Cl_2, C_6H_6, dioxane, THF		[142, 157]
Poly(dimethylsiloxane) (PDMS)	$CHCl_3$, CH_2Cl_2, C_6H_6, dioxane, hexane, THF	Single NMR signal	[158]
Polyurethane (PU)	acetone, $CHCl_3$, CH_2Cl_2, DMF, hexane, THF, TFE		[162]
Poly(ethyleneoxide) (PEO)	acetone, $CHCl_3$, CH_2Cl_2, CH_3OH, CH_3CN, dioxane, DMF, DMSO, H_2O, THF, TFE, toluene		[163]

1.2.3.   Macroscopic and molecular orientational order in a partially ordered phase

The common feature of all media presented above is the existence of anisotropic forces between their molecules, leading to the long range orientational order of the molecules of the phase. From this it follows that the anisotropic part of the physical properties such as the optical refractive index n, the magnetic susceptibility χ, and the electric permettivity ε, are not null anymore and can be measured. The simplest way to detect the presence of orientational order in a liquid sample is to observe it through a polarizing miscoscope. The coloured and complex patterns qualitatively reveal that the sample is birefringent and hence anisotropic in nature, but this experiment does not give a way of quantifying the extent of orientational order. In order to do that, it is necessary to produce a sample in which all the local directors are at the same orientation with respect to an external direction [169]. This can be achieved by confining appropriately the sample between closely spaced glass plates or by application of polarized magnetic or electric fields. These uniformly, macroscopically ordered samples can then be used to measure components $A_{\parallel d}$ or $A_{\perp d}$ relative to the single macroscopic director $\hat{d}$, where A is either n^2, χ or ε. These values can be used to define a macroscopic order parameter S_{mac} [169], as:

$$S_{mac} = \frac{A_{\parallel d} - A_{\perp d}}{\Delta A} \tag{1.2}$$

where ΔA is the maximum value of $A_{\parallel d} - A_{\perp d}$ which may be measurable in a single crystal sample.

S_{mac} is a very useful indication of the extent of orientational order in the liquid crystalline phase but is not a precise measure of the molecular oriention al order in the phase [169]. To describe the orientation of a single molecule relative to the director $\hat{d}$, it is useful to define from now properly the reference frames and their notation used in this thesis (see Figure 1.9):

- LAB frame: the LABoratory frame, a $\{X, Y, Z\}$ Cartesian frame with the Z-axis parallel to the alignment axis imposed by a uniaxial external field. In the following it will be the external magnetic field $\vec{B}_0$;

- DIR frame: the DIRector frame, a $\{x_d, y_d, z_d\}$ Cartesian frame with the z_d-axis parallel to the average director of the anisotropic phase;

- MOL frame: the MOLecular frame, a $\{a, b, c\}$ Cartesian frame fixed on the molecule or a rigid fragment of the molecule.
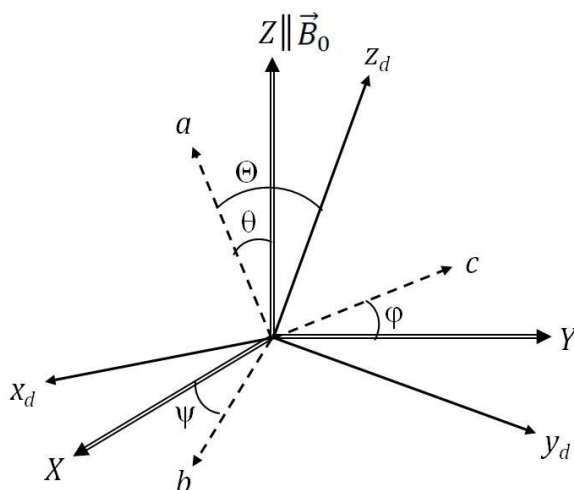
Figure 1.9. Laboratory, director and molecular frames and their relationships.

The molecule is first considered to be rigid and cylindrically symmetric about an axis a so that the orientation of the k-th molecule is specified completely by the angle Θ between the axes a and $\vec{z}_d$.

The quantities n^2, χ and ε are each second rank tensor so that [169]:

$$A_{\parallel d} - A_{\perp d} = \left[A_{aa} - \frac{1}{2}(A_{bb} + A_{cc}) \right] \left(\frac{3}{2}\cos^2\Theta - \frac{1}{2} \right) \tag{1.3}$$

Averaging over the orientations of all the molecules then gives [169]:

$$A_{\parallel d} - A_{\perp d} = \left[A_{aa} - \frac{1}{2}(A_{bb} + A_{cc}) \right] P_2(\cos\Theta) \tag{1.4}$$

where

$$P_2(\cos\Theta) = \langle \frac{3}{2}\cos^2\Theta - \frac{1}{2} \rangle \tag{1.5}$$

is an order parameter for rigid, cylindrically symmetric molecules. The angular brackets denotes an average over either the ensemble or time. If $\left[A_{aa} - \frac{1}{2}(A_{bb} + A_{cc}) \right]$ can be measured and equated to ΔA then $P_2(\cos\Theta)$ is equal to S_{mac}. Therefore, for rigid cylindrically symmetric molecules there is an equivalence between the macroscopic and molecular interpretations of an order parameter. However, most molecules, even if rigid, are not cylindrically symmetric and in these cases the order parameters are the components of the Saupe matrix defined as [169]:

$$S_{\alpha\beta}^d = \langle \frac{3\cos\Theta_\alpha \cos\Theta_\beta - \delta_{\alpha\beta}}{2} \rangle \tag{1.6}$$

where Θ_α is the angle between the director and the molecular axis α and $\delta_{\alpha\beta}$ is the Kronecker delta ($\delta_{\alpha\beta}$ = 1 if α=β and 0 otherwise). The Saupe ordering matrix is a 3X3 real, symmetric

$(S_{\alpha\beta} = S_{\beta\alpha})$, traceless $(\sum_\alpha S_{\alpha\alpha} = 0)$ tensor, hence there are a maximum of five independent non-zero elements, S_{aa}, $(S_{bb} - S_{cc})$, S_{ab}, S_{ac} and S_{bc}. Expressing these elements in spherical coordinates (r, θ, ψ), it is easy to derive the following limits [170]:

$$-\frac{1}{2} \leq S_{aa}, S_{bb}, S_{cc} \leq 1$$

$$-\frac{3}{4} \leq S_{ab}, S_{ac}, S_{bc} \leq \frac{3}{4} \qquad (1.7)$$

It is worth to point out that it is not possible to obtain the five independent order parameters from the measurement of the n, χ or ε anisotropies, but this is possible using NMR spectroscopy [169]. Indeed, what is directly probed *via* NMR spectroscopy of a partially ordered sample is typically the $S_{\alpha\beta}$ ordering matrix relative to the Z axis of the LAB frame, that is the direction of the external magnetic field. The relation between $S_{\alpha\beta}$ and $S_{\alpha\beta}^d$ is the following [171]:

$$S_{\alpha\beta} = S_{\alpha\beta}^d \cdot P_2(cos\theta_{dZ}) \qquad (1.8)$$

where $P_2(cos\theta_{dZ}) = (3cos^2\theta_{dZ} - 1)/2$ and θ_{dZ} is the angle between $Z \parallel \vec{B}_0$ and the liquid crystal director, $\hat{d}$. It is evident that when $\hat{d}$ is parallel to $\vec{B}_0$, then $S_{\alpha\beta} = S_{\alpha\beta}^d$. This is the case of liquid crystalline solvents with positive diamagnetic anisotropy we dealt with in this Ph.D. thesis. For this reason in the following we will always refer to molecular order parameters omitting the subscript d.

In thermotropic liquid crystals the orientational order parameters of solute molecules are typically on the order of 10^{-1}-10^{-2} [171]. In lyotropics and other low order aligning media the order parameters of solutes are only of the order 10^{-5}-10^{-3}, that is much smaller than that in thermotropic LCs [171]. Note that the order of the mesogen molecules themselves is invariably much higher, in the 0.5-0.85 range [172] and then for achieving such a weak solute alignment in the strongly oriented medium, interaction between solute and solvent must be very weak.

1.3.   Principles of NMR spectroscopy

Nuclear Magnetic Resonance (NMR) spectroscopy is now a commonly used method to investigate properties of both mesogen molecules and partially oriented solutes.

Research on oriented mesogens is particularly interesting due to their multiple applications. Among thermotropic low-molecular-weight LCs, ferroelectric rod-like smectogens [173-175] and banana-shaped liquid crystals [33-34, 176] were the most studied LCs in the last

decades due to their high potentialities for liquid-crystal display technology. Also discotic LCs were found to be very promising for application in nonlinear optics and charge/ions transport [177]. At the frontier between chemistry and biology, lyotropic LCs and biological LCs represent the second family of LCs that was object of recent intriguing research [178] thanks to their potential applications spanning from biomimetic technology [179] to drug delivery vehicles [180-181]. Aiming at investigating these liquid-crystalline systems, NMR spectroscopy is a well-adapted technique. Indeed, by combining information from different NMR experiments it is possible to study properties like structure, order and dynamics, that have a significant role in the technological and biological applications of these materials. ^{13}C [182] and especially ^{2}H [183] NMR spectroscopies have been extensively used to study molecular- and phase- structure and order parameters of thermotropics like commercial nematics and smectics [184-185], ferroelectric smectogens [42, 186-187], biaxial nematic phase of banana-shaped LC materials [188-190], discotic LCs [191-192], LC dendrimers [36-37], LC polymers and elastomers [193-195]. The structural and ordering study of lyotropic liquid crystals is more challenging since they are highly heterogeneous systems. Anyway, several NMR experiments can be carried out, possibly combining the complementary properties of different nuclei, such as ^{13}C, ^{1}H, ^{15}N, ^{14}N, ^{31}P, ^{2}H, and ^{19}F [196-200]. Besides structural and ordering studies, NMR spectroscopy has been widely used to investigate the molecular dynamics in liquid-crystalline materials, which can be rather complex due to the occurrence of several kinds of motions and to the partial overlapping among their characteristic times [201-203]. For this purpose, ^{1}H relaxation dispersion measurements together with ^{13}C and ^{2}H linewidth and relaxation studies have been employed to characterize (*i*) single-molecular motions, including internal motions (such as rotations around single or double bonds and *trans-gauche* isomerizations of alkyl chains) [204-206] and single-molecular diffusion motions [207-209] and (*ii*) collective motions (that is the motion of groups of molecules fluctuating or diffusing in anisotropic ways, maintaining a symmetry which reflects that of the mesophase), such as the order director fluctuation in uniaxial phases [210-212] and the layer undulation in smectic phases [213-214].

Together with the NMR study of mesogenic molecules themselves, a huge research field is addressed to the investigation of solute molecules dissolved in partially ordered solvents. Due to the ordering of the solvent molecule, also the solute molecules tend to have a preferred orientation and residual anisotropic spectral parameters can be observed in NMR experiments. At the beginning these anisotropic observables were essentially used for the determination of structural parameters (with up to 10^{-3} Å of accuracy in bond length and 10^{-1} degree in bond angles) and orientational order parameters in small rigid molecules dissolved in highly ordering liquid crystalline solvents [3, 215]. Over the years the liquid crystal NMR

technique was extended to the study of flexible molecules, where not only structural and orientational information, but also conformational equilibria can be investigated. The extreme complexity of the [1]H-spectra (the most studied nucleus) of small flexible compounds dissolved in thermotropics generally required some methods to simplify the spectral analysis and limited the technique to highly symmetric molecules with no more than 8-10 spins [216-218]. The methodological and instrumental development as well as the advent of new aligning media allowed then larger and asymmetrically substituted flexible molecules to be investigated [5, 92, 219], up to larger biomolecular systems, such proteins or nucleic acids [54, 67, 172, 220]. The widespread interest in the investigation of solutes' properties by liquid crystal NMR spectroscopy mainly resides in the possibility to have access, unlike any other technique, to experimental information about three-dimensional structure and conformational distribution directly in a liquid phase.

Whatever the kind of molecule - mesogen or solute - its NMR spectra in an anisotropic environment are dominated by second rank tensorial properties partially averaged by the anisotropic molecular tumbling. Intermolecular interactions are averaged to zero by molecular translational diffusion so that the intramolecular interactions can be detected without the complications of intermolecular ones which dominate the NMR spectra of solids [11]. In order to understand the general factors determining the structure taken by the spectra of nuclei in partially oriented media, it is first necessary to discuss the principal contributions to the nuclear spin Hamiltonian. The intent of this section is thus not to deeply explore the theoretical basis of NMR spectroscopy (many reviews and books already did in comprehensive and elegant way), but to underline those fundamental concepts that are necessary to understand the source of such an astonishingly informative technique.

1.3.1.   Nuclear spin Hamiltonian

A NMR spectrum of an *ensemble* of *N* spins contains typically two kinds of information which may be classed as static and dynamic. The static information is contained in the position and intensities of the lines, whereas the dynamic information in the spin-lattice and spin-spin relaxation times of the nuclei [6, 11]. We will treat here only the static part; for a general treatment of the spin Hamiltonian the reader is referred to references [221-222].

Frequencies and intensities are obtained by solving the time-independent Schrödinger equation:

$$\widehat{H}|\Psi_n\rangle = E_n|\Psi_n\rangle \tag{1.9}$$

where $\widehat{H}$ is the Hamiltonian operator of the considered system and E_n is the energy eigenvalue corresponding to the n-th eigenstate $|\Psi_n\rangle$.

The nuclear spin Hamiltonian can be written as sum of Hamiltonians accounting for the different interactions [6]:

$$\widehat{H} = \sum_\lambda \widehat{H}_\lambda = \widehat{H}_Z + \widehat{H}_\sigma + \widehat{H}_J + \widehat{H}_D + \widehat{H}_Q + \widehat{H}_{SR} \tag{1.10}$$

where $\widehat{H}_Z$, $\widehat{H}_\sigma$, $\widehat{H}_J$, $\widehat{H}_D$ and $\widehat{H}_Q$ are the terms accounting respectively for the Zeeman and the shielding interaction, the indirect and the direct spin-spin coupling and the quadrupolar coupling. Each of them will be discussed in section 1.3.2. $\widehat{H}_{SR}$ is the spin-rotation coupling that accounts for the interactions of the nuclear spins with magnetic fields generated by the rotational motions of the molecules [223]. Albeit it is a dominant relaxation mechanism in gases, it is of marginal importance in liquid- and solid-state NMR, then it will be neglected in the following.

Each generic interaction $\widehat{H}_\lambda$, and then the nuclear spin Hamiltonian, can be written using either Cartesian or irreducible spherical tensor form. Both will be used since there are useful to underline different aspects.

In the Cartesian representation the various terms of the spin Hamiltonian can be expressed as scalar product [11]:

$$\widehat{H}_\lambda = \widehat{U}_\lambda^T \cdot \check{T}_\lambda \cdot \widehat{V}_\lambda \tag{1.11}$$

where $\check{T}_\lambda$ is a second rank Cartesian tensor representing the λ-th interaction, $\widehat{U}_\lambda$ and $\widehat{V}_\lambda$ are the vector operators of two interacting physical quantities, which can be two spins or a spin and an external magnetic field, and the superscript T (omitted for simplicity in the following) stands for transposed. [1]

It does exist a Principal Axis Frame or Principal Axis System (PAS), which is a particular molecular frame in which a selected interaction $\check{T}_\lambda$ is described by a diagonal tensor. Note that the frame is principal for that specific interaction and, in general, different interactions have different principal axis systems.

Generally speaking, even though the Cartesian representation of a tensor is often the easiest way of visualizing its components and their meaning in the chosen basis, from a purely mathematical point of view it may be preferable to express tensors in terms of their

---

[1] We assume, here and throughout the thesis, to work in a Cartesian (rectangular) coordinate system, so (*i*) there is no need to distinguish between covariant and contravariant tensors, thus the notation with indices as subscripts will be always used, and (*ii*) a second rank tensor and the matrix by which it can be represented have the same transformation laws upon a change of basis, thus allowing tensor or matrix to be used indistinctly.

irreducible form. Indeed, any second rank Cartesian tensor can be always decomposed into three tensors [224]:

$$\check{T}_\lambda = T_\lambda^{(0)} + T_\lambda^{(1)} + T_\lambda^{(2)} \tag{1.12}$$

In the Cartesian notation each term is represented by a 3X3 matrix: $T_\lambda^{(0)}$ is the diagonal matrix $\frac{1}{3}Tr(\check{T}_\lambda) \cdot \mathbf{1}$, that corresponds to a scalar component proportional to the trace of the tensor; $T_\lambda^{(1)}$ is an antisymmetric tensor having three independent components; and finally $T_\lambda^{(2)}$ is a traceless symmetric matrix with five independent components. In principle, this decomposition does not require any basis change but it is convenient to use spherical coordinates in order to obtain objects possessing simple transformation properties under rotations. The obtained irreducible tensors expressed in spherical coordinates are called irreducible spherical tensors [224]. An irreducible spherical tensor of rank l is composed of $2l + 1$ components $T_\lambda^{(l,m)}$, where m goes from $-l$ to $+l$ in unitary step. In this notation, the Hamiltonian of a spin interaction λ can be expressed as a sum over scalar products of two irreducible spherical tensors, in the following way [11, 225]:

$$\widehat{H}_\lambda = \sum_l \sum_{m=-l}^{+l} (-1)^m T_\lambda^{(l,m)} \, \widehat{A}_\lambda^{(l,-m)} \tag{1.13}$$

where $T_\lambda^{(l,m)}$ are the irreducible spherical components of the tensor representing the λ-th interaction and $\widehat{A}_\lambda^{(l,-m)}$ is the appropriate nuclear spin operator.

Since NMR investigations are aimed at molecular properties whereas the observable quantities are measured in the LAB frame, a continuous change of reference frame is needed. Basic tools for rotating the reference frame in Cartesian and spherical notation are recalled in Appendix A1.

NMR experiments are usually performed with a static magnetic field which is very high, such that interaction with it is several order of magnitude bigger than other interactions (sometimes quadrupolar interaction may be significative for nuclei with very high nuclear quadrupolar constants). It is possible thus to consider interaction with B_0 as the predominant and to treat other interactions as a perturbative correction to the energy. In this approximation, called *secular* or *high field approximation* (HFA), the only part of the spin Hamiltonian that is relevant for the various internal interactions is the one commuting with the interaction term with B_0, while non commuting terms will be discarded [11]. In the Cartesian representation this corresponds to take only the component of the Cartesian tensor in the Z direction (defined as the direction of the field B_0), that is T_{zz}, which is called its secular part. In the irreducible spherical representation it implies to neglect tensor components with $m \neq 0$,

that is, to retain only the $T^{(l,0)}$ terms. Note that in the case of uniaxial phases with $\hat{d} \parallel \vec{B}_0$ we do not need the HFA in order to delete non-secular terms and $m \neq 0$ terms vanish because of the $D_{\infty h}$ symmetry of the phase [11].

It is possible to simplify further the NMR Hamiltonian in the irreducible spherical form. Because all NMR observable quantities are described by second rank tensors, it is possible to retain only terms with $l = 0,1,2$. Moreover, for symmetric second rank tensor terms with $l = 1$ disappear and only components with $l = 0$ and $l = 2$ do not vanish. [2] Combining these arguments with HFA, equation (1.13) may be re-written as [225]:

$$\hat{H}_\lambda = T_\lambda^{(0,0)} \hat{A}_\lambda^{(0,0)} + T_\lambda^{(2,0)} \hat{A}_\lambda^{(2,0)} \tag{1.14}$$

The spherical notation clearly shows that in general there are rotationally invariant contributions (those with $l = 0$), which is the only part surviving in isotropic phase spectra, and anisotropic contributions (those with $l = 2$).

1.3.2.   NMR interactions

Spherical tensor notation has been appropriate so far since this facilitates the identification of which components can be simplify in the Hamiltonian, but it is more useful to use a Cartesian frame when considering individual contributions $\hat{H}_\lambda$. Thus, the spin operators are best represented in term of $\hat{I}_{i,z}$ and the raising and lowering operators $\hat{I}_{i,\pm}$. [3]

Before describing the individual contributions to the Hamiltonian it is useful to write the general relationship between the ZZ-component of the second rank tensor $\breve{T}_\lambda$ and its components in a molecular frame $T_{\alpha\beta}$ [11].

$$T_{zz} = \sum_{\alpha,\beta} cos\theta_{\alpha z} T_{\alpha\beta} cos\theta_{\beta z} \tag{1.15}$$

where $\theta_{\alpha z}$ is the angle between the Z-axis in the LAB frame and the α axis in the MOL frame. By addition and subtraction of the trace of $\breve{T}_\lambda$, we get:

$$T_{zz} = \frac{1}{3}(T_{aa} + T_{bb} + T_{cc}) + \frac{2}{3}\sum_{\alpha,\beta}\frac{1}{2}(3cos\theta_{\alpha z}cos\theta_{\beta z} - \delta_{\alpha\beta})T_{\alpha\beta} \tag{1.16}$$

---

[2] Note that, while dipolar and quadrupolar tensors are recognized to be symmetric, the symmetry of chemical shift and indirect spin-spin coupling tensors has not yet been demonstrated. Even in this case, however, terms with $l = 1$ may be neglected without significant errors in the routine NMR.
[3] The raising and lowering operators are defined as:

$\hat{I}_{i,+} = \hat{I}_{i,x} + i\hat{I}_{i,y}$
$\hat{I}_{i,-} = \hat{I}_{i,x} - i\hat{I}_{i,y}$

where $\delta_{\alpha\beta}$ is the Kronecker delta (unity if α=β and zero otherwise).

For

$$T^{iso} = \frac{1}{3}(T_{aa} + T_{bb} + T_{cc}) = \frac{1}{3}Tr(\breve{T}) \tag{1.17}$$

and

$$T^{aniso} = \frac{2}{3}\sum_{\alpha,\beta}\frac{1}{2}(3cos\theta_{\alpha z}cos\theta_{\beta z} - \delta_{\alpha\beta})T_{\alpha\beta} \tag{1.18}$$

we have

$$T_{zz} = T^{iso} + T^{aniso} \tag{1.19}$$

Only quantities T^{iso} are measurable in isotropic solutions. The direct dipolar couplings and quadrupolar interactions are both traceless, so they give no observable splitting in isotropic phase spectra, although they influence the linewidth and relaxation times. On the other hand, the quantities T^{aniso} appear in and can dominate the partially oriented spectra.

Nuclear Zeeman interaction and shielding interaction

The interaction of spin moments with the static magnetic field is described by a Zeeman Hamiltonian given by:

$$\widehat{H}_Z = -\sum_i \mu_i B_0 = -\hbar\sum_i \gamma_i B_0 \hat{I}_{i,z} = \hbar\sum_i \omega_{i,0}\hat{I}_{i,z} \tag{1.20}$$

where $\mu_i = \gamma_i \hbar \hat{I}_{i,z}$ is the magnetic dipolar moment, $\hbar = h/2\pi$, with h the Planck's constant, γ_i is the magnetogyric ratio, B_0 is the static magnetic field aligned with $\vec{Z}$-axis in the laboratory frame and $\omega_{i,0} = -\gamma_i B_0$ can be identified as the Larmor frequency of spin I_i.

The external static magnetic field induces currents in the electron clouds surrounding the nuclei, which in turn generate an induced magnetic field. The induced magnetic field is proportional to the static field B_0 and interacts with nuclear spins through the shielding tensor $\breve{\sigma}$. In the HFA, the associated Hamiltonian has the following form:

$$\widehat{H}_\sigma = \hbar\sum_i \gamma_i \sigma_{i,zz} B_0 \hat{I}_{i,z} = -\hbar\sum_i \omega_{i,0}\, \sigma_{i,zz}\hat{I}_{i,z} \tag{1.21}$$

where $\sigma_{i,zz}$ is the ZZ-component of the tensor $\breve{\sigma}$.

It is common to combine the Zeeman interaction with the static magnetic field and the shielding interaction by introducing the modified Zeeman interaction or chemical shift interaction, $\widehat{H}_\delta$, that is defined as the interaction between the nuclear magnetic dipole moment and the effective magnetic field at the nucleus i [6].

$$\hat{H}_\delta = -\hbar \sum_i \gamma_i (1 - \sigma_{i,zz}) B_0 \hat{I}_{i,z} = \hbar \sum_k \omega_{i,0}(1 - \sigma_{i,zz})\hat{I}_{i,z} \tag{1.22}$$

As seen for a generic second rank tensor $\breve{T}_\lambda$, it is possible to write $\sigma_{i,zz}$ as [225]:

$$\sigma_{i,zz} = \sigma_i^{iso} + \sigma_i^{aniso} \tag{1.23}$$

then the equation (1.22) becomes:

$$\hat{H}_\delta = -\hbar \sum_i \gamma_i (1 - \sigma_i^{iso} - \sigma_i^{aniso}) B_0 \hat{I}_{i,z} \tag{1.24}$$

where of course $\sigma_i^{iso} = \frac{1}{3}(\sigma_{aa} + \sigma_{bb} + \sigma_{cc})$ is the isotropic contribution normally measured in conventional liquid samples, and $\sigma_i^{aniso} = \frac{2}{3}\sum_{\alpha,\beta}\frac{1}{2}(3cos\theta_{\alpha z}cos\theta_{\beta z} - \delta_{\alpha\beta})\sigma_{\alpha\beta}$ is the anisotropic contribution that appears in partially ordered liquid samples.

In molecules with high symmetry (possessing at least a threefold symmetry axis) σ_i^{aniso} reduces to the shielding anisotropy term $\Delta\sigma_i = \sigma_{aa} - \frac{1}{2}(\sigma_{bb} + \sigma_{cc})$ [171]. Despite its measurement is of considerable importance in partially ordered systems, its treatement falls outside the purpose of this thesis and more information can be found in references [171 and refs. therein, 226-227].

Scalar or indirect spin-spin coupling

The indirect spin-spin coupling interaction represents the indirect magnetic interaction of nuclear spins with each other mediated by bonding electrons. The most general form of $\hat{H}_J$ is [6]:

$$\hat{H}_J = \sum_{i<j} \hat{I}_i \cdot \breve{J}_{ij} \cdot \hat{I}_j \tag{1.25}$$

where $\breve{J}_{ij}$ is a second-rank tensor. In the HFA, the only terms remaining in the equation are those which involve spin operators commuting with $\hat{I}_z$, the total Z component of spin angular momentum [6]:

$$\hat{H}_J = \sum_{i<j} \left\{ J_{ij,zz}\hat{I}_{i,z}\hat{I}_{j,z} + \frac{1}{4}(J_{ij,xx} + J_{ij,yy})(\hat{I}_{i,+}\hat{I}_{j,-} + \hat{I}_{i,-}\hat{I}_{j,+}) \right\} \tag{1.26}$$

As before, the components in the (X, Y, Z) space-fixed axis system can be expressed in terms of molecule-fixed axes (a, b, c) as [6]:

$$\frac{1}{4}(J_{ij,xx} + J_{ij,yy}) = \frac{1}{2}J_{ij}^{iso} - \frac{1}{4}J_{ij}^{aniso} \tag{1.27}$$

and

$$J_{ij,zz} = J_{ij}^{iso} + J_{ij}^{aniso} \tag{1.28}$$

with again $J_{ij}^{iso} = \frac{1}{3}(J_{aa} + J_{bb} + J_{cc})$ the isotropic contribution and $J_{ij}^{aniso} = \frac{2}{3}\sum_{\alpha,\beta}\frac{1}{2}(3cos\theta_{\alpha z}cos\theta_{\beta z} - \delta_{\alpha\beta})J_{\alpha\beta}$ the anisotropic contribution, that is non-zero only in partially ordered solvents [171, 228-229].

Substituting equations (1.27) and (1.28) into equation (1.26) gives [6, 170]:

$$\hat{H}_J = \sum_{i<j} J_{ij}^{iso}\left\{\hat{I}_{i,z}\hat{I}_{j,z} + \frac{1}{2}(\hat{I}_{i,+}\hat{I}_{j,-} + \hat{I}_{i,-}\hat{I}_{j,+})\right\} + \sum_{i<j} J_{ij}^{aniso}\left\{\hat{I}_{i,z}\hat{I}_{j,z} - \frac{1}{4}(\hat{I}_{i,+}\hat{I}_{j,-} + \hat{I}_{i,-}\hat{I}_{j,+})\right\} \quad (1.29)$$

Dipolar or direct spin-spin coupling

The through-space or direct dipolar spin-spin interaction corresponds to the classical coupling between magnetic dipoles. Every spin magnetic moment generates a magnetic field a second spin can interact with: the interaction is mutual and does not involve the electron clouds.

The classical interaction energy E between two magnetic dipole moments $\vec{\mu}_i$ and $\vec{\mu}_j$ is given by [170]:

$$E = \frac{\vec{\mu}_i \cdot \vec{\mu}_j}{r_{ij}^{\,3}} - \frac{3(\vec{\mu}_i \cdot \vec{r}_{ij})(\vec{\mu}_j \cdot \vec{r}_{ij})}{r_{ij}^{\,5}} \quad (1.30)$$

where $\vec{r}_{ij}$ is the vector from $\vec{\mu}_i$ to $\vec{\mu}_j$ with magnitude r_{ij}.

In quanto-mechanical form, treating $\vec{\mu}_i$ and $\vec{\mu}_j$ as operators, the equation becomes:

$$\hat{H}_D = 2 \cdot \sum_{i<j} \hat{I}_i \cdot \breve{D}_{ij} \cdot \hat{I}_j = \sum_{i<j} \frac{\mu_0}{4\pi}\frac{h\,\gamma_i\gamma_j}{4\pi^2 r_{ij}^5}\left[r_{ij}^2\delta_{\alpha\beta} - 3r_{ij,\alpha}r_{ij,\beta}\right]\hat{I}_{i,\alpha}\hat{I}_{j,\beta} \quad (1.31)$$

The indices α and β label the LAB axes and $r_{ij,\alpha}$ is the α component of $\vec{r}_{ij}$.

Introducing the polar coordinates (r,θ,ψ) [4] and by employing the ladder operators the dipolar Hamiltonian can be written as [170]:

$$\hat{H}_D = \sum_{i<j} \frac{\mu_0}{4\pi}\frac{\gamma_i\gamma_j}{r_{ij}^3}\frac{h}{4\pi^2}\{A + B + C + D + E + F\} \quad (1.32)$$

where

$$A = (1 - cos^2\theta_{ij})\hat{I}_{i,z}\hat{I}_{j,z}$$

$$B = -\frac{1}{4}(1 - cos^2\theta_{ij})(\hat{I}_{i,+}\hat{I}_{j,-} + \hat{I}_{i,-}\hat{I}_{j,+})$$

$$C = -\frac{3}{2}sin\theta_{ij}\,cos\theta_{ij}\,e^{-i\psi}(\hat{I}_{i,+}\hat{I}_{j,z} + \hat{I}_{i,z}\hat{I}_{j,+})$$

---

[4] To convert from Cartesian to polar coordinates, consider that:
$Z = r\,cos\theta$
$X = r\,sin\theta cos\psi$
$Y = r\,sin\theta sin\psi$

$$D = -\frac{3}{2}sin\theta_{ij}\,cos\theta_{ij}\,e^{+i\psi}(\hat{I}_{i,-}\hat{I}_{j,z} + \hat{I}_{i,z}\hat{I}_{j,-}) = C^*$$

$$E = -\frac{3}{4}sin^2\theta_{ij}\,e^{-2i\psi}\,\hat{I}_{i,+}\hat{I}_{j,+}$$

$$F = -\frac{3}{4}sin^2\theta_{ij}\,e^{+2i\psi}\,\hat{I}_{i,-}\hat{I}_{j,-} = E^* \tag{1.33}$$

with μ_0 the vacuum permeability, h the Planck's constant, γ_i and γ_j the magnetogyric ratios of the nuclei i and j and θ_{ij} the angle between the internuclear vector r_{ij} and the magnetic field.

In the HFA, the contribution from the terms from C to F becomes negligible and these terms can therefore be dropped from $\hat{H}_D$. Under this approximation thus only the secular terms A and B contribute to the NMR spectrum and the dipolar Hamiltonian can be written as [170]:

$$\hat{H}_D = \sum_{i<j}\frac{\mu_0}{4\pi}\frac{\gamma_i\gamma_j h}{4\pi^2 r_{ij}^3}\,(1 - 3cos^2\theta_{ij})\left\{\hat{I}_{i,z}\hat{I}_{j,z} - \frac{1}{4}(\hat{I}_{i,+}\hat{I}_{j,-} + \hat{I}_{i,-}\hat{I}_{j,+})\right\} \tag{1.34}$$

The spatial part of the interaction is the ZZ-component of the dipolar tensor $\breve{D}_{ij}$, so that [170, 225]:

$$\hat{H}_D = 2\sum_{i<j}D_{ij,zz}\left\{\hat{I}_{i,z}\hat{I}_{j,z} - \frac{1}{4}(\hat{I}_{i,+}\hat{I}_{j,-} + \hat{I}_{i,-}\hat{I}_{j,+})\right\} \tag{1.35}$$

with

$$D_{ij,zz} = D_{ij}^{aniso} = -\frac{1}{2}\cdot\frac{\mu_0\gamma_i\gamma_j h}{16\pi^3 r_{ij}^3}(3cos^2\theta_{ij} - 1) = -\frac{1}{2}\frac{K_{ij}}{r_{ij}^3}(3cos^2\theta_{ij} - 1) \tag{1.36}$$

where K_{ij} is a constant for a given pair of nuclei denoted as:

$$K_{ij} = \frac{\mu_0\gamma_i\gamma_j h}{16\pi^3} \tag{1.37}$$

Note here that the dipolar tensor is traceless thus it is purely anisotropic.

Total spin-spin coupling

Comparing equations (1.29) and (1.35) for $\hat{H}_J$ and $\hat{H}_D$ it is seen that the multiplier of the spin operator for J_{ij}^{aniso} has the same form as that of $D_{ij,zz}$ and therefore J_{ij}^{aniso} is also called pseudo-dipolar coupling. $\hat{H}_J$ and $\hat{H}_D$ can then be combined to give the Hamiltonian for the total coupling [6]:

$$\hat{H}_T = \hat{H}_J + \hat{H}_D = \sum_{i<j}(J_{ij}^{iso} + 2D_{ij,zz} + J_{ij}^{aniso})\hat{I}_{i,z}\hat{I}_{j,z}$$

$$+ \frac{1}{2}\left(J_{ij}^{iso} - D_{ij,zz} - \frac{1}{2}J_{ij}^{aniso}\right)(\hat{I}_{i,+}\hat{I}_{j,-} + \hat{I}_{i,-}\hat{I}_{j,+}) \tag{1.38}$$

The total splitting that can be measured in a spectrum between spins i and j is:

$$T_{ij} = \left| J_{ij}^{iso} + J_{ij}^{aniso} + 2D_{ij,zz} \right| \text{ (non} - \text{equivalent nuclei)} \tag{1.39}$$

$$T_{ij} = \frac{3}{2} \left| J_{ij}^{aniso} + 2D_{ij,zz} \right| \text{ (equivalent nuclei)} \tag{1.40}$$

with T_{ij} the total spin-spin coupling and $|...|$ the absolute value bars. [5]

From the analysis of a spectrum in isotropic phase one may obtain values of J_{ij}^{iso}, while analysis of a spectrum of oriented molecules yields values of ($J_{ij}^{iso} + J_{ij}^{aniso} + 2D_{ij,zz}$). This means one can have by subtraction separate values of J_{ij}^{iso} and ($2D_{ij,zz} + J_{ij}^{aniso}$) but not of $D_{ij,zz}$ and J_{ij}^{aniso}.

For nuclear pairs ^{1}H-^{1}H and ^{13}C-^{1}H the ratio $J_{ij}^{aniso}/D_{ij,zz}$ has be found to be of the order of 10^{-4} and 10^{-3}, thus J_{ij}^{aniso} is safely neglected, leading to a relative error of the order of 3×10^{-4} [3, 228]. In general, every J_{HX}^{aniso} between a proton and a general X nucleus is small enough to be neglected [228]. For example the value of $J_{ij}^{aniso}/D_{ij,zz}$ in the case of ^{19}F-^{1}H couplings was estimated to be of about 10^{-3} [3]. In such cases, the total splitting observable between two nuclei can be rewritten as [11]:

$$T_{ij} = \left| J_{ij}^{iso} + 2D_{ij,zz} \right| \text{ (non} - \text{equivalent nuclei)} \tag{1.41}$$

$$T_{ij} = 3 \left| D_{ij,zz} \right| \text{ (equivalent nuclei)} \tag{1.42}$$

Contrarily, in couplings between two nuclei other than ^{1}H (such as ^{13}C, ^{14}N, ^{15}N, ^{19}F, ^{29}Si, ^{31}P, ^{77}Se, ^{111}Cd, ^{113}Cd, ^{119}Sn, ^{199}Hg) contribution of J_{ij}^{aniso} was found to be small but significant [228 and refs. therein] and several liquid crystal NMR studies were focused on estimating accurately its size and comparing it to the corresponding theoretically computed value, especially in the case of ^{13}C-^{13}C couplings [230-234], ^{14,15}N-^{13}C couplings [233-235], ^{19}F-^{13}C and ^{19}F-^{19}F couplings [236-241].

Unfortunately, *J* anisotropies are not so simple to determine and in this thesis we will neglect them not only for ^{1}H-^{1}H, ^{1}H-^{13}C and ^{1}H-^{19}F couplings, as usually done, but also in the case of ^{13}C-^{19}F and ^{19}F-^{19}F couplings. This can be justified considering that the ratio $J_{ij}^{aniso}/D_{ij,zz}$ for nuclear pairs such as ^{13}C-^{19}F and ^{19}F-^{19}F does not exceed values of 10^{-2} - 10^{-1} [3, 236, 238], and then neglecting it does not invalidate the degree of accuracy achieved in our analysis.

---

[5] Note that the symbol T_{ij} used here for the total spin-spin coupling is different from the T generic interaction defined before.

Quadrupolar interaction

Nuclei with spin moment higher than 1/2 experience a non-spherical distribution of the electric charge around the nucleus producing an electric quadrupole moment and, in the presence of an external electric field gradient, there is a contribution to the Hamiltonian.

The general case of a quadrupole interaction comparable with the Zeeman term is complex because the magnetic field direction is not a unique axis of quantization of the nuclear spin angular momentum [225]. However, most studies in partially oriented phases involve the much simpler case where the quadrupolar interaction is much smaller than the Zeeman term, and the Hamiltonian for this situation is given here. In this case [225]:

$$\widehat{H}_Q = \sum_i \hat{I}_i \cdot \breve{Q}_i \cdot \hat{I}_i = \sum_i \frac{q_{i,zz}}{4I_i(2I_i - 1)}\left[3\hat{I}_{i,z}\hat{I}_{i,z} - I_i(I_i + 1)\right] \tag{1.43}$$

The term $q_{i,zz}$ is given by

$$q_{i,zz} = \frac{eQ_i V_{i,zz}}{h} \tag{1.44}$$

where eQ_i is the nuclear electric quadrupole moment of nucleus i and $V_{i,zz}$ is the partially averaged component of the electric field gradient tensor measured at the nucleus, and in the direction of $\vec{B}_0$. Note that, as the dipolar interaction, also the quadrupolar tensor is purely anisotropic.

1.4.   Relationship between NMR observables and structure, order and conformational equilibrium

In the previous section we outlined the interactions that are responsible for the typical features displayed by the spectrum of a molecule dissolved in a liquid crystalline medium. However, we did not explain yet how these experimental data are linked to orientational and conformational information. Indeed, the equations above are incomplete, since we neglected molecular motions, which happens in a quicker time-scale that NMR ones, and thus average NMR interactions. Molecular motions include reorientational motions (the molecule rotates as a whole with respect to a chosen direction) and internal motions, namely translational, vibrational and rotational motions. It is convenient in the following to separate the case of (*i*) rigid molecules, showing only fast, high frequency, small-amplitude vibrational motions (in the 10^{-12} s range) and (*ii*) flexible molecules, showing large-amplitude, low frequency, torsional motions, typically internal rotations and ring puckering (spanning timescales ranging from 10^{-9} s to 10^{-1} s) [218].

1.4.1.   Rigid compounds

If we consider again the observed ZZ-component of a generic second rank tensor $\breve{T}_\lambda$ and its components $T_{\alpha\beta}$ in the molecular frame and we take equilibrium averages over the relevant motions in the mesophase, we get [11]:

$$\langle T_{zz}\rangle = T^{iso} + T^{aniso} = T^{iso} + \frac{2}{3}\sum_{\alpha,\beta}\langle\frac{3cos\theta_{\alpha z}cos\theta_{\beta z} - \delta_{\alpha\beta}}{2}T_{\alpha\beta}\rangle \qquad (1.45)$$

with $\theta_{\alpha z}$ the angle between the Z-axis in the LAB frame and the molecule-fixed α-axis and $\delta_{\alpha\beta}$ the Kronecker delta symbol. The angular brackets of equation (1.45) denote averaging over all the relevant molecular motions that, for rigid molecules (*i.e.*, lacking of low-frequency internal torsional degrees of freedom), reduce to small-amplitude, high-frequency "hard" molecular vibrations (typically, bond stretchings and bond angle bendings) and reorientational motions. When the only internal degrees of freedom are vibrational motions, internal and reorientational (or tumbling) motions can be decoupled to a good approximation [11, 218]. In this rigid molecule case the following expression holds:

$$T^{aniso} = \frac{2}{3}\sum_{\alpha,\beta}\langle\frac{3cos\theta_{\alpha z}cos\theta_{\beta z} - \delta_{\alpha\beta}}{2}\rangle T_{\alpha\beta} = \frac{2}{3}\sum_{\alpha,\beta}S_{\alpha\beta}T_{\alpha\beta} \qquad (1.46)$$

where the

$$S_{\alpha\beta} = \langle\frac{3cos\theta_{\alpha z}cos\theta_{\beta z} - \delta_{\alpha\beta}}{2}\rangle \qquad (1.47)$$

are the elements of the Saupe ordering matrix described in 1.2.3.

It is thus implicit from equation (1.46) that the anisotropic contribution of each NMR interaction is directly associated to the orientational parameters $S_{\alpha\beta}$ of the molecules in the ordered medium. It is worth to underline that for rigid molecules a single order matrix is needed to describe the molecular orientational order [218]. This is no longer true for the flexible molecule case.

Depending on the symmetry of the molecule and the suitable choice of the coordinate system, the number of independent elements of the ordering matrix required to describe molecular orientation varies from zero to five. The number of non-zero, independent elements of the Saupe order matrix has been calculated for a molecule belonging to all the point groups [170] and this is resumed in Table 1.3. Note that the Saupe matrix can always be diagonalized to give, in this case, a matrix with only two independent non-zero elements.

Table 1.3. Independent non-zero elements of the Saupe order matrix for various point groups.

Point group	$S_{\alpha\beta}$
C_1, C_i	$S_{aa}, (S_{bb} - S_{cc}), S_{ab}, S_{bc}, S_{ac}$
C_2, C_{2h}, C_s	$S_{aa}, (S_{bb} - S_{cc}), S_{bc}$
C_{2v}, D_2, D_{2h}	$S_{aa}, (S_{bb} - S_{cc})$
C_n, C_{nh}, C_{nv} (n = 3-6)	S_{aa}
$C_{\infty h}, D_{\infty h}$	S_{aa}
D_{2d}	S_{aa}
D_n, D_{nd}, D_{nh} (n = 3-5)	S_{aa}
D_6, D_{6h}	S_{aa}
S_4, S_6	S_{aa}
K_h, O, O_h, T, T_d	all $S_{\alpha\beta}$ = 0 [6]

In this Ph.D. thesis the key NMR interaction we are focused on to obtain structural and orientational information is the dipolar interaction. Expressing $D_{ij,zz}$ for a totally rigid molecule in a uniaxial phase in the molecular frame we get [6, 170, 225]:

$$D_{ij,zz} = \frac{2}{3} \sum_{\alpha,\beta} S_{\alpha\beta} D_{ij,\alpha\beta} =$$

$$-\frac{K_{ij}}{r_{ij}^3} \left[\frac{1}{2} S_{aa} \left(3\cos^2\theta_{ija} - 1 \right) + \frac{1}{2} (S_{bb} - S_{cc})\left(\cos^2\theta_{ijb} - \cos^2\theta_{ijc} \right) \right.$$

$$\left. + 2S_{ab}\cos\theta_{ija}\cos\theta_{ijb} + 2S_{ac}\cos\theta_{ija}\cos\theta_{ijc} + 2S_{bc}\cos\theta_{ijb}\cos\theta_{ijc} \right]$$

$$(1.48)$$

where

$$D_{ij,\alpha\beta} = -\frac{\mu_0 \gamma_i \gamma_j h}{32\pi^3 r_{ij}^3} \left(3\cos\theta_{ij\alpha}\cos\theta_{ij\beta} - \delta_{\alpha\beta} \right) = -\frac{1}{2}\frac{K_{ij}}{r_{ij}^3} \left(3\cos\theta_{ij\alpha}\cos\theta_{ij\beta} - \delta_{\alpha\beta} \right) \quad (1.49)$$

and K_{ij} as in equation (1.37).

The number of terms in equation (1.48) can be reduced if any of the principal axes of *S* can be identified from the symmetry of the molecule.

---

[6] Molecules with sufficiently high symmetry (tetrahedral, octahedral, cubic) are expected not to orient (*S* value is zero) even in an anisotropic environment, and hence the dipolar couplings in such systems should average to zero. However, in actual practice, dipolar splittings are observed [242-246], as a result of the vibration-reorientation coupling (see section 1.4.3).

It is evident the extremely informative content enclosed inside dipolar couplings: their edition gives direct access to geometrical as well as orientational parameters of the molecules oriented in the aligning medium. However, these two kinds of information, structure and orientation, cannot be separated easily. As a general rule, to interpret the dipolar couplings derived from the analysis of NMR spectra in terms of molecular structure and orientation, the measurable dipolar couplings should be at least equal to the total number of S values and geometrical parameters to be determined. In general, for a system of N interacting spins and without any symmetry, we have $N(N-1)/2$ dipolar couplings to determine five elements of the ordering matrix and $3(N-2)$ coordinates. The minimum number of interacting spins required to derive information for such system is given by the following expression [3, 4]:

$$[N(N-1)/2] - 5 - 3(N-2) \geq 0 \qquad (1.50)$$

The minimum value of N required to satisfy the conditions of equation is 7. By similar arguments, it can be shown that in C_s symmetry molecules, $N \geq 5$, and with C_2 symmetry, the condition is $N \geq 4$. In most cases, anyway, the geometry is assumed and just some critical geometrical parameters may be varied in the iterative procedure. Even in this way, the number of independent dipolar couplings determined experimentally has to be greater than the total number of the structural and order parameters to be determined, otherwise the system is said to be underdetermined, and it is not possible to extract the complete structural information without making some other assumptions [3, 4].

Together with dipolar interaction, that affects spectra of all magnetic nuclei, the second purely anisotropic contribution to the spin Hamiltonian is the quadrupolar splitting. The latter exists only for nuclei with I ≥ 1, and among them deuterium was the most studied. The relationship between $q_{i,zz}$ and its components $q_{i,\alpha\beta}$ in a molecular frame can be expressed as [170, 225]:

$$q_{i,zz} = q_i^{aniso} = \frac{2}{3}\sum_{\alpha,\beta} S_{\alpha\beta}\, q_{i,\alpha\beta} = q_{i,aa}\left[S_{aa} + \frac{1}{3}\eta_i(S_{bb} - S_{cc})\right] \qquad (1.51)$$

where

$$\eta_i = \frac{q_{i,bb} - q_{i,cc}}{q_{i,aa}} \qquad (1.52)$$

is the asymmetry parameter.

In this thesis we exclusively dealt with the deuterium nucleus (I = 1), for which the principal axis a lies approximately along the bond C-^{2}H. We define thus $q_{CD} = q_{i,aa}$ and $S_{CD} = S_{i,aa}$ (with $D = {}^2$H). Since normally η_i is not very large (its values fall in the range $-0.15 \leq \eta_i \leq 0.15$) [11], it can be neglected and we get:

$$\hat{H}_Q = \frac{q_{i,zz}}{4}\left[3\hat{I}_z\hat{I}_z - I(I+1)\right] = \frac{q_{CD}S_{CD}}{4}\left[3\hat{I}_z\hat{I}_z - I(I+1)\right] \qquad (1.53)$$

Taking into account the selection rule we have for a single nucleus two transitions in the deuterium NMR spectrum with a splitting:

$$\Delta v_Q = \frac{3}{2}q_{CD}S_{CD} \qquad (1.54)$$

For C-^{2}H bonds, q_{CD} has typical values depending on hybridation state of the carbon bonded to a given deuteron: it is approximately equal to 170 ± 5 kHz, 185 ± 5 kHz and 200 ± 5 kHz, for sp^3, sp^2 and sp carbons, respectively [11]. It is easy therefore to obtain the order parameters S_{CD} from the quadrupole-split doublets.

Traditionally, specifically totally or partially deuterated samples were employed in order to overcome the limitation of the low natural deuterium sensitivity (1.45 x 10^{-6} with respect to proton). The technique has been and is extensively used for structural and orientational studies of solutes and above all for investigations of orientational order, phase type, and molecular dynamics of several liquid crystals [183 and refs. therein, 247 and refs. therein]. The success of ^{2}H-NMR is mainly due to the relative simplicity of deuterium spectra compared to those of the corresponding protonated molecules. Indeed, since dipolar couplings are usually considerably smaller than quadrupolar splitting, ^{2}H-spectra are often observed as superpositions of simple well-resolved quadrupolar doublets [225]. As discussed in the following, this feature is also exploited as method for spectral simplification (see section 1.5.2). On the other hand, the preparation of deuterated molecules to yield observable resonances represents a major disadvantage, since synthetical strategies for labeling organic compounds with deuterium are complex, expensive and time-consuming. However, thanks to the development of high-field, high-sensitivity NMR instrumentation (remember the *S/N* ratio is proportional to $(B_0)^{3/2}$ for a given experimental time [96]), the natural abundance deuterium (NAD) spectroscopy is become a viable alternative and it is now possible to obtain natural abundance ^{2}H-NMR spectra of molecules dissolved in ordered media in a reasonable time [248 and refs. therein]. An important technological development that made NAD spectroscopy easier to apply is the availability of selective deuterium cryogenic probes, whose receiver coils and preamplifiers are cooled to very low temperatures by helium gas for high resolution, liquids spectrometers. As a result, these probes allow a gain in signal sensitivity of a factor 3 to 4 compared with standard high resolution probes [249] and have essentially overcome the problem of low sensitivity of deuterium nucleus. Note that, despite ^{2}H-^{2}H spin couplings are absent in a NAD spectrum due to the very low probability of having two deuterons in the same isotopomer (2.40·10^{-6} %), ^{2}H-^{1}H couplings are still present, so that

proton decoupling is highly recommended. Unfortunately, the classical low-power decoupling allowed with cryoprobes is large enough to properly decouple the ^{2}H-^{1}H dipolar interactions in low ordering samples, but it does not work perfectly in thermotropic samples. A better technical solution has been the use of solid state NMR spectrometers equipped with more than adequate proton decoupling power to give resolved resonance on static liquid crystalline samples [185].

Thanks to these recent advances, the quadrupolar interaction is increasingly used as routine tool, and its role in spectral analysis and data interpretation is seen as complementary to that of dipolar couplings. Indeed, it is worth noting that no information on the sign of Δv_Q is contained in a ^{2}H-NMR spectrum. There is a similar problem with dipolar couplings, unless sophisticated sign-sensitive pulse sequences are used. It has be demonstrated that comparing quadrupolar and dipolar data may help in the assignment of both signs [185]. In particular, for a specific ^{13}C-^{1}H (^{13}C-^{2}H) bond, one can take advantage of a useful relationship between the direct ^{13}C-^{1}H dipolar coupling and the corresponding quadrupolar splitting. Since the two local order parameters can be assumed equal to within about 5% ($S_{CD} = S_{CH}$) [250 and refs. therein], the ratio $\Delta v_{CD}/^1D_{CH}$ is approximately independent of the two order parameters, and it is equal to [250]:

$$\frac{\Delta v_{CD}}{^1D_{CH}} = -\frac{24 q_{CD}\pi^3 r_{CH}^3}{\mu_0 \gamma_C \gamma_H h}$$
(1.55)

It is demonstrated that this ratio $|\Delta v_{CD}/^1D_{CH}|$ lies approximately in the range 10–12 [185, 250].

1.4.2.   Flexible compounds and conformational problem

The presence of conformational flexibility, that is large, low frequency torsional motions, considerably complicates the interpretation of the NMR data compared to the case of rigid molecule. Indeed, in the case of flexible molecules we must deal with the effect of two simultaneous motional averagings: the averaging process due to the tumbling motion of the compound (as for rigid compounds) and the averaging process due to conformational flexibility, which implies the existence of a number of different rotamers [11, 218]. The flexible molecule exists thus in more than one conformation each with its own probability and its own Saupe ordering matrix. If the rate of conformer interconversion is in the slow exchange NMR limit, a separate spectrum would be obtained for each conformer. The analysis of these spectra would yield separate conformer geometries and order tensors, while conformer

probabilities would be obtained from relative integrated intensities. Most case of interest, however, are in the fast exchange NMR limit, and a single, statistically averaged spectrum is measured [11, 217].

To explicitely take into account both the orientational overall motion and the internal rotation one, it is possible to define a singlet (the conformational probability of a molecule is independent on the probability of its neighbours) orientational distribution function, $P_{LC}(\Omega, \{\phi\})$. It is more useful at this point to deepen the conformational problem for the specific case of the dipolar interaction $D_{ij,zz}$ rather than a generic interaction T_{zz}, since it will be the informative observable used in all the following studies.

In a uniaxial liquid crystalline medium where the director aligns along the external applied magnetic field, the averaged D_{ij}^{obs} dipolar coupling between the i-th and j-th nuclei of a flexible molecule can be written as [251]:

$$D_{ij}^{obs} = \frac{2}{3} \int P_{LC}(\Omega, \{\phi\}) \, D_{ij}(\Omega, \{\phi\}) d\Omega d\{\phi\} \qquad (1.56)$$

where $D_{ij}(\Omega, \{\phi\})$ is [251]:

$$D_{ij}(\Omega, \{\phi\}) = \langle \mathbf{s}(\Omega) : \mathbf{D}_{ij}(\{\phi\}) \rangle \qquad (1.57)$$

Here $\Omega = \{\alpha, \beta, \gamma\}$ denotes the set of Euler angles characterizing the orientation of the mesophase director in the chosen molecular frame, the angular brackets $\langle ... \rangle$ indicate the statistical average over the small-amplitude high-frequency molecular vibrational modes (torsion ϕ excluded) and the symbol ":" represents the inner product of the two tensors.

The elements of the tensor $\mathbf{s}(\Omega)$ correspond to [251]:

$$s_{\alpha\beta}(\Omega) = \frac{3cos\theta_{\alpha z}cos\theta_{\beta z} - \delta_{\alpha\beta}}{2} \qquad (1.58)$$

where $\theta_{\alpha z}$ is the instantaneous angle between the director and the molecular axes (a, b, c), and $\delta_{\alpha\beta}$ is the Kronecker delta function.

The term $\mathbf{D}_{ij}(\{\phi\})$ is the geometry-dependent dipolar coupling tensor expressed in the molecular frame [251]:

$$D_{ij,\alpha\beta}(\{\phi\}) = -\frac{1}{2} K_{ij} \frac{3cos\theta_\alpha(\{\phi\})cos\theta_\beta(\{\phi\}) - \delta_{\alpha\beta}}{r_{ij}^3(\{\phi\})} \qquad (1.59)$$

with K_{ij} as in equation (1.37).

The function $P_{LC}(\Omega, \{\phi\})$ describes the properly normalised orientational-conformational probability distribution function of the solute in the partially ordered environment. In other words, it represents the probability of finding the mesophase director Ω-oriented in the solute-fixed frame when the probe-molecule is in its $\{\phi\}$ conformation in the aligned solution. This quantity can be related to the total singlet orientational energy

$U_{TOT}(\Omega, \{\phi\})$. The latter can be built as "mean-torque" potential by adding together an anisotropic, intermolecular potential, $U_{ext}(\Omega, \{\phi\})$ (which depends on both orientational and internal angles and vanishes in the isotropic phase) and an internal rotational potential, $U_{int}(\{\phi\})$ (which is independent of the orientation and depends only on the conformational state, and hence the bond rotational potentials) [169, 217, 252]:

$$U_{TOT}(\Omega, \{\phi\}) = U_{ext}(\Omega, \{\phi\}) + U_{int}(\{\phi\}) \tag{1.60}$$

In this assumption the $P_{LC}(\Omega, \{\phi\})$ becomes [217]:

$$P_{LC}(\Omega, \{\phi\}) = \frac{exp\{-[U_{ext}(\Omega, \{\phi\}) + U_{int}(\{\phi\})]/k_B T\}}{\int exp\{-[U_{ext}(\Omega, \{\phi\}) + U_{int}(\{\phi\})]/k_B T\} \, d\Omega \, d\{\phi\}} \tag{1.61}$$

with T the absolute temperature and k_B the Boltzmann constant.

The probability of finding a molecule in an anisotropic phase in a particular conformation $\{\phi\}$ independent of its orientation can be derived by summing over all the orientations [217]:

$$P_{LC}(\{\phi\}) = \int P_{LC}(\Omega, \{\phi\}) \, d\Omega \tag{1.62}$$

A convenient way to express the $P_{LC}(\Omega, \{\phi\})$ is to consider it as a product of a $P_\phi(\{\phi\})$ and a $P_\Omega(\Omega, \{\phi\})$ [251]:

$$P_{LC}(\Omega, \{\phi\}) = P_\phi(\{\phi\})P_\Omega(\Omega, \{\phi\}) \tag{1.63}$$

where

$$P_\Omega(\Omega, \{\phi\}) = \frac{exp[-U_{ext}(\Omega, \{\phi\})/k_B T]}{Q} \tag{1.64}$$

with

$$Q = \int exp[-U_{ext}(\Omega, \{\phi\})/k_B T] d\{\phi\} \, d\Omega \tag{1.65}$$

and

$$P_\phi(\{\phi\}) = P_{iso}(\{\phi\})\frac{W(\{\phi\})Z_{iso}}{Z} \tag{1.66}$$

where

$$W(\{\phi\}) = \int exp[-U_{ext}(\Omega, \{\phi\})/k_B T] d\Omega \tag{1.67}$$

$$Z = \int W(\{\phi\})P_{iso}(\{\phi\}) \, d\{\phi\} \tag{1.68}$$

$$Z_{iso} = \int P_{iso}(\{\phi\}) \, d\{\phi\} \tag{1.69}$$

The distribution function $P_{iso}(\{\phi\})$ represents the real target of conformational studies in liquids. Unlike $P_\phi(\{\phi\})$, $P_{iso}(\{\phi\})$ is, in principle, free from possible conformational effects induced by the orientational ordering of the mesophase. So, it should be considered the real conformational distribution of our solute in a conventional liquid sharing, at the

temperature studied, the same physical properties (determining the thermodynamics of the solution, as polarity, density etc.) of the liquid crystalline solvent used, with the exception of the ordering strength [251]. $P_{iso}(\{\phi\})$ can be written as a function of $U_{int}(\{\phi\})$ as in the following [217]:

$$P_{iso}(\{\phi\}) = \frac{exp\{-[U_{int}(\{\phi\})]/k_B T\}}{\int exp\{-[U_{int}(\{\phi\})]/k_B T\}\, d\{\phi\}} \tag{1.70}$$

Note that $P_{iso}(\{\phi\})$ and $P_{LC}(\{\phi\})$ are in general not equal, with the difference between them increasing as the orientational order increases [169]. For instance, differences of up to 30% were found for liquid crystal 5CB [253]. However, for low-order small solutes the differences are usually negligible [217, 254-257].

In order to simplify equation (1.56) a series of approximations can be adopted. Firstly, it is quite usual to assume that internal vibrations and overall reorientational (tumbling) motions of the molecule can be decoupled in Equation (1.57), because the dependence of $\mathbf{s}(\Omega)$ on the vibrational state of the molecule is believed to be small enough to be neglected to a good approximation [251, 257-259]. Thus Equation (1.56) can be re-written as [251]:

$$D_{ij}^{obs} = \frac{2}{3}\int P_\phi(\{\phi\}) \sum_{\alpha\beta} S_{\alpha\beta}(\{\phi\})\langle D_{ij,\alpha\beta}(\{\phi\})\rangle d\{\phi\} \tag{1.71}$$

where

$$S_{\alpha\beta}(\{\phi\}) = \frac{\int s_{\alpha\beta}(\Omega)P_\Omega(\Omega,\{\phi\})d\Omega}{\int P_\Omega(\Omega,\{\phi\})d\Omega} \tag{1.72}$$

are the familiar solute orientational order parameters of the Saupe ordering matrix.

Moreover, the dependence of the order parameters on the vibrational state is usually assumed to be much smaller than their dependence on the bond rotational angles, and it can be neglected to a good approximation. Neglecting vibrational motion reduces equation (1.71) to [257]:

$$D_{ij}^{obs} = -\frac{1}{2}K_{ij}\int \frac{P_\phi(\{\phi\})}{r_{ij}^3(\{\phi\})}\cdot [S_{aa}(\{\phi\})\big(3cos^2\theta_{ij,a}(\{\phi\}) - 1\big)$$

$$+(S_{bb}(\{\phi\}) - S_{cc}(\{\phi\}))\left(cos^2\theta_{ij,b}(\{\phi\}) - cos^2\theta_{ij,c}(\{\phi\})\right)$$

$$+4S_{ab}(\{\phi\})cos\theta_{ij,a}(\{\phi\})cos\theta_{ij,b}(\{\phi\})$$

$$+4S_{ac}(\{\phi\})cos\theta_{ij,a}(\{\phi\})cos\theta_{ij,c}(\{\phi\})$$

$$+4S_{bc}(\{\phi\})cos\theta_{ij,b}(\{\phi\})cos\theta_{ij,c}(\{\phi\})] \tag{1.73}$$

with

$$\frac{2}{3}\sum_{\alpha\beta} S_{\alpha\beta}(\{\phi\})\langle D_{ij,\alpha\beta}(\{\phi\})\rangle = -\frac{1}{2}\frac{K_{ij}}{r_{ij}^3(\{\phi\})}\cdot [S_{aa}(\{\phi\})\big(3cos^2\theta_{ij,a}(\{\phi\}) - 1\big)$$

$$+(S_{bb}(\{\phi\}) - S_{cc}(\{\phi\}))\left(cos^2\theta_{ij,b}(\{\phi\}) - cos^2\theta_{ij,c}(\{\phi\})\right)$$

$$+4S_{ab}(\{\phi\})cos\theta_{ij,a}(\{\phi\})cos\theta_{ij,b}(\{\phi\})$$

$$+4S_{ac}(\{\phi\})cos\theta_{ij,a}(\{\phi\})cos\theta_{ij,c}(\{\phi\})$$

$$+4S_{bc}(\{\phi\})cos\theta_{ij,b}(\{\phi\})cos\theta_{ij,c}(\{\phi\})] \tag{1.74}$$

It is tempting to assume that the dependence of $S_{\alpha\beta}(\{\phi\})$ on $\{\phi\}$ can also be neglected, but although this is often done when dipolar couplings are used to study protein structures, it is likely to lead to major errors in the function $P_{LC}(\{\phi\})$ and the structures derived when there is an appreciable degree of intramolecular motion present in the molecule [257]. It is worth to remark the dependence of $S_{\alpha\beta}(\{\phi\})$ on the molecular conformation defined by the torsional angles $\{\phi\}$ has an important consequence: it is not possible to describe the orientational order by a single Saupe order matrix, but it is necessary to recognize that the elements of this matrix depend on the internal coordinates, that is they are conformationally dependent [216].

The implications of equations (1.73) and (1.74) are quite significant: the experimental observables involve products of conformational probabilities and orientational factors and they cannot be determined individually [217-218]. Therefore, for a solution of equation (1.73) either the Saupe order matrix $S_{\alpha\beta}$ (one for each conformer) or the conformer populations should be known. In the absence of any reliable equation relating the $S_{\alpha\beta}$ elements of different conformers all that we can do is to test theoretical models [218]. Even so, the number of unknowns *versus* the number of independent variables is often critical and, if flexible systems are to be described exactly, a huge amount of experimental data would be necessary to describe all degrees of freedom. Definitely, one has to be aware that the more conformational flexibility the compound exhibits the less determined the system will be and the more assumptions have to be made with our current means of data interpretation [217-218]. In other words, the chance that conformation determination can be solved exactly decreases with increasing flexibility of the compounds.

1.4.2.1. Theoretical approaches describing the interdependent conformational orientational problem

To extract useful information from the experimental dipolar couplings in a flexible molecule, it is clear a theoretical tool has to be adopted in order to treat the interdependent conformational-orientational problem. Ultimately, we need models: (*i*) to shape the

conformational distribution function, *i.e.* to introduce a set of potential/probability parameters, and (*ii*) to treat, in some way, the conformational dependence of the order parameters. Several such approaches have been considered for the interpretation of dipolar couplings. The simplest possible model, the Rotamer Isomeric State (RIS) model [260-261], assumes that only a small set of minimum-energy structures is populated. More realistic models allow for continuous bond rotations. Two different approaches have been attempted in the past: the Additive Potential (AP) methods [253], an "approximate" approach whose aim is to reduce equation (1.73) to manageable expressions by using some physically justifiable approximations; the Maximum Entropy (ME) method [262-263], an "unbiased" method based on Information Theory. More recently, a hybrid approach was proposed, that is based on a combination of both AP and ME approach and it is called Additive Potential Maximum Entropy (APME) method [264]. All these approaches will be presented in the following sections. Note other models have been proposed in the past, based, for instance, on the idea that the anisotropic intermolecular potential is dominated by short-range anisotropic interactions depending on the conformer size and shape [265-267], but they will not be discussed in this thesis.

i. The RIS model

For some molecules a reasonable approximation of the conformational distribution is that only a set of few discrete minimum energy conformations is accessible to the molecule, that is only the minimum energy structures are populated on a bond rotational pathway. This approximation is often referred to as the Rotamer Isomeric State (RIS) model approximation [260-261]. In such approximation the internal potential function can be written as:

$$U_{int}(\{\phi\}) = -\sum_n^N V_n \delta(\{\phi\} - \{\phi_n\}) \qquad (1.75)$$

where N is the number of minima potential functions and $\{\phi_n\}$ is the set of internal coordinates corresponding to the n-th conformer. $\delta(\{\phi\} - \{\phi_n\})$ is the Kronecker's delta function which is 1 if $\{\phi\} = \{\phi_n\}$ and 0 otherwise. From this potential it is possible to derive the probability for the n-th conformer, $p(n)$, so that the dipolar coupling can be written as [217]:

$$D_{ij}^{obs} = \frac{2}{3} \sum_n^N \sum_{\alpha,\beta} p(n) S_{\alpha\beta}(n) D_{ij,\alpha\beta}(n) \qquad (1.76)$$

The molecule is thus described as a collection of rigid conformations, having each orientational order $S_{\alpha\beta}(n)$ and weight $p(n)$. The adjustable parameters in the fitting procedure of calculated *versus* experimental dipolar couplings are the products $p(n)S_{\alpha\beta}(n)$, implying that all $p(n)$ values that give physically meaningful $S_{\alpha\beta}(n)$ values represent possible solutions.

The RIS model works well if only a set of symmetry-related conformations is populated. A good example is represented by benzaldehyde, that is interconverting between two, planar conformations which are related by a mirror plane (Scheme 1.1) [216].
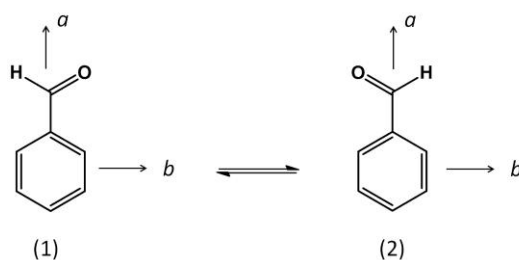
Scheme 1.1.

If all other conformations are neglected:

$$S_{aa}(1) = S_{aa}(2), \qquad S_{bb}(1) = S_{bb}(2), \qquad S_{cc}(1) = S_{cc}(2)$$
$$S_{ab}(1) = -S_{ab}(2)$$
$$S_{bc}(1) = S_{bc}(2) = 0$$
$$S_{ac}(1) = S_{ac}(2) = 0$$

The observed and calculated dipolar couplings can be brought into agreement by adjusting the values of these order parameters [216]. It is obvious that the number of parameters increases rapidly when equilibria among non-symmetry related conformers are involved since each conformation is described by its own probability $p(n)$ and its own ordering matrix $S_{\alpha\beta}(n)$ [217].

Of course the RIS approximation is more robust if the real conformational distribution has a discrete number of very sharp maxima and it becomes inappropriate when rotation about a bond is described by a continuous function $P_{LC}(\{\phi\})$.

ii. The AP methods

These methods are based on modeling $U_{ext}(\Omega, \{\phi\})$ and $U_{int}(\{\phi\})$, the components of the mean potential $U_{TOT}(\Omega, \{\phi\})$. Several ways of modeling $U_{ext}(\Omega, \{\phi\})$ and $U_{int}(\{\phi\})$ individually have been proposed, but just some of them are discussed in the following.

For molecule containing one or more rotor groups the so-called AP-Independent Fragment model has been the most commonly used approach to model $U_{ext}(\Omega, \{\phi\})$. This model was first introduced by Marčelja [268] and subsequently modified by Emsley *et al.* [253]. According to this approach, the $U_{ext}(\Omega, \{\phi\})$ can be written as [216]:

$$U_{ext}(\Omega, \{\phi\}) = -\varepsilon_{2,0}(\{\phi\})C_{2,0}(\Omega) - 2\mathrm{Re}\varepsilon_{2,2}(\{\phi\})C_{2,2}(\Omega) \qquad (1.77)$$

where $C_{2,m}(\Omega)$ are modified spherical harmonics. $\varepsilon_{2,m}(\{\phi\})$ are elements of a suitable conformation-dependent solute-solvent interaction tensor expressed with respect to the principal axes for each conformation $\{\phi\}$; they are related to the strength of the interaction between the molecular mean field and the molecule in the conformation described by the angles $\{\phi\}$ [269]. The sum in equation (1.77) does not contain odd terms because of the symmetry of the phase ($D_{\infty h}$) and it can be truncated at the second order term to a good approximation when used to calculate second-rank quantities, particularly when the ordering is small [269 and refs. therein].

The peculiar feature of the AP method is that these conformationally dependent interaction tensors $\varepsilon_{2,m}(\{\phi\})$ can be written as a sum of conformationally independent contributions from each rigid fragment j in which the molecule can be decomposed [217]:

$$\varepsilon_{2,m}(\{\phi\}) = \sum_p \sum_j \varepsilon_{2,p}^j D_{p,m}^2\left(\left\{\Omega_\phi^j\right\}\right) \qquad (1.78)$$

here j runs on the number of fragments and $\left\{\Omega_\phi^j\right\}$ is the set of Euler angles that describes the orientation of the j-fragment in the molecule with respect to fixed axes in a rigid fragment of the molecule. Therefore, the Wigner rotation matrix $D_{p,m}^2\left(\left\{\Omega_\phi^j\right\}\right)$ relates the principal axes of ε^j to the molecular reference frame. In this way, with $\varepsilon_{2,p}^j$ as adjustable terms, it is possible to express the continuous dependence of the order parameters on the set of internal coordinates. It should be noted that the number of unknowns is strongly reduced as all the order parameters for each conformer can be calculated starting from few unknown $\varepsilon_{2,p}^j$, the number of which depend on the number and the local symmetry of the fragments in the molecule. As a general operative rule they should be the minimum number that assures the independence of the order parameters while keeping their correct symmetry. For instance, there will be just one contribution, $\varepsilon_{2,0}^j$, from a fragment with cylindrical symmetry and two,

$\varepsilon_{2,0}^j$ and $\varepsilon_{2,2}^j$, from a fragment with lower symmetry, provided that the principal axes for ε^j are known [216].

Thanks to the AP method, relatively large molecules can be treated and their conformational distribution obtained. As an example, consider here the mesogen molecule of 4-pentyl-4'cyanobiphenyl (5CB) [169], whose structure is reported in Figure 1.10.
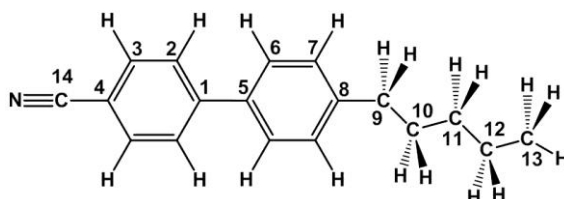
Figure 1.10. Structure and labeling of 4-pentyl-4'-cyanobiphenyl (5CB).

There are six bonds about which rotation occurs, and if a simplified, discrete conformational model is used in which the molecules are considered to move between positions of local minimum energy, there are 216 discrete conformational forms [169]. This is based on the C–C–C–C chain segments being either in a *trans* or one of the two energetically equivalent *gauche* forms, the plane $C_8C_9C_{10}$ being orthogonal (90° or 270°) to the attached ring, and the two rings being in one of four equivalent minimum energy positions generated by rotation about the C_1–C_5 bond. Symmetry considerations reduce the number of conformations which are different in energy to 14, and so there are 28 values of the $\varepsilon_{2,m}(\{\phi\})$ in equation (1.77) [169]. The powerful AP model allows to greatly reduce the number of interaction parameters. In fact, by assuming a C_{2v} symmetry for the ring and only cylindrically symmetric fragments in the alkyl chain, only four fragment tensors are required to describe the whole mesogenic molecule: $\varepsilon_{2,0}(\mathrm{R})$ and $\varepsilon_{2,2}(\mathrm{R})$ for the biaxial cyanobiphenyl group, $\varepsilon_{2,0}(\mathrm{C}-\mathrm{C})$ and $\varepsilon_{2,0}(\mathrm{C}-\mathrm{H})$ for the C-C and C-H bonds in the alkyl chain [169].

When dealing with very flexible molecules such as alkyl chains, the independent fragment model does not always produce $\varepsilon(\{\phi\})$ matrix which accounts correctly for the shape of the conformer. In these cases, it may be preferable to use the AP-Correlated Fragment or "Chord" model [270-271], which adds terms to $U_{ext}(\Omega,\{\phi\})$ depending on the relative orientation of different fragments. In this model Photinos *et al*. considered fragments with cylindrical symmetry, such as C-C bonds, and proposed a potential of mean torque of the form [216]:

$$U_{ext}(\Omega,\{\phi\}) = -\sum_i w_i P_2\left(cos\theta_i\right) - \sum_{i\neq j} w_{ij} P_{ij}\left(s^i, s^{i+j}\right) \qquad (1.79)$$

where

$$P_2(cos\theta_i) = \frac{1}{2}(3cos^2\theta_i - 1) \tag{1.80}$$

and

$$P_{ij}(s^i, s^{i+j}) = \frac{1}{2}(3cos\theta_i cos\theta_{i+j} - s^i \cdot s^{i+j}) \tag{1.81}$$

where θ_i is the angle between the i-th C-C bond and the director, s^i and s^{i+j} are unit vectors along the i-th and $(i+j)$-th C-C bonds (see Figure 1.11). The w_i and w_{ij} terms are the interaction strengths. For the case of an alkane, the w_i are all given the same value of w_0 and so the w_{ij} can be denoted as w_j.
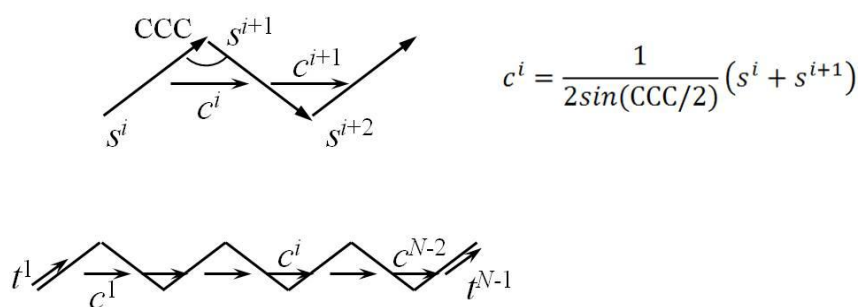
Figure 1.11. The unit vectors used in the chord model (from refs. [270-271]).

It has been also showed [270-271] that an equivalent representation for $U_{ext}(\Omega, \{\phi\})$ is obtained by considering not bonds but chords c^i joining the midpoints of adiacent bonds. In this chord representation, and including only nearest neighbor chord correlations (corresponding to bond correlations of next-nearest neighbors) [216]:

$$U_{ext}(\Omega, \{\phi\}) = -\left\{g_0 \sum_{i=1}^{N-2} P(c^i, c^i) + w_0^t[P(t^1, t^1) + P(t^{N-1}, t^{N-1})]\right\} \tag{1.82}$$

where $g_0 = [2sin^2(CCC/2)]w_0$ and $w_0^t = \frac{1}{2}w_0$. The first and last bonds are denoted by unit vectors t^1 and t^{N-1}.

In this thesis flexible molecules without long alkyl chains were investigated and the AP-Independent Fragment model was found to be an easy and reliable approach to shape $U_{ext}(\Omega, \{\phi\})$ in all cases. As a consequence, in the following we will refer to this method simply as the"AP method".

To fully describe $P_{LC}(\Omega, \{\phi\})$ and finally $P_{iso}(\{\phi\})$, the AP approach requires an appropriate model for the $U_{int}(\{\phi\})$. Models for $U_{int}(\{\phi\})$ may vary, and are often specific to

the molecule under consideration and the amount of experimental data available from which they may be characterized.

The conventional way to deal with internal potential of a flexible molecule is to use a truncated Fourier cosine series such as [257, 272-278]:

$$U_{int}(\{\phi\}) = \sum_k V_k \cos(k\phi) \tag{1.83}$$

whit k = 0,1,2,3… taking values to give the right periodicity of potential. The series has to be kept as shorter as possible compatibly with a correct description of the overall shape of the rotational potential of the molecule (at least near to the expected potential minima) [257]. Such a treatment is rather easy for single rotors but becomes more and more complex as the shape of the potential does and as the number of rotors increases, and this is even more problematic in the case of cooperative motions. In fact, not only the number of terms increases but their value is not independently linked to the shape of the potential itself, that is, it is their combination that contributes to the shape. In this case there are essentially two options: (*i*) adding more terms in order to obtain a very general function, which may entail excessive parameterization, (*ii*) fixing a number of constraints, which could further bias the solutions [217]. Moreover, even when the set of experimental data is large enough, fitting calculated to observed dipolar couplings by varying Fourier coefficients has the general problem that changing these coefficients affects the whole bond rotation potential and not just one parameter [255].

To overcome such drawbacks an approach based on the Direct Probability Description (DPD) of the conformational distribution was introduced [257]. According to this model, $P_{LC}(\{\phi\})$ can be written as a sum (for interdependent conformations) or product (for independent states) of Gaussian functions. Thus, in a molecule with d independent rotors and n_j minima for the j-th rotor, the general form can be written as:

$$P_{LC}(\{\phi\}) = \prod_{i=1}^d \left(\sum_{j,k,\dots}^{n_j,n_k,\dots n_d} A_{i,j,k,\dots d} \, exp\left(\frac{-\left(\phi_i - \phi_{i,j,k,\dots d}^o\right)^2}{2h_{i,j,k,\dots d}^2} \right) \right) \tag{1.84}$$

where $\phi_{i,j,k,\dots d}^o$ are the maxima position angles and $A_{i,j,k,\dots d}$ their relative weights. The distribution width of each Gaussian is given by $2h_{i,j,k,\dots d}$, defined as [279]:

$$h_{i,j,k,\dots d} = \frac{\text{FWHM}}{2\sqrt{2\ln 2}} \tag{1.85}$$

where FWHM, defined experimentally, is the full-width-at-half-maximum.

The variables can then be varied independently, but with the constraint that $P_{LC}(\{\phi\})$ is normalized [257].

From the equation:

$$P_{LC}(\Omega,\{\phi\}) = \frac{P_\Omega(\Omega,\{\phi\})P_{iso}(\{\phi\})W(\{\phi\})Z_{iso}}{Z} \tag{1.86}$$

it is straightforward to calculate the distribution $P_{iso}(\{\phi\})$. Indeed, since $P_{iso}(\{\phi\})$ is the real target of conformational studies, the model was subsequently modified in order to directly expand $P_{iso}(\{\phi\})$, instead of $P_{LC}(\Omega)$, in terms of Gaussian functions [254-255, 269] and this will be the method applied in the following.

Compared with the Fourier expansion approach, the DPD method has particular advantages: (*i*) a smaller number of parameters is required to give a correct description of the probability; (*ii*) each parameter in the expansion influences only one particular aspect of the probability distribution (maximum positions, the width and height at the maxima giving the conformer relative population and so on), and (*iii*) conformational parameters are usually less correlated. This makes very easy to describe even complicated conformational probability density functions (even those needed to deal with cooperative motions) through a few Gaussian functions centered at properly chosen angles (the locations of the maxima) [257, 279].

It is clear that, depending on modeling the mean potential, all the AP methods have the limitation of providing biased estimates of the distribution functions. However, they do have some important advantages with respect to other models, first of all the possibility to obtain both $P_{LC}(\Omega,\{\phi\})$ and $P_{iso}(\{\phi\})$ [216]. The molecules of interest chosen in this Ph.D. thesis were all investigated by using the AP method for the treatment of the ordering interactions combined with the Direct Probability Description (DPD) of the torsional distribution. Such approach will be referred to as AP-DPD method.

Technically speaking, all the calculations required to extract the desired information from the experimental dipolar couplings, *via* the proper theoretical model, are carried out through a dedicated software, the AnCon package [280], developed in the LXNMR S.C.An. laboratory. The strategy adopted while using this software is showed in a flowchart in Figure 1.12. The determination of structure, order and conformational distribution of the molecule under investigation is obtained by fitting a set of calculated dipolar couplings (obtained by a trial set of orientational, geometrical and conformational parameters) against the experimental ones, while iterating on a set of unknown parameters till their optimized values. Such unknowns can be collected into three categories: (*i*) geometrical parameters, namely bond distances and angles, (*ii*) orientational parameters, whose number and nature varies with the molecule and the model used to fit the data, and (*iii*) potential parameters, including those parameters required to shape the internal potential. For rigid molecules just geometrical and orientational (namely the Saupe order parameters) unknowns are included in the calculation.

For flexible molecules, also potential parameters must be considered. In the case of the AP-DPD approach used for all the flexible molecules of this Ph.D. thesis, the orientational parameters are the set of $\varepsilon_{2,p}^{j}$ solute-solvent interaction tensor elements while the potential unknowns are represented by the parameters needed to model the conformational probability in terms of Gaussian functions (namely the $\phi_{i,j,k,\dots d}^{o}$, $A_{i,j,k,\dots d}$ and $h_{i,j,k,\dots d}$ parameters).
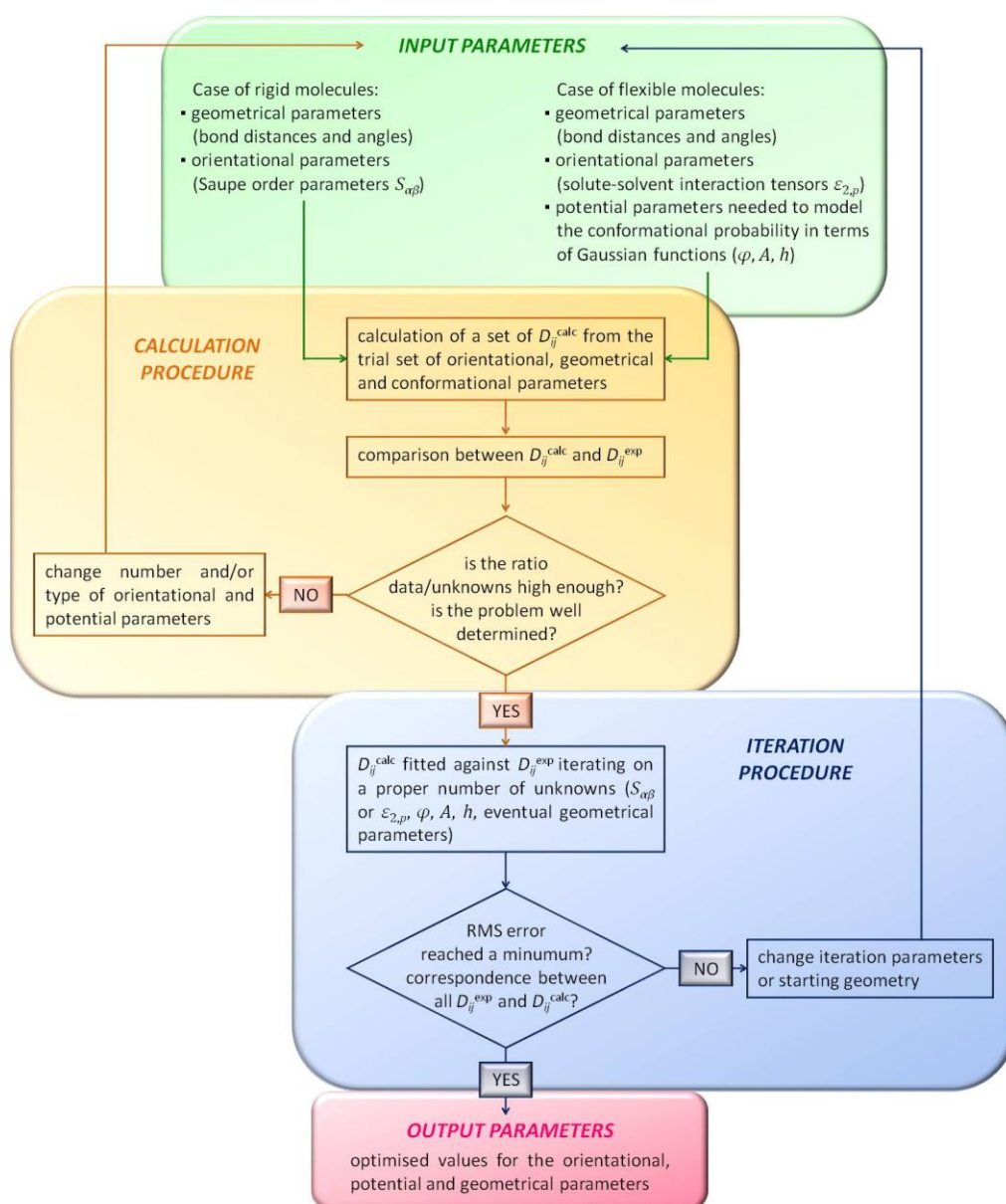

Figure 1.12. Flowchart showing the strategy adopted by the AnCon package.

Of course, the ratio data/unknowns should be kept as high as possible to assure an high determinacy. Iteration parameters and observed dipolar couplings are read and passed to a minimization routine which calls the routine for the calculation of dipolar couplings. Dipolar

couplings are calculated for each selected conformation, averaged on the whole distribution, and then fitted against their observed counterpart. A new set of iteration parameters is produced and the whole procedure repeated until the root mean square between the N calculated and observed dipolar couplings:

$$\text{RMS} = \sum_{i,j}^{N} \sqrt{\frac{\left(D_{ij}^{obs} - D_{ij}^{calc}\right)^2}{N}} \tag{1.87}$$

reaches a minimum.

To avoid local minima, procedure is repeated starting from different initial values.

iii. The ME approach

Another approach for obtaining $P_{LC}(\Omega, \{\phi\})$ is this so-called Maximum Entropy method, suggested first by Zannoni [262-263] an subsequently demonstrated by application to the study of substituted biphenyls dissolved in liquid cristalline solvents [281-282]. According to this approach it is not possible to determine the "real" conformational distribution, or the molecular order parameters, but only the most likely $P_{LC}(\Omega, \{\phi\})$ distribution that is compatible with the set of observables and can be written as [216]:

$$P_{LC}(\Omega, \{\phi\}) = \frac{exp\left\{-\sum_k \lambda_k T_k^{(2,0)}(\Omega, \{\phi\})\right\}}{\int P_{LC}(\Omega, \{\phi\}) sin\beta \; d\beta \; d\gamma \; d\{\phi\}} \tag{1.88}$$

where $T_k^{(2,0)}(\Omega, \{\phi\})$ is the spherical tensor component of a set of k dipolar or quadrupolar interaction, expressed in a frame fixed in a rigid part of the molecule. λ_k are adjustable parameters, whose values are varied in order to bring calculated and observed data into agreement.

The ME method is very attractive in that no assumptions are necessary about the functional form of the rotational potentials. On the other hand it has a drawback, that is it cannot yield $P_{iso}(\{\phi\})$, the probability distribution for an isotropic phase, but it just derives the entire probability distribution function [216]. Another intrinsic problem in the ME method is the dependence of its results on the orientational order of the solute molecule [283-284]. Indeed, by the ME method we achieve qualitative information which has also as much quantitative character as the orientational order increases. In the ideal case of perfect order the dipolar couplings depend only on the internal coordinates, so that they bring with themselves pure pieces of information on the conformational motion. Contrarily, as the molecular order decreases, *i.e.* as dipolar data approaches zero, the probability distribution

obtained by ME approach becomes flatter and flatter. This generally occurs for solutes with low orientational order, thus only qualitative results can be extracted by ME method from their spectral analysis [217]. In general, in order to obtain more peaked distributions by the ME approach, extended data sets and the use of strongly orienting mesophase are required [217].

To overcome the problem of flatness of the resulting ME distribution as far as the orientational order of the solute molecule decreases, a Constrained Maximum Entropy (CME) method was proposed [284], that adds additional constraints for which a parallelism of the type "absence of data-absence of order" does not exist. Since ME results are typically in very good agreement with quantum chemical calculations, *ab initio* calculations on the isolated molecule were used as a source of information.

Taking into account all pros and cons, the question of whether the unbiased ME or the biased AP approach gives the most accurate distribution is not easily answered and the choice strongly depends on the specific solute/solvent system. Anyway, comparisons between results obtained for the same solute from both methods did not reveal significative differences in the shape of the conformational distribution, though highlighting the strong effect of the orientational ordering on the ME distributions, as reported for 4-nitro-1-(2,2,2-trifluoroethoxy)benzene (ME and AP approach applied in [273]), ethylbenzene (refs. [272] and [284] for the AP and ME method, respectively), benzyl chloride (refs. [278] and [284] for the AP and ME/CME method, respectively) and biphenyl (studied in ref. [276] *via* the AP and ME method).

iv. The APME approach

In the last decade, a novel approach for the description of the conformational distribution function from the NMR parameters entered the field. This procedure was constructed as combination of the AP and ME approaches and it is referred to as the Additive Potential Maximum Entropy (APME) method [264]. This new approach overcomes some serious limitations of the two previous models: (*i*) unlike the AP approach, it does not require an *a priori* knowledge of the functional form of the intramolecular potential; (*ii*) in contrast with the ME approach, it correctly describes also systems with low orientational order. To date, few examples are reported where the APME model has been applied for thermotropic [285-286] or lyotropic [287-289] samples. However, it seems to be a very promising tool for conformational investigation of flexible molecules when the functional form of the torsion

angles becomes more and more complicated and especially when dissolved in weakly ordered systems.

1.4.3.   *Vibrational corrections to dipolar couplings*

Since both rigid and flexible molecules undergo vibrational motions, their effects should be taken into account in the edition of dipolar couplings, especially when geometrical data derived from various physical techniques are compared.

An expansion for small amplitudes of vibration provides the relation [171, 290]:

$$D_{ij}^{exp} = D_{ij}^{eq} + D_{ij}^{a} + D_{ij}^{h} + D_{ij}^{non-rigid} \tag{1.89}$$

D_{ij}^{eq} corresponds to the molecular equilibrium structure that minimizes the electronic potential within the Born-Oppnheimer approximation. D_{ij}^{a} is the anharmonic term which for a pair of nuclei at distance R on the z axis is given by $D_{ij}^{a} = -3\langle\Delta z\rangle D_{ij}^{eq}/R$, where $\langle\Delta z\rangle$ is the average z-vibration amplitude. D_{ij}^{h} is the harmonic term which is given by $D_{ij}^{h} = 6(C^{\parallel} - C\perp Dijeq/R2$, where C∥ and C⊥ are the diagonal terms of the covariance matrix of vibrations. Finally, $D_{ij}^{non-rigid}$ is the non-rigid term, and it represents the contribution arising from the correlation of vibrational and reorientational motions [3, 291-292]. For this reason, it is also known as vibration-reorientation coupling. This term becomes particularly evident in spectra of tetrahedral molecules, isotropic by symmetry (all $S_{\alpha\beta}$ are calculated to be zero, see Table 1.3), that show unexpected splittings when aligned in liquid crystals. The contribution of the non-rigid term to the dipolar coupling will be discussed in chapter 2 for the highly symmetric molecule of tetramethylallene.

Owing to their R^{-2} dependence, the harmonic vibrational corrections are particularly large for directly bonded nuclei such as in direct ^{13}C-^{1}H bonds or between geminal protons in methyl and methylene protons [217]. It has been calculated, for example, that for ^{13}C-^{1}H bonds in benzene, D_{ij}^{h} is approximatively 8% of D_{ij}^{exp} and the neglect of such correction leads to an error in the bond length of 2.7% [228, 259]. The prior requirement for the application of these corrections is the availability of a valence force field of the studied molecule. Harmonic force fields obtained from the analysis of a vibrational spectrum are not easy to be found in literature and when available they are limited to small simples molecules. However, thanks to theoretical improvement of computational methods, it is now possible to calculate force fields with a reasonable accuracy also for relatively complex molecules. From a force field and

assuming the corresponding molecular geometry, some computer programs [293-294] derive then normal coordinates, vibrational frequencies, covariance matrices of quadratic displacements and, finally, D_{ij}^h coupling. In some cases, a mixed approach combining calculated normal modes and experimental vibrational frequencies was adopted in calculating the covariance matrix elements and this demonstrated to improve the quality of the estimation [230, 255-256, 279, 295]. The computation of anharmonic terms is more complicated. However, though programs were developed to compute the effects of anharmonic vibrations [296], it has been pointed out that the structure calculated after the application of the harmonic corrections is internally consistent and comparable directly with the geometrical data obtained with other techniques [3, 215]. Therefore, the contribution of the anharmonic term to the observed dipolar coupling is typically neglected.

Unfortunately, the extension of vibrational corrections to flexible molecules is not straightforward. Indeed, the conformational dependence of observed dipolar couplings has to be translated into a conformational dependence of the harmonic force field which complicates further the calculation of the vibrational corrections. A central problem is for which conformation(s) to calculate the force field. In a "massive" approach all the force fields (one for each conformation explored) are calculated and used in the determination of the vibrational corrections. This method is of course CPU expensive and consequently very often too hard to follow. In a "light" approach, only force fields corresponding to the more stable conformers are calculated and used. This method is not particularly expensive and its successful application in several papers [230, 255-256, 279, 295] is easily justified by considering that the increasing error in neglecting contributions from conformers away from the minima is rapidly cut off by the Boltzmann probability factor of those conformers.

A notable point is that the importance of vibrational corrections to dipolar couplings is related to the precision with which D_{ij}^{obs} can be measured. Since dipolar couplings of up to several thousand Hertz are observed in strongly orienting systems, opposed to only some Hertz (or tens of Hertz) in weakly aligning media, a greater relative precision can be achieved in the former case. This means that in thermotropic LCs al least the harmonic vibrational corrections should be taken into account. However, for samples in highly ordered media studied in this Ph.D. thesis, only $^nD_{HH}$ (with n ≥ 3) were considered, for which, as a general rule, vibrational corrections are relatively unimportant [217]. Hence, we safely neglected them in all cases. Contrarily, in conformational studies on solutes dissolved in PBLG systems performed in this project, RDCs between nuclei other ^{1}H were observed, requiring in principle the inclusion of vibrational corrections in the calculations. Anyway, in all cases, it can be assumed that the

error derived from neglecting vibrational corrections falls within the "intrinsic" degree of error due to the edition of dipolar couplings. Note, for instance, that the largest vibrational corrections observed for a monosaccharide dissolved in a lyotropic LC are around 0.3 Hz and 0.1 Hz for $^1D_{CH}$ and $^2D_{HH}$ coupling, respectively, that is ~10% of the amplitude of D_{ij} [297]. When compared to absolute errors on D_{ij}^{obs} associated with all NMR experiments we used, such corrections can be considered not relevant. Therefore, we neglected vibrational corrections for all PBLG systems, without noticeably affecting the conformational results.

1.5.   *NMR methodology in partially ordered phases*

Conveying the idea of the orientational order adopted by a solute dissolved in an aligning medium and understanding to what extent such orientational order affects its NMR spectrum may be difficult, but this becomes striking looking at an example, as the one reported in Figure 1.13. The same solute, *trans*-stilbene, gives different single-quantum (SQ) ^{1}H spectra when dissolved in different phases, the THF-d_8 isotropic phase, and the two anisotropic phases represented by the lyotropic PBLG/THF-d_8 mixture and thermotropic liquid crystal ZLI1132. These two anisotropic phases, PBLG and ZLI1132, can be considered as illustrative of what we have more generally in a highly and weakly ordering media.

Two main comparisons should be addressed. Firstly, NMR spectra of oriented molecules, both in lyotropic and thermotropic solvents (Figure 1.13 (b) and (c)), are characterized by a greater number of transitions than conventional high-resolution NMR spectra in conventional liquids (Figure 1.13 (a)), *i.e.* they are more complex. This is obviously due to the presence of dipolar interactions between the most or the totality of the active spins in the molecule. A direct consequence is that the definition of weak and strong coupling in spectra of oriented molecules depends on the strength of both dipolar and indirect spin-spin couplings compared to chemical shifts, unlike the strength of only the indirect spin-spin couplings in the conventional liquid-state NMR spectra. Another important point is that even dipolar couplings between equivalent nuclei influence the NMR spectrum. A group which is magnetically equivalent and provides a single resonance line in the isotropic phase gives rise to a multiplicity of lines in oriented systems [3, 4]. For example, in benzene in the isotropic phase, all six protons have the same chemical shift, and the indirect spin-spin couplings do not affect the spectrum, giving rise to a A_6 spin system. Contrarily, in the oriented phase the spectrum of benzene is designated as AA'A''A'''A''''A''''' (72 transitions) and it depends upon all the direct

as well as the indirect coupling constants [3, 4]. Furthermore, for oriented molecules, even fully equivalent groups A_n (where n is the number of fully equivalent spin-1/2 nuclei) give rise to a multiplicity of n transitions with a separation equal to $3D_{ij}$ between adjacent transitions [3, 4].
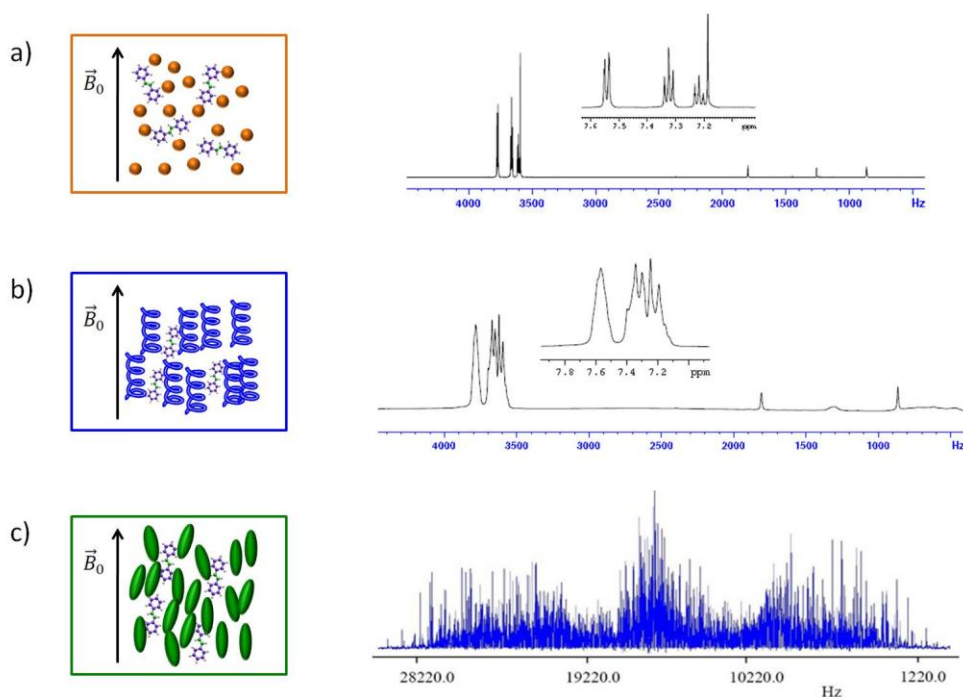
Figure 1.13. SQ ^{1}H spectra of *trans*-stilbene dissolved in (a) THF-d$_8$, (b) PBLG/ THF-d$_8$ mixture and (c) ZLI1132.

In general, for N interacting spins I=1/2, the maximum number of lines appearing in the single-quantum NMR spectrum of a compound partially oriented in a mesophase can be calculated using equation [298-299]:

$$\text{number of transitions} = \frac{(2N)!}{(N-1)!\,(N+1)!} \qquad (1.90)$$

For example, for systems with five, six, seven and eight interacting spins, there are 210, 792, 3003, and 11440 allowed transitions, respectively. Hence, for every addition of an interacting spin, the number of allowed transitions increases by nearly fourfold. However, elements of symmetry in the spin system decrease the number of different transitions, simplifying the spectra. For example, a completely unsymmetrical six-spin system will show 792 transitions in the ^{1}H SQ spectrum, while a more symmetrical molecule such as benzene, exhibits only 72 transitions in the SQ proton spectrum [298-299].

The second - even more important in the context of this thesis - comparison we should make is between spectra of solutes dissolved in lyotropic and thermotropic solvents, as the ones reported in Figure 1.13 (b) and (c). If in both cases the same anisotropic Hamiltonian influences the spectral pattern, why are these spectra so different? The answer clearly resides in the different ordering power of the solvent (lyotropic *versus* thermotropic liquid crystal), that directly affects the entity of dipolar couplings, and this in turn results in significantly different spectral patterns. Typically values of the solute's orientational order parameter are on the order of 10^{-1}-10^{-2} in thermotropic LCs and in the range 10^{-3} to 10^{-5} in organic solutions of poly-γ-benzyl-L-glutamate (PBLG). This difference has two main consequences. (*i*) First, the spectra of solutes dissolved in highly ordering liquid crystals are characterized by the presence of a very high number of distinct transitions evenly dispersed over a few 10^{4} Hz frequency range and exhibiting strong second order features [4]. Contrarily, in mixtures of PBLG and organic co-solvent the dipolar couplings are often small values compared to Larmor frequency differences [99-100], *i.e*, dipolar and scalar couplings are of the same order of magnitude. Therefore, spectra may sometimes retain first-order features or, more often, they display second order effects that are much weaker than in thermotropic LCs. (*ii*) Secondly, unlike thermotropics, the exact measurement of scalar couplings is a crucial step in PBLG samples. Indeed, while in thermotropic LCs scalar couplings can be even roughly estimated, since the contribute they give to the total coupling is much smaller than the corresponding dipolar couplings, in weakly ordered media a precise edition of scalar couplings is essential to avoid transferring a significant error in the extraction of the dipolar couplings. The measurement of dipolar couplings in PBLG samples, therefore, has the prerequisite of performing two series of precise measurements, one in isotropic solution yielding the scalar coupling constants J_{ij} and one in anisotropic solution yielding the total coupling constants T_{ij} [219]. The value of D_{ij} can then be obtained from the difference of the former two.

Being the differences in the spectra of highly and weakly ordered solutes so prominent, it is evident that the extraction of the experimental data set poses specific issues according to the ordering power of the aligning medium. This means that the adopted operational strategies may be different.

1.5.1.   NMR experiments

The different degree of complexity between highly and weakly ordered samples influences the NMR experiments one can perform in order to gather a data set that is as large as possible.

The total absence of first-order features in spectra of molecules in strong aligning media poses some obvious limitations. Therefore, monodimensional proton spectra are the most used and actually the maximum number of interacting spins in a molecule from which a resolved [1]H-spectrum can be obtained is about 12 [225]. For some small molecules, 1D ^{13}C-spectra and especially carbon satellite spectra of protons [254-255, 279, 295] can be useful to extend the data set. Besides the more common monodimensional spectra, some 2D and 3D pulse sequences have been specifically developed for thermotropic liquid crystalline samples [300-303], the most relevant being spin-echo techniques [304-305], 2D COSY and modified Z-COSY techniques [305-307] and 2D heteronuclear correlation experiments [308-310]. Further improvements were made by introducing the 2D separated-local field (SLF) ^{13}C experiments [182] and their several implementations, including 2D and 3D proton-detected local field (PDLF) techniques [185, 311-314], and 2D SLF ^{13}C combined with off-magic angle spinning techniques [128, 315-316]. Both SLF and PDLF experiments require, however, high power proton decoupling, which can be achieved only with spectrometers designed to study solid samples.

Unlike thermotropic samples, spectra in weakly ordering phases generally retain some first-order features so, in principle, most 1D and 2D experiments for measuring scalar couplings in isotropic samples can be used to extract dipolar couplings from spectra of lyotropic samples [166, 317]. However, in practice, the required precision for measuring RDCs is usually higher than that for scalar couplings and consequently existing methods have been strongly revised and extended in the past decades [166, 317]. A variety of excellent 2D state-of-the-art pulse sequences initially developed for isotropics have been successfully applied on PBLG samples, the most popular being homonuclear *J*-resolved experiments [318-319] for the determination of [1]H-^{1}H couplings, E.COSY (exclusive correlation spectroscopy) methods [320-323] for the sign-sensitive determination of $^nJ_{HH}/^nD_{HH}$, adequately modified HSQC [324-331] and heteronuclear *J*-resolved [297, 332-334] experiments for the edition of one-bond as well as long-range [13]C-^{1}H dipolar couplings. The first-order nature of spectra in PBLG medium offers an additional advantage: it is possible to select signals from a given pair of spins in the molecule so that just one desired coupling can be selectively edited. Following this principle homonuclear [335-343] and heteronuclear [344-347] SElective ReFocusing (SERF) experiments

have been reported. As a further development, the use of selective pulses may be combined with the spatial frequency encoding approach. This means the pulse is effectively applied on a broad range of chemical shifts according to their spatial position in the NMR tube, as if different selective experiments were run on different parts of the NMR tube at the same time [348-350].

Both in highly and weakly ordered media, the presence of other magnetically active heteronuclei may be an interesting alternative to get additional information by recording NMR spectra of such spins. Fluorine and phosphorous NMR spectroscopies, for example, were demonstrated to be particularly attractive, thanks to higher sensitivity with respect to ^{13}C. Indeed ^{19}F and ^{31}P are 100% naturally abundant spins ½ nuclei and possess relatively high magnetogyric ratios, providing respectively about 83% and 7% of the proton NMR sensitivity for a given magnetic field. For these reasons they were exploited both in thermotropic [236, 351-352] and lyotropic [112, 353-355] solvents.

Another magnetically active nucleus that has recently gained more and more attention is ^{2}H. Indeed, since at natural abundance level ^{2}H-^{2}H spin–spin couplings are not detected, the NAD 1D ^{2}H-{^{1}H} spectra in ordered media simply consist of the superposition of independent quadrupolar doublets. For large molecules, the correlation between the two components for each quadrupolar doublet is not always simple to achieve, mainly due to overlapping of peaks. To overcome this limitation, several two-dimensional autocorrelation deuterium NMR experiments referred to as QUOSY (for QUadrupole Ordered SpectroscopY) have been developed [356], among which the Q-COSY and Q-resolved sequences were found to be the most useful [357-358]. Even if NAD spectroscopy has been showed to offer advantages for studying thermotropic samples [359], it is in lyotropic systems that the technique has really gained a leading position and has been also extensively applied for enantiomeric discrimination [184-185, 248, 360-366].

In principle the number and the variety of NMR pulse sequences that can be used to measure dipolar couplings is greater for lyotropic than thermotropic samples. However, it is worth to underline that even in polypeptidic liquid crystalline solvents the edition of the desired couplings is not always trivial with existing methods and significant signal overlaps may prevent from a fast and/or simple interpretation of complex multiplicities. Therefore, despite the extremely broad array of experiments already available for the measurement of dipolar couplings in PBLG systems, there is still the continuous need for the design of new pulse sequences.

1.5.2. *Spectral analysis*

As highlighted in the previous paragraph, the difference in the degree of orientational order and then in the extent of first- or second-order spectral features substantially distinguishes spectra of solutes dissolved in thermotropic or lyotropic LCs. This has an obvious consequence in the strategy adopted for spectral analysis, too.

A first-order analysis similar to that of isotropic liquids is generally possible in weakly ordered liquid crystals such as organic solutions of PBLG. In this case, once measured the scalar couplings J_{ij}^{iso} from the isotropic sample and the total couplings T_{ij} from the anisotropic one, the values of D_{ij} can then be obtained such as:

$$D_{ij} = \frac{\pm T_{ij} - (\pm J_{ij}^{iso})}{2} \ (\text{non} - \text{equivalent nuclei}) \qquad (1.91)$$

$$D_{ij} = \frac{\pm T_{ij}}{3} \ (\text{equivalent nuclei}) \qquad (1.92)$$

However, care must be taken concerning the sign. As only the absolute values of coupling constants are observed in conventional spectra, both sign and value of D_{ij} can be edited only if the signs of J_{ij}^{iso} and T_{ij} are known. The determination of the sign is typically straightforward for $^1D_{CH}$, since the sign of $^1J_{CH}$ are known to be positive [367] and in the PBLG phase $^1J_{CH}$ are generally larger than corresponding $^1D_{CH}$ [99-100]. The situation is more complex for $^nD_{CH}$ (with n≠1) and $^nD_{HH}$. Some measurement methods which also provide the sign of scalar coupling constants (see section 1.5.1) or other considerations taken by literature (for instance J_{HH} between aromatic protons are positive [368]) can be exploited, but even in this case two possible values of D_{ij} can be obtained starting from the absolute values of T_{ij} observed in conventional spectra. Finally, for totally unknown signs of J_{ij}^{iso} and T_{ij}, up to four values of D_{ij} are possible. It is evident that methods for choosing the "correct value" of D_{ij} are thus essential.

In thermotropic liquid crystals, a first-order analysis of the spectra similar to those of liquids is generally not possible and spectral simulation packages are essential for the edition of all dipolar couplings. Just in few cases signal overlap and strong coupling in spectra of large molecules dissolved in a PBLG phase may also require the use of such graphical interfaces. Several iterative computer programs suitably modified by the inclusion of the dipolar couplings are commonly used [369-372]. An home-made graphical package dubbed ARCANA [373] was developed in the LXNMR S.C.An. group, and it is the software used in all the spectral analysis of solutes dissolved in thermotropic solvents considered in this thesis. The strategy adopted for

the analysis of the spectra is shown in the form of a flowchart in Figure 1.14. It consists essentially of few steps:

step 1. A spectrum is calculated from a trial set of input parameters and it is compared to the experimental one;

step 2. As many as possible calculated to experimental frequencies are assigned;

step 3. Trial sub-sets of spectral parameters are modified iteratively by the Castellano Bothner-By algorithm [374] to fit experimental frequencies;

step 4. The simulated spectrum is re-calculated and steps 2 and 3 are repeated while assigning/deleting lines and modifying the parameters iteration set; the iteration procedure is continued until good correspondence between the calculated and experimental spectrum is reached and the root-mean-square error between the calculated and experimental line positions reaches a minimum.

It is worth remarking that the spectral analysis *via* ARCANA software bypasses the problem of sign discussed for lyotropic samples, since both sign and value of D_{ij} are obtained in the output file. Note that the iteration procedure uses only line frequencies; it is the operator who, on the basis of intensities and line distribution, makes the proper assignments. It is evident then that an expert operator is needed, his role fundamental in step 2.

Step 1 remains the critical point in the procedure given the nature of anisotropic spectra. The trial spectrum computed should closely resemble the experimental one such that a sufficient number of transitions can be assigned for subsequent iteration and refinement of the parameters. It is thus evident that, without a judicious choice of the starting parameter set, the number of lines and the lack of first order features are such that there is no chance of success. The starting parameters for the iterative spectral analysis include chemical shifts, indirect spin-spin couplings, and direct dipolar couplings. Starting values for the chemical shifts and indirect spin-spin couplings are usually taken from spectra of isotropic samples. The dipolar couplings constitute the bigger problem. They may be calculated assuming the molecular geometry and certain guessed values for the orientational tensor components but the analysis is often quite complex because, even if an appropriate molecular geometry can be guessed, the degrees of order are difficult to predict [3, 4]. Definitively, it is with the intuition, experience and sometimes also the luck of scientists working in the field that the trial spectra can be simulated with reasonable resemblance to the experimental ones so that the complicated spectra can be analyzed.
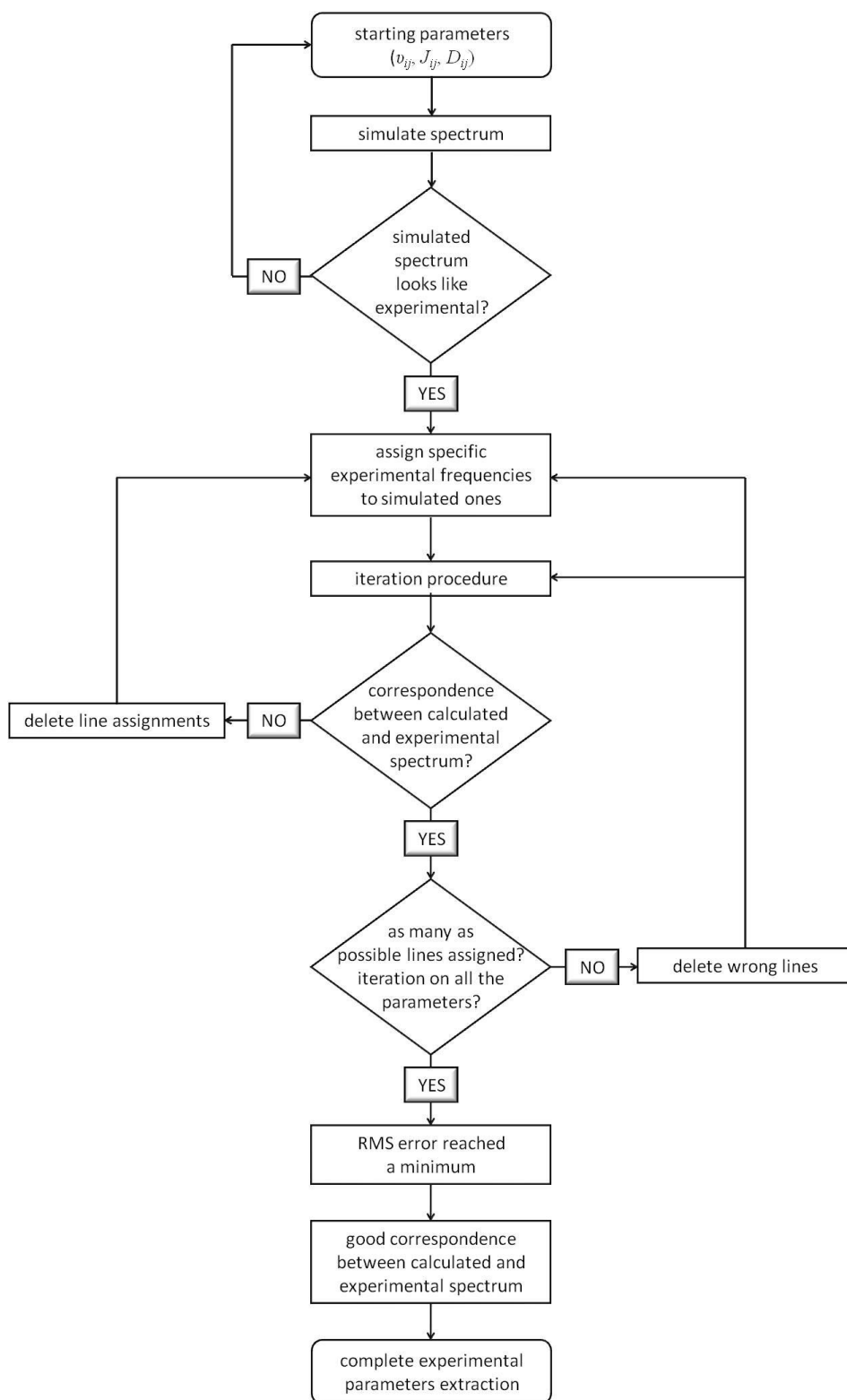
Figure 1.14. Flowchart showing the strategy adopted for analysis of the NMR spectra of oriented molecules.

Even with the help of a simulation program, the high intrinsic complexity that characterize 1D proton spectra in thermotropic liquid crystals imposes an upper limit on the

number of interacting spins for which the spectral analysis can be carried out conveniently. The difficulty obviously increases with the increase in the number of spins, with the decrease in the symmetry and with solute flexibility. Severe overlap between transitions in unsymmetrical spin systems containing more than about 8 spins makes analysis of single-quantum spectra often too complicated and virtually impossible [298]. If elements of symmetry are present in the spin system, the resulting spectrum is simplified and, in such conditions, spectra of up to 12 interacting spins can be analyzed [251, 256, 258]. In order to overcome this practical limitation, several techniques, both experimental and methodological, have been and are being developed to aid in the analysis of the complex spectrum, and we give in the following a brief description of the most popular:

1. *Isotopic substitution*

Isotopic substitution, and in particular partially or totally deuteration of samples, is one of the oldest procedure suggested for the simplification of the spectra of strongly oriented molecules. As deuterium splits signals in more complex way (I = 1) and the D_{HD} couplings are small ($\gamma_D \cong \gamma_H/6.5$) the common strategy is recording SQ ^{1}H spectra with deuterium decoupling [375-379]. In this way it is possible to dramatically simplify the proton spectrum (*i.e.* deuteration and [2]H-decoupling reduces the spin system) while keeping - in first approximation - the same order and the same internal potential. The extracted dipolar couplings can then be safely transferred back to the analysis of the ^{1}H spectrum recorded for the fully protonated solute [257, 272]. Another method that has been used to aid the analysis is to deuterate and estimate the order parameters from the deuteron NMR spectrum. The order parameters thus derived are used, assuming a molecular structure for a fixed conformation, to estimate the starting parameters for the analysis of the complicated proton NMR spectrum [276]. Since specific deuteration is generally synthetically challenging, time consuming and, in some cases, impractical, this method has not found widespread application, but with the enhanced sensitivity of the spectrometers, the natural abundance ^{2}H-NMR spectra can be alternatively employed to derive orientation information.

2. *Off Magic Angle (OMAS) or Variable Angle Sample (VASS) Spinning experiments*

A convenient method for systematically scaling anisotropic interactions in orientationally ordered systems is provided by spinning the sample about an axis that makes an angle α with the external magnetic field [215]. If the rate of spinning exceeds the rate of director reorientation, the director aligns along the spinning axis instead of along the magnetic field. When α equals 54.7° (the "magic angle"), the anisotropic interactions vanish. When spinning close to the magic angle the anisotropic interactions, including the dipole-dipole interaction,

are scaled by a factor $R = (1/2)(3cos^2\alpha - 1)$, and first order features can then be introduced in the spectrum [127-128]. The technique is referred to as "off magic angle spinning" or "variable angle spinning", since it can be performed, in principle, at different angles, and it has be exploited both for thermotropic [380-382] and lyotropic [126, 383-385] systems. However, the usefulness of this method is limited by interference of lines from the liquid crystal medium. The use of fully deuterated liquid crystals as solvents may be helpful in such cases [215].

   3. *Multiple Quantum (MQ) spectroscopy* [298-299, 386]

MQ NMR is concerned with the indirect observation of transitions between energy levels differing in total spin quantum number by $\Delta M \neq \pm 1$. The main benefit lies in the fact that there are fewer transitions in the high-order MQ spectra, leading then to a dramatic simplification of the spectrum of a solute dissolved in a liquid crystalline solvent [300-301, 387-389]. The number of M-quantum transitions in a system of N nuclei (I = 1/2) without symmetry is given by [298-299]:

$$\text{number of } M - \text{quantum transitions} = \frac{(2N)!}{(N-M)!\,(N+M)!} \qquad (1.93)$$

It must be pointed that the frequencies of the resonances in the MQ-NMR spectra are governed by exactly the same parameters as those in conventional single-quantum NMR spectra, so they contain the same information. In principle, the N-1 and N-2 quantum spectra contain sufficient transitions to solve the spectrum completely for all of the spectral parameters for most spin systems [298]. In many cases, the analysis of the high-order MQ-NMR spectra has been used to provide initial spectral parameters that have been used as starting point for the more complex analysis of the single-quantum spectrum [272, 279, 390-393].

   4. *Automated spectral fitting routines*

There have been many attempts to develop totally automatic computer procedures for spectral analysis [394-399]. The automatic programs avoid the assigning of experimental to calculated transitions, but their usefulness decreases significantly when the guess starting parameters are far from their real values or when the system has a large number of independent spectral parameters [215]. More recently, novel methods based on Evolutionary Strategies and Genetic Algorithms [400-407] have been developed. A fascinating example of the potentiality of Genetic Algorithm is the successfull analysis of the very complicated ^{1}H spectrum of pentane as a solute in nematic liquid crystalline solvents [401]. Pentane is a highly flexible molecule whose proton spectrum consists of roughly 20000 transitions with many overlapping lines and few distinguishing features, making it essentially impossible to analyse

with the traditional "line-assignment" technique. However, it should be noted that the use of evolutionary algorithms for the spectral analysis requires as a prerequisite a good starting set of parameters or a good estimation of the solute degree of orientational order. In the case of pentane, initial estimates of the dipolar couplings were done by considering nine RIS structures and assuming values for their conformational probabilities and by using a model for estimating solute conformer order parameters. Then, despite evolutionary strategies might represent an important breakthrough in spectral analysis of complicated spectra offering the possibility of extending investigations to more complicated spin systems than ever envisaged in the past, the need for a good starting set of parameters is still of undoubtable importance.

5. *Molecular dynamics*

Recently, atomistic molecular dynamics simulations of liquid crystalline systems have proven to be a reliable way to reproduce mesogens' properties as well as solutes' experimental dipolar couplings [408-413]. The simulated D_{ij} can be used as an useful starting point to aid in spectral analysis in cases that would be otherwise impossible to solve in a reasonable time. Their application in conjunction with evolutionaty algorithms has been very recently illustrated in the case of n-pentane dissolved in 5CB [409]. In this thesis the usefulness of the strategy when combined with classical spectral "line-assignment" analysis carried out by an operator will be investigated in chapter 3 in the case of biphenyl.

Despite in principle several methods to simplify the spectral analysis do exist, in practice each of the developed techniques has some practical difficulties, and hence so far none has been used as a routine method. However, the availability of ultrahigh-field magnetic fields and the sensitivity enhancement in the modern spectrometers as well as the improvements in atomistic simulation methods and the enormous power of modern computer technology are likely to provide more advances in the field.

1.6.   Conclusion

This first chapter has been intended to outline the basic tools of NMR spectroscopy in partially ordered media, which will be applied in the next chapters to the study of different rigid and flexible molecules. What it should be emphasized is that dipolar couplings characterizing spectra of partially ordered solutes are an astonishing source of information, but it is not trivial to get it since (*i*) more or less sophisticated NMR experiments have to be performed in order to obtain resolved spectra from which D_{ij}^{exp} could be measured and (*ii*) *a*

priori knowledge of molecular structure and theoretical models are necessary in order to give to such D_{ij}^{exp} a physical meaning, that is in order to get information on orientational order, structure and conformational equilibrium. It can be useful to resume with a flowchart the whole analytical strategy presented in this chapter and adopted in the following studies (Figure 1.15).
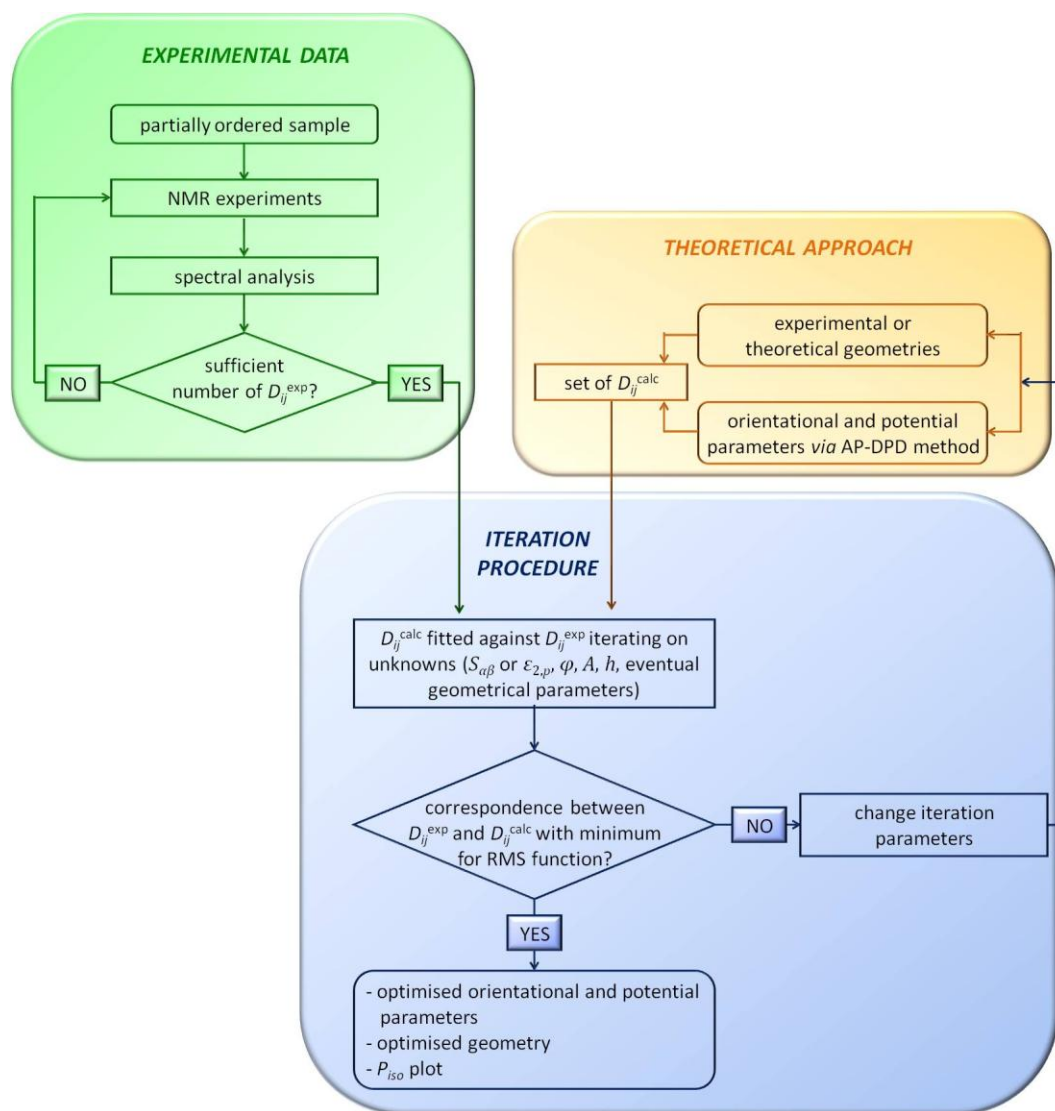
Figure 1.15. Flowchart showing the whole analytical strategy adopted for structural, orientational and conformational studies of partially ordered molecules.

References

[1] A. Saupe, G. Englert, High-resolution nuclear magnetic resonance spectra of oriented molecules, *Phys. Rev. Lett.* 11, **1963**, 462-464

[2] A. Saupe, Recent results in the field of liquid crystals, *Angew. Chem. Int. Ed.*, 7, **1968**, 97-112

[3] P. Diehl, Structure of rigid molecules dissolved in liquid crystalline solvents, in *Encyclopedia of Magnetic Resonance*, John Wiley & Sons, Ltd. **2007**

[4] N. Suryaprakash, Structure of molecules by NMR spectroscopy using liquid crystal solvents, *Concepts Magn. Reson.*, 10, **1998**, 167-192

[5] R. M. Gschwind, Residual dipolar couplings - A valuable NMR parameter for small organic molecules, *Angew. Chem. Int. Ed.* 44, **2005**, 4666-4668

[6] J. W. Emsley, J. C. Lindon, The nuclear Hamiltonian for partially oriented molecules, in *NMR Spectroscopy Using Liquid Crystal Solvents*, Pergamon Press, Oxford, **1975**, chap. 2, ISBN: 0080199194

[7] G. R. Luckhurst, G. W. Gray, *The Molecular Physics of Liquid Crystals*, G. R. Luckhurst and G. W. Gray eds., Academic Press, London, **1979**, chap. 17, ISBN: 9780124589506

[8] E. B. Priestley, Liquid crystal mesophases, in *Introduction to Liquid Crystals*, Springer-Verlag US, **1976**, chap. 1, ISBN: 9781468421774

[9] J. W. Emsley, J. C. Lindon, Liquid crystals, in *NMR Spectroscopy Using Liquid Crystal Solvents*, Pergamon Press, Oxford, **1975**, chap. 1, ISBN: 0080199194

[10] P. Collings, M. Hird, *Introduction to Liquid Crystals: Chemistry and Physics*, Taylor&Francis Ltd., **1997**, ISBN: 0748406433

[11] C. A. Veracini, NMR spectra in liquid crystals. The partially averaged spin Hamiltonian, in *Nuclear Magnetic Resonance of Liquid Crystals*, J. W. Emsley ed., Reidel, Dordrecht, **1985**, chap. 5, ISBN: 9027718784

[12] P. G. de Gennes, *The Physics of Liquid Crystals*, Oxford, **1975**, ISBN: 9780198517856

[13] N. A. Plate, *Liquid-Crystal Polymers*, Plenum Press, New York, **1993**, ISBN: 9780306442193

[14] R. A. Weiss, C. K. Ober, *Liquid-Crystalline Polymers*, volume 435, American Chemical Society, **1990**, ISBN: 9780841218499

[15] H. K. Bisoyi, S. Kumar, Liquid-crystal nanoscience: an emerging avenue of soft self-assembly, *Chem. Soc. Rev.*, 40, **2011**, 306-319

[16] H. W. Lee, W. You, S. Barman, S. Hellstrom, M. C. LeMieux, J. H. Oh, S. Liu, T. Fujiwara, W. M. Wang, B. Chen, Y. W. Jin, J. M. Kim and Z. Bao, Lyotropic liquid-crystalline solutions of high-concentration dispersions of single-walled carbon nanotubes with conjugated polymers, *Small*, 5, **2009**, 1019-1024

[17] S. Zhang, S. Kumar, Carbon nanotubes as liquid crystals, *Small*, 4, **2008**, 1270-1283

[18] W. Song, I. A. Kinloch, A. H. Windle, Nematic liquid crystallinity of multiwall carbon nanotubes, *Science*, 302, **2003**, 1363-1363

[19] K. Binnemans, Ionic liquid crystals, *Chem. Rev.*, 105, **2005**, 4148-4204

[20] H. Ohno, *Electrochemical Aspects of Ionic Liquids*, Wiley: New York, **2005**, ISBN: 9780471762515

[21] J. Dupont, R. F. de Souza, P. A. Z. Suarez, Ionic liquid (molten salt) phase organometallic catalysis, *Chem. Rev.*, 102, **2002**, 3667-3692

[22] P. Wasserscheid, T. Welton, *Ionic Liquids in Synthesis*, Wiley-VCH, Weinheim, **2002**, ISBN: 9783527312399

[23] M. J. Earle, K. R. Seddon, Ionic liquids. Green solvents for the future, *Pure Appl. Chem.*, 72, **2000**, 1391-1398

[24] P. Wasserscheid, W. Keim, Ionic liquids - New "solutions" for transition metal catalysis, *Angew. Chem. Int. Ed.*, 39, **2000**, 3772-3789

[25] C. Rodríguez-Abreu, C. Aubery Torres, G. J. T. Tiddy, Chromonic liquid crystalline phases of pinacyanol acetate: characterization and use as templates for the preparation of mesoporous silica nanofibers, *Langmuir*, 27, **2011**, 3067-3073

[26] S.-W. Tam-Chang, L. Huang, Chromonic liquid crystals: properties and applications as functional materials, *Chem. Commun.*, **2008**, 1957-1967

[27] J. Lydon, Chromonic liquid crystal phases, *Curr. Opin. Colloid Interface Sci.*, 3, **1998**, 458-466

[28] J. P. F. Lagerwall, G. Scalia, A new era for liquid crystal research: Applications of liquid crystals in soft matter nano-, bio- and microtechnology, *Curr. Appl. Phys.*, 12, **2012**, 1387-1412

[29] D. Haristoy, S. Mery, B. Heinrich, L. Mager, J. F. Nicoud, D. Guillon, Structure and photoconductive behaviour of a sanidic liquid crystal, *Liq. Cryst.*, 27, **2000**, 321-328

[30] I. G. Voigt-Martin, P. Simon, S. Bauer, H. Ringsdorf, Structure and defects in sanidic liquid crystalline polymers. 1, *Macromolecules*, 28, **1995**, 236-242

[31] K. Geese, M. Prehm, C. Tschierske, Bent-core mesogens with thiophene units, *J. Mater. Chem.*, 20, **2010**, 9658-9665

[32] K. Gomola, L. Guo, E. Gorecka, D. Pociecha, J. Mieczkowski, K. Ishikawa, H. Takezoe, First symmetrical banana compounds exhibiting SmAP$_R$ mesophase and unique transition between two orthogonal polar phases, *Chem. Commun.*, **2009**, 6592-6594

[33] A. Jákli, C. Bailey, J. Harden, Physical properties of banana liquid crystals, in *Thermotropic Liquid Crystals. Recent Advances*, A. Ramamoorthy ed., Springer, Dordrecht, The Netherlands, **2007**, chap. 2, ISBN: 9781402053276

[34] R. A. Reddy, C. Tschierske, Bent-core liquid crystals: polar order, superstructural chirality and spontaneous desymmetrisation in soft matter systems, *J. Mater. Chem.* 16, **2006**, 907-961

[35] G. Pelzl, S. Diele, W. Weissflog, Banana-shaped compounds - A new field of liquid crystals, *Adv. Mater.*, 11, **1999**, 707-724

[36] D. A. Markelov, V. V. Matveev, P. Ingman, M. N. Nikolaeva, E. Lähderanta, V. A. Shevelev, N. I. Boiko, NMR studies of carbosilane dendrimer with terminal mesogenic groups, *J. Phys. Chem. B*, 114, **2010**, 4159-4165

[37] V. Domenici, M. Cifelli, C. A. Veracini, N. I. Boiko, E. V. Agina, V. P. Shibaev, Order and dynamics of a liquid crystalline dendrimer by means of ^{2}H NMR spectroscopy, *J. Phys. Chem. B*, 112, **2008**, 14718-14728

[38] B. Donnio, D. Guillon, Liquid crystalline dendrimers and polypedes, in *Supramolecular Polymers, Polymeric Betains, Oligomers*, *Adv. Polym. Sci.*, K. S. Lee ed., Springer-Verlag, Berlin-Heidelderg-New York, Germany, 201, **2006**, 45-155, ISBN: 9783540319245

[39] D. Demus, J. Goodby, G. W. Gray, H.-W. Spiess, V. Vill, *Handbook of Liquid Crystals, vol.2A: Low Molecular Weight Liquid Crystals I*, Wiley-VCH, Verlag, **1998**, ISBN: 9783527292714

[40] P.S. Persham, *Structure of Liquid Crystal Phases (Lecture Notes in Physics)*, World Scientific Publishing Co Pte Ltd, **1988**, ISBN: 9789971506681

[41] K. K. Chan, P. S. Pershan, L. B. Sorensen, F. Hardouin, X-ray studies of transitions between nematic, smectic- A_1, -A_2, and -A_d phases, *Phys. Rev. A*, 34, **1986**, 1420-1433

[42] C. A. Veracini, M. Geppi, Liquid crystalline samples: chiral smectic phases, in *Encyclopedia of Magnetic Resonance*, John Wiley & Sons, Ltd., **2007**

[43] J. P. F. Lagerwall, F. Giesselmann, Current topics in smectic liquid crystal research, *Chem. Phys. Chem.*, 7, **2006**, 20-45

[44] D. Galland, F. Volino, On the interpretation of NMR data of non-rigid molecules in nematic phases: a serve test of the single conformation model, *J. Phys. II*, 1, **1991**, 209-223

[45] E. Lafontaine, J. P. Bayle, J. Courtieu, High resolution NMR in cholesteric medium: visualization of enantiomers, *J. Am*. *Chem*. *Soc*., 111, **1989**, 8294-8296

[46] B. W. Koenig, J.-S. Hu, M. Ottiger, S. Bose, R. W. Hendler, A. Bax, NMR measurement of dipolar couplings in proteins aligned by transient binding to purple membrane fragments, *J. Am. Chem. Soc.*, 121, **1999**, 1385-1386

[47] J. Sass, F. Cordier, A. Hoffmann, M. Rogowski, A. Cousin, J. G. Omichinski, H. Löwen, S. Grzesiek, Purple membrane induced alignment of biological macromolecules in the magnetic field, *J. Am. Chem. Soc.*, 121, **1999**, 2047-2055

[48] G. Siegal, J. van Duynhoven, M. Baldus, Biomolecular NMR: recent advances in liquids, solids and screening, *Curr. Opin. Chem. Biol.*, 3, **1999**, 530-536

[49] B. Bendiak, Sensitive through-space dipolar correlations between nuclei of small organic molecules by partial alignment in a deuterated liquid solvent, *J. Am. Chem. Soc.*, 124, **2002**, 14862-14863

[50] P. Haberz, F. Rodriguez-Castañeda, J. Junker, S. Becker, A. Leonov, C. Griesinger, Two new chiral EDTA-based metal chelates for weak alignment of proteins in solution, *Org. Lett.*, 8, **2006**, 1275-1278

[51] M John, G. Pintacuda, A. Y. Park, N. E. Dixon , G. Otting, Structure determination of protein-ligand complexes by transferred paramagnetic shifts, *J. Am. Chem. Soc.*, 128, **2006**, 12910-12916

[52] J. Wöhnert, K. J. Franz, M. Nitz, B. Imperiali, H. Schwalbe, Protein alignment by a coexpressed lanthanide-binding tag for the measurement of residual dipolar couplings, *J. Am. Chem. Soc.*, 125, **2003**, 13338-13339

[53] I. Bertini, C. Luchinat, G. Parigi, Paramagnetic constraints: an aid for quick solution structure determination of paramagnetic metalloproteins, *Concepts Magn. Reson.*, 14, **2002**, 259-286

[54] N. Tjandra, J. G. Omichinski, A. M. Gronenborn, G. M. Clore, A. Bax, Use of dipolar ^{1}H-^{15}N and ^{1}H-^{13}C couplings in the structure determination of magnetically oriented macromolecules in solution, *Nat. Struct. Biol.*, 4, **1997**, 732-738

[55] N. Tjandra, S. Grzesiek, A. Bax, Magnetic field dependence of nitrogen-proton *J* splittings in ^{15}N-enriched human ubiquitin resulting from relaxation interference and residual dipolar coupling, *J. Am. Chem. Soc.*, 118, **1996**, 6264-6272

[56] J. R. Tolman, J. M. Flanagan, M. A. Kennedy, J. H. Prestegard, Nuclear magnetic dipole interactions in field-oriented proteins: information for structure determination in solution, *Proc. Natl. Acad. Sci. U.S.A.*, 92, **1995**, 9279-9283

[57] A. S. Tracey, Lyotropic liquid crystalline samples, in *Encyclopedia of Magnetic Resonance,* John Wiley & Sons, Ltd., **2007**

[58] A. M. Figueiredo Neto, S. R. A. Salinas, *The Physics of Lyotropic Liquid Crystals: Phase transitions and Structural Properties*, Oxford University Press Inc., New York, **2005**, ISBN: 9780198525509

[59] G. Burducea, Lyotropic liquid crystals: structural polymorphism, *Romanian Rep. Phys.*, 56, **2004**, 87-100

[60] C. L. Khetrapal, A. C. Kunwar, A. S. Tracey, P. Diehl, Nuclear magnetic resonance studies in lyotropic liquid crystals, in *NMR Basic Principles and Progress*, *Vol. 9, Lyotropic Liquid Crystals*, P. Diehl, E. Fluck, and R. Kosfeld eds., pp. 3-74, Springer-Verlag, Berlin, **1975**, ISBN: 9780387073033

[61] J. R. Tolman, K. Ruan, NMR residual dipolar couplings as probes of biomolecular dynamics, *Chem. Rev.*, 106, **2006**, 1720-1736

[62] A. Bax, A. Grishaev, Weak alignment NMR: a hawk-eyed view of biomolecular structure, *Curr. Opin. Struct. Biol.*, 15, **2005**, 563-570

[63] M. Blackledge, Recent progress in the study of biomolecular structure and dynamics in solution from residual dipolar couplings *Prog. Nucl. Magn. Reson. Spectrosc.*, 46, **2005**, 23-61

[64] J. H. Prestegard, C. M. Bougault, A. I. Kishore, Residual dipolar couplings in structure determination of biomolecules, *Chem. Rev.*, 104, **2004**, 3519-3540

[65] A. Annila, P. Permi, Weakly aligned biological macromolecules in dilute aqueous liquid crystals, *Concepts Magn. Reson.*, 23A, **2004**, 22-37

[66] C. Griesinger, J. Meiler, W. Peti, Angular restraints from residual dipolar couplings for structure refinement, in *Protein NMR for the millennium* R. Krishna and L. J. Berliner eds., New York, Kluwer Academic/Plenum Publ., **2003**, chap. 7, ISBN: 9780306474484

[67] N. Tjandra, A. Bax, Direct measurement of distances and angles in biomolecules by NMR in a dilute liquid crystalline medium, *Science*, 278, **1997**, 1111-1114

[68] C. B. Tan, B. M. Fung, G. Cho, Phospholipid bicelles that align with their normals parallel to the magnetic field, *J. Am. Chem. Soc.*, 124, **2002,** 11827-11832

[69] M. Ottiger, A. Bax, Characterization of magnetically oriented phospholipid micelles for measurement of dipolar couplings in macromolecules, *J. Biomol. NMR*, 12, **1998**, 361-372

[70] R. S. Prosser, J. S. Hwang, R. R. Vold, Magnetically aligned phospholipid bilayers with positive ordering: a new model membrane system, *Biophys. J.*, 74, **1998**, 2405-2418

[71] C. R. Sanders II, J. P. Schwonek, Characterization of magnetically orientable bilayers in mixtures of dihexanoylphosphatidylcholine and dimyristoylphosphatidylcholine by solid-state NMR, *Biochemistry*, 31, **1992**, 8898-8905

[72] Z. Shi, R. W. Woody, N. R. Kallenbach, Is polyproline II a major backbone conformation in unfolded proteins?, *Adv. Protein Chem.*, 62, **2002**, 163-240

[73] R. V. Pappu, G. D. Rose, A simple model for polyproline II structure in unfolded states of alanine-based peptides, *Protein Sci*., 11, **2002**, 2437-2455

[74] M. Ottiger, A. Bax, Bicelle-based liquid crystals for NMR-measurement of dipolar couplings at acidic and basic pH values, *J. Biomol. NMR*, 13, **1999**, 187-191

[75] L. G. Barrientos, C. Dolan, A. M. Gronenborn, Characterization of surfactant liquid crystal phases suitable for molecular alignment and measurement of dipolar couplings, *J. Biomol. NMR*, 16, **2000**, 329-337

[76] R. S. Prosser, J. A. Losonczi, I. V. Shiyanovskaya, Use of a novel aqueous liquid crystalline medium for high-resolution NMR of macromolecules in solution, *J. Am. Chem. Soc.*, 120, **1998**, 11010-11011

[77] M. Rückert, G. Otting, Alignment of biological macromolecules in novel nonionic liquid crystalline media for NMR experiments, *J. Am. Chem. Soc.*, 122, **2000**, 7793-7797

[78] S. Vyas, C. J. Hernandez, M. P. Augustine, Ordering of alkali halide salts dissolved in bacteriophage Pf1 solutions: A nuclear magnetic resonance study, *J. Chem. Phys.*, 116, **2002**, 7109-7115

[79] M. Zweckstetter, A. Bax, Characterization of molecular alignment in aqueous suspensions of Pf1 bacteriophage, *J. Biomol. NMR*, 20, **2001**, 365-377

[80] M. R. Hansen, L. Mueller, A. Pardi, Tunable alignment of macromolecules by filamentous phage yields dipolar coupling interactions, *Nat. Struct. Biol.*, 5, **1998**, 1065-1074

[81] L. G. Barrientos, J. M. Louis, A. M. Gronenborn, Characterization of the cholesteric phase of filamentous bacteriophage *fd* for molecular alignment, *J. Magn. Reson.*, 149, **2001**, 154-158

[82] G. M. Clore, M. R. Starich, A. M. Gronenborn, Measurement of residual dipolar couplings of macromolecules aligned in the nematic phase of a colloidal suspension of rod-shaped viruses, *J. Am. Chem. Soc.*, 120, **1998**, 10571-10572

[83] S. M. Douglas, J. J. Chou, W. M. Shih, DNA-nanotube-induced alignment of membrane proteins for NMR structure determination, *Proc. Natl. Acad. Sci. USA*, 104, **2007**, 6644-6648

[84] J. Lorieau, L. Yao, A. Bax, Liquid crystalline phase of G-tetrad DNA for NMR study of detergent-solubilized proteins, *J. Am. Chem. Soc.*, 130, **2008**, 7536-7537

[85] K. Fleming, D. Gray, S. Matthews, Cellulose crystallites, *Chem. A Eur. J.*, 7, **2001**, 1831-1836

[86] K. Fleming, D. Gray, S. Prasannan, S. Matthews, Cellulose crystallites: a new and robust liquid crystalline medium for the measurement of residual dipolar couplings, *J. Am. Chem. Soc.*, 122, **2000**, 5224-5225

[87] X. M. Dong, D. G. Gray, Effect of counterions on ordered phase formation in suspensions of charged rodlike cellulose crystallites. *Langmuir*, 13, **1997**, 2404-2409

[88] F. Camerel, J. C. R. Gabriel, P. Batail, Magnetically induced large mesoporous single-domain monoliths using a mineral liquid crystal as a template, *Adv. Funct. Mater.*, 13, **2003**, 377-381

[89] H. Desvaux, J. C. P. Gabriel, P. Berthault, F. Camerel, First use of a mineral liquid crystal for measurement of residual dipolar couplings of a nonlabeled biomolecule, *Angew. Chem. Int. Ed.*, 40, **2001**, 373-376

[90] J. C. P. Gabriel, P. Davidson, Mineral liquid crystals from self-assembly of anisotropic nanosystems, *Top. Curr. Chem.*, 226, **2003**, 119-172

[91] C. M. Thiele, Use of RDCs in rigid organic compounds and some practical considerations concerning alignment media, *Conc. Magn. Reson. Part A*, 30A, **2007**, 65-80

[92] J. Yan, E. R. Zartler, Application of residual dipolar couplings in organic compounds, *Magn. Reson. Chem.*, 43, **2005**, 53-64

[93] C. M. Thiele, Simultaneous assignment of all diastereotopic protons in strychnine using RDCs: PELG as alignment medium for organic molecules, *J. Org. Chem.*, 69, **2004**, 7403-7413

[94] L. Verdier, P. Sakhaii, M. Zweckstetter, C. Griesinger, Measurement of long range H,C couplings in natural products in orienting media: a tool for structure elucidation of natural products, *J. Magn. Reson.*, 163, **2003**, 353-359

[95] C. M. Thiele, S. Berger, Probing the diastereotopicity of methylene protons in strychnine using residual dipolar couplings, *Org. Lett.*, 5, **2003**, 705-708

[96] M. Sarfati, P. Lesot, D. Merlet, J. Courtieu, Theoretical and experimental aspects of enantiomeric differentiation using natural abundance multinuclear nmr spectroscopy in chiral polypeptide liquid crystals, *Chem. Commun.*, **2000**, 2069-2081

[97] D. Merlet, A. Loewenstein, W. Smadja, J. Courtieu, P. Lesot, Quantitative description of the facial discrimination of molecules containing a prochiral group by NMR in a chiral liquid crystal, *J. Am. Chem. Soc.*, 120, **1998**, 963-969

[98] A. Meddour, P. Berdagué, A. Hedli, J. Courtieu, P. Lesot, Proton-decoupled carbon-13 NMR spectroscopy in a lyotropic chiral nematic solvent as an analytical tool for the measurement of the enantiomeric excess, *J. Am. Chem. Soc.*, 119, **1997**, 4502-4508

[99] P. Lesot, D. Merlet, J. Courtieu, J. Emsley, T. T. Rantala, J. Jokisaari, Calculation of the molecular ordering parameters of (±)-3-butyn-2-ol dissolved in an organic solution of poly(γ-benzyl-L-glutamate), *J. Phys. Chem. A*, 101, **1997**, 5719-5724

[100] P. Lesot, Y. Gounelle, D. Merlet, A. Loewenstein, J. Courtieu, Measurement and analysis of the molecular ordering tensors of two enantiomers oriented in a polypeptide liquid crystalline system, *J. Phys. Chem.*, 99, **1995**, 14871-14875; (correction), 100, **1995**, 14569

[101] I. Canet, J. Courtieu, A. Loewenstein, A. Meddour, J. M. Péchiné, Enantiomeric analysis in a polypeptide lyotropic liquid crystal by deuterium NMR, *J. Am. Chem. Soc.*, 117, **1995**, 6520-6526

[102] A. Meddour, I. Canet, A. Loewenstein, J. M. Péchiné, J. Courtieu, Observation of enantiomers, chiral by virtue of isotopic substitution, through deuterium NMR in a polypeptide liquid crystal, *J. Am. Chem. Soc.*, 116, **1994**, 9652-9656

[103] H. Toriumi, T. Yamazaki, A. Abe, E. T. Samulski, Deuterium N.M.R. studies of polypeptides I. Sidechain orientation in poly(γ-benzyl L-glutamate) and the mechanism of the cholesteric sense inversion, *Liq. Cryst.*, 1, **1986**, 87-96

[104] K. Czarniecka, E. T. Samulski, Polypeptide liquid crystals: a deuterium NMR study, *Mol. Cryst. Liq. Cryst.*, 63, **1981**, 205-214

[105] M. Panar, W. D. Phillips, Magnetic ordering of poly-γ-benzyl-L-glutamate solutions, *J. Am. Chem. Soc.*, 90, **1968**, 3880-3882

[106] E. T. Samulski, A. V. Tobolsky, Some unusual properties of poly(γ-benzyl L-glutamate) films cast in strong magnetic fields, *Macromolecules*, 1, **1968**, 555-557

[107] E. T. Samulski, Liquid crystalline order in polypeptides in *Liquid-Crystalline Order in Polymers*, A. Blumstein ed., Academic press, New York, **1978**, chap. 5, ISBN: 9780121086503

[108] J. C. Mitchell, A. E. Woodward, P. Doty, Polypeptides. XVI. The polydispersity and configuration of low molecular weight poly-γ-benzyl-L-glutamates, *J. Am. Chem. Soc.*, 79, **1957**, 3955-3960

[109] P. Doty, J. H. Bradbury, A. M. Holtzer, Polypeptides. IV. The molecular weight, configuration and association of poly-γ-benzyl-L-glutamate in various solvents, *J. Am. Chem. Soc.*, 78, **1956**, 947-954

[110] A. Solgadi, L. Jean, M.-C. Lasne, J. Rouden, J. Courtieu, A. Meddour, NMR in chiral polypeptide liquid crystals: the problem of amines, *Tetrahedron: Asymmetry*, 18, **2007**, 1511-1516

[111] O. Lafon, P. Lesot, M. Rivard, M. Chavarot, F. Rose-Munch, E. Rose, Enantiomeric analysis of planar chiral (η^6-arene)chromium tricarbonyl complexes using NMR in oriented solvents, *Organometallics*, 24, **2005**, 4021-4028

[112] M. Rivard, F. Guillen, J.-C. Fiaud, C. Aroulanda, P. Lesot, Efficient enantiodiscrimination of chiral monophosphine oxides and boranes by phosphorus coupled ^{13}C NMR spectroscopy in the presence of chiral ordering agents, *Tetrahedron: Asymmetry*, 14, **2003**, 1141-1152

[113] C. Aroulanda, V. Boucard, F. Guibé, J. Courtieu, D. Merlet, Weakly oriented liquid-crystal NMR solvents as a general tool to determine relative configurations, *Chem. Eur. J.*, 9, **2003**, 4536-4539

[114] P. Lesot, M. Sarfati, J. Courtieu, Natural abundance deuterium NMR spectroscopy in polypeptide liquid crystals as a new and incisive means for the enantiodifferentiation of chiral hydrocarbons, *Chem. Eur. J.*, 9, **2003**, 1724-1745

[115] C. Aroulanda, P. Lesot, D. Merlet, J. Courtieu, Structural ambiguities revisited in two bridged ring systems exhibiting enantiotopic elements, using natural abundance deuterium NMR in chiral liquid crystals, *J. Phys. Chem. A*, 107, **2003**, 10911-10918

[116] C. Aroulanda, M. Sarfarti, J. Courtieu, P. Lesot, Investigation of the enantioselectivity of three polypeptide liquid-crystalline solvents using NMR spectroscopy, *Enantiomer*, 6, **2001**, 281-287

[117] C. Aroulanda, D. Merlet, J. Courtieu, P. Lesot, NMR experimental evidence of the differentiation of enantiotopic directions in C_s and C_{2V} molecules using partially oriented, chiral media, *J. Am. Chem. Soc.*, 123, **2001**, 12059-12066

[118] M. Sarfati, C. Aroulanda, J. Courtieu, P. Lesot, Enantiomeric recognition of chiral invertomers through NMR in chiral oriented phases: a study of *cis*-decalin, *Tetrahedron: Asymmetry*, 12, **2001**, 737-744

[119] P. Lesot, A. Meddour, J. Courtieu, A. Loewenstein, Visualization of enantiomers in a polypeptide liquid-crystal solvent through carbon-13 NMR spectroscopy, *J. Chem. Soc. Faraday Trans.*, 91, **1995**, 1371-1375

[120] J.-L. Canet, A. Fadel, J. Salaun, I. Canet-Fresse, J. Courtieu, Enantiomeric excess analysis of sesquiterpene precursors through proton decoupled deuterium NMR in cholesteric lyotropic liquid crystal, *Tetrahedron: Asymmetry*, 4, **1993**, 31-34

[121] C. Canlet, D. Merlet, P. Lesot, A. Meddour, A. Loewenstein, J. Courtieu, Deuterium NMR stereochemical analysis of *threo-erythro* isomers bearing remote stereogenic centres in racemic and non-racemic liquid crystalline solvents, *Tetrahedron: Asymmetry*, 11, **2000**, 1911-1918

[122] W. Smadja, S. Auffret, P. Berdagué, D. Merlet, C. Canlet, J. Courtieu, J.-Y. Legros, A. Boutros, J.-C. Fiaud, Visualisation of axial chirality using ^{2}H-{^{1}H} NMR in poly(γ-benzyl-L-glutamate), a chiral liquid crystal solvent, *Chem. Commun.*, **1997**, 2031-2032

[123] P. Lesot, O. Lafon, H. B. Kagan, C.-A. Fan, Study of molecular rotational isomerism using deuterium NMR in chiral oriented solvents, *Chem. Commun.*, **2006**, 389-391

[124] R. Berger, J. Courtieu, R. R. Gil, C. Griesinger, Matthias Köck, P. Lesot, B. Luy, D. Merlet, A. Navarro-Vázquez, M. Reggelin, U. M. Reinscheid, C. M. Thiele, M. Zweckstetter, Is enantiomer assignment possible by NMR spectroscopy using residual dipolar couplings from chiral nonracemic alignment media? - A critical assessment, *Angew. Chem. Int. Ed.*, 51, **2012**, 8388-8391

[125] L. Ziani, P. Lesot, A. Meddour, J. Courtieu, Empirical determination of the absolute configuration of small chiral molecules using natural abundance ^{2}H NMR in chiral liquid crystals, *Chem. Commun.*, **2007**, 4737-4739

[126] C. M. Thiele, Scaling the alignment of small organic molecules in substituted polyglutamates by variable-angle sample spinning, *Angew. Chem. Int. Ed.*, 44, **2005**, 2787-2790

[127] J. Courtieu, J. P. Bayle, B. M. Fung, Variable angle sample spinning NMR in liquid crystals, *Prog. Nucl. Magn. Reson. Spectrosc.*, 26, **1994**, 141-169

[128] J. Courtieu, D. W. Alderman, D. M. Grant, Spinning near the magic angle: a means of obtaining first-order dipolar NMR spectra of molecules dissolved in nematic liquid crystals, *J. Am. Chem. Soc.*, 103, **1981**, 6783-6784

[129] M. M. Green, J. W. Park, T. Sato, A. Teramoto, S. Lifson, R. L. B. Selinger, J. V. Selinger, The macromolecular route to chiral amplification, *Angew. Chem. Int. Ed.*, 38, **1999**, 3138-3154

[130] T. Sato, J. Nakamura, A. Teramoto, M. M. Green, Cholesteric pitch of lyotropic polymer liquid crystals, *Macromolecules*, 31, **1998**, 1398-1405

[131] T. Sato, Y. Sato, Y. Umemura, A. Teramoto, Y. Nagamura, J. Wagner, D. Weng, Y. Okamoto, K. Hatada, M. M. Green, Polyisocyanates and the interplay of experiment and theory in the formation of lyotropic cholesteric states, *Macromolecules*, 26, **1993**, 4551-4559

[132] M. Dama, S. Berger, Polyacetylenes as a new alignment medium to measure residual dipolar couplings for chiral organic molecules, *Tetrahedron Lett.*, 53, **2012**, 6439-6442

[133] K. Maeda, E. Yashima, Dynamic helical structures: detection and amplification of chirality, *Top. Curr. Chem.*, 265, **2006**, 47-88

[134] K. Okoshi, K. Sakajiri, J. Kumaki, E. Yashima, Well-defined lyotropic liquid crystalline properties of rigid-rod helical polyacetylenes, *Macromolecules*, 38, **2005**, 4061-4064

[135] M. Dama, S. Berger, Polyisocyanides as a new alignment medium to measure residual dipolar couplings for small organic molecules, *Org. Lett.*, 14, **2012**, 241-243

[136] G. A. Metselaar, S. J. Wezenberg, J. J. L. M. Cornelissen, R. J. M. Nolte, A. E. Rowan, Lyotropic liquid-crystalline behavior of polyisocyanodipeptides, *J. Polym. Sci., Part A: Polym. Chem.*, 45, **2007**, 981-988

[137] T. Kajitani, K. Okoshi, S.-I. Sakurai, J. Kumaki, E. Yashima, Helix-sense controlled polymerization of a single phenyl isocyanide enantiomer leading to diastereomeric helical polyisocyanides with opposite helix-sense and cholesteric liquid crystals with opposite twist-sense, *J. Am. Chem. Soc.*, 128, **2006**, 708-709

[138] L. Arnold, A. Marx, C. M. Thiele, M. Reggelin, Polyguanidines as chiral orienting media for organic compounds, *Chem. Eur. J.*, 16, **2010**, 10342-10346

[139] J. Kim, B. M. Novak, A. J. Waddon, Lyotropic liquid crystalline properties of poly(*N,N′*-di-*n*-hexylguanidine), *Macromolecules*, 37, **2004**, 1660-1662

[140] J. Kim, B. M. Novak, A. J. Waddon, Liquid crystalline properties of polyguanidines, *Macromolecules*, 37, **2004**, 8286-8292

[141] B. Deloche, E. T. Samulski, Short-range nematic-like orientational order in strained elastomers: a deuterium magnetic resonance study, *Macromolecules*, 14, **1981**, 575-581

[142] B. Luy, K. Kobzar, H. Kessler, An easy and scalable method for the partial alignment of organic molecules for measuring residual dipolar couplings, *Angew. Chem. Int. Ed.*, 43, **2004**, 1092-1094

[143] R. Tycko, F. J. Blanco, Y. Ishii, Alignment of biopolymers in strained gels: a new way to create detectable dipole-dipole couplings in high-resolution biomolecular NMR, *J. Am. Chem. Soc.*, 122, **2000**, 9340-9341

[144] J. J. Chou, S. Gaemers, B. Howder, J. M. Louis, A. Bax, A simple apparatus for generating stretched polyacrylamide gels, yielding uniform alignment of proteins and detergent micelles, *J. Biomol. NMR*, 21, **2001**, 377-382

[145] Y. Ishii, M. A. Markus, R. Tycko, Controlling residual dipolar couplings in high resolution NMR of proteins by strain induced alignment in a gel, *J. Biomol. NMR*, 21, **2001**, 141-151

[146] H.-J. Sass, G. Musco, S. J. Stahl, P. T. Wingfield, S. Grzesiek, Solution NMR of proteins within polyacrylamide gels: diffusional properties and residual alignment by mechanical stress or embedding of oriented purple membranes, *J. Biomol. NMR*, 18, **2000**, 303-309

[147] T. Cierpicki, J. H. Bushweller, Charged gels as orienting media for measurement of residual dipolar couplings in soluble and integral membrane proteins, *J. Am. Chem. Soc.*, 126, **2004**, 16259-16266

[148] T. S. Ulmer, B. E. Ramirez, F. Delaglio, A. Bax, Evaluation of backbone proton positions and dynamics in a small protein by liquid crystal NMR spectroscopy, *J. Am. Chem. Soc.*, 125, **2003**, 9179-9191

[149] S. Meier, D. Haussinger, S. Grzesiek, Charged acrylamide copolymer gels as media for weak alignment, *J. Biomol. NMR*, 24, **2002**, 351-356

[150] G. Kummerlöwe, M. Udaya Kiran, B. Luy, Covalently cross-linked gelatin allows chiral distinction at elevated temperatures and in DMSO, *Chem. Eur. J.*, 15, **2009**, 12192-12195

[151] C. Naumann, P. W. Kuchel, Prochiral and chiral resolution in ^{2}H NMR Spectra: solutes in stretched and compressed gelatin gels, *J. Phys. Chem. A*, 112, **2008**, 8659-8664

[152] C. Naumann, W. A. Bubb, B. E. Chapman, P. W. Kuchel, Tunable-alignment chiral system based on gelatin for NMR spectroscopy, *J. Am. Chem. Soc.*, 129, **2007**, 5340-5341

[153] K. Kobzar, H. Kessler, B. Luy, Stretched gelatin gels as chiral alignment media for the discrimination of enantiomers by NMR spectroscopy, *Angew. Chem. Int. Ed.*, 44, **2005**, 3145-3147

[154] J. Ma, G. I. Goldberg, N. Tjandra, Weak alignment of biomacromolecules in collagen gels: an alternative way to yield residual dipolar couplings for NMR measurements, *J. Am. Chem. Soc.*, 130, **2008**, 16148-16149

[155] U. Eliav, G. Navon, Collagen fibers as a chiral agent: a demonstration of stereochemistry effects, *J. Am. Chem. Soc.*, 128, **2006**, 15956-15957

[156] J. C. Freudenberger, S. Knör, K. Kobzar, D. Heckmann, T. Paululat, H. Kessler, B. Luy, Stretched poly(vinyl acetate) gels as NMR alignment media for the measurement of residual dipolar couplings in polar organic solvents, *Angew. Chem. Int. Ed.*, 44, **2005**, 423-426

[157] B. Luy, K. Kobzar, S. Knör, J. Furrer, D. Heckmann, H. Kessler, Orientational properties of stretched polystyrene gels in organic solvents and the suppression of their residual ^{1}H NMR signals, *J. Am. Chem. Soc.*, 127, **2005**, 6459-6465

[158] J. C. Freudenberger, P. Spiteller, R. Bauer, H. Kessler, B. Luy, Stretched poly (dimethylsiloxane) gels as NMR alignment media for apolar and weakly polar organic solvents: an ideal tool for measuring RDCs at low molecular concentrations, *J. Am. Chem. Soc.*, 126, **2004**, 14690-14691

[159] R. R. Gil, C. Gayathri, N. V. Tsarevsky, K. Matyjaszewski, Stretched poly(methyl methacrylate) gel aligns small organic molecules in chloroform. Stereochemical analysis and diastereotopic proton NMR assignment in ludartin using residual dipolar couplings and ^{3}J coupling constant analysis, *J. Org. Chem.*, 73, **2008**, 840-848

[160] G. Kummerlöwe, J. Auernheimer, A. Lendlein, B. Luy, Stretched poly(acrylonitrile) as a scalable alignment medium for DMSO, *J. Am. Chem. Soc.*, 129, **2007**, 6080-6081

[161] P. Haberz, J. Farjon, C. Griesinger, A DMSO-compatible orienting medium: towards the investigation of the stereochemistry of natural products, *Angew. Chem., Int. Ed.*, 44, **2005**, 427-429

[162] P. Kaden, J. C. Freudenberger, B. Luy, Noncovalently and covalently cross-linked polyurethane gels as alignment media and the suppression of residual polymer signals using diffusion- filtered spectroscopy, *Magn. Reson. Chem.*, 50, **2012**, S22-S28

[163] C. Merle, G. Kummerlöwe, J. C. Freudenberger, F. Halbach, W. Stöwer, C. L. v. Gostomski, J. Höpfner, T. Beskers, M. Wilhelm, B. Luy, Crosslinked poly(ethyleneoxide) as a versatile alignment medium for the measurement of residual anisotropic NMR parameters, *Angew. Chem. Int. Ed.*, 52, **2013**, 10309-10312

[164] G. Kummerlöwe, F. Halbach, B. Laufer, B. Luy, Precise measurement of RDCs in water and DMSO based gels using a silicone rubber tube for tunable stretching, *The Open Spectrosc. J.*, 2, **2008**, 29-33

[165] P. W. Kuchel, B. E. Chapman, N. Müller, W. A. Bubb, D. J. Philp, A. M. Torres, Apparatus for rapid adjustment of the degree of alignment of NMR samples in aqueous media: verification with residual quadrupolar splittings in ^{23}Na and ^{133}Cs spectra, *J. Magn. Reson.*, 180, **2006**, 256-265

[166] G. Kummerlöwe, E. F. McCord, Steve F. Cheatham, S. Niss, R. W. Schnell, B. Luy, Tunable alignment for all polymer gel/solvent combinations for the measurement of anisotropic NMR parameters, *Chem. Eur. J.*, 16, **2010**, 7087-7089

[167] S. S. D. Büchler, G. Kummerlöwe, B. Luy, Naturally occurring biodegradable polymers as the basis of chiral gels for the distinction of enantiomers by partially oriented NMR spectroscopy, *Int. J. Artif. Organs*, 34, **2011**, 134-138

[168] G. Kummerlöwe, B. Luy, Residual dipolar couplings as a tool in determining the structure of organic molecules, *Trends Anal. Chem.*, 28, **2009**, 483-493

[169] J. W. Emsley, NMR methods of studying orientational order in the liquid crystalline and isotropic phases of mesogenic samples, *Liq. Cryst.*, 32, **2005**, 1515-1524

[170] C. A. de Lange, E. E. Burnell, Basics of NMR of molecules in uniaxial anisotropic environment, in *NMR of Ordered Liquids*, E. E. Burnell and C. A. de Lange eds., Kluwer Academic, Dordrecht, **2003**, chap. 1, ISBN: 1402013434

[171] J. Jokisaari, Anisotropy of shielding and coupling in liquid crystalline solutions, in *Encyclopedia of Magnetic Resonance,* John Wiley & Sons, Ltd., **2011**

[172] A. Bax, J. J. Chou, B. E. Ramirez, Liquid crystalline samples: application to macromolecular structure determination, in *Encyclopedia of Magnetic Resonance*, John Wiley & Sons, Ltd., **2007**

[173] M. Hird, Ferroelectricity in liquid crystals-materials, properties and applications, *Liq. Cryst.*, 38, **2011**, 1467-1493

[174] S. T. Lagerwall, *Ferroelectric and Antiferroelectric Liquid Crystals*, Wiley-VCH, New York, **1999**, ISBN: 9783527613588

[175] J. W. Goodby, R. Blinc, N. A. Clark, S. T. Lagerwall, M. A. Osipov, S. A. Pikin, T. Sakurai, K. Yoshino, B. Zeks, *Ferroelectric Liquid Crystals, Principle, Properties and Applications*, Gordon and Breach Science Publishers, London, **1991**, ISBN: 9782881242823

[176] H. Takezoe, Y. Takanishi, Bent-core liquid crystals: their mysterious and attractive world, *Jpn. J. Appl. Phys.*, 45, **2006**, 597-625

[177] B. R. Kaafarani, Discotic liquid crystals for opto-electronic applications, *Chem. Mater.*, 23, **2011**, 378-396

[178] I. W. Hamley, Liquid crystal phase formation by biopolymers, *Soft Matter*, 6, **2010**, 1863-1871

[179] A. D. Rey, Liquid crystal models of biological materials and processes, *Soft Matter*, 6, **2010**, 3402-3429

[180] P. V. Patel, J. B. Patel, R. D. Dangar, K. S. Patel, K. N. Chauhan, Liquid crystal drug delivery system, *Int. J. Pharm. Appl. Sci.*, 1, **2010**, 118-123

[181] C. Guo, J. Wang, F. Cao, R. J. Lee, G. Zhai, Lyotropic liquid crystal systems in drug delivery, *Drug Discovery Today*, 15, **2010**, 23-24

[182] B. M. Fung, Liquid crystalline samples: carbon-13 NMR, in *Encyclopedia of Magnetic Resonance*, John Wiley & Sons, Ltd., **2007**

[183] R. Y. Dong, Liquid crystalline samples: deuterium NMR, in *Encyclopedia of Magnetic Resonance*, John Wiley & Sons, Ltd., **2007**

[184] J. W. Emsley, P. Lesot, G. De Luca, A. Lesage, D. Merlet, G. Pileio, The conformation and orientational order of a 1,2-disubstituted ethane nematogenic molecule (I22) in liquid crystalline and isotropic phases studied by NMR spectroscopy, *Phys. Chem. Chem. Phys.*, 12, **2010**, 2895-2914

[185] J. W. Emsley, P. Lesot, G. De Luca, A. Lesage, D. Merlet, G. Pileio, A comparison of proton-detected ^{13}C local field experiments with deuterium NMR at natural abundance for studying liquid crystals, *Liq. Cryst.*, 35, **2008**, 443-464

[186] A. Marini, V. Domenici, ^{2}H, ^{13}C NMR and a*b initio* calculations applied to the SmC* phase: methodology and case studies, *Ferroelectrics*, 395, **2010**, 46-59

[187] M. Cifelli, V. Domenici, A. Marini, C. A. Veracini, NMR studies of the ferroelectric SmC* phase, *Liq. Cryst*. 37, **2010**, 935-948

[188] V. Domenici, Order and dynamics of rod-like and banana-shaped liquid crystals by ^{2}H NMR, *Pure Appl. Chem.*, 79, **2007**, 21-37

[189] T. J. Dingemans, L. A. Madsen, N. A. Zafiropoulos, W. B. Lin, E. T. Samulski, Uniaxial and biaxial nematic liquid crystals, *Philos. Trans. R. Soc. A*, 364, **2006**, 2681-2696

[190] G. R. Luckhurst, V-shaped molecules: new contenders for the biaxial nematic phase, *Angew. Chem. Int. Ed.*, 44, **2005**, 2834-2836

[191] S. V. Dvinskikh, D. Sandström, H. Zimmermann, A. Maliniak, Carbon-13 NMR spectroscopy applied to columnar liquid crystals, *Prog. Nucl. Magn. Reson. Spectrosc.*, 48, **2006**, 85-107

[192] S. V. Dvinskikh, H. Zimmermann, A. Maliniak, D. Sandström, Separated local field spectroscopy of columnar and nematic liquid crystals, *J. Magn. Reson.*, 163, **2003**, 46-55

[193] S. Kundu, G. Feio, L. F. V. Pinto, P. L. Almeida, J. L. Figueirinhas, M. H. Godinho, Deuterium NMR study of orientational order in cellulosic network microfibers, *Macromolecules*, 43, **2010**, 5749-5755

[194] V. Domenici, G. Ambrožič, M. Čopič, A. Lebar, I. Drevenšek-Olenik, P. Umek, B. Zalar, B. Zupančič, M. Žigon, Interplay between nematic ordering and thermomechanical response in a side-chain liquid single crystal elastomer containing pendant azomesogen units, *Polymer*, 50, **2009**, 4837-4844

[195] R. Storz, A. Komp, A. Hoffmann, H. Finkelmann, Phase biaxiality in smectic-A side-chain liquid crystalline elastomers, *Macromol. Rapid Commun.*, 30, **2009**, 615-621

[196] L. Shi, X. D. Wu, L. D. Lu, X. J. Yang, X. Wang, Molecular mechanism for formation of polyaniline lamella from a lyotropic liquid crystal: an NMR study, *J. Phys. Chem. B*, 113, **2009**, 2725-2733

[197] J. Schiller, M. Muller, B. Fuchs, K. Baete, A. Klaus, D. Huster, ^{31}P NMR spectroscopy of phospholipids: from micelles to membranes, *Curr. Anal. Chem.*, 3, **2007**, 283-301

[198] J. H. Ma, C. Guo, Y. L. Tang, H. Z. Liu, ^{1}H NMR spectroscopic investigations on the micellization and gelation of PEO–PPO–PEO block copolymers in aqueous solutions, *Langmuir*, 23, **2007**, 9596-9605

[199] D. Capitani, A. Yethiraj, E. E. Burnell, Memory effects across surfactant mesophases, *Langmuir*, 23, **2007**, 3036-3048

[200] R. Y. Dong, ^{14}N spin relaxation study in the hexagonal phase of a lyotropic liquid crystal, *Mol. Phys.*, 99, **2001**, 637-641

[201] M. Cifelli, Translational self-diffusion measurements in thermotropics by means of static field gradients NMR diffusometry, in *Nuclear Magnetic Resonance Spectroscopy of Liquid Crystals*, R. Y. Dong ed., World Scientific, Singapore, **2009**, chap. 9, ISBN: 9789814273664

[202] V. Domenici, C. A. Veracini, Dynamics of liquid crystals by means of deuterium NMR relaxation, in *Nuclear Magnetic Resonance Spectroscopy of Liquid Crystals*, R. Y. Dong ed., World Scientific, Singapore, **2009**, chap. 8, ISBN: 9789814273664

[203] P. J. Sebastiao, C. Cruz, A. C. Ribeiro, Advances in proton NMR relaxometry in thermotropic liquid crystals, in *Nuclear Magnetic Resonance Spectroscocpy of Liquid Crystals*, R. Y. Dong ed., World Scientific, Singapore, **2009**, chap. 5, ISBN: 9789814273664

[204] V. Domenici, Quantitative analysis of ^{2}H NMR T_{1Q}, T_{1Z} and T_2 relaxation times in the SmA phase of a liquid crystal dendrimer, *Phys. Chem. Chem. Phys.*, 11, **2009**, 8496-8506

[205] V. Domenici, M. Geppi, C. A. Veracini, R. Y. Dong., Molecular dynamics of a ferroelectric smectogen in its smectic phases by means of ^{2}H NMR spectroscopy, *Liq. Cryst.*, 33, **2006**, 479-484

[206] V. Domenici, M. Geppi, C. A. Veracini, A. V. Zakharov, Molecular dynamics in the smectic A and C* phases in a long-chain ferroelectric liquid crystal: ^{2}H NMR, dielectric properties, and a theoretical treatment, *J. Phys. Chem. B*, 109, **2005**, 18369-18377

[207] T. Apih, V. Domenici, A. Gradisek, V. Hamplova, M. Kaspar, P. J. Sebastiao, M. Vilfan, ^{1}H NMR relaxometry study of a rod-like chiral liquid crystal in its isotropic, cholesteric, TGBA*, and TGBC* phases, *J. Phys. Chem. B*, 114, **2010**, 11993-12001

[208] A. E. Frise, T. Ichikawa, M. Yoshio, H. Ohno, S. V. Dvinskikh, T. Kato, I. Furó, Ion conductive behaviour in a confined nanostructure: NMR observation of self-diffusion in a liquid-crystalline bicontinuous cubic phase, *Chem. Commun.*, 46, **2010**, 728-730

[209] R. Y. Dong, NMR study of diffusive processes in novel liquid crystalline phases, *Thin Solid Films*, 517, **2008**, 1367-1379

[210] A. Vogel, K. T. Tan, H. Waldmann, S. E. Feller, M. F. Brown, D. Huster, Flexibility of ras lipid modifications studied by ^{2}H solid-state NMR and molecular dynamics simulations, *Biophys. J.*, 93, **2007**, 2697-2712

[211] D. Frezzato, G. J. Moro, M. Tittelbach, G. Kothe, Transverse nuclear spin relaxation induced by director fluctuations in a nematic liquid crystal polymer. Evaluation of the anisotropic elastic constants, *J. Chem. Phys.*, 119, **2003**, 4060-4069

[212] M. F. Brown, R. L. Thurmond, S. W. Dodd, D. Otten, K. Beyer, Elastic deformation of membrane bilayers probed by deuterium NMR relaxation, *J. Am. Chem. Soc.*, 124, **2002**, 8471-8484

[213] A. Van-Quynh, P. J. Sebastião, D. A. Wilson, G. H. Mehl, Detecting columnar deformations in a supermesogenic octapode by proton NMR relaxometry, *Eur. Phys. J. E*, 31, **2010**, 275-283

[214] A. Carvalho, P. J. Sebastião, A. C. Ribeiro, H. T. Nguyen, M. Vilfan, Molecular dynamics in tilted bilayer smectic phases: a proton nuclear magnetic resonance relaxometry study, *J. Chem. Phys.*, 115, **2001**, 10484-10492

[215] C. L. Khetrapal, G. A. Nagana Gowda, NMR of partially ordered solutes with emphasis on structure determination, in *NMR of Ordered Liquids*, E. E. Burnell and C. A. de Lange eds., Kluwer Academic, Dordrecht **2003**, chap. 7, ISBN: 1402013434

[216] J. W. Emsley, Liquid crystalline samples: structure of nonrigid molecules, in *Encyclopedia of Magnetic Resonance*, John Wiley & Sons, Ltd, **2007**

[217] G. Celebre, M. Longeri, NMR studies of solutes in liquid crystals: small flexible molecules, in *NMR of Ordered Liquids*, E. E. Burnell and C. A. de Lange eds., Kluwer Academic, Dordrecht, **2003**, chap. 14, ISBN: 1402013434

[218] C. A. Veracini, M. Longeri, Studies of solutes with internal rotors, in *Nuclear Magnetic Resonance of Liquid Crystals*, J. W. Emsley ed., Reidel, Dordrecht, **1985**, chap. 6, ISBN: 9027718784

[219] C. M. Thiele, Residual dipolar couplings (RDCs) in organic structure determination, *Eur. J. Org. Chem.* **2008**, 5673-5685

[220] A. Bax, N. Tjandra, High-resolution heteronuclear NMR of human ubiquitin in an aqueous liquid crystalline medium, *J. Biomol. NMR*, 10, **1997**, 289-292

[221] C. P. Slitcher, *Principles of Magnetic Resonance: with examples from solid state physics*, Harper & Row, New York, **1963**

[222] A. Abragam, *Principles of Nuclear Magnetism*, Oxford University Press, London, **1961**

[223] M. H. Levitt, Nuclear spin Hamiltonian, in *Spin Dynamics. Basics of Nuclear Magnetic Resonance*, John Wiley & Sons Ltd., Chichester, **2001**, chap. 7, ISBN: 0471489220

[224] M. E. Rose, *Elementary Theory of Angular Momentum*, Dover Publication, Inc., New York, **1995**, ISBN: 9780486684802

[225] J. W. Emsley, Liquid crystals: general considerations, in *Encyclopedia of Magnetic Resonance*, John Wiley & Sons, Ltd, **2007**

[226] J. Lounila, J. Jokisaari, Anisotropies in spin-spin coupling constants and chemical shifts as determined from the NMR spectra of molecules oriented by liquid crystal solvents, *Prog. Nucl. Magn. Reson. Spectrosc.*, 15, **1982**, 249-290

[227] J. W. Emsley, J. C. Lindon, Anisotropy in chemical shift, in *NMR Spectroscopy Using Liquid Crystal Solvents*, Pergamon Press, Oxford, **1975**, chap. 8, ISBN: 0080199194

[228] J. Vaara, J. Jokisaari, R. E. Wasylishen, D. L. Bryce, Spin-spin coupling tensors as determined by experiment and computational chemistry, *Prog. Nucl. Magn. Reson. Spectrosc.*, 41, **2002**, 233-304

[229] J. W. Emsley, J. C. Lindon, Anisotropy in nuclear spin-spin coupling, in *NMR Spectroscopy Using Liquid Crystal Solvents*, Pergamon Press, Oxford, **1975**, chap. 7, ISBN: 0080199194

[230] G. De Luca, M. Longeri, G. Pileio, P. Lantto, NMR spectroscopy investigation of the cooperative nature of the internal rotational motions in acetophenone, *Chem. Phys. Chem.*, 6, **2005**, 2086-2098

[231] J. Kaski, P. Lantto, J. Vaara, J. Jokisaari, Experimental and theoretical *ab Initio* study of the ^{13}C-^{13}C spin-spin coupling and ^{1}H and ^{13}C shielding tensors in ethane, ethene, and ethyne, *J. Am. Chem. Soc.*, 120, **1998**, 3993-4005

[232] J. Kaski, J. Vaara, J. Jokisaari, ^{13}C–^{13}C spin–spin coupling tensors in benzene as determined experimentally by liquid crystal NMR and theoretically by *ab initio* calculations, *J. Am. Chem. Soc.*, 118, **1996**, 8879-8886

[233] J. Lounila, M. Ala-Korpela, J. Jokisaari, A special method for analyzing anisotropic nuclear magnetic resonance parameters: acetonitrile in liquid crystals, *J. Chem. Phys.*, 93, **1990**, 8514-8523

[234] P. Diehl, J. Jokisaari, J. Amrein, T. Väänänen, P. Pyykkö, Determination of the ^{13}C-^{13}C and ^{13}C-^{15}N coupling constant anisotropies of acetonitrile partially oriented by nematic liquid crystals, *J. Magn. Reson.*, 48, **1982**, 495-502

[235] Y. Hiltunen, J. Jokisaari, J. Lounila, A. Pulkkinen, Anisotropy of the proton and carbon-13 chemical shifts and of the carbon-13-nitrogen-14 spin-spin couplings of methyl isocyanide as determined by NMR in nematic mesogens, *J. Am. Chem. Soc.*, 111, **1989**, 3217-3220

[236] J. W. Emsley, G. De Luca, A. Lesage, M. Longeri, F. B. Mallory, C. W. Mallory, The indirect through-space F-F coupling in peri-difluoronaphthalene: is it anisotropic?, *Phys. Chem. Chem. Phys.*, 10, **2008**, 6534-6543

[237] E. M. Brown, P. D. McCaffrey, D. A. Wann, D. W. H. Rankin, Accurate structures from combined gas electron diffraction and liquid crystal NMR data; the importance of anisotropy of indirect couplings for 1,4-difluorobenzene, *Phys. Chem. Chem. Phys.*, 10, **2008**, 738-742

[238] P. Lantto, J. Kaski, J. Vaara, J. Jokisaari, Spin-spin coupling tensors in fluoromethanes, *Chem. Eur. J.*, 6, **2000**, 1395-1406

[239] J. Vaara, J. Kaski, J. Jokisaari, Indirect fluorine coupling anisotropies in *p*-difluorobenzene: implications to orientation and structure determination of fluorinated liquid crystals, *J. Phys. Chem. A*, 103, **1999**, 5675-5684

[240] J. Jokisaari, Y. Hiltunen, J. Lounila, Methyl fluoride–[13]C in nematic liquid crystals: anisotropy of the indirect [13]C–[19]F spin–spin coupling and of the ^{1}H, ^{13}C, and ^{19}F chemical shielding, *J. Chem. Phys.*, 85, **1986**, 3198-3202

[241] A. Pulkkinen, J. Jokisaari, T. Väänänen, ^{1}H and ^{19}F NMR study with carbon-13 satellites of *para*-difluorobezene in various nematic liquid crystals: structure and *J*-coupling anisotropy, *J. Mol. Struct.*, 144, **1986**, 359-369

[242] E. E. Burnell, C. A. de Lange, ^{1}H and ^{2}H NMR of methanes partially oriented in liquid-crystal phases: separation of rigid and nonrigid molecule effects, *J. Chem*. *Phys*., 76, **1982**, 3474-3479

[243] J. G. Snijders, C. A. de Lange, E. E. Burnell, Vibration-rotation coupling in anisotropic environments: NMR of methanes in liquid crystals, *J. Chem*. *Phys*., 77, **1982**, 5386-5396

[244] R. Ader, A. Loewenstein, Proton and deuteron magnetic resonance of methanes, silanes and GeH$_3$D dissolved in nematic liquid crystals, *Mol. Phys.*, 30, **1975**, 199-208

[245] R. Ader, A. Loewenstein, Nuclear magnetic resonance spectra of deuterated methanes and 2,2-dimethylpropane in nematic liquid crystals, *Mol. Phys.*, 24, **1972**, 455-457

[246] L. C. Snyder, S. Meiboom, NMR of tetrahedral molecules in a nematic solvent, *J. Chem. Phys.*, 44, **1966**, 4057-4058

[247] V. Domenici, The role of NMR in the study of partially ordered materials: perspectives and challenges, *Pure Appl Chem.*, 83, **2011**, 67-94

[248] P. Lesot, J. Courtieu, Natural abundance deuterium NMR spectroscopy: developments and analytical applications in liquids, liquid crystals and solid phases, *Prog. Nucl. Magn. Reson. Spectrosc.*, 55, **2009**, 128-159

[249] Y. W. Kim, W. L. Earl, R. E. Norberg, Cryogenic probe with low-loss transmission line for nuclear magnetic resonance, *J. Magn. Reson.*, 116, **1995**, 139-144

[250] J. W. Emsley, P. Lesot, D. Merlet, The orientational order and conformational distributions of the two enantiomers in a racemic mixture of a chiral, flexible molecule dissolved in a chiral nematic liquid crystalline solvent, *Phys. Chem. Chem. Phys.*, 6, **2004**, 522-530

[251] G. Celebre, G. De Luca, M. Longeri, Exploiting the information content of dipolar couplings: determination of the temperature dependence of the inter-ring twist angle of biphenyl dissolved in uniaxial mesophases, *Liq. Cryst.*, 37, **2010**, 923-933

[252] J. W. Emsley, G. R. Luckhurst, The effect of internal motion on the orientational order parameters for liquid crystalline systems, *Mol. Phys.*, 41, **1980**, 19-29

[253] J. W. Emsley, G. R. Luckhurst, C. P. Stockley, A theory of orientational ordering in uniaxial liquid crystals composed of molecules with alkyl chains, *Proc. R. Soc. Lond. A*, 381, **1982**, 117-138

[254] G. Celebre, G. De Luca, J. W. Emsley, M. Longeri, D. Merlet, G. Pileio, N. Suryaprakash, Obtaining the structure and bond rotational potential of a substituted ethane by NMR spectroscopy of solutions in nematic liquid-crystalline solvents, *J. Chem. Phys.*, 123, **2005**, 194907.1-9

[255] G. Celebre, M. Concistré, G. De Luca, M. Longeri, G. Pileio, J. W. Emsley, The structure of acrolein in a liquid crystal phase, *Chem. Eur. J.*, 11, **2005**, 3599-3608

[256] G. Celebre, G. De Luca, M. Longeri, G. Pileio, J. W. Emsley, Is styrene planar in liquid phases?, *J. Chem. Phys.*, 120, **2004**, 7075-7084

[257] G. Celebre, G. De Luca, J. W. Emsley, E. K. Foord, M. Longeri, F. Lucchesini, G. Pileio, The conformational distribution in diphenylmethane determined by nuclear magnetic resonance spectroscopy of a sample dissolved in a nematic liquid crystalline solvent, *J. Chem. Phys.*, 118, **2003**, 6417-6426

[258] C. Aroulanda, G. Celebre, G. De Luca, M. Longeri, Molecular ordering and structure of quasi-spherical solutes by liquid crystal NMR and Monte Carlo simulations: the case of norbornadiene, *J. Phys. Chem. B*, 110, **2006**, 10485-10496

[259] P. Diehl, Molecular structure from dipolar coupling, in *Nuclear Magnetic Resonance of Liquid Crystals*, J. W. Emsley ed., Reidel, Dordrecht, **1985**, chap. 7, ISBN: 9027718784

[260] P. J. Flory, *Statistical Mechanics of Chain Molecules*, Interscience Publishers, New York, **1969**

[261] S. W. Sinton, D. B. Zax, J. B. Murdoch, A. Pines, Multiple-quantum N.M.R. study of molecular structure and ordering in a liquid crystal, *Mol. Phys.*, 53, **1984**, 333-362

[262] L. Di Bari, C. Forte, C. A. Veracini, C. Zannoni, An internal order approach to the investigation of intramolecular rotations in liquid crystals by NMR: 3-phenyl-thiophene in PCH and phase IV, *Chem. Phys. Lett.*, 143, **1988**, 263-269

[263] C. Zannoni, An internal order parameter formalism for non-rigid molecules, in *Nuclear Magnetic Resonance of Liquid Crystals*, J. W. Emsley ed., Reidel, Dordrecht, **1985**, chap. 2, ISBN: 9027718784

[264] B. Stevensson, D. Sandström, A. Maliniak, Conformational distribution functions extracted from residual dipolar couplings: A hybrid model based on maximum entropy and molecular field theory, *J. Chem. Phys.*, 119, **2003**, 2738-2746

[265] D. S. Zimmerman, E. E. Burnell, Anisotropic short range potentials for solutes in nematic liquid crystals, *Mol. Phys.*, 78, **1993**, 687-702

[266] L. C. Ter Beek, D. S. Zimmerman, E. E. Burnell, The orientation of molecules with internal rotation in nematic phases, *Mol. Phys.*, 80, **1993**, 177-189

[267] A. Ferrarini, G. J. Moro, P.L. Nordio, G.R. Luckhurst, A shape model for molecular ordering in nematics, *Mol. Phys.*, 77, **1992**, 1-15

[268] S. Marčelja, Chain ordering in liquid crystals. I. Even-odd effect, *J. Chem. Phys.*, 60, **1974**, 3599-3604

[269] M. Concistré, G. De Luca, M. Longeri, G. Pileio, J. W. Emsley, The structure and conformations of 2-thiophenecarboxaldehyde obtained from partially averaged dipolar couplings, *Chem. Phys. Chem.*, 6, **2005**, 1483-1491

[270] D. J. Photinos, E. T. Samulski, H. Toriumi, Alkyl chains in a nematic field. 1. A treatment of conformer shape, *J. Phys. Chem.*, 94, **1990**, 4688-4694

[271] D. J. Photinos, E. T. Samulski, H. Toriumi, Alkyl chains in a nematic field. 2. Temperature and chain length dependence of orientational ordering, *J. Phys. Chem.*, 94, **1990**, 4694-4700

[272] C. Algieri, F. Castiglione, G. Celebre, G. De Luca, M. Longeri, J. W. Emsley, The structure of ethylbenzene as a solute in liquid crystalline solvents *via* analysis of proton NMR spectra, *Phys. Chem. Chem. Phys.*, 2, **2000**, 3405-3413

[273] J. W. Emsley, I. D. Wallington, D. Catalano, C. A. Veracini, G. Celebre, M. Longeri, Comparison of the maximum entropy and additive potential methods for obtaining rotational potentials from the NMR spectra of samples dissolved in liquid crystalline solvents. The case of 4-nitro-1-(β,β,β-trifluoroethoxy) benzene, *J. Phys. Chem.*, 97, **1993**, 6518-6523

[274] J. W. Emsley, T. J. Home, G. Celebre, M. Longeri, H. Zimmermann, Conformation of the ethoxy group in 4-ethoxy-4'-cyanobipheny, *J. Phys. Chem.*, 96, **1992**, 1929-1934

[275] G. Celebre, G. De Luca, M. Longeri, J. W. Emsley, Internal rotation potential function for anisole in solution: a liquid crystal NMR study, *J. Phys. Chem.*, 96, **1992**, 2466-2470

[276] G. Celebre, G. De Luca, M. Longeri, D. Catalano, C. A. Veracini, J. W. Emsley, Structure of biphenyl in a nematic liquid-crystalline solvent**, *J. Chem. Soc. Faraday Trans.*, 87, **1991**, 2623-2627

[277] G. Celebre, M. Longeri, E. Sicilia, J. W. Emsley, The angle of twist between the two phenyl rings in the nematic liquid crystal 4-n-pentyl-4'-cyanobiphenyl, *Liq. Cryst.*, 7, **1990**, 731-737

[278] G. Celebre, M. Longeri, J. W. Emsley, The nature of the internal rotational barrier in benzyl chloride. An interpretation of the dipolar coupling constants obtained from the analysis of the proton N.M.R. spectra of samples dissolved in liquid crystal solvents, *Mol. Phys.*, 64, **1988**, 715-723

[279] G. Celebre, M. Concistré, G. De Luca, M. Longeri, G. Pileio, Intrinsic information content of NMR dipolar couplings: a conformational investigation of 1,3-butadiene in a nematic phase, *Chem. Phys. Chem.*, 7, **2006**, 1930-1943

[280] G. Pileio, Ph.D. Thesis, Università della Calabria, Rende, Italy, **2005**

[281] R. Berardi, F. Spinozzi, C. Zannoni, Maximum entropy internal order approach to the study of intramolecular rotations in liquid crystals, *J. Chem. Soc. Faraday Trans.*, 88, **1992**, 1863-1873

[282] D. Catalano, L. Di Bari, C. A. Veracini, G. N. Shilstone, C. Zannoni, A maximum-entropy analysis of the problem of the rotameric distribution for substituted biphenyls studied by ^{1}H nuclear magnetic resonance spectroscopy in nematic liquid crystals, *J. Chem. Phys.*, 94, **1991**, 3928-3935

[283] G. Cinacchi, G. Prampolini, DFT study of the torsional potential in ethylbenzene and ethoxybenzene: the smallest prototypes of alkyl- and alkoxy-aryl mesogens, *J. Phys. Chem. A*, 107, **2003**, 5228-5232

[284] G. Cinacchi, M. Longeri, C. A. Veracini, Internal rotation in alkyl benzene derivatives: maximum entropy and constrained maximum entropy analysis of the dipolar couplings of samples dissolved in a nematic liquid crystal solvent, *Phys. Chem. Chem. Phys.*, 4, **2002**, 5582-5589

[285] A. B. Sahakyan, A. G. Shahkhatuni, A. A. Shahkhatuni, H. A. Panosyan, Torsion sensitivity in NMR of aligned molecules: study on various substituted biphenyls, *Magn. Reson. Chem.*, 46, **2008**, 144-149

[286] J. Thaning, B. Stevensson, A. Maliniak, Molecular structure extracted from residual dipolar couplings: diphenylmethane dissolved in a nematic liquid crystal, *J. Chem. Phys.*, 123, **2005**, 044507.1-6

[287] J. Thaning, C.-J. Högberg, B. Stevensson, A. P. Lyubartsev, A. Maliniak, Molecular conformations in a phospholipid bilayer extracted from dipolar couplings: a computer simulation study, *J. Phys. Chem. B*, 111, **2007**, 13638-13644

[288] C. Landersjö, B. Stevensson, R. Eklunda, J. Östervall, P. Söderman, G. Widmalm, A. Maliniak, Molecular conformations of a disaccharide investigated using NMR Spectroscopy, *J. Biomol. NMR*, 35, **2006**, 89-101

[289] B. Stevensson, C. Landersjö, G. Widmalm, A. Maliniak, Conformational distribution function of a disaccharide in a liquid crystalline phase determined using NMR spectroscopy, *J. Am. Chem. Soc.*, 124, **2002**, 5946-5947

[290] E. E. Burnell, C. A. de Lange, J. B. S. Barnhoorn, I. Aben, P. F. Levelt, Molecules with large-amplitude torsional motion partially oriented in a nematic liquid crystal: ethane and isotopomers, *J. Phys. Chem. A*, 109, **2005**, 11027-11036

[291] J. Lounila, P. Diehl, A general theory for the correlation between vibration and rotation of partially oriented molecules and for its effects on the NMR parameters, *J. Magn. Reson.*, 56, **1984**, 254-261

[292] J. Lounila, P. Diehl, The effects of the correlation between vibration and rotation of partially oriented molecules on the N.M.R. parameters, *Mol. Phys.*, 52, **1984**, 827-845

[293] S. Sykora, J. Vogt, H. Bosiger, P. Diehl, Vibrational corrections in NMR spectra of oriented molecules, *J. Magn. Reson.*, 36, **1979**, 53-60

[294] P. Diehl, W. Niederberger, The vibrationally averaged molecular structure: a comparison of NMR data for oriented benzene with results from electron diffraction and raman spectroscopy, *J. Magn. Reson.*, 9, **1973**, 495-502

[295] M. Concistré, L. De Lorenzo, G. De Luca, M. Longeri, G. Pileio, G. Raos, Conformational analysis of 2,2'-bithiophene: a ^{1}H liquid crystal NMR study using the ^{13}C satellite spectra, *J. Phys. Chem. A*, 109, **2005**, 9953-9963

[296] J. Lounila, R. Wasser, P. Diehl, Effects of anharmonic vibrations on molecular properties, *Mol. Phys.*, 62, **1987**, 19-31

[297] T. N. Pham, S. L. Hinchley, D. W. H. Rankin, T. Liptaj, D. Uhrín, Determination of sugar structures in solution from residual dipolar coupling constants: methodology and application to methyl-β-D-xylopyranoside, *J. Am. Chem. Soc.*, 126, **2004**, 13100-13110

[298] L. D. Field, Multiple quantum spectroscopy in liquid crystalline solvents, in *Encyclopedia of Magnetic Resonance*, John Wiley & Sons, Ltd., **2007**

[299] L. D. Field, Multiple quantum NMR spectroscopy in orientationally ordered fluids, in *NMR of Ordered Liquids*, E. E. Burnell and C. A. de Lange eds., Kluwer Academic, Dordrecht, **2003**, chap 4, ISBN: 1402013434

[300] A. Kumar, N. Suryaprakash, Two-dimensional NMR of molecules oriented in liquid crystals - Recent development, in *Encyclopedia of Magnetic ResonanceI*, John Wiley & Sons, Ltd., **2009**

[301] A. Kumar, Two-dimensional NMR of molecules oriented in liquid crystalline phases, in *Encyclopedia of Magnetic Resonance*, John Wiley & Sons, Ltd, **2007**

[302] A. Kumar, Applications of two-dimensional NMR to oriented molecules, *Curr*. *Sci*., 57, **1988**, 109-120

[303] C. L. Khetrapal, A. Kumar, A. C. Kunwar, P. C. Mathias, K. V. Ramanathan, Two-dimensional NMR spectra of oriented molecules, *J. Magn. Reson.*, 37, **1969**, 349-351

[304] D. L. Turner, Two-dimensional spin-echo spectroscopy of oriented systems, *J. Magn. Reson.*, 46, **1969**, 213-226

[305] J. W. Emsley, D. L. Turner, A. M. Giroud, M. Longeri, Spin-echo and autocorrelation experiments as an aid in the analysis of complex spectra from liquid-crystalline samples, *J. Chem. Soc. Faraday Trans. 2*, 81, **1985**, 603-611

[306] R. C. R. Grace, A. Kumar, Flip-angle dependence of non-equilibrium states yielding information on connectivity of transitions and energy levels of oriented molecules, *J. Magn*. *Reson*., 99, **1992**, 81-92

[307] K. Rukmani, A. Kumar, Symmetry filtering of the NMR spectra of oriented molecules into irreducible representations using two-dimensional correlation spectroscopy, *Chem. Phys. Lett.*, 133, **1987**, 485-490

[308] B. Bikash, G. M. Raghav, N. Suryaprakash, ^{13}C-^{1}H HSQC experiment of probe molecules aligned in thermotropic liquid crystals: sensitivity and resolution enhancement in the indirect dimension, *J. Magn. Reson.*, 185, **2007**, 221-229

[309] H. S. V. Deepak, A. Joy, N. Suryaprakash, Determination of natural abundance ^{15}N–^{1}H and ^{13}C–^{1}H dipolar couplings of molecules in a strongly orienting media using two-dimensional inverse experiments, *Magn. Reson. Chem.,* 44, **2006**, 553-565

[310] J. W. Emsley, D. Merlet, K. J. Smith, N. Suryaprakash, Selective detection of the proton NMR spectra of molecules containing rare spins at natural abundance in liquid crystalline samples *J. Magn. Reson.*, 154, **2002**, 303-310

[311] S. Caldarelli, Local field experiments in liquid crystals, in *Encyclopedia of Magnetic Resonance*, John Wiley & Sons, Ltd., **2009**

[312] M. Hong, A. Pines, S. Caldarelli, Measurement and assignment of long-range C-H dipolar couplings in liquid crystals by two-dimensional NMR spectroscopy, *J. Phys*. *Chem*., 100, **1996**, 14815-14822

[313] S. Caldarelli, M. Hong, L. Emsley, A. Pines, Measurement of carbon-proton dipolar couplings in liquid crystals by local dipolar field NMR spectroscopy, *J. Phys*. *Chem*., 100, **1996**, 18696-18701

[314] S. Caldarelli, A. Lesage, L. Emsley, Long-range dipolar couplings in liquid crystals measured by three-dimensional NMR spectroscopy, *J. Am*. *Chem*. *Soc*., 118, **1996**, 12224-12225

[315] B. M. Fung, J. Afzal, Carbon-13 NMR of liquid crystals. Spinning near the magic angle with proton-proton dipolar decoupling *J. Am. Chem. Soc.*, 108, **1986**, 1107-1108

[316] B. M. Fung, J. Afzal, T. L. Foss, M. H. Chau, Nematic ordering of 4-n-alkyl- 4′-cyanobiphenyls studied by carbon-13 NMR with off-magic-angle spinning, *J. Chem. Phys. A*, 85, **1986**, 4808-4814

[317] B. Luy, A. Frank, H. Kessler, Conformational analysis of drugs by nuclear magnetic resonance spectroscopy, in *Molecular Drug Properties. Measurement and Prediction*, R. Mannhold ed., Wiley-VCH Verlag GmbH & Co. KGaA, Weinheim, **2008**, chap. 9, ISBN: 9783527317554

[318] G. A. Morris, Two-dimensional *J*-resolved spectroscopy, in *Encyclopedia of Nuclear Magnetic Resonance*, John Wiley & Sons, Ltd., **2007**

[319] W. P. Aue, J. Karhan, R. R. Ernst, Homonuclear broad-band decoupling and 2-dimensional *J*-resolved NMR spectroscopy, *J. Chem. Phys.*, 64, **1976**, 4226-4227

[320] P. Tzvetkova, S. Simova, B. Luy, P.E.HSQC: A simple experiment for simultaneous and sign-sensitive measurement of ($^1J_{CH}$ + D_{CH}) and ($^2J_{HH}$ + D_{HH}) couplings, *J. Magn. Reson.*, 186, **2007**, 193-200

[321] C. Griesinger, O. W. Sørensen, R. R. Ernst, Practical aspects of the E.COSY technique. Measurement of scalar spin-spin coupling constants in peptides, *J. Magn. Reson.*, 75, **1987**, 474-492

[322] C. Griesinger, O. W. Sørensen, R. R. Ernst, Correlation of connected transitions by two-dimensional NMR spectroscopy, *J. Chem. Phys.*, 85, **1986**, 6837-6852

[323] C. Griesinger, O. W. Sørensen, R. R. Ernst, Two-dimensional correlation of connected NMR transitions, *J. Am. Chem. Soc.*, 107, **1985**, 6394-6396

[324] B. Yu, H. van Ingen, D. I. Freedberg, Constant time INEPT CT-HSQC (CTi-CT-HSQC) - A new NMR method to measure accurate one-bond *J* and RDCs with strong ^{1}H-^{1}H couplings in natural abundance, *J. Magn. Reson.*, 228, **2013**, 159-165

[325] K. Kobzar, B. Luy, Analyses, extensions and comparison of three experimental schemes for measuring ($^nJ_{CH}$ + D_{CH})-couplings at natural abundance, *J. Magn. Reson.*, 186, **2007**, 131-141

[326] J. Furrer, M. John, H. Kessler, B. Luy, J-spectroscopy in the presence of residual dipolar couplings: determination of one-bond coupling constants and scalable resolution, *J. Biomol. NMR*, 37, **2007**, 231-243

[327] P. Nolis, J. F. Espinosa, T. Parella, Optimum spin-state selection for all multiplicities in the acquisition dimension of the HSQC experiment, *J. Magn. Reson.*, 180, **2006**, 39-50

[328] J. Farjon, W. Bermel, C. Griesinger, Resolution enhancement in spectra of natural products dissolved in weakly orienting media with the help of ^{1}H homonuclear dipolar decoupling during acquisition: application to ^{1}H–^{13}C dipolar couplings measurements, *J. Magn. Reson.*, 180, **2006**, 72-82

[329] V. M. Marathias, I. Goljer, A. C. Bach II, Simultaneous determination of ^{1}H–^{1}H and ^{1}H–^{13}C residual dipolar couplings in a chiral liquid crystal solvent using a natural abundance HSQC experiment, *Magn. Reson. Chem.*, 43, **2005**, 512-519

[330] K. Fehér, S. Berger, K. Kövér, Accurate determination of small one-bond heteronuclear residual dipolar couplings by F1 coupled HSQC modified with a G-BIRD$^{(r)}$ module, *J. Magn. Reson.*, 163, **2003**, 340-346

[331] T. Carlomagno, W. Peti, C. Griesinger, A new method for the simultaneous measurement of magnitude and sign of $^1D_{CH}$ and $^1D_{HH}$ dipolar couplings in methylene groups, *J. Biomol. NMR*, 17, **2000**, 99-109

[332] U. R. Prabhu, S. R. Chaudhari, N. Suryaprakash, Visualization of enantiomers and determination of homo- and hetero-nuclear residual dipolar and scalar couplings: the natural abundant ^{13}C edited J/D-resolved NMR techniques, *Chem. Phys. Lett.*, 500, **2010**, 334-341

[333] T. N. Pham, T. Liptaj, K. Bromek, D. Uhrín, Measurement of small one-bond proton–carbon residual dipolar coupling constants in partially oriented ^{13}C natural abundance oligosaccharide samples: analysis of heteronuclear [1]J$_{CH}$-modulated spectra with the BIRD inversion pulse, *J. Magn. Reson.*, 157, **2002**, 200-209

[334] G. Bodenhausen, R. Freeman, D.L. Turner, Two-dimensional J spectroscopy: proton-coupled carbon-13 NMR, *J. Chem. Phys.*, 65, **1976**, 839-840

[335] J. Farjon, D. Merlet, SERF-filtered experiments: new enantio-selective tools for deciphering complex spectra of racemic mixtures dissolved in chiral oriented media, *J. Magn. Reson.*, 210, **2011**, 24-30

[336] L. Beguin, N. Giraud, J.M. Ouvrard, J. Courtieu, D. Merlet, Improvements to selective refocusing phased (SERFph) experiments, *J. Magn. Reson.*, 199, **2009**, 41-47

[337] J. Farjon, L. Ziani, L. Beguin, D. Merlet, J. Courtieu, Selective NMR excitations in chiral analysis, *Annu. Rep. NMR*, 61, **2007**, 283-293

[338] J.M. Nuzillard, Biselective refocusing pulses and the SERF experiment, *J. Magn. Reson.*, 187, **2007**, 193-198

[339] B. Baishya, U. R. Prabhu, N. Suryaprakash, Enantiomeric discrimination by double quantum excited selective refocusing (DQ-SERF) experiment, *J. Phys. Chem. B*, 111, **2007**, 12403-12410

[340] L. Beguin, J. Courtieu, L. Ziani, D. Merlet, Simplification of the ^{1}H NMR spectra of enantiomers dissolved in chiral liquid crystals, combining variable angle sample spinning and selective refocusing experiments, *Magn. Reson. Chem.*, 44, **2006**, 1096-1101

[341] P. Nolis, A. Roglans, T. Parella, IFSERF, an isotope-filtered SERF experiment for the precise measurement of proton–proton coupling constants between chemically equivalent protons, *J. Magn. Reson.*, 173, **2005**, 305-309

[342] J. Farjon, D. Merlet, P. Lesot, J. Courtieu, Enantiomeric excess measurements in weakly oriented chiral liquid crystal solvents through 2D ^{1}H selective refocusing experiments, *J. Magn. Reson.*, 158, **2002**, 169-172

[343] T. Facke, S. Berger, SERF, a new method for H,H spin-coupling measurement in organic chemistry, *J. Magn. Reson. Ser. A*, 113, **1995**, 114-116

[344] N. Nath, N. Suryaprakash, Spin-selective correlation experiment for measurement of long-range J couplings and for assignment of (R/S) enantiomers from the residual dipolar couplings and DFT, *J. Phys. Chem. B*, 115, **2011**, 6868-6875

[345] N. Nath, N. Suryaprakash, Enantiodiscrimination and extraction of short and long range homo- and hetero-nuclear residual dipolar couplings by a spin selective correlation experiment, *Chem. Phys. Lett.*, 496, **2010**, 175-182

[346] N. Nath, B. Baishya, N. Suryaprakash, Visualization of enantiomers using natural abundant ^{13}C-filtered single and double quantum selective refocusing experiments: application to small chiral molecules, *J. Magn. Reson.*, 200, **2009**, 101-108

[347] J. Farjon, J.P. Baltaze, P. Lesot, D. Merlet, J. Courtieu, Heteronuclear selective refocusing 2D NMR experiments for the spectral analysis of enantiomers in chiral oriented solvents, *Magn. Reson. Chem.*, 42, **2004**, 594-599

[348] D. Merlet, L. Beguin, J. Courtieu, N. Giraud, Spin–spin coupling edition in chiral liquid crystal NMR solvent, *J. Magn. Reson.*, 209, **2011**, 315-322

[349] N. Giraud, L. Beguin, J. Courtieu, D. Merlet, Nuclear magnetic resonance using a spatial frequency encoding: application to *J*-edited spectroscopy along the sample, *Angew. Chem. Int. Ed.*, 49, **2010**, 3481-3484

[350] K. Zangger, H. Sterk, Homonuclear broadband-decoupled NMR spectra, *J. Magn. Reson.*, 124, **1997**, 486-489

[351] G. De Luca, J. W. Emsley, E. Salager, A. Lesage, A general strategy for obtaining $^{19}F–^{19}F$ and $^{13}C–^{19}F$ residual dipolar couplings in perfluorocarbons from the NMR spectroscopy of liquid crystalline samples, *Phys. Chem. Chem. Phys.*, 12, **2010**, 7968-7976

[352] B. Aldridge, G. De Luca, M. Edgar, S. J. Edgar, J. W. Emsley, M. I. C. Furby, M. Webster, The structure of 2,2'-difluorobiphenyl in solid crystalline and liquid crystalline phases, *Liq. Cryst.*, 24, **1998**, 569-581

[353] J. Yan, F. Delaglio, A. Kaerner, A.D. Kline, H. Mo, M. J. Shapiro, T.A. Smitka, G. A. Stephenson, E. R. Zartler, Complete relative stereochemistry of multiple stereocenters using only residual dipolar couplings, *J. Am. Chem. Soc.*, 126, **2004**, 5008-5017

[354] B. Luy, J. J. Barchi, J. P. Marino, S^{3}E-E.COSY Methods for the measurement of ^{19}F associated scalar and dipolar coupling constants, *J. Magn. Reson.*, 152, **2001**, 179-184

[355] B. Luy, J. P. Marino, Measurement and application of ^1H-^{19}F dipolar couplings in the structure determination of 2'-fluorolabeled RNA, *J. Biom. NMR*, 20, **2001**, 39-47

[356] D. Merlet, B. Ancian, J. Courtieu, P. Lesot, Two-dimensional deuterium NMR spectroscopy of chiral molecules oriented in a polypeptide liquid crystal: applications for the enantiomeric analysis through natural abundance deuterium NMR, *J. Am. Chem. Soc.*, 121, **1999**, 5249-5258

[357] O. Lafon, P. Lesot, D. Merlet, J. Courtieu, Modified z-gradient filtering as a mean to obtain phased deuterium autocorrelation 2D NMR spectra in oriented solvents, *J. Magn. Reson.*, 171, **2004**, 135-142

[358] D. Merlet, M. Sarfati, B. Ancian, J. Courtieu, P. Lesot, Description of natural abundance deuterium 2D-NMR experiments in weakly ordered liquid-crystalline solvents using a tailored Cartesian spin-operator formalism, *Phys. Chem Chem. Phys.*, 2, **2000**, 2283-2290

[359] C. L. Khetrapal, K. V. Ramanathan, N. Suryaprakash, S. Vivekanandan, Natural abundance ^2H NMR spectra of molecules oriented in liquid crystals, *J. Magn. Reson.*, 135, **1998**, 265-266

[360] P. Lesot, O. Lafon, Experimental detection of achiral and chiral naturally abundant $^{13}C–^2H$ isotopomers by 2D-NMR in liquids and chiral oriented solvents, *Anal. Chem.*, 84, **2012**, 4569-4573

[361] Z. Serhan, I. Billault, A. Borgogno, A. Ferrarini, P. Lesot, Analysis of NAD 2D-NMR spectra of saturated fatty acids in polypeptide aligning media by experimental and modeling approaches, *Chem. Eur. J.*, 18, **2012**, 117-126

[362] I. Billault, A. Ledru, M. Ouetrani, Z. Serhan, P. Lesot, R. J. Robins, Probing substrate-product relationships by natural abundance deuterium 2D NMR spectroscopy in liquid-crystalline solvents: the case of the epoxidation of linoleate to vernoleate by two different plant enzymes, *Anal. Bioanal. Chem.*, 402, **2012**, 2985-2998

[363] P. Lesot, C. Aroulanda, Analytical potentials of natural abundance deuterium NMR spectroscopy in achiral thermotropics and polypeptide chiral liquid crystals, in *NMR Spectroscopy of Liquid Crystals*, R. Dong ed., Elsevier, **2009**, chap. 2, ISBN: 9789814273664

[364] J. W. Emsley, P. Lesot, J. Courtieu, D. Merlet,The effect of a chiral nematic solvent on the orientational order and conformational distribution of a flexible prochiral solute, *Phys. Chem. Chem. Phys.*, 6, **2004**, 5331-5337

[365] P. Lesot, D. Merlet, A. Loewenstein, J. Courtieu, Enantiomeric visualization using proton-decoupled natural abundance deuterium NMR in poly(-benzyl-L-glutamate) liquid crystalline solutions, *Tetrahedron: Asymmetry*, 9, **1998**, 1871-1881

[366] D. Merlet, B. Ancian, W. Smadja, J. Courtieu, P. Lesot, Analysis of natural abundance deuterium NMR spectra of enantiomers in chiral liquid crystals *via* 2D auto-correlation experiments, *Chem. Commun.*, **1998**, 2301-2302

[367] H. O. Kalinowski, S. Berger, S. Braun, *Carbon-13 NMR Spectroscopy*, John Wiley and Sons, Chichester, UK, **1988**, ISBN: 9780471913061

[368] F. W. Wehrli, A. P. Marchand, S. Wehrli, *Interpretation of Carbon-13 NMR Spectra*, Wiley, Chichester, New York, **1988**, ISBN: 9780471917427

[369] XSIM Program Package ©, K. Marat, University of Manitoba, Winnipeg, MB, Canada, **1997**

[370] P. Diehl, H. Kellerhals, E. Lustig, Computer assistance in the analysis of high resolution NMR spectra, in *NMR Basic Principles and Progress*, vol. 6, P. Diehl, E. Fluck and R. Kosfeld eds., Springer-Verlag, Berlin, **1972**, ISBN: 9780387055329

[371] P. Diehl, H. P. Kellerhals, W. Niederberger, The structure of toluene as determined by NMR of oriented molecules, *J. Magn. Reson.*, 4, **1971**, 352-357

[372] P. Diehl, C. L. Khetrapal, H. P. Kellerhals, The N.M.R. spectrum of pyridine oriented in the nematic phase, *Mol. Phys.*, 15, **1968**, 333-337

[373] G. Celebre, G. De Luca, M. Longeri, E. Sicilia, Graphical interactive strategy for the analysis of NMR spectra in liquid crystalline phases, *J. Chem. Inf. Comput. Sci.*, 34, **1994**, 539-545

[374] S. Castellano, A. A. Bothner-By, Analysis of NMR spectra by least squares, *J. Chem. Phys.*, 41, **1964**, 3863-3869

[375] E. Ciampi, G. De Luca, J. W. Emsley, Measurement of interproton, nuclear spin dipolar couplings in liquid crystalline samples by combining variable angle sample spinning, isotope dilution, and deuterium decoupling, *J. Magn. Reson.*, 129, **1997**, 207-211

[376] R. C. Hewitt, S. Meiboom, L. C. Snyder, Proton NMR in nematic liquid crystalline solvents: the use of deuterium decoupling, *J. Chem. Phys.*, 58, **1973**, 5089-5095

[377] L. C. Snyder, S. Meiboom, Theory of proton NMR with deuteron decoupling in nematic liquid crystalline solvent, *J. Chem. Phys.*, 58, **1973**, 5096-5103

[378] S. Meiboom, R. C. Hewitt, L. C. Snyder, Developments in NMR in liquid crystalline solvents, *Pure Appl. Chem.*, 32, **1972**, 251-261

[379] J. W. Emsley, J. C. Lindon, J. M. Tabony, T. H. Wilmshurst, Simplification of the ^{1}H nuclear magnetic resonance spectra of partially oriented molecules by partial deuteriation and deuterium decoupling, *J. Chem. Soc. D, Chem. Commun.*, **1971**, 1277-1278

[380] C. Qian, P. Thureau, R. W. Martin, Variable angle spinning (VAS) experiments for strongly oriented systems: methods development and preliminary results, *Magn. Reson. Chem.*, 46, **2008**, 351-355

[381] G. H. J. Park, R. W. Martin, D. Sakellariou, A. Pines, A. G. Shahkhatuni, A. A. Shahkhatuni, H. A. Panosyan, Variable angle spinning (VAS) NMR study of solvent effects in liquid crystalline solutions of ^{13}C–iodomethane, *Chem. Phys. Lett.*, 399, **2004**, 196-199

[382] J. Courtieu, D. W. Alderman, D. M. Grant, J. P. Bayle, Director dynamics and NMR applications of nematic liquid crystals, spinning at various angles from the magnetic field, *J. Chem. Phys.*, 77, **1982**, 723-730

[383] G. Zandomeneghi, P. T. F. Williamson, A. Hunkeler, B. H. Meier, Switched-angle spinning applied to bicelles containing phospholipid-associated peptides, *J. Biomol. NMR*, 25, **2003**, 125-132

[384] F. Tian, J.A. Losonczi, M. W. F. Fischer, J. H. Prestegard, Sign determination of dipolar couplings in field-oriented bicelles by variable angle sample spinning (VASS), *J. Biomol. NMR*, 15, **1999**, 145-150

[385] A. Kimura, N. Kuni, H. Fujiwara, Orientation and conformation of met-enkephalin in a liquid crystal as studied by magic-angle and near-magic angle spinning two dimensional NMR spectroscopy, *J. Phys. Chem.*, 100, **1996**, 14056-14061

[386] G. Bodenhausen, Multiple-quantum NMR, *Prog. Nucl. Magn. Reson. Spectrosc.*, 14, **1980**, 137-173

[387] L. D. Field, G. K. Pierens, K. J. Cross, M. L. Terry, Multiple quantum NMR spectroscopy of molecules aligned in liquid crystalline solvents, *J. Magn. Reson.*, 97, **1992**, 451-465

[388] G. K. Pierens, T. A. Carpenter, Z. D. Colebrook, L. D. Field, L. D. Hall, Selection of multiple quantum of molecules in liquid crystalline solution using pulsed magnetic field gradients, *J. Magn. Reson.*, 99, **1992**, 398-402

[389] G. P. Drobny, Multiple quantum NMR: studies of molecules in ordered phases, *Ann. Rev. Phys. Chem.*, 36, **1985**, 451-489

[390] F. Castiglione, G. Celebre, G. De Luca, M.Longeri, The NMR spectra of samples dissolved in liquid–crystalline phases: automatic analysis with the aid of multiple quantum spectra - The case of flexible molecules, *J. Magn. Reson.*, 142, **2000**, 216-228

[391] G. Celebre, F. Castiglione, M.Longeri, J. W. Emsley, The NMR spectra of samples dissolved in liquid-crystalline phases. Automatic analysis with the aid of multiple-quantum spectra, *J. Magn. Reson. Ser. A*, 121, **1996**, 139-146

[392] T. Chandrakumar, J. M. Polson, E. E. Burnell, A multiple-quantum ^{1}H NMR study of conformational biasing of biphenyl in a nematic liquid crystal, *J. Magn. Reson. Ser. A*, 118, **1996**, 264-271

[393] J. M. Polson, E. E. Burnell, Multiple-quantum ^{1}H NMR study of partially oriented biphenylene, *J. Magn. Reson. Ser. A*, 106, **1994**, 223-228

[394] V. Zinin, A. Il'yasov, H. Thiele, G. Hägele, U. Weber, WIN-DAISY: Application to oriented molecules. Analysis and simulation of NEMA-NMR spectra, *Appl. Magn. Reson.*, 8, **1995**, 311-317

[395] D. S. Stephenson, G. Binsch, The molecular structure of cyclopentene in solution as obtained from a nematic phase proton N.M.R. study, *Mol. Phys.*, 43, **1981**, 697-710

[396] G. Binsch, *Computational Methods in Chemistry*, J. Bargon ed., Plenum Press, New York, **1980**, ISBN: 9780306404559

[397] S. Stephenson, G. Binsch, Automated analysis of high-resolution NMR spectra. I. Principles and computational strategy, *J. Magn. Reson.*, 37, **1980**, 395-409

[398] D. S. Stephenson, G. Binsch, Automated analysis of high-resolution NMR spectra III - The nematic phase spectra of three allyl halides, *Org. Magn. Reson.*, 14, **1980**, 226-233

[399] D. P. Diehl, S. Sýkora, J. Vogt, Automatic analysis of NMR spectra: an alternative approach, *J. Magn. Reson.*, 19, **1975**, 67-82

[400] E. E. Burnell, C. A. de Lange, W. L. Meerts, Novel strategies for solving highly complex NMR spectra of solutes in liquid crystals, in *Nuclear Magnetic Resonance Spectroscopy of Liquid Crystals*, R. Dong ed., World Scientific Review, **2009**, chap. 1, ISBN: 9789814273664

[401] W. L. Meerts, C. A. de Lange, A. C. J. Weber, E. E. Burnell, Evolutionary algorithms to solve complicated NMR spectra, *J. Chem. Phys.*, 139, **2009**, 044504.1-8

[402] A. C. J. Weber, X. Yang, R. Y. Dong, W. L. Meerts, E. E. Burnell, Solute order parameters in liquid crystals from NMR spectra solved with evolutionary algorithms: application of double Maier-Saupe Kobayashi-McMillan theory, *Chem. Phys. Lett.*, 476, **2009**, 116-119

[403] W. L. Meerts, C. A. de Lange, A. C. J. Weber, E. E. Burnell, A simple two-step automatic assignment procedure for complicated NMR spectra of solutes in liquid crystals using genetic algorithms, *Chem. Phys. Lett.*, 441, **2007**, 324-346

[404] W. L. Meerts, M. Schmitt, Application of genetic algorithms in automated assignments of high-resolution spectra, *Int. Rev. Phys. Chem.*, 25, **2006**, 353-406

[405] W. L. Meerts, M. Schmitt, G. C. Groenenboom, New applications of the genetic algorithms in the automated analysis of high resolution spectra, *Can. J. Chem.*, 82, **2004**, 804-819

[406] N. Hansen, S. Kern, Evaluating the CMA evolution strategy on multimodal test functions, in *Parallel Problem Solving from Nature PPSN VIII*, vol. 3242, X. Yao et al. ed., LNCS, Springer, **2004**

[407] N. Hansen, A. Ostermeier, Completely derandomized self-adaptation in evolution strategies, *Evolutionary Computation*, 9, **2001**, 159-195

[408] M. F. Palermo, A. Pizzirusso, L. Muccioli, C. Zannoni, An atomistic description of the nematic and smectic phases of 4-*n*-octyl-4'-cyanobiphenyl (8CB), *J. Chem. Phys.*, 138, **2013**, 204901.1-16

[409] A. C. J. Weber, A. Pizzirusso, L. Muccioli, C. Zannoni, W. L. Meerts, C. A. de Lange, E. E. Burnell, Efficient analysis of highly complex nuclear magnetic resonance spectra of flexible solutes in ordered liquids by using molecular dynamics, *J. Chem. Phys.*, 136, **2012**, 174506.1-7

[410] A. Pizzirusso, M. B. Di Cicco, G. Tiberio, L. Muccioli, R. Berardi, C. Zannoni, Alignment of small organic solutes in a nematic solvent: the effect of electrostatic interactions, *J. Phys. Chem. B*, 116, **2012**, 3760-3771

[411] A. Pizzirusso, R. Berardi, L. Muccioli, M. Ricci, C. Zannoni, Predicting surface anchoring: molecular organization across a thin film of 5CB liquid crystal on silicon, *Chem. Sci.*, 3, **2012**, 573-579

[412] A. Pizzirusso, M. Savini, L. Muccioli, C. Zannoni, An atomistic simulation of the liquid-crystalline phases of sexithiophene, *J. Mat. Chem.*, 21, **2011**, 125-133

[413] G. Tiberio, L. Muccioli, R. Berardi, C. Zannoni, Towards in silico liquid crystals. Realistic transition temperatures and physical properties for *n*-cyanobiphenyls via molecular dynamics simulations, *Chem. Phys. Chem.*, 10, **2009**, 125-136

Chapter 2

STRUCTURAL AND ORIENTATIONAL ANALYSIS OF RIGID MOLECULES

2.1.   Introduction

The spin-spin dipolar couplings that dominate the spectra of rigid molecules dissolved in liquid crystalline phases can give access to valuable information about structure and order. Several reviews report the extensive use of the method for molecular as well as macromolecular structure determination [1-2]. In this Ph.D. thesis, we mainly used some small rigid compounds as "probes" with the purpose of getting interesting considerations about the orientational and positional ordering phenomena. The investigation of the degree of order may evidently be carried out both for solute and solvent molecules and in this chapter both issues will be addressed.

The Saupe orientational order parameters of compounds dissolved in liquid crystalline media have been widely exploited in the past as a key to understand the basic mechanism for the orientational order acting in an anisotropic fluid and to formulate more or less simple models for the liquid crystal environment [3]. In this regard, especially small rigid well characterized solutes, whose spectrum is amenable to analysis, are often chosen as probes of the intermolecular potential. A case in point are molecules which possess a tetrahedral or higher symmetry. In the early years of liquid crystal NMR, it came as a surprise that such solutes, when dissolved in a nematic phase, showed spectral splittings that, under the assumption of rigidity of the molecular structure, should not be there [4-5]. To approach such issue a number of simple molecules like hydrogen, methane, ethane and their deuterated and tritiated isotopologues, whose electronic structure and vibrational force fields are well known, were studied as solutes in nematic phases [6-15]. Actually, this unexpected behavior is interpreted as arising from a sort of interplay between vibrational and reorientational solute motion and it is taken into account in the non-rigid, vibration-reorientation contribution $D_{ij}^{non-rigid}$ to the observed dipolar couplings (equation (1.89)). Therefore, in contrast to the initial point of view [4, 16-17], solute-solvent interactions do not lead to any significant "distortion" or "deformation" of the solute molecule [6, 18 and refs. therein], but only affect to some extent the rotational part of the wavefunction, while leaving the vibrational and electronic parts essentially untouched. Although the $D_{ij}^{non-rigid}$ contribution completely dominates in methane and other tetrahedral molecules, it may be supposed to become less significant in other less symmetrical solutes. Currently, the assessment of its relative weight is a debated question [18], mainly because the term $D_{ij}^{non-rigid}$ is hardly estimated by available experimental procedures; therefore it is usually considered as an adjustable parameter [6, 18] or its value is transferred from that of similar groups in different, simpler molecules [19-20].

Anyway, when the orientational ordering of the molecule is very small and some of the other contributions can be safely neglected, it is still possible to appreciate the experimental value of the non-rigid term. This is the case of the *quasi*-spherical D_{2d} symmetry tetramethylallene molecule (TMA) dissolved in uniaxial nematic solvents. Aiming at attempting an experimental assessment of the vibration-reorientation correlation in weakly oriented molecules, we studied the peculiar orientational behavior of TMA dissolved in the I52 nematic solvent. Section 2.2 reports the results we obtained.

The application of NMR spectroscopy for studying the order of the molecules that constitute the liquid crystalline phase is a more difficult proposition from a purely experimental point of view. Indeed, such mesogenic molecules normally possess a plethora of coupled spins and interconvert among many different conformations. Their high resolution ^{1}H spectra, averaged over all conformers, are thus composed of a huge number of mostly unresolved lines and are impossible to analyze without a tool for spectral simplification. Deuterium NMR spectroscopy has proven to be the most popular alternative strategy for measurement of order parameters in various mesophases [21-24]. Over the last decade, interest in smectic rather than nematic liquid crystals has experienced a renaissance, with active research in both materials themselves and their promising technological applications. Smectics are characterized by a layered structure, with the constituent particles having not only a long-range orientational order, but also a *quasi*-long-range one-dimensional positional order along the axis perpendicular to the layers [25]. For the investigation of orientational order parameters many spectroscopic and diffractometric techniques are used (Raman [26-27] and fluorescence depolarization [28] spectroscopies, or X-rays and neutron diffraction techniques [29-30]). Among them, NMR has already played and will play in the near future a major role [22, 31-32], particularly ^{2}H NMR, since orientational order parameters can be obtained in a straightforward way by simple quadrupolar splitting measurements. Contrarily, for the measurement of positional order parameters, no straightforward experiment is available at present. Recently, a novel method to estimate the positional order parameters of a smectogenic liquid crystal solvent from knowledge of the orientational order parameters of a number of rigid probe solutes dissolved therein has been proposed [33]. The technique was applied as first example to the smectogen 4,4'-di-*n*-heptylazoxybenzene (HAB), in which the solutes 1,4-dichlorobenzene and naphthalene were dissolved. Following this approach, during this thesis project the bilayer and partially bilayer smectic A liquid crystals HAB and 8OCB (4-*n*-octyloxy-4'-cyanobyphenyl) have been further investigated, leading to the determination of both the positional order parameters of the solvents and the positional distribution functions of the solute molecules.

In the following paragraphs then the main theme, *i.e.* the degree of order in an anisotropic sample, will be investigated focusing on two different aspects: (*i*) in section 2.2 the very small orientational order of the highly symmetric molecule of TMA dissolved in a nematic phase will be exploited as limit condition for measuring, within some approximations, the vibration-reorientation contribution affecting the observed $^1D_{CH}$; (*ii*) section 2.3 will report two applications of a recently suggested route for the determination of the latter's positional order parameters through the solutes orientational order parameters. In all cases, the solute is represented by a rigid small molecule, and the solvent is a highly orienting, nematic or smectic, thermotropic liquid crystalline phase.

2.2. *Study of highly symmetric rigid solutes in uniaxial nematics: the vibration-reorientation contribution to dipolar couplings in very weak orientational ordering conditions*

The orientational order of a solute dissolved in a nematic liquid crystal arises from the anisotropy, $\Delta F = F_\parallel - F_\perp$, of the liquid crystal mean field, which often has cylindrical symmetry around the direction of the space-fixed magnetic field direction, Z. The potential, U, that describes the interaction leading to solute orientational order in this anisotropic mean field is given by [34]:

$$U = -\frac{1}{3}\Delta F \sum_{\alpha o} \zeta_{\alpha\beta}(Q_m)\, S_{\alpha\beta}(\Omega) \tag{2.1}$$

with the orientation operator

$$S_{\alpha\beta}(\Omega) = \frac{3cos\theta_{\alpha z}cos\theta_{\beta z} - \delta_{\alpha\beta}}{2} \tag{2.2}$$

where α and β axes are in the MOL frame, $cos\theta_{\alpha z}$ is the direction cosine between the Z-axis in the LAB frame and the α axis in the MOL frame and $\delta_{\alpha\beta}$ is the Kronecker delta function. Q_m stands for the m-th vibrational normal mode and finally the $\zeta_{\alpha\beta}$ tensor denotes some electronic property of the solute that can couple with the liquid-crystal solvent field.

This simple model gives a picture of the liquid crystal environment as providing an average second-rank mean field tensor, F_{ij}, that interacts with some second-rank tensorial property, ζ_{ij}, of the solute molecule. Tensor ζ_{ij} is supposed to be determined by the electronic structure and hence the geometry of the solute molecule, and therefore depends on its vibrational coordinates. The potential U is a function of both the vibrational normal modes Q_m of the solute and of the Euler angles Ω that describe its orientation, so it couples

reorientational and vibrational motions. Such potential is treated as a perturbation on the freely rotating and vibrating solute molecule. In a complete perturbation treatment, it was found [6, 15, 19, 34] that only the solute rotational wavefunctions were somewhat affected and that the anisotropic dipolar couplings could be expressed as a sum of various terms.

Consider the following general expression for a dipolar couplings between two nuclei i and j [35]:

$$D_{ij}^{obs} = \sum_{\alpha,\beta} \langle \, d_{ij,\alpha\beta} \, S_{\alpha\beta}(\Omega) \rangle_{\substack{vibrations, \\ rotations}} \tag{2.3}$$

where

$$d_{ij,\alpha\beta} = -\frac{\mu_0 \gamma_i \gamma_j h}{16\pi^3} \cdot \frac{cos\theta_{ij\alpha}cos\theta_{ij\beta}}{r_{ij}^3} \tag{2.4}$$

with μ_0 the vacuum permeability, h the Planck's constant, γ_i and γ_j the magnetogyric ratios of the nuclei i and j, and $\theta_{ij\alpha}$ the angle between the α-axis in the MOL frame and the internuclear vector r_{ij}. The angular brackets of equation (2.3) denote averaging over all the relevant molecular motions, namely the vibrational and reorientational motions of the molecule.

Within the perturbation theory, D_{ij}^{obs} is decomposed in the following contributions [6, 19, 35]:

$$D_{ij}^{obs} = D_{ij}^{eq} + D_{ij}^{a} + D_{ij}^{h} + D_{ij}^{non-rigid} \tag{2.5}$$

In this equation there are two sorts of terms:

- the first three terms, D_{ij}^{eq}, D_{ij}^{a} and D_{ij}^{h}, where averaging over vibrations and reorientations can be carried out independently, leading to contributions of the type:

$$D_{ij}^{w} = \sum_{\alpha,\beta} \langle \, d_{ij,\alpha\beta} \rangle_{vibrations} \langle S_{\alpha\beta}(\Omega) \rangle_{rotations} ; \quad w = eq, a, h \tag{2.6}$$

- the fourth term, $D_{ij}^{non-rigid}$, where this separation cannot be made:

$$D_{ij}^{non-rigid} = \sum_{\alpha,\beta} \langle \, d_{ij,\alpha\beta} \, S_{\alpha\beta}(\Omega) \rangle_{\substack{vibration, \\ rotations}} \tag{2.7}$$

D_{ij}^{eq} is usually the dominant contribution, but the other terms are by no means negligible if one wants to extract accurate bond distances and bond lengths. Moreover, for small degrees of orientational order the relative importance of the non-rigid term compared to the other contributions tends to increase, preventing from accurate solute structure determinations.

The four terms can be written in their explicit form as in the following:

$$D_{ij}^{eq} = d_{ij,\alpha\beta}^{eq} S_{\alpha\beta}$$

$$D_{ij}^{a} = \sum_{m} \left(\frac{\partial d_{ij,\alpha\beta}}{\partial Q_m} \right)^{eq} \langle \, Q_m \rangle_T S_{\alpha\beta}$$

$$D_{ij}^{h} = \frac{1}{2} \sum_{m,n} \left(\frac{\partial^2 d_{ij,\alpha\beta}}{\partial Q_m \partial Q_n} \right)^{eq} \langle Q_m Q_n \rangle_T S_{\alpha\beta}$$

$$D_{ij}^{non-rigid} = \frac{1}{3} \Delta F \sum_{m} \left(\frac{\partial d_{ij,\alpha\beta}}{\partial Q_m} \right)^{eq} \left(\frac{\partial \zeta_{kl}}{\partial Q_m} \right)^{eq} \frac{1}{\omega_m^2} \langle S_{\alpha\beta}(\Omega) S_{kl}(\Omega) \rangle_{rotations} \qquad (2.8)$$

where ω_m is the vibrational frequency of the m-th normal mode, the k and l subscripts run over the components of the second-rank tensorial property ζ_{kl} of the solute molecule, and $S_{\alpha\beta} = \langle S_{\alpha\beta}(\Omega) \rangle_{rotations}$ are the Saupe order parameters that describe the orientational order of the solute in the anisotropic solvent.

From equations (2.8) it is evident that the first three terms, D_{ij}^{eq}, D_{ij}^{a} and D_{ij}^{h}, are proportional to the Saupe order parameters $S_{\alpha\beta}$, so that they can be written according to the following generalized formula:

$$D_{ij}^{w} = -\frac{1}{2} K_{ij} \sum_{\alpha,\beta} S_{\alpha\beta} \left(\Phi_{ij,\alpha\beta}^{w} \right); \quad w = eq, a, h \qquad (2.9)$$

where $K_{ij} = \mu_0 \gamma_i \gamma_j h / 16\pi^3$ and $\Phi_{ij,\alpha\beta}^{w}$ are generic terms. These three contributions to the dipolar couplings can be calculated directly from the known equilibrium geometry and from the anharmonic and harmonic force fields, without any knowledge about the mechanism(s) that determine the solute partial orientation in the nematic solvent. Expressions for the derivatives $\left(\partial d_{ij,\alpha\beta} / \partial Q_m \right)^{eq}$ and $\left(\partial^2 d_{ij,\alpha\beta} / \partial Q_m \partial Q_n \right)^{eq}$ have been given in various places [15, 36-38]. The situation is entirely different for the non-rigid contribution to the dipolar coupling. Indeed, $D_{ij}^{non-rigid}$ has a more complex orientational dependence, of the type $\langle S_{\alpha\beta}(\Omega) S_{kl}(\Omega) \rangle_{rotations}$. Moreover, it depends on the quantity $\left(\partial \zeta_{kl} / \partial Q_m \right)^{eq}$ that is unknown as long as the orienting mechanism is unknown. In the case of methane, a well-characterized molecule that possesses an equilibrium structure with tetrahedral symmetry, this term is the only contribution to the dipolar couplings and it is responsible of the unexpected anisotropic splitting in its NMR spectrum. Hence, the importance of this term can be studied independent from other complications. Although the mechanism(s) that are at the root of the interaction between solute and solvent field are not known, the relevant $\left(\partial \zeta_{kl} / \partial Q_m \right)^{eq}$ parameters can be fitted to the experimentally observed dipolar couplings. In all other less symmetrical solutes, the experimental assessment of the single non-rigid contribution becomes more difficult because, of course, only the whole sum giving the observed D_{ij}^{obs} is known from the experiment. Therefore, $D_{ij}^{non-rigid}$ is admittedly complicated to obtain and it is usually considered as an adjustable parameter [6].

Anyway, a peculiar - and particularly favorable - situation is found when the orientational ordering of the molecule is very small and some of the other contributions to the observed dipolar couplings can be safely neglected. In these cases, the value of the $D_{ij}^{non-rigid}$ term can be experimentally calculated. Such a situation may occur when a highly symmetric rigid solute is dissolved in an uniaxial nematic thermotropic liquid crystal. In this context we studied the case of the tetramethylallene (TMA), a *quasi*-spherical molecule possessing a D_{2d} symmetry, dissolved in the nematic solvent 4-ethyl-2-fluoro-4'-[2-(*trans-4-n*-pentylcyclohexyl)ethyl]biphenyl, commonly known as I52. Structure, molecular frame, and atom numbering of TMA and chemical structure of I52 are reported in Figure 2.1. In the numbering of TMA, the carbon and protons of a first methyl group were labeled as [13]C1, H2, H3, and H4, while the other equivalent methyl protons they are coupled to are considered as groups and are labeled 5, 6, and 7. Note that the symmetry of the molecule in the non-chiral nematic LC requires only one order parameter (namely, S_{aa}) to describe the orientational ordering of the solute (see Table 1.3 in chapter 1).
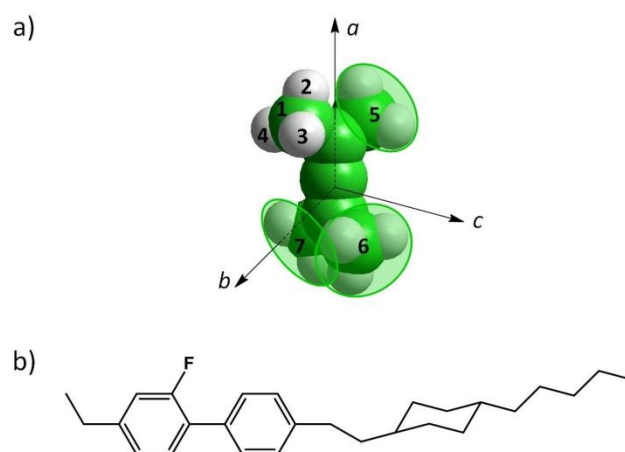
Figure 2.1. (a) "Balls" structure, atomic labeling and molecular frame of the D_{2d} symmetry tetramethylallene (TMA) and (b) topological structure of the liquid crystal I52.

2.2.1.   *Analysis of proton and carbon spectra of TMA dissolved in I52*

Proton and carbon spectra of a sample of TMA/I52 (∼2.3 wt %, see Appendix A3) were recorded on a Bruker Avance 500 MHz instrument (11.74 T) equipped with a BBI probe and analyzed by the homemade iterative program ARCANA [39], in order to collect the experimental [1]H-^{1}H and [1]H-^{13}C dipolar couplings. Spectra were recorded upon cooling from the isotropic phase, throughout the range of the nematic phase, with 40-50 min intervals of

thermostabilization for each value of the working temperature, T. A preliminary T calibration curve was performed and an accuracy of 0.5 K on the T-control was provided by a standard variable-temperature unit BVT-2000 and a B-TO2000 thermocouple.

It is common to introduce a reduced temperature, T_{red}, defined as the ratio between the working temperature, T, and the nematic-isotropic phase-transition temperature of the solution, T_{NI}:

$$T_{red} = \frac{T}{T_{NI}} \qquad (2.10)$$

This dimensionless quantity allows a direct comparison of temperature values regardless of sample concentration or temperature unity control of the spectrometer. In terms of reduced temperature the ^{1}H spectra were collected in the range 0.70 - 0.99. Figure 2.2 shows the experimental ^{1}H spectra at some different values of T_{red}.
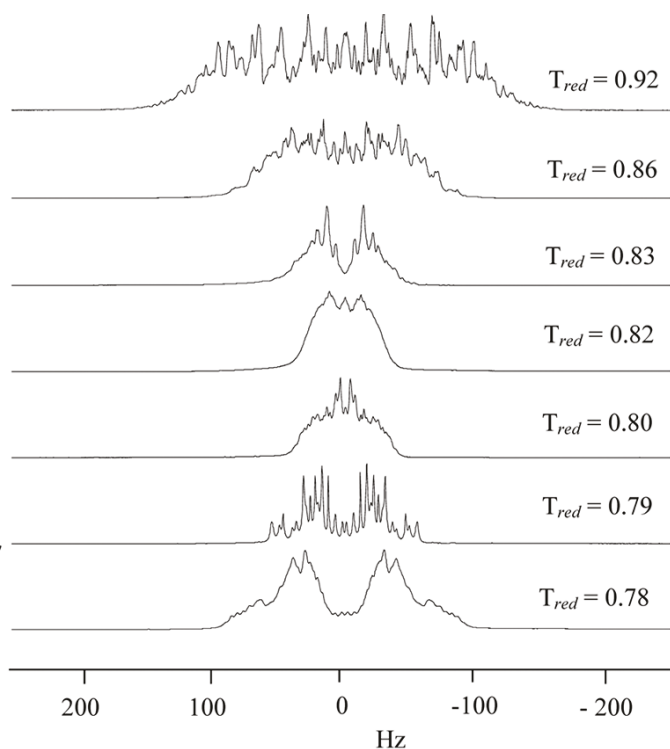
Figure 2.2. 500 MHz experimental ^{1}H spectra of TMA dissolved in I52 at different values of T_{red}.

Unfortunately, as a result of the low ordering of the solute and the high number of transitions of the 12-spin system, some spectra appear crowded with quite broad lines, so that an extremely thorough analysis was possible only for some more resolved spectra. Two crucial features, however, can be clearly appreciated: (*i*) all the spectra are characterized by a whole spectral width of only a few tens of Hertz, indicating a very weak orientational order of the

molecule; (*ii*) a peculiar behavior can be observed on cooling, that is the spectral width initially decreases until it reaches its minimum value at T_{red} = 0.82 (where the narrowest spectrum is recorded), then it starts to increase again at lower temperatures. The latter point is particularly intriguing and it may suggest two possible explanations: S_{aa} changes its sign (scenario *a*) or reaches a minimum/maximum (scenario *b*) at about T_{red} = 0.82. As discussed in the following, even if the hypothesis *a* of the change of sign appears the most intuitive, it is not fully satisfactory because it conflicts with other reasonable considerations that can be made about our system.

The more resolved ^{1}H spectrum corresponds to the T_{red} = 0.79, where the D_{26} is zero (see below) and the proton NMR spectrum is simply described by two coupled methyl groups (*i.e.* the same 6-spin system as that of acetone). This explains the relatively simple spectrum obtained. The comparison between the experimental and fitted spectrum at this T_{red} is displayed in Figure 2.3.
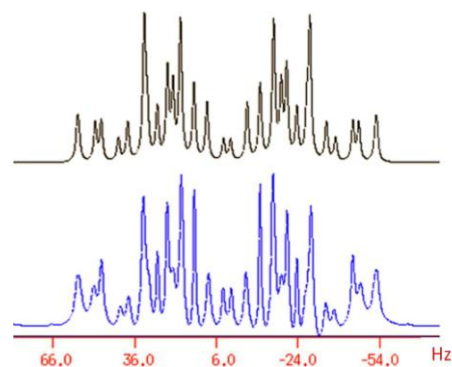
Figure 2.3. Comparison between the experimental (on the bottom) and the calculated (on the top) spectra for the best case (T_{red} = 0.79). The dipolar couplings used to obtain the calculated spectrum are those reported in Table 2.1. Moreover, only J_{25} has been set slightly different from 0 (J_{25} = -0.2 Hz) to reproduce some fine features of the spectrum.

The analysis of the proton spectra at T_{red} = 0.77, 0.79, 0.83 and 0.86 gave the set of three D_{HH} reported in the last three lines of Table 2.1. Despite the low resolution of the spectra, the D_{ij}^{obs} values we extracted are the only ones able to reproduce, at best, our experimental spectra and can thus be considered reliable enough to carry out our study at a semi-quantitative level. The main problem is that, together with the magnitudes, only the relative signs of the three D_{HH} couplings can be determined from the proton spectra.

To resolve such ambiguity, ^{13}C NMR spectra revealed essential, since $^1D_{CH}$ (corresponding to D_{12}^{obs}) is the only D_{ij}^{obs} for which the magnitude and absolute sign can be

assigned unequivocally. Each ^{13}C NMR spectrum resulted to be basically composed by the lines resulting from the C1 carbon coupled with the three equivalent protons H2, H3, and H4, so producing a quadruplet from which the D_{12} dipolar coupling constant was extracted by fixing J_{12} = +127 ±0.3 Hz (value obtained from the isotropic spectrum of TMA in CDCl$_3$). Unfortunately, the ^{13}C spectra showed a satisfactory signal-to-noise ratio only at three T_{red}, in common with the ^{1}H spectra, namely 0.79, 0.83 and 0.86. The values extracted at these T_{red} are reported in the first line of Table 2.1.

Table 2.1. Observed dipolar couplings D_{ij}^{obs} (in Hz) of TMA in I52.

T_{red}	0.77	0.79	0.83	0.86
D_{12}	not determined	9.92 ± 0.10	4.82 ± 0.17	2.92 ± 0.47
D_{23}	14.87 ± 0.30	9.70 ± 0.20	9.13 ± 0.11	12.26 ± 0.20
D_{25}	-14.89 ± 0.25	-8.11 ± 0.10	-7.61 ± 0.11	-10.07 ± 0.18
D_{26}	2.61 ± 0.60	0.04 ± 0.15	2.18 ± 0.50	4.29 ± 0.60

2.2.2. Data interpretation and calculation of the order parameter

Two possible scenarios, *a* and *b*, were considered for the explanation of the experimental observations. Although none of them is fully satisfactory in explaining all the observations, both converge in indicating that the contribution to the dipolar couplings accounting for the vibrational-reorientational correlation plays a very important role.

Scenario a. The first hypothesis is that the three D_{HH} couplings change sign at some T_{red} between 0.79 and 0.83 as a consequence of the fact that S_{aa} crosses through 0. According to the literature, the non-rigid contribution for the long-range D_{26} as well as the anharmonic and harmonic contributions for all three interproton couplings are usually very small or even negligible [40-45] (less than 1%). Following these assumptions, we can simply write from equation (2.5):

$$D_{23}^{obs} \approx D_{23}^{eq} + D_{23}^{non-rigid}$$
$$D_{25}^{obs} \approx D_{25}^{eq} + D_{25}^{non-rigid}$$
$$D_{26}^{obs} \approx D_{26}^{eq} \tag{2.11}$$

Contrarily, the anharmonic and harmonic contributions to D_{12}^{obs} cannot be neglected:

$$D_{12}^{obs} \approx D_{12}^{eq} + D_{12}^{a} + D_{12}^{h} + D_{12}^{non-rigid} \tag{2.12}$$

The surviving term D_{26}^{eq} is seen to vanish at T_{red} about 0.79 (see Table 2.1), and this could be read as a symptom that S_{aa} is about 0 at that T_{red}. As a consequence, the contributions D_{23}^{eq}, D_{25}^{eq} and D_{12}^{eq} should vanish at T_{red} = 0.79, too, so that:

$$\left(D_{23}^{obs}\right)_{T_{red}=0.79} \approx \left(D_{23}^{non-rigid}\right)_{T_{red}=0.79}$$

$$\left(D_{25}^{obs}\right)_{T_{red}=0.79} \approx \left(D_{25}^{non-rigid}\right)_{T_{red}=0.79}$$

$$\left(D_{12}^{obs}\right)_{T_{red}=0.79} \approx (D_{12}^{a})_{T_{red}=0.79} + \left(D_{12}^{h}\right)_{T_{red}=0.79} + \left(D_{12}^{non-rigid}\right)_{T_{red}=0.79} \quad (2.13)$$

There are, however, a couple of considerations that argue against this very simple and physically sensible interpretation of the data. First of all, the values of D_{23}^{obs} and D_{25}^{obs} reported in Table 2.1 seem too large to be due exclusively to the non-rigid term. This prompted us to test indirectly the influence of the non-rigid contributions on D_{23}^{obs} and D_{25}^{obs} by plotting the ratio $D_{23}^{obs}/D_{25}^{obs}$ as a function of the T_{red}. Since our D_{2d} molecule requires that all except non-rigid contributions to the D_{ij} be proportional to the S_{aa} order parameter, the ratios between the experimental dipolar couplings are expected to be essentially independent of T when the non-rigid contributions are negligible. The ratio $D_{23}^{obs}/D_{25}^{obs}$ for the four considered T_{red} is shown in Figure 2.4.
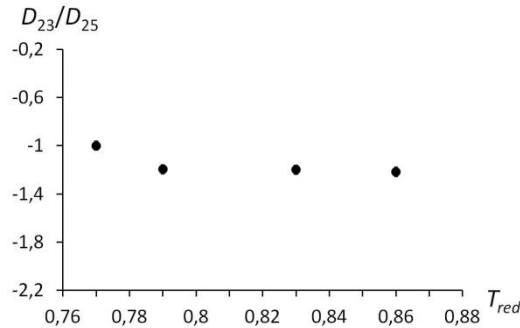

Figure 2.4. D_{23}/D_{25} ratio and corresponding error as a function of the reduced temperature.

A temperature-independence of the $D_{23}^{obs}/D_{25}^{obs}$ ratio is observed, more markedly between T_{red} = 0.79 and T_{red} = 0.86, suggesting that both D_{23}^{obs} and D_{25}^{obs} are approximately devoid of non-rigid effects. In this case, since the harmonic and anharmonic terms scale as S_{aa}, thus entailing very small corrections to the already small couplings, we should reject what was said above, and on the contrary, we should write:

$$D_{23}^{obs} \approx D_{23}^{eq}$$

$$D_{25}^{obs} \approx D_{25}^{eq} \quad (2.14)$$

A second criticism against the scenario a is based on the decreasing of D_{12}^{obs} with increasing T_{red}. Such reduction should be due to an additional, opposite in sign, contribution to the non-rigid term. Admitting that D_{12}^{eq} is much greater than D_{12}^a, D_{12}^h, and considering that D_{12}^{eq} has opposite sign with respect to S_{aa}, in order to have a negative additional contribution to $D_{12}^{non-rigid}$ at T_{red} = 0.83, we should have a positive order parameter. In the scenario a, where S_{aa} changes its sign crossing through 0 at $T_{red} \approx 0.79$, this means that the order parameter is negative at temperatures lower than T_{red} = 0.79 and becomes positive for higher temperatures. This result seems counterintuitive, because the solute would prefer the parallel alignment for higher temperatures (where the orientational thermal disorder is higher) whereas it would adopt a more hampered perpendicular orientation when the temperature is lower and the thermal disorder is less important. Assuming the more reasonable trend for S_{aa}, that is positive for T_{red} < 0.79 and negative for T_{red} > 0.79, the behavior of D_{12}^{obs} as a function of the T_{red} becomes inexplicable, because after T_{red} = 0.79, D_{12}^{eq} is positive and adds up to $D_{12}^{non-rigid}$ so that an increase of D_{12}^{obs} with the increase in temperature should be expected. These two argumentations make the hypothesis a not completely satisfactory.

Scenario b. If the change of sign of S_{aa} does not occur, the order parameter has to be necessarily negative (as a result of the D_{12}^{obs} trend), and the dipolar couplings pass through a minimum/maximum when S_{aa} reaches its smallest possible magnitude. Looking at Figure 2.5, it is realized that the three interproton dipolar couplings share their minimum magnitude at the same $(T_{red})_{min}$ of about 0.82 (exactly the temperature where the experimental ^{1}H spectrum shows its narrowest spectral width), while the minimum of the [13]C-^{1}H dipolar coupling falls at T_{red} > 0.86.
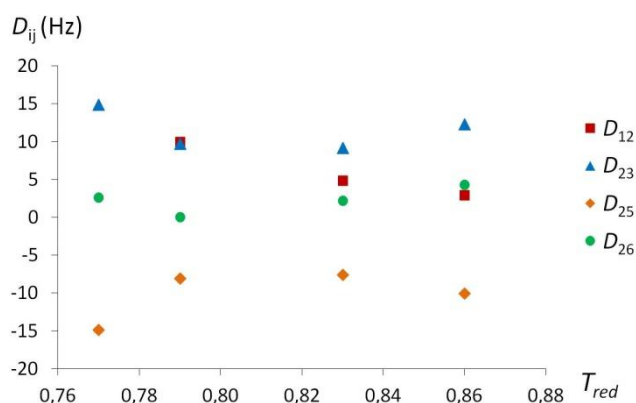
Figure 2.5. Behaviors of D_{12} (red square), D_{23} (blue triangle), D_{25} (orange rhombus) and D_{26} (green circle) as a function of T_{red} when S_{aa} < 0 is assumed.

Keeping the approximation of neglecting the vibrational contributions we get:

$$D_{23}^{obs} \approx D_{23}^{eq}$$

$$D_{25}^{obs} \approx D_{25}^{eq}$$

$$D_{26}^{obs} \approx D_{26}^{eq} \qquad (2.15)$$

Following this assumption, it is very simple to calculate the values of S_{aa} (reported in Table 2.2 and shown in Figure 2.6) from the interproton dipolar couplings D_{23} and D_{25} at the different temperatures. In the calculation we adopted the following standard regular geometries for the molecule: C=C = 1.31 Å, C-C$_{Me}$ = 1.50 Å, C-H = 1.11 Å, C$_{Me}$ĈC$_{Me}$ = 120°, and regular tetrahedral structures. For the description of the rotation of methyl groups when calculating intermethyl couplings, we used the usual 120° three site jump model, exploiting the 3-fold symmetry of the methyl groups and "freezing" them in their sterically less hindered conformations (RIS model). Note that the observed D_{26} couplings have been excluded in this case from the calculation of the order parameter because they are too small and affected by large relative errors. Their inclusion leads to the same values of S_{aa} even though affected by quite high relative errors. D_{12} was not used in the calculation due to its vibrational dependence.

Table 2.2. Values of the order parameter S_{aa} and the calculated dipolar couplings D_{23}^{calc} and D_{25}^{calc} (in Hz) of TMA in I52 at different reduced temperatures. The RMS between observed and calculated D_{ij} is also reported.

T_{red}	0.77	0.79	0.83	0.86
D_{23}^{calc}	14.29	8.52	8.01	10.68
D_{25}^{calc}	-15.42	-9.20	-8.65	-11.53
RMS	0.55	1.13	1.08	1.52
S_{aa}	-0.0119 ± 0.0005	-0.0070 ± 0.0009	-0.0070 ± 0.0009	-0.009 ± 0.0013

In Figure 2.6, it is seen that the minimum of magnitude of the S_{aa} order parameter falls at $(T_{red})_{min} \approx 0.82$, the temperature where the interproton dipolar couplings are simultaneously the smallest ones in magnitude and the ^{1}H spectrum is the narrowest one.
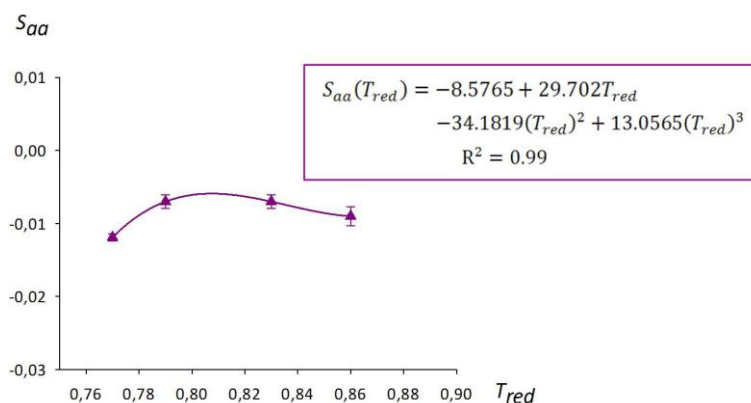
Figure 2.6. Behavior of the S_{aa} order parameter as a function of T_{red}. The cubic fitting of the curve is also shown. The value S_{aa}=0 at T_{red} = 1 has been added as a boundary condition for the fitting of the curve.

A first important conclusion then is that the hypothesis *b*, the presence of a minimum of magnitude for S_{aa}, appears to be the most reasonable explanation for the observed data. What is more, we tried at this point to evaluate at a semi-quantitative level the different contributions playing a role in the remaining C-H coupling D_{12}^{obs}.

2.2.3.   Quantification of the vibration-reorientation contribution

From equation (2.5) we can write:

$$\Delta_{12} \equiv D_{12}^{obs} - D_{12}^{eq} \approx D_{12}^{a} + D_{12}^{h} + D_{12}^{non-rigid} \tag{2.16}$$

where the D_{12}^{eq} are calculated by using the S_{aa} values of Table 2.2. In Table 2.3, the obtained D_{12}^{eq} and Δ_{12} are reported.

Table 2.3. Values of D_{12}^{eq} and Δ_{12} (in Hz) of TMA in I52 at different reduced temperatures obtained by using the S_{aa} values of Table 2.2. The errors affecting the D_{12}^{eq} values have been estimated, by error propagation, from the corresponding errors on the order parameter.

T_{red}	0.79	0.83	0.86
D_{12}^{eq}	6.36 ± 0.25	5.98 ± 0.48	7.97 ± 1.11
Δ_{12}	3.56 ± 0.35	-1.16 ± 0.68	-5.05 ± 1.58

By following equation (2.9), the sum of harmonic and anharmonic contributions can be collected as:

$$D_{12}^a + D_{12}^h = -S_{aa}\Gamma_{12} \tag{2.17}$$

where

$$\Gamma_{12} = \frac{1}{2}K_{ij}\left(\Phi_{12,aa}^a + \Phi_{12,aa}^h\right) \tag{2.18}$$

Then equation (2.16) becomes:

$$\Delta_{12} \approx -S_{aa}\Gamma_{12} + D_{12}^{non-rigid} \tag{2.19}$$

Since S_{aa} as a function of T_{red} is known from the interproton dipolar couplings, if we are able to determine the Γ_{12} term of equation (2.18), we can thus quantitatively assess, within the approximations used in the derivation, the $D_{12}^{non-rigid}$ contribution from equation (2.19).

To evaluate Γ_{12} without force fields and theoretical calculations about harmonic and anharmonic vibrational corrections affecting D_{12}^{obs}, it can be useful to plot Δ_{12} as a function of T_{red} (Figure 2.7).

$$\Delta_{12}(T_{red}) = 590.0644 - 1313.9702T_{red}$$
$$+723.8776(T_{red})^2$$
$$R^2 = 0.98$$
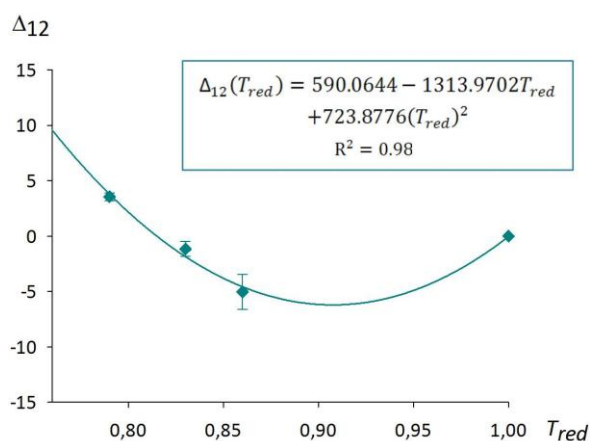
Figure 2.7. Behavior of Δ_{12} as a function of T_{red}. The quadratic fitting of the curve is also shown. The value $\Delta_{12} = 0$ at $T_{red} = 1$ has been added as a boundary condition.

Note that Δ_{12} crosses through 0, changing its sign, at $T_{red} = 0.82$, that is the $(T_{red})_{min}$ of the three interproton dipolar couplings. Because when $\Delta_{12} = 0$ then $D_{12}^{obs} = D_{12}^{eq}$, this result seems to suggest that at least at $T_{red} = 0.82$, only the equilibrium contributions survive for all the dipolar couplings, including D_{12}^{obs}. This can occur when the single D_{12}^a, D_{12}^h and $D_{12}^{non-rigid}$ are negligibly small (as we assumed for interproton couplings in the whole temperature range), or when it does exist a perfect balance of the effects, such that from equation (2.19) we got:

$$\left(D_{12}^{non-rigid}\right)_{T_{red}=0.82} = \Gamma_{12}(S_{aa})_{T_{red}=0.82} \tag{2.20}$$

Equation (2.20) cannot be directly exploited to determine $D_{12}^{non-rigid}$, because the non-rigid contribution itself is involved. On the other hand, if we consider Γ_{12} to be independent of T_{red} (which is a reasonable approximation), we can exploit the fact that the function $\Delta_{12}(T_{red})$ reaches its minimum at T_{red} = 0.91 (see Figure 2.7); so, its derivative calculated there must vanish. Then the following relation holds:

$$\left(\frac{\partial \Delta_{12}}{\partial T_{red}}\right)_{T_{red}=0.91} = -\Gamma_{12}\left(\frac{\partial S_{aa}}{\partial T_{red}}\right)_{T_{red}=0.91} + \left(\frac{\partial D_{12}^{non-rigid}}{\partial T_{red}}\right)_{T_{red}=0.91} = 0 \tag{2.21}$$

So that Γ_{12} is given by:

$$\Gamma_{12} = \left(\frac{\partial D_{12}^{non-rigid}}{\partial T_{red}}\right)_{T_{red}=0.91} \bigg/ \left(\frac{\partial S_{aa}}{\partial T_{red}}\right)_{T_{red}=0.91} = \frac{B}{A} \tag{2.22}$$

with

$$A = \left(\frac{\partial S_{aa}}{\partial T_{red}}\right)_{T_{red}=0.91} \tag{2.23}$$

$$B = \left(\frac{\partial D_{12}^{non-rigid}}{\partial T_{red}}\right)_{T_{red}=0.91} \tag{2.24}$$

By introducing equation (2.22) in equation (2.19) we obtain the following explicit general equation giving the $D_{12}^{non-rigid}$ contribution as a function of T_{red}:

$$D_{12}^{non-rigid}(T_{red}) \approx \Delta_{12}(T_{red}) + S_{aa}(T_{red})\Gamma_{12} = \Delta_{12}(T_{red}) + S_{aa}(T_{red})\frac{B}{A} \tag{2.25}$$

In order to use such equation, we should be able to evaluate the terms A and B. The term A can be calculated by the equation corresponding to the cubic fitting shown in Figure 2.6:

$$S_{aa}(T_{red}) = -8.5765 + 29.702T_{red} - 34.1819(T_{red})^2 + 13.0565(T_{red})^3 \tag{2.26}$$

Then we have:

$$A = \left(\frac{\partial S_{aa}}{\partial T_{red}}\right)_{T_{red}=0.91} = 29.702 - 68.3638(0.91) + 39.1695(0.91)^2 = -0.0728 \tag{2.27}$$

The calculation of B is more complicated. Assuming B is constant within a very narrow range of T_{red} in the proximity of the minimum of Δ_{12} (T_{red} = 0.91), we will consider the following limit expressions:

$$D_{12}^{non-rigid}(T_{red} = 0.91) \approx \Delta_{12}(0.91) + S_{aa}(0.91)\frac{B}{A} \tag{2.28}$$

$$\lim_{T_{red}\to 0.91^+} D_{12}^{non-rigid}(T_{red}) \equiv D_{12}^{non-rigid}(0.91) \tag{2.29}$$

$$\lim_{T_{red}\to 0.91^-} D_{12}^{non-rigid}(T_{red}) \equiv D_{12}^{non-rigid}(0.91) \tag{2.30}$$

The limits reported above for equations (2.29) and (2.30) (approaching 0.91 from the right and left but, of course, never reaching exactly 0.91) have been calculated numerically from equation (2.25), by exploiting equation (2.26) for the evaluation of the function $S_{aa}(T_{red})$ and the equation corresponding to the quadratic fitting of $\Delta_{12}(T_{red})$, shown in Figure 2.7:

$$\Delta_{12}(T_{red}) = 590.0644 - 1313.9702 T_{red} + 723.8776(T_{red})^2 \qquad (2.31)$$

By using the A value of equation (2.27), equations (2.29) and (2.30) converge to equation (2.28) for B = -3.487.

Finally, by introducing the A and B values in equation (2.25) we obtain:

$$D_{12}^{non-rigid}(T_{red}) \approx \Delta_{12}(T_{red}) + 47.9 S_{aa}(T_{red}) \qquad (2.32)$$

By calculating the non-rigid contributions for $D_{12}^{non-rigid}$ at the three experimental temperatures, we obtained the results reported in Table 2.4.

Table 2.4. Values of $D_{12}^{non-rigid}$ (in Hz) of TMA in I52 at different reduced temperatures. The errors have been estimated, by error propagation, starting from those affecting the Δ_{12} and the order parameters.

T_{red}	0.79	0.83	0.86
$D_{12}^{non-rigid}$	3.44 ± 0.39	-2.15 ± 0.72	-5.00 ± 1.64

Knowing $D_{12}^{non-rigid}$, D_{12}^{obs}, and D_{12}^{eq} as functions of T_{red}, we can also obtain, by difference, the contribution $(D_{12}^{a} + D_{12}^{h})$ *vs* T_{red}. The behaviors of the different contributions are plotted in Figure 2.8. It is worth emphasizing that the information emerging from the figure should be considered only at a semi-quantitative level. It can be seen that in the scenario *b*, the non-rigid contribution (blue large-dashed line) basically represents the whole Δ_{12} (red small-dashed line). In other words, the difference between D_{12}^{obs} and D_{12}^{eq} dipolar coupling terms seems to be essentially due to the reorientation-vibration correlation, while the sum of the harmonic and anharmonic contributions (yellow dotted line) plays a very minor role. This predominance is reasonably due to the fact that our solute is a very symmetric and *quasi-spherical* molecule, so that a very low orientational ordering (linearly affecting D_{12}^{a} and D_{12}^{h}) has to be expected. TMA in I52 possesses then a "methane-like" behavior, which can be associated with that described not only for methane [5, 13-15, 46-51] but also for other very symmetric (about spherical) molecules [4, 16-17, 50, 52] dissolved in uniaxial orienting mesophases. Of course, the imperfect reliability of our observed dipolar couplings and/or the adopted assumptions and approximations are likely to bias our results and conclusions. For instance, the scenario *b* describes a situation where the order parameter would have a

minimum of magnitude at $(T_{red})_{min}$ = 0.82. Hypothetical suggestions to explain such trend may include competition between opposite ordering/disordering mechanisms and collective phase order effects due to the TMA doping, but definitely there are no resolutive explanations and the issue will be addressed in the future. However, although the calculations are evidently approximate, we are convinced that the significant predicted values of $D_{12}^{non-rigid}$ are physically sensible, thus representing a very important contribution to the experimental D_{12}^{obs}.
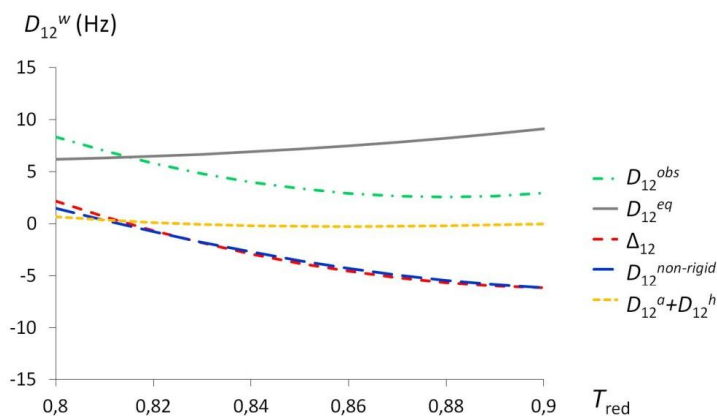
Figure 2.8. Different D_{12} contributions as a function of T_{red}: $D_{12}^{non-rigid}$ (blue large-dashed line), D_{12}^{a} + D_{12}^{h} (yellow dotted line), and D_{12}^{eq} (gray solid line). For comparison, $D_{12}^{obs} = D_{12}^{eq} + D_{12}^{a} + D_{12}^{h} + D_{12}^{non-rigid}$ (green dotted-dashed line) and $\Delta_{12} = D_{12}^{obs} - D_{12}^{eq} = D_{12}^{a} + D_{12}^{h} + D_{12}^{non-rigid}$ (red small-dashed line) have been plotted. The large errors affecting the curves are not shown in the figure.

2.2.4. Conclusions

The essence of the phenomenon of reorientation-vibration coupling has been investigated and a semi-quantitative assessment of the non-rigid contribution to the ^{13}C-^{1}H dipolar coupling has been derived, within some approximations, from NMR study of the very weak orientationally ordered molecule TMA in I52. Two possible interpretations of the experimental observations have been presented and discussed with their pros and cons. In any case, the main result is that the reorientation-vibration interaction represents a fundamental contribution to the value of the observed experimental dipolar coupling, further confirming the conclusions given in the past for perfectly symmetric molecules dissolved in liquid crystalline phases. Although the amounts of approximations used probably affects the accuracy in the outcome, final results can be considered quite plausible in indicating the magnitude of $D_{12}^{non-rigid}$. These results have been published in a paper [53] reported at the end of the thesis.

2.3.   Study of rigid probe solutes in smectic phases: determination of positional order parameters

The distinctive feature of smectic liquid crystals is their layered structure [54]. This means their constituent particles both have an orientational order, as in the more common nematic phase, and a *quasi* long-range one-dimensional positional order. As described in chapter 1, smectics further differentiate on the basis of the orientation that molecule long axes preferentially take with respect to the layer normal and of the degree of positional order within a given layer. In the simplest case, the smectic A (SmA) phase, particles preferentially orient along the layer normal (the director $\hat{d}$ points along the smectic layer normal) [55-56] and possess a short-range, liquid-like in-layer positional order. This state of affairs readily complicates when molecules do not preferentially arrange side-by-side but in some shifted configuration, as in the case of the bilayer A_2 and interdigitated bilayer A_d smectic phases.

The degree of orientational and positional order is quantitatively expressed by a number of order parameters. Whereas several experimental techniques are able to measure orientational order parameters [26-32], perhaps surprisingly there is no straightforward experimental method to quantitatively assess the extent of layering.

Positional order can be readily quantified through a series of parameters τ_k, defined as [56-57]:

$$\tau_k = \frac{1}{\delta} \int_0^{\delta} dz \, cos\left(2\pi k \frac{z}{\delta}\right) \rho(z) \qquad (2.33)$$

with $\rho(z)$ the distribution function of z, the molecular centre displacement from the mid-layer position resolved along the director $\hat{d}$, δ the layer spacing and k a positive integer. Note that the definition of equation (2.33) implies that $z = 0$ corresponds to the center of a layer, where $\rho(z)$ takes its maximum value. These parameters τ_k quantify the extent of layering with $\tau_k = 0$ meaning absence of a layered structure and $\tau_k = 1$ corresponding to molecules locked in the mid-layer positions. Positional order parameters can be measured of course both for the liquid crystal solvent Σ (τ_k^{Σ}) and the solute σ (τ_k^{σ}).

Yet the very value borne by these parameters is experimentally hard to know for a molecular smectic liquid crystal. Diffraction techniques would appear as the most suited to investigate positional order in smectics. Such methods provide accurate values of the layer spacing, δ, that for a SmA phase turns out of the order of the molecular length. Unfortunately, they cannot provide as straightforwardly also the values of the parameters τ_k. Indeed, it can be shown [29] that the quantities directly measured in a diffraction experiment, *i.e.* the relative scattering intensities of the k-th layer diffracted peak, I_{00k}, are proportional to $\tau_k{}^2$,

but the constant of proportionality, that is the value of I_{00k} for the perfectly ordered smectic, I_{00k}^P, is unknown. Particular assumptions on I_{00k}^P may lead to an estimate of ratios of the type $\tau_{k'}/\tau_{k''}$, though, in practice, only peaks up to the second only can be detected, so that solely the ratio τ_2/τ_1 can be effectively measured in a diffraction experiment [57]. In order to obtain values of the parameters τ_k, the use of a Gaussian shape for $\rho(z)$ was proposed in the past [58-60]. To further improve such procedure, two methods have been recently reported, that lead to the measurement of the parameter τ_1 for a range of smectogenic materials [61-62].

In recent years, the problem of determining positional order parameters in smectics was being addressed from viewpoints other than the traditional one based on diffraction techniques and NMR spectroscopy is at the heart of these new attempts. Two different pathways were followed. In one case, proton NMR was used to determine the diffusion coefficients in the N and SmA phases and then these data were related to the τ_k's *via* a theoretical model validated by computer simulations [63]. In the other cases, rigid and relatively small molecules were dissolved in a smectogenic solvent and their Saupe ordering matrices determined *via* liquid-crystal NMR spectroscopy. The aim of these studies is to exploit the fine changes that the orientational order parameters of certain solutes may undergo upon the onset of layering to get information on the positional order of the smectic liquid crystalline solutions. These studies can be further subdivided in two groups depending on how they analyse solutes' $S_{\alpha\beta}$ matrix. This analysis has important consequences on what can be unveiled about the structure of the smectic liquid-crystalline solutions. A first series [64-68] makes use of mean-field models, developed from the classic Maier-Saupe and McMillan theories, and their outputs are the positional order parameters of the solutes. In the second group instead [33, 69], a statistical thermodynamic density-functional theory (ST-DFT), developed from the classic Onsager theory, is used that expresses solutes' positional-orientational distribution function in terms of the solvent's positional-orientational distribution. The main advantage is this method allows the determination not only of the positional distribution functions of the solute molecules (from which the τ_k^σ solute's positional order parameters can be derived), but also of positional distribution function of the solvent, which leads to the desired τ_k^Σ solvent's positional order parameters. Note that as the solutions are sufficiently dilute (~2-3% by mole fraction), these parameters should not differ from those characterizing the pure smectic solvent.

This part of the Ph.D. work belongs to the above-mentioned second group. The method has been recently applied to the determination of the positional order parameter of the smectogenic liquid crystal solvent 4,4'-di-*n*-heptylazoxybenzene (HAB) through the probe

solutes 1,4-dichlorobenzene (DCB) and naphthalene (NFT) [33]. In the present project, new experimental data for the Saupe ordering matrices of the solutes biphenylene (BIF) and pyrene (PYR) dissolved in the nematic and smectic A phases of HAB were determined and then merged with those previously determined to form a larger set, with which potentialities and limits of the ST-DFT-based methodology can be better assessed.

As stated before, the study of smectic LCs when modified forms of the conventional non-polar monolayer smectic A phase are considered is more complicated. Encouraged by the results obtained for a typical SmA phase, the ST-DFT methodology has been then tested on such a more delicate situation. In particular we chose as liquid crystalline solvent of interest the partial bilayer smectic A phase of the 4-*n*-octyloxy-4'-cyanobyphenyl (8OCB), a member of the well-known *n*-alkoxycyanobiphenyl series of liquid crystal molecules (*n*OCB).

All this part of the project was carried out in collaboration with Prof. Giorgio Cinacchi at the University of Madrid, who first developed the ST-DFT method. Therefore, in the following paragraphs a description of the NMR experiments and a discussion of the data acquired will be given, with emphasis on the information one can extract from them. A very concise picture of the methodology underlying the ST-DFT approach will be given as essential tool to understand the results. For an accurate theoretical description of the methodology, including calculation details and implementation for the smectic A_d case, the reader is referred to the first papers [33, 69] and those published during this thesis [70-71].

2.3.1. Concise recall of the methodology

The key point of the ST-DFT approach is that, for those particular binary mixtures whose one of the component, the liquid crystal solvent Σ, is in large majority with respect to the second component, the solute σ, the following relationship between the positional-orientational distribution function of solute $\rho_\sigma(z, \Omega)$ and the positional-distribution function of the solvent $\rho_\Sigma(z', \Omega')$ stands [33]:

$$\rho_\sigma(z,\Omega) = \frac{1}{\Lambda} e^{-2\Psi \int_{-\infty}^{+\infty} dz' \int d\Omega' \rho_\Sigma(z',\Omega') A_{\sigma\Sigma}(z-z', \Omega, \Omega')} \quad (2.34)$$

where Λ is a normalization constant, z and z' define the position of the solute's and solvent's center of mass along $\hat{d}$, and Ω are the usual Euler angles defining the orientational state. Ψ is a prefactor which helps correct in an effective way for the neglect of higher-order terms involving ever more complicated integrals. It is a solvent property only that can be interpreted as the solvent's effective density. Finally, $A_{\sigma\Sigma}(z - z', \Omega', \Omega)$ is a specific function measuring

the solute-solvent interactions. A more rigorous derivation is given in references [33, 69]; here the purpose is only to illustrate that, in the very dilute limit, $\rho_\sigma(z, \Omega)$ is linked to the positional-orientational distribution function of the solvent *via* the function $A_{\sigma\Sigma}$. Note that the dilute limit is the condition under which we operate since, if the solutions are dilute, it is reasonable to expect that these parameters are, at most, only slightly different from those of the pure smectic liquid crystal.

In a good approximation [72], $\rho_\Sigma(z', \Omega')$ can be written as depending on three parameters: the layer spacing δ, the solvent orientational order parameter η, and the smectic amplitude λ, a parameter that accounts for the strength of the positional mean-field potential energy. Therefore, in combination with equation (2.29), within this approximation, the positional-orientational distribution function of the solute $\rho_\sigma(z, \Omega)$ depends solely on four parameters: Ψ, λ, δ, and η. The NMR investigation of the solvent allows the experimental determination of the term η, while other parameters can be determined by a fitting procedure of the experimental Saupe ordering matrices of a number of solutes $[S_{\alpha\beta}]_\sigma^{exp}$, obtained by means of NMR, to the corresponding ones calculated by the ST-DFT, $[S_{\alpha\beta}]_\sigma^{calc}$. The quantity one is required to minimize is:

$$\tilde{\chi}^2 = \frac{1}{\upsilon} \sum_\sigma \sum_{\alpha\beta} \left\{ [S_{\alpha\beta}]_\sigma^{exp} - [S_{\alpha\beta}]_\sigma^{calc} \right\}^2 \tag{2.35}$$

with υ the number of data minus the number of parameters and the two sums running over the solute molecules dissolved and the independent elements of their respective Saupe ordering matrices.

From the above, some key points are now clear: (*i*) NMR spectroscopy is a particularly indicated technique since it gives access to essential experimental data both for the solvent (the parameter η) and for the solute (the Saupe ordering matrices $[S_{\alpha\beta}]_\sigma^{exp}$); (*ii*) small rigid molecules act as probes of the smectic solvent structure and provide the set of Saupe ordering matrices necessary for the fitting procedure; (*iii*) aiming at fitting the three parameters Ψ, λ and δ, a large set of Saupe ordering matrices of different solutes is preferable. In the following such methodology will be applied to the smectogenic liquid crystal solvents HAB and 8OCB.

To make the just described methodology, ST-DFT combined with liquid crystal NMR, more clear, it is useful to resume the main points in a flowchart (Figure 2.9).

$$\text{TARGET} \implies \tau_k = \frac{1}{\delta}\int_0^\delta dz\, cos\left(2\pi k\frac{z}{\delta}\right)\rho(z)$$

$\tau_k = 0$ absence of a layered structure
$\tau_k = 1$ molecules locked in the mid-layer positions

ST-DFT MODELISATION

CASE of SOLUTE σ: modelisation of $\rho_\sigma(z,\Omega)$ $\implies$ τ_k^σ

CASE of SOLVENT Σ: modelisation of $\rho_\Sigma(z',\Omega')$ $\implies$ τ_k^Σ

$$\rho_\sigma(z,\Omega) = \frac{1}{\Lambda}e^{-2\Psi\int_{-\infty}^{+\infty}dz'\int d\Omega'\rho_\Sigma(z',\Omega')A_{\sigma\Sigma}(z-z',\ \Omega,\ \Omega')}$$

$\rho_\sigma(z,\Omega)$ is the probability density to find a solute molecule σ in the state defined by the position z of its centre of mass along the director and its orientation specified by the usual set of Euler angles Ω
$A_{\sigma\Sigma}(z,\Omega)$ is a function measuring solute-solvent interactions

$\rho_\Sigma(z',\Omega') \rightarrow$ depends on $\rightarrow$
δ (layer spacing)
λ (smectic amplitude)
η (solvent orientational order parameter)

$\rho_\Sigma(z',\Omega')$ is the probability density to find a solvent molecule Σ in the state defined by the position z' of its centre of mass along the director and its orientation specified by the usual set of Euler angles Ω'

$$[S_{\alpha\beta}]_\sigma^{calc}$$

$$\tilde\chi^2 = \frac{1}{v}\sum_\sigma\sum_{\alpha\beta}\left\{[S_{\alpha\beta}]_\sigma^{exp} - [S_{\alpha\beta}]_\sigma^{calc}\right\}^2$$

Keypoint: model for $\rho_\Sigma(z',\Omega')$

$$[S_{\alpha\beta}]_\sigma^{exp}$$

$S_{aa}^{PAS} \equiv \eta$ $\leftarrow$ Euler transformations $\leftarrow$ S_{aa}^{MOL}

Experimental D_{HH} for the solute $\leftarrow$ **NMR EXPERIMENTAL DATA** $\rightarrow$ Experimental D_{HD} and/or Δu_Q for the solvent

Figure 2.9. Flowchart showing the ST-DFT - liquid crystal NMR methodology proposed for the determination of positional order parameters.

2.3.2.   The smectic A phase of 4,4'-di-n-heptyl-azoxybenzene (HAB)

Collecting a large set of solutes' ordering Saupe matrices is an experimentally demanding condition, hard to be fulfilled. When such condition is not met, a simpler version of the procedure can alternatively be applied by exploiting the knowledge of Ψ in the nematic phase and extrapolating its value down into the smectic phase [66-68], together with making a reasonable assumption on the value of the smectic layer spacing. Thus, only λ would remain to be determined and, from this, the solvent smectic order parameters could be estimated. This strategy was the one exploited in ref. [33] for determining the τ_k parameters for HAB using DCB and NFT as probe molecules. Besides the theoretical limitations of this first example, the main experimental drawback was represented by the relatively small amount of experimental data. Therefore, being the method promising, a more extended data set was the goal to pursue. This part of the Ph.D. thesis fits into such a context and aims at investigating by NMR spectroscopy two dilute solutions (approximately 2.0% by mole fraction) prepared by dissolving the rigid solutes biphenylene (BIF) and pyrene (PYR) in a mixture of HAB and HAB-d$_4$

(deuterated in the *ortho* positions with respect to the alkyl chains, provided by Prof. C. A. Veracini from University of Pisa) in order to measure the solvent's second-rank orientational order parameter η and the Saupe ordering matrices of the solutes. For details on samples preparation see Appendix A3. This new data set was then merged with the one previously obtained from DCB and NFT in the same solvent and the resulting overall data set analyzed with the ST-DFT theory to provide the smectic solvent's positional order parameters along with the positional-orientational distribution functions of the various solutes. In Figure 2.10 the structure of the solvent and the solute molecules considered are reported, together with the molecular reference frame chosen for these solutes molecules. For sake of completeness also the chemical structure of DCB and NFT are displayed.
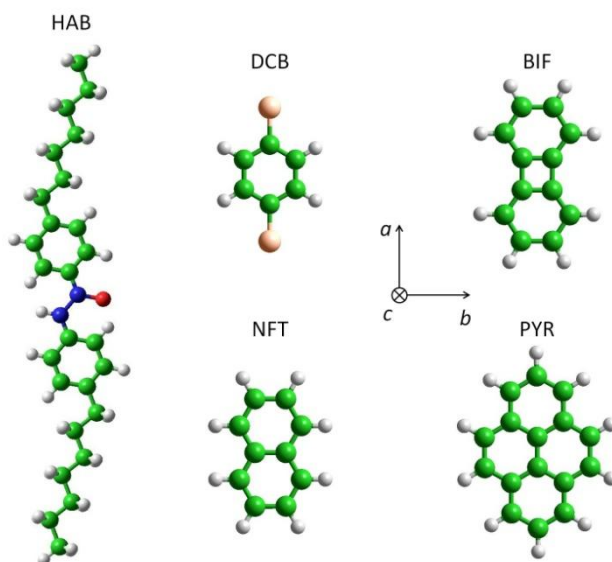
Figure 2.10. "Ball-and-stick" structures of the solvent and solute molecules, referred to with their respective label defined in the text. The (a, b, c) axes of the molecular reference frame adopted for the solute molecules are also shown.

2.3.2.1. Experiments

[1]H spectra of the solutes and ^{2}H spectra of the solvent were recorded on a Bruker Avance 500 MHz spectrometer (11.74 T) equipped with BBI probe, a temperature control unit BVT-2000 and a B-TO2000 thermocouple. Spectra were recorded upon cooling from the isotropic phase, with 40-50 min intervals of thermostabilization for each T value, spanning both the nematic and the smectic A liquid-crystal phases, that is in the temperature range 313 K - 333 K for the first sample, BIF/HAB-d$_4$/HAB (T_{NI} = 343 K), and in the range 307 K - 328 K for

the second sample, PYR/HAB-d$_4$/HAB (T_{NI} = 338 K). In terms of reduced temperatures, this corresponds to the range 0.91-0.97 for both samples, where the transition between the nematic and smectic A phases, T_{SN}, is recorded at 0.94.

All proton spectra were analyzed through an iterative procedure using ARCANA software [39]. Figure 2.11 reports, as an example, the calculated and the experimental ^{1}H spectra in HAB at T_{red} = 0.93 for BIF and PYR, respectively. The final experimental data, that is the residual dipolar couplings D_{ij}, are given, for each reduced temperature, in Table 2.5 for BIF and in Table 2.6 for PYR. In order to easily follow their trend *versus* the reduced temperature, plots are also given in Figures 2.12 and 2.13 for BIF and PYR, respectively. The Saupe ordering matrices were obtained, fixing standard molecular geometries, from the residual dipolar couplings for the two solutes and are reported in Tables 2.7 and 2.8.
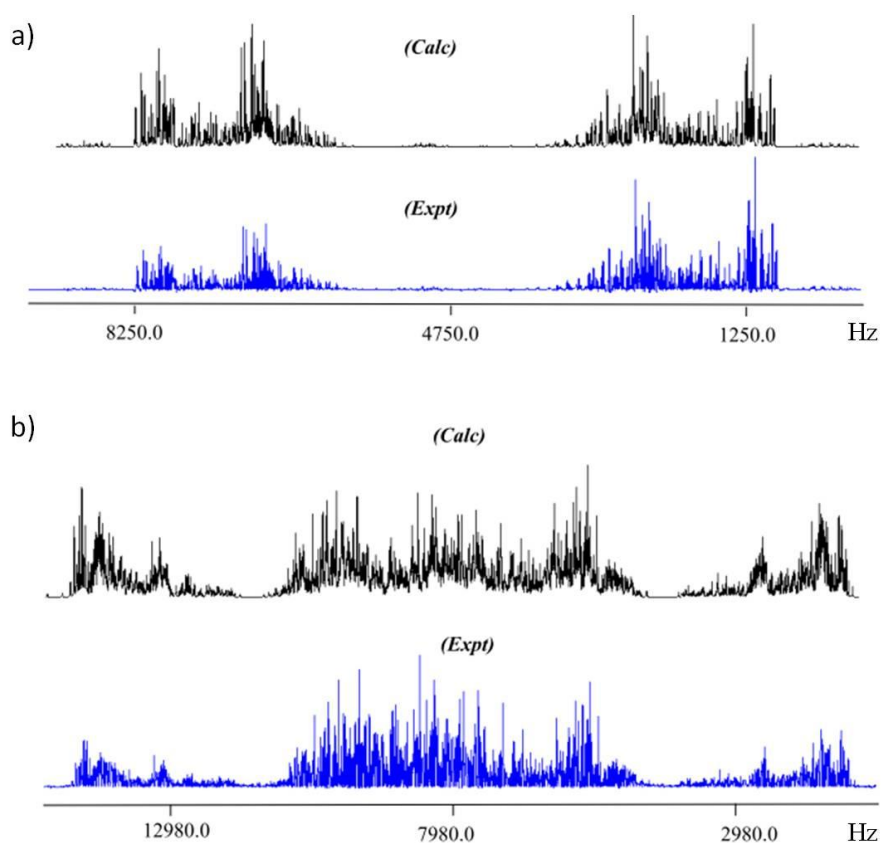
Figure 2.11. Calculated and experimental ^{1}H-NMR spectra of (a) BIF and (b) PYR in HAB at T_{red} = 0.93. A Gaussian multiplication was applied prior to Fourier transform.

Table 2.5. Experimental D_{ij} (in Hz) obtained at different T_{red} from the spectral analysis of BIF in HAB by ARCANA software. The transition between the nematic and smectic A phases is recorded at T_{red} = 0.94. The chemical structure provides the hydrogen atom numbering.
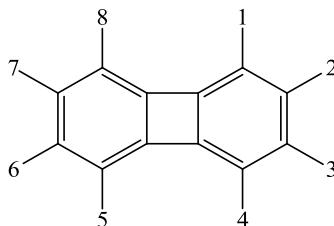
T_{red}	D_{12}	D_{13}	D_{14}	D_{15}	D_{16}
0.97	-1349.93 ± 0.08	-75.07 ± 0.11	13.24 ± 0.31	-39.94 ± 0.33	-60.57 ± 0.10
0.96	-1444.93 ± 0.08	-78.38 ± 0.12	17.11 ± 0.36	-40.76 ± 0.35	-65.06 ± 0.12
0.95	-1512.69 ± 0.06	-80.26 ± 0.08	19.47 ± 0.24	-43.02 ± 0.24	-68.11 ± 0.08
0.94	-1572.97 ± 0.05	-83.03 ± 0.06	19.83 ± 0.19	-45.46 ± 0.22	-70.62 ± 0.06
0.93	-1634.03 ± 0.04	-88.10 ± 0.05	20.25 ± 0.15	-46.78 ± 0.15	-73.46 ± 0.05
0.92	-1661.51 ± 0.04	-90.88 ± 0.04	18.68 ± 0.16	-48.01 ± 0.13	-74.73 ± 0.04
0.91	-1679.02 ± 0.04	-93.08 ± 0.05	17.46 ± 0.16	-48.67 ± 0.17	-75.38 ± 0.05

T_{red}	D_{17}	D_{18}	D_{23}	D_{26}	D_{27}
0.97	-125.54 ± 0.09	-529.65 ± 0.25	124.17 ± 0.31	-44.91 ± 0.31	-56.90 ± 0.25
0.96	-135.06 ± 0.10	-568.15 ± 0.25	151.58 ± 0.34	-49.29 ± 0.33	-60.69 ± 0.26
0.95	-141.27 ± 0.07	-595.34 ± 0.17	171.23 ± 0.25	-51.48 ± 0.24	-63.94 ± 0.18
0.94	-147.15 ± 0.05	-620.20 ± 0.14	183.44 ± 0.18	-52.78 ± 0.20	-66.58 ± 0.16
0.93	-152.51 ± 0.05	-642.55 ± 0.11	175.21 ± 0.15	-55.44 ± 0.15	-69.26 ± 0.11
0.92	-154.93 ± 0.04	-652.48 ± 0.10	167.01 ± 0.13	-56.02 ± 0.13	-70.24 ± 0.10
0.91	-156.39 ± 0.04	-658.69 ± 0.11	158.09 ± 0.15	-56.78 ± 0.15	-70.53 ± 0.11

Table 2.6. Experimental D_{ij} (in Hz) obtained at different T_{red} from the spectral analysis of PYR in HAB by ARCANA software. The transition between the nematic and smectic A phases is recorded at T_{red} = 0.94. The chemical structure provides the hydrogen atom numbering.
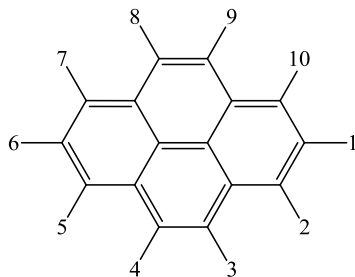
T_{red}	D_{12}	D_{13}	D_{14}	D_{15}	D_{16}
0.97	-554.17 ± 0.09	-154.98 ± 0.14	-84.65 ± 0.14	-56.82 ± 0.10	-43.02 ± 0.16
0.96	-569.45 ± 0.08	-161.67 ± 0.12	-86.89 ± 0.12	-60.24 ± 0.09	-46.20 ± 0.15
0.95	-578.34 ± 0.07	-166.66 ± 0.11	-91.04 ± 0.12	-60.71 ± 0.08	-46.87 ± 0.13
0.94	-586.90 ± 0.06	-171.01 ± 0.10	-94.70 ± 0.09	-64.21 ± 0.07	-49.80 ± 0.10
0.93	-592.99 ± 0.05	-175.54 ± 0.09	-96.13 ± 0.09	-65.42 ± 0.07	-51.36 ± 0.09
0.92	-597.84 ± 0.07	-178.06 ± 0.11	-99.92 ± 0.11	-68.87 ± 0.07	-53.65 ± 0.11
0.91	-601.79 ± 0.07	-183.01 ± 0.12	-102.03 ± 0.11	-69.39 ± 0.08	-54.57 ± 0.11

T_{red}	D_{23}	D_{24}	D_{25}	D_{27}	D_{28}
0.97	-1654.15 ± 0.09	-291.28 ± 0.10	-115.05 ± 0.12	-48.67 ± 0.16	-37.78 ± 0.14
0.96	-1733.40 ± 0.07	-308.14 ± 0.07	-118.41 ± 0.10	-51.07 ± 0.14	-39.46 ± 0.11
0.95	-1798.50 ± 0.06	-319.87 ± 0.07	-123.35 ± 0.09	-53.88 ± 0.12	-39.58 ± 0.10
0.94	-1864.45 ± 0.06	-331.40 ± 0.06	-127.18 ± 0.08	-54.04 ± 0.10	-42.46 ± 0.09
0.93	-1911.60 ± 0.05	-341.11 ± 0.05	-131.37 ± 0.07	-54.44 ± 0.10	-43.42 ± 0.09
0.92	-1974.15 ± 0.06	-352.22 ± 0.07	-135.20 ± 0.08	-55.30 ± 0.12	-43.58 ± 0.11
0.91	-2015.29 ± 0.06	-359.85 ± 0.07	-139.14 ± 0.08	-58.66 ± 0.13	-44.41 ± 0.10

T_{red}	D_{29}	D_{210}	D_{34}	D_{38}	D_{39}
0.97	-24.12 ± 0.15	-4.46 ± 0.16	-2269.34 ± 0.12	-12.84 ± 0.19	-1.23 ± 0.20
0.96	-22.40 ± 0.11	0.27 ± 0.14	-2383.02 ± 0.09	-12.40 ± 0.16	-0.82 ± 0.17
0.95	-22.31 ± 0.10	1.70 ± 0.12	-2474.10 ± 0.08	-12.06 ± 0.14	0.37 ± 0.13
0.94	-22.20 ± 0.09	4.88 ± 0.11	-2572.08 ± 0.07	-11.05 ± 0.12	0.76± 0.12
0.93	-22.02 ± 0.08	10.58 ± 0.10	-2642.06 ± 0.07	-10.79 ± 0.11	1.88 ± 0.11
0.92	-21.12 ± 0.10	12.30 ± 0.12	-2734.75 ± 0.08	-10.49 ± 0.15	4.03 ± 0.16
0.91	-20.44 ± 0.10	15.41 ± 0.12	-2796.91 ± 0.09	-10.35 ± 0.15	4.25 ± 0.15
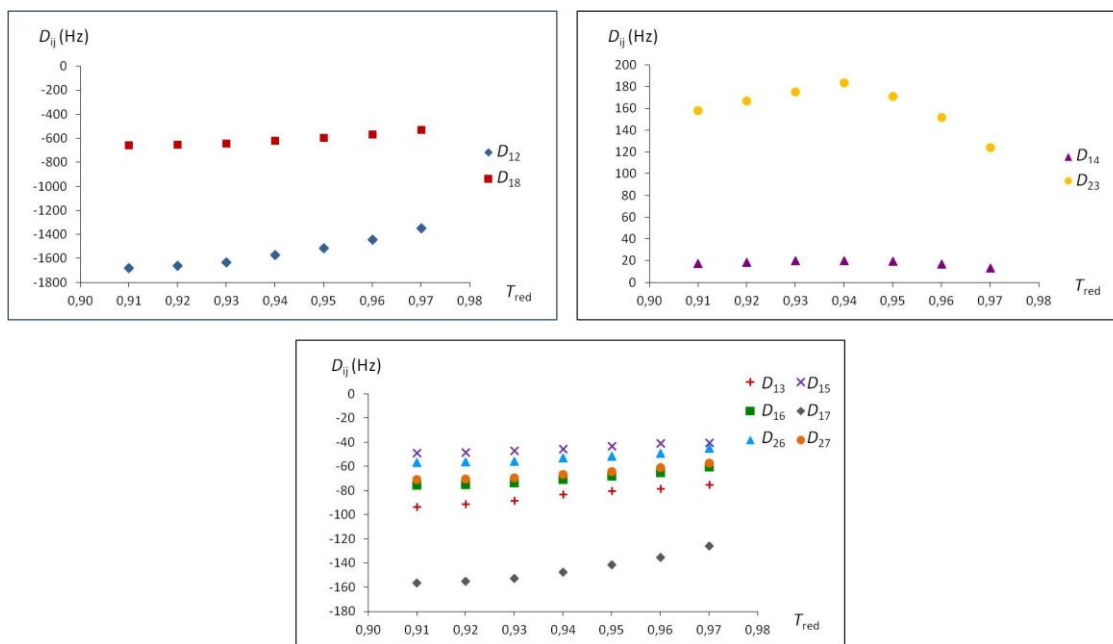
Figure 2.12. Experimental dipolar couplings obtained from the spectral analysis of BIF in HAB, as function of T_{red}.
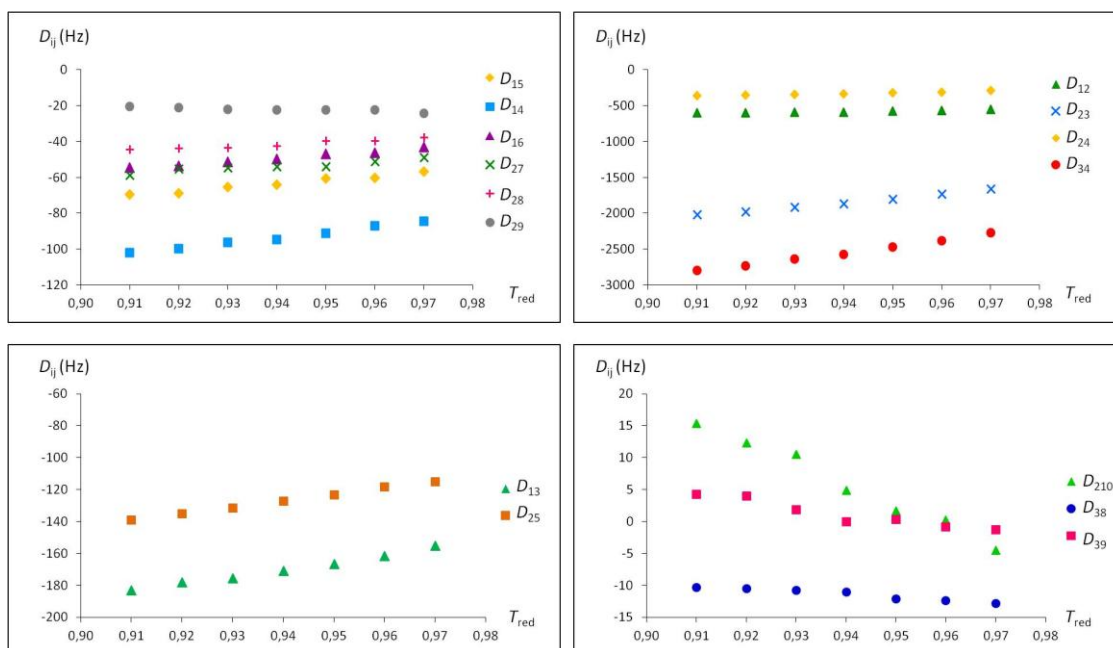
Figure 2.13. Experimental dipolar couplings obtained from the spectral analysis of PYR in HAB, as function of T_{red}.

Table 2.7. Elements of the Saupe ordering matrix for BIF in HAB as a function of reduced temperature.

T_{red}	S_{aa}	$S_{bb} - S_{cc}$
0.97	0.2560 ± 0.0003	0.2261 ± 0.0004
0.96	0.2767 ± 0.0003	0.2382 ± 0.0002
0.95	0.2882 ± 0.0003	0.2469 ± 0.0003
0.94	0.3002 ± 0.0003	0.2561 ± 0.0004
0.93	0.3111 ± 0.0003	0.2689 ± 0.0004
0.92	0.3158 ± 0.0003	0.2757 ± 0.0003
0.91	0.3210 ± 0.0003	0.2855 ± 0.0003

Table 2.8. Elements of the Saupe ordering matrix for PYR in HAB as a function of reduced temperature.

T_{red}	S_{aa}	$S_{bb} - S_{cc}$
0.97	0.2876 ± 0.0016	0.2903 ± 0.0028
0.96	0.3038 ± 0.0027	0.2998 ± 0.0023
0.95	0.3150 ± 0.0029	0.3080 ± 0.0023
0.94	0.3271 ± 0.0028	0.3152 ± 0.0022
0.93	0.3375 ± 0.0025	0.3196 ± 0.0019
0.92	0.3477 ± 0.0028	0.3262 ± 0.0024
0.91	0.3561 ± 0.0027	0.3300 ± 0.0020

The deuterium spectra of the solvent were used to obtain the numerical values of the solvent's second-rank orientational order parameter η, following a standard procedure [73-74]. The ^{2}H spectrum of HAB-d$_4$ consists of a pair of doublets due to the quadrupolar splitting Δv_Q of the four deuterated *ortho* positions (with respect to the alkyl chains) and the additional dipole-dipole coupling D_{HD} between the deuterium in *ortho* and the proton in *meta* position (see Figure 2.14). The heteronuclear dipolar coupling between a deuterium and a proton produces a splitting given by [73]:

$$D_{HD} = -\frac{\gamma_H \gamma_D h}{4\pi^2 r_{HD}^3} S_{aa} \qquad (2.36)$$

where r_{HD} is the H-D distance (equal to 2.48 Å) and $\gamma_H \gamma_D h/4\pi^2$ = 1.844·10^4 Hz Å^3.

D_{HD} depends on only one order parameter, S_{aa}, which is expected to be positive (D_{HD} will thus be negative). Since S_{aa} is expressed in the molecular fragment-fixed frame, a rotation has to be performed in order to obtain it in the PAS frame (see Figure 2.14). Assuming from literature an angle of 16.8° between the principal axis of HAB and the direction D-H of the two

rings [74], and using conventional rotational matrices of director cosine, we calculated the $S_{aa}^{PAS} \equiv \eta$ solvent orientational order parameters at different T_{red} listed in Table 2.9. Note that extracted data are consistent with the orientational order parameters recently reported for pure HAB [75] obtained by the analysis of several NMR observables (^{13}C chemical shift anisotropies, ^{1}H-^{2}H and ^{13}C-^{2}H dipolar couplings, and ^{2}H quadrupolar splittings) supplemented by quantum chemical density functional theory calculations, and claimed to be more reliable than the ones obtained by the traditional approach, based on the simpler analysis of ^{2}H spectra. The η values obtained after proper rotation from quadrupolar splittings were also used to confirm the values of Table 2.9.
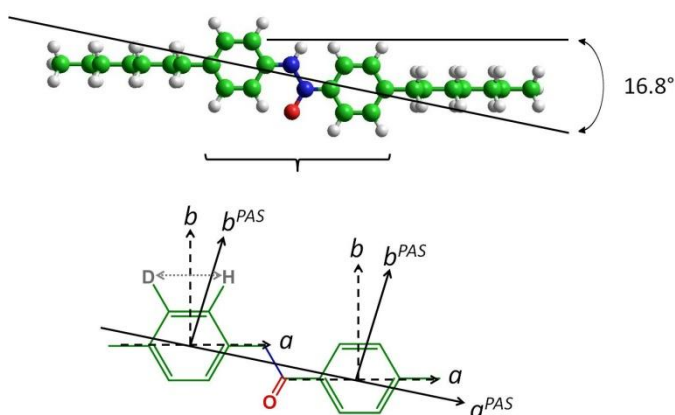
Figure 2.14. Location of the molecular frame fixed on each phenyl ring (a, b, c) and of the principal frame $(a^{PAS}, b^{PAS}, c^{PAS})$ with respect to which the solvent orientational order paremeter η is defined. Axes c and c^{PAS}, not shown, define right-handed Cartesian systems.

Table 2.9. Mean value of the solvent's orientational order parameter η as a function of the reduced temperature. The error estimated for them is 10% (from resolution of ^{2}H spectra and by error propagation).

T_{red}	η
0.97	0.65
0.96	0.68
0.95	0.71
0.94	0.72
0.93	0.75
0.92	0.78
0.91	0.80

2.3.2.2. Data analysis

The analysis of the whole set of experimental data in HAB, composed of the ordering matrices of DCB, NFT, BIF, and PYR as a function of temperature, requires a proper model for solute-solvent interactions. The choice is driven by a compromise between the desire of preserving the chemical identity of the molecules under consideration and the one of keeping the calculations as simple as possible. Following an intermediate choice, both solute and solvent molecules were described at the atomistic, chemically detailed level. Atom-atom interactions were taken of the hard sphere type, with each sphere radius equal to the corresponding atom or group (the united atom approximation was used for methylene and methyl groups in the alkyl chains of HAB) van der Waals radius [76]. To reduce computational burden, the solvent was allowed to adopt a single conformation, having the central core planar, the dihedral angles defined by the first two methylene groups of the chains and the corresponding phenyl ring set, respectively, at ±90° and the two chains in an *all trans* conformation.

After parametrization of the solvent distribution function, the parameters (Ψ, λ and δ) are determined by fitting the predicted elements of solute Saupe ordering matrices with those obtained experimentally. Two series of fittings were performed: (1) the phase was assumed nematic throughout the temperature range explored, λ was set equal to 0 and δ thus left undefined, so that Ψ was the sole parameter left to vary; (2) the phase was assumed smectic A throughout the temperature range explored, λ was varied together with Ψ, while δ was fixed at the value of 28.9 Å as reported in a past diffraction experiment [77]. Note that as the experimental data set was large enough, there was no need to make any extrapolation of the result for Ψ in the N phase down to the SmA phase, as done in the previous work [33].

Table 2.10 gives the values of the quantity $\tilde{\chi}^2$ resulting from the two series of fittings. Its trend is in good agreement with the known phase sequence: while $\tilde{\chi}^2{}_N$ increases with decreasing temperature, $\tilde{\chi}^2{}_{SmA}$ has in general the opposite behavior. This means that, as expected, the addition of the parameter λ leads to progressively better fittings. Nonetheless, $\tilde{\chi}^2{}_N$ remains smaller for the first two highest temperatures, while at T_{red} = 0.95 the two values of $\tilde{\chi}^2$ are essentially equivalent, indicating that, for the three highest temperatures, the extra parameter added does not improve the quality of the fitting obtained by varying the sole parameter Ψ. This is consistent with the N character of the liquid-crystalline solutions for T_{red} ≥ 0.95. The addition of λ leads to fittings of a substantially better quality for T_{red} ≤ 0.94, where the liquid crystalline solutions are indeed in the SmA phase. While $\tilde{\chi}^2{}_{SmA}$ does decrease in

general with temperature, it does not do so at the lowest temperature considered (T_{red} = 0.91), at which its value is comparable to the one obtained at T_{red} = 0.95. There is no evident reason for that at the moment.

**Table 2.10.** Parameters of the two series of fitting as a function of reduced temperature.

T_{red}	$10^4\,\tilde{\chi}^2{}_{N}$	$10^4\,\tilde{\chi}^2{}_{SmA}$
0.97	5.73	6.66
0.96	5.90	6.52
0.95	6.11	5.93
0.94	6.60	4.92
0.93	7.94	3.77
0.92	9.65	3.56
0.91	12.11	5.88

The main result of the analysis of the $\left[S_{\alpha\beta}\right]_{\sigma}^{exp}$ are the solvent's positional order parameters τ_k^{Σ}, that are reported in Figure 2.15 as a function of reduced temperature for k = 1,2,3. The error in these parameters was estimated assuming a 10% error in the value of η. Values of τ_k^{Σ} reported in Figure 2.15 are consistent with those previously obtained with the same methodology using a smaller experimental data set derived only from the probe solutes DCB and NFT [33]. Moreover, similar values of the positional order parameters were found for HAB through a different method, based on the NMR measurement of self-diffusion coefficients in the liquid crystalline phase [63].
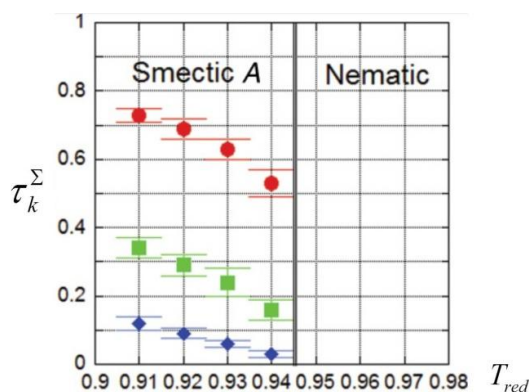
Figure 2.15. Solvent's positional order parameters τ_k^{Σ} as a function of reduced temperature: τ_k^{Σ} = 1 (red circles), τ_k^{Σ} = 2 (green squares), and τ_k^{Σ} = 3 (blue diamonds). In the nematic phase there is no positional order.

By-products of the analysis are the solutes' positional-orientational distribution functions $\rho_\sigma(z, \Omega)$, from which the positional order parameters of the solutes can be calculated. Figure 2.16 shows these parameters as a function of the reduced temperature for k = 1,2. Noteworthy is the negative value of τ_1, indicating that the solutes prefer to reside in the interlayer regions. This confirms what was previously found elsewhere [33, 66-69]. The positive value of τ_2 is just a further reflection of the layered nature of the SmA phase.
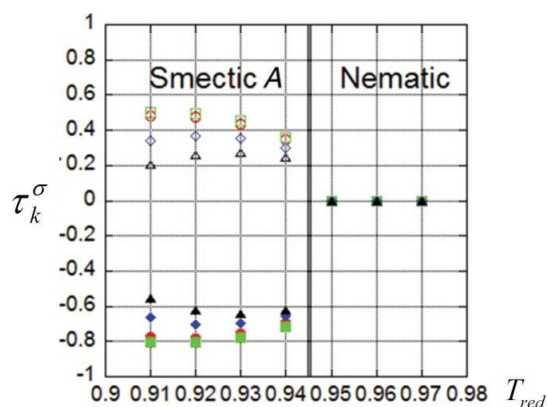
Figure 2.16. Solutes' positional order parameters τ_k^σ as a function of reduced temperature: DCB (red circles), NFT (green squares), BIF (blue diamonds), and PYR (black triangles). Full symbols correspond to k = 1, while empty symbols to k = 2.

2.3.3.   *The partial bilayer smectic* A_d *phase of 4-n-octyloxy-4'-cyanobiphenyl (8OCB)*

Encouraged by the promising results obtained for the conventional smectic A phase of HAB, the performances of the proposed methodology, combining a statistical thermodynamic density functional theory (ST-DFT) with liquid crystal NMR spectroscopy, has been tested on a more delicate solvent which displays a partial bilayer SmA$_d$ phase. In particular the liquid crystal medium we started with was the 4-*n*-octyloxy-4'-cyanobyphenyl (8OCB), a member of the well-known *n*OCB series of liquid crystal molecules. This series of compounds, together with the series of *n*-alkylcyanobiphenyls (*n*CB), was first reported in the '70s [78] and they have been the object of a wealth of studies ever since. Provided *n* is large enough, a nematic phase and, for *n* ≥ 8, also a SmA phase form. Soon after their synthesis, X-ray diffraction studies were carried out that revealed that the layer spacing δ in the SmA phase of the higher alkyl and alkoxy homologues were between once and twice a molecular length [79-81]. It was readily recognized that this had to be due to some sort of dimerisation, induced by the strong dipole moment borne by the terminal cyano groups, which interact between them and with

the phenyl groups of the biphenyl moiety: as a result, a partial bilayer SmA phase, labelled SmA$_d$, turns out; its structure is schematically given in Figure 2.17.
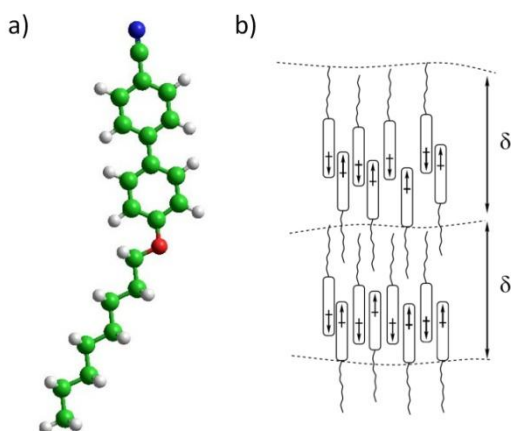
Figure 2.17. (a) "Ball-and-stick" structure of the 8OCB solvent molecule and (b) schematic illustration of a partial bilayer smectic A$_d$ phase it creates, with molecules tending to pair up in a slipped-parallel configuration.

The picture deducted from the diffraction experiments later received several confirmations (see, for instance, ref. [82]), more recently also from a few computer simulation studies conducted on atomistic models of 8CB [83-86]. These computational studies also confirmed how the layered structure of the SmA$_d$ of this compound is somewhat loose, supporting then the well-known very weak, second-order character of the nematic-smectic phase transition in these compounds [87-88]. Though, to the best of our knowledge, similar simulations are not available on 8OCB, it is very likely that what found for 8CB applies also to its alkoxy counterpart, given the many similarities shared by the two compounds. It is thus evident that the loose, partial bilayer character of its structure, linked to the very weak, second-order character of the nematic-smectic phase transition in compounds of this sort, would seem to play against a smooth extension of the previous results to this case. It is in fact not warranted that solutes' orientational order parameters do show any detectable sign of entering a smectic phase.

2.3.3.1. Experiments

The solute molecules employed in the present work were 1,4-dichlorobenzene (DCB), biphenylene (BIF) and pyrene (PYR), whose structures are reported in Figure 2.10, along with

the axes of their molecular reference frame. Dilute solutions (approximately 3.0% by mole fraction) were prepared by dissolving BIF and PYR in a mixture of 8OCB and 8OCB-d$_8$ (deuterated in the biphenyl fragment, prepared by Prof. H. Zimmermann), while DCB were dissolved in 8OCB. For details on samples preparation see Appendix A3.

^{1}H spectra of the solutes and ^{2}H spectra of the solvent were recorded at different common reduced temperatures T_{red} on a Bruker Avance 500MHz spectrometer (equipped with BBI probe, BVT-2000 temperature control unit and B-TO2000 thermocouple) upon cooling from the isotropic phase, with 40-50 min intervals of thermostabilization for each T value. In particular, ^{1}H spectra of the solutes were recorded and analysed using the home-made program ARCANA [39] in the temperature range 320 K - 344 K for the first solution, DCB/8OCB (T_{NI} = 347 K), in the range 325 K – 348 K for the second solution, BIF/8OCB-d$_8$/8OCB (T_{NI} = 352 K), and in the range 323 K – 334 K for the third solution, PYR/8OCB-d$_8$/8OCB (T_{NI} = 350 K). In terms of reduced temperatures, this corresponds to the range 0.92-0.99 for samples containing DCB and BIF, spanning both the nematic (in the range 0.97-0.99) and the smectic-A$_d$ (in the range 0.92-0.95) liquid-crystal phases, and to the range 0.92-0.95 for the sample containing PYR. Note that for the last sample it was possible to analyze the proton spectra only at low temperatures in the SmA$_d$ phase. Indeed, due to their low quality, in terms of linewidth and signal-to-noise ratio, it proved impossible to analyze such complex spectra (10 spins) at higher temperatures in the N phase. In Figure 2.18 the calculated and experimental ^{1}H spectra of DCB, BIF and PYR in the liquid crystal solvent at T_{red} = 0.93 are reported.

The experimental residual dipolar couplings D_{ij} extracted from spectral analysis are listed for each temperature, in Tables 2.11, 2.12 and 2.13, and reported graphically in Figures 2.19, 2.20 and 2.21, for DCB, BIF and PYR, respectively. The Saupe ordering matrices for the three solutes were obtained from the corresponding set of residual dipolar coupling data upon adoption of standard molecular geometries and are reported in Tables 2.14, 2.15, and 2.16.
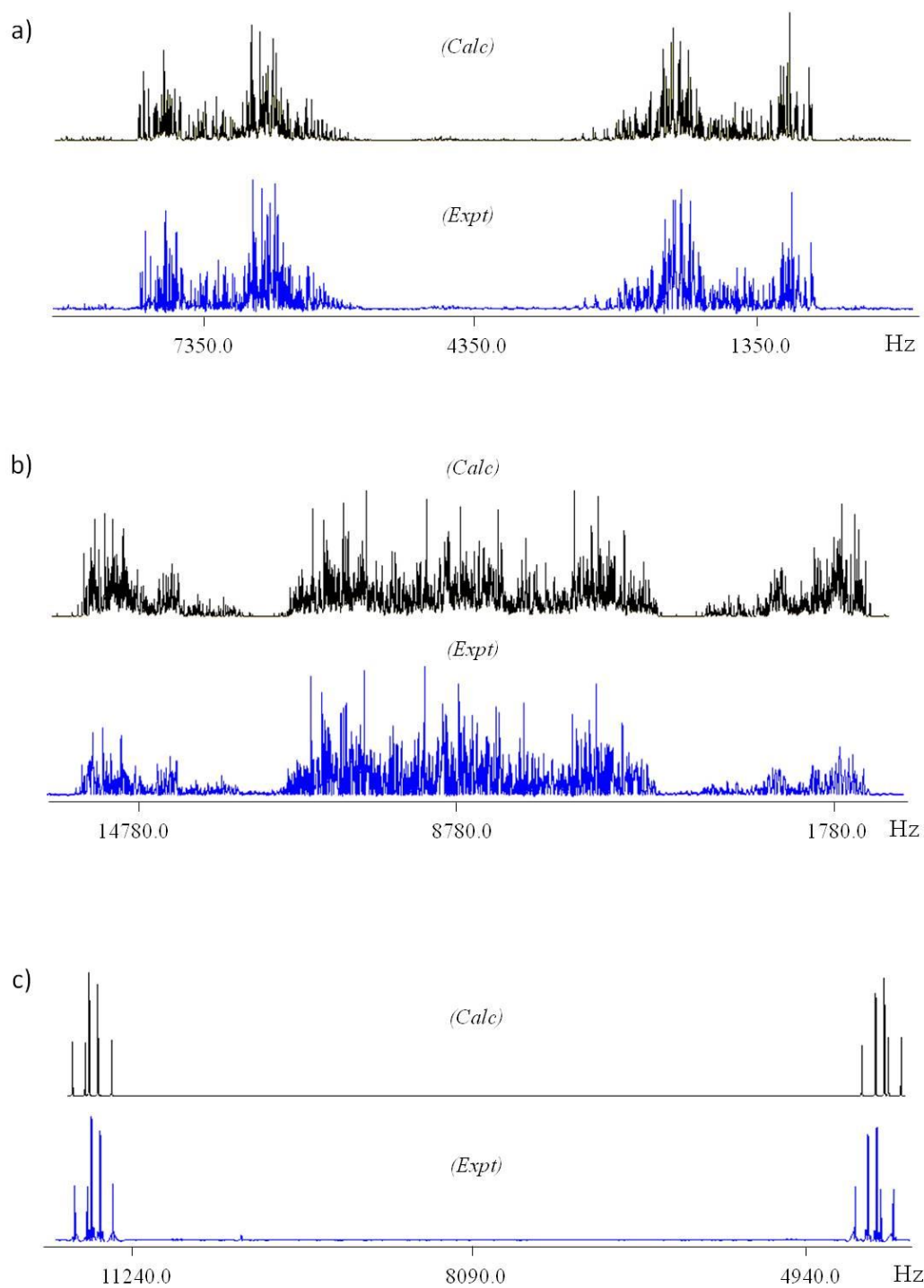
Figure 2.18. Calculated and experimental ^{1}H-NMR spectra of (a) BIF, (b) PYR and (c) DCB in 8OCB at T_{red} = 0.93. A gaussian multiplication was applied prior to Fourier transform.

Table 2.11. Experimental D_{ij} (in Hz) obtained at different T_{red} from the spectral analysis of DCB in 8OCB by ARCANA software. The transition between the nematic and smectic-A phases is recorded at about T_{red} = 0.96. The chemical structure provides the hydrogen atom numbering.
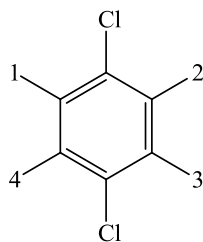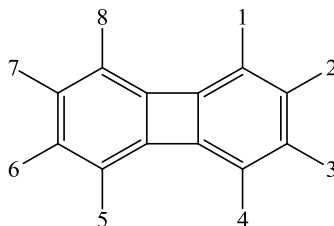

T_{red}	D_{12}	D_{13}	D_{23}
0.99	59.35 ± 0.07	-29.10 ± 0.08	-1797.19 ± 0.07
0.98	65.48 ± 0.10	-33.04 ± 0.11	-2020.42 ± 0.10
0.97	68.17 ± 0.09	-35.02 ± 0.09	-2125.43 ± 0.08
0.95	72.03 ± 0.09	-36.91 ± 0.09	-2244.50 ± 0.07
0.94	74.22 ± 0.06	-37.81 ± 0.07	-2303.16 ± 0.05
0.93	77.01 ± 0.03	-38.91 ± 0.03	-2396.70 ± 0.03
0.92	78.88 ± 0.06	-39.03 ± 0.06	-2412.36 ± 0.06
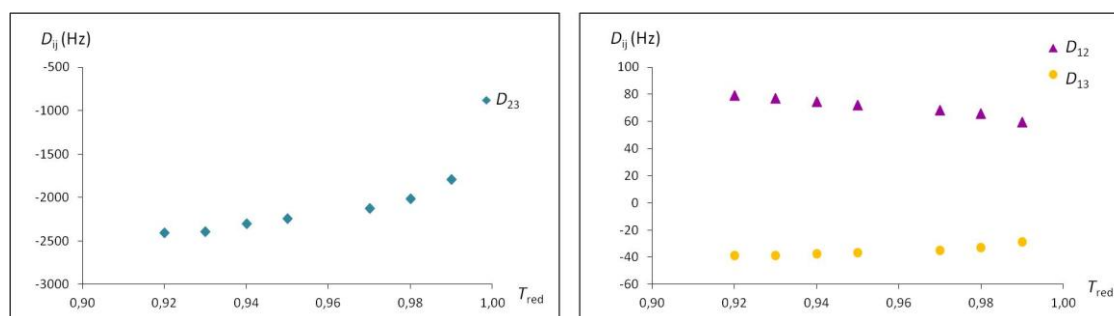
Figure 2.19. Experimental dipolar couplings obtained from the spectral analysis of DCB in 8OCB, as function of T_{red}.

Table 2.12. Experimental D_{ij} (in Hz) obtained at different T_{red} from the spectral analysis BIF in 8OCB/8OCB-d$_8$ by ARCANA software. The transition between the nematic and smectic-A phases is recorded at about T_{red} = 0.96. The chemical structure provides the hydrogen atom numbering.

T_{red}	D_{12}	D_{13}	D_{14}	D_{15}	D_{16}
0.99	-1292-98 ± 0.08	-75.27 ± 0.10	-11.29 ± 0.35	-38.65 ± 0.38	-58.32 ± 0.11
0.98	-1387.49 ± 0.11	-80.34 ± 0.14	4.17 ± 0.51	-43.39 ± 0.46	-63.14 ± 0.16
0.97	-1482.65 ± 0.07	-86.53 ± 0.10	12.06 ± 0.34	-44.34 ± 0.33	-66.97 ± 0.10
0.95	-1597.19 ± 0.07	-91.65 ± 0.11	12.36 ± 0.32	-46.74 ± 0.34	-72.20 ± 0.11
0.94	-1662.52 ± 0.06	-93.79 ± 0.09	16.24 ± 0.23	-48.35 ± 0.25	-75.38 ± 0.08
0.93	-1739.29 ± 0.06	-96.17 ± 0.07	18.53 ± 0.25	-50.56 ± 0.25	-78.29 ± 0.08
0.92	-1801.83 ± 0.05	-96.21 ± 0.06	21.92 ± 0.21	-51.89 ± 0.22	-81.41 ± 0.07

T_{red}	D_{17}	D_{18}	D_{23}	D_{26}	D_{27}
0.99	-113.98 ± 0.09	-487.16 ± 0.23	85.45 ± 0.32	-41.00 ± 0.35	-54.12 ± 0.25
0.98	-125.38 ± 0.11	-539.56 ± 0.35	100.16 ± 0.50	-44.52 ± 0.46	-60.12 ± 0.35
0.97	-137.73 ± 0.08	-579.29 ± 0.21	109.45 ± 0.33	-49.33 ± 0.31	-62.73 ± 0.20
0.95	-148.39 ± 0.09	-625.75 ± 0.22	133.55 ± 0.30	-53.87 ± 0.31	-66.83 ± 0.22
0.94	-154.70 ± 0.07	-652.01 ± 0.19	150.34 ± 0.24	-56.60 ± 0.24	-69.58 ± 0.21
0.93	-162.57 ± 0.07	-683.95 ± 0.16	178.22 ± 0.23	-59.15 ± 0.23	-73.39 ± 0.17
0.92	-168.91 ± 0.06	-709.50 ± 0.22	206.85 ± 0.19	-61.46 ± 0.22	-77.15 ± 0.15

Table 2.13. Experimental D_{ij} (in Hz) obtained at different T_{red} from the spectral analysis PYR in 8OCB/8OCB-d$_8$ by ARCANA software. Only ^{1}H spectra in the SmA$_d$ range could be analyzed. The chemical structure provides the hydrogen atom numbering.


T_{red}	D_{12}	D_{13}	D_{14}	D_{15}	D_{16}
0.95	-695.22 ± 0.38	-180.66 ± 0.64	-93.79 ± 0.58	-59.87 ± 0.49	-47.19 ± 0.58
0.94	-717.25 ± 0.06	-188.03 ± 0.10	-99.06 ± 0.10	-66.21 ± 0.08	-52.08 ± 0.12
0.93	-728.17 ± 0.07	-192.80 ± 0.11	-102.05 ± 0.11	-67.99 ± 0.08	-53.60 ± 0.12
0.92	-731.32 ± 0.07	-194.81 ± 0.10	-103.60 ± 0.10	-69.77 ± 0.08	-53.99 ± 0.12

T_{red}	D_{23}	D_{24}	D_{25}	D_{27}	D_{28}
0.95	-1862.04 ± 0.38	-326.75 ± 0.41	-128.89 ± 0.49	-55.27 ± 0.78	-46.38 ± 0.71
0.94	-1961.02 ± 0.06	-344.87 ± 0.07	-131.78 ± 0.09	-57.01 ± 0.11	-46.92 ± 0.09
0.93	-2019.41 ± 0.07	-354.93 ± 0.07	-136.01 ± 0.09	-59.95 ± 0.13	-47.82 ± 0.10
0.92	-2043.68 ± 0.07	-359.40 ± 0.07	-137.88 ± 0.09	-60.64 ± 0.12	-49.00 ± 0.10

T_{red}	D_{29}	D_{210}	D_{34}	D_{38}	D_{39}
0.95	-32.71 ± 0.63	-24.65 ± 0.82	-2517.23 ± 0.57	-17.46 ± 0.86	-6.96 ± 0.14
0.94	-32.50 ± 0.09	-23.12 ± 0.12	-2657.81 ± 0.08	-16.56 ± 0.13	-6.45 ± 0.17
0.93	-32.05 ± 0.10	-21.25 ± 0.13	-2740.09 ± 0.09	-16.40 ± 0.13	-6.08 ± 0.14
0.92	-31.93 ± 0.10	-18.98 ± 0.12	-2774.83 ± 0.09	-16.32 ± 0.14	-5.47 ± 0.15
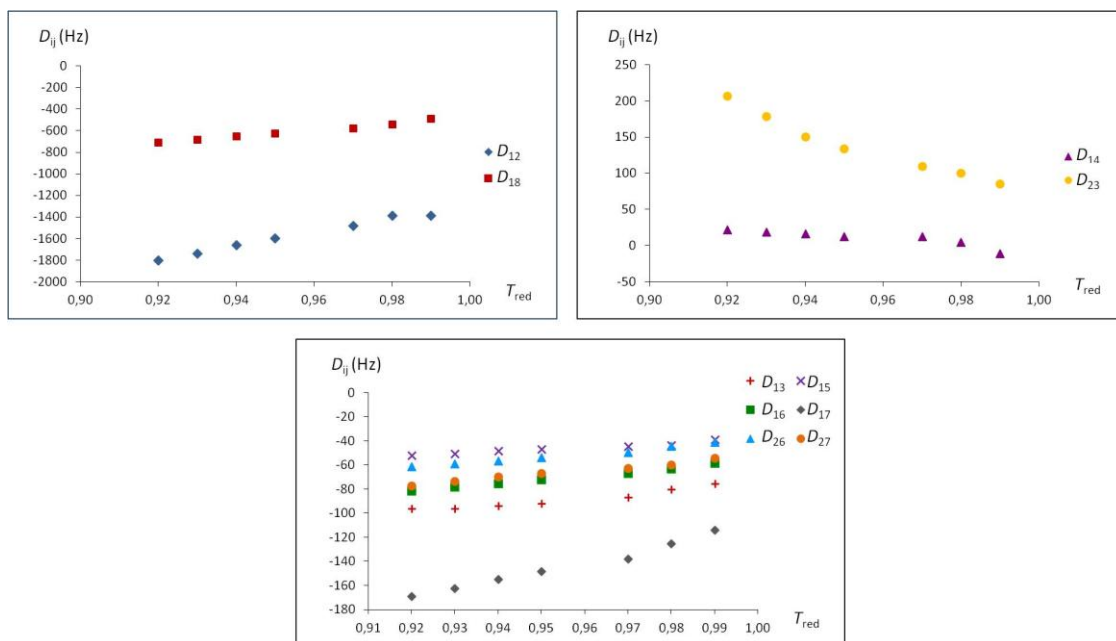
Figure 2.20. Experimental dipolar couplings obtained from the spectral analysis of BIF in 8OCB, as function of T_{red}.
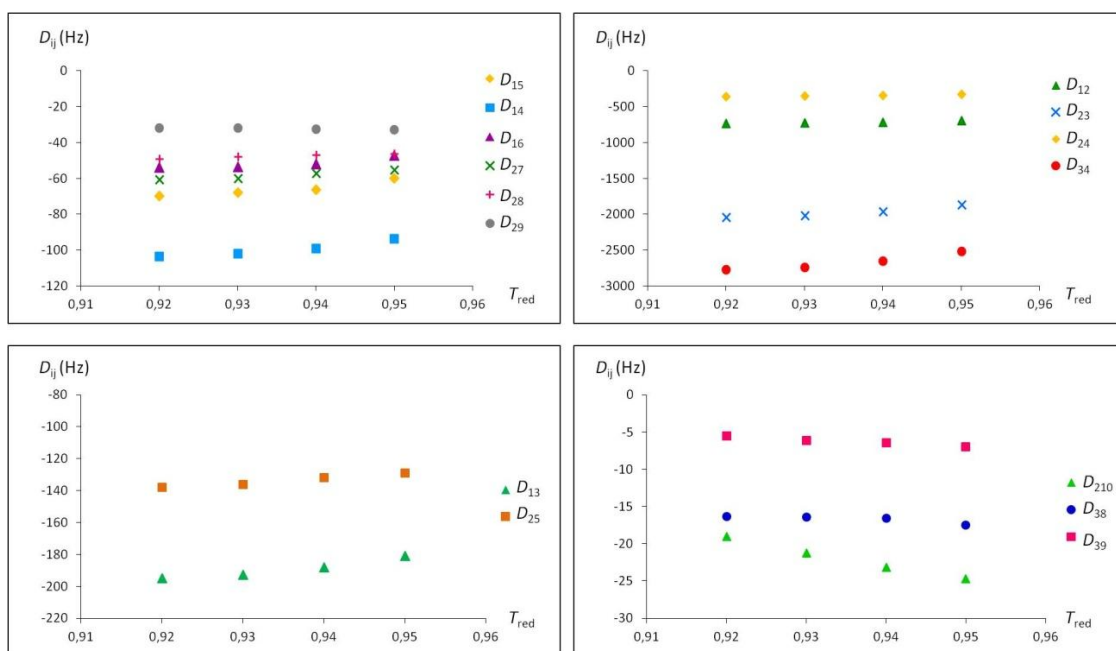
Figure 2.21. Experimental dipolar couplings obtained from the spectral analysis of PYR in 8OCB, as function of T_{red}.

Table 2.14. Elements of the Saupe ordering matrix for DCB in 8OCB as a function of reduced temperature.

T_{red}	S_{aa}	$S_{bb} - S_{cc}$
0.99	0.2068 ± 0.0001	0.1379 ± 0.0008
0.98	0.2307 ± 0.0001	0.1525 ± 0.0010
0.97	0.2729 ± 0.0001	0.1829 ± 0.0009
0.95	0.2881 ± 0.0001	0.1929 ± 0.0008
0.94	0.2957 ± 0.0001	0.1977 ± 0.0010
0.93	0.3077 ± 0.0001	0.2057 ± 0.0008
0.92	0.3097 ± 0.0001	0.2055 ± 0.0011

Table 2.15. Elements of the Saupe ordering matrix for BIF in 8OCB/8OCB-d$_8$ as a function of reduced temperature.

T_{red}	S_{aa}	$S_{bb} - S_{cc}$
0.99	0.2415 ± 0.0009	0.2211 ± 0.0011
0.98	0.2617 ± 0.0010	0.2377 ± 0.0011
0.97	0.2810 ± 0.0003	0.2549 ± 0.0004
0.95	0.3037 ± 0.0003	0.2720 ± 0.0004
0.94	0.3163 ± 0.0002	0.2805 ± 0.0003
0.93	0.3324 ± 0.0003	0.2901 ± 0.0003
0.92	0.3447 ± 0.0004	0.2954 ± 0.0005

Table 2.16. Elements of the Saupe ordering matrix for PYR in 8OCB/8OCB-d$_8$ as a function of reduced temperature.

T_{red}	S_{aa}	$S_{bb} - S_{cc}$
0.95	0.3217 ± 0.0038	0.3486 ± 0.0026
0.94	0.3373 ± 0.0034	0.3637 ± 0.0024
0.93	0.3480 ± 0.0033	0.3713 ± 0.0024
0.92	0.3531 ± 0.0034	0.3738 ± 0.0023

The ^{2}H spectra of the solvent were recorded and analysed, in the range of T_{red} between 0.92 and 0.99, only for the samples of BIF and PYR, containing deuterated 8OCB. According to standard procedures [89-90] it was possible to obtain the numerical values of the solvent's second-rank orientational order parameter η listed in Table 2.17.

The analysis of the ^{2}H spectrum of 8OCB-d$_8$ gives the quadrupolar splitting Δv_Q of the deuterated positions in the biphenyl fragment, which, assuming the quadrupolar tensor axially symmetric along the C-D direction, are directly related to the order parameter S_{CD} by (see chapter 1):

$$\Delta v_Q = \frac{3}{2} q_{CD} S_{CD} \tag{2.37}$$

Assuming the typical value for sp^2 carbon of q_{CD} = 185 kHz [91], it is easy to obtain the order parameters S_{CD} from the quadrupole-split doublets. From standard geometries a simple rotation of 60° provided the η solvent orientational order parameters expressed in the PAS frame (see Figure 2.22).
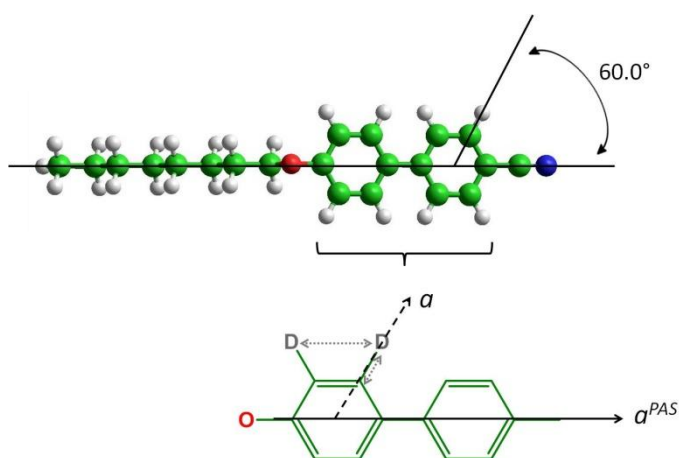
Figure 2.22. Location of a axis in the molecular frame fixed on each phenyl ring and a^{PAS} axis in the principal frame with respect to which the solvent orientational order paremeter η is defined. The a^{PAS} axis coincides with the molecule main axis direction (passing through the oxygen atom, the carbon atom bonded to it, the two carbon atoms joining the two phenyl groups, the carbon atom bonded to the cyano group and the carbon and nitrogen atoms of the latter).

Note that the quadrupolar doublet is further split into three lines by the vicinal ^{2}H-^{2}H dipolar coupling [92]:

$$D_{DD} = -\frac{\gamma_D^2 h}{4\pi^2 r_{DD}^3} S_{aa} \tag{2.38}$$

The S_{aa} order parameter is already expressed in the PAS system (the direction ^{2}H-^{2}H is parallel to the principal a axis, see Figure 2.22) so it represents the η parameter. Such dipolar data were used to further confirm the values of η reported in Table 2.17.

Table 2.17. Mean value of the solvent's orientational order parameter η as a function of the reduced temperature. The error estimated for them is 10%. (from resolution of ^{2}H spectra and by error propagation).

T_{red}	η
0.99	0.44
0.98	0.47
0.97	0.50
0.96	0.56
0.95	0.61
0.94	0.62
0.93	0.64
0.92	0.67

2.3.3.2. Data analysis

In the analysis of the experimental data *via* the ST-DFT method, the centre of a 8OCB molecule was taken coincident with the position of its oxygen atom. With regards to solute-solvent interactions, we followed again the intermediate choice that involves modeling these interactions at an atomistic, chemically detailed level yet retaining only the repulsive part of the atom-atom interactions and assuming the latter of the hard-sphere type. To reduce computational burden further, some simplifications were adopted: (*i*) the alkyl chain was kept in its fully extended, *all trans*, conformation; (*ii*) the hydrogen atoms of the liquid crystal molecule were grouped together with the carbon atom they are bonded to and each group so formed was described by a single hard sphere; (*iii*) according to previous quantum chemical calculations, the chemical bond joining the first two methylene groups of the chain was constrained to lie on the plane of the oxygen atom and nearby phenyl group [93] and the dihedral angle between the two phenyl groups was set at the value of 42° [94]. An implementation of the ST-DFT method was necessary in this case to account for the partial bilayer nature of the 8OCB smectic liquid crystal, which implies the presence of two classes of solvent molecules, having the cyano group parallel or anti-parallel to the arbitrarily chosen direction of the layer normal. All details are reported in ref. [70].

After parametrization of the solvent distribution function, three series of fittings were performed. In a first series the data in the N phase (available for DCB and BIF only) were considered. For each of three temperatures, S_{aa} and $S_{bb} - S_{cc}$ of the two compounds were fitted, using the corresponding value of η in Table 2.17, constraining $\lambda = 0$ and letting Ψ be the

sole parameter to vary. In a second series, the data in the smectic phase, this time including PYR, were analysed assuming that the solutes remain in a N phase, *i.e.* constraining $\lambda = 0$ and varying Ψ only. The values of $\tilde{\chi}^2$ for both these fittings are reported in the second and third column of Table 2.18. In both case the value of $\tilde{\chi}^2$ increases with decreasing temperature. Unlike the previously described case of HAB, the experimental data set available for 8OCB was not large enough for allowing a contemporary fitting on both the λ and Ψ terms in the smectic phase. Thus, we resort to the alternative strategy already exploited [33], which consists in extrapolating the result for Ψ obtained in the N phase down to the SmA$_d$ phase, taking advantage of it being slightly dependent on temperature. δ was fixed at the value determined experimentally ($\delta = 32$Å [79]), so that λ was the sole parameter left to vary. The last column of Table 2.18 gives the results of this fitting. One can observe that the two series of fittings in the last two columns of Table 2.18 are essentially of the same quality, with the fittings assuming the phase as smectic just slightly better, as measured by the values of $\tilde{\chi}^2$. This result can be thought of as consistent with the loose character of the layered structure in the smectic phase of 8OCB.

Table 2.18. Parameters of the three series of fittings as a function of reduced temperature.

T_{red}	$10^3 \, \tilde{\chi}^2{}_{\text{N}}$ [a]	$10^3 \, \tilde{\chi}^2{}_{\text{SmA}}$ [b]	$10^4 \, \tilde{\chi}^2{}_{\text{SmA}}$ [c]
0.99	0.36		
0.98	0.57		
0.97	1.17		
0.95		1.52	1.40
0.94		1.98	1.80
0.93		2.38	2.00
0.92		2.54	2.00

[a] results from fitting in the N phase, varying Ψ only
[b] results from fitting in the SmA$_d$, assumed as a N phase, varying Ψ only
[c] results from fitting in the SmA$_d$, obtained by extrapolating the result for Ψ obtained in the N phase, varying λ only

From the analysis of the $\left[S_{\alpha\beta}\right]_\sigma^{exp}$, the solvent's positional order parameters τ_k^Σ can be calculated. τ_k^Σ for k=1,2,3, shown in Figure 2.23 as a function of the reduced temperature, appears immediately smaller and affected by a larger uncertainty than the ones previously determined for HAB at the same reduced temperatures. Comparing our results for 8OCB with the ones obtained over the years for the series of *n*-alkyl and *n*-alkoxy cyanobiphenyls [61-62,

83, 95], it is to remark the values of τ_1 found in this work for 8OCB are consistent with values found for 8CB (comprised between 0.4 and 0.6) by diffraction based methods [61, 95].
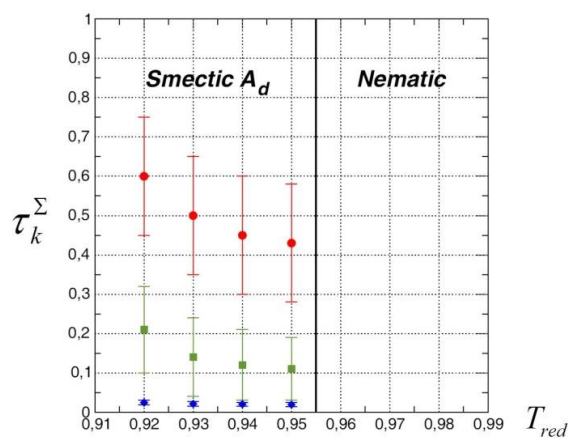
Figure 2.23. Solvent's positional order parameters τ_k^{Σ} as a function of reduced temperature: k = 1 (red circles), k = 2 (green squares), and k = 3 (blue diamonds).

The ST-DFT analysis gives as by-products the solutes' positional-orientational distribution functions $\rho_\sigma(z, \Omega)$, shown in Figure 2.24. It is clear the solutes prefer, as usual, to lie in the regions where the terminal chains of the liquid crystal molecule are more likely located. The extent of the partitioning is considerable: a solute has nearly 90% probability to be found dwelling in the chain region. Dwelling in the core or in the chain regions is associated to a different degree of orientational ordering for the three solutes. It is of interest to see that for DCB and BIF S_{aa} is always larger than $S_{bb} - S_{cc}$, be a solute in the core or in the chain regions, whereas for PYR $S_{aa} \simeq S_{bb} - S_{cc}$ all across the layers. This would mean that, while DCB and BIF behave as ordinary rod-like particles, tending to be more aligned to the layer normal when they are in the core rather than in the chain regions, the orientational order of PYR changes little across a layer, its a- and c-axes always tending to be parallel and perpendicular to the director, respectively, and its b-axis more isotropically distributed.
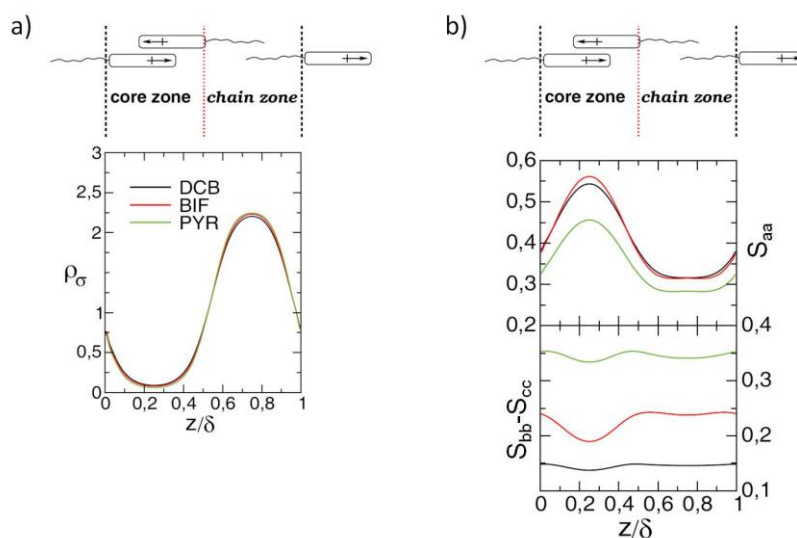
Figure 2.24. (a) Positional distribution functions ρ_σ and (b) orientational order parameters S_{aa} (on the top) and $S_{bb} - S_{cc}$ (on the bottom) for the three solutes, DCB (black), BIF (red) and PYR (green) as a function of the position inside the liquid crystalline phase.

2.3.4. Conclusions

In this section some recent applications of a new methodology for the determination of the solvent's positional order parameters, exploiting a combination of liquid crystal NMR spectroscopy and a statistical thermodynamic density functional theory (ST-DFT), are presented. The approach has been applied first on the conventional SmA liquid crystal HAB, and then on the more delicate case of the interdigitated SmA_d liquid crystal 8OCB. Depending on the amounts of experimental data, a "full" or "simple" version of the methodology have been applied. However, in both case we obtained realistic results in good agreement with the data available from diffraction methods. The presented methodology represents thus a complementary or alternative tool with respect to standard methods, all relying on diffraction experiments, and it would be of interest in perspective to extend it to a smectic C phase. Consider, additionally, that this methodology rests upon the partitioning of small solutes in intra- and inter-layer regions of a smectic liquid crystal and their experiencing different orientational torques in the different regions, and that the similar portioning behavior of small solutes in lipid bilayers is of basic importance in biochemistry and pharmacology [96-98]. It is tempting therefore to speculate on how the present approach could be adapted to contribute to this issue.

2.4. Conclusion

This second chapter showed how the application of ^{1}H, ^{13}C and ^{2}H 1D NMR spectroscopy to rigid probes molecules dissolved in highly orienting thermotropic phases allows to collect valuable experimental data useful to face two arduous issues.

In section 2.2 the highly symmetric molecule of TMA dissolved in the uniaxial nematic I52 solvent was chosen as example of solutes experiencing very weak orientational ordering conditions. The investigation of the peculiar ^{1}H spectral behavior obtained under cooling revealed in turn an interesting trend for the S_{aa} order parameter, from which, under some approximations, a semi-quantitative assessment of the non-rigid contribution to the $^1D_{CH}$ could be derived.

In section 2.3 some rigid solutes, DCB, BIF, NFT and PYR, dissolved in LCs displaying both nematic and smectic phase were used as probes to derive the solvent's positional order parameters, that are typically hard to obtain by standard diffraction techniques. This recently proposed methodology, which combines NMR spectroscopy in liquid crystals and a ST-DFT approach, gave realistic results when applied on the apolar SmA phase of HAB and the interdigitated SmA$_d$ phase of 8OCB.

A basic conclusion should be inferred: when the attention of NMR researchers is focused on more and more complex and flexible systems, it should not be forgotten that rigid small molecules still retain a great interest. It is just the expertise scientists have gained over the years in studying relatively simple solutes that may be now smartly exploited for contributing to more general problems, as the determination of the non-rigid contribution to dipolar couplings or of the positional order parameters in smectic LCs.

References

[1] P. Diehl, Structure of rigid molecules dissolved in liquid crystalline solvents, in *Encyclopedia of Magnetic Resonance*, John Wiley & Sons, Ltd., **2007**

[2] A. Bax, J. J. Chou, B. E. Ramirez, Liquid crystalline samples: application to macromolecular structure determination, in *Encyclopedia of Magnetic Resonance*, John Wiley & Sons, Ltd., **2007**

[3] C. A. de Lange, E. E. Burnell, Theory, models and simulations, in *NMR of Ordered Liquids*, E. E. Burnell and C. A. de Lange eds., Kluwer Academic, Dordrecht, **2003**, part III, ISBN: 1402013434

[4] D. Bailey, A. D. Buckingham, F. Fujiwara, L. W. Reeves, High-resolution nuclear magnetic resonance spectra of tetrahedral molecules and ions in anisotropic environments, *J. Magn. Reson.*, 18, **1975**, 344-357

[5] L. C. Snyder, S. Meiboom, NMR of tetrahedral molecules in a nematic solvent, *J. Chem. Phys.*, 44, **1966**, 4057-4058

[6] E. E. Burnell, C. A. de Lange, D. Capitani, G. Angelini, O. Ursini, ^{3}H NMR of the tritiated isotopologues of methane in nematic liquid-crystal solvents, *Chem. Phys. Lett.*, 486, **2010**, 21-26

[7] L. C. ter Beek, E. E. Burnell, Dideuterium as solute in nematic liquid crystals, *Chem. Phys. Lett.*, 426, **2006**, 96-99

[8] E. E. Burnell, C. A. de Lange, A. L. Segre, D. Capitani, G. Angelini, G. Lilla, J. B. S. Barnhoorn, Tritium nuclear magnetic resonance study of T_2, HT, and DT dissolved in nematic solvents, *Phys. Rev. E*, 55, **1997**, 496-503

[9] A. J. van der Est, E. E. Burnell, J. Lounila, Molecular hydrogen in nematic liquid crystals. Unusual isotope effects, *J. Chem. Soc. Faraday Trans. 2*, 84, **1988**, 1095-1108

[10] C. A. de Lange, J. G. Snijders, E. E. Burnell, On the orientation of small molecules in anisotropic solvents, in *Nuclear Magnetic resonance of Liquid Crystals*, J. W. Emsley ed., Reidel, Dordrecht, **1985**, chap. 8, ISBN: 9027718784

[11] P. B. Barker, A. J. van der Est, E. E. Burnell, G.N. Patey, C. A. de Lange, J. G. Snijders, NMR of deuterium in liquid crystal mixtures, *Chem. Phys. Lett.*, 107, **1984**, 426-430

[12] G. N. Patey, E. E. Burnell, J. G. Snijders, C. A. de Lange, Molecular solutes in nematic liquid crystals: orientational order and electric field gradients, *Chem. Phys. Lett.*, 99, **1983**, 271-274

[13] J. G. Snijders, C. A. de Lange, E. E. Burnell, Vibration-rotation coupling in anisotropic environments. II. Quadrupolar couplings of methanes in liquid crystals, *J. Chem. Phys.*, 79, **1983**, 2964-2969

[14] E. E. Burnell, C. A. de Lange, ^{1}H and ^{2}H NMR of methanes partially oriented in liquid-crystal phases: separation of rigid and nonrigid molecule effects, *J. Chem. Phys.*, 76, **1982**, 3474-3479

[15] J. G. Snijders, C. A. de Lange, E. E. Burnell, Vibration-rotation coupling in anisotropic environments: NMR of methanes in liquid crystals, *J. Chem. Phys.*, 77, **1982**, 5386-5395

[16] P. Diehl, A. C. Kunwar, H. Zimmermann, ^{1}H, ^{115}Sn, ^{17}Sn, and ^{119}Sn NMR studies on tetramethyltin in nematic and isotropic phases, *J. Magn. Reson.*, 30, **1978**, 621-623

[17] I. Y. Wet, C. S. Johnson Jr., NMR spectra of pseudotetrahedral molecules dissolved in a nematic liquid-crystal mixture, *J. Magn. Reson.*, 23, **1976**, 259-264

[18] C. A. de Lange, W. L. Meerts, A. C. J. Weber, E. E. Burnell, Scope and limitations of accurate structure determination of solutes dissolved in liquid crystals, *J. Phys. Chem. A*, 114, **2010**, 5878-5887

[19] E. E. Burnell, C. A. de Lange, J. B. S. Barnhoorn, I. Aben, P. F. Levelt, Molecules with large-amplitude torsional motion partially oriented in a nematic liquid crystal: ethane and isotopomers, *J. Phys. Chem. A*, 109, **2005**, 11027-11036

[20] J. B. S. Barnhoorn, C. A. de Lange, ^{1}H, ^{19}F and ^{2}H NMR of monofluoromethane and deuterated analogues partially oriented in nematic liquid crystals, *Mol. Phys.*, 88, **1996**, 1-20

[21] J. W. Emsley, Liquid crystals: general considerations, in *Encyclopedia of Magnetic Resonance*, John Wiley & Sons, Ltd., **2007**

[22] R. Y. Dong , Liquid crystalline samples: deuterium NMR, in *Encyclopedia of Magnetic Resonance*, John Wiley & Sons, Ltd., **2007**

[23] J. C. Rowell, W. D. Phillips, L. R. Melby, M. Panar, NMR studies of some liquid crystal systems, *J. Chem. Phys.*, 43, **1965**, 3442-3454

[24] W. D. Phillips, J. C. Rowell, L. R. Melby, Quadrupole splittings in the deuterium magnetic resonance spectra of liquid crystals, *J. Chem. Phys.*, 41, **1964**, 2551-2552

[25] P. J. Collings, M. Hird, *Introduction to Liquid Crystals: Chemistry and Physics,* Taylor & Francis, London, **1997**, ISBN: 0748406433

[26] C. D. Southern, H. F. Gleeson, Using the full Raman depolarisation in the determination of the order parameters in liquid crystal systems, *Eur. Phys. J. E*, 24, **2007**, 119-127

[27] P. S. Pershan, Raman studies of orientational order in liquid crystals, in *The Molecular Physics of Liquid Crystals*, G. R. Luckhurst and G. W. Gray eds., Academic Press, London, **1979**, chap. 17, ISBN: 9780124589506

[28] A. Arcioni, R. Tarroni, C. Zannoni, Fluorescence depolarization in liquid crystals, in *Polarized Spectroscopy of Ordered Systems*, B. Samori' and E. Thulstrup eds., Kluwer, Dordrecht, **1988**, chap. 18, ISBN: 9789400930391

[29] A. J. Leadbetter, Structural studies of nematic, smectic A and smectic C phases, in *The Molecular Physics of Liquid Crystals*, G. R. Luckhurst and G. W. Gray eds., Academic, London, **1979**, chap. 13, ISBN: 9780124589506

[30] J. Doucet, X-ray studies of ordered smectic phases, in *The Molecular Physics of Liquid Crystals*, G. R. Luckhurst and G. W. Gray eds., Academic, London, **1979**, chap. 14, ISBN: 9780124589506

[31] C. A. Veracini, M. Geppi, Liquid crystalline samples: chiral smectic phases, in *Encyclopedia of Magnetic Resonance*, John Wiley & Sons, Ltd., **2007**

[32] J. Charvolin, B. Deloche, Nuclear magnetic resonance studies of molecular behavior, in *The Molecular Physics of Liquid Crystals*, G. R. Luckhurst and G. W. Gray eds., Academic, London, **1979**, chap. 15, ISBN: 9780124589506

[33] G. Celebre, G. Cinacchi, G. De Luca, Solvent smectic order parameters from solute nematic order parameters, *J. Chem. Phys.*, 129, **2008**, 094509.1-8

[34] J. G. Snijders, C. A. de Lange, E. E. Burnell, On the orientation mechanism of small molecules in liquid crystalline environments, *Israel J. Chem.*, 23, **1983**, 269-281

[35] E. E. Burnell, C. A. de Lange, NMR as a tool in the investigation of fundamental problems in ordered liquids, *Solid State Nucl. Magn. Reson.*, 28, **2005**, 73-90

[36] A. J. van der Est, E. E. Burnell, J. B. S. Barnhoorn, C. A. de Lange, J. G. Snijders, Acetylene in nematic liquid crystals: a vibrational analysis of the observed dipolar couplings, *J. Chem. Phys.*, 89, **1988**, 4657-4665

[37] S. Sýkora, J. Vogt, H. Bösiger, P. Diehl, Vibrational corrections in NMR spectra of oriented molecules, *J. Magn. Reson.*, 36, **1979**, 53-60

[38] N. J. D. Lucas, The influence of vibrations on molecular structure determinations from N.M.R. in liquid crystals, *Mol. Phys.*, 22, **1971**, 147-154

[39] G. Celebre, G. De Luca, M. Longeri, E. Sicilia, Graphical interactive strategy for the analysis of NMR spectra in liquid crystalline phases, *J. Chem. Inf. Comput. Sci.*, 34, **1994**, 539-545

[40] G. Celebre, G. De Luca, M. Longeri, G. Pileio, Calculated *versus* "experimental" force fields: the influence in the structure determination of benzene by NMR spectroscopy in liquid crystal solvents, *Mol. Cryst. Liq. Cryst.*, 465, **2007**, 289-299

[41] C. Aroulanda, G. Celebre, G. De Luca, M. Longeri, Molecular ordering and structure of *quasi*-spherical solutes by liquid crystal NMR and Monte Carlo simulations: the case of norbornadiene, *J. Phys. Chem. B*, 110, **2006**, 10485-10496

[42] G. De Luca, M. Longeri, G. Pileio, P. Lantto, NMR spectroscopy investigation of the cooperative nature of the internal rotational motions in acetophenone, *Chem. Phys. Chem.*, 6, **2005**, 2086-2098

[43] J. Kaski, P. Lantto, J. Vaara, J. Jokisaari, Experimental and theoretical *ab initio* study of the ^{13}C–^{13}C spin–spin coupling and ^{1}H and ^{13}C shielding tensors in ethane, ethene, and ethyne, *J. Am. Chem. Soc.*, 120, **1998**, 3993-4005

[44] J. Kaski, J. Vaara, J. Jokisaari, ^{13}C–^{13}C spin–spin coupling tensors in benzene as determined experimentally by liquid crystal NMR and theoretically by *ab initio* calculations, *J. Am. Chem. Soc.*, 118, **1996**, 8879-8886

[45] P. Diehl, Molecular structure from dipolar coupling, in *Nuclear Magnetic Resonance of Liquid Crystals*, J. W. Emsley ed., Reidel, Dordrecht, **1985**, chap. 7, ISBN: 9027718784

[46] A. J. Van der Est, P. B. Barker, E. E. Burnell, C. A. de Lange, J. G. Snijders, N.M.R. of methanes in liquid crystal mixtures, *Mol. Phys.*, 56, **1985**, 161-169

[47] J. Lounila, P. Diehl, The effects of the correlation between vibration and rotation of partially oriented molecules on the N.M.R. parameters, *Mol. Phys.*, 52, **1984**, 827-845

[48] E. E. Burnell, C. A. de Lange, Effects of interaction between molecular internal motion and reorientation on NMR of anisotropic liquids, *J. Magn. Reson.*, 39, **1980**, 461-480

[49] A. Loewenstein, Relaxation times, diffusion coefficients and high frequency NMR measurements of methane dissolved in MBBA, *Chem. Phys. Lett.*, 38, **1976**, 543-546

[50] R. Ader, A. Loewenstein, Proton and deuteron magnetic resonance of methanes, silanes and GeH$_3$D dissolved in nematic liquid crystals, *Mol. Phys.*, 30, **1975**, 199-208

[51] R. Ader, A. Loewenstein, Nuclear magnetic resonance spectra of deuterated methanes and 2,2-dimethylpropane in nematic liquid crystals, *Mol. Phys.*, 24, **1972**, 455-457

[52] A. J. Montana, B. P. Dailey, NMR studies of spherical molecules dissolved in smectic liquid crystal solvents, *J. Magn. Reson.*, 22, **1976**, 117-124

[53] G. Celebre, G. De Luca, M. E. Di Pietro, Experimental assessment of the vibration-reorientation contribution to liquid crystal NMR dipolar couplings: the case of tetramethylallene dissolved in a nematic mesophase, *J. Phys. Chem. B*, 115, **2011**, 11119-11126

[54] P. G. de Gennes, J. Prost, *The Physics of Liquid Crystals, 2nd edition*, Clarendon Press, Oxford, **1995**, ISBN: 9780198517856

[55] E. B. Priestley, Liquid crystal mesophases, in *Introduction to Liquid Crystals*, E. B. Priestley, P. J. Wojtowicz, and P. Sheng eds., Plenum Press, New York, **1974**, chap. 1, ISBN: 9780306308581

[56] G. W. Gray, Liquid crystals and molecular structure - Smectics, in *The Molecular Physics of Liquid Crystals*, G. R. Luckhurst and G. W. Gray eds., Academic Press, London, **1979**, chap. 12, ISBN: 9780124589506

[57] P. J. Wojtowicz, Introduction to the molecular theory of smectic-A liquid crystals, in *Introduction to Liquid Crystals*, E. B. Priestley, P. J. Wojtowicz and P. Sheng eds., Plenum Press, New York, **1974**, chap. 7, ISBN: 9780306308581

[58] Y. Takanishi, A. Ikeda, H. Takezoe, A. Fukuda, Higher smectic-layer order parameters in liquid crystals determined by X-ray diffraction and the effect of antiferroelectricity, *Phys. Rev. E*, 51, **1995**, 400-406

[59] J. Watanabe, M. Hayashi, Thermotropic liquid crystals of polyesters having a mesogenic *p,p'*-bibenzoate unit. 2. X-ray study on smectic mesophase structures of BB-5 and BB-6, *Macromolecules*, 22, **1989**, 4083-4088

[60] A. J. Leadbetter, E. K. Norris, Distribution functions in three liquid crystals from X-ray diffraction measurements, *Mol. Phys.*, 38, **1979**, 669-686

[61] G. G. Alexander, S. M. King, R. M. Richardson, H. Zimmermann, Determination of the translational order parameter for smectic liquid crystals using small-angle neutron scattering, *Liq. Cryst.*, 37, **2010**, 961-968

[62] N. Kapernaum, F. Giesselmann, Simple experimental assessment of smectic translational order parameters, *Phys. Rev. E*, 78, **2008**, 062701.1-3

[63] M. Cifelli, G. Cinacchi, L. De Gaetani, Smectic order parameters from diffusion data, *J. Chem. Phys.*, 125, **2006**, 164912-164918

[64] A. C. J. Weber, X. Yang, R. Y. Dong, E. E. Burnell, The smectic effect on solute order parameters rationalized by double Maier–Saupe Kobayashi–McMillan theory, *J. Chem. Phys.*, 132, **2010**, 034503.1-8

[65] A. C. J. Weber, X. Yang, R. Y. Dong, W. L. Meerts, E. E. Burnell, Solute order parameters in liquid crystals from NMR spectra solved with evolutionary algorithms: application of double Maier–Saupe Kobayashi–McMillan theory, *Chem. Phys. Lett.*, 476, **2009**, 116-119

[66] A. Yethiraj, R. Y. Dong, E. E. Burnell, The smectic potential in a liquid crystal with a reentrant nematic phase: NMR of solutes, *Chem. Phys. Lett.*, 441, **2007**, 245-249

[67] A. Yethiraj, A. C. J. Weber, R. Y. Dong, E. E. Burnell, NMR determination of smectic ordering of probe molecules, *J. Phys. Chem. B*, 111, **2007**, 1632-1639

[68] A. Yethiraj, Z. Sun, R. Y. Dong, E. E. Burnell, NMR measurement of smectic ordering and nematic-smectic-A coupling in a liquid crystal, *Chem. Phys. Lett.*, 398, **2004**, 517-521

[69] G. Cinacchi, Ordering of biaxial solutes in a smectic solvent, *Chem. Phys. Lett.*, 416, **2005**, 238-245

[70] M. E. Di Pietro, G. Celebre, G. De Luca, H. Zimmermann, G. Cinacchi, Smectic order parameters *via* liquid crystal NMR spectroscopy: application to a partial bilayer smectic A phase, *Eur. Phys. J. E*, 35, **2012**, 112.1-10

[71] M. E. Di Pietro, G. Celebre, G. De Luca, G. Cinacchi, Rigid probe solutes in a smectic-A liquid crystal: an unconventional route to the latter's positional order parameters, *Phys. Rev. E*, 84, **2011**, 061703.1-7

[72] M. A. Bates, G. R. Luckhurst, Computer simulation studies of anisotropic systems. XXX. The phase behavior and structure of a Gay-Berne mesogen, *J. Chem. Phys.*, 110, **1999**, 7087-7108

[73] Y. Sasanuma, Conformational and orientational characteristics of chain molecules placed in a nematic field: *n*-decane and 1,6-dimethoxyhexane dissolved in 4'-methoxybenzylidene-4-*n*-butylaniline (MBBA), *J. Phys. II*, 3, **1993**, 1759-1778

[74] D. Catalano, C. Forte, C. A. Veracini, J. W. Emsley, G. N. Shilstone, Solute-solvent interactions in the nematic and smectic A phases of 4,4'-di-*n*-heptylazoxybenzene studied by deuteron NMR, *Liq. Cryst.*, 2, **1987**, 357-371

[75] L. Calucci, M. Geppi, A. Marini, C. A. Veracini, Orientational order in liquid crystals by combining ^{2}H and ^{13}C nuclear magnetic resonance spectroscopy and density functional theory calculations, *Phys. Rev. E*, 82, **2010**, 041702.1-8

[76] A. Bondi, van der Waals volumes and radii, *J. Phys. Chem.*, 68, **1964**, 441-451

[77] E. H. Pape, On packing in smectics: X-ray diffraction study on the homologous series 4,4'-di-*n*-alkyl-azoxybenzenes, *Mol. Cryst. Liq. Cryst.*, 102, **1984**, 271-280

[78] G. W. Gray, K. J. Harrison, J. A. Nash, New family of nematic liquid crystals for displays, *Electron. Lett.*, 9, **1973**, 130-131

[79] A. J. Leadbetter, J. C. Frost, J. P. Gaughan, G. W. Gray, A. Mosley, The structure of smectic A phases of compounds with cyano end groups, *J. Phys. France*, 40, **1979**, 375-380

[80] A. J. Leadbetter, R. M. Richardson, C. N. Colling, The structure of a number of nematogens, *J. Phys. Colloques*, 36, **1975**, C1.37-43

[81] J. E. Lydon, C. J. Coakley, A structural study of the smectic mesophases of two biphenyl compounds and an X-ray investigation of the miscibility criterion, *J. Phys. Colloques*, 36, **1975**, C1.45- 48

[82] P. E. Cladis, D. Guillon, F. R. Bouchet, P. L. Finn, Reentrant nematic transitions in cyano-octyloxybiphenyl (8OCB), *Phys. Rev. A*, 23, **1981**, 2594-2601

[83] M. F. Palermo, A. Pizzirusso, L. Muccioli, C. Zannoni, An atomistic description of the nematic and smectic phases of 4-*n*-octyl-4′-cyanobiphenyl (8CB), *J. Chem. Phys.*, 138, **2013**, 204901.1-16

[84] J. Zhang, J. Su, H. Guo, An atomistic simulation for 4-cyano-4′-pentylbiphenyl and its homologue with a reoptimized force field, *J. Phys. Chem. B*, 115, **2011**, 2214-2227

[85] L. De Gaetani, G. Prampolini, Computational study through atomistic potentials of a partial bilayer liquid crystal: structure and dynamics, *Soft Matter*, 5, **2009**, 3517-3526

[86] Y. Lansac, M. A. Glaser, N. A. Clark, Microscopic structure and dynamics of a partial bilayer smectic liquid crystal, *Phys. Rev. E*, 64, **2001**, 051703.1-12

[87] A. A. Zywociński, S. A. Wieczorek, J. Stecki, High-resolution volumetric study of the smectic-*A*–to–nematic transition in 4-(*n*-pentyl)phenylthiol-4′-(*n*-octyloxy)benzoate (8¯S5) and octyloxycyanobiphenyl (8OCB), *Phys. Rev. A*, 36, **1987**, 1901-1907

[88] J. Thoen, H. Marynissen, W. Van Dael, Temperature dependence of the enthalpy and the heat capacity of the liquid-crystal octylcyanobiphenyl (8CB), *Phys. Rev. A*, 26, **1982**, 2886-2905

[89] J. W. Emsley, Measurement of orientational ordering by NMR, in *Nuclear Magnetic Resonance of Liquid Crystals*, J. W. Emsley ed., Reidel, Dordrecht, **1985**, chap. 15, ISBN: 9027718784

[90] J. W. Emsley, J. C. Lindon, NMR spectra from quadrupolar nuclei, in *NMR Spectroscopy Using Liquid Crystal Solvents*, Pergamon Press, Oxford, **1975**, chap. 6, ISBN: 0080199194

[91] E. H. Hardy, R. Witt, M. D. Zeidler, A new method for the determination of the dynamic isotope effect and the deuterium quadrupole coupling constant in liquids, *J. Magn. Reson.*, 134, **1998**, 300-307

[92] V. Domenici, M. Geppi, C. A. Veracini, NMR in chiral and achiral smectic phases: structure, orientational order and dynamics, *Prog. Nucl. Magn. Reson. Spectrosc.*, 50, **2007**, 1-50

[93] G. Cinacchi, G. Prampolini, DFT study of the torsional potential in ethylbenzene and ethoxybenzene: the smallest prototypes of alkyl- and alkoxy-aryl mesogens, *J. Phys. Chem. A*, 107, **2003**, 5228-5232

[94] S. Tsuzuki, T. Uchimaru, K. Matsumura, M. Mikami, K. Tanabe, Torsional potential of biphenyl: a*b initio* calculations with the Dunning correlation consisted basis sets, *J. Chem. Phys.*, 110, **1999**, 2858-2862

[95] A. J. Leadbetter, J. L. A. Durrant, M. Rugman, The density of 4-*n*-octyl-4-cyano-biphenyl (8CB), *Mol. Cryst. Liq. Cryst.*, 34, **1977**, 231-235

[96] J. L. MacCallum, D. P. Tieleman, Computer simulation of the distribution of hexane in a lipid bilayer: spatially resolved free energy, entropy, and enthalpy profiles, *J. Am. Chem. Soc.*, 128, **2005**, 125-130

[97] T. Hessa, H. Kim, K. Bihlmaier, C. Lundin, J. Boekel, H. Andersson, I. M. Nilsson, S. H. White, G. von Heijne, Recognition of transmembrane helices by the endoplasmic reticulum translocon, *Nature*, 433, **2005**, 377-381

[98] S. H. White, G. I. King, J. E. Cain, Location of hexane in lipid bilayers determined by neutron diffraction, *Nature*, 290, **1981**, 161-163

Chapter 3

STRUCTURAL, ORIENTATIONAL AND CONFORMATIONAL ANALYSIS

OF FLEXIBLE MOLECULES

3.1.   Introduction

In the previous chapter the molecules we considered are rigid objects, but they constitute only a small part of the reality. Most of compounds are in fact flexible and undergo not only small-amplitude vibrational motions but above all large-amplitude, low frequency, torsional motions. This means a flexible molecule switches constantly between some more stable conformations, and it does exist as an average structure. Torsional internal motions are rapid enough, on the NMR timescale, that the dipolar couplings and the quadrupolar splittings which are obtained by analysis of the NMR spectrum of a liquid crystalline sample are averages over these motions. *Via* these averaged values, it is thus possible to investigate by liquid crystal NMR techniques the molecular internal motions and then the flexibility of molecules in solution.

NMR studies of flexible molecules in liquid crystalline phases are mainly of two kinds, those of the mesogens themselves (or smaller molecules that mimic part of them) and of non-mesogenic solutes. In this thesis the emphasis was given to studies of solutes dissolved in liquid crystalline phases, aimed at determining their conformational distribution. The knowledge of three-dimensional structure and conformational equilibrium of flexible organic solutes in liquid phase represents indeed a fundamental subject both for theory and applications and the molecules under investigation in this Ph.D. thesis try to cover as many areas of interest as possible.

From a theoretical point of view, investigating the molecular conformational equilibrium has represented a challenging and intriguing topic. Efforts for example have been concentrated in rationalizing the influence of the phase on the changes in the dihedral angles observed for some molecules in different state of matters [1-3], or in explaining the detailed mechanisms of chemical reaction pathways in terms of steric hindrance and conformational arrangements [4-5]. Over the years, the theoretical conformational analysis *via* molecular modeling calculations has gained an impressive importance as technique for investigating structures, determining spatial and thermodynamic properties, calculating conformational energies, exploring orientational behaviors and conformational potentials [6-10]. Besides the interest in itself, an experimental and/or theoretical description of potential surfaces and conformational distributions is intimately linked to a plethora of applications. In fact, it is generally recognized that the spatial arrangement that a compound adopts can deeply affects its chemical reactivity, molecular packing and biological activity. This gains a special interest in the life science and medicinal chemistry, since the conformational distribution may guide the interactions the therapeutic agents create with endogenous ligands as well as specific delivery

systems [11-15]. The elucidation of their three-dimensional structure and conformational description can be then of valuable help for the rational drug design and screening processes as well as for the pharmaceutical formulation development.

From the above, it is obvious that a tool allowing structural and conformational analysis of flexible molecules is extremely meaningful in multiple fields. The possibility of performing such investigation in a liquid environment is even more interesting, since it is the state of matter where molecules generally interact and, if bioactive, play their role. NMR spectroscopy evidently satisfies both requirements. Classical NMR strategy for investigating molecular structure and conformation in solution has, for a considerable time, relied on scalar spin-spin couplings measurements, for torsional constraints [16-17], the nuclear Overhauser effect (nOe) measurements, for short and medium-range distance constraints [18], or a combination of these two. However, standard NMR parameters are short ranged in nature, thus these methods have limitations for obtaining connectivity information between atoms which are far apart and are often insufficient for an unequivocal structural and conformational determination, particularly when the measurement averages over two or more conformers [15, 19-22]. Moreover, NOESY experiments may be very time-consuming if mixing time is not well defined, because a build-up curve is required in this case. Giving access to anisotropic observables, NMR spectroscopy in ordering liquid crystalline phases provides with a reliable alternative and makes it possible to obtain an amount of experimental information not available with other techniques. Indeed, thanks to their dependence on the spin-spin distances and on the orientations of the internuclear vectors with respect to the external magnetic field, dipolar couplings represent a valuable probe of long-range constraints of even spatially remote parts of molecules, typically absent in *J*-coupling and nOe measurements, and can thus provide with an unique insight into the conformational design of organic compounds.

Despite the extremely informative content, the effective application of liquid crystal NMR techniques to the conformational problem meets some difficulties in the extraction as well as the interpretation of experimental data. A first obstacle is related to the complexity of NMR spectra in partially ordered media, which rises quickly with the increase in the size of the spin networks. In thermotropic LCs, analysis of single-quantum ^{1}H spectra (proton being the most studied magnetically active nucleus) of spin systems larger than 10 nuclei is a very hard task and spectral analysis needs the help of simulation programs. In this Ph.D. thesis we used the home-made software ARCANA [23]. An alternative strategy may reside in the use of automated spectral fitting routines like Genetic Algorithms [24-27]. In all cases, the availability of a good set of input parameters for the iterative spectral analysis remains a crucial step (see chap. 1 section 1.5.2). Whereas input values for chemical shifts and indirect couplings are

usually taken from spectra of isotropic samples, guessing adequate starting values for dipolar couplings is a real problem. This point will be central in section 3.2 in the case of biphenyl. In lyotropic LCs, some graphical packages can be sometimes used (MestRe, NMRSIM, PANIC or ARCANA), but this is not generally required, since second-order features are typically weak and a first-order spectral analysis is often possible. This does not mean that in PBLG phases the extraction of the desired large set of D_{ij} is trivial, because of significant signal overlaps and complex multiplet structures. Moreover, since experimental RDCs that can be obtained in PBLG phases have typically small magnitude (Hz or tens of Hz), (*i*) the percentage error in the measured D_{ij}^{obs} is, for the same absolute error, generally greater than in thermotropic spectra, and (*ii*) only the largest dipolar interactions can be practically measured, so that the number of collected data is not always large enough for a subsequent conformational analysis. These issues will be discussed in more detail for the anti-inflammatory molecules described in section 3.3. Attempting to extract as many D_{ij}^{obs} as possible, various NMR experiments on different nuclei may be combined. However, even though a broad array of 1D and 2D NMR pulse sequences is already available, we will see for example in the case of diflunisal (section 3.3.1.1) that there is always the need for new experiments allowing a simple and time-saving edition of experimental dipolar couplings.

A second difficulty one has to face in the study of the conformational problem is related to the interpretation of the experimental data. Indeed, in order to yield the desired conformational information from the dipolar couplings set, some basic initial information must be available and some assumptions must be made [28]. First, we need starting values for molecular structure. This kind of information can be derived from data of other techniques available in literature or mostly from molecular modelling calculations. Secondly, we have to choose a proper method to model the solute-solvent anisotropic orientational potential and the intramolecular potential from which $P_{LC}(\Omega, \{\phi\})$, and possibly $P_{iso}(\{\phi\})$, can be obtained. From this point of view, the simplest case of flexible molecules to be studied is represented by single rotors. The choice for a "reasonable" shape of the potential barrier is rather easy, and a description through a small number of terms with a limited number of adjustable parameters turned out to be generally adequate. Many example exist [2, 29-43] whose experimental data have been fitted by different methods, RIS, AP or ME. A more complex case is represented by molecules which display two rotations. Moreover, for some two-rotor molecules it may be necessary to allow for cooperative rather than independent rotations [44-48] and in these cases the reproduction of potential surfaces is not trivial. It is logical that the extension of such methodology for the treatment of the conformational problem to molecules displaying more

degrees of flexibility becomes a formidable task. With the increase in bond rotations within a molecule, it becomes impracticable to sample enough points for each rotation, in order to be able to characterize the functional form of the potentials by NMR. In some cases a dramatically simplification of the conformational distribution taking into account only the conformers at the minima in the rotational potential (the RIS model) is sufficient [49]. Alternatively, residual dipolar couplings alone or combined with nOe data and/or long range scalar coupling constants can be used to refine structures or validate a minimum energy conformation obtained by molecular modelling calculations [15, 50-58].

In an effort to organize logically this chapter, the studies will be presented following a certain degree of complexity. For this reason, the single-rotor molecule of biphenyl will be presented as first example. Then, the class of anti-inflammatory drugs will be investigated, starting from single rotors (diflunisal and phenylsalicylic acid), towards more complex cases like naproxen, displaying two non-coupled rotations. In the last part, we will discuss the cooperative motions of *trans*-stilbene and *trans*-4,4'-dichlorostilbene, two prototype molecules for a series of stilbenoids endowed with multiple biological activities and involved in a variety of human pathological processes. The choice of the suitable liquid crystalline phase will be explained each time according to the nature of the solute, *i.e.* taking into account number of spin and symmetry.

3.2.   Starting set of dipolar couplings for spectral analysis from molecular dynamics: the case of biphenyl in thermotropic nCB

Biphenyl is a well-known single-rotor molecule that has attracted researchers' interest for years. It interconverts among four symmetry-related structures characterized by a dihedral angle φ between the two ring planes (see Figure 3.1). Such molecule represents a building block for the rigid core of many mesogens [59-60] and the value of φ plays an important role in determining the physical properties of such materials and their molecular packing [61-62]. From the theoretical viewpoint, the investigation of the torsional distribution is interesting since it offers insights into the competitive interactions that are responsible of the inter-ring torsion: the conjugation of the π electronic system *versus* the repulsive forces between hydrogen atoms at *ortho* positions. It has be found that the value of φ at the global minimum of the torsional potential, φ_M, shows a strong dependence on the phase of the material, ranging from values of about 45° in the gas phase [63-66], 30-40° in solution [67-69], to 0°-10° in the solid phase [70-76]. Moreover, the torsional angle φ_M plays a role in determining the

reactivity of biphenylic molecules, too. It has been found for example that when biphenyl is enclosed in the binding pocket of the biphenyl dioxygenase, an enzyme involved in degradation pathways of biphenyls and polychlorinated biphenyls in bacteria, it is the staggered arrangement of the substrate that is bounded and fixed by the aminoacid residues of the protein's active site [77]. To contribute to this debated subject, some researchers faced the issue using liquid crystal NMR spectroscopy. Several ^{1}H-NMR studies of the conformational distribution of biphenyl and substituted analogues as solutes in different strongly ordering nematic solvents have been reported [2, 43, 78-83], that gave values for φ_M in the range 32-38°, depending on the method (RIS, ME or AP) chosen for the analysis of the experimental D_{HH}.

Unfortunately, the single-quantum spectrum of the biphenyl molecule, a 10-spin system, is quite complicated and its spectral analysis was achieved only resorting to deuteration as method for simplifying the spectrum [2]. The quadrupolar splittings from the [2]H-spectrum of the totally deuterated molecule were measured and used to calculate the values of the order parameters, which were exploited in turn, by assuming a regular hexagonal structure (aromatic C-C bonds = 1.40 Å, inter-ring C-C bond = 1.46 Å, C-H bonds = 1.08 Å, and all angles equal to 120°), to estimate trial values for the dipolar couplings. As for biphenyl, the availability of a good set of input parameters, and in particular of dipolar couplings, is probably the main obstacle in the iterative analysis of proton spectra of solutes dissolved in highly ordering media. Next to deuteration and isotopic substitution in general, several strategies have been proposed to aid in the analysis, but none of them has proven to be resolutive.

In this context, from the collaboration between the LXNMR S.C.An. group at the University of Calabria and the LCGroup at the University of Bologna, a new potential procedure was suggested. The idea is related to the recent advances in atomistic molecular dynamics (MD) simulations of liquid crystalline systems made by the team of Prof. Zannoni, which demonstrated to be promising in reproducing real experimental results of the phase itself and of solutes dissolved therein [84-88]. A particularly appealing outcome was the ability in reproducing properties like phase transition temperatures, orientational order parameters and [13]C-^{1}H residual dipolar couplings of commercial standard mesogenic compounds like 4-*n*-pentyl-4'-cyanobiphenyl (5CB) and 4-*n*-octyl-4'-cyanobiphenyl (8CB) [89]. Though, for a given temperature, the dipolar couplings simulated for the mesogenic molecules were systematically higher than the experimental ones, indicating some defects in predicting the orientational order of the phase, the results are interesting. The logical following question is whether or not (*i*) residual dipolar couplings can be simulated also for flexible solutes partially ordered in such liquid crystalline phases and (*ii*) these MD couplings can be used as starting parameters for the analysis of their NMR experimental spectrum. In a first recent test [90], MD simulated dipolar

couplings for the flexible molecule of *n*-pentane dissolved in 5CB seemed to provide a good starting point for analysis of the experimental NMR spectrum using an evolutionary strategy algorithm, even if again the MD couplings for a given temperature are larger in magnitude than the NMR ones. Evolutionary strategies are essentially brute-force methods that will always be able to reach convergence if reasonable ranges for the dipolar couplings are defined beforehand. The questionable point may be eventually to define to what extent a CPU-time is acceptable or not. A more effective proof of the reliability of MD simulated dipolar couplings of a partially ordered solute should repose on evaluating if such MD couplings well reproduce the experimental values obtained by a standard operator-mediated spectral analysis and, even more, if such simulated set is good enough to be used as starting input set in the iterative analysis. With this aim, the LXNMR S.C.An. group and the LCGroup have tackled a joint experimental and MD-simulated ^{1}H NMR study at different temperatures of the flexible aromatic π-conjugated molecule of biphenyl, employed as a probe dissolved in the well known liquid crystalline solvents 5CB (exhibiting only a nematic phase) and 8CB (exhibiting both a nematic and a smectic A phase, see Appendix A2). The contribution of this Ph.D. work relates in particular to the experimental study of biphenyl (2P) in 8CB (Figure 3.1).
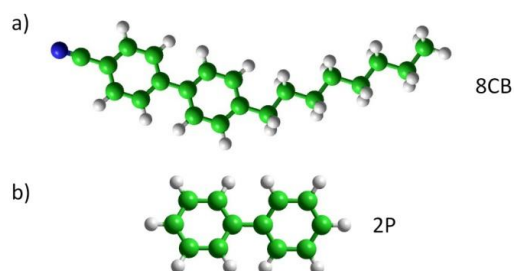
Figure 3.1. "Balls and cylinders" structure of (a) the liquid crystal 8CB and (b) biphenyl (2P).

The choice of biphenyl as solute for the comparison is largely justified by the amount of experimental liquid crystal NMR investigations already done and by the wide expertise acquired within the LXNMR S.C.An. group in the analysis of its spectra in thermotropic phases as well as the interpretation of the extracted D_{ij} using proper theoretical models. However, note that, though many NMR studies of biphenyl have appeared, the case of biphenyl in *n*-alkylcyanobiphenyl (*n*CB) liquid crystals has never been treated before. By similar arguments, the choice of 5CB and 8CB as liquid crystalline solvents is due to the recent development and validation made by the LCGroup of a force field (FF) for *n*CB, that proved to be able to reproduce transition temperatures within a few degrees from experiment and to obtain a

good agreement with the available NMR data [89, 91]. Through this validated FF, the alignment of 2P in 8CB was simulated by molecular dynamics, providing a set of MD dipolar couplings to be compared with the experimental ones obtained by an operator-mediated analysis of its NMR ^{1}H spectrum. In the following a direct comparison aimed at "quantifying" the predictivity of liquid crystal modeling will be presented, followed by a brief discussion on the real applicability of the MD simulated dipolar couplings as good set of input parameters for the iterative spectral analysis.

3.2.1.   *Comparison between experimental and MD simulated results*

In order to compare NMR and MD data, the experimental and simulated systems should be kept as similar as possible. For NMR experiments we used a dilute sample of 2P/8CB (2.8 wt%), added of 1,3,5-trichlorobenzene (TCB) as orientational probe (see Appendix A3 for details on sample preparation). Proton spectra were recorded on a Bruker Avance 500MHz (11.74 T) instrument, equipped with a Bruker BVT-2000 temperature control unit (accuracy of 0.5 K on the T-control), at temperatures ranging from 273.0 K to 307.0 K (0.88-0.99 in terms of $T_{red} = T/T_{NI}$, where the SmA phase is in the range 0.88-0.96), allowing for a thermostabilization of 40-50 min for each temperature. Spectral analysis was performed through the program ARCANA [23], yielding the [1]H-^{1}H dipolar couplings reported in columns "exp" of Table 3.1. Figure 3.2 reports, as an example, the calculated and the experimental ^{1}H spectra at T_{red} = 0.97.

16820.0 15820.0 14820.0 13820.0 12820.0 11820.0 10820.0 9820.0 8820.0 7820.0 6820.0 5820.0 4820.0 3820.0 2820.0 1820.0 820.0   Hz
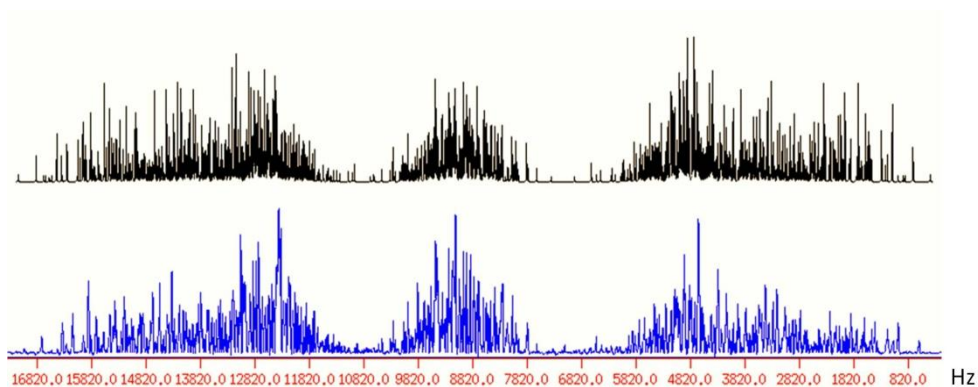
Figure 3.2. Calculated (on the top) and experimental (on the bottom) ^{1}H-NMR spectra of 2P in 8CB at T_{red} = 0.97. The RMS agreement is 0.97.

To compare with NMR experiments, a solution of 2P in 8CB at 2.7 wt% (added of TCB) has been simulated by the MD technique [92] in the range of temperature between 294.0 K and 306.0 K (0.963-1.003 in terms of T_{red}). Note that this system, composed of 1892 molecules of 8CB, 8 of TCB and 100 of 2P, is the biggest that can be simulated for approaching the experimental concentration. Both solutes and solvent have been described with atomistic detail, using for the 8CB the previously validated force field. Simulation details will be reported in a paper that is currently in preparation [93].

Before discussing NMR and MD results in terms of dipolar coupling values, it is interesting to compare experimental and simulated transition temperatures. The experimental values were obtained by observing the solution through a polarizing optical microscope equipped with temperature unit and high resolution camera and confirmed from the NMR spectral pattern. The corresponding values for the simulated system can be obtained by plotting the macroscopic orientational order parameter $\langle P_2 \rangle$ (defined as in chapter 1 section 1.2.3) against the temperature (Figure 3.3). Note that (*i*) simulations are very time-consuming (about six months were required to collect points in the whole range of temperature) and (*ii*) for $\langle P_2 \rangle$ < 0.3 the phase is considered to be isotropic. For these reasons only one value of simulated $\langle P_2 \rangle$ (corresponding to T = 306.0 K) is reported in the isotropic range.
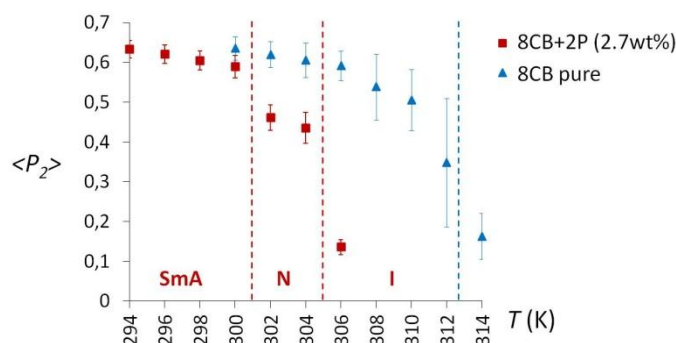
Figure 3.3. MD simulated orientational order parameter as a function of temperature for pure 8CB [91] (blue) and 8CB with 2P as solute (red). The simulated transition temperatures are indicated by dashed vertical lines.

Results from both experiments and simulations are summarised in Figure 3.4. Consider first the nematic-isotropic transition temperature, T_{NI}. For the pure 8CB, the experimental value of T_{NI} is 313.5 K [59] and the simulated one is 312.5 K [91]. From NMR experiments it is observed that, as expected, dissolving 2P in 8CB reduces the LC order, leading to a shift of T_{NI} to lower temperatures (T_{NI}^{exp} = 311.0 K). In simulations, when 2P is present, the T_{NI}^{sim} has been estimated to be 305.0 K, and this is revealed by a significant decrease of ordering between

304.0 K and 306.0 K (Figure 3.3). Although a downshift of this transition temperature is expected because of the addition of the solute, and also taking into account the significant statistical error usually affecting the determination of T_{NI} in the simulations (~4-5 K), the consequences of doping 8CB with a small quantity of biphenyl appear to be significantly overestimated when compared to the real ones. In other words, the simulations describe a situation where the doping of the solvent compromises in a significant way the ordering of the studied system, causing an extreme narrowing of the nematic range. Contrarily, if we compare the smectic A - nematic transition temperature, T_{SN}, a better agreement can be observed between experimental and simulated results. From Figure 3.4 it can be seen that T_{SN} is estimated to occur at around 301.0 K and 303.0 K from the simulations and the NMR experiments, respectively, that is few degrees below the T_{SN} for pure 8CB at 306.5 K [59]. Note that MD simulations do not cover the temperature range below 294.0 K (gray zone in Figure 3.4), which corresponds approximately to the crystal - smectic A transition temperature T_{KS} for the pure 8CB [59]. On the contrary T_{KS} for the experimental sample was recorded at 270.0 K, hence indicating a significant influence on the solvent's order caused by the addition of solute.
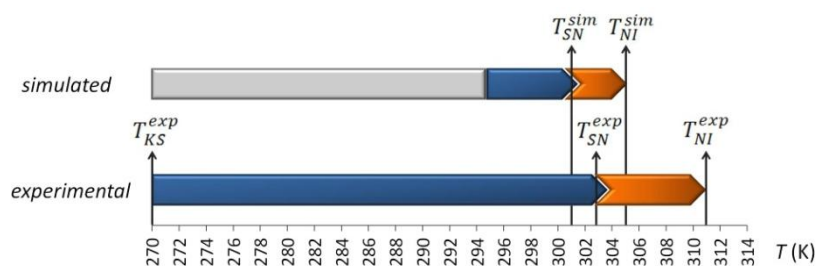
Figure 3.4. Comparison between simulated and experimental transition temperatures for 8CB with 2P as solute. Nematic and smectic ranges are in orange and blue, respectively. Gray area represents the temperature range not considered in MD simulations.

The main target of this study is a comparison of experimental and simulated data in terms of dipolar couplings. In the NMR technique, these quantities can be derived from the analysis of the spectral lines, while in the simulation they are calculated from atomic coordinates, relating them to the direction of maximum alignment of the sample, that is assumed to be coincident with the direction of the magnetic field used in the experiment. The dipolar couplings of a given solute are thus intrinsically dependent on the average order of the liquid crystal solvent, which is directly transferred to the solute through intermolecular interactions. Moreover, dipolar couplings contain the ensemble average of the molecular

internal degrees of freedom. Therefore reproducing RDCs for biphenyl with a simulation implied a sufficiently realistic description of its intramolecular potential.

The discrepancies observed in the transition temperatures for the experimental and simulated cases are of course translated in terms of magnitude of dipolar couplings at a specific temperature, preventing from a comparison of dipolar couplings at the same absolute temperature. However, despite these differences, an effective comparison between simulated and experimental dipolar couplings is possible when considering same values of T_{red}. Table 3.1 and Figure 3.5 report the experimental and MD simulated dipolar couplings of selected hydrogen pairs as a function of T_{red}. It can be seen that there is a acceptable general correspondence between experimental and MD simulated dipolar couplings at the same T_{red}. This denotes a fair ability of MD simulations to reproduce the conformation of 2P and its order, induced by the liquid crystal, and their temperature dependence. Looking at single couplings more carefully, one can observe that the worst agreement occurs for two intra-ring dipolar couplings, $D_{12'} = D_{34'}$ and $D_{25} = D_{46}$. Though in both cases D_{ij}^{sim} is 2.5 - 3 times greater than D_{ij}^{exp} (see Table 3.1), the discrepancy is much more evident in Figure 3.5 for $D_{25} = D_{46}$, as an obvious consequence of the absolute magnitude of the two couplings. Though at present no evidence definitely explains why molecular dynamics simulations fail in reproducing such couplings, a couple of considerations have to be made. Concerning $D_{12'} = D_{34'}$, it should be noted that its magnitude is very small. Therefore, even if the percentage error is large ($D_{ij}^{sim} - D_{ij}^{exp}$ is about 150-200% than D_{ij}^{exp}), the absolute error (around 10 Hz) is similar to those observed for other dipolar couplings (see, for instance, $D_{14} = D_{14'} = D_{23} = D_{23'}$, $D_{16} = D_{35}$ or $D_{15} = D_{36}$) or even less (*i.e.* $D_{12} = D_{34}$ or $D_{13} = D_{13'}$). Concerning $D_{25} = D_{46}$, it should be considered that the angle between the orientation of the internuclear vector $r_{25} = r_{46}$ and the main molecular axis a is near to the "magic angle". As a consequence, even very small geometrical changes have a great effect on the entity of the corresponding dipolar coupling. It can be supposed then that the simulated value for such coupling is affected by a larger indeterminacy.

Table 3.1. Experimental and simulated ^{1}H-^{1}H dipolar couplings (all values in Hz) for biphenyl in 8CB at different reduced temperatures. The chemical structure provides the hydrogen atom numbering. Errors on simulated D_{HH} are estimated through the "blocking" method described in ref. [94].
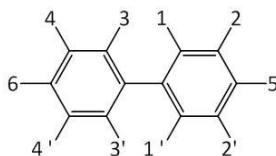
T_{red}	$D_{12}= D_{34}$		$D_{13}= D_{13'}$		$D_{11'}= D_{33'}$	
	exp	*sim*	*exp*	*sim*	*exp*	*sim*
0.880	-3766.82 ± 0.05		-1284.43 ± 0.10		236.76 ± 0.15	
0.890	-3686.11 ± 0.04		-1252.34 ± 0.08		229.61 ± 0.13	
0.910	-3565.24 ± 0.05		-1205.94 ± 0.09		218.99 ± 0.15	
0.920	-3481.88 ± 0.05		-1174.29 ± 0.11		212.47 ± 0.17	
0.930	-3391.12 ± 0.03		-1140.11 ± 0.07		205.33 ± 0.12	
0.940	-3290.35 ± 0.03		-1102.17 ± 0.06		196.66 ± 0.10	
0.960	-3158.86 ± 0.03		-1054.30 ± 0.06		187.44 ± 0.10	
0.963		-3177 ± 9		-924 ± 5		164 ± 1
0.970	-3022.42 ± 0.03	-3094 ± 13	-1004.91 ± 0.06	-895 ± 8	177.16 ± 0.10	156 ± 2
0.977		-3003 ± 15		-867 ± 9		150 ± 2
0.980	-2556.68 ± 0.05		-844.09 ± 0.11		145.95 ± 0.17	
0.983		-2891 ± 25		-833 ± 10		141 ± 3
0.990	-2348.86 ± 0.08	-2205 ± 23	-771.09 ± 0.16	-623 ± 10	132.39 ± 0.28	99 ± 3
0.996		-2055 ± 47		-578 ± 11		90 ± 4

T_{red}	$D_{22'}= D_{44'}$		$D_{14}= D_{14'} = D_{23}= D_{23'}$		$D_{24}= D_{24'}$	
	exp	*sim*	*exp*	*sim*	*exp*	*sim*
0.880	235.85 ± 0.15		-317.02 ± 0.05		-119.63 ± 0.10	
0.890	229.37 ± 0.12		-313.98 ± 0.04		-117.27 ± 0.08	
0.910	218.66 ± 0.14		-303.63 ± 0.05		-113.54 ± 0.09	
0.920	212.03 ± 0.17		-300.79 ± 0.05		-110.33 ± 0.11	
0.930	204.32 ± 0.11		-289.01 ± 0.03		-107.82 ± 0.06	
0.940	197.51 ± 0.10		-280.65 ± 0.03		-105.08 ± 0.06	
0.960	186.44 ± 0.10		-269.17 ± 0.03		-100.57 ± 0.06	
0.963		165 ± 1		-272 ± 1		-102.1 ± 0.3
0.970	176.90 ± 0.11	157 ± 2	-257.51 ± 0.03	-264 ± 1	-96.17 ± 0.07	-99.4 ± 0.4
0.977		151 ± 2		-257 ± 1		-96.6 ± 0.5
0.980	145.85 ± 0.17		-217.93 ± 0.05		-81.45 ± 0.11	
0.983		142 ± 3		-248 ± 1		-93 ± 1

T_{red}	exp	sim	exp	sim	exp	sim
0.990	131.69 ± 0.28	99 ± 3	-200.64 ± 0.08	-189 ± 1	-75.47 ± 0.17	-71 ± 1
0.996		90 ± 4		-176 ± 2		-66 ± 2

T_{red}	$D_{12'}= D_{34'}$		$D_{16}= D_{35}$		$D_{15}= D_{36}$	
	exp	sim	exp	sim	exp	sim
0.880	1.55 ± 0.07		-222.26 ± 0.12		-473.00 ± 0.12	
0.890	0.30 ± 0.05		-217.02 ± 0.11		-464.04 ± 0.10	
0.910	-1.07 ± 0.06		-210.28 ± 0.12		-449.47 ± 0.13	
0.920	-2.06 ± 0.06		-205.12 ± 0.16		-439.59 ± 0.15	
0.930	-2.56 ± 0.05		-200.03 ± 0.09		-428.38 ± 0.09	
0.940	-3.57 ± 0.04		-193.89 ± 0.08		-417.12 ± 0.08	
0.960	-4.47 ± 0.04		-186.30 ± 0.09		-400.61 ± 0.09	
0.963		-14 ± 1		-190 ± 1		-405 ± 1
0.970	-5.05 ± 0.04	-16 ± 1	-178.78 ± 0.08	-185 ± 1	-383.78 ± 0.09	-396 ± 2
0.977		-16 ± 1		-180 ± 1		-385 ± 3
0.980	-6.37 ± 0.07		-151.70 ± 0.14		-325.68 ± 0.14	
0.983		-17 ± 1		-173 ± 1		-371 ± 3
0.990	-6.77 ± 0.11	-17 ± 1	-139.88 ± 0.23	-133 ± 1	-298.88 ± 0.22	-285 ± 3
0.996		-17 ± 1		-124 ± 3		-266 ± 6

T_{red}	$D_{26}= D_{45}$		$D_{25}= D_{46}$		D_{56}	
	exp	sim	exp	sim	exp	sim
0.880	-90.35 ± 0.12		-2.22 ± 0.12		-71.74 ± 0.09	
0.890	-88.93 ± 0.10		-9.93 ± 0.10		-70.33 ± 0.07	
0.910	-86.03 ± 0.12		-21.28 ± 0.12		-67.84 ± 0.08	
0.920	-83.19 ± 0.16		-31.28 ± 0.15		-66.33 ± 0.09	
0.930	-81.89 ± 0.09		-34.48 ± 0.09		-64.82 ± 0.06	
0.940	-79.84 ± 0.08		-39.89 ± 0.08		-62.76 ± 0.06	
0.960	-76.72 ± 0.09		-46.66 ± 0.08		-60.14 ± 0.05	
0.963		-77.6 ± 0.2		-130 ± 6		-61.2 ± 0.3
0.970	-73.25 ± 0.08	-75.7 ± 0.3	-51.75 ± 0.08	-139 ± 6	-57.76 ± 0.05	-60 ± 1
0.977		-73.4 ± 0.4		-142 ± 7		-58 ± 1
0.980	-61.52 ± 0.13		-58.70 ± 0.13		-49.21 ± 0.09	
0.983		-71 ± 1		-148 ± 6		-56 ± 1
0.990	-56.39 ± 0.22	-54 ± 1	-62.23 ± 0.21	-149 ± 6	-44.66 ± 0.14	-43 ± 1
0.996		-50 ± 1		-147 ± 5		-40 ± 3
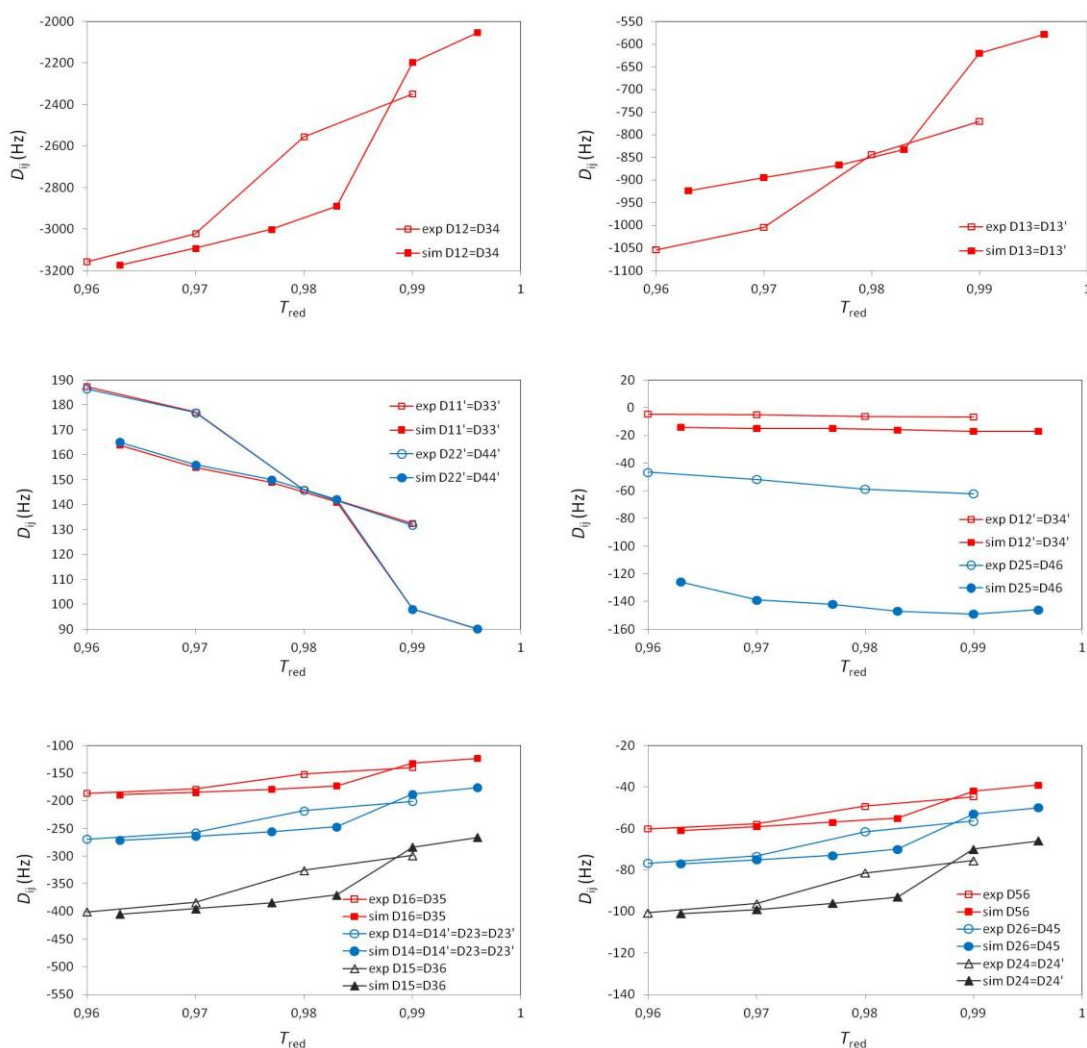
Figure 3.5. Comparison of experimental (empty symbols) and simulated (filled symbols) dipolar couplings as function of T_{red} in 2P/8CB system. Lines are reported as eye-guide.

Encouraged by the satisfactory overall agreement, the next step is obviously to evaluate whether or not the set of MD dipolar couplings can be used as starting parameters for a operator-mediated analysis of the experimental NMR spectra. To investigate this possibility, we input the initial dipolar couplings obtained from MD into the ARCANA program in order to calculate a trial spectrum to be compared with the experimental one. The iterative analysis described in chap. 1 was carried out and it was possible to finally assign a high number of transitions, achieving a low RMS, while iterating on all parameters (chemical shifts and D_{ij}). This result demonstrates the differences found for some couplings (namely $D_{12'}= D_{34'}$ and $D_{25}= D_{46}$) do not invalidate the operator's task. Hence, MD atomistic simulations seem to represent a viable strategy to provide a starting set of parameters for the analysis of NMR

spectra of orientationally ordered solutes in anisotropic environments when no other information is available.

As seen in chapter 1 section 1.4.2, experimental dipolar couplings in flexible molecules are directly linked to the probability distribution function $P_{LC}(\Omega, \{\phi\})$, which in turn can be related to the intermolecular potential, $U_{ext}(\Omega, \{\phi\})$, and the internal rotational potential, $U_{int}(\{\phi\})$. Hence, as last comparison, it is interesting to look at the torsional free energies of biphenyl in 8CB calculated by molecular dynamics simulations and obtained experimentally. Indeed, in MD simulations and NMR experiments this relationship D_{ij} - torsional potential is "read" in the opposite sense. In fact, in order to calculate from the atomic coordinates and the orientation of internuclear vectors the D_{ij}, especially the inter-ring ones, MD simulations require a precise description of the phenyl-phenyl torsional potential to be inserted in the force field. Therefore, knowing the profile of $U_{int}(\{\phi\})$ is a prerequisite for computing the averaged dipolar couplings. From the experimental viewpoint, dipolar couplings are the observed quantities that are directly extracted from the spectral analysis. They contain in themselves the conformational information but proper theoretical models and some assumptions are needed in order to finally get the conformational equilibrium described. Thus, the D_{ij} are essential if one wants to obtain, *via* liquid crystal NMR, the solute's $U_{int}(\{\phi\})$. In the case of biphenyl, the theoretical approach used to treat the conformational problem was the AP-DPD method, as already done by Celebre *et al.* for biphenyl dissolved in the thermotropic LCs I52, MM (55 wt% ZLI1132/EBBA magic mixture) and HAB [78].

Biphenyl belongs to the D_{2h} point group if the inter-ring angle φ is equal to 0° and D_{2d} if φ = 90°. For all other values of φ, it possesses a D_2 symmetry. Therefore, if the molecular axis system is chosen to be coincident with the PAS for the Saupe matrix (the bc plane bisects the inter-ring angle φ, and axis a is along the molecular long axis (see Figure 3.6)), only two independent order parameters (namely, S_{aa} and $S_{bb} - S_{cc}$) are needed to describe completely the solute ordering in achiral nematics (see Table 1.3 in chapter 1).

Within the AP method, the fragmental contributions required to construct (*via* equation (1.78)) the solute-solvent interaction tensors, are chosen to be those of the rings, $\varepsilon_{2,0}(R)$ and $\varepsilon_{2,2}(R)$. As usual, the two phenyl ring fragments are assumed to keep a rigid C_{2v} symmetry structure as they rotate relative to each other. According to the DPD approach, the normalized $P_{iso}(\{\phi\})$ is modeled as a sum of Gaussian functions as in the following [78]:

$$P_{iso}(\{\phi\}) = \frac{\sum_{i=1}^{2} exp\left[-\left(\frac{\varphi - ((-1)^i \varphi_M)}{h}\right)^2 / 2\right] + exp\left[-\left(\frac{\varphi - ((-1)^i (\pi - \varphi_M))}{h}\right)^2 / 2\right]}{4h\sqrt{2\pi}}$$

$$(3.1)$$

where φ_M is the most probable value of the twist angle, and h gives the width at half maximum height, as in equation (1.85).
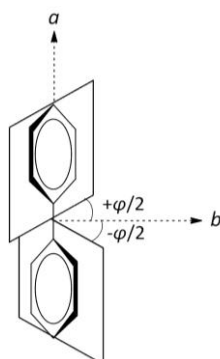
Figure 3.6. Molecular reference frame chosen in biphenyl molecule. Axis c, not shown, defines a right-handed Cartesian system.

Once the theoretical apparatus is established, the experimental D_{HH} of Table 3.1 have to be fitted against the calculated ones by using the program AnCon [95], while varying the orientational ($\varepsilon_{2,0}(R)$ and $\varepsilon_{2,2}(R)$) and conformational (φ_M and h) parameters, until a satisfying RMS (equation (1.87)) is reached. In this specific case, 10 sets (one for each temperature) of D_{HH} are available. Therefore, following a well established procedure [78], we performed a simultaneous fit of the 10 temperature-dependent data sets (12 D_{HH} x 10 temperatures = 120 D_{HH}), adjusting 31 parameters, that is 10 pairs of $\varepsilon_{2,0}(R)$ and $\varepsilon_{2,2}(R)$ (one pair for each temperature), 10 values of φ_M (one for each temperature) and a single value of h (assumed to be common for all the temperatures). In the fitting procedure the geometry was fixed as the one optimised in [78], assuming it does not change significantly within the range of temperatures studied. As an example, Table 3.2 reports the resulting φ_M and h parameters along with the calculated order parameters S_{aa} and $S_{bb} - S_{cc}$ obtained from the conformational analysis at two chosen temperature, 290.0 K (smectic A phase) and 305.0 K (nematic phase). These results are perfectly in agreement with those found for the same molecule dissolved in the thermotropic LCs I52, MM and HAB [78], where, at T_{red} ~0.93, φ_M was found in the range 35.4° - 36.3°.

Table 3.2. Order parameters and values of φ_M and h for biphenyl dissolved in 8CB at two chosen temperatures.

	T (K) / T_{red}	
	290.0 / 0.93	305.0 / 0.98
φ_M (degree)	35.37 ± 0.12	35.51 ± 0.12
h (degree)	11.93 ± 0.28	11.93 ± 0.28
S_{aa}	0.425 ± 0.004	0.321 ± 0.005
$S_{bb} - S_{cc}$	0.182 ± 0.005	0.152 ± 0.003

Finally, it is interesting to compare the effective torsional free energy obtained for biphenyl in 8CB by MD simulations with the same potential calculated experimentally *via* the AP/DPD method. In particular, Figure 3.7 displays the torsional potentials obtained at two different temperatures (one in the nematic and one in the smectic phase) by both MD simulations and the AP/DPD approach. Observing Figure 3.7 a couple of considerations emerges immediately: (*i*) the simulated profile is qualitatively similar to the experimental one, in terms of position of the minima and width of the potential wells; (*ii*) both in the simulated and in the experimental curves, there are no changes in the torsional energy of biphenyl when it is dissolved in the nematic or smectic phase of 8CB. Note, however, that a quantitative comparison between the simulated and the experimental torsional potentials cannot be made, since conformational analysis *via* AP-DPD method does not allow a quantitative description of the torsional barriers. This means that, while an effective difference of ~2 kcal/mol is observed between the values of the maxima at 0° and 90° in the simulated torsional distributions, the energy gaps shown in the experimental curves are not realistic.
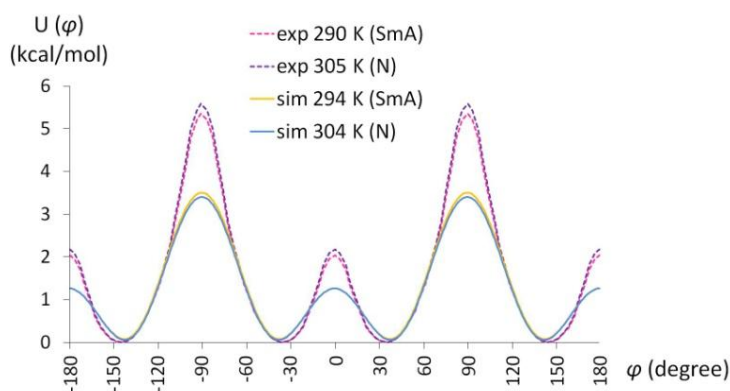
Figure 3.7. Torsional potential for biphenyl in 8CB obtained experimentally in the nematic (T = 305.0 K, violet dashed line) and smectic (T= 290.0 K, pink dashed line) phases with the AP-DPD method and calculated in the nematic (T = 304.0 K, blue solid line) and smectic (T= 290.0 K, yellow solid line) phases *via* MD simulations.

3.2.2. Conclusions

With the aim of overcoming one of the main problems faced in the spectral analysis of partially ordered solutes, that is the need for a good starting set of spectral parameters, atomistic simulations of liquid crystalline systems may represent a new effective tool. In this section the results obtained by MD simulations for the system biphenyl/8CB were compared with NMR experimental outcomes. Despite not negligible differences in terms of transitions temperatures emerge from the comparison, the set of simulated D_{ij} is rather in agreement with the experimental one and allows a standard "line-assignment" operator-mediated spectral analysis when used as starting set of parameters. Same considerations were derived from a similar procedure performed on a sample of 2P dissolved in 5CB (data not shown). The strategy is applied here to the relatively simple molecule of biphenyl (a single-rotor with 4 symmetry-related conformations) but it might represent in the future a viable solution in the NMR spectral analysis of more complex compounds dissolved in anisotropic media when no other information is available.

3.3. Conformational investigation in solution of anti-inflammatory drugs by NMR spectroscopy in weakly ordering media

As stated in section 3.1, the conformational problem is a crucial point when dealing with flexible molecules endowed with biological or pharmacological activity. Indeed, a fundamental topic in medicinal chemistry is the investigation of the relationship between conformation and drug activity. It is well recognized that the spatial arrangement adopted by a bioactive molecule affects the interactions it creates with endogenous ligands, influencing its biological activity, pharmacokinetic properties and metabolic degradation pathways [11-12, 14-15]. Additionally, an area of growing interest is the development of vehicles for the controlled delivery of the active agent. Even in this case, conformational equilibria may play an important role [13, 96]. Several experimental techniques, namely X-ray, solid-state fluorescence and solid state NMR spectroscopies, offer well established protocols for collecting useful data in solid systems. Anyway, it is obvious that investigating conformational distribution in solution can be substantially more interesting, being the liquid medium the environment where the bioactive molecule interacts with its partner or is released by a delivery system. Over the years, liquid state NMR spectroscopy, based on *J*-couplings and nOe measurements, has proven to provide with clues about the conformation the drug can adopt

in solution [97]. However, the technique shows at least a couple of limitations. Firstly, the information it can give is evidently short-range: [3]J-couplings are limited to dihedral angles *via* three covalent bonds, while through space nOe connectivities show a r^{-6} dependence (r being the internuclear distance) and can then be found only up to ~5 Å in favorable cases. In order to obtain the relative orientation of remote centers, multiple nOe or J-coupling connections have to be performed in series to transverse the entire molecule. As soon as the chain of short-range information is broken, distant parts of a molecule cannot be correlated anymore and the whole structure refinement is bound to fail [98-99]. A second, perhaps not immediate, drawback is that only the most stable conformation(s) can be detected, but no information on the potential energy surface can be yield. The knowledge of the most likely conformer matches well with the classic "lock-and-key" model for drug-ligand interactions, which suggests a drug will interact with a target only if its shape, *i.e.* the most populated conformation, is complementary to the active site [11]. Anyway, this model offers an oversimplified picture of the interaction processes in living organisms and it does not take into account the conformational heterogeneity of the substrates. Therefore, it has been replaced by the more dynamic "conformational selection" model, which considers that a macromolecular ligand can sample a vast ensemble of drug's conformations and consequently each thermally accessible conformer other than the lowest energy may play important roles in molecular recognition [11, 14]. In other words, also weakly populated, higher energy conformations may be responsible for recognizing and binding to partners.
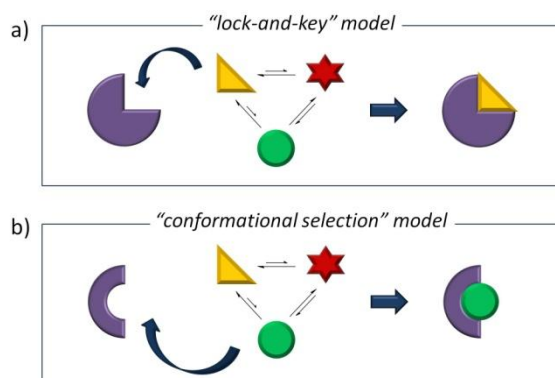
Figure 3.8. (a) "Lock-and-key" and (b) "conformational selection" models describing interaction processes in living organisms.

A landmark case is that of the neurotransmitter acetylcholine, that can exist in *trans*, *gauche* and eclipsed conformations. Liquid state NMR studies and X-ray crystallography indicate that, despite the *gauche* conformation is predominant in solution [100], the bound

conformations of this flexible molecule appear to differ substantially with receptor subtype, that is the *gauche* form is the active conformation at nicotinic receptors [101-102], whereas the *anti* form binds to the muscarinic receptors [103]. Moreover, theoretical conformational analysis revealed that only the completely extended conformation of acetylcholine and its analogues is productive for the enzymatic hydrolysis by the degradative enzyme acetylcholinesterase [12, 104]. It is clear the estimating only the most stable conformer may be no longer sufficient. The proposed methodology, *i.e.* NMR spectroscopy in partially ordered media combined with AP-DPD model, represents an alternative and/or complementary tool for conformational studies of flexible bioactive molecules. Its strength resides in measurement of D_{ij} that (*i*) depend on both the internuclear distance (with a r^{-3} dependence) and the orientation of the internuclear vector relative to the external magnetic field, making it generally possible to correlate distant parts of the molecule, and (*ii*) for flexible molecules are averaged not only on the vibrational but also over the torsional internal motions, containing then information on the conformational equilibrium. The achievement of this kind of fine conformational description is evidently dependent on the complexity of the molecule, and the treatment of the conformational problem becomes more and more intricate with the increasing number of spins and degrees of flexibility. Drug molecules are typically highly substituted, unsymmetrical, very flexible compounds, that is far from those presented till now in this thesis (rigid molecules in chapter 2 and biphenyl in section 3.2). Their investigation in thermotropic LCs as the ones we described for the previous studies is thus a formidable task, that has been up to now limited to molecules with no more than 10-12 spins (see section 3.4). The alternative strategy we chose to apply is the use of weakly ordering liquid crystalline media like PBLG mixtures that, preserving some first-order character of spectra, facilitates the extraction of residual dipolar couplings (RDCs). Even simplifying the spectral analysis, the extraction of the sufficient number of experimental informative data may present some limitations, as discussed in 3.1. Moreover, the theoretical treatment poses an upper limit to the degree of torsional flexibility that can be described. The description of the conformational potential is attemptable, within some assumptions, for molecules with no more than two or three bond rotations and in all cases the *a priori* knowledge of molecular structures is required. As illustration of the potentiality together with the limitations of the technique we present here the conformational investigation *via* NMR in PBLG phases of some nonsteroidal anti-inflammatory drugs (NSAIDs). NSAIDs are a class of drugs that provide analgesic, antipyretic and anti-inflammatory effects and the most prominent members (namely aspirin, ibuprofen and naproxen) are available over the counter in most countries. They act by inhibiting the enzyme cyclooxygenase (COX) [105-106], and reducing then the formation of

thromboxane and prostaglandins, messenger molecules in cellular processes like inflammation, platelet aggregation and pyresis [107]. We have considered two of the most common families, salicylates and 2-arylpropionic acids (or profens). Concerning the first class, we report in section 3.3.1 the conformational investigation of the molecule of diflunisal (DFL, Figure 3.9). The presence of two fluorine atoms in its structure led to the development of a new pulse sequence in order to overcome the problem of the arduous NMR data extraction. Moreover, the comparison of its torsional distribution with that of its non-fluorinated analogue, the phenylsalicylic acid (APS, Figure 3.9), allowed to derive some considerations about the influence that the substitution of proton by fluorine atoms (simply referred to as [1]H-^{19}F substitution in the following) has on structure and conformational equilibrium. Both DFL and APS display a single bond rotation, very similar to that of biphenyl, thus the AP-DPD approach has been used again for their theoretical description. Note that this is one of the first examples of extension of the Additive Potential model to flexible molecules dissolved in weakly orienting phases [108-109]. Therefore, even if relatively simple, the case of DFL and APS are useful also as test to confirm the efficacy and robustness of the AP-DPD approach when applied to lyotropic systems. More complicated from this viewpoint is the treatment of conformational distribution of profen derivatives. The molecule of naproxen (NAP, Figure 3.24) was chosen as illustrative of two-rotor molecules with non-coupled rotations and results obtained for its conformational analysis will be presented in section 3.3.2. It is worthwhile remarking that similar investigations were undertaken on two other compounds of the same class, namely flurbiprofen (2-(2-fluoro-4-biphenyl)propanoic acid) and ibuporofen (2-(4-(2-methylpropyl)phenyl)propanoic acid). The former displays two non-coupled torsions, like naproxen, and was mainly chosen for investigating the effect on the torsional potential of the fluorine atom in *ortho* position relative to the inter-ring C-C single bond. The aim was to compare the inter-ring torsional distribution obtained for such mono-fluorinated molecule with those already obtained for the non-fluorinated biphenyl molecule and the bifluorinated molecule of diflunisal. Preliminary conformational results have been obtained from [1]H-^{1}H, [1]H-^{19}F, [1]H-^{13}C and [19]F-^{13}C dipolar couplings extracted for a sample of flurbiprofen dissolved in PBLG/CDCl$_3$, suggesting a good agreement with molecular modelling calculations. Unfortunately, the superposition of several lines as well as the presence of non neglectable second order effects prevented from collecting an experimental data set large enough to accurately describe the torsional potential. More sophisticated NMR experiments on the same sample and/or change in organic co-solvent will be explored as alternative solutions. In the attempt to extend the methodology to anti-inflammatory drugs possessing a greater number of torsional degrees and/or coupled rotations, we selected ibuprofen as test compound.

Indeed, the treatment of the two coupled rotations of its methylpropyl substituent, together with the additional torsion of the propionic fragment with respect to the central phenyl ring, is theoretically challenging. From the experimental viewpoint, ^{1}H and ^{13}C spectra of a sample of ibuprofen dissolved in PBLG/CDCl$_3$ are promising, since the double substitution on the phenyl ring allows for signals that are sufficiently far apart to precisely measure an acceptable number of residual dipolar couplings. It is to verify if such data set is really enough to perform a conformational analysis that takes into account all the degrees of flexibility in the molecule. Since the results for flurbiprofen and ibuprofen are only partial and they cannot be completed before the end of the Ph.D., they will not be included in the following discussion and only outcomes for the molecule of naproxen will be presented.

3.3.1.   Single rotor: diflunisal and and its non-fluorinated analogue, phenylsalicylic acid

The 2',4'-difluoro-4-hydroxy[1,1'-biphenyl]-3-carboxylic acid, commonly known as diflunisal (DFL, Figure 3.9) is a FDA-approved cyclooxygenase inhibitor, difluorphenyl-derivate of aspirin, presenting similar analgesic and anti-inflammatory therapeutic indications and side effects. It was first sold under the brand name Dolobid®, marketed by Merck & Co., but generic versions are now widely available.
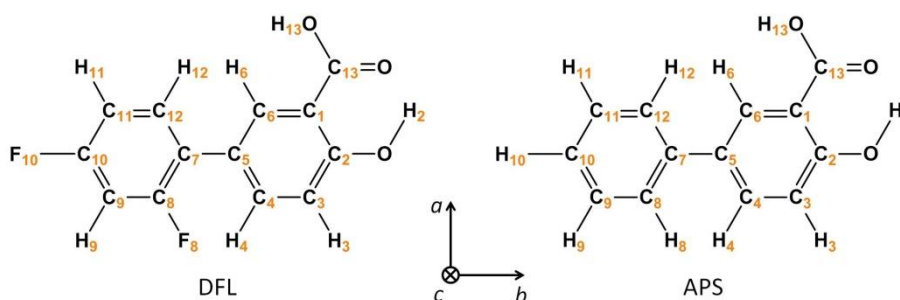
Figure 3.9. Topological structure and atomic labelling of diflunisal and phenylsalicylic acid, referred to with their respective label defined in the text. The (a, b, c) axes of the molecular reference frame adopted for the molecules are also shown.

The structural and conformational problem in complexes that DFL forms with polymeric matrices or metals as well as target proteins has been investigated in solid state by both computational techniques and X-ray, solid-state fluorescence and solid-state NMR measurements [110-117]. Aiming to explore the conformational distribution of DFL directly in

a liquid medium, we resort to NMR spectroscopy combined to the use of PBLG phases. It is worth to underline here that the ability of the polypeptic fibers to readily dissolve in common low viscosity organic solvents allows to overcome the problem of sparing water solubility of the DFL.

From Figure 3.9, it can be seen that the presence of an hydrogen bond between -C_{13}=O and -O-H_2, confirmed by theoretical calculations and NMR spectral evidences, reduces to one the degree of flexibility of the molecule. This means that the conformational study of DFL is the description of a single inter-ring torsion angle φ, defined as the dihedral angle C_4-C_5-C_7-C_8.

In the optic of studying the conformational equilibrium of the molecule of DFL, another structural feature has to be taken into account, that is the presence of two fluorine atoms in the same aromatic ring. This has a dual importance in this thesis project. (*i*) From an experimental point of view, ^{19}F NMR is extremely advantageous in order to gather a more extended data set. ^{19}F is a 100% naturally abundant ½-nuclear spin and it possesses a high magnetogyric ratio, providing 83% of the proton NMR sensitivity for a given magnetic field. Moreover, the ^{19}F chemical shift is exquisitely sensitive to changes in the local environment, making it a very attractive nucleus for NMR studies of various complex molecules [118-123]. It has been demonstrated for example that J_{HF} can provide insights for structural elucidation and conformational design of organic compounds. Indeed Karplus-type relationships have been described for $^{3}J_{HF}$ [124-125], allowing their exploitation for conformational analysis [126-127] and many studies show how much long-range scalar $^{n}J_{HF}$ couplings (n > 3) could report on local bond geometries [128-130]. More information can be obtained of course in anisotropic media by ^{1}H-^{19}F residual dipolar couplings [131-132]. Though D_{HF} are very informative, their use is often hindered by the inherent difficulties in their measurement. This is exactly what occurs in the case of diflunisal, where the very large number of long and short-range residual dipolar couplings between all the magnetically active nuclei in the molecule makes standard spectra overcrowded and extremely complicated to analyse. This prompted us to develop a new frequency spatially encoded heteronuclear ^{1}H-^{19}F selective refocusing NMR experiment (GET-SERF) [133] that allows editing in one single 2D experiment all couplings between a selected fluorine site and all the proton nuclei of the molecule. (*ii*) The presence of fluorine atoms also makes diflunisal a good model molecule to study the influence of ^{19}F nucleus on bond rotation. Next to the interest in fundamental research, this subject has implications in drug synthesis, too. At present, the replacement of hydrogen atoms by fluorine is a well-established practice adopted by pharmaceutical chemists to obtain fluorinated compounds displaying similar biological activity to their hydrogen natural analogues but greater resistance to metabolic degradation and improved bioavailability [134-137]. Indeed, though fluorine atom is still the

substituent with the smallest size that can be used as replacement for the C-H bond in drug design, it is known that it can have an influence on inter- and intramolecular forces and the substitution ^{1}H-^{19}F can alter the physical and chemical properties of compounds, because of its electronegativity, low polarisability and bond strength [138-139]. In the case of diflunisal, it is expected that fluorine atom in 2' position affects rotation about the inter-ring bond. Compared to other halogens, the presence of fluorine in biphenyl-like molecules has a much smaller influence on the φ value (the optimized twist angle was found *in vacuo* to be of 42.5°, 45.1° and 59.9° for biphenyl, 2-fluorobiphenyl and 2-chlorobiphenyl, respectively, by B3LYP/6-311+G* calculations [140]) and the torsional barrier (for instance, in 2-fluoro substituted biphenyls it is found to be barely detectable [141]). Albeit small, an influence does exist and the similarity, in terms of bulkiness, between ^{19}F and ^{1}H is currently not unanimously recognised [141]. In this thesis, aiming to probe whether the ^{19}F nuclei have or not significant effects on the structure and/or conformational distribution of the DFL, we decided to investigate its non-fluorinated analogue, the 4-hydroxy[1,1'-biphenyl]-3-carboxylic acid (or phenylsalicylic acid, APS, structure and numbering reported in Figure 3.9). To make the discussion clearer, the molecule of DFL will be presented first, followed by the case of APS, with a comparison between the two compounds in terms of structure and torsional potential.

3.3.1.1. Diflunisal

i. NMR experiments. Development of a new gradient encoded SERF experiment for the trivial edition of ^{1}H-^{19}F couplings

With the aim of probing the conformational distribution of the investigated molecule we firstly need a large set of experimental data, represented by the observed dipolar couplings D_{ij}^{obs}. Indeed, what is directly read from the anisotropic spectra is the total coupling constant $T_{ij} = |J_{ij} + 2D_{ij,zz}|$ (note that there are no fully equivalent nuclei in the DFL molecule). This means that to edit D_{ij}^{obs} two series of measurements were performed: one on the isotropic sample (DFL in THF-d$_8$), to obtain the scalar couplings J_{ij}^{obs}, and one on the anisotropic sample, to get access to the total couplings T_{ij}^{obs}. As liquid crystalline phases we chose those commonly used in the LRMN group at the University of Paris-Sud, that is solutions of poly-γ-benzyl-L-glutamate (PBLG) and racemic mixtures, named PBG, of PBLG and its enantiomer PBDG. Although the easily commercially available L-enantiomer (PBLG) is the solvent typically used

for most studies, in this work we prepared two samples of DFL, in the chiral PBLG/THF and achiral PBG/THF phase (see Appendix A3 for more details). The idea was to highlight whether or not the chirality of the phase influences the conformational distribution. In the following more emphasis will be given to the chiral sample DFL/PBLG/THF, since the procedure carried out on the achiral sample DFL/PBG/THF led to same considerations.

1D NMR ^{1}H, ^{19}F, ^{19}F-{^{1}H}, ^{13}C, ^{13}C-{^{1}H} and ^{13}C-{^{19}F} spectra were recorded on both the isotropic and anisotropic samples of DFL. Spectral assignment of the peaks was performed on the basis of ^{1}H-^{1}H COSY, ^{1}H-^{13}C and ^{19}F-^{13}C HSQC, ^{1}H-^{13}C and ^{19}F-^{13}C HMBC correlation experiments. All the ^{1}H, ^{19}F and ^{13}C spectra were recorded at 300 K on a liquid high-resolution Bruker Avance 400MHz spectrometer (9.4 T) equipped with a standard variable-temperature unit (BVT-3000) and a BBI or QXO probe with a z field-gradient coil. The ^{19}F lock channel of QXO probe was used for the fluorine pulses.

J_{ij} and T_{ij} couplings between nuclear pairs ^{1}H-^{1}H, ^{1}H-^{13}C and ^{19}F-^{13}C were measured from experiments as 2D ^{1}H-^{13}C J-resolved, ^{1}H-^{1}H SERF and 1D ^{13}C-{^{1}H}. The extraction of J_{HF} and T_{HF} couplings in the diflunisal molecule revealed more difficult. As seen in Figure 3.10, an immediate measurement of ^{1}H-^{19}F couplings is complicated in spectra (a) and (b) of the isotropic sample and almost impossible in spectra (c) and (d) of the anisotropic sample. We tried then to develop a simple pulse sequence allowing the trivial, precise and quick edition of such coupling constants.

As ^{1}H and ^{19}F have similar NMR properties, in order to design a new NMR tool aiming to simply edit spectral ^{1}H-^{19}F couplings, it is reasonable to start from NMR methodological strategies already developed for simplifying ^{1}H-^{1}H spectral patterns. In the case of the homonuclear proton-proton couplings, an appealing approach is based on the use of semi-selective pulses. In particular, an efficient 2D NMR method for the measurement of a single specific J_{HH} coupling in isotropic media, the SElective ReFocusing (SERF) experiment, was developed in 1995 by Fäcke and Berger [142]: by replacing the two hard pulses of a standard ^{1}H-^{1}H J-resolved method by selective and doubly selective RF pulses, this sequence simplifies the proton NMR spectra by selecting a coupling between a pair of nuclei and allows the detection of the desired information. The SERF experiment was then successfully improved and applied on a variety of compounds [143-150].
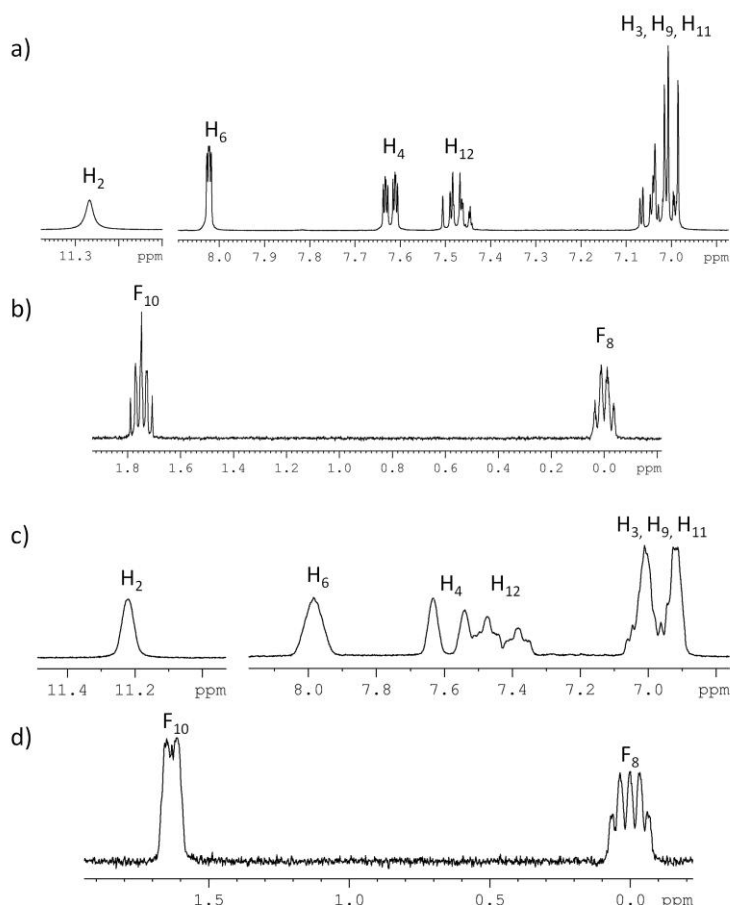
Figure 3.10. (a) 1D ^{1}H and (b) ^{19}F broadband excitation spectra of diflunisal in THF-d$_8$. (c) 1D ^{1}H and (d) ^{19}F broadband excitation spectra recorded on diflunisal in PBLG/THF at 300 K. In both (b) and (d) F$_8$ signal was arbitrary set at 0 ppm, whereas in (a) and (c) residual ^{1}H lines of solvent were used as internal reference.

With the purpose to extract the ^{1}H-^{19}F couplings, we adapted the SERF standard sequence replacing the doubly semi-selective π pulse on proton nuclei at the center of the t_1 evolution time by a doubly semi-selective π pulse on proton and fluorine. This new heteronuclear ^{1}H-^{19}F SERF experiment is denoted HF-SERF [133] and the pulse sequence is reported in Figure 3.11 (a). Consider how it acts in the simplest case of two nuclei, proton A and fluorine X: the first semi-selective π/2 pulse is applied at υ_A, the proton resonance frequency, which is the nucleus to be detected in the t_2 acquisition time. After an evolution time t_1/2 two semi-selective π pulses are applied on A and X nuclei. Then only the desired coupling evolves during the t_1 delay, whereas all the other couplings and the chemical shifts are refocused. In other words, one gets on the 2D map the signal corresponding to A with the full coupling multiplicity in the F$_2$ dimension and only the coupling between A and X in the F$_1$ domain. After tilt of the 2D spectrum, the selected couplings are removed from the direct

dimension, allowing a simplification of the spectral pattern. The phase of the signal is modulated by the coupling during t_1 and thus the resulting lines are "phase-twisted", so that the 2D spectrum is generally processed in magnitude mode.
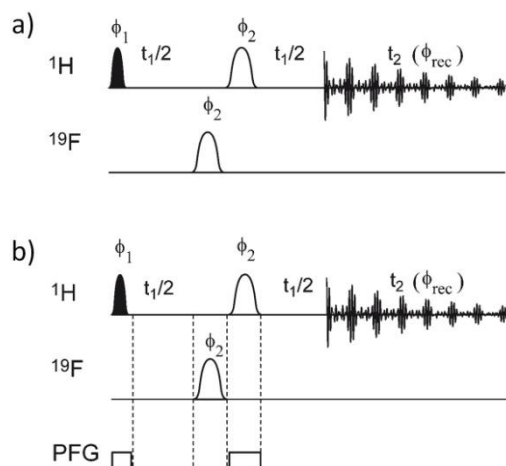
Figure 3.11. Pulse sequences for the (a) HF-SERF and (b) GET-SERF experiments. Black and white ellipse shapes correspond to $\pi/2$- and π-shaped pulses, respectively. The $\pi/2$ and π pulses used here are the E-BURP and RE-BURP shape pulses [151-152]. On the pulsed-field gradient (PFG) channel white rectangular bars refer to the application of a rectangular-shaped z-field gradient. The phase cycle is: $\phi_1 = \phi_{rec} = $ x, -x, x, -x; $\phi_2 = $ x, x, -x, -x.

Note that in the latest years, heteronuclear ^{1}H-^{13}C selective refocusing experiments have been developed to benefit from the chemical shift dispersion of the ^{13}C nucleus [153-156]. Unlike ^{19}F, ^{13}C is a rare and poor sensitive spin. Therefore, even if only selective pulse on proton nucleus is necessary, such sequences often require NMR methods for enhancing signal intensity before acquisition (*i.e.* INEPT transfer) and a filter for eliminating ^{1}H-^{12}C coherences. The high sensitivity and abundance of ^{19}F explain why the ^{1}H-^{13}C selective refocusing experiments are not an adapted solution to resolve ^{1}H-^{19}F couplings. An alternative approach for the extraction of ^{1}H-^{19}F couplings could be the homonuclear *J*-resolved experiments where the heteronuclear couplings are read on the F_2-trace. Though commonly used [157-159], this method is not always efficient because, due to the numerous J_{HF}, the spectrum is not always resolved enough to edit the couplings and, even well resolved, the assignment of couplings could remain difficult. The HF-SERF experiment approach proposed here permits to overcome these difficulties.

However, one of the main drawbacks of the SERF-type experiments, and then of HF-SERF, is that in each spectrum only the couplings between the nuclei covered by the selective pulses (*i.e.* the selected proton and fluorine sites) are edited on the 2D map. As a consequence

several spectra should be acquired in order to gather the measurements of all couplings within the molecule, thus multiplying the experiments to be performed and therefore requiring a significant experimental time. To overcome this limitation, as previously proposed by Giraud *et al.* [160], the frequency encoding approach can be used. Indeed, the simultaneous application of a pulsed field gradient along the sample allows surmounting the problem by effectively applying the pulse on a broad range of chemical shifts according to their spatial position in the NMR tube [160-164]. In other words, in a Gradient encoded homonuclear SERF experiment (G-SERF) it becomes possible, thanks to the creation of a spatial frequency encoding along the sample, to run different selective experiments on different parts of the NMR tube and thus to individually assign and measure, in a single 2D spectrum, all the homonuclear couplings experienced by a given proton site in the molecule. In order to trivially edit in one single NMR experiment all ^{1}H-^{19}F couplings, we combined the frequency encoding approach to the HF-SERF pulse sequence, and we developed the new Gradient Encoded heTeronuclear ^{1}H-^{19}F SElective ReFocusing NMR experiment (GET-SERF) experiment [133], whose pulse sequence is shown in Figure 3.11 (b). The application of two weak field gradients in correspondence of the proton selective pulses allows to carry out this selective experiment on each proton in separate "slices", editing all the ^{1}H-^{19}F couplings between a given fluorine site X and every others protons of the compound, within one single 2D spectrum. Note that in the HF-SERF pulse sequence of Figure 3.11 (a) the two semi-selective π pulses on A and X nuclei at the end of the evolution time $t_1/2$ are applied sequentially in order to permit the encoding in the GET-SERF experiment.

We applied the novel GET-SERF experiment to the diflunisal molecule dissolved both in THF-d_8 and PBLG/THF phase, collecting in each 2D spectrum all the scalar or total couplings between the selected fluorine site and all the protons of the molecule. Figure 3.12 shows the GET-SERF spectra recorded on diflunisal dissolved in THF-d_8, selecting each time F_8 (spectrum (a)) or F_{10} (spectrum (b)). In order to optimize the spatial encoding, the spectral width was limited to the aromatic region.

Consider the spectrum (a), where the offset of the non-encoded semi-selective pulse in the refocusing block was set at the F_8 resonance frequency, so as to edit every coupling involving this selected fluorine. The first frequency encoded π/2 pulse excites the proton spins having different chemical shifts in different cross sections of the sample and subsequently the selective refocusing block allows every interaction undergone by these protons to be refocused, except their couplings with F_8. The resulting spectrum is thus the sum of four sub-spectra originating from every slice in the sample. All the three cross sections corresponding to υ_6, υ_4, υ_{12} (with υ_i the resonance frequency of the *i*-th nucleus) have a doublet structure in the

indirect domain, with splittings J_{H6F8}, J_{H4F8}, and J_{H12F8}, respectively. The last cross section corresponds to the three different protons, H_3, H_9 and H_{11}. In this case, the chemical shift difference is lower than the excitation band frequency, then interactions among them will not be refocused and will appear in the F_1 dimension together with their couplings with F_8. For this reason, a doublet of doublet with splitting J_{H9H11} and J_{H9F8} and a doublet with the same splitting J_{H9H11} are observed at ν_9 and ν_{11}, respectively. H_3 is not coupled to H_9, H_{11} or F_8 and it gives a singlet signal in the F_1 dimension. Note how the separation of the information in different dimensions makes it trivial to assign the different couplings to each proton. Artifacts visible in this cross section can be attributed to second-order coupling effects which for strongly coupled spin systems contribute to the creation of coherences that follow the same coherence transfer pathway as the desired signals and cannot be removed by standard phase cycling and gradient selection procedures. Analysis as well as individuation of methods for their suppression is out of the scope of this project.

This experiment has also been successfully applied on the F_{10} resonance (spectrum (b) of Figure 3.12). It is observed that H_6 and H_4 are not coupled with F_{10}, while H_{12} has a doublet structure in the indirect domain, with splitting J_{H12F10}. In the last cross section, a doublet of doublet with splittings J_{H9H11} and J_{H9F10} and a doublet of doublet with splittings J_{H9H11} and J_{H11F10} are observed at ν_9 and ν_{11}, respectively. Again, H_3 gives a singlet signal because it is not coupled to H_9, H_{11} or F_{10}.

One could argue that [1]H-[19]F J-couplings in such a system composed of only two fluorine nuclei could be extracted from simpler classical experiments as selective decoupling. However, compared to a 1D proton spectrum, a better resolution is obtained with the GET-SERF experiments, thanks to the inhomogeneity refocusing.

In order to extract the [1]H-^{19}F total couplings, the GET-SERF experiment was applied on the anisotropic sample, where the additional very large number of long and short-range residual dipolar couplings makes the spectra even more complicated and often impossible to analyse. Figure 3.13 (a) shows the GET-SERF spectrum of the sample DFL/PBLG/THF where the offset of the non-encoded inversion pulse is set at ν_8. In this case, the 1D proton and fluorine spectra are too complex to unambiguously edit the whole set of heteronuclear couplings using simpler classical experiments (Figure 3.10), supporting our effort to develop the GET-SERF experiment. The 2D map is the sum of three sub-spectra originating from different slices of the sample. The cross section corresponding to ν_6 shows clearly a doublet in the indirect domain with splitting T_{H6F8}. Unlike the isotropic sample, the signals at ν_4 and ν_{12} are not far enough to allow the individual extraction in different slices of the NMR tube and they are collected together so that both T_{H4H12} and their couplings with F_8 will appear in the indirect dimension. In
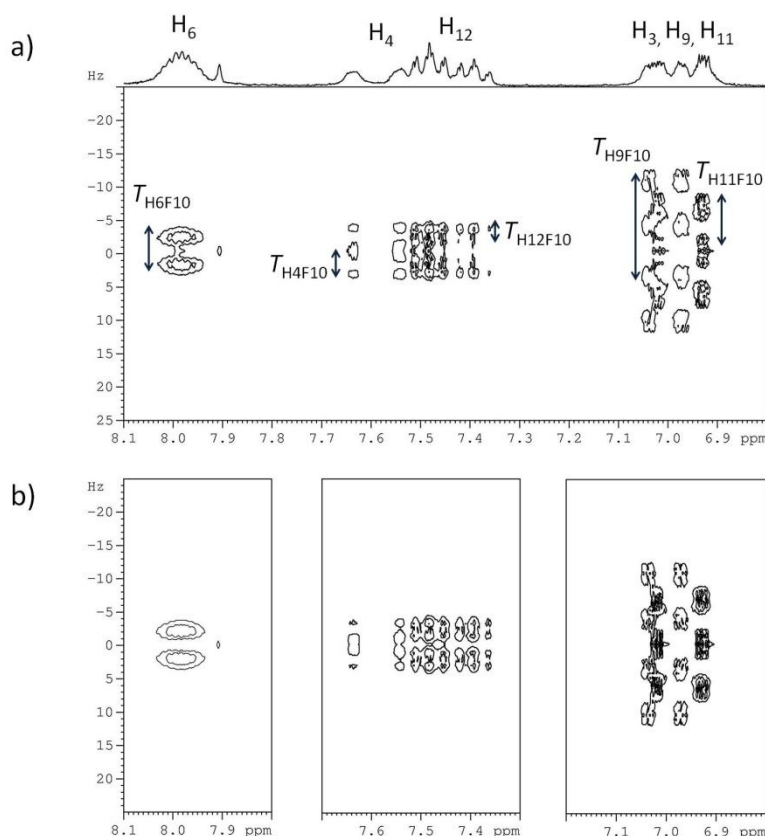
particular a doublet with splitting T_{H4H12} and a doublet of doublet with T_{H4H12} and T_{H12F8} splittings are visible at υ_4 and υ_{12}, respectively. Similar considerations on the cross section containing signals from H_3, H_9 and H_{11} lead to the extraction of the coupling constants T_{H9F8}, T_{H9H11}, T_{H3H9} and T_{H3H11}. This experiment has also been successfully applied on the F_{10} resonance and is presented in Figure 3.14 (a).
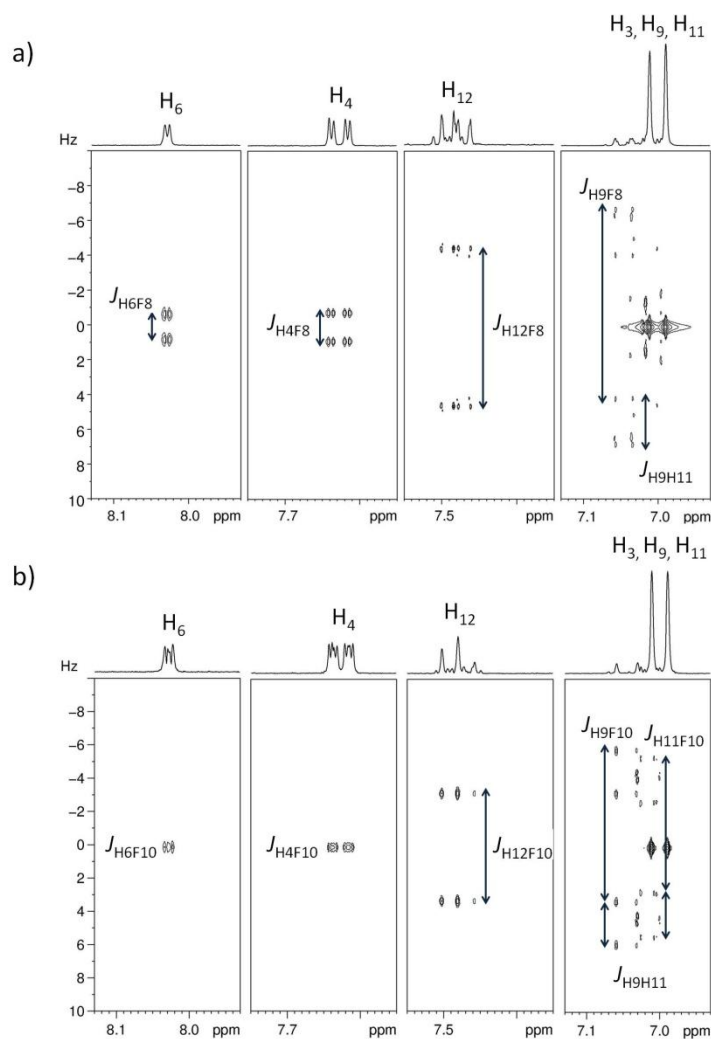
Figure 3.12. 2D GET-SERF tilted spectra at 300 K of diflunisal in THF-d$_8$ where the offset of the non-encoded inversion pulse is set at (a) υ_8 and (b) υ_{10}. Each F_1-trace obtained for a given proton H$_i$ (at υ_i) is modulated by the heteronuclear coupling H$_i$-F$_8$ (or H$_i$-F$_{10}$) selectively edited as well as by all homonuclear couplings H$_i$-H$_j$ it is submitted to. Each GET-SERF spectrum was recorded using a data matrix of 4096 (t_2) x 512 (t_1) with four scans per t_1 increment. The relaxation delays were 1 s. A zero filling to 1024 data points was applied in t_1 and sine functions in both dimensions were applied prior to double Fourier transform. The duration of the encoded RE-BURP refocusing and the E-BURP excitation pulses on the proton channel was 49.5 ms corresponding to a frequency width of 100 Hz. The sample was spatially encoded by a rectangular z pulsed field gradient of strength 0.3 G/cm. The duration of the RE-BURP refocusing pulse on the fluorine channel was 16.5 ms corresponding to a frequency width of 300 Hz. Each spectrum was recorded in 4.5 h.
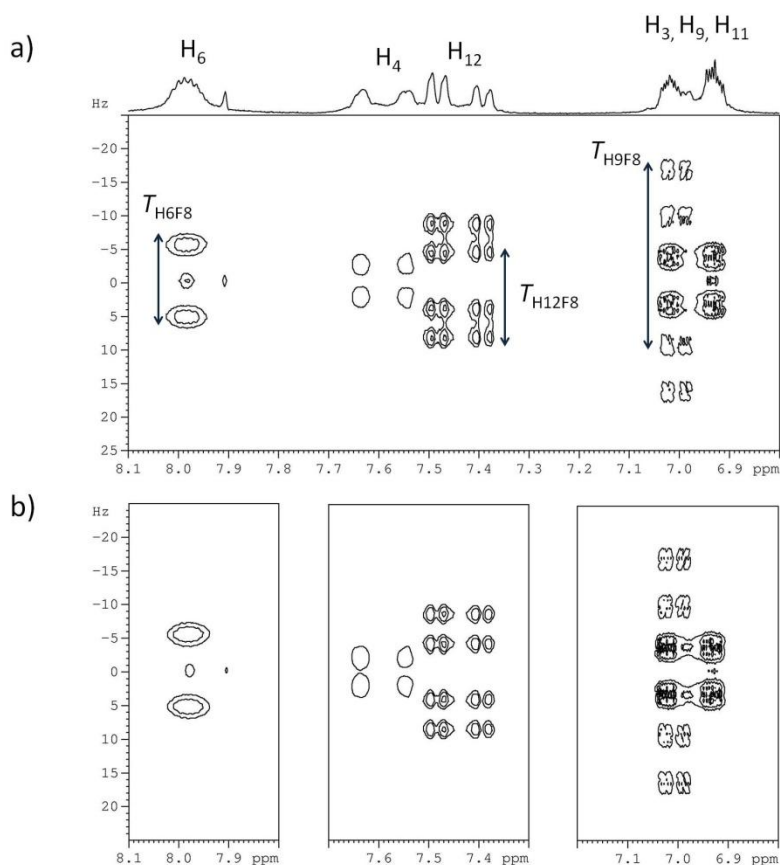
Figure 3.13. (a) 2D GET-SERF tilted spectrum recorded on diflunisal in PBLG/THF at 300 K. The offset of the non-encoded inversion pulse is set at υ_8. This spectrum was recorded in 13 min. (b) Set of three HF-SERF tilted spectra recorded on the same sample under same experimental conditions. The offsets of the selective pulses were set at υ_8 on the fluorine channel for all experiments, and at υ_6, $\upsilon_{4,12}$ or $\upsilon_{3,9,11}$ on the proton channel, respectively. Each 2D spectrum was recorded in 13 min, *i.e.* 39 min for the whole set of HF-SERF experiments. Both the GET-SERF and the three HF-SERF tilted spectra were recorded using a data matrix of 2048 (t_2) x 64 (t_1) with four scans per t_1 increment. The relaxation delays were 1.5 s. Data were processed using zero-filling up to 256 points and a sine filter in t_1. On the proton channel the duration of the soft pulses was 27.5 ms corresponding to a frequency width of 180 Hz, while on the fluorine channel the duration of the RE-BURP pulse was 12.4 ms corresponding to a frequency width of 400 Hz. In the GET-SERF spectrum the sample was spatially encoded by a rectangular z pulsed field gradient of strength 0.2 G/cm.

Figure 3.14. (a) 2D GET-SERF tilted spectrum recorded on diflunisal in PBLG/THF at 300K. The offset of the non-encoded inversion pulse is set at υ_{10}. This spectrum was recorded in 13 min. (b) Set of three HF-SERF tilted spectra recorded on the same sample under same experimental conditions. The offset of the selective pulses were set at υ_{10} on the fluorine channel for all experiments, and at υ_6, $\upsilon_{4,12}$ or $\upsilon_{3,9,11}$ on the proton channel, respectively. Each 2D spectrum was recorded in 13 min, *i.e* 39 min for the whole set of HF-SERF experiments. Both the GET-SERF and the three HF-SERF tilted spectra were recorded using a data matrix of 2048 (t_2) x 64 (t_1) with four scans per t_1 increment. The relaxation delays were 1.5 s. Data were processed using zero-filling up to 256 points and a sine filter in t_1. On the proton channel the duration of the soft pulses was 27.5 ms corresponding to a frequency width of 180 Hz, while on the fluorine channel the duration of the RE-BURP pulse was 12.4 ms corresponding to a frequency width of 400 Hz. In the GET-SERF spectrum the sample was spatially encoded by a rectangular z pulsed field gradient of strength 0.2 G/cm.

To stress the advantages derived by the use of spatial frequency encoding we compared the GET-SERF experiments with the series of three HF-SERF experiments, run under the same experimental conditions on the anisotropic sample, which allows to gather the same collection of data (Figures 3.13 (b) and 3.14 (b)). Despite the same correlation pattern can be observed in both kinds of spectra, it has to be mentioned that the gradient encoding approach is intrinsically less sensitive than the non-encoded experiment, because only a spatially restricted cross section of the sample is responsible for the signal at a given resonance frequency. In the case of diflunisal, a 4-fold difference in intensity is observed between the

broadband and the encoded spectra recorded under the same experimental conditions (Figure 3.15). Note that the loss in sensibility is, in this case, lower than previously reported [160], due to the small spectral width to be encoded.
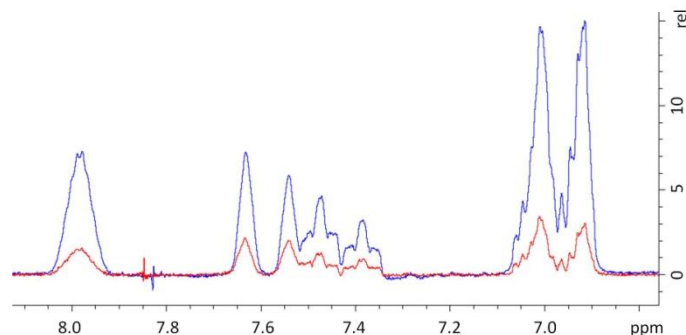
Figure 3.15. Comparison between the standard broadband ^{1}H 1D spectrum (blue) and the ^{1}H 1D spectrum spatially encoded by a rectangular z pulsed field gradient of strength 0.2 G/cm (red), recorded on diflunisal in PBLG/THF at 300K.

As a consequence of the reduced sensibility of an encoded spectrum with respect to the non-encoded one, a greater number of scans and a longer experimental time are in principle required to obtain the same sensitivity for a single map. In the case of diflunisal, however, we can observe that the result of the gradient encoded experiment is still sensitive enough to be valuably exploited. Moreover, to collect every coupling involving F_8 (or F_{10}) spin at least three HF-SERF experiments are necessary, leading finally to a total protocol that is longer than the spatial encoding approach (see Figures 3.13 and 3.14). More generally, for a spin system composed of n non-equivalent proton nuclei coupled to m fluorine sites, $n \times m$ HF-SERF spectra have to be recorded to measure every ^{1}H-^{19}F coupling constant. The design of the GET-SERF pulse sequence, which allows n spins to be individually probed, and their coupling to the m-th nucleus to be selected, reduces the number of experiments required for the same coupling network to m. This constitutes a further proof of the potentiality of gradient encoded selective refocusing spectroscopy as a tool for acquiring more rapidly all the information about large spin networks.

Thanks to the novel GET-SERF experiment the totality of ^{1}H-^{19}F couplings was then measured for the diflunisal molecule. These coupling constants, together with the ^{1}H-^{1}H, ^{1}H-^{13}C and ^{19}F-^{13}C *J* and *T*, are reported in the third and fourth columns of Table 3.3.

Table 3.3. Experimental chemical shifts δ_k^{iso}, scalar couplings J_{ij}^{obs}, total couplings T_{ij}^{obs}, dipolar couplings D_{ij}^{obs} and quadrupolar splittings $\Delta\nu_{CD_k}$ determined by the NMR analysis of DFL dissolved in THF-d_8 and PBLG/THF. Errors are estimated from spectral resolution. In the last column, the D_{ij}^{calc} values are also reported for comparison. The whole agreement between D_{ij}^{obs} and D_{ij}^{calc} is given by the RMS.

i	j	J_{ij}^{obs} (Hz)	T_{ij}^{obs} (Hz)	$D_{ij}^{obs \, (a)}$ (Hz)	$D_{ij}^{calc \, (b)}$ (Hz)
C-H couplings					
C_3	H_3	162.9 ± 0.2	222.8 ± 0.6	30.0 ± 0.4	30.0
C_3	H_4	0.0 ± 0.2	-18.0 ± 0.6	-9.0 ± 0.4	-10.0
C_4	H_4	160.0 ± 0.2	110.2 ± 0.6	-24.9 ± 0.4	-24.8
C_4	H_6	8.7 ± 0.2	9.6 ± 0.6	0.5 ± 0.4	1.1
C_6	H_4	7.9 ± 0.2	8.4 ± 0.6	0.3 ± 0.4	0.4
C_6	H_6	162.5 ± 0.2	226.1 ± 0.6	31.8 ± 0.4	31.7
C_9	H_9	165.9 ± 0.2	175.2 ± 0.6	4.7 ± 0.4	4.4
C_9	H_{11}	5.5 ± 0.2	7.1 ± 0.6	0.8 ± 0.4	1.1
C_{11}	H_{11}	166.0 ± 0.2	193.6 ± 0.6	13.8 ± 0.4	13.8
C_{12}	H_{12}	162.8 ± 0.2	170.1 ± 0.6	3.7 ± 0.4	4.1
C-F couplings					
C_8	F_8	-247.7 ± 0.3	-231.7 ± 0.6	8.0 ± 0.5	8.3
C_8	F_{10}	12.0 ± 0.3	9.3 ± 0.6	-1.4 ± 0.5	-1.3
C_9	F_8	26.3 ± 0.6	20.1 ± 0.6	-3.1 ± 1.1	-3.4
C_9	F_{10}	26.3 ± 0.6	20.1 ± 0.6	-3.1 ± 1.1	-3.2
C_{10}	F_8	12.1 ± 0.3	11.3 ± 0.6	-0.4 ± 0.5	-0.4
C_{10}	F_{10}	-246.6 ± 0.3	-311.9 ± 0.6	-32.7 ± 0.5	-32.5
C_{12}	F_8	4.7 ± 0.3	6.5 ± 0.6	0.9 ± 0.5	0.9
C_{12}	F_{10}	9.4 ± 0.3	6.5 ± 0.6	-1.5 ± 0.5	-1.5
H-H couplings					
H_3	H_4	8.6 ± 0.1	-36.4 ± 0.4	-22.5 ± 0.3	-23.0
H_3	H_6	0.5 ± 0.1	4.5 ± 0.4	2.0 ± 0.3	1.3
H_4	H_6	2.4 ± 0.1	5.2 ± 0.3	1.4 ± 0.2	1.7
H_4	H_9	0.0 ± 0.1	-2.9 ± 0.4	-1.5 ± 0.3	-1.1
H_4	H_{11}	0.0 ± 0.1	-2.9 ± 0.4	-1.5 ± 0.3	-1.0
H_4	H_{12}	0.0 ± 0.1	-5.0 ± 0.2	-2.5 ± 0.2	-2.3
H_6	H_9	0.0 ± 0.1	-4.5 ± 0.4	-2.3 ± 0.3	-2.4
H_6	H_{11}	0.0 ± 0.1	-4.5 ± 0.4	-2.3 ± 0.3	-2.2
H_6	H_{12}	0.0 ± 0.1	-10.1 ± 0.3	-5.1 ± 0.2	-5.4
H_9	H_{11}	2.6 ± 0.1	7.2 ± 0.2	2.3 ± 0.2	2.2
H_{11}	H_{12}	8.7 ± 0.1	-35.7 ± 0.4	-22.2 ± 0.3	-22.1
H-F couplings					
H_4	F_8	1.7 ± 0.1	0.0 ± 0.5	-0.9 ± 0.3	-0.7
H_4	F_{10}	0.0 ± 0.5	-2.1 ± 0.5	-1.1 ± 0.5	-0.7

H_6	F_8	1.5 ± 0.1	-11.1 ± 0.5	-6.3 ± 0.3	-6.6
H_6	F_{10}	0.0 ± 0.5	-3.9 ± 0.5	-2.0 ± 0.5	-1.6
H_9	F_8	10.9 ± 0.1	-26.8 ± 0.5	-18.9 ± 0.3	-18.3
H_9	F_{10}	9.1 ± 0.1	14.4 ± 0.5	2.7 ± 0.3	2.1
H_{11}	F_8	-1.0 ± 0.1	0.0 ± 0.5	0.5 ± 0.3	0.5
H_{11}	F_{10}	8.1 ± 0.1	7.0 ± 0.5	-0.6 ± 0.3	-1.0
H_{12}	F_8	9.0 ± 0.1	12.8 ± 0.5	1.9 ± 0.3	1.8
H_{12}	F_{10}	6.4 ± 0.1	1.9 ± 0.5	-2.3 ± 0.3	-2.6
F-F couplings					
F_8	F_{10}	7.2 ± 0.2	4.1 ± 0.4	-1.6 ± 0.3	-1.5

RMS		0.31 Hz

k	$\delta_k^{iso\ (c)}$ (ppm)	$\Delta\nu_{CD_k}$ (Hz)
H_2	11.26 ± 0.05	-249.4 ± 0.5
H_3	7.00 ± 0.05	-359.9 ± 0.5
H_4	7.62 ± 0.05	324.0 ± 0.5
H_6	8.02 ± 0.05	-368.2 ± 0.5
H_9	7.03 ± 0.05	-40.9 ± 0.5
H_{11}	7.01 ± 0.05	-162.0 ± 0.5
H_{12}	7.47 ± 0.05	-36.5 ± 0.5
C_1	110.7 ± 0.3	
C_2	160.1 ± 0.3	
C_3	115.6 ± 0.3	
C_4	133.9 ± 0.3	
C_5	123.7 ± 0.3	
C_6	128.6 ± 0.3	
C_7	122.5 ± 0.3	
C_8	157.9 ± 0.3	
C_9	102.1 ± 0.3	
C_{10}	160.3 ± 0.3	
C_{11}	109.5 ± 0.3	
C_{12}	129.4 ± 0.3	
C_{13}	170.0 ± 0.3	
F_8	0.0 ± 0.1	
F_{10}	1.8 ± 0.1	

[a] calculated from $D_{ij}^{obs} = \left[\pm T_{ij}^{obs} - (\pm J_{ij}^{iso})\right]/2$ (see chapter 1 section 1.5.2)

[b] from the AP-DPD method (see below)

[c] chemical shifts are given from calibration with THF signal (at 1.72 ppm and 25.37 ppm for proton and carbon-13, respectively), while in the absence of internal standard for the fluorine, the chemical shifts of F_8 was calibrated at 0 ppm

A crucial point is that, in all the experiments we performed, only the absolute values of the indirect and total coupling constants is measured from spectra, leading to an uncertainty in the signs and magnitudes of the values of the D_{ij}^{obs} to be used in the following conformational analysis. A common strategy [165-167] was adopted here to solve this uncertainty for the one-bond ^{1}H-^{13}C dipolar couplings, $^1D_{CH}$, by measuring from natural abundance deuterium (NAD) spectra the corresponding quadrupolar splittings $\Delta\nu_{CD_k}$ for the k-th deuterium nucleus. The difficulties in the assignment of the quadrupolar doublets in the 1D ^{2}H-{^{1}H} spectrum were overcome by recording the NAD 2D autocorrelation Q-COSY spectrum reported in Figure 3.16 [168-169].
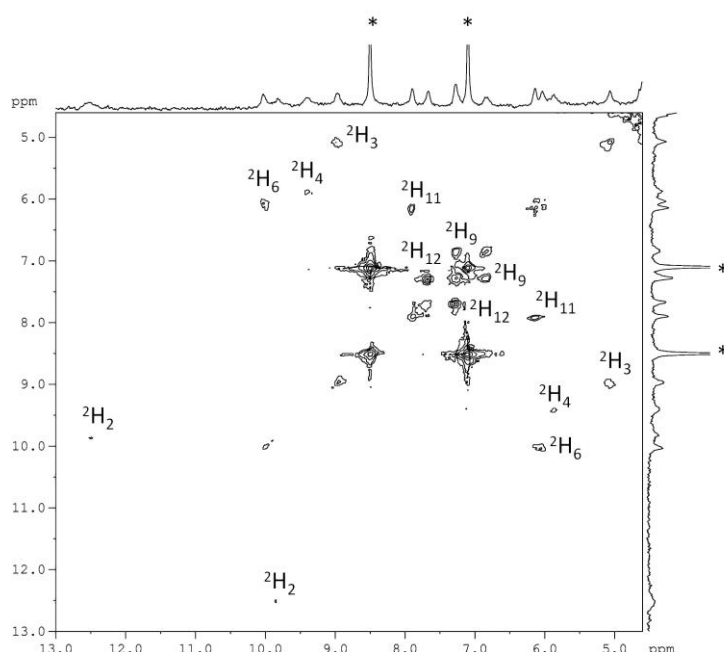
Figure 3.16. Q-COSY Fz spectrum recorded on diflunisal in PBLG/THF at 300 K in 57 h. The data acquired had 2048 (t_2) x 512 (t_1) points with 592 scans per t_1 increment. An exponential filtering (LB = 4.0 Hz and 2.0 Hz) is applied respectively in the F$_1$ and F$_2$ dimension and the data were symmetrized. The WALTZ-16 sequence was used to decouple the protons. Peaks labeled with an asterisk are from the solvent stabilizer (butylated hydroxytoluene, BHT).

The basic idea of this experiments is to obtain a 2D contour plot in which the correlation peaks appearing between the two components of each quadrupole doublet reflect their connectivity, as in a classical 2D COSY spectrum. By comparison with the 1D spectrum it is thus simple to attribute unambiguously each doublet on the basis of chemical shifts. By applying a 45° tilt, the individual quadrupolar doublets could hence be extracted from the columns of the 2D spectrum, allowing the edition of $\Delta\nu_{CD_k}$ at each deuterium position

reported in Table 3.3. The 1D and 2D ^{2}H NMR spectra were recorded on a high-resolution Bruker Avance II 600MHz spectrometer (14.1 T) equipped with a 5-mm selective ^{2}H cryoprobe. Temperature was carefully fed-back at 300 K by a standard variable-temperature unit (BVT-3000).

As discussed in chapter 1 (section 1.4.1), for a specific [13]C-[1]H ([13]C-^{2}H) bond, the ratio $|\Delta v_{CD}/{}^1D_{CH}|$ lies approximately in the range 10-12 [108, 170]. Hence, as the ${}^1J_{CH}$ scalar couplings are always positive [171], by a simple comparison of the two experimental ${}^1D_{CH}$ possible values with the expected one predicted by the ratio $|\Delta v_{CD}/{}^1D_{CH}|$, the correct magnitude and sign was unambiguously determined. Once we got a starting reliable set of dipolar couplings, the determination of the rest of the D_{ij}^{obs} was carried out, in the different fragments first and in the total molecule then, by a trial and error process. This means that, for each single coupling, one assumes one by one a possible value (sign and magnitude) and evaluates the consistence with the structure and the complete set of dipolar couplings [172 and refs therein]. From the totality of the experimental couplings, only those whose sign and value were assigned with a high level of confidence were included in the analysis, for a total of 40 D_{ij}^{obs} (reported in the fifth column of Table 3.3).

ii. Molecular modelling calculations

Although the NMR collected data set on the sample is large, in order to determine the complete structure and the energy differences defining the conformational distribution, we also need the geometry of the most stable conformers and a good estimate of the potential energy surface (PES). For this reason we performed molecular modelling calculations for an isolated molecule by a density functional theory (DFT) approach. Structures and locations of the lowest minimum energy forms for the DFL molecule were estimated *in vacuo* with the functional B3LYP and the basis set 6-31++G** using the Gaussian09 software package [173]. The bond lengths and angles are, to a good approximation, independent on the conformational state, so the minimum energy structure was used to perform a rigid PES scan for the torsion angle φ = C_4-C_5-C_7-C_8 over the 0°-360° range with a 5°-step sampling (Figure 3.17).

From Figure 3.17 it is seen that four minimum energy conformers were found: (*i*) a couple of "*trans*" conformers with F_8 opposite to the carboxylic group (φ = ±43.2°) corresponding to the absolute minima (where the normalized potential energy, E_{pot}^{norm}, is fixed

to be 0 kJ/mol), and (*ii*) a couple of "*cis*" conformers with F_8 on the same side to the carboxylic group (φ = ±135.2°) corresponding to the relative minima (E_{pot}^{norm} ~1.18 kJ/mol). The theoretical Boltzmann distribution can be roughly calculated from the potential energy values as:

$$P_{theo}(\varphi) = exp\left(- E_{pot}^{norm}/RT\right) \tag{3.2}$$

with T the absolute temperature and R the ideal gas constant. From equation (3.2) we derived relative percentages of 30% for each "*trans*" conformer and 20% of each "*cis*" conformer.

Note that in order to exclude significant solvent effects, geometry optimization jobs were also performed taking into account in the calculation tetrahydrofuran as medium by means of the default Polarizable Continuum Model (PCM) [174] implemented in the Gaussian package. No significant difference in terms of structure and relative energies of the most stable conformers emerged between the gas and liquid state.
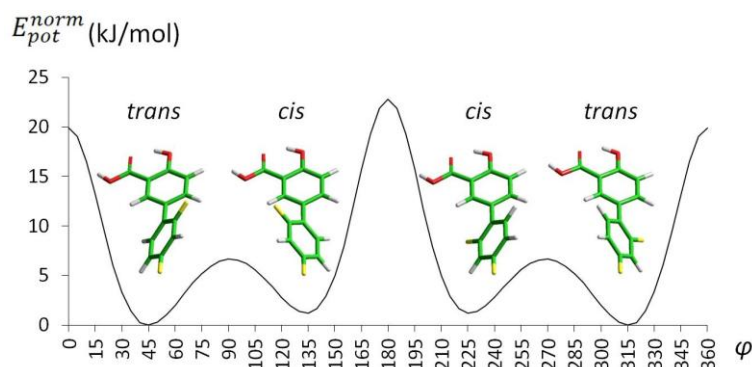
Figure 3.17. Normalized potential energy as a function of φ = $C_4C_5C_7C_8$ obtained for DFL from B3LYP/6-31++G** calculations, including structures of the corresponding minimum energy conformers.

iii. Conformational analysis

To extract the desired conformational information from the observed dipolar couplings in the flexible molecule of diflunisal, we used the AP-DPD approach, which, as discussed in chapter 1, is a combination of Additive Potential model for the treatment of the ordering interactions, with the Direct Probability Description of the torsional distribution. Within the AP model, we can describe DFL by six fragment tensors $\varepsilon_{2,p}^{j}$ (the MOL frame is reported in Figure 3.9):

- $\varepsilon_{2,0}^{ring\ A}$ and $\varepsilon_{2,2}^{ring\ A}$, for the C_{2v}-symmetry fluorinated ring (ring A)
- $\varepsilon_{2,0}^{ring\ B}$ and $\varepsilon_{2,2}^{ring\ B}$, for the C_{2v}-symmetry salicylic ring (ring B)

- $\varepsilon_{2,0}^{C-F}$, for the monoaxial component along the C_8-F_8 bond direction
- $\varepsilon_{2,0}^{C-C}$, for the monoaxial component along the C_1-C_{13} bond direction.

In the DPD approach, the isotropic probability distribution $P_{iso}(\{\phi\})$ is described in terms of Gaussian functions. For diflunisal, $P_{iso}(\{\phi\})$ corresponds to the torsional probability distribution around the inter-ring angle φ, the $P_{iso}(\varphi)$, which can be directly modelled as a sum of four Gaussian functions corresponding to the two non-equally probable couples of conformers:

$$P_{iso}(\varphi) \propto \left\{ \frac{A_1}{2} \cdot exp\left[-\frac{(\varphi - \varphi_1^{max})^2}{2h_1^2} \right] + \frac{A_1}{2} \cdot exp\left[-\frac{(\varphi - 360 + \varphi_1^{max})^2}{2h_1^2} \right] \right.$$

$$\left. + \frac{A_2}{2} \cdot exp\left[-\frac{(\varphi - 180 + \varphi_2^{max})^2}{2h_2^2} \right] + \frac{A_2}{2} \cdot exp\left[-\frac{(\varphi - 180 - \varphi_2^{max})}{2h_2^2} \right] \right\} \quad (3.3)$$

where φ_1^{max} and φ_2^{max} are the most probable values of the torsion angle, A_1 and A_2 are the relative weights of the two couples (we also fixed the constraint $A_1 + A_2 = 1$) and, finally, h_1 and h_2 give the width at half maximum height of each Gaussian according to equation (1.85).

Being the theoretical apparatus defined, the software AnCon [95] was used to fit the experimental dipolar couplings of Table 3.3, while fixing molecular geometry as from molecular modelling calculations and by iterating on a pertinent number of unknowns (namely, the orientational parameters represented by the six $\varepsilon_{2,p}^{j}$ and the potential terms represented by φ_1^{max}, φ_2^{max}, $h_1 = h_2$ and $A_1 = 1 - A_2$), until an acceptable value for the RMS target function is reached. Note that we have, for 10 unknowns, 40 D_{ij}^{obs} (21 for the fluorinated ring, 9 for the salicylic ring, 10 between the two rings). Therefore, the problem should be overdetermined from the ratio (independent target D_{ij})/(adjustable parameters) = 40/10 = 4. However, because of the strong interdependence between the potential terms, and especially because of the small magnitude of the experimental D_{ij}^{obs}, the system does not converge when a simultaneous iteration is performed. As a consequence, we adjusted the different parameters of equation (3.3) step by step. After optimization, a good agreement between D_{ij}^{obs} and D_{ij}^{calc} (reported in the last column of Table 3.3) has been obtained, as one can appreciate in Figure 3.18. The optimized parameters and the torsional potential $P_{iso}(\varphi)$ calculated by this approach are shown in the second column of Table 3.4 and in Figure 3.19 (red solid line), respectively.

D_{ij}^{calc} (Hz)
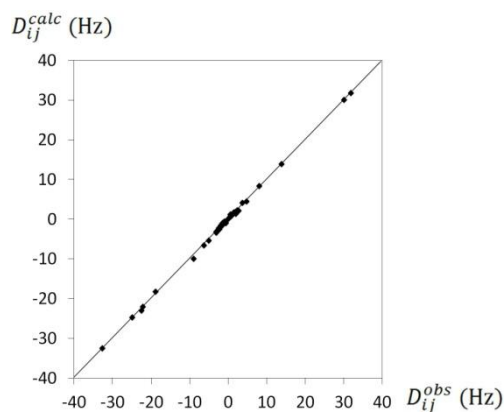
Figure 3.18. Observed *versus* theoretical dipolar couplings obtained for the diflunisal respectively from NMR experiments and by the AP-DPD approach.

Table 3.4. Optimized values of the iteration parameters used in the conformational analysis with the AP-DPD approach of the DFL molecule dissolved in PBLG/THF and PBG/THF.

	DFL in PBLG/THF	DFL in PBG/THF
φ_1^{max} (degree)	45.5 ± 2.1	45.2 ± 2.1
φ_2^{max} (degree)	41.1 ± 1.2	41.6 ± 1.1
$h_1 = h_2$ (degree)	10.5 ± 1.8	10.7 ± 2.2
A_1	0.56 ± 0.02	0.56 ± 0.05
$\varepsilon_{2,0}^{ring\,A}$ (RT)	-0.03 ± 0.01	-0.012 ± 0.003
$\varepsilon_{2,2}^{ring\,A}$ (RT)	-0.02 ± 0.01	-0.009 ± 0.002
$\varepsilon_{2,0}^{C-F}$ (RT)	-0.00040 ± 0.00001	-0.0006 ± 0.0001
$\varepsilon_{2,0}^{ring\,B}$ (RT)	0.04 ± 0.01	0.026 ± 0.003
$\varepsilon_{2,2}^{ring\,B}$ (RT)	-0.018 ± 0.005	-0.026 ± 0.001
$\varepsilon_{2,0}^{C-C}$ (RT)	0.0087 ± 0.0005	0.0097 ± 0.0002
RMS	0.35	0.43

The $P_{iso}(\varphi)$ is characterized by a couple of "*trans*" conformers (absolute maxima), having φ_1^{max} = ±45.5° and a relative percentage of 56%, and a couple of "*cis*" conformers (relative maxima), having φ_2^{max} = ±41.1° and a relative percentage of 44%. This solution is in good agreement with molecular modelling calculations, with only small changes in the values of the probability ratio between the two couples of conformers and the torsion angles corresponding to the maxima positions. The similarity between experimental and theoretical results is straightaway to catch in Figure 3.19, where the theoretical probability distribution, $P_{theo}(\varphi)$, calculated from the potential energy values obtained by DFT calculations is plotted (green dashed line) together with the $P_{iso}(\varphi)$.
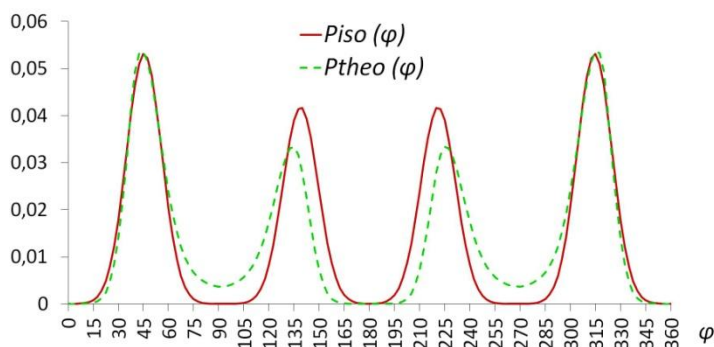
Figure 3.19. Experimental (red solid line) and theoretical (green dashed line) torsional probability distributions as a function of φ obtained for the diflunisal, respectively by the AP-DPD approach and from B3LYP/6-31G** calculations. Both curves are obtained by varying φ over the 0°-360° range with a 5°-step sampling.

For sake of completeness we remark that the same analysis was carried out on the achiral DFL/PBG/THF system, leading to the same conclusions (optimized values of the iteration parameters are reported for comparison in the third column of Table 3.4). Testing the same achiral molecule in both PBLG and PBG phases proves there are no effects on the conformational equilibrium resulting from the chirality of the medium and supports the reliability of the proposed methodology for the conformational analysis of compounds possessing stereocenters.

3.3.1.2. Phenylsalicylic acid

The molecule of APS, the analogue of DFL without the fluorine atoms, was investigated with the intent of probing any effect of the ^{19}F nuclei on the structure and/or conformational distribution. The same procedure described for DFL was used for the APS, too. Then, we will only focus on the results in order to highlight eventual similarities and differences between the two compounds.

i. NMR experiments

[1]H-^{1}H and [1]H-^{13}C indirect and total spin-spin couplings were measured from 2D [1]H-[13]C *J*-resolved and [1]H-^{1}H SERF experiments performed on the isotropic (APS in THF-d$_8$) and anisotropic (APS in PBLG/THF) samples (see Appendix A3). The extracted values of J_{ij}^{obs} and

T_{ij}^{obs} and the calculated D_{ij}^{obs} are reported, together with experimental chemical shifts δ_k^{iso}, in Table 3.5.

Table 3.5. Experimental chemical shifts δ_k^{iso}, scalar couplings J_{ij}^{obs}, total couplings T_{ij}^{obs} and dipolar couplings D_{ij}^{obs} determined by the NMR analysis of APS dissolved in THF-d$_8$ and PBLG/THF. Errors are estimated from spectral resolution. In the last column, the D_{ij}^{calc} values are also reported for comparison. The whole agreement between D_{ij}^{obs} and D_{ij}^{calc} is given by the RMS.

i	j	J_{ij}^{obs} (Hz)	T_{ij}^{obs} (Hz)	$D_{ij}^{obs\ (a)}$ (Hz)	$D_{ij}^{calc\ (b)}$ (Hz)
C-H couplings					
C_1	H_3	5.3 ± 0.3	6.6 ± 0.6	0.7 ± 0.5	0.7
C_1	H_4	0.0 ± 0.3	-2.0 ± 0.6	-1.0 ± 0.5	-0.5
C_3	H_3	162.1 ± 0.3	213.9 ± 0.6	25.9 ± 0.5	25.6
C_3	H_4	0.0 ± 0.3	-11.6 ± 0.6	-5.8 ± 0.5	-5.7
C_4	H_4	158.1 ± 0.3	115.5 ± 0.6	-21.3 ± 0.5	-21.3
C_4	H_6	8.1 ± 0.3	9.3 ± 0.6	0.6 ± 0.5	0.7
C_6	H_3	-1.2 ± 0.5	0.0 ± 0.6	0.6 ± 0.6	0.6
C_6	H_4	7.1 ± 0.3	7.4 ± 0.6	0.2 ± 0.5	0.1
C_6	H_6	160.4 ± 0.3	211.6 ± 0.8	25.6 ± 0.5	25.9
C_8	H_8	159.1 ± 0.3	192.0 ± 0.8	16.5 ± 0.5	16.8
C_9	H_9	161.3 ± 0.3	195.1 ± 0.6	16.9 ± 0.5	16.7
C_{10}	H_9	0.0 ± 0.3	8.2 ± 0.6	4.1 ± 0.5	4.0
C_{10}	H_{10}	160.9 ± 0.3	102.4 ± 0.8	-29.3 ± 0.5	-30.0
C_{10}	H_{11}	0.0 ± 0.3	8.2 ± 0.6	4.1 ± 0.5	4.0
C_{11}	H_{11}	161.3 ± 0.3	195.1 ± 0.6	16.9 ± 0.5	16.7
C_{13}	H_6	4.5 ± 0.3	0.0 ± 0.6	-2.3 ± 0.5	-2.3
H-H couplings					
H_3	H_4	8.6 ± 0.1	-12.8 ± 0.4	-10.7 ± 0.3	-10.0
H_3	H_6	0.5 ± 0.1	3.3 ± 0.4	1.4 ± 0.3	1.1
H_4	H_6	2.5 ± 0.1	4.7 ± 0.4	1.1 ± 0.3	0.8
H_4	H_8	0.0 ± 0.1	-4.1 ± 0.4	-2.1 ± 0.3	-2.1
H_4	H_{12}	0.0 ± 0.1	-4.1 ± 0.4	-2.1 ± 0.3	-2.1
H_6	H_8	0.0 ± 0.1	-11.3 ± 0.4	-5.7 ± 0.3	-5.7
H_6	H_9	0.0 ± 0.1	-3.2 ± 0.6	-1.6 ± 0.4	-1.2
H_6	H_{10}	0.0 ± 0.1	-2.9 ± 0.6	-1.5 ± 0.4	-1.0
H_6	H_{11}	0.0 ± 0.1	-3.2 ± 0.6	-1.6 ± 0.4	-1.2
H_6	H_{12}	0.0 ± 0.1	-11.3 ± 0.4	-5.7 ± 0.3	-5.7
H_8	H_9	7.8 ± 0.1	-13.7 ± 0.6	-10.8 ± 0.4	-10.2

H_8	H_{10}	1.2 ± 0.1	0.0 ± 0.6	-0.6 ± 0.4	-0.9
H_8	H_{11}	0.7 ± 0.1	2.4 ± 0.6	0.9 ± 0.4	0.7
H_8	H_{12}	1.4 ± 0.1	5.8 ± 0.6	2.2 ± 0.4	2.0
H_9	H_{10}	7.4 ± 0.1	18.0 ± 0.6	5.3 ± 0.4	5.3
H_9	H_{11}	1.4 ± 0.1	6.0 ± 0.6	2.3 ± 0.4	2.0
H_9	H_{12}	0.7 ± 0.1	2.4 ± 0.6	0.9 ± 0.4	0.7
H_{10}	H_{11}	7.4 ± 0.1	18.0 ± 0.6	5.3 ± 0.4	5.3
H_{10}	H_{12}	1.2 ± 0.1	0.0 ± 0.6	-0.6 ± 0.4	-0.9
H_{11}	H_{12}	7.8 ± 0.1	-13.7 ± 0.6	-10.8 ± 0.4	-10.2

RMS	0.35 Hz

k	δ_k^{iso} (c) **(ppm)**
H_2	11.17 ± 0.07
H_3	7.00 ± 0.07
H_4	7.75 ± 0.07
H_6	8.12 ± 0.07
H_8, H_{12}	7.56 ± 0.07
H_9, H_{11}	7.38 ± 0.07
H_{10}	7.26 ± 0.07
C_1	113.7 ± 0.3
C_2	162.9 ± 0.3
C_3	118.7 ± 0.3
C_4	134.9 ± 0.3
C_5	133.0 ± 0.3
C_6	129.3 ± 0.3
C_7	141.0 ± 0.3
C_8, C_{12}	127.3 ± 0.3
C_9, C_{11}	129.6 ± 0.3
C_{10}	127.7 ± 0.3
C_{13}	173.0 ± 0.3

[a] calculated as $D_{ij}^{obs} = \left[\pm T_{ij}^{obs} - (\pm J_{ij}^{iso})\right]/2$ (see chapter 1 section 1.5.2)

[b] from the AP-DPD method (see below)

[c] the chemical shifts are given from calibration with THF signal (at 1.72 ppm and 25.37 ppm for proton and carbon-13, respectively)

ii. Molecular modelling calculations

As for DFL, *in vacuo* molecular modelling calculations for an isolated molecule were performed on APS by the Gaussian09 software package (B3LYP/6-31++G**) [173]. Fixing the structure of the minimum energy conformer, a rigid PES scan was carried out for the torsion angle $\varphi = C_4\text{-}C_5\text{-}C_7\text{-}C_8$ over the 0°-360° range with a 5°-step sampling (Figure 3.20). As expected for symmetry reasons, four equally probable minimum energy conformers resulted from the molecular modelling calculations of APS. Torsion angle values of the conformers are respectively $\varphi = \pm39.1°$ and $180°\pm39.1°$.

From a purely geometrical viewpoint it is reasonable the replacement $^1H\text{-}^{19}F$ in APS with respect to DFL affects some bond lengths and angles. In Appendix A4 we report for comparison the optimised geometries obtained for a *trans* and a *cis* minimum energy conformers of DFL and for one of the four equally probable minimum energy conformers of APS. Besides the obvious difference in the length of the C-F bonds (~1.35 Å) compared to the corresponding C-H bonds (~1.086 Å), it is more interesting to note that the presence of protons instead of fluorine atoms in APS molecule affects almost all internal angles of ring A as well as angles between the inter-ring $C_5\text{-}C_7$ bond and each phenyl ring.
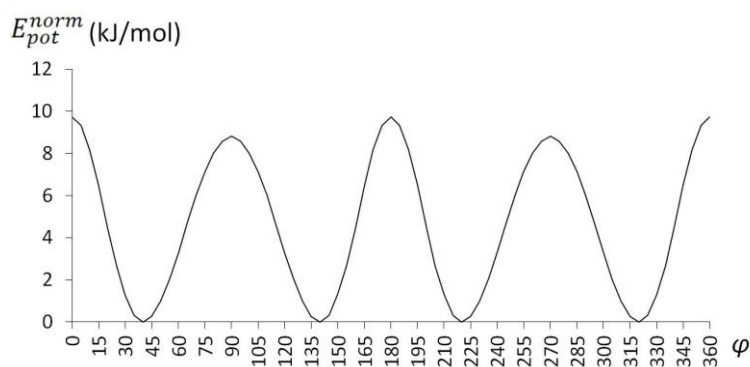
Figure 3.20. Normalized potential energy as a function of $\varphi = C_4\text{-}C_5\text{-}C_7\text{-}C_8$ obtained for APS from B3LYP/6-31++G** calculations.

iii. Conformational analysis and comparison between the conformational probability distribution of the fluorinated and non-fluorinated molecule

Similarly to DFL, the AP-DPD approach was applied to treat the conformational problem for the phenylsalicylic acid.

Within the AP model, the molecule is described by five fragment tensors $\varepsilon_{2,p}^j$:

- $\varepsilon_{2,0}^{ring\ A}$ and $\varepsilon_{2,2}^{ring\ A}$, for the C_{2v}-symmetry unsubstituted ring (ring A)

- $\varepsilon_{2,0}^{ring\ B}$ and $\varepsilon_{2,2}^{ring\ B}$, for the C_{2v}-symmetry salicylic ring (ring B)

- $\varepsilon_{2,0}^{C-C}$, for the monoaxial component along the C_1-C_{13} bond direction

When modelling the torsional distribution for APS, the symmetry of one ring (compared to DFL) has to be taken into account. Then, $P_{iso}(\varphi)$ is simply the sum of four Gaussian functions with equal weight:

$$P_{iso}(\varphi) \propto \left\{ exp\left[-\frac{(\varphi - \varphi^{max})^2}{2h^2} \right] + exp\left[-\frac{(\varphi - 360 + \varphi^{max})^2}{2h^2} \right] \right.$$
$$\left. + exp\left[-\frac{(\varphi - 180 + \varphi^{max})^2}{2h^2} \right] + exp\left[-\frac{(\varphi - 180 - \varphi^{max})^2}{2h^2} \right] \right\} \qquad (3.4)$$

where φ^{max} represents the most probable value of the torsion angle and h gives the width at half maximum height of the Gaussians, as in equation (1.85).

As above, the orientational parameters (the five $\varepsilon_{2,p}^{j}$) together with the potential terms (φ^{max} and h) are the unknowns in the iterative fitting procedure of the D_{ij}^{obs} of Table 3.5 (molecular geometry is taken from molecular modelling calculations). With respect to DFL the amount of both the target D_{ij} and the adjustable parameters is reduced. In particular, because of the symmetry of one ring with respect to the DFL, there are 27 independent D_{ij}^{obs} (10 for ring A, 13 the salicylic ring and only 4 between the two rings) and 7 unknowns. Calculations were performed by varying φ^{max}, with a parametrical adjustment of h. The best fit between D_{ij}^{obs} and D_{ij}^{calc} (reported for comparison in the last column of Table 3.5) was reached (see Figure 3.21) for the optimized parameters reported in Table 3.6, corresponding to the $P_{iso}(\varphi)$ shown in Figure 3.22 (blue line), characterized by four equally probable conformers having φ^{max} = ±40° and 180° ±40°. This result is evidently in close agreement with the values obtained for an isolated molecule by the DFT calculation.
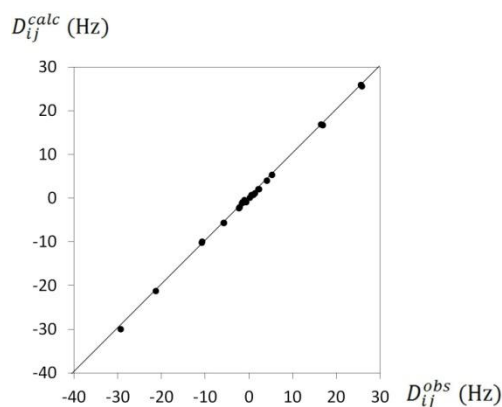
Figure 3.21. Observed *versus* theoretical dipolar couplings obtained for the phenylsalicylic acid respectively from NMR experiments and by the AP-DPD approach.

Table 3.6. Optimized values of the iteration parameters used in the conformational analysis with the AP-DPD approach of the APS molecule dissolved in PBLG/THF.

	APS in PBLG/THF
φ^{max} (degree)	40 ± 15
h (degree)	27.5 ± 2.5 (after parameterization)
$\varepsilon_{2,0}^{ring\ A}$ (RT)	-0.005 ± 0.002
$\varepsilon_{2,2}^{ring\ A}$ (RT)	-0.0152 ± 0.0009
$\varepsilon_{2,0}^{ring\ B}$ (RT)	0.009 ± 0.002
$\varepsilon_{2,2}^{ring\ B}$ (RT)	-0.0014 ± 0.0008
$\varepsilon_{2,0}^{C-C}$ (RT)	0.0064 ± 0.0002
RMS	0.31
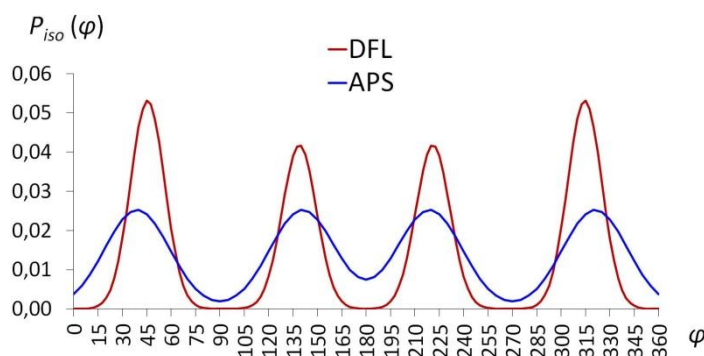
Figure 3.22. Comparison between experimental torsional probability distributions obtained in PBLG/THF for phenylsalicylic acid (blue line) and diflunisal (red line), as a function of φ. Both curves are obtained by varying φ over the 0°-360° range with a 5°-step sampling.

A comparison between the conformational probability distributions (reported in Figure 3.22) obtained for the fluorinated DFL (red line) and non-fluorinated APS (blue line) molecules in the PBLG/THF solvent immediately reveals two main differences, in the exact position of the maxima and in the width of the Gaussian functions. Firstly, the inter-ring torsion angles found for the most stable conformers of APS are slightly smaller than those resulted in the analysis of DFL (about 3° between the average $(\varphi_1^{max} + \varphi_2^{max})/2$ in DFL and φ^{max} in APS). This result could be merely associated to the greater van der Waals radius of the fluorine nucleus compared to the proton [175], implying a weak steric hindrance effect in the rotation around the C_5-C_7 bond. Indeed, if one looks at the error associated to φ^{max} value in APS it is evident that the torsion angle value can cover a large range, including the φ_1^{max} and φ_2^{max} values found for DFL. Secondly, the peaks characterizing the $P_{iso}(\varphi)$ distribution of APS appear less sharp than those obtained for the DFL. From a physical point of view, this could suggest that

the presence of ^{19}F nuclei makes DFL be more confined in proximity of its conformational minima with respect to APS. However, it should be remarked that the sharpness of the peaks is related to the magnitude of the h parameter and the data set collected for APS was not sufficient to make the software able to converge when the h parameter is put as a variable in the iteration process. The value of 27.5° ±2.5 reported in Table 3.6 comes thus from a parametrical adjustment process of 5° ≤ h ≤ 35°, yielding the best fitting between D_{ij}^{calc} and D_{ij}^{obs} in the window ranging from h = 25° to h = 30°. Hence, a value of h greater than $h_1 = h_2$ found in DFL seems to be necessary in order to reproduce the experimental dipolar couplings for APS, suggesting a difference in the rotational barriers for the fluorinated and non-fluorinated compounds.

3.3.2.   Two and more rotations: profens

The second family of NSAIDs considered in this Ph.D. thesis is that of the 2-arylpropionic acid derivatives, commonly known as profens, whose general structure is reported in Figure 3.23. In particular, naproxen, flurbiprofen and ibuprofen were selected as molecules of interest. Results for the former will be presented here, while preliminary studies started on flurbiprofen and ibuprofen will be left out.
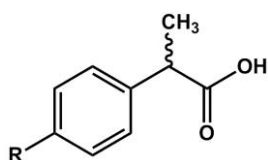
Figure 3.23. Structure of 2-arylpropionic acids (profens) composed of three basic units: the propionic acid side chain, the central aryl moiety and a hydrophobic terminal residue R.

Profens are chiral bioactive compounds, most of them traditionally marketed as racemic mixtures. Indeed, individual enantiomers differ in both pharmacokinetics and pharmacodynamics [176-178], and in particular *in vitro* and *in vivo* studies demonstrated that the anti-inflammatory activity, *i.e.* the ability of inhibiting COX, is largely stereospecific for the *S*-enantiomers [179-182]. However, since *R*-enantiomer is generally inactive, its presence in the formulation can be easily justified when compared to the complicated and expensive methods for enantioselective synthesis and enantiomeric purification. Moreover, most compounds usually undergo a unidirectional chiral inversion from *R*- to *S*-isomer in biological

systems [183-187], so that the *R*-enantiomer acts as a prodrug for the *S*-isomer and contributes to the pharmacodynamics of the racemate. Naproxen represents an exception because it is internationally sold as *S*-enantiomer due to the potential toxicity of the *R*-isomer [188]. Currently, also ibuprofen is being marketed in several European countries as the stereochemically pure *S*-(+)-enantiomer [188] because of relevant difference between physical properties of the racemate and *S*-ibuprofen (dexibuprofen) [189-193]. Moreover, the general recent trend pursued by many companies is toward reevaluating drugs previously marketed as racemates and marketing them as single-enantiomer, in order to improve its therapeutic efficacy and to extend patent protection [188]. Therefore, the need for convenient and effective techniques for the differentiation and the study of enantiomers as well as the measurement of enantiomeric purity is continuously growing [194-199]. Next to the investigation of methods for enantiomeric synthesis and chiral discrimination, a quite large number of papers focused on studying the three dimensional structure of this class of anti-inflammatory drugs, with the aim of predicting the localization of interaction sites, rationalizing their accommodation inside the receptor cavity and designing new anti-inflammatory drugs with improved activities [107, 200-204]. In this context, our purpose is to offer a contribution by accurately describe the conformational equilibrium of such molecules in a liquid state, by exploiting the potentiality of liquid crystal NMR spectroscopy. For the arguments presented in section 3.3, the structural and conformational analysis of profens is quite impossible to perform by NMR spectroscopy in thermotropic LCs, at least without an extremely good set of starting parameters. Moreover, these molecules possess a higher number of magnetically active nuclei with respect to diflunisal. Thus, we resort again to PBLG phases that, inducing a smaller degree of order, facilitate the extraction of residual dipolar couplings. Even so, the structural and conformational analysis poses some difficulties. Experimentally speaking, collecting a large set of independent RDCs is not trivial, and this was the main obstacle encountered in the study of naproxene and flurbiprofen. From a theoretical viewpoint, the presence of two or more degree of flexibility makes the torsional potential description challenging, compared to the single-rotor case seen in the previous section. Naproxen and flurbiprofen were chosen as model compounds for molecules which display two rotations that are far enough to be considered as independent, while the study of ibuprofen was intended to deal with the more delicate case of cooperative rotations. Note that the use of PBLG-organic co-solvent mixtures has the additional advantage of overcoming the problem of very poor water solubility of the chosen drugs. Finally, it is worth remarking that the attractive well-recognized qualities of NMR spectroscopy in chiral PBLG phases as a tool for enantiomeric discrimination [165, 205-212] could in principle be exploited also for these chiral

drugs. However, enantiodiscrimination studies were out of the scope of this Ph.D. thesis. For the conformational and structural analysis, PBLG was still used instead of the achiral PBG phase, as a consequence of its simpler and cheaper commercially availability. This required pure isomers to be used as solutes, in order to avoid difficulty in the differentiation of superposed spectra of each enantiomer.

3.3.2.1. Naproxen

The S-(+)-2-(6-methoxy-2-naphthalen)propanoic acid (Figure 3.24), commonly known as naproxen (NAP), is used as a therapeutic agent for the treatment of rheumatoid and osteoarthritis. Originally introduced in prescription form as Naprosyn® by Syntex in 1976 and as the over-the-counter drug Aleve® by Bayer in 1994, NAP is currently sold under various tradenames including Anaprox®, Antalgin®, Apranax®, Midol Extended Relief®, Naprelan®, Synflex® and so on. It exhibits analgesic, anti-pyretic, and anti-inflammatory activity and was recently reported to be effective in the prevention of bladder cancer progression [201]. The S-enantiomer of NAP is 28-fold more active as anti-inflammatory than the R-isomer [213], which is reported to be a liver toxin [214] and to incidentally causes gastrointestinal disorders [215]. As a consequence, NAP and its sodium salt are internationally delivered as the pure S-(+)-isomers.
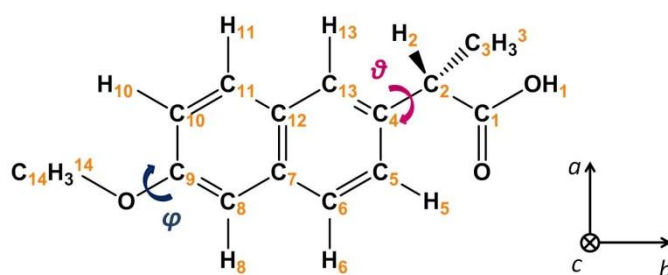
Figure 3.24. Topological structure, atomic labelling and torsional angles of S-(+)-naproxen (NAP). The (a, b, c) axes of the molecular reference frame adopted are also shown.

The NAP molecule possesses two flexible substituents that may take different orientations with respect to the naphthalene ring and lead to several stable isomers: the methoxy group and the propionic fragment, that is the chain bearing the asymmetric carbon. The conformational investigation of NAP resides then in the description of two dihedral angles: φ, defined as the dihedral angle C_8-C_9-O-C_{14}, and ϑ, defined as the dihedral angle C_{13}-

C_4-C_2-H_2 (Figure 3.24). The crystal structure of NAP and its sodium salt have been determined by X-ray measurements [216-219] and computer modelling for crystal structure prediction found very different crystal packing for the enantiomeric and racemic form [220]. The scarce solubility of NAP in water can be substantially enhanced after inclusion in cyclodextrins and analogues. Structure and intermolecular interactions of the resulting complexes were studied in solid state and in solution by molecular modelling as well as X-ray diffractometry and ^{1}H NMR spectroscopy [221-223]. Theoretical calculations were performed also in the gas and liquid phase [203, 224]. An attempt to experimentally refine the spatial arrangement of NAP in solution was done by two-dimensional [1]H nOe measurements, which indicated that, while for the methoxy group a single well defined conformation (φ = C_8-C_9-O-C_{14} ~0°) can be assumed to be almost exclusively populated, the description of the torsion around the C_2-C_4 axis is more complex [225]. Indeed, nOe data seem to be better reproduced taking into account an average of more theoretical calculated conformations with respect to a mono-conformational model. However, experimental outcomes are not sufficient to unambiguously distinguish between the models. Aiming at overcoming the limitations related to a conformational analysis by nOe measurements we decided to exploit the potentiality of NMR in liquid crystalline phases for describing the torsional probability distribution of *S*-naproxen.

i. NMR experiments

In order to extract the large set of experimental dipolar couplings necessary for the conformational analysis of NAP, a series of 1D and 2D NMR spectra was recorded on the isotropic and anisotropic samples (see Appendix A3) to obtain respectively the scalar J_{ij}^{obs} and the total T_{ij}^{obs} coupling constants. Unfortunately, ^{1}H signals of THF fall very near to signals from aliphatic protons of NAP (*i.e.* H_2, H_3 and H_{14}), preventing from an accurate measurement of T_{ij} when the molecule of interest is dissolved in PBLG/THF. For this reason proton and carbon spectra were recorded on a sample obtained by using totally deuterated THF as organic co-solvent.

All spectra were recorded at 300 K on a liquid high-resolution Bruker Avance 400MHz spectrometer (9.4 T) equipped with a standard variable-temperature unit (BVT-3000) and a BBI or QXO probe with a z field-gradient coil. Spectral assignment of the peaks was performed by 1D ^{1}H, ^{13}C, [13]C-{[1]H} spectra and 2D ^{1}H-^{1}H COSY, ^{1}H-^{13}C HSQC and HMBC correlation experiments. J_{HH} and T_{HH} were measured from homonuclear *J*-resolved and SERF experiments.

Note that in PBLG phases even dipolar couplings between the three equivalent protons of each methyl groups (H_3 and H_{14}) influence the NMR spectrum. For instance, H_3 gives a doublet of triplets due to the coupling with the proton directly attached to the asymmetric carbon (H_2) and to the dipolar couplings between the three equivalent protons of the methyl group. Albeit not well resolved in the ^1H 1D spectrum (Figure 3.25 (a)), this multiplet structure is evident in the homonuclear SERF experiment shown in Figure 3.25 (b). We underline that, even though signals of H_2 and H_{14} are superposed in the single-quantum ^1H spectrum, the positions of each proton in distinct fragments of the molecule avoids ambiguities in the assignment of each coupling to a specific nuclear pair.
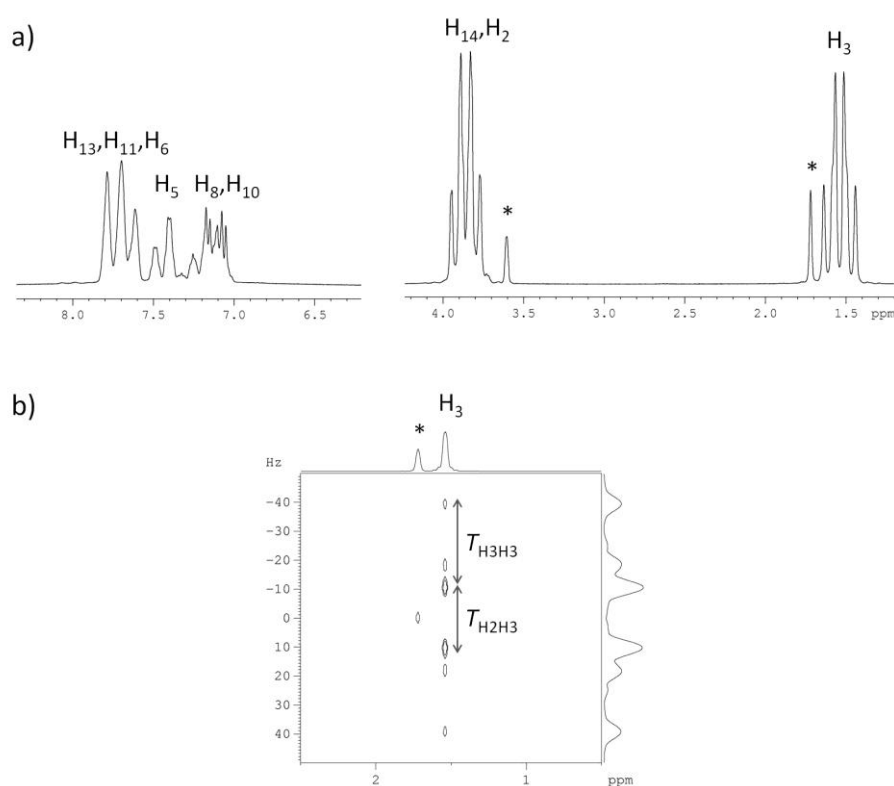
Figure 3.25. (a) 1D ^1H spectrum recorded on *S*-naproxen in PBLG/THF-d_8 at 300 K. (b) 2D SERF tilted spectrum of the same sample where the offsets of the selective pulses were set at υ_3 on the F_2 dimension and at $\upsilon_{2,14}$ on the F_1 dimension. The SERF spectrum was recorded in 26 min using a data matrix of 2048 (t_2) x 64 (t_1) with 16 scans per t_1 increment. The relaxation delays were 1 s. Data were processed using zero-filling up to 256 points and a sine filter in both dimensions. The duration of the RE-BURP refocusing and the E-BURP excitation pulses was 12.4 ms corresponding to a frequency width of 400 Hz. Solvent peaks are labeled with asterisks.

The ^1H-^{13}C *J*-resolved experiment was not resolved enough to allow the measurement of all desired long-range couplings, especially those between spins belonging to different fragments of the molecule (*i.e.* methoxy group, naphthalene, propionic acid). Therefore, we

applied the heteronuclear selective refocusing ^{13}C-^{1}H NMR experiments, HETSERF, originally developed by Bax and Freeman for the measurement of long-range ^{1}H-^{13}C scalar couplings in isotropic media [226], and applied after to the extraction short- and long-range total spin-spin couplings in solutes dissolved in chiral liquid crystals [156]. The basic pulse sequence, reported in Figure 3.26, is based on the heteronuclear *J*-resolved 2D experiment but involves a 180° shaped proton RF pulse for selecting a single type of proton in the studied molecule. Then, after a double Fourier transformation, the couplings between the selected proton and all the interacting carbon atoms are observed in the indirect dimension while the ^{13}C-{^{1}H} spectrum appears in the F$_2$ dimension.
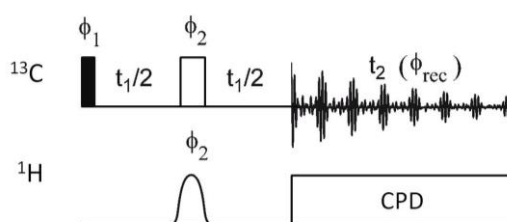
Figure 3.26. Pulse sequence for the HETSERF experiment. Black and white rectangles correspond respectively to π/2- and π-shaped pulses, while white ellipse shape corresponds to π RE-BURP shape pulse. On the proton channel rectangular bar refers to the application of a classical WALTZ-16 decoupling sequence. The 16-steps phase cycle is: $\phi_1 = \phi_{rec}$ = x, -x, x, -x, y, -y, y, -y, -x, x, -x, x, -y, y, -y, y; ϕ_2 = x, x, -x, -x, y, y, -y, -y, -x, -x, x, x, -y, -y, y, y.

While retaining the advantage of the large chemical shift range of ^{13}C spectra, this experiment (*i*) reduces the multiplicity of proton coupled ^{13}C lines resulting in increased sensitivity and (*ii*) leads to narrower linewidths thanks to the refocusing of field inhomogeneities during t_1. One severe limitation of HETSERF experiment is related to the superposition of proton signals. Indeed, a single proton can be selected only when its signal is far enough, *i.e.* if its chemical environment is sufficiently different, from the others. In the molecule of NAP the overlap of aromatic ^{1}H signals (see Figure 3.25 (a)) prevents from applying HETSERF experiment to all protons in the molecule. However, the pulse sequence proved to be a valuable aid for editing critical dipolar couplings between aromatic carbons and aliphatic protons. As an example, Figures 3.27 and 3.28 display the HETSERF spectra recorded selecting H$_2$ and H$_{14}$ on the proton channel, respectively on the isotropic and anisotropic sample, together with selected signals from the corresponding proton-coupled ^{13}C 1D spectra. It can be observed that the heteronuclear selective spectra allows: (*i*) scalar couplings such as $^2J_{C4H2}$, $^3J_{C5H2}$ or $^3J_{C13H2}$, which are already seen in the 1D spectrum, to be precisely measured and

unequivocally assigned (Figure 3.27) and (*ii*) total couplings such as $^2T_{C4H2}$, $^3T_{C5H2}$, and $^4T_{C8H14}$, which cannot be measured in the 1D spectrum, to be easily edited (Figure 3.28).
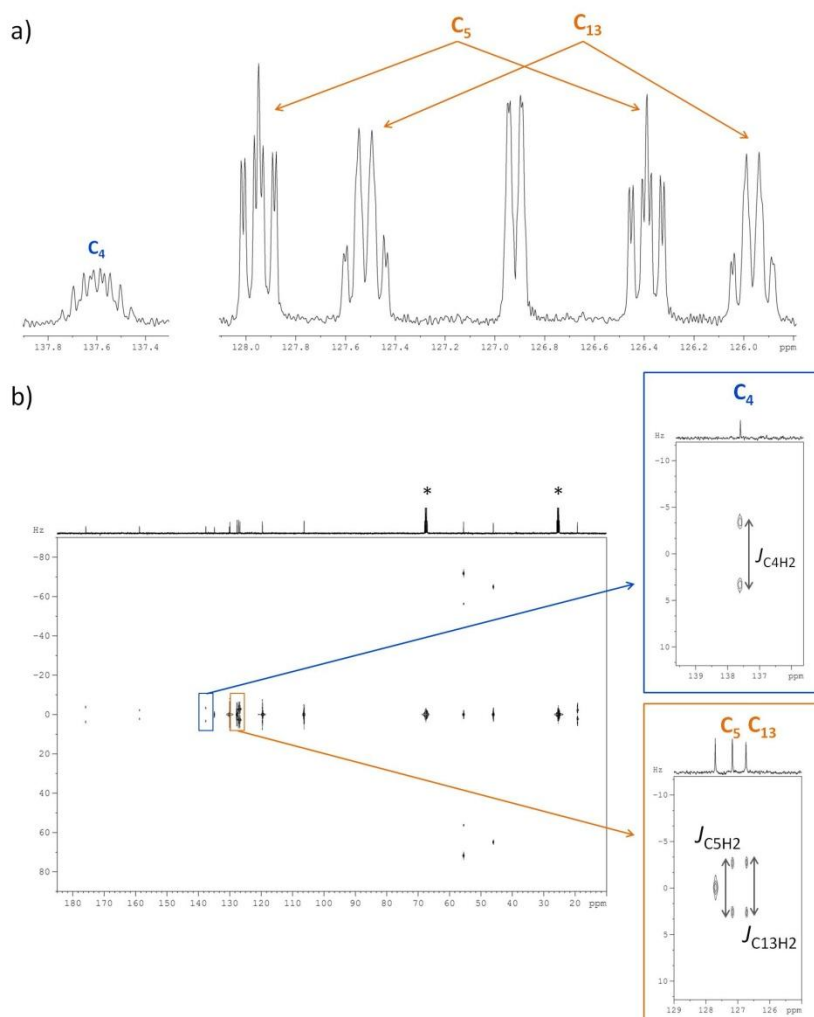
Figure. 3.27. (a) Signals of some selected aromatic carbons (C_4, C_5 and C_{13}) extracted from the 1D proton-coupled ^{13}C spectrum of *S*-naproxen in THF-d$_8$. The spectrum was recorded by using 32768 points and 8192 scans and processed using zero-filling up to 65536 points. (b) 2D HETSERF spectrum of the same sample where the offsets of the π selective pulse on the proton channel was set at $\upsilon_{2,14}$. The HETSERF spectrum was recorded in 5.5 h using a data matrix of 4096 (t_2) x 512 (t_1) with 16 scans per t_1 increment. The relaxation delays were 1.5 s. Data were processed using zero-filling up to 1024 points and no filter. The duration of the RE-BURP refocusing pulse was 49.5 ms corresponding to a frequency width of 100 Hz. Enlarged maps of selected carbon signals (C_4, C_5 and C_{13}) are also shown. Solvent peaks are labeled with asterisks.
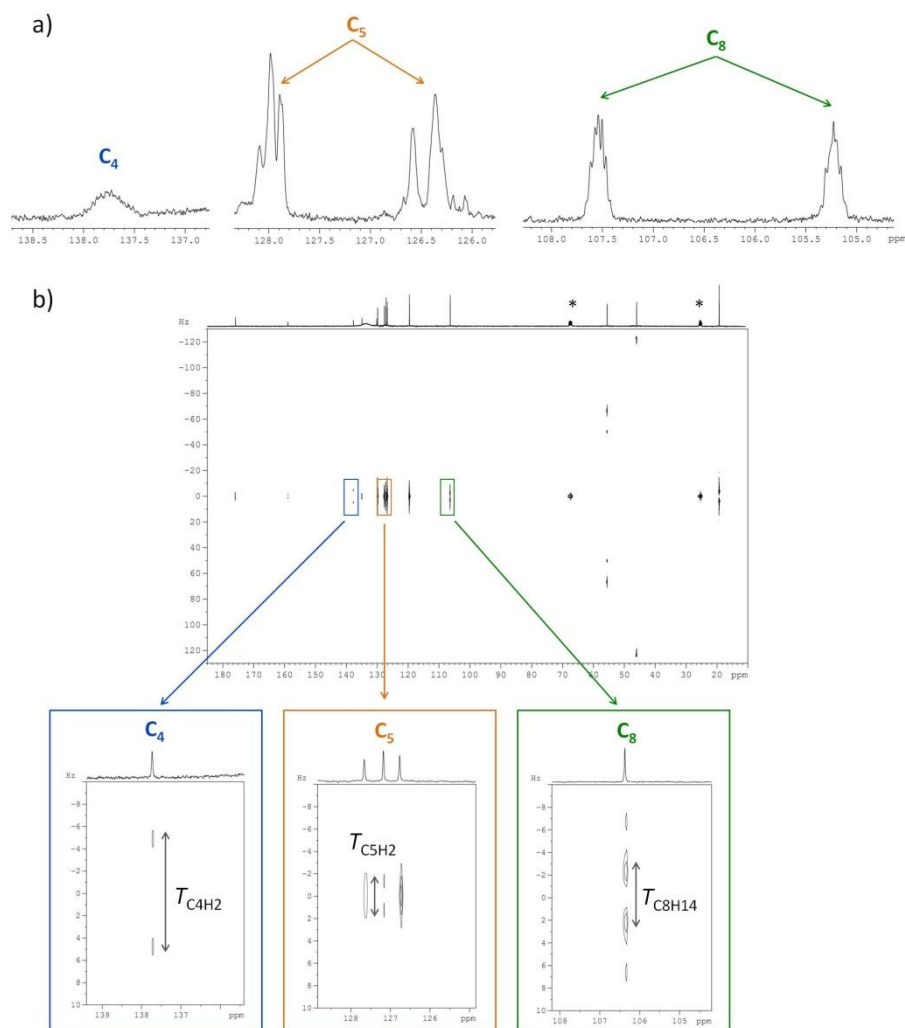
Figure. 3.28. (a) Signals of some selected aromatic carbons (C_4, C_5 and C_8) extracted from the 1D proton-coupled ^{13}C spectrum of *S*-naproxen in PBLG/THF-d$_8$. The spectrum was recorded at 300 K by using 32768 points and 4096 scans and processed using zero-filling up to 65536 points and an exponential filter (LB = 0.5 Hz). (b) 2D HETSERF spectrum of the same sample where the offsets of the π selective pulse on the proton channel was set at $\upsilon_{2,14}$. The HETSERF spectrum was recorded in 2 h using a data matrix of 4096 (t_2) x 288 (t_1) with 16 scans per t_1 increment. The relaxation delays were 1 s. Data were processed using zero-filling up to 512 points and no filter. The duration of the RE-BURP refocusing pulse was 16.5 ms corresponding to a frequency width of 300 Hz. Enlarged maps of selected carbon signals (C_4, C_5 and C_8) are also shown. Solvent peaks are labeled with asterisks.

By combining different experiments a large set of scalar and total coupling constants was finally collected, whose values are reported in the third and fourth columns of Table 3.7.

As for diflunisal, only the absolute values of the indirect and total coupling constants is measured from spectra, thus requiring the measurement of quadrupolar splittings in order to solve the uncertainty in the signs and magnitudes of $^1D_{CH}$. NAD 1D ^{2}H-{^{1}H} and 2D *Q*-COSY spectra cannot be conveniently performed on the sample NAP/PBLG/THF-d$_8$, because signals deriving from the deuterated solvent completely hide signals from deuterium sites at natural

abundance in the molecule of interest. For this reason, another sample was prepared dissolving NAP in PBLG/THF, while keeping the same concentration of solute (~8 wt%) and polymer (~15 wt%) (see Appendix A3). Deuterium spectra were recorded on a high-resolution Bruker Avance II 600MHz spectrometer (14.1 T) equipped with a 5-mm selective ^{2}H cryoprobe. Temperature was carefully fed-back at 300K by a standard variable-temperature unit (BVT-3000). The Δv_{CD_k} measured at different deuterium positions are reported in Table 3.7. In the aliphatic region only quadrupolar doublets for methyl protons H_3 and H_{14} could be individuated, since peaks of H_2 are of lower intensity and then easily hidden from solvent signals.

Table 3.7. Experimental chemical shifts δ_k^{iso}, scalar couplings J_{ij}^{obs}, total couplings T_{ij}^{obs}, dipolar couplings D_{ij}^{obs} and quadrupolar splittings Δv_{CD_k} determined by the NMR analysis of NAP dissolved in THF-d$_8$, PBLG/THF-d$_8$ and PBLG/THF. Errors are estimated from spectral resolution. In the last column, the D_{ij}^{calc} values are also reported for comparison. The whole agreement between D_{ij}^{obs} and D_{ij}^{calc} is given by the RMS.

i	j	J_{ij}^{obs} (Hz)	T_{ij}^{obs} (Hz)	D_{ij}^{obs} [a] (Hz)	D_{ij}^{calc} [b] (Hz)
C-H couplings					
C_2	H_2	129.7 ± 0.6	246.3 ± 0.6	58.3 ± 0.6	58.3
C_2	H_5	3.4 ± 0.4	6.5 ± 0.6	1.6 ± 0.5	1.4
C_3	H_2	-4.2 ± 0.4	7.0 ± 0.6	5.6 ± 0.5	5.3
C_3	H_3	128.4 ± 0.6	115.7 ± 0.6	-6.4 ± 0.6	-6.6
C_4	H_2	-6.7 ± 0.4	-9.3 ± 0.8	-1.3 ± 0.6	-2.0
C_4	H_3	4.5 ± 0.6	4.4 ± 0.6	-0.1 ± 0.6	-0.4
C_4	H_5	0.0 ± 0.4	14.7 ± 0.8	7.4 ± 0.6	6.9
C_5	H_2	5.2 ± 0.4	3.0 ± 0.8	-1.1 ± 0.6	-1.1
C_5	H_5	156.9 ± 0.6	171.2 ± 0.8	7.2 ± 0.7	7.3
C_5	H_{13}	7.8 ± 0.4	11.2 ± 0.6	1.7 ± 0.5	1.8
C_6	H_6	157.7 ± 0.6	238.0 ± 0.6	40.2 ± 0.6	39.5
C_7	H_5	8.2 ± 0.4	6.4 ± 0.8	-0.9 ± 0.7	-1.2
C_8	H_8	157.9 ± 0.6	233.1 ± 0.6	37.6 ± 0.6	37.8
C_8	H_{11}	-1.3 ± 0.6	0.0 ± 0.6	0.7 ± 0.6	0.8
C_8	H_{14}	0.0 ± 0.6	-4.4 ± 0.8	-2.2 ± 0.7	-2.4
C_{10}	H_8	5.7 ± 0.6	9.4 ± 0.6	1.9 ± 0.6	1.8
C_{10}	H_{10}	160.1 ± 0.6	176.0 ± 0.6	8.0 ± 0.6	7.9
C_{11}	H_8	0.0 ± 0.6	1.5 ± 0.6	0.8 ± 0.6	0.8
C_{11}	H_{11}	159.2 ± 0.6	234.2 ± 0.8	37.5 ± 0.7	38.2
C_{11}	H_{13}	5.1 ± 0.6	-4.5 ± 0.6	-4.8 ± 0.6	-4.5
C_{13}	H_2	6.0 ± 0.4	0.0 ± 0.8	-3.0 ± 0.7	-3.5

C$_{13}$	H$_5$	6.2 ± 0.4	9.1 ± 0.8	1.5 ± 0.7	1.5
C$_{13}$	H$_{13}$	156.7 ± 0.6	232.6 ± 0.8	38.0 ± 0.8	38.5
C$_{14}$	H$_8$	0.0 ± 0.6	-6.8 ± 0.6	-3.4 ± 0.6	-3.7
C$_{14}$	H$_{14}$	143.6 ± 0.6	132.9 ± 0.6	-5.4 ± 0.6	-5.2
H-H couplings					
H$_2$	H$_3$	7.2 ± 0.2	20.5 ± 0.8	6.7 ± 0.5	6.5
H$_2$	H$_5$	0.0 ± 0.2	-6.8 ± 0.2	-3.4 ± 0.2	-3.2
H$_3$	H$_3$	0.0 ± 0.2	-29.0 ± 0.8	-9.7 ± 0.5	-9.8
H$_3$	H$_5$	0.0 ± 0.2	1.0 ± 0.2	0.5 ± 0.2	0.4
H$_5$	H$_6$	8.5 ± 0.2	-35.7 ± 0.4	-22.1 ± 0.3	-22.6
H$_5$	H$_8$	0.0 ± 0.2	-6.2 ± 0.4	-3.1 ± 0.3	-3.1
H$_5$	H$_{14}$	0.0 ± 0.2	-2.0 ± 0.2	-1.0 ± 0.2	-0.8
H$_6$	H$_8$	1.2 ± 0.2	-33.9 ± 0.4	-17.6 ± 0.3	-17.2
H$_6$	H$_{10}$	0.0 ± 0.2	1.8 ± 0.4	0.9 ± 0.3	0.6
H$_6$	H$_{11}$	0.0 ± 0.2	4.3 ± 0.4	2.2 ± 0.3	1.6
H$_6$	H$_{13}$	0.9 ± 0.2	4.3 ± 0.4	1.7 ± 0.3	1.6
H$_6$	H$_{14}$	0.0 ± 0.2	-4.1 ± 0.2	-2.1 ± 0.2	-2.1
H$_8$	H$_{10}$	2.6 ± 0.2	9.5 ± 0.4	3.5 ± 0.3	3.4
H$_8$	H$_{11}$	0.7 ± 0.2	4.3 ± 0.4	1.8 ± 0.3	1.6
H$_8$	H$_{14}$	-0.3 ± 0.1	28.8 ± 0.4	-14.6 ± 0.3	-14.8
H$_{10}$	H$_{11}$	8.9 ± 0.2	-39.8 ± 0.4	-24.4 ± 0.3	-23.8
H$_{11}$	H$_{13}$	0.6 ± 0.2	-32.8 ± 0.4	-16.7 ± 0.3	-17.4
H$_{14}$	H$_{14}$	0.0 ± 0.2	-22.0 ± 0.4	-7.3 ± 0.3	-7.4

RMS		0.40 Hz

k	δ_k^{iso} [c] (ppm)	$\Delta\nu_{CD_k}$ (Hz)
H$_2$	3.79 ± 0.05	-
H$_3$	1.51 ± 0.05	63.0 ± 0.8
H$_5$	7.42 ± 0.05	-99.9 ± 0.8
H$_6$	7.68 ± 0.05	-342.5 ± 0.8
H$_8$	7.17 ± 0.05	-345.9 ± 0.8
H$_{10}$	7.09 ± 0.05	-80.3 ± 0.8
H$_{11}$	7.68 ± 0.05	-342.5 ± 0.8
H$_{13}$	7.69 ± 0.05	-342.5 ± 0.8
H$_{14}$	3.85 ± 0.05	60.7 ± 0.8
C$_1$	175.8 ± 0.3	
C$_2$	46.0 ± 0.3	
C$_3$	19.2 ± 0.3	
C$_4$	137.6 ± 0.3	

C_5	127.2 ± 0.3
C_6	127.7 ± 0.3
C_7	134.9 ± 0.3
C_8	106.3 ± 0.3
C_9	158.8 ± 0.3
C_{10}	119.6 ± 0.3
C_{11}	129.9 ± 0.3
C_{12}	130.1 ± 0.3
C_{13}	126.7 ± 0.3
C_{14}	55.5 ± 0.3

[a] calculated from $D_{ij} = \left[\pm T_{ij}^{obs} - (\pm J_{ij}^{iso})\right]/2$ (non-equivalent nuclei) or $D_{ij}^{obs} = \pm T_{ij}^{obs}/3$ (equivalent nuclei)

[b] from the AP-DPD method (see below)

[c] chemical shifts are given from calibration with THF signal (at 1.72 ppm and 25.37 ppm for proton and carbon-13, respectively)

ii. Molecular modeling calculations

As seen before, the *a priori* knowledge of the geometry of the most stable conformers and a good estimate of the potential energy surface (PES) is required. Hence, a molecular dynamics calculation was first performed by the MD module of HyperChem™ software package [227] with the semiempirical AM1 method, in order to individuate approximately structures and locations of the lowest minimum energy conformers for the NAP molecule *in vacuo*. An accurate geometry optimization was performed then on the minimum energy structures at DFT level by means of the B3LYP hybrid density functional using the 6-31++G** basis set provided by the Gaussian03 software package [228]. Theoretical calculations predict four minimum energy conformers, whose relative energies together with the most relevant structural parameters related to the geometry of the flexible substituents are reported in Table 3.8.

For both conformers I and II, the O-C_{14} bond lies in the plane of the aromatic ring and the methoxy group adopts a *cis* orientation with respect to the C_8-C_9 aromatic bond (φ = C_8-C_9-O-C_{14} ~0°). The isomers involving the *trans* geometry of the methoxy group (φ = C_8-C_9-O-C_{14} ~180°) and the same geometry of the chiral side chain (III and IV) are about 6 kJ/mol less stable than their *cis* analogues. Calculating roughly the Boltzmann population distribution of the four conformers from their relative energies (equation (3.2)), we obtain that isomers I and II count for more than 90% with respect to conformers III and IV. The conformational preference for the *cis* configuration of the methoxy group has already been found for naproxen and

analogues [220, 225, 229]. In general, in the absence of overriding steric effects from substituents on adjacent ring positions, a methoxy group attached to an aromatic ring is known to adopt a conformation with its heavy atoms in the ring plane [46, 230-232]. The stability of this coplanar conformation is accepted to be mainly defined by the conjugation between the oxygen in-plane lone pairs and the aromatic π system [230] and/or the electrostatic interaction between the methyl and the proximate ring atoms [233]. If the system is not symmetrical with respect to the methoxy C_{ipso} - C_{para} axis, coplanar conformers are generally not equally populated and in this case the *cis* orientation of the methoxy group to the aromatic C–C bond with the larger π bond order is preferred [234-235].

Table 3.8. Relative energies and selected dihedral angles of the four lowest minimum energy conformers obtained for NAP from B3LYP/6-31++G** calculations.

conformers	I	II	III	IV
E_{pot}^{norm} (kJ/mol)	0.00	1.18	6.31	7.25
φ = C_8-C_9-O-C_{14} (degree)	0.48	0.05	179.97	-179.98
ϑ = C_{13}-C_4-C_2-H_2 (degree)	5.61	-173.29	5.13	-173.93
C_{13}-C_4-C_2-C_3 (degree)	-115.12	66.01	-115.63	65.32
C_{13}-C_4-C_2-C_1 (degree)	121.42	-57.56	120.89	-58.25
P_{theo} (%) [a]	56.9	35.4	4.6	3.1

[a] Calculated by equation $P_{theo}(\varphi) = exp\left(-E_{pot}^{norm}/RT\right)$

The two isomers I and II of Table 3.8 (and the two isomers III and IV) differ by the torsion angle ϑ of the chiral substituent around the C_2-C_4 axis. The dihedral angle ϑ is, respectively, 5.61° and -173.29° for isomers I and II. This means the two bulky methyl and carboxylic acid groups are located on each side of naphthalene plane in both isomers to minimize steric repulsion and the hydrogen atom directly bound to the stereogenic carbon atom (α-hydrogen) lies almost in the naphthalene plane. Thus, the two isomers correspond to a rotation of about 180° of the whole chiral substituent around the C_2-C_4 bond. Conformation I (and III) seems to be slightly stabilized with regard to conformation II (and IV), with relative percentages of about 60% and 40% respectively. The *quasi*-planarity of the α-hydrogen atom relative to the aromatic ring is in agreement with previous results [203, 220, 236-237]. Note, however, that in literature slightly different outcomes are reported in some cases, with additional relative minima for ϑ = C_{13}-C_4-C_2-H_2 at about 134°, that is with the C_2-C_3 bond lying almost in the plane of the naphthalene ring [225, 238]. In order to further verify our

theoretical results, optimized PES scans (*i.e.* allowing for bond lengths and angles relaxation of the structure) were performed separately (thanks to the limited interactions between the methoxy group and the propionic acid group) for the torsion angle φ and ϑ, over the 0°-360° range with a 5°-step sampling (Figure 3.29).
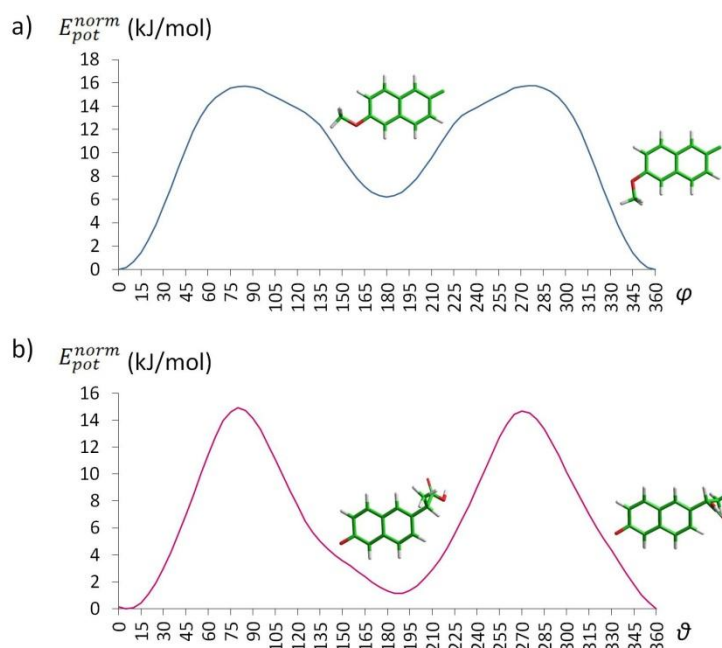
Figure 3.29. Normalized potential energy as a function of (a) φ = C_8-C_9-O-C_{14} and (b) ϑ = C_{13}-C_4-C_2-H_2, obtained for NAP from B3LYP/6-31++G** calculations, including spatial arrangement of the corresponding fragment at the lowest minimum energies.

The one dimensional scan for φ (Figure 3.29 (a)) revealed again two minima, in which the methoxy group adopt coplanar conformations relative to the naphthalene ring. From the one dimensional scan for ϑ (Figure 3.29 (b)) it can be observed that the potential wells for the rotation of the chiral side chain are not perfectly symmetric. Nevertheless, at ϑ ~135° no real minima can be observed. Hence, the conformer exhibiting the C_2-C_3 bond almost in the plane of the naphthalene ring is not a minimum energy structure. Note, finally, that also changing the functional and the basis set from B3LYP/6-31++G** to MP2/6-31G gave similar results.

iii. Conformational analysis

Once collected a large set of experimental D_{ij}^{obs} and calculated the geometries of the most stable conformers, the conformational analysis can be performed by using the AP-DPD

approach. As assumed in the molecular modeling calculations, torsional potentials for the two dihedral angles φ and ϑ are non-cooperative motions, due to the limited interactions between the methoxy group and the propionic acid group. Therefore, the more convenient strategy to describe the conformational distribution for this molecule is a two-step approach:

1) each non-cooperative motion is first treated separately, in order to quickly optimize the orientational and potential parameters, avoiding huge computational burden;

2) the two non-cooperative rotations are treated together, in order to describe the potential surface for the whole molecule.

Torsional potential for the dihedral angle φ = C$_8$-C$_9$-O-C$_{14}$

For describing by the AP model the 2-methoxynaphthalene fragment (composed of the naphthalene, *N*, and the methoxy, *M*, group), 4 fragment tensors $\varepsilon_{2,p}^j$ are required:

- $\varepsilon_{2,0}^N$ and $\varepsilon_{2,2}^N$, for the naphthalene fragment (*N*)
- $\varepsilon_{2,0}^{C-O}$, for the monoaxial component along the C$_9$-O bond direction
- $\varepsilon_{2,0}^{O-CH_3}$, for the monoaxial component along the O-C$_{14}$ bond direction.

Within the Direct Probability Description model the torsional probability distribution around φ can be modelled as a sum of two Gaussian functions centered at 0° and 180°. Some convergence problems sometimes occur if the centers of a Gaussian coincides with the boundaries of the space that is sampled. In these cases a common trick is to change the space boundaries. To overcome this usual obstacle, a more general expression has been designed in the LXNMR S.C.An. group to describe the sum of two Gaussian functions separated by 180°. The $P_{iso}(\varphi)$ function for the 2-methoxynaphthalene fragment of *S*-naproxen can be then written as:

$$P_{iso}(\varphi) = \left(\frac{|cos\varphi| - cos\varphi}{2} + A_\varphi cos\varphi \right) \cdot exp\left[-\frac{sin^2(\varphi - \varphi^{max})}{2h_\varphi^2} \right] \tag{3.5}$$

where φ^{max} is the first most probable value of the torsion angle (the second one being 180°+φ^{max}), A_φ is the relative weight of the first Gaussian (the relative weight of the second Gaussian is fixed to be equal to $1 - A_\varphi$) and, finally, h_φ gives the width at half maximum height of each Gaussian according to equation (1.85).

With this theoretical apparatus and fixing molecular geometry as from molecular modelling calculations (the used molecular geometry is reported in Appendix A5), a subset of D_{ij}^{obs} of Table 3.7 (that is those corresponding to the 2-methoxynaphthalene portion of the molecule) was fitted by using the software AnCon [95], iterating on the orientational

parameters $\varepsilon_{2,p}^{j}$ and the potential terms φ^{max} and A_{φ} separately, and parametrically adjusting h_{φ}, until an acceptable value for the RMS target function is reached. Overall, we have 23 independent D_{ij}^{obs} (16 for *N*, 2 for *M* and 5 between the two fragments) for 7 unknowns. After optimization we obtained the torsional potential $P_{iso}(\varphi)$ reported in Figure 3.30, which is characterized by an absolute maximum at 0° with relative percentage of 87% and a relative maximum at 180° with relative percentage of 13%.
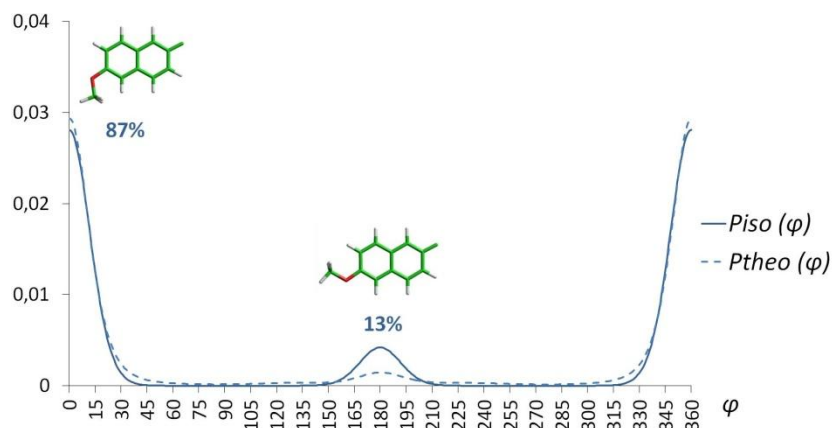
Figure 3.30. Experimental (solid line) and theoretical (dashed line) torsional probability distributions as a function of φ obtained for *S*-naproxen respectively by the AP-DPD approach and from B3LYP/6-31G** calculations.

This solution confirms the coplanar arrangement of the methoxy group with a preference for the *cis* configuration relative to the C_8-C_9 bond which has been found by DFT theoretical calculations. The agreement between experimental and theoretical results can be easily seen in Figure 3.30 where the theoretical probability distribution, $P_{theo}(\varphi)$, calculated from the potential energy values obtained by DFT calculations is plotted (blue dashed line) together with the $P_{iso}(\varphi)$ obtained from AP-DPD approach (blue solid line). A slight change in the probability ratio between the two conformer is observed (90:10 in $P_{theo}(\varphi)$ *versus* 87:13 in experimental $P_{iso}(\varphi)$), but it is worth underlining that this ratio is extremely sensitive to the geometry of the methoxy group with respect to the naphthalene fragment, especially to the angle OC_9C_8. In our calculation such angle is fixed at 125.76° as from molecular modelling results, but it can be seen from Figure 3.31 that, for small changes of its value, the best fit between D_{ij}^{obs} and D_{ij}^{calc} (with RMS values being invariably of 0.44-0.45) is reached for a significantly different probability ratio of the conformers. In other words, an acceptable correspondence between D_{ij}^{obs} and D_{ij}^{calc} can be achieved for a wide range of values for the

angle OC_9C_8, while simultaneously varying the probability distribution of the two most stable conformers.
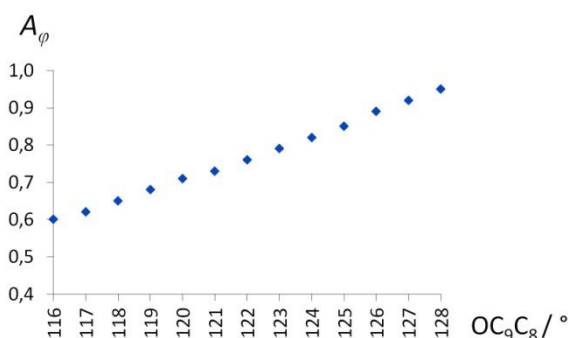
Figure 3.31. Optimized values of A_φ as a function of the angle OC_9C_8 calculated for *S*-naproxen by the AP-DPD approach while fixing φ^{max} = 0° and h_φ = 12.

Torsional potential for the dihedral angle ϑ = C$_{13}$-C$_4$-C$_2$-H$_2$

The second torsional potential to be investigated in the molecule of NAP is that around the dihedral angle ϑ. Hence, we consider in this case the *S*-(+)-2-(2-naphthyl)propanoic acid (composed of the naphthalene, *N*, and the propanoic acid, *P*). Within the AP model, this portion of the molecule can be described by six fragment tensors $\varepsilon_{2,p}^{j}$:

- $\varepsilon_{2,0}^{N}$ and $\varepsilon_{2,2}^{N}$, for the naphthalene fragment (*N*)
- $\varepsilon_{2,0}^{C-C}$, for the monoaxial component along the C_4-C_2 bond direction
- $\varepsilon_{2,0}^{C-H}$, for the monoaxial component along the C_2-H_2 bond direction
- $\varepsilon_{2,0}^{C-CH_3}$, for the monoaxial component along the C_2-C_3 bond direction
- $\varepsilon_{2,0}^{H-CH_3}$, for the monoaxial component along the H_2-C_3 direction.

The same expression used previously for the torsional potential of the methoxy group works well for the rotation of the propanoic fragment, since the two lowest energy conformers derive from a rotation of about 180° of the whole chiral substituent around the C_2-C_4 bond. The torsional probability distribution about ϑ is then written as:

$$P_{iso}(\vartheta) = \left(\frac{|cos\vartheta| - cos\vartheta}{2} + A_\vartheta cos\vartheta \right) \cdot exp\left[-\frac{sin^2(\vartheta - \vartheta^{max})}{2h_\vartheta^2} \right] \qquad (3.6)$$

where ϑ^{max} and 180°+ϑ^{max} are the most probable values of the torsion angle, A_ϑ is the relative weight of the Gaussian centered at ϑ^{max} (the relative weight of the Gaussian centered at 180°+ϑ^{max} is equal to $1 - A_\vartheta$) and, finally, h_ϑ gives the width at half maximum height of each Gaussian according to equation (1.85).

The orientational parameters (the six $\varepsilon_{2,p}^{j}$) and potential terms (ϑ^{max}, A_ϑ and h_ϑ) represents the 9 unknowns that the software AnCon iterates on, while fitting the subset of 27 independent D_{ij}^{obs} (16 for *N*, 7 for *P* and 4 between the two fragments) of Table 3.7 corresponding to the naphthylpropanoic portion of the molecule. As previously, calculations were performed by fixing molecular geometry as from molecular modelling calculations (Appendix A5) and by varying ϑ^{max} and A_ϑ separately, with a parametrical adjustment of h_ϑ. The torsional potential $P_{iso}(\vartheta)$ obtained after optimization is reported in Figure 3.32 (pink solid line), together with the theoretical probability distribution, $P_{theo}(\varphi)$ (pink dashed line) calculated from the potential energy values obtained by DFT calculations.
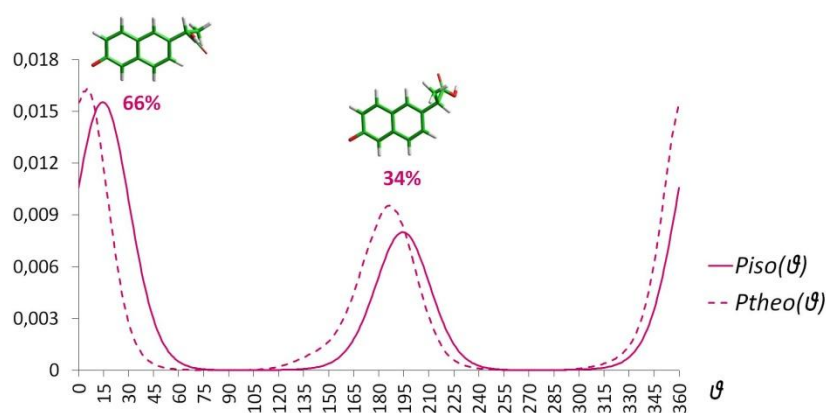
Figure 3.32. Experimental (solid line) and theoretical (dashed line) torsional probability distributions as a function of ϑ obtained for *S*-naproxen respectively by the AP-DPD approach and from B3LYP/6-31G** calculations.

Experimental $P_{iso}(\vartheta)$ displays an absolute maximum at 15.8° with relative percentage of 66% and a relative maximum at 195.8° with relative percentage of 34%. The experimental curve is similar to the theoretical one, confirming again the *quasi*-planarity of the α-hydrogen atom relative to the aromatic ring with a slight preference for the *cis* configuration relative to the C_4-C_{13} bond. A shift of ϑ^{max} value (and consequently 180°+ϑ^{max}) from about 6° in DFT calculations to 15.8° in the AP-DPD conformational analysis can be observed. However, it should be remarked that even if the iteration process converges for ϑ^{max} = 15.8°, a similar acceptable correspondence between D_{ij}^{obs} and D_{ij}^{calc} can be obtained for a wider range of ϑ^{max} values. In Figure 3.33 we report as an example the minimum RMS AnCon converges to, while varying ϑ^{max} from -30° to 60°. The curve is almost flat and the RMS error is practically indiscernible in the range 10°-25°. This trend may indicate that: (*i*) the spatial arrangement of the propionic group relative to the naphthalene is not very fixed, *i.e.* the α-hydrogen prefers

lying almost in the naphthalene plane in the *cis* configuration relative to the C_4-C_{13} bond, but it is not well confined in this position, and it fluctuates adopting different arrangements between ϑ = 10° and ϑ = 25°; and/or (*ii*) the experimental data we extracted from spectra of NAP dissolved in PBLG/THF-d_8 between the two fragments are not numerous and large enough to individuate a peaked preferred position, but rather a limited region of space where the lateral chain is confined. In both cases, even though the conformational information we gain is not extremely precise, we have experimental evidence that restrict the most probable values adopted in solution by the angle ϑ from the 0-360° whole space to a small range of 15° degrees.

RMS
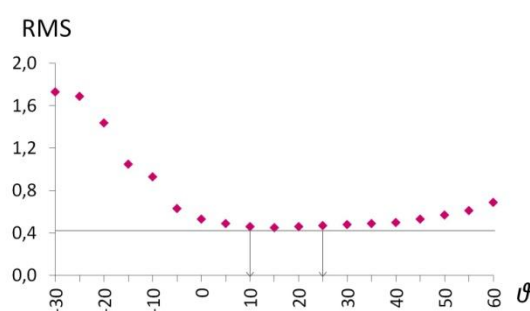
Figure 3.33. RMS value as a function of ϑ^{max} calculated for *S*-naproxen by the AP-DPD approach while fixing A_ϑ = 0.66 and h_ϑ = 17.

Torsional potentials for the non-coupled rotations around φ = C_8-C_9-O-C_{14} and ϑ = C_{13}-C_4-C_2-H_2

Since the propanoic and the methoxy groups are relatively far from each other in the molecular structure, it can be safely assumed that the rotations around the two dihedral angles φ and ϑ are non-cooperative motions. Hence, once treated each motion separately, it is quite simple to describe the whole molecular potential surface, since the total probability distribution function $P_{iso}(\varphi, \vartheta)$ is simply the product between the single probability distribution for each torsion:

$$P_{iso}(\varphi, \vartheta) = P_{iso}(\varphi) \cdot P_{iso}(\vartheta) \qquad (3.7)$$

As for the definition of the fragment tensors $\varepsilon_{2,p}^{j}$ for the whole molecule, it is to remember that in the AP model the conformationally dependent interaction tensors $\varepsilon_{2,m}(\{\phi\})$ necessary to define the intermolecular potential $U_{ext}(\Omega, \{\phi\})$, can be written as the sum of the conformationally independent $\varepsilon_{2,p}^{j}$ from each rigid fragment. Hence, in the case of *S*-naproxen, we just need to add the interaction tensors defined for the two substructures considered before. A simplification is obtained considering that the direction of the C_9-O and C_4-C_2 bonds is parallel, thus $\varepsilon_{2,0}^{C-O} = \varepsilon_{2,0}^{C-C}$. Definitely, 7 $\varepsilon_{2,p}^{j}$ are required:

- $\varepsilon_{2,0}^N$ and $\varepsilon_{2,2}^N$ for the *N* fragment
- $\varepsilon_{2,0}^{O-CH_3}$ for the *M* fragment
- $\varepsilon_{2,0}^{C-H}$, $\varepsilon_{2,0}^{C-CH_3}$, $\varepsilon_{2,0}^{H-CH_3}$ for the *P* fragment
- $\varepsilon_{2,0}^{C-O} = \varepsilon_{2,0}^{C-C}$ for connecting *N*, *P* and *M*.

These seven orientational parameters represent the unknowns that the software AnCon iterates on, while fitting the 34 independent D_{ij}^{obs} (16 for *N*, 7 for *P*, 2 for *M*, 4 between *N* and *P*, and 5 between *N* and *M*) of Table 3.7. The six potential terms (φ^{max}, ϑ^{max}, A_φ, A_ϑ, h_φ and h_ϑ) were taken from the optimised values of the single rotations, whereas molecular geometry was fixed again as from molecular modelling calculations (Appendix A5). A satisfactory RMS error of 0.40 was reached, with a good correspondence between D_{ij}^{obs} and D_{ij}^{calc} (reported in the last column of Table 3.7), as it can be seen in Figure 3.34. The optimized parameters and the torsional distribution $P_{iso}(\varphi, \vartheta)$ are shown in Table 3.9 and Figure 3.35, respectively.

Table 3.9. Optimized values of the iteration parameters used in the conformational analysis with the AP-DPD approach of the NAP molecule dissolved in PBLG/THF-d$_8$.

	NAP in PBLG/THF-d$_8$
φ^{max} (degree)	0.15 ± 10.0
ϑ^{max} (degree)	15.80 ± 5.9
A_φ	0.87 ± 0.02
A_ϑ	0.66 ± 0.03
h_φ (degree)	12.0
h_ϑ (degree)	17.0
$\varepsilon_{2,0}^N$ (RT)	-0.0096 ± 0.0003
$\varepsilon_{2,2}^N$ (RT)	-0.0045 ± 0.0003
$\varepsilon_{2,0}^{C-O} = \varepsilon_{2,0}^{C-C}$ (RT)	0.0059 ± 0.0002
$\varepsilon_{2,0}^{C-H}$ (RT)	-0.0123 ± 0.0003
$\varepsilon_{2,0}^{C-CH_3}$ (RT)	-0.0076 ± 0.0006
$\varepsilon_{2,0}^{H-CH_3}$ (RT)	0.0054 ± 0.0006
$\varepsilon_{2,0}^{O-CH_3}$ (RT)	0.0073 ± 0.0003
RMS	0.40
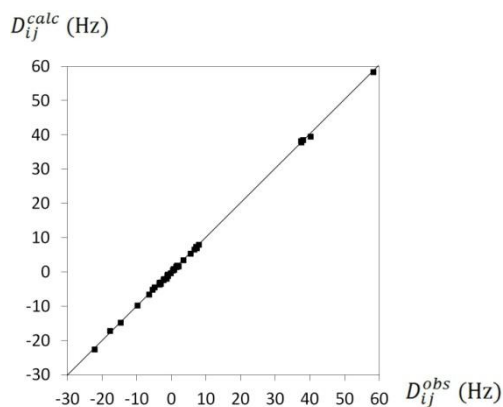
Figure 3.34. Observed *versus* theoretical dipolar couplings obtained for NAP respectively from NMR experiments and by the AP-DPD approach.
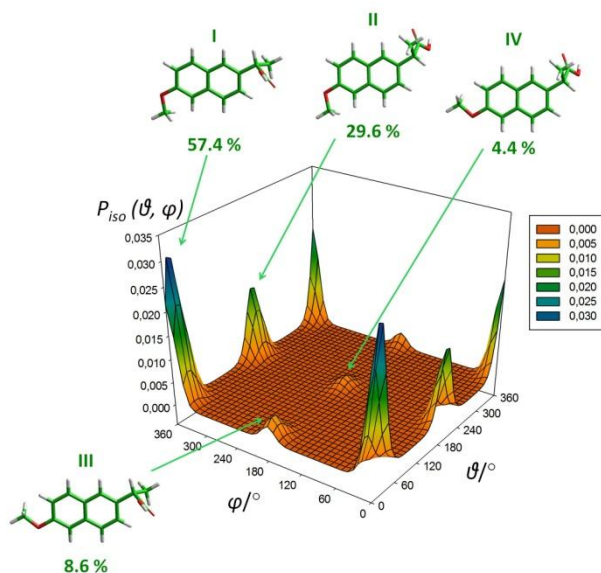
Figure 3.35. Experimental probability distribution $P_{iso}(\varphi, \vartheta)$ obtained by AP-DPD approach for *S*-naproxen dissolved in PBLG/THF-d$_8$, including structures of minimum energy conformers and their relative abundance.

Four minimum energy conformers can be seen in the experimental potential surface obtained by the AP-DPD approach. Conformers I and II, having φ = C$_8$-C$_9$-O-C$_{14}$ ~0° and and ϑ = C$_{13}$-C$_4$-C$_2$-H$_2$ respectively equal to ~15° and ~195° are the most stable conformers, with relative percentages of 57.4% and 29.6%. The isomers III and IV involving the *trans* geometry of the methoxy group (φ = C$_8$-C$_9$-O-C$_{14}$ ~180°) and the same geometry of the chiral side chain (ϑ = C$_{13}$-C$_4$-C$_2$-H$_2$ equal to ~15° and ~195°, respectively) are less stable than their *cis* analogues, showing relative percentages of 8.6% and 4.4%. Comparing D_{ij}^{obs} and D_{ij}^{calc} reported in the last two columns of Table 3.7, it can be observed that the conformational equilibrium between

these four isomers provides a good fit of experimental dipolar couplings (Figure 3.34). An acceptable reproduction cannot be achieved with a mono-conformational model, that is considering just one most stable conformer. Therefore, NMR in PBLG phases reveals an efficace technique to acquire conformational information on two-rotor bioactive molecules in solution starting from experimental NMR data. Albeit a margin of error has to be considered around the optimised values found for torsional angles, it is possible to gather reliable experimental information on the preferred spatial arrangements adopted by the flexible molecule in a liquid medium.

3.3.3. Conclusions

Examples reported in this section prove that NMR spectroscopy in weakly orienting PBLG phases, combined with the AP-DPD approach, is a valuable tool for investigating the structure and the conformational equilibrium of anti-inflammatory drugs displaying one or two torsional degrees.

From the study of diflunisal and its non-fluorinated analogue, phenylsalicylic acid, (section 3.3.1) some interesting remarks can be derived. First, in order to overcome the difficulties in the extraction from standard spectra of DFL of proton-fluorine couplings, necessary for tackling the conformational analysis, the new GET-SERF pulse sequence has been developed. Combining selective refocusing and spatial encoding approaches, this experiment allows the trivial edition of all long and short range ^{1}H-^{19}F scalar or dipolar couplings in one single NMR experiment. The probability distribution of DFL dissolved in the polypeptidic PBLG/THF solvent shows a couple of *trans* conformers with φ_1^{max} = ±45.5° and relative percentage of 56% and a couple of *cis* conformers with φ_2^{max} = ±41.1° and a relative percentage of 44%, in very good agreement with the theoretical results obtained at DFT level. Moreover, the similar experimental outcomes in both chiral (PBLG/THF) and achiral (PBG/THF) phases proves there are no effects on the conformational equilibrium resulting from the chirality of the medium. Finally, APS has been studied under similar conditions to probe the influence the fluorine nuclei have on the conformational equilibrium of the diflunisal. Results seem to suggest a smoothing in the rotational barriers.

In section 3.3.2 the same promising strategy has been applied to the naproxen molecule, whose torsional description implies two non-cooperative rotations to be considered. In agreement with DFT theoretical calculations, four minimum energy structures have been

individuated by treating the experimental D_{ij}^{obs} with the AP-DPD approach: a couples of more stable conformers (I and II, with relative percentages of 57.4% and 29.6%, respectively) with the methoxy group in the *cis* arrangement (φ = C$_8$-C$_9$-O-C$_{14}$ ~0°) and α-hydrogen atom *quasi-*planar relative to the aromatic ring (ϑ = C$_{13}$-C$_4$-C$_2$-H$_2$ equal to ~15° and ~195, respectively); a couple of less stable conformers (III and IV, relative percentages of 8.6% and 4.4%, respectively) involving the *trans* geometry of the methoxy group (φ = C$_8$-C$_9$-O-C$_{14}$ ~180°) and the same geometry of the chiral side chain (ϑ = C$_{13}$-C$_4$-C$_2$-H$_2$ equal to ~15° and ~195°, respectively).

From these three examples we can conclude that (*i*) the use of PBLG phases seems to be a promising approach in the study of conformational equilibria of complex flexible molecules, otherwise impossible to treat using thermotropic solvents and (*ii*) the AP-DPD model appears as a solid method also for weakly ordered solutes. At the same time, it is evident that in order to achieve an accurate conformational description one has to face a series of difficulties: (*i*) multiple adapted NMR experiments have to be combined - and eventually designed - in order to extract a set of experimental data that is as large and accurate as possible; (*ii*) a reliable geometry is necessary, to be kept fixed in the iteration procedure. However, the existence of a broad array of weakly ordering phases, providing with a different degree of order and, for lyotropic systems, with different aligning medium/solvent combinations, together with the recognized efficacy of AP-DPD approach, make NMR in these phases a promising competitive tool for conformational investigations of small flexible bioactive molecules.

3.4. Conformational investigation in solution of stilbenoids by NMR spectroscopy in highly and weakly ordering media

The last family of molecules investigated in this Ph.D. thesis is that of *trans*-stilbenoids, *i.e.* derivatives of *trans*-diphenylethene, commonly known as *trans*-stilbene (*t*-St), reported in Figure 3.36 (a).

t-St and its derivatives show several interesting biological and technological properties that could be affected, to a certain extent, by the rotameric distribution of the molecule. Green plants of various taxonomic groups naturally biosynthesize stilbenoic compounds, the most common being resveratrol (*trans*-3,4′,5-trihydroxystilbene), piceatannol (*trans*-3,3′,4′,5-tetrahydroxystilbene) or rhapontigenin (*trans*-3,3′,5-trihydroxy-4′-methoxystilbene), that act as

protective agents against adverse conditions, such as microbial attacks or environmental stress [239-241]. These naturally occurring stilbenic compounds have been reported to possess multiple biological activities, including antioxidant [242], antiproliferative and proapoptotic [243-245], anti-ciclooxygenase [246], estrogenic/antiestrogenic [247], antiplatelet and vasodilating [248-250], antifungal [251] and antiallergic [252] properties. As a consequence, the last decades have witnessed intense research devoted to understanding the mechanisms underlying the activities of these natural compounds [253-257] as well as designing and evaluating synthetic analogues like the popular *trans*-4,4'-dihydroxystilbene [258-263]. These compounds are indeed very promising since they can play an important role in the prevention and the treatment of a wide variety of human pathological processes, like inflammation [264-265], atherosclerosis [266] and cardiovascular diseases [267-268]. They can delay the onset of age-related diseases, such as diabetes [269], can found application in hormonal and anticancer therapies [270-275] and may be an important tool for the early diagnosis of Alzheimer's disease [276-277].

From the viewpoint of technology and material science, *t*-St is a well-known building block of several commercially available liquid crystals and it has been included in many macromolecular backbones, such as polymers or dendrimers, for inducing liquid crystalline behavior [278-279]. *t*-St represents also the shortest oligomer of the poly(*p*-phenylenevinylene) family, conjugated polymers presenting semiconducting characteristics together with mechanical flexibility and low manufacturing costs [280]. Finally, stilbene and its related substitute analogues are associated with photochemical and photophysical phenomena and are among the most widely investigated organic chromophores [281]. Photosystems including stilbenic molecules are used in LEDs, photoresistors, photoconductive devices, imaging and optical switching techniques, materials for nonlinear optic and laser dyes [282] and stilbene moieties have been exploited as photoresponsive groups to functionalize devices such as hydrogels or polymeric vescicles for the photochemically controlled drug release [283-284].

As said above, all these properties could depend (totally or, at least, partly) on the spatial arrangement the molecule adopts and this is why the structure and conformational distribution of *trans*-stilbene has attracted much interest over the last decades. The structures and the point groups of the presumed three most stable conformations for *t*-St are shown in Figure 3.36 (b) (the sign convention for internal rotations is shown in Figure 3.36 (a)): C_{2h} (full planar molecule), C_2 (disrotatory, propeller-like conformation, where the rings are tilted at the same angle with respect to the ene plane, *i.e.* $\phi_1 = \phi_2$) and C_i (conrotatory conformation,

where the rings are parallel to each other, *i.e.* tilted at angles equal in magnitude but opposite in sign: $\phi_1 = -\phi_2$).
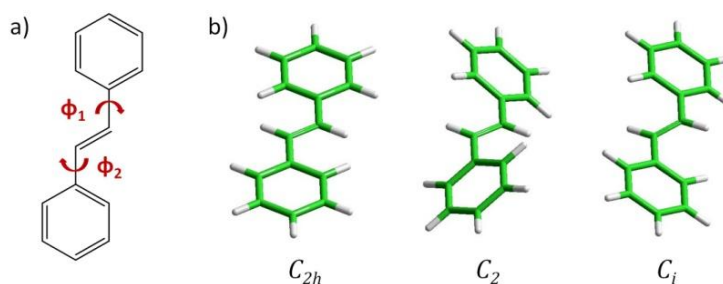
Figure 3.36. (a) Topological structure and torsional angles and (b) possible conformers with corresponding point groups of *trans*-stilbene (*t*-St).

The torsional distribution of the π -conjugated *t*-St molecule is the result of the balance between different forces, that are the steric repulsions of the phenyl groups and the vinyl system and the loss in conjugation energy stabilization of the π systems. As for biphenyl (section 3.2), the conformational equilibrium of *t*-St is, in principle, affected by the phase of the material. It has been found that in solid phase the *t*-St molecule tends to be basically planar or at most just slightly twisted [285-291], so that its symmetry is either C_{2h} or C_i. Experimental results in gas phase are quite controversial, some works leading to a C_{2h} or at most C_i structure for the isolated molecule [292-299], while others finding out exclusively a twisted structure [300-303]. The results of theoretical calculations are also not uniform, giving planar or twisted structures depending on the methods and basis sets used [304-316]. Being the torsional distribution so questionable in solid and gas state, it is obvious that in the intermediate liquid state the debate is totally open. Raman spectroscopy studies in fluid phases found out both a C_2 symmetry [317-319] and a planar form [314]. Evidence from vibrational spectra seemed to indicate the molecule is planar in solution [320], whereas NMR experiments in isotropic phase suggested for *t*-St in solution a twisted structure, from studies on the conformational dependence of deuterium-induced isotopic effects [321] or a flat molecular geometry, from considerations on ^{1}H chemical shifts [322].

In a so wide plethora of theoretical and experimental outcomes, we decided to investigate the conformational distribution of *trans*-stilbene in solution by the liquid crystal NMR spectroscopy. Since *t*-St has been largely studied by different experimental and theoretical techniques, if we want to add meaningful information, we have to seek for a methodology that can give results as strong as possible. Hence, the idea is (*i*) to dissolve the *t*-St solute in thermotropic phases in order to extract from the ^{1}H spectrum - that, even if

complex, is amenable to analysis - an accurate set of D_{ij}^{obs}, from which a reliable conformational and structural refinement can be derived, and (*ii*) to dissolve then the same molecule in a PBLG phase, in order to compare results from both phases and especially to collect evidence about the accuracy and reliability of the data extracted by NMR spectroscopy in weakly ordering phases. At this point, which strategy to use for analysing the complex NMR spectrum of *t*-St in thermotropic LCs? *t*-St is a 12-spin system and even if it possesses a symmetric structure, when dissolved in thermotropic LCs, it gives very challenging NMR spectra. Several different methods for spectral simplification have been proposed in the past and one of the most popular is the isotopic substitution (see section 1.5.2). Though deuterium has been traditionally chosen for replacing ^{1}H, in the case of *t*-St we decided to substitute protons in *para* positions with chlorine atoms, reducing thus the number of magnetically active spins from 12 to 10. We synthesised then the *trans*-4,4'-dichlorostilbene (DCS), that can be considered a prototype molecule for 4,4'-disubstituted analogs of *trans*-stilbene, such as the *trans*-4,4'-dihydroxystilbene, which is endowed with interesting biological properties [258-259, 262, 271]. A rigorous investigation of the conformational equilibrium of these derivatives, and then of DCS, can help in shedding more light on the mechanisms by which they play their role. Of course, van der Waals radius and electric properties of chlorine differ from proton. Although the substitution at *para* positions minimises the effect on rotations deriving from the greater steric hindrance of Cl, the replacement Cl-^{1}H may have some influences on the molecular torsional equilibrium, that are worth to be explored.

In order to present clearly all the mentioned points for the two molecules, *t*-St and DCS, in the different phases, ZLI1132 and PBLG, the discussion will be organised in the following way: the NMR spectral analysis and conformational investigation of DCS and *t*-St dissolved in the nematic solvent ZLI1132 will be reported first (section 3.4.1), comparing the conformational distributions found for the chlorinated and non-chlorinated analogues; then, the molecule of *t*-St dissolved in a PBLG phase will be studied in section 3.4.2, with a final comparison between orientational and conformational outcomes of the highly and weakly ordered sample.

3.4.1. *trans*-4,4'-Dichlorostilbene and trans-stilbene in ZLI1132

The conformation equilibria of DCS and *t*-St in the nematic solvent ZLI1132 are investigated in this section, with (*i*) a comparison between results found for the chlorinated

and non-chlorinated analogues and (*ii*) a comparison between the conformational distributions found for *t*-St in solution by the AP-DPD approach and *in vacuo* from theoretical calculations.

3.4.1.1. Synthesis of trans-4,4'-dichlorostilbene and NMR experiments

DCS has been synthesized following the procedure described in [323] (Scheme 3.1). The 4-chlorobenzyldiethylphosphonate (1.19 g, 4.53 mmol) and sodium methoxide (10% excess) were dissolved in dry dimethylformamide (25 mL) in a 250 mL three-necked flask fitted with a thermometer, calcium chloride guard tube, dropping funnel and magnetic stirrer. A solution of 4-chlorobenzaldehyde (640 mg, 4.57 mmol) in dry dimethylformamide (10 mL) was added dropwise, with stirring and cooling in an ice-bath (the temperature of the reaction was kept between 30 °C and 40 °C). The reaction mixture was left stirring at room temperature for ~20 h, then hydrolyzed with water (25 mL). The precipitated product was collected on a filter, washed with water and freed of the solvent at reduced pressure. The *trans*-4,4'-dichlorostilbene obtained was further purified by column chromatography with Merk 60 silica gel (70–230 mesh) and with hexane as eluent. Finally, the solid DCS weighed 810 mg (3.2 mmol, yield equal to 42%). From NMR characterization in THF we got: $\delta_{H(ortho)}$ = 7.47 ppm (d, $^3J_{HH}$ = 8.5 Hz, 4H); $\delta_{H(meta)}$ = 7.28 ppm (d, $^3J_{HH}$ = 8.5 Hz, 4H); $\delta_{H(ene)}$ = 7.14 ppm (s, 2H); $\delta_{C(meta)}$ = 128.57 ppm ($^1J_{CH}$ = 163.8 Hz); $\delta_{C(ene)}$ = 127.88 ppm ($^1J_{CH}$ = 154.5 Hz); $\delta_{C(orto)}$ = 127.74 ppm ($^1J_{CH}$ = 159.5 Hz).
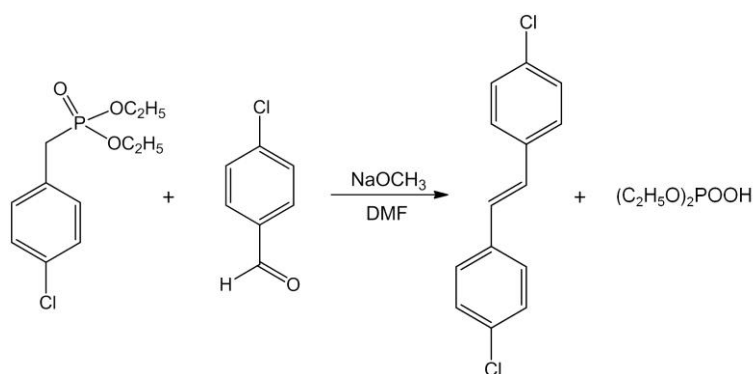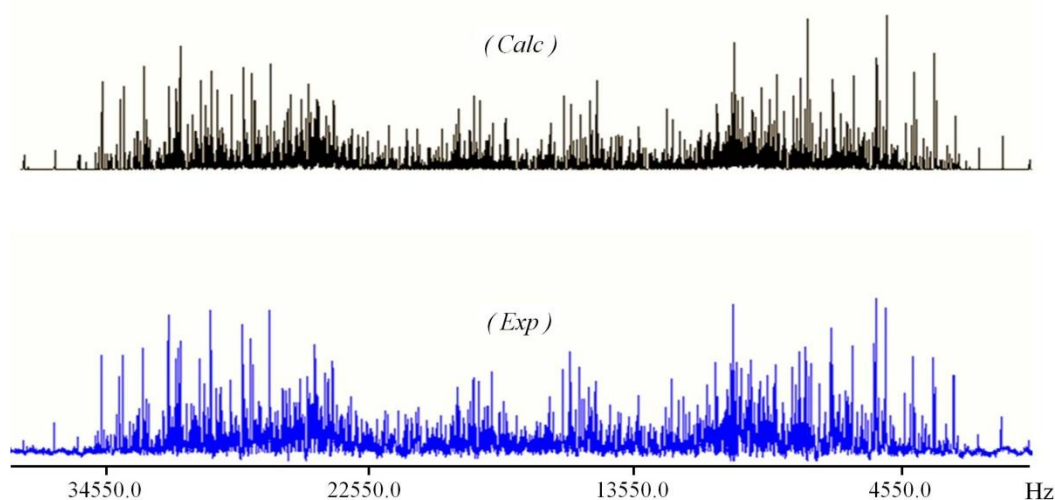

Scheme 3.1.

Spectral analysis of DCS

DCS so synthetized was dissolved at approximately 2.6 wt% in the commercial nematic solvent ZLI1132 (see Appendix A3) and its ^{1}H spectrum (shown in Figure 3.37) was recorded at

room temperature (298 K) on a Bruker Avance 500 MHz (11.74 T) instrument, equipped with a Bruker BVT-2000 temperature control unit.


Figure 3.37. The 500 MHz ^{1}H NMR experimental spectrum (bottom, in blue) of *trans*-4,4'-dichlorostilbene dissolved in the liquid crystalline nematic mesophase ZLI1132 at 298 K. For comparison, the spectrum calculated by using the D_{ij}^{obs} spectral parameters (obtained from the analysis and reported in Table 3.10) is also shown, in black, at the top of the figure.

The analysis of such spectrum is clearly not trivial, even if it is "simpler" than for *t*-St (see below, Figure 3.39). The first step requires a quite good estimation of the spectral parameters, which must be close enough to the correct set, so that the trial parameters can be used in a successful iterative analysis. As usual, the starting values of chemical shifts δ_{ij} (defined as the difference between the δ_i and δ_j chemical shifts) and the scalar couplings J_{ij} were taken from the routine analysis of the proton NMR spectrum of an isotropic solution of DCS dissolved in THF. Looking for a set of D_{ij} good enough to reproduce at best (or, at least, in an acceptable way) the basic features of the spectrum of DCS, starting values for dipolar couplings were guessed assuming the molecular geometry and certain tentative values for the the longitudinal order parameter S_{aa} and the biaxiality order parameter $S_{bb} - S_{cc}$ (see Figure 3.38 for the definition of the $\{a, b, c\}$ molecular frame). In particular, two different sets of D_{ij} were produced by fixing the geometry of the molecule in both planar, C_{2h} symmetry, and slightly non-planar, C_2 symmetry, conformation. The D_{ij}^{trial} obtained by fixing the molecule in the planar conformation and adjusting, by trial and error, the longitudinal and the biaxiality order parameters, turned out to give simulated trial spectra (corresponding to different sets of D_{ij}^{trial} obtained as functions of the S_{ij} variables) invariably showing a distribution of lines

completely incompatible with the experimental one. Therefore, they were rejected, together with the hypothesis of the full planarity of the molecule. This was the first significant, "model-free" symptom indicating the molecule is not planar in solution. On the contrary, a reasonable set of starting dipolar couplings was predicted by assuming a non-planar C_2 conformation with a torsion angle ϕ_1 = ϕ_2 of about 17° and two trial order parameters having the values S_{aa} = 0.6 and $S_{bb} - S_{cc}$ = 0.12. In this case, the trial spectrum showed a certain similarity, in terms of total width and lines distribution, with the experimental one. Hence, the set of dipolar couplings obtained in this way has been used as starting set of parameters in the spectral analysis that was successfully carried out by using the home-made program ARCANA [23], obtaining a satisfactory RMS of 0.78. The set of resulting observed D_{HH} is reported in the third column of Table 3.10, whereas the calculated spectrum is shown in Figure 3.37 (top).
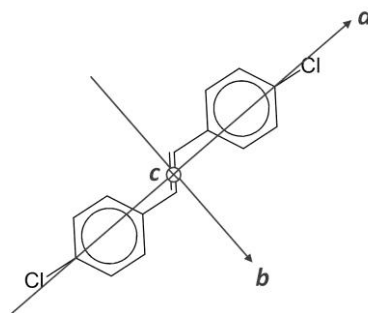
Figure 3.38. Definition of the $\{a, b, c\}$ molecular frame for DCS (the c axis, perpendicular to the (ab) plane where the vinyl group lies, defines a right-handed Cartesian system).

Table 3.10. Experimental chemical shifts $\delta_{ij} = \delta_i - \delta_j$, scalar couplings J_{ij} and dipolar couplings D_{ij}^{obs}, determined from the analysis of ^{1}H NMR spectrum of *trans*-4,4'-dichlorostilbene dissolved in ZLI1132. In the last column, the D_{ij}^{calc} are reported for comparison. The whole agreement is given by the RMS between AP-DPD-calculated and observed dipolar couplings. The chemical structure provides the hydrogen atom numbering.
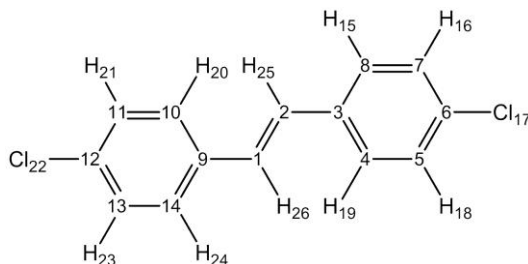

i, j	J_{ij} (Hz)	D_{ij}^{obs} (Hz)	$D_{ij}^{calc\,(a)}$ (Hz)
15, 16	8.0	-4860.10 ± 0.02	-4860.20
15, 18		31.86 ± 0.03	31.09
15, 19	2.0	371.32 ± 0.06	370.09
15, 20		-458.92 ± 0.03	-459.33
15, 21		-165.66 ± 0.02	-164.26
15, 25		-1881.08 ± 0.04	-1881.07
15, 26		-2965.13 ± 0.05	-2965.13
16, 18	2.0	373.17 ± 0.05	374.87
16, 21		-76.77 ± 0.04	-75.50
16, 25		-440.17 ± 0.05	-439.78
16, 26		-442.16 ± 0.05	-442.32
25, 26	17.5	1020.72 ± 0.07	1020.22
		δ_{ij}	
15, 16		-115.23 ± 0.04	
25, 16		-206.54 ± 0.04	
	RMS	0.85 Hz	

[a] from the AP-DPD method (see below)

Spectral analysis of t-St

The D_{ij}^{obs} obtained for the 10-spin system DCS were used as starting point for the analysis of the extremely complex ^{1}H spectrum (reported in Figure 3.39), recorded at 298 K on the same Bruker Avance 500 MHz instrument, on a sample at approximately 3.6 wt% of *t*-St in ZLI1132 (see Appendix A3 for sample preparation). Being the molecule a 12-spin system and

taking into account molecular symmetry, the spectrum is affected by 19 independent dipolar coupling constants.
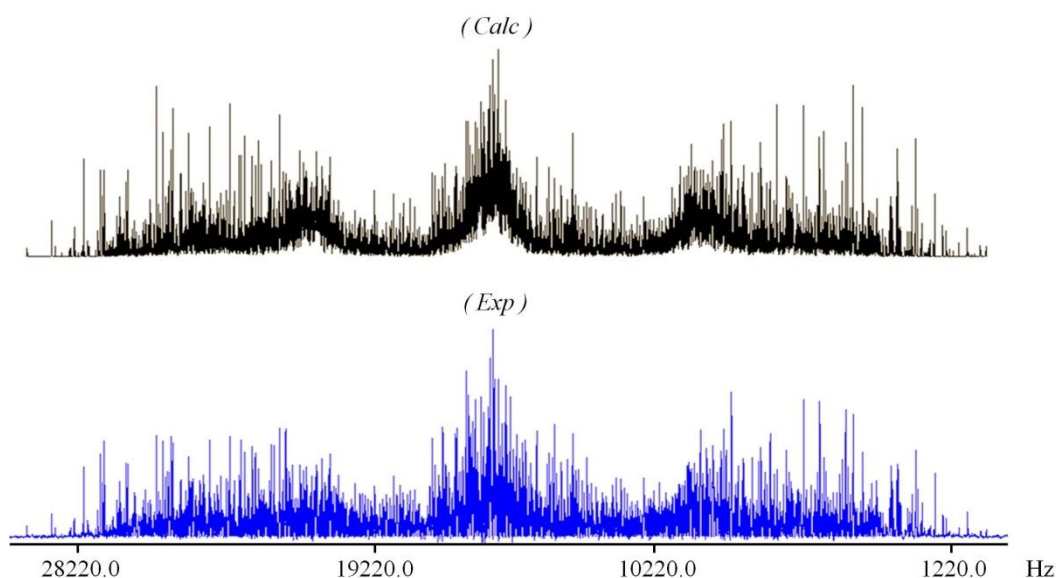
Figure 3.39. The 500 MHz ^{1}H NMR experimental spectrum (bottom, in blue) of *trans*-stilbene dissolved in the liquid crystalline nematic mesophase ZLI1132 at 298 K. For comparison, the spectrum calculated by using the D_{ij}^{obs} spectral parameters (obtained from the analysis and reported in Table 3.11) is also shown, in black, at the top of the figure.

By fixing again the molecule in the C_2 conformation with a torsion angle $\phi_1 = \phi_2$ of about 15°, the longitudinal and biaxiality order parameters were varied parametrically in order to reproduce the 12 independent D_{ij}^{obs} extracted from the spectral analysis of the chlorinated compound. The best correspondence was achieved for the two order parameters S_{aa} = 0.590 and $S_{bb} - S_{cc}$ = 0.134, allowing a good estimation of the other 7 dipolar couplings for the *t*-St. The spectrum of *t*-St simulated with this set of D_{ij}^{trial}, properly scaled, was sufficiently close, in terms of total width and lines distribution, to the observed one and this led to the successful analysis by ARCANA software [23], obtaining a RMS of 0.88 Hz. The whole set of final spectral parameters is reported in Table 3.11, whereas the calculated spectrum is shown in Figure 3.39 (top).

Table 3.11. Experimental chemical shifts $\delta_{ij} = \delta_i - \delta_j$, scalar couplings J_{ij} and dipolar couplings D_{ij}^{obs}, determined from the analysis of ^{1}H NMR spectrum of *trans*-stilbene dissolved in ZLI1132. In the last column, the D_{ij}^{calc} are reported for comparison. The whole agreement is given by the RMS between AP-DPD-calculated and observed dipolar couplings. The chemical structure provides the hydrogen atom numbering.
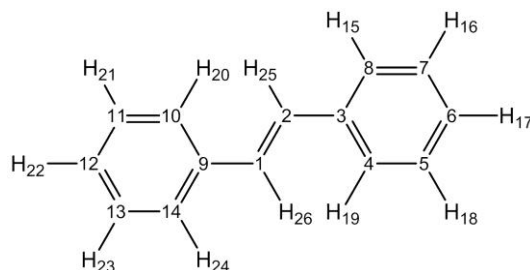
i, j	J_{ij} (Hz)	D_{ij}^{obs} (Hz)	$D_{ij}^{calc\ (a)}$ (Hz)
15, 16	8.0	-4004.33 ± 0.03	-4004.85
15, 17	2.0	-507.48 ± 0.06	-507.37
15, 18		-1.48 ± 0.04	-0.69
15, 19	2.0	247.46 ± 0.08	246.73
15, 20		-397.17 ± 0.05	-399.16
15, 21		-140.41 ± 0.04	-138.98
15, 22		-104.60 ± 0.06	-103.64
15, 25		-1732.91 ± 0.07	-1732.84
15, 26		-2462.52 ± 0.08	-2462.51
16, 17	6.0	-20.45 ± 0.06	-19.85
16, 18	2.0	246.98 ± 0.08	248.33
16, 21		-64.74 ± 0.06	-63.36
16, 22		-50.75 ± 0.06	-49.68
16, 25		-364.85 ± 0.09	-364.74
16, 26		-380.11 ± 0.09	-376.75
17, 22		-39.58 ± 0.08	-39.82
17, 25		-271.60 ± 0.14	-270.23
17, 26		-254.36 ± 0.14	-256.08
25, 26	17.5	681.36 ± 0.10	676.55

i, j		δ_{ij}	
15, 17		-459.39 ± 0.06	
16, 17		-444.85 ± 0.07	
25, 17		-666.61 ± 0.07	
		RMS	1.67 Hz

[a] from the AP-DPD method (see below)

3.4.1.2. Conformational and orientational analysis

The sets of experimental D_{ij}^{obs} extracted from the analysis of the two spectra (Tables 3.10 and 3.11) have been exploited to investigate structure and conformational equilibrium of the two molecules, using the AP-DPD theoretical model. In treating the two symmetric stilbenic molecules, the phenyl rings and the vinyl rigid fragments were assumed, as usually done in literature [28, 31], to keep a fixed structure as they rotate relative to each other. Moreover, each ring was assumed to have a C_{2v} symmetry, so requiring a couple of interaction parameters $\varepsilon_{2,0}(R)$ and $\varepsilon_{2,2}(R)$, while the ene group, assumed as effectively described by an axially-symmetric interaction tensor, needs a single independent element $\varepsilon_{2,0}^{C=C}$, the component along the C=C bond direction. According to the DPD method, the $P_{iso}(\phi_1,\phi_2)$ was modelled directly as a sum of bidimensional Gaussian functions, by using the following general form:

$$P_{iso}(\phi_1,\phi_2) \propto \sum_{\text{over the different } C_x-\text{symmetry structures}} \frac{A_{C_x}}{n_{C_x}}$$

$$\cdot \sum_{k=1}^{n_{C_x}} exp\left[-\left(\frac{sin^2\big(\phi_1 - (\phi_1^{max})_{C_x}^k\big)}{2h_1^2} + \frac{sin^2\big(\phi_2 - (\phi_2^{max})_{C_x}^k\big)}{2h_2^2}\right)\right] \qquad (3.8)$$

where n_{C_x} is the number of rotamers belonging to the C_x point group and A_{C_x} is the global relative weight of the C_x structures (so that $\sum_{(\text{over all the } C_x)} A_{C_x} = 1$). $(\phi_i^{max})_{C_x}^k$ represents, for the i-th torsion, the twist angle corresponding to the k-th of the the n_{C_x} most probable conformations with C_x symmetry. Finally, h_1 and h_2 give the width at half maximum height along each dimension of the bidimensional Gaussians. Note that the use of sinusoidal functions in the exponent of the Gaussians, introduced here for the first time, assures the right periodicity of the probability distribution, simplifying its analytical expression with respect to those used in past papers [29-31, 45, 78, 170, 324-325].

Once the theoretical apparatus is established, the experimental dipolar couplings have to be fitted *via* the software AnCon [95], while fixing a molecular geometry and simultaneously iterating on a number of unknowns, that is the three orientational parameters ($\varepsilon_{2,0}(R)$, $\varepsilon_{2,2}(R)$ and $\varepsilon_{2,0}^{C=C}$), the potential terms (represented by the $\phi_1^{max} = \pm\phi_2^{max}$ angle, the $h_1 = h_2$ value and the $A_{C_2} = 1 - A_{C_i}$ weight of Equation (3.8)), and some selected geometrical parameters, in order to minimize the RMS target function. For *t*-St we have 19 independent D_{HH} and in particular 12 connecting the different rigid subunits of the molecules (6 between each ring and the central ene group and 6 between the two rings). For the DCS, out of the 12 independent D_{HH}, 7 couple protons of different fragments. For this reason, calculations were

performed first by fitting the D_{HH} obtained for *t*-St, in order to adjust not only orientational and potential terms, but also selected bond lengths and valence angles, hence refining molecular geometries. Fixing the same optimised structure for the DCS, its potential surface was then explored by fitting 12 independent D_{HH}, with iteration on orientational and potential parameters.

Geometry of rigid fragments

For the *trans*-stilbene, a first otpimization was performed on the rigid phenyl ring (structure, labelling and fragment-fixed frame reported in Figure 3.40).
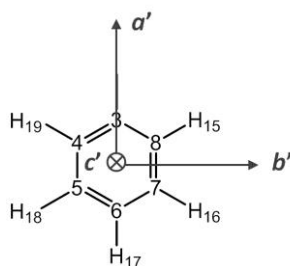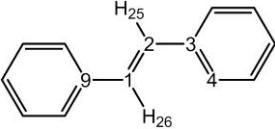
Figure 3.40. Reference frame fixed on the phenyl rigid fragment of the *trans*-stilbene molecule (the c' axis defines a right-handed Cartesian system).

From the whole set of observed interproton dipolar couplings of Table 3.11, we have for the phenyl ring subunit a subset of 6 intraring $D_{ij}^{obs}(ring)$ values (of course, the two ring subunits in the molecule have been assumed to be structurally identical). Note that, from the ^{1}H NMR spectrum, we cannot have direct information on the carbon geometries of the molecule. Hence, only a "virtual" skeleton of the molecule can be hypothesized and assumed, compatible with the proton coordinates, able to reproduce the observed D_{ij}^{obs}. First of all, we fixed the proton coordinates correspondingly to an "all-120°" regular hexagon with $\overline{CC}$ = 1.40 Å and $\overline{CH}$ =1.09 Å. This implies for the rings a C_{2v} local symmetry, that is consistent with the nuclear spin symmetry. Then, we adjusted the local order parameters, $S_{a'a'}^{ring}$ and $(S_{b'b'} - S_{c'c'})^{ring}$, and the $C_7\hat{C}_8H_{15}$ angle (similarly, also the $C_5\hat{C}_4H_{19}$ angle has been correspondingly changed to keep the C_{2v} symmetry of the rings) in order to reproduce the 6 intraring dipolar couplings (3 degrees of freedom *versus* 6 experimental data represents a good overdetermination of the system). The final results were: $C_7\hat{C}_8H_{15}$ = 119.25°, $S_{a'a'}^{ring}$ = 0.5068

and $(S_{b'b'} - S_{c'c'})^{ring}$ = 0.1754. These ring geometries were then kept fixed in all subsequent calculations.

For the vinyl fragment only one local direct coupling is experimentally available (the $D_{25,26}^{obs}$ coupling constant). Hence, we were forced to start by borrowing the geometries of this subunit from theoretical calculations, carried out by the MP2/6-31G ** method, reported in the second column of Table 3.12 (see section 3.4.1.3), and iterating on them only when we considered the entire molecule.

Table 3.12. Starting and refined geometries of the vinyl group.

Geometrical parameter	Initial value [a]	Refined value [b]
$r_{12}(\text{Å})$	1.352	1.337
$r_{23}(\text{Å})$	1.466	1.477
$C_1\hat{C}_2C_3$ (degree)	124.83	125.54
$C_2\hat{C}_3C_4$ (degree)	120.80	122.49
$C_1\hat{C}_2H_{25}$ (degree)	118.78	120.24

[a] from MP2/6-31G** theoretical calculations
[b] from the iterative procedure carried out by Ancon software on the whole molecule

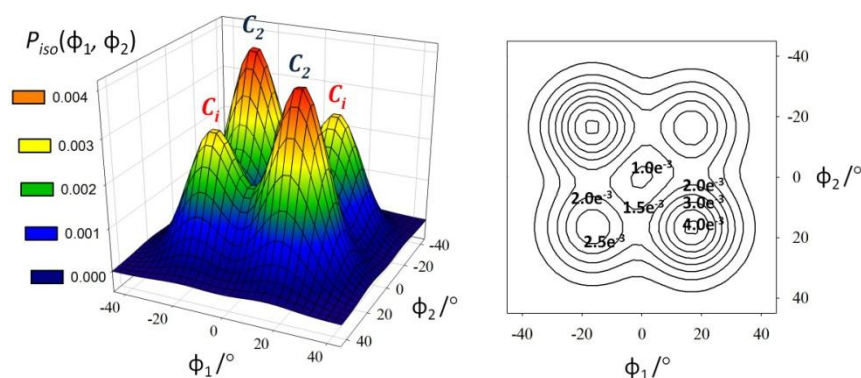***Conformational distribution and orientational ordering of t-St***

Starting with the optimised geometries of the ring and the theoretical geometry of the vinyl group, we tried to reproduce the whole set of D_{ij}^{obs} measured for *t*-St (Table 3.11), simultaneously iterating on the $\varepsilon_{2,0}(R)$, $\varepsilon_{2,2}(R)$ and $\varepsilon_{2,0}^{C=C}$ interaction tensor parameters, the potential terms $\phi_1^{max} = \pm\phi_2^{max}$, $h_1 = h_2$ and $A_{C_2} = 1 - A_{C_i}$, and the geometrical parameters of the ene group, until the RMS reached an acceptable value. The ratio between 19 target D_{ij} (of which 12 inter-fragment) and 6 adjustable parameters makes the problem well determined. It is worth emphasizing that ϕ_1^{max}, h_1 and A_{C_2} can be varied independently, but with the constraint that $P_{iso}(\phi_1,\phi_2)$, sampled in this case every 3° torsional steps, is normalized (in particular, because of the molecular symmetry, we normalized the distribution function for $-45° \leq \phi_1, \phi_2 \leq 45°$).The refinement of the initial geometries used for the vinyl fragment provided with a better reproduction of the whole set of the observed couplings for

the whole molecule. Note that the final refined values, reported in the third column of Table 3.12, are similar to the starting ones, so that the used geometries can be considered reliable. By the slight refining of the vinyl geometries and by the optimized values of iteration parameters (reported in Table 3.13) we were finally successful in reproducing the observed direct couplings with a low RMS of 1.67 Hz (the single dipolar couplings D_{ij}^{calc} calculated by this approach are reported, for comparison, in the last column of Table 3.11).

The surface $P_{iso}(\phi_1, \phi_2)$ resulting from the procedure described above and the corresponding contour plot are shown in Figure 3.41. The main feature of the obtained $P_{iso}(\phi_1, \phi_2)$ function is represented by the existence of four symmetry related maxima of the probability function, corresponding to the C_2 (absolute maxima) and C_i (relative maxima) structures characterized by having, respectively, $\phi_1^{max} = \phi_2^{max}$ and $\phi_1^{max} = -\phi_2^{max}$, with $\phi_1^{max} = 16.8°$. Note that the planar structure with C_{2h} is not a minimum.

Table 3.13. Optimized values of the iteration parameters used in the conformational analysis with the AP-DPD approach of the *t*-St molecule dissolved in ZLI1132.

	t-St in ZLI1132
$\phi_1^{max} = \pm\phi_2^{max}$ (degree)	16.80 ± 0.02
A_{C_2}	0.59 ± 0.01
$h_1 = h_2$ (degree)	10 (after parameterization)
$\varepsilon_{2,0}(R)$ (RT)	1.349 ± 0.002
$\varepsilon_{2,2}(R)$ (RT)	0.650 ± 0.001
$\varepsilon_{2,0}^{C=C}$ (RT)	0.473 ± 0.006
RMS	1.67

Figure 3.41. Experimental probability distribution $P_{iso}(\phi_1, \phi_2)$ for *t*-St dissolved in the nematic solvent ZLI1132 at 298 K, obtained by the liquid crystal NMR conformational analysis (both the 3D surface and its contour plot are shown).

Even though the main objective of this study is the conformational analysis, it can be interesting to briefly discuss here the orientational ordering of *t*-St in the thermotropic LC ZLI1132 at 298 K. This will lead to some useful considerations when compared to the orientational behaviour in the PBLG phase (section 3.4.2.2). For the C_2 conformation, the order parameters given in the PAS of the Saupe matrix (see Figure 3.42 for the definition of the $\{a, b, c\}$ molecular frame and of the η angle, giving the location of the PAS) are the following: S_{aa} = 0.525 and $S_{bb} - S_{cc}$ = 0.174, with η = 44.92°. In the same molecular frame, *i.e.* the PAS of the S matrix of C_2, the C_i order parameters are: S_{aa} = 0.506, $S_{bb} - S_{cc}$ = 0.176, S_{bc} = ±0.055, S_{ab} ∼0.0 and S_{ac} = ∓0.029 (the ± and ∓ signs are referred to the two possible forms of C_i, namely $\{\phi_1^{max}$ = +16.8°; ϕ_2^{max} = −16.8°$\}$ and $\{\phi_1^{max}$ = -16.8°; ϕ_2^{max} = +16.8°$\}$). It is clear that (*i*) the molecule is basically oriented with the main molecular axis a (Figure 3.42) parallel with respect to the director of the phase, and (*ii*) the orientations of the C_2 and C_i conformers are essentially the same.
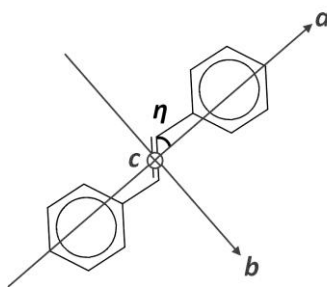
Figure 3.42. Definition of the $\{a, b, c\}$ molecular frame for *trans*-stilbene (the c axis, perpendicular to the (ab) plane where the vinyl group lies, defines a right-handed Cartesian system). Note the η angle describing an integral rotation of the $\{a, b, c\}$ system about the c axis, which locates the principal axis system of the S matrix for the C_2 structure.
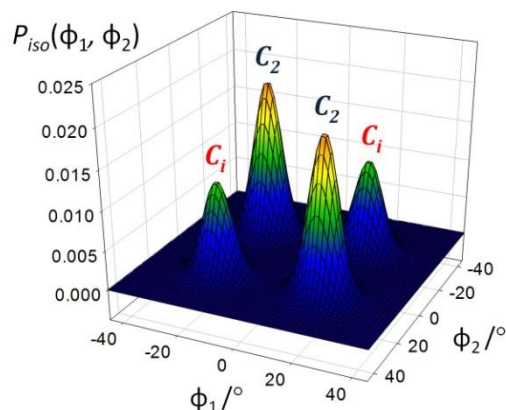
Conformational distribution of DCS

Finally, in order to evaluate the influence resulting of the Cl-^{1}H substitution at the *para* positions on the conformational distribution, also the torsional potential surface of DCS was described by fitting the whole set of 12 independent D_{ij}^{obs} of Table 3.10. We assumed the same geometries of the fragments adopted for *trans*-stilbene and adjusted the $\varepsilon_{2,0}(R)$, $\varepsilon_{2,2}(R)$ and $\varepsilon_{2,0}^{C=C}$ interaction tensor parameters, the $\phi_1^{max} = \pm\phi_2^{max}$ angle, the $h_1 = h_2$ value and the $A_{C_2} = 1 - A_{C_i}$ weight of Equation (3.8). By the optimized values of iteration parameters, reported in Table 3.14, we were finally successful in reproducing the observed direct couplings with a satisfactory RMS of 0.85 Hz. The D_{ij}^{calc} calculated by this approach are reported, for comparison, in the last column of Table 3.10, while the resulting surface $P_{iso}(\phi_1, \phi_2)$ is shown

in Figure 3.43. As for *t*-St, the main feature of the obtained $P_{iso}(\phi_1, \phi_2)$ function is the existence of the four symmetry related maxima of the probability function, corresponding to the C_2 (absolute maxima) and C_i (relative maxima) structures, characterized by having, respectively, $\phi_1^{max} = \phi_2^{max}$ and $\phi_1^{max} = -\phi_2^{max}$, with ϕ_1^{max} = 18.69°.

Table 3.14. Optimized values of the iteration parameters used in the conformational analysis with the AP-DPD approach of the DCS molecule dissolved in ZLI1132.

	DCS in ZLI1132
$\phi_1^{max} = \pm\phi_2^{max}$ (degree)	18.69 ± 0.17
A_{C_2}	0.63 ± 0.01
$h_1 = h_2$ (degree)	4.66 ± 2.64
$\varepsilon_{2,0}(R)$ (RT)	1.702 ± 0.002
$\varepsilon_{2,2}(R)$ (RT)	0.720 ± 0.004
$\varepsilon_{2,0}^{C=C}$ (RT)	0.291 ± 0.015
RMS	0.85

Figure 3.43. Experimental probability distribution $P_{iso}(\phi_1, \phi_2)$ for DCS dissolved in the nematic solvent ZLI1132 at 298 K, obtained by the liquid crystal NMR conformational analysis.

The result obtained about the locations of the stable rotamers of DCS is very close to that of *trans*-stilbene, the magnitude of torsional angles being 18.7° for DCS *versus* 16.8° for *t*-St. This basically indicates very limited effects of the 4,4' Cl-substitution on the positions of the conformational minima, as reasonably expected. Also the relative weights A_{C_x} of the two structures C_2 and C_i in DCS (amounting to A_{C_2} = 63% and A_{C_i} = 37%) are not far from what

found for *trans*-stilbene (where the ratio $A_{C_2} : A_{C_i}$ was 59:41 in percentage). The main difference one can observe between the $P_{iso}(\phi_1, \phi_2)$ distributions obtained for *t*-St and DCS (Figures 3.41 and 3.43) resides in the relative height and width of the maxima. Indeed, the conformational surface obtained for DCS is characterized by peaks that appear sharper and higher than for *trans*-stilbene, suggesting that the chlorinated molecule is more confined in the vicinity of its conformational minima with respect to *t*-St. However, this simple deduction should be more carefully evaluated. The sharpness of the peaks is in fact related to the magnitude of the h_i parameters, determining the width at half-maximum height along each dimension of the bidimensional Gaussian. The value $h_1 = h_2$ = 10° for *t*-St has been obtained by a parametrical adjustment process, so that it is difficult to estimate the possible error affecting it. On the contrary, the smaller value $h_1 = h_2$ = 4.7° for DCS resulted from a fitting of the experimental data where the h parameter has been used as a variable in the computer iteration process. Hence, we can assess it is affected by an error of ±2.64°, leading to a window of possible h values ranging from 2° to 7.5°. This indeterminacy on the "real" value of h makes the results for DCS and *t*-St more similar than it seems apparently.

3.4.1.3. In vacuo theoretical calculations for t-St and comparison with experimental results

In order to corroborate the conformational results obtained experimentally for *trans*-stilbene, we decided to perform also theoretical calculations *in vacuo*. To date, several papers reported calculations for the isolated molecule of *t*-St, with different results depending on the methods and basis sets used, and the controversy is still unresolved [310 and refs. therein]. Computations by means of semiempirical AM1 [326] and PM5 [307], the Hartree-Fock HF [306, 327] and the single point second-order Møller-Plesset MP2 [320] approaches led to a nonplanar structure of C_2 symmetry as global energy minimum, characterized by a torsion angle from 15° to 29°. In sharp contrast, theoretical investigations at the semiempirical PM3 level [315] and DFT level, employing the BLYP, BVWN and B3LYP functionals [311, 320, 327-328], led to the conclusions that the ground-state structure of *trans*-stilbene is planar or practically planar *in vacuo*. Indeed, DFT functionals (producing the planar result) are believed to fail in correctly describing long-range nonbonding interactions [310 and refs. therein], while for these kind of molecules MP2 is considered more reliable [304, 310]. For this reason, we used the MP2/6-31G** method to perform a relaxed PES scan for *t*-St (reported in Figure

3.44), over the 0°-360° range with a 3°-step sampling, using the Gaussian03 (rev. C.02) software package [228].
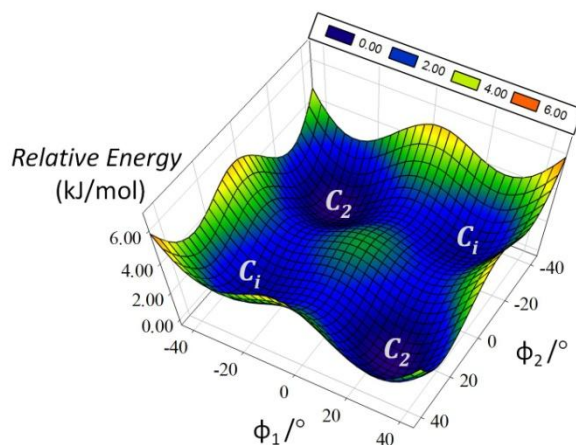
Figure 3.44. The conformational potential energy surface (PES) obtained for *trans*-stilbene from MP2/6-31G** calculations. The locations of absolute and relative minima are labeled by means of their point group symbols. Calculations required 17 days, 17 h and 15 min of CPU time on a server IBM e326, equipped with two processors AMD Opteron 2.6 GHz and 2GB of RAM (O.S.: SUSE Linux Enterprise Server 9 for AMD64).

From the obtained conformational PES shown in Figure 3.44 it is evident the presence of four symmetry related minimum energy conformers: a couple of absolute minima (C_2 structures, where the relative torsional energy, RTE, is fixed to be 0 kJ/mol) and a couple of relative minima (C_i structures corresponding to a RTE ~1.2 kJ/mol), characterized by having, respectively, $\phi_1^{max} = \phi_2^{max}$ and $\phi_1^{max} = -\phi_2^{max}$, with ϕ_1^{max} = 27°. The C_{2h} planar conformation ($\phi_1^{max} = \phi_2^{max}$ = 0°) is neither a minimum nor a saddle point, but rather a local maximum corresponding to a RTE of about 3 kJ/mol. Even though the past literature witnesses that different theoretical approaches can give quite different results, it should be noted that interestingly something very similar to what we have found here has been already obtained by *ab initio* RHF/3-21G calculations [306]. This increases, in our opinion, the reliability of our findings.

In order to make more effective and immediate the comparison between the theoretical results, referred to the isolated molecule, and the experimental liquid crystal NMR results in solution, it is useful to plot the probability resulting from the *ab initio* calculations as a function of ϕ_1 and ϕ_2. The theoretical probability distribution $P_{theo}(\phi_1, \phi_2)$ (normalized for -45° ≤ ϕ_1, ϕ_2 ≤ 45°) is shown in Figure 3.45.
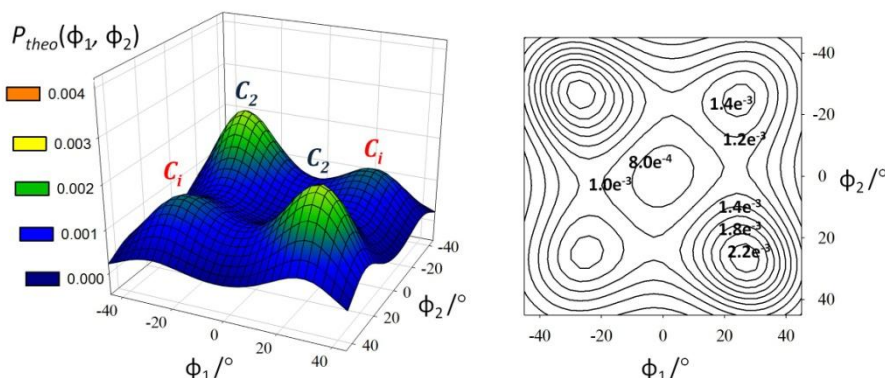
Figure 3.45. Normalized probability distribution $P_{theo}(\phi_1, \phi_2)$ for *trans*-stilbene, obtained from the theoretical PES of Figure 3.44 (both the 3D surface and its contour plot are shown for the sake of clarity).

A comparison of Figures 3.41 and 3.45 immediately reveals significant similarities in the shape of the conformational probability distributions obtained from MP2/6-31G** calculations and the AP-DPD approach. Both the investigations agree in indicating non planar structures as the more stable conformations for the molecule and in particular the same peculiar four peaks of probability belonging to the same symmetries (the two C_2 global and the two C_i local maxima) are found in both cases. Moreover, a crude ratio between the probabilities exactly corresponding to C_2 and C_i structures roughly indicates relative percentages to be about 62% of C_2 against 38% of C_i both in liquid and in gas phase. Important differences, however, have to be noted, in terms of precise locations of the maxima and in their different heights. Firstly, the values of the twist angles experimentally found in solution (ϕ_1^{max} = 16.80°) seem to be smaller with respect to those theoretically predicted *in vacuo* (ϕ_1^{max} = 27°). This result is not surprising. Indeed, it is reasonable that in in the gas phase, where the intermolecular interactions are absent or very weak, the isolated molecule adopts basically a C_2 structure, with a relatively big twist angle (for example it has been found of 32.5° in [303], that is not very dissimilar from our calculated 27°). Contrarily, passing to the liquid phase, intermolecular interactions grow, forcing the molecule toward a less twisted arrangement (*i.e.* smaller twist angle values). Finally, in the solid phase they dominate so that *t*-St is practically planar [286-291]. This behavior is quite usual in conjugated systems, as it has been already discussed for biphenyl in section 3.2. Secondly, from MP2 theoretical calculations, the isolated molecule seems to be "less confined" in the C_2 and C_i high probability conformations with respect to the liquid state, where the probability peaks appear higher and sharper. Nonetheless, discerning with certainty to which extent this difference is

physically sensible is difficult since (*i*) the obtained results may be biased by the adopted methods of investigation of the torsional equilibrium and (*ii*) the term $h_1 = h_2$, giving the width at half maximum height along each dimension of the bidimensional Gaussians, has been parameterized during the AP-DPD calculations.
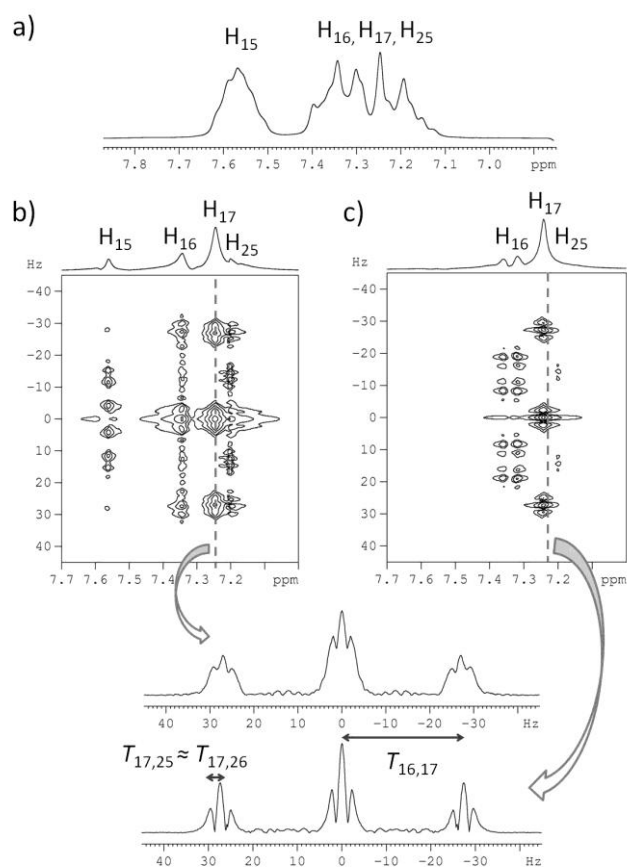
3.4.2.   trans-Stilbene in PBLG/THF-d₈

Once described the conformational and orientational behavior of *trans*-stilbene in a highly ordering LC phase as ZLI1132, the next goal we wanted to pursue is the study of the same solute dissolved in a weakly PBLG-based aligning phase. This allows (*i*) to compare results from both phases, for evaluating the different degree of order induced to the solute and highlighting possible effects on the conformational equilibrium, and (*ii*) to evaluate the extent of information as well as the accuracy of the experimental data that can be extracted by NMR spectroscopy in weakly ordering phases.

3.4.2.1. NMR experiments

Unlike sample of *t*-St in thermotropic ZLI1132, where the analysis of only the 1D ^{1}H spectrum yields a data set that is large enough to be informative in the conformational study, the edition of a sufficiently extended set of experimental dipolar couplings requires not only a series of 1D and 2D NMR spectra to be recorded on different nuclei, but also isotropic spin-spin couplings to be precisely measured. Hence, as seen for the anti-inflammatory drugs of section 3.3, multiple homo- and heteronuclear experiments were carried out on both an isotropic (*t*-St/THF-d₈) and anisotropic (*t*-St/PBLG/THF-d₈) sample (see Appendix A3 for sample preparation), in order to extract respectively the scalar J_{ij}^{obs} and the total T_{ij} coupling constants.

All spectra were recorded at 298 K on a liquid high-resolution Bruker Avance 500MHz spectrometer (11.74 T) equipped with a TBO probe and a standard variable-temperature unit BVT-3000. As usually, spectral assignment of the peaks was performed by 1D ^{1}H, ^{13}C, ^{13}C-{^{1}H} spectra and 2D ^{1}H-^{1}H COSY, ^{1}H-^{13}C HSQC and HMBC correlation experiments, while homo- and heteronuclear *J*-resolved and SERF experiments were used to extract ^{1}H-^{1}H and ^{1}H-^{13}C scalar and total couplings. Unfortunately, spectra are not well resolved and the superposition of

signals from three of the four chemically equivalent protons (see the 1D ^{1}H broadband spectrum in Figure 3.46 (a)) makes it difficult (*i*) to accurately measure [1]H-^{1}H couplings and (*ii*) to apply selective pulses on proton in order to edit specific [1]H-^{13}C couplings. Indeed, even when a visible splitting can be measured from the spectrum, it is difficult to unambiguously assign it to a pair of coupled nuclei. Some tricks can sometimes be exploited in order to extract as many couplings as possible. As an example, Figure 3.46 reports the [1]H-[1]H *J*-resolved spectrum (b) and the SERF-like spectrum resulting from the application of a semi-selective pulse selecting *meta*, *para* and ethylenic protons and excluding *ortho* protons (c).


Figure 3.46. (a) 1D ^{1}H broadband excitation spectrum recorded on *trans*-stilbene in PBLG/THF-d$_8$ at 298 K. (b) Tilted [1]H-[1]H *J*-resolved spectrum recorded on the same sample in 6 h using a data matrix of 2048 (t_2) x 256 (t_1) with 24 scans per t_1 increment. The relaxation delays were 1s. Data were processed using zero-filling up to 4096 (t_2) x 1024 (t_1) points and a sine filter in t_1. (c) Tilted SERF spectrum resulting from the application of semi-selective E-BURP excitation and RE-BURP refocusing pulses on the proton channel at $\upsilon_{16,17,25}$, with duration of 29.1 ms, corresponding to a frequency width of 170 Hz. Spectrum was recorded in 6 h using a data matrix of 2048 (t_2) x 256 (t_1) with 24 scans per t_1 increment. The relaxation delays were 1s. Data were processed using zero-filling up to 1024 points and a sine filter in t_1. Columns extractions corresponding to H$_{17}$ for both *J*-resolved and SERF spectra are also shown.

Signal from H_{17} gives a triplet of triplets in the *J*-resolved spectrum, from which two couplings can be measured. A simple conclusion is these total couplings correspond to H_{16}-H_{17} and H_{15}-H_{17}, that is the nearest nuclear pairs. Looking at SERF spectrum, where only couplings between H_{17}, H_{16} and H_{25} should be present (H_{15} is the only proton having chemical shift far enough from the others to be excluded from the semi-selective pulse) a similar spectral pattern is observed for H_{17}. This means that $T_{15,17}$ is not observed and H_{17} is coupled to H_{25} and H_{26} with a similar coupling constant (*i.e.* the resolution does not allow to appreciate the predictable difference between $T_{17,25}$ and $T_{17,26}$). To be sure only H_{17}, H_{16} and H_{25} have been really selected by the soft pulse, consider that (*i*) no signal at 7.56 ppm (*i.e.* the resonance frequency of H_{15}) is present in the SERF 2D spectrum, and (*ii*) F_2 projection after tilt gives for H_{16} a singlet in the *J*-resolved spectrum (all couplings appear in the F_1 dimension) and a doublet in the SERF spectrum (after tilt of the 2D map, couplings among selected protons appear only in the F_1 dimension, while coupling with H_{15} is refocused and appears in the direct dimension).

Finally, a total amount of 13 independent D_{ij}^{obs} (reported in Table 3.15) between the nuclear pairs ^{1}H-^{1}H and ^{1}H-^{13}C were collected, and in particular 7 for the phenyl ring, 2 for the ene group and 4 between each ring and the ene group. The amount of dipolar couplings extracted so far is evidently lower than the D_{HH} set extracted from a single 1D ^{1}H spectrum in thermotropic phase. It could be of interest in the future to use more and different NMR pulse sequences and/or simulation graphical packages like ARCANA for the spectral analysis, to help in editing a larger number of more accurate couplings. However, an important point emerges. From the experimental viewpoint, the presence of elements of symmetry in the spin system represents a big advantage for highly ordering systems, since they decrease the number of different transitions, simplifying the spectrum. Contrarily, molecular symmetry seems to complicate NMR spectral analysis when the same solutes are dissolved in weakly aligning media, because the number of independent couplings one can hope to extract is reduced. Moreover, in the absence of asymmetric substitutions in the molecular structure, nuclei are more likely to possess a similar chemical environment, *i.e.* their signals are more likely to appear at very close frequencies in the spectrum or even to overlap. The phenomenon is obviously field-dependent and the use of spectrometers operating at higher magnetic fields could be useful in this case.

Table 3.15. Experimental chemical shifts δ_k^{iso}, scalar couplings J_{ij}^{iso}, total couplings T_{ij}^{obs} and dipolar couplings D_{ij}^{obs} determined by the NMR analysis of *t*-St dissolved in THF-d$_8$ and PBLG/THF-d$_8$. In the last column, the D_{ij}^{calc} values are also reported for comparison. The whole agreement is given by the RMS between AP-DPD-calculated and observed dipolar couplings. The chemical structure provides the hydrogen atom numbering.
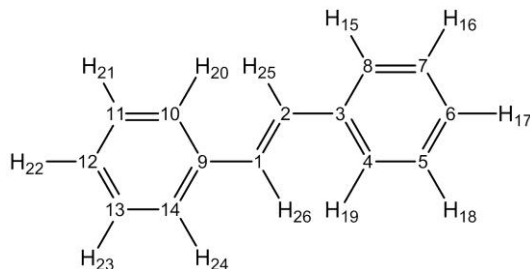
i, j	J_{ij}^{iso} (Hz)	T_{ij}^{obs} (Hz)	D_{ij}^{obs} [a] (Hz)	D_{ij}^{calc} [b] (Hz)
C-H couplings				
1, 20	4.6 ± 0.5	7.4 ± 0.6	1.4 ± 0.6	1.1
1, 25	-3.5 ± 0.8	-12.0 ± 0.6	4.3 ± 0.7	4.4
1, 26	153.4 ± 0.5	249.4 ± 0.2	48.0 ± 0.4	48.1
3, 15	0.0 ± 0.8	13.6 ± 0.6	6.8 ± 0.7	6.2
4, 15	6.6 ± 0.8	9.6 ± 0.6	1.5 ± 0.7	1.5
4, 19	156.4 ± 0.5	211.4 ± 0.6	27.5 ± 0.6	27.8
5, 16	7.7 ± 0.2	10.5 ± 0.2	1.4 ± 0.2	1.4
5, 18	158.7 ± 0.2	213.5 ± 0.2	27.4 ± 0.2	27.3
6, 15	7.6 ± 0.5	7.4 ± 0.6	-0.1 ± 0.6	-0.1
6, 17	160.8 ± 0.5	86.4 ± 0.6	-37.2 ± 0.6	-37.3
H-H couplings				
16, 17	7.5 ± 0.2	27.0 ± 0.5	9.7 ± 0.4	9.1
16, 25	0.0 ± 0.2	-2.8 ± 0.5	-1.4 ± 0.4	-0.9
16, 26	0.0 ± 0.2	-2.8 ± 0.5	-1.4 ± 0.4	-1.2
17, 25	0.0 ± 0.2	-2.2 ± 0.5	-1.1 ± 0.4	-0.7
17, 26	0.0 ± 0.2	-2.2 ± 0.5	-1.1 ± 0.4	-1.0
			RMS	0.35 Hz

k	δ_k^{iso} [c] (ppm)
15	7.56 ± 0.3
16	7.34 ± 0.3
17	7.24 ± 0.3
25	7.20 ± 0.3
1	129.44 ± 0.2
3	138.56 ± 0.2

|	
4	127.25 ± 0.2
5	129.30 ± 0.2
6	128.39 ± 0.2

[a] calculated from $D_{ij}^{obs} = \left[\pm T_{ij}^{obs} - (\pm J_{ij}^{iso})\right]/2$ (see chapter 1 section 1.5.2)

[b] from the AP-DPD method (see below)

[c] chemical shifts are given from calibration with THF signal (at 1.72 ppm and 25.37 ppm for proton and carbon-13, respectively)

3.4.2.2. Conformational and orientational analysis

Albeit the set of experimental D_{ij}^{obs} extracted for *t*-St dissolved in PBLG/THF-d$_8$ is not significantly extended (13 independent D_{ij}^{obs}, but only 4 connecting the phenyl ring with the ene group) and the small values of dipolar couplings are affected by not negligible errors when compared to values in ZLI1132 of Table 3.11, a conformational analysis is still affordable. The software AnCon was used again to reproduce the set of D_{ij}^{obs} measured for *t*-St in PBLG/THF-d$_8$ (Table 3.15), by fixing the molecular geometry previously optimised in ZLI1132. A first test is to verify whether or not the potential distribution obtained from the AP-DPD conformational analysis of *t*-St/ZLI1132 is still consistent with experimental data obtained for the same molecule in PBLG phase. Then, keeping the potential terms $\phi_1^{max} = \pm\phi_2^{max}$, $h_1 = h_2$ and $A_{C_2} = 1 - A_{C_i}$ fixed at their optimized values of Table 3.13 (obtained for *t*-St in ZLI1132), the $\varepsilon_{2,0}(R)$, $\varepsilon_{2,2}(R)$ and $\varepsilon_{2,0}^{C=C}$ interaction tensor parameters were varied until RMS reached an acceptable value. As it can be appreciated in Figure 3.47, the optimised values, reported in Table 3.16, gave a good reproduction of D_{ij}^{obs} with a low RMS of 0.35 Hz. The dipolar couplings D_{ij}^{calc} calculated by this approach are reported, for comparison, in the last column of Table 3.15.
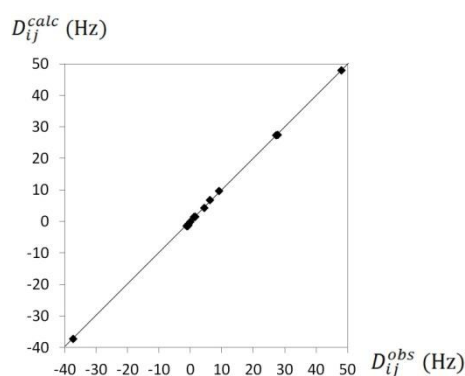

Figure 3.47. Observed *versus* theoretical dipolar couplings obtained for the the *t*-St molecule dissolved in PBLG/THF-d$_8$, respectively from NMR experiments and by the AP-DPD approach.

Table 3.16. Values of the iteration parameters used in the conformational analysis with the AP-DPD approach of the *t*-St molecule dissolved in PBLG/THF-d$_8$.

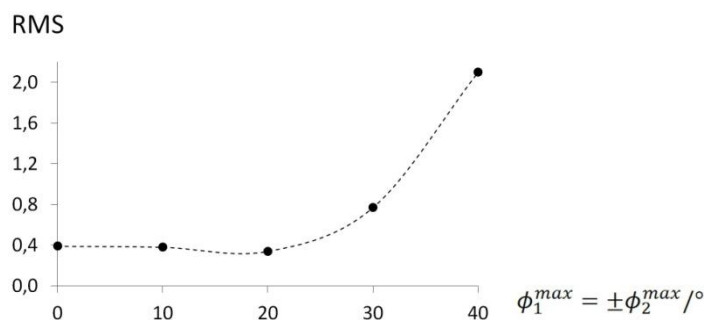|	*t*-St in PBLG/THF-d$_8$
$\phi_1^{max} = \pm\phi_2^{max}$ (degree)	16.80 [a]
A_{C_2}	0.59 [a]
$h_1 = h_2$ (degree)	10 [a]
$\varepsilon_{2,0}(R)$ (RT)	0.00388 ± 0.00003
$\varepsilon_{2,2}(R)$ (RT)	-0.00582 ± 0.00005
$\varepsilon_{2,0}^{C=C}$ (RT)	0.00568 ± 0.00014
RMS	0.35

[a] potential terms from conformational analysis in ZLI1132

The consistence of data in the thermotropic and lyotropic phases represents a satisfactory outcome. Moreover, due to the small values of dipolar couplings, we parametrically changed the potential terms, one by one, and we followed the trend of the RMS target function (and the corresponding reproduction of each single D_{ij}^{obs}). In particular the probability ratio A_{C_2} was varied in the range 0.2-0.8 (Figure 3.48) and the torsion angle $\phi_1^{max} = \pm\phi_2^{max}$ from 0° to 40° (Figure 3.49).
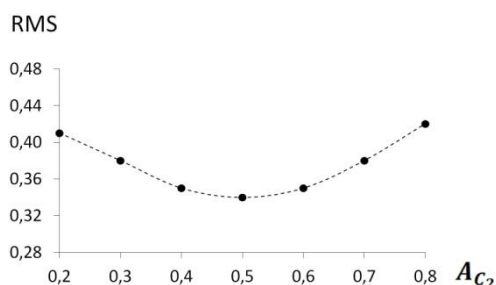
Figure 3.48. RMS value as a function of probability ratio A_{C_2} calculated for *t*-St in PBLG/THF-d$_8$ by the AP-DPD approach while fixing ϕ_1^{max} = 16.80 and h_1 = 10. The curve is also drawn as eye-guide.

It can be observed from Figure 3.48 that the RMS error gradually decreases, reaching a minimum at A_{C_2} ~0.5, and then increases again. The main conclusions are: (*i*) an equilibrium between the two couples of conformers has to be considered in order to reproduce the experimental data set with a low RMS, *i.e.* neither the couple of C_2 conformers nor that of C_i is sufficient alone (this would translate to A_{C_2} = 1 and A_{C_2} = 0, respectively) to fit the D_{ij}^{obs}; (*ii*) situations with $0.4 \leq A_{C_2} \leq 0.6$ cannot be practically distinguished, since in this range not only

RMS is acceptably low but also the differences between each inter-ring D_{ij}^{obs} and its corresponding D_{ij}^{calc} is lower than 0.5.

Figure 3.49. RMS value as a function of $\phi_1^{max} = \pm\phi_2^{max}$ calculated for *t*-St in PBLG/THF-d$_8$ by the AP-DPD approach while fixing A_{C_2} = 0.6 and h_1 = 10. The curve is also drawn as eye-guide.

Despite the lowest RMS value appears at $\phi_1^{max} = \pm\phi_2^{max}$ = 20°, the curve shown in Figure 3.49 is substantially flat - and the RMS error practically indiscernible - in the range 0°-20°, increasing quickly after 20°. As a result, the conformational analysis we performed on the sample *t*-St/PBLG/THF-d$_8$ does not individuate a precise value of the torsion angle but rather a limited range of about 20°. This interval is perfectly in agreement with results found for the thermotropic sample.

Summarising the results obtained for this sample, it can be reasonably said that the our experimental data lead to a $P_{iso}(\phi_1, \phi_2)$ (equation 3.8) characterized essentially by $0 \leq \phi_1^{max} = \pm\phi_2^{max} \leq 20°$ and $0.4 \leq A_{C_2} \leq 0.6$ (fixing $h_1 = h_2$ = 10). Then, even from data in a weakly orienting phase as PBLG/THF-d$_8$, a restricted range for the twist angle of the most probable conformations and for their relative weight is unambiguously determined and the corresponding conformational distribution is the only possible solution to fit experimental data. Hence, when treatment in a thermotropic solvent is not a viable way to obtain conformational information, the use of PBLG phases as alternative solvent can, together with the AP-DPD approach, yield important meaningful results.

Next to the conformational equilibrium, a second valuable information one can get from residual dipolar couplings is the orientational order. As seen in the case of *t*-St dissolved in ZLI1132, the orientations of the C_2 and C_i conformers are essentially the same, and this behaviour is expected to be even more prominent in the weakly orienting PBLG phase. Therefore, we consider here the averaged order parameters rather then those for the single C_2 or C_i conformation. In the PAS of the Saupe matrix (see Figure 3.42 for the definition of the $\{a, b, c\}$ molecular frame and of the η angle, giving the location of the PAS), we obtained: S_{aa} =

0.0019 and $S_{bb} - S_{cc}$ = -0.0024, with η = 37.45°. Table 3.17 sums up the orientational order parameters found for *t*-St in the two phases. Few points are worthy to be noted: (*i*) S_{aa} in PBLG is still positive, even if smaller than in thermotropic solvent ($S_{aa} \sim 0.5$); (*ii*) the biaxiality order parameter $S_{bb} - S_{cc}$ is negative in PBLG/THF-d$_8$ and positive in ZLI1132; (*iii*) S_{bb} is negative in both cases but its absolute value in the low ordering phase is comparable with S_{aa}, while in the thermotropic phase it is three times smaller; (*iv*) S_{cc} is the smallest order parameter in PBLG phase, while in ZLI1132 it is negative and two times greater than S_{bb}. Overall, these evidences would indicate that in the weakly oriented sample the biaxiality order parameter - and in particular S_{bb} - increases at the expense of the longitudinal order parameter S_{aa}. It would be interesting in the future to investigate more deeply if this orientational trend may be driven by some interactions with the phenyl rings in the side chains of PBLG.

Table 3.17. Orientational order parameters found for *t*-St in ZLI1132 and PBLG/THF-d$_8$ mixture.

	t-St in ZLI1132 [a]	*t*-St in PBLG/THF-d$_8$ [b]
S_{aa}	0.525	0.0019
$S_{bb} - S_{cc}$	0.174	-0.0024
S_{bb}	-0.176	-0.0021
S_{cc}	-0.350	0.0003
η (degree)	44.92	37.45

[a] Results for the C_2 conformer given in the PAS of the Saupe matrix for this conformation
[b] Results for the averaged conformation given in the PAS of the averaged Saupe matrix

3.4.3.   Conclusions

In this section, structure, order and conformation of the *trans*-stilbene have been investigated at various levels. Firstly, its orientational and conformational behavior was studied in solution by NMR spectroscopy when dissolved in both a highly (ZLI1132) and a weakly (PBLG/THF-d$_8$) ordering liquid crystal. AP-DPD treatment led to a torsional surface characterized by four more stable symmetry-related conformations, that is a couple of global minima, where the molecule exhibits a propeller-like C_2 symmetry, and a couple of C_i local minima, where the rings are conrotated of the same angle. Data in thermotropic phase clearly individuated minimum conformers existing at $\phi_1^{max} = \phi_2^{max}$ (relative percentage of 59%) and $\phi_1^{max} = -\phi_2^{max}$ (relative percentage of 41%), with ϕ_1^{max} = 16.8°. In PBLG phase, a reduced

number of small residual dipolar couplings allowed to define limited ranges where conformers are more probably confined, $0 \leq \phi_1^{max} = \pm\phi_2^{max} \leq 20°$ and $0.4 \leq A_{C_2} \leq 0.6$. This is a proof of the reliability of NMR in PBLG phases for the conformational study of flexible more complex molecules when their spectra in a thermotropic phase are too hard to be recorded at high resolution and/or analysed. In other words, the agreement between outcomes from the two phases testifies that: (*i*) there is no perceptible influence of the phase on the conformational equilibrium; and (*ii*) conformational information derived from a weakly ordered sample is reliable in individuating restricted intervals that contain the "real" minimum energy conformers. This encourages then the application of NMR in PBLG phase to more complex molecules otherwise impossible to treat. To procede further in the comparison between the highly and weakly oriented sample, the order parameters have been evaluated, observing in the PBLG phase a rise in the biaxiality at the expense of S_{aa}.

As a second point, the similarity between the conformational distributions found for *t*-St in solution and *via* MP2/6-31G** theoretical calculations *in vacuo* seem to suggest that the differences between the conformational behavior of the molecule in solution (where inter- and intramolecular forces act), with respect to the calculations on the isolated molecule (where only intramolecular interactions are considered), are not enough to cancel the main features of the probability distribution. Torsional distributions in the two phases are of course not identical and in particular the calculated potential (Figure 3.41) shows lower barriers, comparable with RT at room temperature. This means that: (*i*) since the preference for one or the other conformation is relatively weak, the system has to be described in terms of the full torsional distribution (*i.e.* at room temperature C_2 and C_i conformations are simultaneously present, and also the planar conformation is not totally absent); (*ii*) the small energy differences may be one reason for the discrepancies between the results of different experiments (small changes of the experimental conditions, as the temperature and/or the solvent, might significantly affect the torsional distribution) and for the discrepancies between theoretical calculations performed at different levels.

Finally, the conformational distribution of *trans*-4,4'-dichlorostilbene, prototype molecule of 4,4'-substituted *trans*-stilbene derivatives endowed with innumerable properties (consider for instance the *trans*-4,4'-dihydroxystilbene), was investigated in the nematic ZLI1132 liquid crystal, with the aim of (*i*) contributing to a better understanding of useful structure-property relationships for 4,4'-disubstituted *trans*-stilbene analogs and (*ii*) evaluating the influence of the Cl-^{1}H substitution at the *para* positions on the conformational distribution. The same C_2 and C_i stable conformations were found having ϕ_1^{max} = 18.69° and, respectively,

A_{C_2} = 63% and A_{C_i} = 37%. Overall, this indicates very limited effects of the 4,4' Cl-substitutions on the positions of the conformational minima, even if the sharper and higher peaks with respect to *trans*-stilbene seem to suggest a slightly greater confinement of the chlorinated molecule in proximity of its conformational minima.

3.5.   Conclusion

In this chapter NMR spectroscopy in liquid crystals revealed a valuable tool for investigating structure, order and conformational equilibria of different flexible molecules possessing one or two torsional degrees. The potentiality of this technique, disclosing such molecular information from residual dipolar couplings directly in a liquid medium, is evident, especially when compared to classical NMR strategies relying on short-range interactions. On the other hand, it is clear that some assumptions must be made and proper theoretical models must be adopted, in order to translate the experimental dipolar couplings into the desired molecular information. The edition of the experimental D_{ij} and their physical interpretation follow different routes and pose different problems depending on the kind of liquid crystalline phase – highly or weakly orienting – that is used as NMR solvent. Complex overcrowded spectra composed of thousands of transitions characterize NMR spectra of highly oriented compounds, but when their analysis is successfully achieved with the aid of graphical packages, it leads to a set of very accurate dipolar couplings with magnitude up to several thousand of Hertz. The treatment of these D_{ij}^{obs} by the AP-DPD approach, unanimously recognized as an efficace and robust method for these systems, gives a reliable description of the torsional probability with a precise location of the minimum energy conformers and very small margins of error. Unique limitation is the difficulty of spectral analysis, that restricts its application to no more than 12-spin symmetric systems. The cases of biphenyl in section 3.2 and stilbenoids in section 3.4 illustrate well the high spectral complexity *versus* high accuracy of extracted D_{ij} and following molecular information that can be obtained for symmetric small solutes dissolved in thermotropic phases. In the case of biphenyl, molecular dynamics simulations were tested as a tool for obtaining a good starting set of spectral parameters, leading to an encouraging agreement between the experimental and simulated sets of D_{ij}. In the case of stilbenoids, the spectral analysis of the 10-spin system *trans*-4,4'-dichlorostilbene in ZLI1132 was achieved by guessing a trial set of order parameters corresponding to a non-planar C_2 structure. The independent D_{ij}^{obs} extracted for the chlorinated compound were used

for facing the more complex 12-spin system of *trans*-stilbene. The accurate sets of D_{ij}^{obs} obtained for both molecules gave detailed $P_{iso}(\phi_1, \phi_2)$ distributions after AP-DPD treatment, corresponding to two C_2 and two C_i minimum conformers existing at $\phi_1^{max} = \phi_2^{max}$ and $\phi_1^{max} = -\phi_2^{max}$ (ϕ_1^{max} = 16.8° and relative percentage of 59% and 41% for *trans*-stilbene, and ϕ_1^{max} = 18.7° and relative percentage of 63% and 37% for *trans*-4,4'-dichlorostilbene).

When asymmetric more complex molecules such as the anti-inflammatory drugs diflunisal and naproxen (section 3.3) are studied, the need for an alternative strategy becomes mandatory and here we chose to resort to weakly orienting PBLG phases as alternative NMR solvents. Compared to thermotropic ones, spectra display weak second-order features and appear simpler to analyse without using graphical packages. Indeed, spectral simplification is often only apparent, because for the extraction of the desired large set of D_{ij} various NMR experiments on different nuclei must be combined. In the absence of available simple and time-saving experiments, new pulse sequence may be designed and this is the case of the new GET-SERF experiment proposed in section 3.3.1.1 for the trivial edition of ^{1}H-^{19}F couplings. If its application appears relatively easy in the case of a difluorinated molecule as diflunisal, it may represent a relevant tool when dealing with more complex molecules. Indeed, for a system containing n and m non-equivalent proton and fluorine sites, m experiments are sufficient in order to selectively extract all ^{1}H-^{19}F couplings in the whole molecule. Another issue to be taken into account when investigating conformational equilibria in weakly ordering media is that the accuracy in the edition of experimental data and in the derived structural and conformational information may be lower than in thermotropics. Indeed, the correct description of rotations is associated with the number and the entity of the inter-fragment D_{ij}. Hence, in the case of diflunisal, a favourable line distribution in the spectra along with the presence of magnetically active heteronuclei allowed to gather a reasonable amount of inter-ring D_{ij} for a quite accurate description of the torsional distribution, with a couple of *trans* conformers, with F$_8$ opposite to the carboxylic group (φ_1^{max} = ±45.5° and relative percentage of 56%), and a couple of *cis* conformers, with F$_8$ on the same side to the carboxylic group (φ_2^{max} = ±41.1° and a relative percentage of 44%). Contrarily, in the case of naproxen or *trans*-stilbene, due to the overlap of signals and/or symmetry of the structure, a smaller number of independent inter-fragment D_{ij}^{obs} was collected, so that no precise values of torsional angles but rather small ranges could be individuated for the major conformers. In particular, four minimum energy structures have been found for naproxen: a couples of more stable conformers (I and II) with the methoxy group in the *cis* arrangement (φ ~0°) and α-hydrogen atom *quasi*-planar relative to the aromatic ring (ϑ equal to ~15° and ~195, respectively), and a

couple of less stable conformers (III and IV) involving the *trans* geometry of the methoxy group (φ ~180°) and the same geometry of the chiral side chain (ϑ equal to ~15° and ~195°, respectively). The conformational equilibrium among these four structure seems to be the only model able to reproduce experimental data. More informative for the direct comparison between highly and weakly ordered media is probably the case of *trans*-stilbene. Analysis in PBLG phase allowed to define restricted ranges where conformers are more likely to be confined (0 $\leq \phi_1^{max} = \pm\phi_2^{max} \leq$ 20° and 0.4 $\leq A_{C_2} \leq$ 0.6). These intervals are perfectly consistent with the more precise location of the minima found in the thermotropic LC. Therefore, examples presented here testifies that the conformational information achieved in PBLG phases is reliable, though sometimes not very precise, and becomes extremely meaningful when no other data in solution are available.

At the end of this third chapter the main conclusions to draw are: (*i*) NMR in liquid crystals is effectively a valuable tool for studying the conformation of small flexible molecules; (*ii*) the AP-DPD model represents a robust approach for treating both highly and weakly ordered solutes; (*iii*) highly and weakly ordering phases possess each their pros and cons and the choice between them should be done by considering spectral complexity and degree of accuracy. For small symmetric molecules accurate molecular information are likely to be accessible from the D_{ij}^{obs} extracted from their spectra in thermotropic LCs. For more complex asymmetric molecules the smarter choice is to use PBLG phases, that reveal a meaningful and reliable source of conformational information when no other investigation in solution is possible.

References

[1] K. Jeong, B. J. Byun, Y. K. Kang, Conformational preferences of glycerol in the gas phase and in water, *Bull. Korean Chem. Soc.*, 33, **2012**, 917-924

[2] G. Celebre, G. De Luca, M. Longeri, D. Catalano, C. A. Veracini, J. W. Emsley, Structure of biphenyl in a nematic liquid-crystalline solvent, *J. Chem. Soc. Faraday Trans.*, 87, **1991**, 2623-2627

[3] R. M. Irwin, J. Laane, Phase-dependent conformation and vibrational spectra of 1,3-disilacyclobutane, *J. Phys. Chem.*, 82, **1978**, 2845-2850

[4] J. Zheng, P. Seal, D. G. Truhlar, Role of conformational structures and torsional anharmonicity in controlling chemical reaction rates and relative yields: butanal + HO_2 reactions, *Chem. Sci.*, 4, **2013**, 200-212

[5] D. Seebach, Uroš Grošelj, W. B. Schweizer, S. Grimme, C. Mück-Lichtenfeld, Experimental and theoretical conformational analysis of 5-benzylimidazolidin-4-one derivatives – a "playground" for studying dispersion interactions and a "windshield-wiper" effect in organocatalysis, *Helv. Chim. Acta*, 93, **2010**, 1-16

[6] P. Matteini, A. Goti, G. Agati, Theoretical conformational analysis of rutin, *Monatsh. Chem.*, 141, **2010**, 793-800

[7] Y. A. Vereshchagina, E. A. Ishmaeva, V. V. Zverev, Theoretical conformational analysis of organophosphorus compounds, *Russ. Chem. Rev.*, 74, **2005**, 297-315

[8] R. Stowasser, R. S. Glass, R. Hoffmann, The dithiacyclooctane cation (DTCO1): conformational analysis, interconversion barriers and bonding, *J. Chem. Soc. Perkin Trans. 2*, **1999**, 1559-1561

[9] P. Birner, S. Kugler, K. Simon, G. Náray-Szabó, Theoretical conformational analysis of substituted phenylbenzoates, *Mol. Cryst. Liq. Cryst.*, 80, **1982**, 11-17

[10] P. Mezey, A. Kucsman, G. Theodorakopoulos, I. G. Csizmadia, Theoretical conformational analysis of a simple sulphilimine model, *Theoret. Chim. Acta (Berl.)*, 38, **1975**, 115-119

[11] D. D. Boehr, R. Nussinov, P. E. Wright, The role of dynamic conformational ensembles in biomolecular recognition, *Nat. Chem. Biol.*, 5, **2009**, 789-796

[12] D. A. Belinskaya, N. N. Shestakova, Theoretical conformational analysis in the determination of productive conformations of substrates for acetylcholinesterase and butyrylcholinesterase, *Russ. J. Bioorg. Chem.*, 31, **2005**, 419-425

[13] J. Z. Hilt, M. E. Byrne, Configurational biomimesis in drug delivery: molecular imprinting of biologically significant molecules, *Adv. Drug Deliv. Rev.*, 56, **2004**, 1599-1620

[14] D. P. Fairlie, J. D. A. Tyndall, R. C. Reid, A. K. Wong, G. Abbenante, M. J. Scanlon, D. R. March, D. A. Bergman, C. L. L. Chai, B. A. Burkett, Conformational selection of inhibitors and substrates by proteolytic enzymes: implications for drug design and polypeptide processing, *J. Med. Chem.*, 43, **2000**, 1271-1281

[15] T. Mavromoustakos, A. Kolocouris, M. Zervou, P. Roumelioti, J. Matsoukas, R. Weisemann, An effort to understand the molecular basis of hypertension through the study of conformational analysis of

losartan and sarmesin using a combination of nuclear magnetic resonance spectroscopy and theoretical calculations, *J. Med. Chem.*, 42, **1999**, 1714-1722

[16] M. Karplus, Vicinal proton coupling in nuclear magnetic resonance, *J. Am. Chem. Soc.*, 85, **1963**, 2870-2871

[17] M. Karplus, Contact electron-spin coupling of nuclear magnetic moments, *J. Chem. Phys.*, 30, **1959**, 11-15

[18] D. Neuhaus, M. P. Williams, *The Nuclear Overhauser Effect in Structural and Conformational Analysis*, 2nd ed., Wiley-VCH, New York, **2000**, ISBN: 9780471246756

[19] R. S. Lipsitz, N. Tjandra, Residual dipolar couplings in NMR structure analysis, *Annu. Rev. Biophys. Biomol. Struct.*, 33, **2004**, 387-413

[20] E. de Alba, N. Tjandra, NMR dipolar couplings for the structure determination of biopolymers in solution, *Prog. Nucl. Magn. Reson. Spectrosc.*, 40, **2002**, 175-197

[21] J. H. Prestegard, H. M. Al-Hashimi, J. R. Tolman, NMR structures of biomolecules using field oriented media and residual dipolar couplings, *Q. Rev. Biophys.*, 33, **2000**, 371-424

[22] J. Cavanagh, *Protein NMR Spectroscopy: Principles and Practice*, Academic Press, New York, **1996**, ISBN: 9780121644901

[23] G. Celebre, G. De Luca, M. Longeri, E. Sicilia, Graphical interactive strategy for the analysis of NMR spectra in liquid crystalline phases, *J. Chem. Inf. Comput. Sci.*, 34, **1994**, 539-545

[24] E. E. Burnell, C. A. de Lange, W. L. Meerts, Novel strategies for solving highly complex NMR spectra of solutes in liquid crystals, in *Nuclear Magnetic Resonance Spectroscopy of Liquid Crystals*, R. Dong ed., World Scientific Review, **2009**, chap. 1, ISBN: 9789814273664

[25] W. L. Meerts, C. A. de Lange, A. C. J. Weber, E. E. Burnell, Evolutionary algorithms to solve complicated NMR spectra, *J. Chem. Phys.*, 139, **2009**, 044504.1-8

[26] W. L. Meerts, C. A. de Lange, A. C. J. Weber, E. E. Burnell, A simple two-step automatic assignment procedure for complicated NMR spectra of solutes in liquid crystals using genetic algorithms, *Chem. Phys. Lett.*, 441, **2007**, 324-346

[27] W. L. Meerts, M. Schmitt, Application of genetic algorithms in automated assignments of high-resolution spectra, *Int. Rev. Phys. Chem.*, 25, **2006**, 353-406

[28] G. Celebre, M. Longeri, NMR studies of solutes in liquid crystals: small flexible molecules, in *NMR of Ordered Liquids*, E. E. Burnell and C. A. de Lange eds., Kluwer Academic, Dordrecht, **2003**, chap 14, ISBN: 1402013434

[29] M. Concistré, L. De Lorenzo, G. De Luca, M. Longeri, G. Pileio, G. Raos, Conformational analysis of 2,2'-bithiophene: a ^{1}H liquid crystal NMR study using the ^{13}C satellite spectra, *J. Phys. Chem. A*, 109, **2005**, 9953-9963

[30] G. Celebre, M. Concistré, G. De Luca, M. Longeri, G. Pileio, J. W. Emsley, The structure of acrolein in a liquid crystal phase, *Chem. Eur. J.*, 11, **2005**, 3599-3608

[31] G. Celebre, G. De Luca, M. Longeri, G. Pileio, J. W. Emsley, Is styrene planar in liquid phases?, *J. Chem. Phys.*, 120, **2004**, 7075-7084

[32] R. Berardi, F. Spinozzi, C. Zannoni, Maximum entropy internal order approach to the study of intramolecular rotations in liquid crystals, *J. Chem. Soc. Faraday Trans.*, 88, **1992**, 1863-1873

[33] L. C. Ter Beek, D. S. Zimmerman, E. E. Burnell, The conformation of 2,2′-dithiophene in nematic solvents determined by ^{1}H-NMR, *Mol. Phys.*, 74, **1991**, 1027-1035

[34] G. Celebre, M. Longeri, J. W. Emsley, The nature of the internal rotational barrier in benzyl chloride. An interpretation of the dipolar coupling constants obtained from the analysis of the proton NMR spectra of samples dissolved in liquid crystal solvents, *Mol. Phys.*, 64, **1988**, 715-723

[35] P. Diehl, J. Jokisaari, J. Amrein, The structure and intramolecular motion of benzaldehyde as studied on the basis of proton spectra with ^{13}C satellites of the oriented molecule, *Org. Magn. Reson.*, 13, **1980**, 451-454

[36] G. Chidichimo, F. Lelj, M. Longeri, N. Russo, C. A. Veracini, Conformational study of 2,2′-biselenophene partially oriented in a nematic liquid crystral phase by PMR spectra including [77]Se satellites, *Chem. Phys. Lett.*, 67, **1979**, 384-387

[37] M. Duchêne, J. W. Emsley, J. C. Lindon, J. Overstall, D. S. Stephenson, The molecular structure and reorientation of parafluorobenzaldehyde dissolved in a smectic mesophase studied using N.M.R. spectroscopy, *Mol. Phys.*, 33, **1977**, 281-286

[38] L. Bellitto, C. Petrongolo, C. A. Veracini, M. Bambagiotti, Conformational studies of molecules partially oriented in nematic phase: nuclear magnetic resonance and theoretical investigation of 2,2′-bifuryl, *J. Chem. Soc. Perkin Trans. II*, **1977**, 314-318

[39] L. D. Field, S. Sternhell, A. S. Tracey, The conformation of biphenyls in nematic liquid crystalline solution. An investigation of the torsional angles in 2,6-dihalogenated derivatives, *J. Am. Chem. Soc.*, 99, **1977**, 5249-5253

[40] J. W. Emsley, D. S. Stephenson, J. C. Lindon, L. Lunazzi, S. Pulga, Structure and conformation of 4,4′-bipyridyl by nuclear magnetic resonance spectroscopy of a nematic solution, *J. Chem. Soc. Perkin Trans. II*, **1975**, 1541-1544

[41] J. Courtieu, Y. Gounelle, C. Duret, P. Gonord, S. K. Kan, Etude structurale de la bipyrimidine par RMN en phase nématique, *Org. Magn. Reson.*, 6, **1974**, 622-624

[42] P. Bucci, M. Longeri, C. A. Veracini, L. Lunazzi, Nematic phase nuclear magnetic resonance investigations of rotational isomerism. III. Conformational preferences and interconversion barrier of 2,2′-bithienyl, *J. Am. Chem. Soc.*, 96, **1974**, 1305-1309

[43] W. Niederberger, P. Diehl, L. Lunazzi, The structure and conformation of 4,4′-dichlorobiphenyl determined by N.M.R. of oriented molecules in nematic solvents, *Mol. Phys.* 26, **1973**, 571-576

[44] G. De Luca, M. Longeri, G. Pileio, P. Lantto, NMR spectroscopy investigation of the cooperative nature of the internal rotational motions in acetophenone, *Chem. Phys. Chem.*, 6, **2005**, 2086-2098

[45] G. Celebre, G. De Luca, J. W. Emsley, E. K. Foord, M. Longeri, F. Lucchesini, G. Pileio, The conformational distribution in diphenylmethane determined by nuclear magnetic resonance spectroscopy of a sample dissolved in a nematic liquid crystalline solvent, *J. Chem. Phys.*, 118, **2003**, 6417-6426

[46] G. Celebre, G. De Luca, M. Longeri, J. W. Emsley, Internal rotation potential function for anisole in solution: a liquid crystal NMR study, *J. Phys. Chem.*, 96, **1992**, 2466-2470

[47] L. Di Bari, M. Persico, C. A. Veracini, Coupled internal rotations in substituted ethoxybenzenes: maximum entropy analysis of nuclear magnetic resonance of nematic solutions data and *ab initio* rotameric distributions, *J. Chem. Phys.*, 96, **1992**, 4782-4791

[48] G. Celebre, M. Longeri, J. W. Emsley, An investigation by N.M.R. spectroscopy of the dependence on internal motion of the orientational ordering of ethoxybenzene and 4-fluoroethoxybenzene when dissolved in a nematic solvent, *Liq. Cryst.*, 6, **1989**, 689-700

[49] M. E. Rosen, S. P. Rucker, C. Schmidt, A. Pines, Two-dimensional proton NMR studies of the conformations and orientations of *n*-alkanes in a liquid-crystal solvent, *J. Phys. Chem.*, 97, **1993**, 3858-3866

[50] E. Säwén, B. Stevensson, J. Östervall, A. Maliniak, G. Widmalm, Molecular conformations in the pentasaccharide LNF-1 derived from NMR spectroscopy and molecular dynamics simulations, *J. Phys. Chem. B*, 115, **2011**, 7109-7121

[51] A. Silipo, Z. Zhang, F. J. Cañada, A. Molinaro, R. J. Linhardt, J. Jiménez-Barbero, Conformational analysis of a dermatan sulfate-derived tetrasaccharide by NMR, molecular modeling, and residual dipolar couplings, *Chem. Bio. Chem.*, 9, **2008**, 240-252

[52] N. Cramer, S. Helbig, A. Baro, S. Laschat, R. Diestel, F. Sasse, D. Mathieu, C. Richter, G. Kummerlöwe, B. Luy, H. Schwalbe, Synthesis and biological properties of cylindramide derivatives: evidence for calcium-dependent cytotoxicity of tetramic acid lactams, *Chem. Bio. Chem.*, 9, **2008**, 2474-2486

[53] U. M. Reinscheid, J. Farjon, M. Radzom, P. Haberz, A. Zeeck, M. Blackledge, C. Griesinger, Effect of the solvent on the conformation of a depsipeptide: NMR-derived solution structure of hormaomycin in DMSO from residual dipolar couplings in a novel DMSO-compatible alignment medium, *Chem. Bio. Chem.*, 7, **2006**, 287-296

[54] J. Klages, C. Neubauer, M. Coles, H. Kessler, B. Luy, Structure refinement of cyclosporin A in chloroform by using RDCs measured in a stretched PDMS-gel, *Chem. Bio. Chem.*, 6, **2005**, 1672-1678

[55] T. N. Pham, S. L. Hinchley, D. W. H. Rankin, T. Liptaj, D. Uhrín, Determination of sugar structures in solution from residual dipolar coupling constants: methodology and application to methyl *β*-D-xylopyranoside, *J. Am. Chem. Soc.*, 126, **2004**, 13100-13110

[56] D. I. Freedberg, An alternative method for pucker determination in carbohydrates from residual dipolar couplings: a solution NMR study of the fructofuranosyl ring of sucrose, *J. Am. Chem. Soc.*, 124, **2002**, 2358-2362

[57] H. F. Azurmendi, C. A. Bush, Conformational studies of blood group A and blood group B oligosaccharides using NMR residual dipolar couplings, *Carbohydr. Res.*, 337, **2002**, 905-915

[58] M. Martin-Pastor, C. A. Bush, Refined structure of a flexible heptasaccharide using ^{1}H-^{13}C and ^{1}H-^{1}H NMR residual dipolar couplings in concert with NOE and long range scalar coupling constants, *J. Biomol. NMR*, 19, **2001**, 125-139

[59] P. Collings, M. Hird, *Introduction to Liquid Crystals: Chemistry and Physics*, Taylor&Francis Ltd., **1997**, ISBN: 0748406433

[60] H. Kelker, R. Hatz, *Handbook of Liquid Crystals*, Verlag Chemie, Weinheim, **1980**, ISBN: 9783527254811

[61] L. Venkataraman, J. E. Klare, C. Nuckolls, M. S. Hybertsen, M. L. Steigerwald, Dependence of single-molecule junction conductance on molecular conformation, *Nature*, 442, **2006**, 904-907

[62] K. Tashiro, J. Hou, M. Kobayashi, T, Inoue, X-ray structure analyses and vibrational spectral measurements of the model compounds of the liquid-crystalline arylate polymers. Finding out the Raman bands characteristic of the twisted biphenyl structure in association with the solid-to-liquid crystalline phase transition, *J. Am. Chem. Soc.*, 112, **1990**, 8273-8279

[63] M. P. Johansson, J. Olsen, Torsional barriers and equilibrium angle of biphenyl: reconciling theory with experiment, *J. Chem. Theory Comput.*, 4, **2008**, 1460-1471

[64] I. Cacelli, G. Prampolini, Torsional barriers and correlations between dihedrals in *p*-polyphenyls, *J. Phys. Chem. A*, 107, **2003**, 8665-8670

[65] J. C. Sancho-García, J. L. Brédas, J. Cornil, Assessment of the reliability of the Perdew–Burke–Ernzerhof functionals in the determination of torsional potentials in π-conjugated molecules, *Chem. Phys. Lett.*, 377, **2003**, 63-68

[66] A. Almeniggen, O. Bastiansen, L. Fernholt, B. N. Cyvin, S. J. Sandal, Structure and barrier of internal rotation of biphenyl derivatives in the gaseous state: part 1. The molecular structure and normal coordinate analysis of normal biphenyl and pedeuterated biphenyl, *J. Mol. Struct.*, 128, **1985**, 59-76

[67] S. Charbonnier, S. T. Beguemsi, Y. T. N'Guessan, D. Legoff, A. Proutiere, R. Viani, Dihedral angle of biphenyl compounds studied by theoretical calculations (dipole induced dipole, molecular mechanics) and experimental methods (electro-optic measurements, infrared spectroscopy), *J. Mol. Struct.*, 158, **1987**, 109-125

[68] R. J. Pulham, D. Steele, Vibrational spectra of 4,4'-difluorobiphenyl-d_8 and the structure of biphenyls in solution, *J. Raman Spectrosc.*, 15, **1984**, 217-223

[69] V. J. Eaton, D. Steele, Dihedral angle of biphenyl in solution and the molecular force field, *J. Chem. Soc. Faraday Trans. 2*, 69, **1973**, 1601-1608

[70] D. H. Barich, R. J. Pugmire, D. M. Grant, R. J. Iuliucci, Investigation of the structural conformation of biphenyl by solid state ^{13}C NMR and quantum chemical NMR shift calculations, *J. Phys. Chem. A*, 105, **2001**, 6780-6784

[71] S. Ando, T. Hironaka, H. Kurosu, I. Ando, ^{13}C NMR chemical shift as a probe for estimating the conformation of aromatic groups in the solid state. 1. Biphenyls, *Magn. Reson. Chem.*, 38, **2000**, 241-250

[72] H. Calleau, J. L. Baodour, C. M. E. Zeyen, Structural phase transition in polyphenyls. VII. A neutron diffraction study of the structural phase transition in biphenyl-d_{10}, *Acta Crystallogr. B*, 35, **1979**, 426-432

[73] Y. Delugeard, G. P. Charbonneau, Biphenyl: three-dimensional data and new refinement at 293 K, *Acta Crystallogr. B*, 33, **1977**, 1586-1588

[74] A. Bree, M. Edelson, A study of the second order phase transition in biphenyl at 40 K through raman spectroscopy, *Chem. Phys. Lett.*, 46, **1977**, 500-504

[75] G. P. Charbonneau, Y. Delugeard, Structural transition in polyphenyls. III. Crystal structure of biphenyl at 110 K, *Acta Cryst. B*, 32, **1976**, 1420-1423

[76] A. Hargreaves, S. H. Rizvi, The crystal and molecular structure of biphenyl, *Acta Crystallogr. B*, 15, **1962**, 365-373

[77] Y. Furusawa, V. Nagarajan, M. Tanokura, E. Masai, M. Fukuda, T. Senda, Crystal structure of the terminal oxygenase component of biphenyl dioxygenase derived from *Rhodococcus sp.* strain RHA1, *J. Mol. Biol.*, 342, **2004**, 1041-1052

[78] G. Celebre, G. De Luca, M. Longeri, Exploiting the information content of dipolar couplings: determination of the temperature dependence of the inter-ring twist angle of biphenyl dissolved in uniaxial mesophases, *Liq. Cryst.*, 37, **2010**, 923-933

[79] A. B. Sahakyan, A. G. Shahkhatuni, A. A. Shahkhatuni, H. A. Panosyan, Torsion sensitivity in NMR of aligned molecules: study on various substituted biphenyls, *Magn. Reson. Chem.*, 46, **2008**, 144-149

[80] G. Celebre, G. De Luca, G. Mazzone, The combined use of deuterium NMR and computer simulations for conformational investigation of flexible molecules in nematic solutions, *J. Mol. Struct.: Theochem*, 728, **2005**, 209-214

[81] T. Chandrakumar, J. M. Polson, E. E. Burnell, A multiple-quantum ^{1}H NMR study of conformational biasing of biphenyl in a nematic liquid crystal, *J. Magn. Reson. A*, 118, **1996**, 264-271

[82] R. Berardi, F. Spinozzi, C. Zannoni, A new maximum entropy conformational analysis of biphenyl in liquid crystal solution, *Mol. Cryst. Liq. Cryst.*, 290, **1996**, 245-253

[83] D. Catalano, L. Di Bari, C. A. Veracini, G. N. Shilstone, C. Zannoni, A maximum-entropy analysis of the problem of the rotameric distribution for substituted biphenyls studied by ^{1}H nuclear magnetic resonance spectroscopy in nematic liquid crystals, *J. Chem. Phys.*, 94, **1991**, 3928-3935

[84] A. Pizzirusso, R. Berardi, L. Muccioli, M. Ricci, C. Zannoni, Predicting surface anchoring: molecular organization across a thin film of 5CB liquid crystal on silicon, *Chem. Sci.*, 3, **2012**, 573-579

[85] A. Pizzirusso, M. B. Di Cicco, G. Tiberio, L. Muccioli, R. Berardi, C. Zannoni, Alignment of small organic solutes in a nematic solvent: the effect of electrostatic interactions, *J. Phys. Chem. B*, 116, **2012**, 3760-3771

[86] T. A. Papadopoulos, L. Muccioli, S. Athanasopoulos, A. B. Walker, C. Zannoni, D. Beljonne, Does supramolecular ordering influence exciton transport in conjugated systems? Insight from atomistic simulations, *Chem. Sci.*, 2, **2011**, 1025-1032

[87] A. Pizzirusso, M. Savini, L. Muccioli, C. Zannoni, An atomistic simulation of the liquid-crystalline phases of sexithiophene, *J. Mat. Chem.*, 21, **2011**, 125-133

[88] R. Berardi, L. Muccioli, C. Zannoni, Can nematic transitions be predicted by atomistic simulations? A computational study of the odd-even effect, *Chem. Phys. Chem.*, 5, **2004**, 104-111

[89] G. Tiberio, L. Muccioli, R. Berardi, C. Zannoni, Towards in silico liquid crystals. Realistic transition temperatures and physical properties for *n*-cyanobiphenyls *via* molecular dynamics simulations, *Chem. Phys. Chem.*, 10, **2009**, 125-136

[90] A. C. J. Weber, A. Pizzirusso, L. Muccioli, C. Zannoni, W. L. Meerts, C. A. de Lange, E. E. Burnell, Efficient analysis of highly complex nuclear magnetic resonance spectra of flexible solutes in ordered liquids by using molecular dynamics, *J. Chem. Phys.*, 136, **2012**, 174506.1-7

[91] M. F. Palermo, A. Pizzirusso, L. Muccioli, C. Zannoni, An atomistic description of the nematic and smectic phases of 4-*n*-octyl-4'-cyanobiphenyl (8CB), *J. Chem. Phys.*, 138, **2013**, 204901.1-16

[92] W. E. Palke, D. Catalano, G. Celebre, J. W. Emsley. Molecular dynamics simulation of biphenyl dissolved in a liquid crystalline solvent: a test of theoretical methods of deriving rotational potentials from partially averaged nuclear spin dipolar couplings, *J. Chem. Phys.*, 105, **1996**, 7026-7033

[93] A. Pizzirusso, L. Muccioli, C. Zannoni, M. Longeri, G. Celebre, G. De Luca, M. E. Di Pietro, Alignment of biphenyl in nematic and smectic liquid crystals. Comparing atomistic simulations and proton NMR experiments for 5CB and 8CB solutions, *in preparation*

[94] H. Flyvbjerg , H. G. Petersen, Error estimates on averages of correlated data, *J. Chem. Phys.*, 91, **1989**, 461-466

[95] G. Pileio, Ph.D. Thesis, Università della Calabria, Rende, Italy, **2005**

[96] P. Cairo, F. Ortuso, S. Alcaro, E. Fontananova, E. Tocci, E. Drioli, β-Cyclodextrin interactions with three drugs used in inflammatory pathologies: an experimental and theoretical study, *Chem. Phys. Lett.*, 454, **2008**, 374-381

[97] B. Luy, A. Frank, H. Kessler, Conformational analysis of drugs by nuclear magnetic resonance spectroscopy, in *Molecular Drug Properties. Measurement and Prediction*, R. Mannhold ed., Wiley-VCH Verlag GmbH & Co. KGaA, Weinheim, **2008**, chap. 9, ISBN: 9783527317554

[98] G. Kummerlöwe, B. Luy, Residual dipolar couplings as a tool in determining the structure of organic molecules, *Trends Anal. Chem.*, 28, **2009**, 483-493

[99] J. Yan, E. R. Zartler, Application of residual dipolar couplings in organic compounds, *Magn. Reson. Chem.*, 43, **2005**, 53-64

[100] P. Partington, J. Feeney, A. S. V. Burgen, The conformation of acetylcholine and related compounds in aqueous solutions as studied by nuclear magnetic resonance spectroscopy, *Mol. Pharmacol.*, 8, **1972**, 269-277

[101] T. H. Cerlie, S. E. Van-Rossum-Fikkert, W. J. Van Dijk, K. Brej, A. B. Smit, T. Sixma, Nicotine and carbamylcholine binding to nicotinic receptors as studied in AChBP crystal structures, *Neuron*, 41, **2004**, 907-914

[102] R. W. Behling, T. Yamane, G. Navon, L. W. Jelinski, Conformation of acetylcholine bound to the nicotinic acetylcholine receptor, *Proc. Natl. Acad. Sci. U.S.A.*, 85, **1988**, 6721-6724

[103] H. Furukawa, T. Hamada, M. K. Hayashi, T. Haga, Y. Muto, H. Hirota, S. Yokoyama, K. Nagasawa, M. Ishiguro, Conformation of ligands bound to the muscarinic acetylcholine receptor, *Mol. Pharmacol.*, 62, **2002**, 778-787

[104] N. N. Shestakova, E. V. Rozengart, A. E. Khovanskikh, B. S. Zhorov, V. A. Govyrin, Determination of productive conformations of acetylcholinesterase substrates using theoretical conformational analysis, *Bioorg. Khim.*, 15, **1989**, 335-344

[105] W. L. Smith, D. L. DeWitt, R. M. Garavito, Cyclooxygenase: structural, cellular, and molecular biology, *Annu. Rev. Biochem.*, 69, **2000**, 145-182

[106] J. R. Vane, Y. S. Bakhle, R. M. Botting, Cyclooxygenases 1 and 2, *Annu. Rev. Pharmacol. Toxicol.*, 38, **1998**, 97-120

[107] B. S. Selinsky, K. Gupta, C. T. Sharkey, P. J. Loll, Structural analysis of NSAID binding by prostaglandin H_2 synthase: time-dependent and time-independent inhibitors elicit identical enzyme conformations, *Biochemistry*, 40, **2001**, 5172-5180

[108] J. W. Emsley, P. Lesot, D. Merlet, The orientational order and conformational distributions of the two enantiomers in a racemic mixture of a chiral, flexible molecule dissolved in a chiral nematic liquid crystalline solvent, *Phys. Chem. Chem. Phys.*, 6, **2004**, 522-530

[109] J. W. Emsley, P. Lesot, J. Courtieu, D. Merlet, The effect of a chiral nematic solvent on the orientational order and conformational distribution of a flexible prochiral solute, *Phys. Chem. Chem. Phys.*, 6, **2004**, 5331-5337

[110] S. Fountoulaki, F. Perdih, I. Turel, D. P. Kessissoglou, G. Psomas, Non-steroidal anti-inflammatory drug diflunisal interacting with Cu(II). Structure and biological features, *J. Inorg. Biochem.*, 105, **2011**, 1645-1655

[111] T. N. Pham, S. A. Watson, A. J. Edwards, M. Chavda, J. S. Clawson, M. Strohmeier, F. G. Vogt, Analysis of amorphous solid dispersions using 2D solid-state NMR and [1]H T_1 relaxation measurements, *Mol. Pharm.*, 7, **2010**, 1667-1691

[112] J. Ghuman, P. A. Zunszain, I. Petitpas, A. A. Bhattacharya, M. Otagiri, S. Curry, Structural basis of the drug-binding specificity of human serum albumin, *J. Mol. Biol.*, 353, **2005**, 38-52

[113] H. G. Brittain, B. J. Elder, P. K. Isbester, A. H. Salerno, Solid-state fluorescence studies of some polymorphs of diflunisal, *Pharm. Res.*, 22, **2005**, 999-1006

[114] S. L. Adamski-Werner, S. K. Palaninathan, J. C. Sacchettini, J. W. Kelly, Diflunisal analogues stabilize the native state of transthyretin. Potent inhibition of amyloidogenesis, *J. Med. Chem.*, 47, **2004**, 355-374

[115] W. I. Cross, N. Blagden, R. J. Davey, A whole output strategy for polymorph screening: combining crystal structure prediction, graph set analysis, and targeted crystallization experiments in the case of diflunisal, *Cryst. Growth Des.*, 3, **2003**, 151-158

[116] R. Pignatello, M. Ferro, G. De Guidi, G. Salemi, M. A. Vandelli, S. Guccione, M. Geppi, C. Forte, G. Puglisi, Preparation, characterisation and photosensitivity studies of solid dispersions of diflunisal and Eudragit RS100[®] and RL100[®], *Int. J. Pharm.*, 218, **2001**, 27-42

[117] H. Mao, P. J. Hajduk, R. Craig, R. Bell, T. Borre, S. W. Fesik, Rational design of diflunisal analogues with reduced affinity for human serum albumin, *J. Am. Chem. Soc.*, 123, **2001**, 10429-10435

[118] U. H. N. Dürr, S. Afonin, B. Hoff, G. de Luca, J. W. Emsley, A. S. Ulrich, Alignment of druglike compounds in lipid bilayers analyzed by solid-state ^{19}F-NMR and molecular dynamics, based on dipolar couplings of adjacent CF$_3$ groups, *J. Phys. Chem. B*, 116, **2012**, 4769-4782

[119] S. L. Grage, U. H.N. Dürr, S. Afonin, P. K. Mikhailiuk, I. V. Komarov, A. S. Ulrich, Solid state ^{19}F NMR parameters of fluorine-labeled amino acids. Part II: aliphatic substituents, *J. Magn. Reson.*, 191, **2008**, 16-23

[120] S. L. Grage, J. Salgado, U. Dürr, S. Afonin, R. W. Glaser, A. S. Ulrich, Solid state ^{19}F-NMR of biomembranes, in *Perspectives on Solid State NMR in Biology, Focus on Structural Biology*, vol. 1, S. R. Kiihne and H. J. M. deGroot eds., Kluwer Academic Publishers, **2001**, chap. 8, ISBN: 9789048157440

[121] M. A. Danielson, J. J. Falke, Use of ^{19}F NMR to probe protein structure and conformational changes, *Annu. Rev. Biomol. Struct.*, 25, **1996**, 163-195

[122] F. Rastinejad, C. Evilia, P. Lu, Studies of nucleic acids and their protein interactions by ^{19}F NMR, *Methods Enzymol.*, 261, **1995**, 560-575

[123] J. T. Gerig, Fluorine NMR of proteins, *Prog. Nucl. Magn. Reson. Spectrosc.*, 26, **1994**, 293-370

[124] C. Thibaudeau, J. Plavec, J. Chattopadhyaya, A new generalized Karplus-type equation relating vicinal proton-fluorine coupling constants to H–C–C–F torsion angles, *J. Org. Chem.*, 63, **1998**, 4967-4984

[125] K. L. Williamson, Y.-F. Li, F. H. Hall, S. Swager, Dihedral angle and bond angle dependence of vicinal proton–fluorine spin–spin coupling, *J. Am. Chem. Soc.*, 88, **1966**, 5678-5680

[126] A. Solladié-Cavallo, L. Jierry, L. Bouérat, M. Schmitt, Conformation of tri- and tetra-substituted 2-fluoro cyclohexanones: proton non-equivalence, F–H and F–C coupling constants, conformational dependence of $^3J_{FH}$ and $^4J_{FH}$, *Tetrahedron*, 58, **2002**, 4195-4199

[127] Y. G. Gakh, A. A. Gakh, A. M. Gronenborn, Fluorine as an NMR probe for structural studies of chemical and biological systems, *Magn. Reson. Chem.*, 38, **2000**, 551-558

[128] A. V. Afonin, Through space spin–spin coupling [19]F–[1]H as the base for comparative analysis of conformational equilibrium in fluorine-substituted aryl vinyl selenides and sulfides, *Russ. J. Org. Chem.*, 46, **2010**, 1313-1316

[129] M. Hennig, M. L. Munzarová, W. Bermel, L. G. Scott, V. Sklenář, J. R. Williamson, Measurement of long-range [1]H–[19]F scalar coupling constants and their glycosidic torsion dependence in 5-fluoropyrimidine-substituted RNA, *J. Am. Chem. Soc.*, 128, **2006**, 5851-5858

[130] S. Jaime-Figueroa, L. J. Kurz, Y. Liu, R. Cruz, Synthesis and experimental study of through-space hydrogen–fluorine and carbon–fluorine spin–spin coupling in 4,5-substituted 1-acetyl-8-fluoronaphthalenes, *Spectrochim. Acta Part A*, 56, **2000**, 1167-1178

[131] J. Yan, F. Delaglio, A. Kaerner, A. D. Kline, H. Mo, M. J. Shapiro, T. A. Smitka, G. A. Stephenson, E. R. Zartler, Complete relative stereochemistry of multiple stereocenters using only residual dipolar couplings, *J. Am. Chem. Soc.*, 126, **2004**, 5008-5017

[132] B. Luy, J.-P. Marino, Measurement and application of [1]H-^{19}F dipolar couplings in the structure determination of 2'-fluorolabeled RNA, *J. Biomol. NMR*, 20, **2001**, 39-47

[133] M. E. Di Pietro, C. Aroulanda, D. Merlet, GET-SERF, a new gradient encoded SERF experiment for the trivial edition of [1]H-^{19}F couplings, *J. Magn. Reson.*, 234, **2013**, 101-105

[134] K. Müller, C. Faeh, F. Diederich, Fluorine in pharmaceuticals: looking beyond intuition, *Science*, 317, **2007**, 1881-1886

[135] K. L. Kirk, Selective fluorination in drug design and development: an overview of biochemical rationales, *Curr. Top. Med. Chem.*, 6, **2006**, 1447-1456

[136] J. P. Bégué, D. Bonnet-Delpon, Recent advances (1995–2005) in fluorinated pharmaceuticals based on natural products, *J. Fluor. Chem.*, 127, **2006**, 992-1012

[137] R. Filler, Y. Kobayashi, L. M. Yagupolskii, *Organofluorine Compounds in Medicinal Chemistry and Biomedical Applications*, Elsevier, Amsterdam, The Netherlands, **1993**, ISBN: 9780444897688

[138] K. L. Kirk, Fluorine in medicinal chemistry: recent therapeutic applications of fluorinated small molecules, *J. Fluor. Chem.*, 127, **2006**, 1013-1029

[139] K. Reichenbächer, H. I. Süss, J. Hulliger, Fluorine in crystal engineering - ''the little atom that could'', *Chem. Soc. Rev.*, 34, **2005**, 22-30

[140] F. Grein, Twist angles and rotational energy barriers of biphenyl and substituted biphenyls, *J. Phys. Chem. A*, 106, **2002**, 3823-3827

[141] A. Mazzanti, L. Lunazzi, R. Ruzziconi, S. Spizzichino, M. Schlosser, The torsional barriers of 2-hydroxy- and 2-fluorobiphenyl: small but measurable, *Chem. Eur. J.*, 16, **2010**, 9186-9192

[142] T. Fäcke, S. Berger, SERF, a new method for H,H spin-coupling measurement in organic chemistry, *J. Magn. Reson. Ser. A*, 113, **1995**, 114-116

[143] J. Farjon, D. Merlet, SERF-filtered experiments: new enantio-selective tools for deciphering complex spectra of racemic mixtures dissolved in chiral oriented media, *J. Magn. Reson.*, 210, **2011**, 24-30

[144] L. Beguin, N. Giraud, J. M. Ouvrard, J. Courtieu, D. Merlet, Improvements to selective refocusing phased (SERFph) experiments, *J. Magn. Reson.*, 199, **2009**, 41-47

[145] B. Baishya, U. R. Prabhu, N. Suryaprakash, Enantiomeric discrimination by double quantum excited selective refocusing (DQ-SERF) experiment, *J. Phys. Chem. B*, 111, **2007**, 12403-12410

[146] J. M. Nuzillard, Biselective refocusing pulses and the SERF experiment, *J. Magn. Reson.*, 187, **2007**, 193-198

[147] J. Farjon, L. Ziani, L. Beguin, D. Merlet, J. Courtieu, Selective NMR excitations in chiral analysis, *Annu. Rep. NMR*, 61, **2007**, 283-293

[148] L. Beguin, J. Courtieu, L. Ziani, D. Merlet, Simplification of the ^{1}H NMR spectra of enantiomers dissolved in chiral liquid crystals, combining variable angle sample spinning and selective refocusing experiments, *Magn. Reson. Chem.*, 44, **2006**, 1096-1101

[149] P. Nolis, A. Roglans, T. Parella, IFSERF, an isotope-filtered SERF experiment for the precise measurement of proton–proton coupling constants between chemically equivalent protons, *J. Magn. Reson.*, 173, **2005**, 305-309

[150] J. Farjon, D. Merlet, P. Lesot, J. Courtieu, Enantiomeric excess measurements in weakly oriented chiral liquid crystal solvents through 2D ^{1}H selective refocusing experiments, *J. Magn. Reson.*, 158, **2002**, 169-172

[151] R. Freeman, Shaped radiofrequency pulses in high resolution NMR, *Prog. Nucl. Magn. Res.*, 32, **1998**, 59-106

[152] H. Geen, R. Freeman, Band-selective radiofrequency pulses, *J. Magn. Reson.*, 93, **1991**, 93-141

[153] N. Nath, N. Suryaprakash, Spin-selective correlation experiment for measurement of long-range J couplings and for assignment of (R/S) enantiomers from the residual dipolar couplings and DFT, *J. Phys. Chem. B,* 115, **2011**, 6868-6875

[154] N. Nath, N. Suryaprakash, Enantiodiscrimination and extraction of short and long range homo- and hetero-nuclear residual dipolar couplings by a spin selective correlation experiment, *Chem. Phys. Lett.*, 496, **2010**, 175-182

[155] N. Nath, B. Baishya, N. Suryaprakash, Visualization of enantiomers using natural abundant ^{13}C-filtered single and double quantum selective refocusing experiments: application to small chiral molecules, *J. Magn. Reson.*, 200, **2009**, 101-108

[156] J. Farjon, J. P. Baltaze, P. Lesot, D. Merlet, J. Courtieu, Heteronuclear selective refocusing 2D NMR experiments for the spectral analysis of enantiomers in chiral oriented solvents, *Magn. Reson. Chem.*, 42, **2004**, 594-599

[157] A. Jegorov, P. Sedmera, V. Havlicek, M. Husak, S. Pakhomova, B. Kratochvil, M. Kuchar, P. Bulej, Spectroscopic and structural study of flobufen, *J. Fluorine Chem.*, 73, **1995**, 213-219

[158] M. Barfield, E. W. Della, P. E. Pigou, S. R. Walter, Nuclear spin–spin coupling via nonbonded interactions. Importance of bridgehead interactions on vicinal carbon-13–fluorine-19 and long-range proton–fluorine-19 coupling constants in 1-fluorobicycloalkanes, *J. Am. Chem. Soc.*, 104, **1982**, 3549-3552

[159] L. D. Hall, S. Sukumar, Applications of homonuclear two-dimensional *J* spectroscopy: an alternative to broad band heteronuclear and homonuclear decoupling, *J. Am. Chem. Soc.*, 101, **1979**, 3120-3121

[160] N. Giraud, L. Beguin, J. Courtieu, D. Merlet, Nuclear magnetic resonance using a spatial frequency encoding: application to *J*-edited spectroscopy along the sample, *Angew. Chem. Int. Ed.*, 49, **2010**, 3481-3484

[161] J. A. Aguilar, A. A. Colbourne, J. Cassani, M. Nilsson, G. A. Morris, Decoupling two-dimensional NMR spectroscopy in both dimensions: pure shift NOESY and COSY, *Angew. Chem. Int. Ed.*, 51, **2012**, 6460-6463

[162] D. Merlet, L. Beguin, J. Courtieu, N. Giraud, Spin–spin coupling edition in chiral liquid crystal NMR solvent, *J. Magn. Reson.*, 209, **2011**, 315-322

[163] A. Aguilar, S. Faulkner, M. Nilsson, G. A. Morris, Pure shift ^{1}H NMR: a resolution of the resolution problem?, *Angew Chem. Int. Ed.*, 49, **2010**, 3901-3903

[164] K. Zangger, H. Sterk, Observation of coupling across the ice–water interface by 2D time domain NMR, *J. Magn. Reson.*, 124, **1997**, 486-489

[165] M. Sarfati, P. Lesot, D. Merlet, J. Courtieu, Theoretical and experimental aspects of enantiomeric differentiation using natural abundance multinuclear nmr spectroscopy in chiral polypeptide liquid crystals, *Chem. Commun.*, **2000**, 2069-2081

[166] A. Meddour, P. Berdagué, A. Hedli, J. Courtieu, P. Lesot, Proton-decoupled carbon-13 NMR spectroscopy in a lyotropic chiral nematic solvent as an analytical tool for the measurement of the enantiomeric excess, *J. Am. Chem. Soc.*, 119, **1997**, 4502-4508

[167] P. Lesot, A. Meddour, J. Courtieu, A. Loewenstein, Visualization of enantiomers in a polypeptide liquid-crystal solvent through carbon-13 NMR spectroscopy, *J. Chem. Soc. Faraday Trans.*, 91, **1995**, 1371-1375

[168] D. Merlet, B. Ancian, J. Courtieu, P. Lesot, Two-dimensional deuterium NMR spectroscopy of chiral molecules oriented in a polypeptide liquid crystal: applications for the enantiomeric analysis through natural abundance deuterium NMR, *J. Am. Chem. Soc.*, 121, **1999**, 5249-5258

[169] D. Merlet, B. Ancian, W. Smadja, J. Courtieu, P. Lesot, Analysis of natural abundance deuterium NMR spectra of enantiomers in chiral liquid crystals *via* 2D auto-correlation experiments, *Chem. Commun.*, **1998**, 2301-2302

[170] J. W. Emsley, P. Lesot, G. De Luca, A. Lesage, D. Merlet, G. Pileio, A comparison of proton-detected ^{13}C local field experiments with deuterium NMR at natural abundance for studying liquid crystals, *Liq. Cryst.*, 35, **2008**, 443-464

[171] H. O. Kalinowski, S. Berger, S. Braun, *Carbon-13 NMR Spectroscopy*, John Wiley and Sons, Chichester, UK, **1988**, ISBN: 9780471913061

[172] J. W. Emsley, P. Lesot, G. De Luca, A. Lesage, D. Merlet, G. Pileio, The conformation and orientational order of a 1,2-disubstituted ethane nematogenic molecule (I22) in liquid crystalline and isotropic phases studied by NMR spectroscopy, *Phys. Chem. Chem. Phys.*, 12, **2010**, 2895-2914

[173] M. J. Frisch, G. W. Trucks, H. B. Schlegel, G. E. Scuseria, M. A. Robb, J. R. Cheeseman, G. Scalmani, V. Barone, B. Mennucci, G. A. Petersson, H. Nakatsuji, M. Caricato, X. Li, H. P. Hratchian, A. F. Izmaylov, J. Bloino, G. Zheng, J. L. Sonnenberg, M. Hada, M. Ehara, K. Toyota, R. Fukuda, J. Hasegawa, M. Ishida, T. Nakajima, Y. Honda, O. Kitao, H. Nakai, T. Vreven, J. A. Montgomery Jr., J. E. Peralta, F. Ogliaro, M. Bearpark, J. J. Heyd, E. Brothers, K. N. Kudin, V. N. Staroverov, R. Kobayashi, J. Normand, K. Raghavachari, A. Rendell, J. C. Burant, S. S. Iyengar, J. Tomasi, M. Cossi, N. Rega, J. M. Millam, M. Klene, J. E. Knox, J. B. Cross, V. Bakken, C. Adamo, J. Jaramillo, R. Gomperts, R. E. Stratmann, O. Yazyev, A. J. Austin, R. Cammi, C. Pomelli, J. W. Ochterski, R. L. Martin, K. Morokuma, V. G. Zakrzewski, G. A. Voth, P. Salvador, J. J. Dannenberg, S. Dapprich, A. D. Daniels, O. Farkas, J. B. Foresman, J. V. Ortiz, J. Cioslowski, D. J. Fox, *Gaussian 09, Revision A.02*, Gaussian, Inc., Wallingford CT, **2009**

[174] M. Cossi, G. Scalmani, N. Rega, V. Barone, New developments in the polarizable continuum model for quantum mechanical and classical calculations on molecules in solution, *J. Chem. Phys.*, 117, **2002**, 43-54

[175] A. Bondi, van der Waals volumes and radii, *J. Phys. Chem.*, 68, **1964**, 441-451

[176] M. F. Landoni, A. Soraci, Pharmacology of chiral compounds: 2-arylpropionic acid derivatives, *Curr. Drug Metab.*, 2, **2001**, 37-51

[177] A. M. Evans, Pharmacodynamics and pharmacokinetics of the profens: enantioselectivity, clinical implications, and special reference to S(+)-ibuprofen, *J. Clin. Pharmacol.*, 36, **1996**, 7S-15S

[178] P. J. Hayball, Chirality and nonsteroidal anti-inflammatory drugs, *Drugs*, 52, **1996**, 47-58

[179] W. F. Kean, C. J. L. Lock, J. Rischke, R. Butt, W. W. Buchanan, H. Howard-Lock, Effect of R and S enantiomers of naproxen on aggregation and thromboxane production in human platelets, *J. Pharm. Sci.*, 78, **1989**, 324-327

[180] A. Buttinoni, M. Ferrari, M. Colombo, R. Ceserani, Biological activity of indoprofen and its optical isomers, *J. Pharm. Pharmacol.*, 35, **1983**, 603-604

[181] S. S. Adams, P. Bresloff, C. G. Mason, Pharmacological differences between the optical isomers of ibuprofen: evidence for metabolic inversion of (2)-isomer, *J. Pharm. Pharmacol.*, 28, **1976**, 256-257

[182] Z. N. Gaut, H. Baruth, L. O. Randall, C. Ashley, J. R. Paulsrud, Stereoisomeric relationships among anti-inflammatory activity, inhibition of platelet aggregation, and inhibition of prostaglandin synthetase, *Prostaglandins*, 10, **1975**, 59-66

[183] T. Konishi, H. Nishikawa, S. Kitamura, K. Tatsumi, *In vivo* studies on chiral inversion and amino acid conjugation of 2-[4-(3-methyl-2-thienyl)phenyl]propionic acid in rats and dogs, *Drug Metab. Dispos.*, 27, **1999**, 158-60

[184] M. A. Shirley, X. Guan, D. G. Kaiser, G. W. Halstead, T. A. Baillie, Taurine conjugation of ibuprofen in humans and in rat liver in vitro: relationship to metabolic chiral inversion, *J. Pharmacol. Exp. Ther.*, 269, **1995**, 1166-1175

[185] T. A. Baillie, W. J. Adams, D. G. Kaiser, L. S. Olanoff, G. W. Halstead, H. Harpootlian, G. J. V. Glessen, Mechanistic studies of the metabolic chiral inversion of (R)-ibuprofen in humans, *J. Pharmacol. Exp. Ther.*, 249, **1989**, 517-523

[186] J. Caldwell, A. J. Hutt, S. Fournel-Gigleux, The metabolic chiral inversion and dispositional enantioselectivity of the 2-arylpropionic acids and their biological consequences, *Biochem. Pharmacol.*, 37, **1988**, 105-114

[187] T. Yamaguchi, Y. Nakamura, Stereoselective metabolism of 2-phenylpropionic acid in rat. II. Studies on the organs responsible for the optical isomerization of 2-phenylpropionic acid in rat *in vivo*, *Drug Metab. Dispos.*, 15, **1987**, 535-539

[188] I. K. Reza, R. Mehvar, *Chirality in Drug Design and Development*, CRC Press, **2004**, ISBN: 9780824750626

[189] G. Leising, R. Resel, F. Stelzer, S. Tasch, A. Lanziner, G. Hantich, Physical aspects of dexibuprofen and racemic ibuprofen, *J. Clin. Pharmacol.*, 36, **1996**, 3S-6S

[190] S. R. Cox, E. P. Gall, K. K. Forbes, M. Gresham, G. Goris, Pharmacokinetics of the R(-) and S(+) enantiomers of ibuprofen in the serum and synovial fluid of arthritis patients. *J. Clin. Pharmacol.*, 31, **1991**, 88-94

[191] A. M. Evans, R. L. Nation, L. N. Sansom, F. Bochner, A. A. Somogyi, Stereoselective plasma protein binding of ibuprofen enantiomers, *Eur. J. Clin. Pharmacol.*, 36, **1989**, 283-290

[192] K. Williams, R. Day, R. Knihinicki, A. Duffield, The stereoselective uptake of ibuprofen enantiomers into adipose tissue, *Biochem. Pharmacol.*, 35, **1986**, 3403-3405

[193] E. J. D. Lee, K. M. Williams, R. O. Day, G. Graham, D. Champion, Stereoselective disposition of ibuprofen enantiomers in man, *Br. J. Clin. Pharmacol.*, 19, **1985**, 669-674

[194] K. Tanaka, Y. Nakai, H. Takahashi, Efficient NMR chiral discrimination of carboxylic acids using rhombamine macrocycles as chiral shift reagent, *Tetrahedron: Asymmetry*, 22, **2011**, 178-184

[195] N. H. Hashim, S. J. Khan, Enantioselective analysis of ibuprofen, ketoprofen and naproxen in wastewater and environmental water samples, *J. Chromatogr. A*, 1218, **2011**, 4746-4754

[196] L. H. Steenkamp, D. Brady, Decision making in the development of a biocatalytic route for resolution of S-naproxen: from screening to scale-up, *Current research, Technology and Education Topics in Applied Microbiology and Microbial Biotechnology*, 2, **2010**, 980-987

[197] H. Luna, A. Pacheco, A. Solís, H. I. Pérez, N. Manjarrez, J. Cassani, Study towards the improvement of the enantioselective hydrolysis of naproxen esters by sheep liver acetone powder, *J. Biotech. Res.*, 1, **2009**, 21-27

[198] L. O. Healy, J. P. Murrihy, A. Tan, D. Cocker, M. McEnery, J. D. Glennon, Enantiomeric separation of R,S-naproxen by conventional and nano-liquid chromatography with methyl-β-cyclodextrin as a mobile phase additive, *J. Chromatogr. A*, 924, **2001**, 459-464

[199] N. Layh, A. Stolz, J. Böhme, F. Effenberger, H.-J. Knackmuss, Enantioselective hydrolysis of racemic naproxen nitrile and naproxen amide to S-naproxen by new bacteria isolates, *J. Biotechnol.*, 33, **1994**, 175-182

[200] K. C. Duggan, D. J. Hermanson, J. Musee, J. Prusakiewicz, J. L. Scheib, B. D. Carter, S. Banerjee, J. A. Oates, L. J. Marnett, (*R*)-Profens are substrate-selective inhibitors of endocannabinoid oxygenation by COX-2, *Nat. Chem. Biol.*, 7, **2011**, 803-809

[201] K. C. Duggan, M. J. Walters, J. Musee, J. M. Harp, J. R. Kiefer, J. A. Oates, L. J. Marnett, Molecular basis for cyclooxygenase inhibition by the non-steroidal anti-inflammatory drug naproxen, *J. Biol. Chem.*, 285, **2010**, 34950-34959

[202] N. Okulik, A. H. Jubert, Theoretical study on the structure and reactive sites of three non-steroidal anti-inflammatory drugs: ibuprofen, naproxen and tolmetin acids, *J. Mol. Struct.: Theochem*, 769, **2006**, 135-141

[203] Y. G. Smeyers, L. Bouniama, N. J. Smeyersa, A. Ezzamarty, A. Hernandez-Laguna, C. I. Sainz-Diaz, Quantum mechanical and QSAR study of some α-arylpropionic acids as anti-inflammatory agents, *Eur. J. Med. Chem.*, 33, **1998**, 103-112

[204] R. A. Appleton, K. Brown, Conformational requirements at the prostaglandin cyclooxygenase receptor site: a template for designing non steroidal anti inflammatory drugs, *Prostaglandins*, 18, **1979**, 29-34

[205] B. Luy, Distinction of enantiomers by NMR spectroscopy using chiral orienting media, *J. Indian Inst. Sci.*, 90, **2010**, 119-132

[206] B. Böttcher, V. Schmidts, J. A. Raskatov, C. M. Thiele, Determination of the conformation of the key intermediate in an enantioselective palladium-catalyzed allylic substitution from residual dipolar couplings, *Angew. Chem. Int. Ed.*, 49, **2010**, 205-209

[207] A. Solgadi, L. Jean, M.-C. Lasne, J. Rouden, J. Courtieu, A. Meddour, NMR in chiral polypeptide liquid crystals: the problem of amines, *Tetrahedron: Asymmetry*, 18, **2007**, 1511-1516

[208] M. Rivard, F. Guillen, J.-C. Fiaud, C. Aroulanda, P. Lesot, Efficient enantiodiscrimination of chiral monophosphine oxides and boranes by phosphorus coupled ^{13}C NMR spectroscopy in the presence of chiral ordering agents, *Tetrahedron: Asymmetry*, 14, **2003**, 1141-1152

[209] C. Aroulanda, V. Boucard, F. Guibé, J. Courtieu, D. Merlet, Weakly oriented liquid-crystal NMR solvents as a general tool to determine relative configurations, *Chem. Eur. J.*, 9, **2003**, 4536-4539

[210] P. Lesot, M. Sarfati, J. Courtieu, Natural abundance deuterium NMR spectroscopy in polypeptide liquid crystals as a new and incisive means for the enantiodifferentiation of chiral hydrocarbons, *Chem. Eur. J.*, 9, **2003**, 1724-1745

[211] C. Aroulanda, M. Sarfarti, J. Courtieu, P. Lesot, Investigation of the enantioselectivity of three polypeptide liquid-crystalline solvents using NMR spectroscopy, *Enantiomer*, 6, **2001**, 281-287

[212] M. Sarfati, J. Courtieu, P. Lesot, First successful enantiomeric discrimination of chiral alkanes using NMR spectroscopy, *Chem. Commun.*, **2000**, 1113-1114

[213] A. P. Roszkowski, W. H. Rooks II, A. J. Tomolins, L. M. Miller, Antiinflamatory and analgetic propierties of *d*-2-(6'-methoxy-2'-naphtyl)-propionic acid (Naproxen), *J. Pharmacol. Exp. Ther.*, 179, **1971**, 114-123

[214] U. A. Boelsterli, H. J. Zimmerman, A. Kretz-Rommel, Idiosyncratic liver toxicity of nonsteroidal antiinflammatory drugs: molecular mechanisms and pathology, *Crit. Rev. Toxicol.*, 25, **1995**, 207-235

[215] R. A. Sheldon, *Chirotechnology: industrial synthesis of optically active compounds*, Taylor & Francis, **1993**, ISBN: 9780824791438

[216] Y. B. Kim, I. Y. Park, W. R. Lah, The crystal structure of naproxen sodium, ($C_{14}H_{13}O_3Na$), *Arch. Pharm. Res.*, 13, **1990**, 166-173

[217] Y. B. Kim, H. J. Song, I. Y. Park, Refinement of the structure of naproxen, (+)-6-methoxy-α-methyl-2-naphthaleneacetic acid, *Arch. Pharm. Res.*, 10, **1987**, 232-238

[218] K. Ravikumar, S. S. Rajan, V. Pattabhi, E. J. Gabe, Structure of naproxen, $C_{14}H_{14}O_3$, *Acta Crystallogr., Sect. C: Cryst. Struct. Commun.*, 41, **1985**, 280-282

[219] Y. B. Kim, H. J. Song, The molecular structure of (+)-6-methoxy-α-methyl-2-naphthaleneacetic acid determined by X-ray method, *Arch. Pharm. Res.*, 7, **1984**, 137-139

[220] D. E. Braun, M. Ardid-Candel, E. D'Oria, P. G. Karamertzanis, J.-B. Arlin, A. J. Florence, A. G. Jones, S. L. Price, Racemic naproxen: a multidisciplinary structural and thermodynamic comparison with the enantiopure form, *Cryst. Growth Des.*, 11, **2011**, 5659-5669

[221] N. Sadlej-Sosnowska, L. Kozerski, E. Bednarek, J. Sitkowski, Fluorometric and NMR studies of the naproxen–cyclodextrin inclusion complexes in aqueous solutions, *J. Inclusion Phenom. Mol. Recognit. Chem.*, 37, **2000**, 383-394

[222] G. Bettinetti, M. Sorrenti, A. Negri, M. Setti, P. Mura, F. Melani, Interaction of naproxen with alpha-cyclodextrin and its noncyclic analog maltohexaose, *Pharm. Res.*, 16, **1999**, 689-694

[223] S. P. Van Helden, M. J. Van Drooge, A. J. Claessens, A. C. A. Jansen, L. H. Janssen, A molecular modelling study of the distortion of α-cyclodextrin (cyclomaltohexaose) in complexes with guest molecules, *Carbohydr. Res.*, 215, **1991**, 251-260

[224] F. Römer, T. Kraska, A force field for naproxen, *Mol. Simulat.*, 38, **2012**, 152-160

[225] E. Bednarek, W. Bocian, J. Cz. Dobrowolski, L. Kozerski, N. Sadlej-Sosnowska, J. Sitkowski, The conformation of the naproxen anion studied by ^{1}H NMR and theoretical methods, *J. Mol. Struct.*, 559, **2001**, 369-377

[226] A. Bax, R. Freeman, Long-range proton-carbon-13 NMR spin coupling constants, *J. Am. Chem. Soc.*, 104, **1982**, 1099-1100

[227] Release 8.0.3 for Windows, Copyright © **2007** Hypercube, Inc.

[228] Gaussian 03, Revision C.02, M. J. Frisch, G. W. Trucks, H. B. Schlegel,G. E. Scuseria, M.A. Robb, J. R. Cheeseman, J. A. Montgomery Jr., T. Vreven, K. N. Kudin, J. C. Burant, J. M. Millam, S. S. Iyengar, J. Tomasi, V. Barone, B. Mennucci, M. Cossi, G. Scalmani, N. Rega, G. A. Petersson, H. Nakatsuji, M. Hada, M. Ehara, K. Toyota, R. Fukuda, J. Hasegawa, M. Ishida, T. Nakajima, Y. Honda, O. Kitao, H. Nakai, M. Klene, X. Li, J. E. Knox, H. P. Hratchian, J. B. Cross, C. Adamo, J. Jaramillo, R. Gomperts, R. E. Stratmann, O. Yazyev, A. J. Austin, R. Cammi, C. Pomelli, J. W. Ochterski, P. Y. Ayala, K. Morokuma, G. A. Voth, P. Salvador, J. J. Dannenberg, V. G. Zakrzewski, S. Dapprich, A. D. Daniels, M. C. Strain, O. Farkas, D. K. Malick, A. D. Rabuck, K. Raghavachari, J. B. Foresman, J. V. Ortiz, Q. Cui, A. G. Baboul, S. Clifford, J. Cioslowski, B. B. Stefanov, G. Liu, A. Liashenko, P. Piskorz, I. Komaromi, R. L. Martin, D. J. Fox, T. Keith, M. A. Al-Laham, C. Y. Peng, A. Nanayakkara, M. Challacombe, P. M. W. Gill, B. Johnson, W. Chen, M. W. Wong, C. Gonzalez, J. A. Pople, Gaussian, Inc., Pittsburgh PA, **2003**

[229] T. Troxler, S_1–S_0 Electronic spectroscopy and *ab initio* calculations of *cis*-2-methoxynaphthalene, *J. Phys. Chem. A*, 102, **1998**, 4775-4787

[230] D. C. Spellmeyer, P. D. J. Grootenhuis, M. D. Miller, L. F. Kuyper, P. A. Kollman, Theoretical investigations of the rotational barrier in anisole: an *ab initio* and molecular dynamics study, *J. Phys. Chem.*, 94, **1990**, 4483-4491

[231] M. A. Vincent, I. H. Hillier, A theoretical study of methoxy group rotation in anisole, *Chem. Phys.*, 140, **1990**, 35-40

[232] T. Schaefer, G. H. Penner, Long-range ^{13}C,[13]C spin-spin coupling constants in anisole and some derivatives, *Can. J. Chem.*, 66, **1988**, 1635-1640

[233] R. H. Contreras, R. R. Biekofsky, D. G. De Kowalewski, A. M. Orendt, J. C. Facelli, Effects of electronic resonance interaction on methoxy group NMR parameters: theoretical and experimental study of substituted 2-methoxypyridines, *J. Phys. Chem.*, 97, **1993**, 91-93

[234] R. R. Biekofsky, A. B. Pomilio, R. A. Aristegui, R. H. Contreras, A ^{13}C NMR and AM1 study on intramolecular interactions defining the methoxy group conformation in unhindered anisole derivatives, *J. Mol. Struct.*, 344, **1995**, 143-150

[235] L. I. Kruse, C. W. DeBrosse, C. H. Kruse, Study of aromatic functional group conformations in solution by nuclear Overhauser enhancement and relaxation techniques: detection of .pi.-electron density and correlation with chemical reactivity, *J. Am. Chem. Soc.*, 107, **1985**, 5435-5442

[236] K. Löbmann, R. Laitinen, H. Grohganz, C. Strachan, T. Rades, K. C. Gordon, A theoretical and spectroscopic study of co-amorphous naproxen and indomethacin, *Int. J. Pharm.*, 453, **2013**, 80-87

[237] M. M. Velazquez, M. Valero, L. J. Rodriguez, S. M. B. Costa, M. A. Santos, Hydrogen bonding in a non-steroidal anti-inflammatory drug - Naproxen, *J. Photochem. Photobiol. B: Biol.*, 29, **1995**, 23-31

[238] F. Lahmani, K. Le Barbu-Debus, N. Seurre, A. Zehnacker-Rentien, Laser spectroscopy of a chiral drug in a supersonic beam: conformation and complexation of *S*-(+)-naproxen, *Chem. Phys. Lett.*, 375, **2003**, 636-644

[239] C. Rivière, A. D. Pawlusa, J.-M. Mérillon, Natural stilbenoids: distribution in the plant kingdom and chemotaxonomic interest in Vitaceae, *Nat. Prod. Rep.*, 29, **2012**, 1317-1333

[240] M. Okasaka, Y. Takaishi, K. Kogure, K. Fuzukawa, H. Shibata, T. Higuti, G. Honda, M. Ito, O. K. Kodzhimotov, O. Ashurmetov, New stilbene derivatives from *Calligonum leucocladum*, *J. Nat. Prod.*, 67, **2004**, 1044-1046

[241] J. Harmatha, L. Dinan, Biological activities of lignans and stilbenoids associated with plant-insect chemical interactions, *Phytochem. Rev.*, 2, **2003**, 321-330

[242] E. N. Frankel, A. L. Waterhouse, J. E. Kinsella, Inhibition of human LDL oxidation by resveratrol, *Lancet*, 341, **1993**, 1103-1104

[243] H. Piotrowska, M. Kucinska, M. Murias, Biological activity of piceatannol: leaving the shadow of resveratrol, *Mutat. Res.*, 750, **2012**, 60-82

[244] O. P. Mgbonyebi, J. Russo, I. H. Russo, Antiproliferative effect of synthetic resveratrol on human breast epithelial cells, *Int. J. Oncol.*, 12, **1998**, 865-869

[245] M.-V. Clément, J. L. Hirpara, S.-H. Chawdhury, S. Pervaiz, Chemopreventive agent resveratrol, a natural product derived from grapes, triggers CD95 signaling-dependent apoptosis in human tumor cells, *Blood*, 92, **1998**, 996-1002

[246] M. MacCarrone, T. Lorenzon, P. Guerrieri, A. Finazzi Agrò, Resveratrol prevents apoptosis in K562 cells by inhibiting lipoxygenase and cyclooxygenase activity, *Eur. J. Biochem.*, 265, **1999**, 27-34

[247] J. L. Bowers, V. V. Tyulmenkov, S. C. Jernigan, C. M. Klinge, Resveratrol acts as a mixed agonist/antagonist for estrogen receptors α and β, *Endocrinology*, 141, **2000**, 3657-3667

[248] B. Olas, B. Wachowicz, Resveratrol, a phenolic antioxidant with effects on blood platelet functions, *Platelets*, 16, **2005**, 251-260

[249] T. A. Aburjai, Anti-platelet stilbenes from aerial parts of *Rheum palaestinum*, *Phytochemistry*, 55, **2000**, 407-410

[250] S. K. Ko, S. M. Lee, W. K. Whang, Anti-platelet aggregation activity of stilbene derivatives from *Rheum undulatum*, *Arch. Pharm. Res.*, 22, **1999**, 401-403

[251] N. Kim, J. K. Kim, D. Hwang, Y. H. Lim, The possible mechanism of rhapontigenin influencing antifungal activity on Candida albicans, *Med. Mycol.*, 51, **2013**, 45-52

[252] H. Matsuda, N. Tomohiro, K. Hiraba, S. Harima, S. Ko, K. Matsuo, M. Yoshikawa, M. Kubo, Study on anti-Oketsu activity of rhubarb II. Anti-allergic effects of stilbene components from rhei undulati rhizoma (dried rhizome of *Rheum undulatum* cultivated in Korea), *Biol. Pharm. Bull.*, 24, **2001**, 264-267

[253] İ. Gülçin, Antioxidant properties of resveratrol: a structure-activity insight, *Innov. Food Sci. Emerg. Technol.*, 11, **2010**, 210-218

[254] A. N. Queiroz, B. A.Q. Gomes, W. M. Moraes Jr., R. S. Borges, A theoretical antioxidant pharmacophore for resveratrol, *Eur. J. Med. Chem.*, 44, **2009**, 1644-1649

[255] G. A. Locatelli, M. Savio, L. Forti, I. Shevelev, K. Ramadan, L. A. Stivala, V. Vannini, U. Hübscher, S. Spadari, G. Maga, Inhibition of mammalian DNA polymerases by resveratrol: mechanism and structural determinants, *Biochem. J.*, 389, **2005**, 259-268

[256] L. M. Szewczuk, L. Forti, L. A. Stivala, T. M. Penning, Resveratrol is a peroxidase-mediated inactivator of COX-1 but not COX-2: a mechanistic approach to the design of COX-1 selective agents, *J. Biol. Chem.*, 279, **2004**, 22727-22737

[257] L. Frémont, Minireview: biological effects of resveratrol, *Life Sci.*, 66, **2000**, 663-673

[258] G. J. Fan, X. D. Liu, Y. P. Qian, Y. J. Shang, X. Z. Li, F. Dai, J. G. Fang, X. L. Jin, B. Zhou, 4,4'-dihydroxy-*trans*-stilbene, a resveratrol analogue, exhibited enhanced antioxidant activity and cytotoxicity, *Bioorg. Med. Chem.*, 17, **2009**, 2360-2365

[259] M. Savio, T. Coppa, L. Bianchi, V. Vannini, G. Maga, L. Forti, O. Cazzalini, M. C. Lazzè, P. Perucca, E. Prosperi, L. A. Stivala, The resveratrol analogue 4,4'-dihydroxy-*trans*-stilbene inhibits cell proliferation with higher efficiency but different mechanism from resveratrol, *Int. J. Biochem. Cell Biol.*, 41, **2009**, 2493-2502

[260] B. Billack, V. Radkar, C. Adiabouah, *In vitro* evaluation of the cytotoxic and antiproliferative properties of resveratrol and several of its analogs, *Cell. Mol. Biol. Lett.*, 13, **2008**, 553-569

[261] L. F. Zheng, Q. Y. Wei, Y. J. Cai, J. G. Fang, B. Zhou, L. Yang, Z. L. Liu, DNA damage induced by resveratrol and its synthetic analogues in the presence of Cu (II) ions: mechanism and structure-activity relationship, *Free Radic. Biol. Med.*, 41, **2006**, 1807-1816

[262] Y.-J. Cai, J.-G. Fang, L.-P. Ma, L. Yang, Z.-L. Liu, Inhibition of free radical-induced peroxidation of rat liver microsomes by resveratrol and its analogues, *Biochim. Biophys. Acta*, 1637, **2003**, 31-38

[263] K. S. Korach, M. Metzlert, J. A. McLachlan, Estrogenic activity *in vivo* and *in vitro* of some diethylstilbestrol metabolites and analogs, *Proc. Natl. Acad. Sci. USA*, 75, **1978**, 468-471

[264] S. Rotondo, G. Rajtar, S. Manarini, A. Celardo, D. Rotilio, G. de Gaetano, V. Evangelista, C. Cerletti, Effect of *trans*-resveratrol, a natural polyphenolic compound, on human polymorphonuclear leukocyte function, *Br. J. Pharmacol.*, 123, **1998**, 1691-1699

[265] Y. Kimura, H. Okuda, S. Arichi, Effects of stilbenes on arachidonate metabolism in leukocytes, *Biochim. Biophys. Acta*, 834, **1985**, 275-278

[266] N. L. Kerry, M. Abbey, Red wine and fractionated phenolic compounds prepared from red wine inhibit low density lipoprotein oxidation *in vitro*, *Atherosclerosis*, 135, **1997**, 93-102

[267] C. R. Pace-Asciak, O. Rounova, S. Hahn, E. P. Diamandis, D. M. Goldberg, Wines and grape juices as modulators of platelet aggregation in healthy human subjects, *Clin. Chim. Acta*, 246, **1996**, 163-182

[268] C. R. Pace-Asciak, S. Hahn, E. P. Diamandis, G. Soleas, D. M. Goldberg, The red wine phenolics *trans*-resveratrol and quercetin block human platelet aggregation and eicosanoid synthesis: implications for protection against coronary heart disease, *Clin. Chim. Acta*, 235, **1995**, 207-219

[269] J. C. Milne, P. D. Lambert, S. Schenk, D. P. Carney, J. J. Smith, D. J. Gagne, L. Jin, O. Boss, R. B. Perni, C. B. Vu, J. E. Bemis, R. Xie, J. S. Disch, P. Yeeng, J. J. Nunes, A. V. Lynch, H. Yang, H. Galonek, K. Israelian, W. Choy, A. Iffland, S. Lavu, O. Medvedik, D. A. Sinclair, J. M. Olefsky, M. R. Jirousek, P. J. Elliott, C. H. Westphal, Small molecule activators of SIRT1 as therapeutics for the treatment of type 2 diabetes, *Nature*, 450, **2007**, 712-716

[270] F. Belluti, G. Fontana, L. Dal Bo, N. Carenini, C. Giommarelli, F. Zunino, Design, synthesis and anticancer activities of stilbene-coumarin hybrid compounds: identification of novel proapoptotic agents, *Bioorgan. Med. Chem.*, 18, **2010**, 3543-3550

[271] K. V. Balan, Y. Wang, S. W. Chen, J.-C. Chen, L.-F. Zheng, L. Yang, Z.-L. Liu, P. Pantazis, J. H. Wyche, Z. Han, Proteasome-independent down-regulation of estrogen receptor-α (ERα) in breast cancer cells treated with 4,4'-dihydroxy-*trans*-stilbene, *Biochem. Pharmacol.*, 72, **2006**, 573-581

[272] S. Kim, S. Y. Min, S. K. Lee, W.-J. Cho, Comparative molecular field analysis study of stilbene derivatives active against A549 lung carcinoma, *Chem. Pharm. Bull.,* 51, **2003**, 516-521

[273] K. P. L. Bhat, D. Lantvit, K. Christov, R. G. Mehta, R. C. Moon, J. M. Pezzuto, Estrogenic and antiestrogenic properties of resveratrol in mammary tumor models, *Cancer Res.*, 61, **2001**, 7456-7463

[274] T. Hsieh, J. W. Wu, Differential effects on growth, cell cycle arrest, and induction of apoptosis by resveratrol in human prostate cancer cell lines, *Exp. Cell. Res.*, 249, **1999**, 109-115

[275] M. Jang, L. Cai, G. O. Udeani, K. V. Slowing, C. F. Thomas, C. W. W. Beecher, H. H. Fong, N. R. Farnsworth, A. D. Kinghorn, R. G. Mehta, R. C. Moon, J. M. Pezzuto, Cancer chemopreventive activity of resveratrol, a natural product derived from grapes, *Science*, 275, **1997**, 218-220

[276] M. C. Hong, Y. K. Kim, J. Y. Choi, S. Q. Yang, H. Rhee, Y. H. Ryu, T. H. Choi, G. J. Cheon, G. I. An, H. Y. Kim, Y. Kim, D. J. Kim, J.-S. Lee, Y.-T. Chang, K. C. Lee, Synthesis and evaluation of stilbene derivatives as a potential imaging agent of amyloid plaques, *Bioorg. Med. Chem.*, 18, **2010**, 7724-7730

[277] X. Chen, QSAR and primary docking studies of *trans*-stilbene (TSB) series of imaging agents for β-amyloid plaques, *J. Mol. Struct.: Theochem.*, 763, **2006**, 83-89

[278] A. Ravikrishnan, P. Sudhakara, P. Kannan, Stilbene-based liquid crystalline and photocrosslinkable polynaphthylphosphate esters, *J. Mater. Sci.*, 45, **2010**, 435-442

[279] S. Buathong, L. Gehringer, B. Donnio, D. Guillon, Supramolecular organization of dendritic supermolecules into liquid crystalline mesophases, *C. R. Chimie*, 12, **2009**, 138-162

[280] L. Zoppi, A. Calzolari, A. Ruini, A. Ferretti, M. Caldas, Defect-induced effects on carrier migration through one-dimensional poly(*para*-phenylenevinylene) chains, *Phys. Rev. B*, 78, **2008**, 165204.1-6

[281] V. Papper, G. I. Likhtenshtein, Substituted stilbenes: a new view on well-known systems. New applications in chemistry and biophysics, *J. Photochem. Photobiol. A*, 140, **2001**, 39-52

[282] E. C. Buruiana, M. Zamfir, T. Buruiana, Synthesis, characterization and fluorescence study of new polyacrylates containing stilbene, *Eur. Polym. J.*, 43, **2007**, 4316-4324

[283] I. Tomatsu, K. Peng, A. Kros, Photoresponsive hydrogels for biomedical applications, *Adv. Drug Delivery Rev.*, 63, **2011**, 1257-1266

[284] F. Meng, Z. Zhong, J. Feijen, Stimuli-responsive polymersomes for programmed drug delivery, *Biomacromolecules*, 10, **2009**, 197-209

[285] M. Tachon, E. Davies, M. Lamotte, K. A. Muszkat, T. Wismontski-Knittel, Shpolskii spectra of *trans*-1,2-di(2'-pyridyl)ethylene. Identification and evidence for almost planar structure and π type HMO for the trapped rotamer, *J. Phys. Chem.*, 98, **1994**, 11870-11877

[286] K. Ogawa. T. Sano. S. Yoshimura, Y. Takeuchi, K. J. Toriumi, Molecular structure and intramolecular motion of (*E*)-stilbenes in crystals. An interpretation of the unusually short ethylene bond, *J. Am. Chem. Soc.*, 114, **1992**, 1041-1051

[287] J. A. Bouwstra, A. Schouten, J. Kroon, Structural studies of the system *trans*-azobenzene/*trans*-stilbene. II. A reinvestigation of the disorder in the crystal structure of *trans*-stilbene, $C_{14}H_{12}$, *Acta Crystallogr. C*, 40, **1984**, 428-431

[288] J. Bernstein, Refinement of *trans*-stilbene: a comparison of two crystallographic studies, *Acta Crystallogr. B*, 31, **1975**, 1268-1271

[289] A. Hoekstra, P. Meertens, A. Vos, Refinement of the crystal structure of *trans*-stilbene (TSB). The molecular structure in the crystalline and gaseous phases, *Acta Crystallogr. B*, 31, **1975**, 2813-2817

[290] C. J. Finder, M. G. Newton, N. L. Allinger, An improved structure of *trans*-stilbene, *Acta Crystallogr. B*, 30, **1974**, 411-415

[291] J. M. Robertson, I. Woodward, X-ray analysis of the dibenzyl series. IV. Detailed structure of stilbene, *Proc. R. Soc. London Ser. A.*, 162, **1937**, 568-583

[292] W.-Y. Chiang, J. Laane, Fluorescence spectra and torsional potential functions for *trans*-stilbene in its S_0 and S_1 (π, π*) electronic states, *J. Chem. Phys.*, 100, **1994**, 8755-8767

[293] B. B. Champagne, J. F. Pfanstiel, D. F. Plusquellic, D. W. Pratt, W. M. van Herpen, W. L. Meerts, *trans*-Stilbene: a rigid, planar asymmetric top in the zero-point vibrational levels of its S_0 and S_1 electronic states, *J. Phys. Chem.*, 94, **1990**, 6-8

[294] J. S. Baskin, A. H. Zewail, Determination of excited-state rotational constants and structures by Doppler-free picosecond spectroscopy, *J. Phys. Chem.*, 93, **1989**, 5701-5717

[295] L. H. Spangler, R. van Zee, S. C. Blankespoor, T. S. Zwier, Additional evidence for planarity in isolated *trans*-stilbene: a study of α-deuterio-*trans*-stilbene, *J. Phys. Chem.*, 91, **1987**, 6077-6079

[296] L. H. Spangler, R. van Zee, T. S. Zwier, Assignment of the low-frequency modes in *trans*-stilbene. Evidence for planarity in the isolated molecule, *J. Phys. Chem.*, 91, **1987**, 2782-2786

[297] J. S. Baskin, P. M. Felker, A. H. Zewail, Purely rotational coherence effect and time-resolved sub-Doppler spectroscopy of large molecules. II. Experimental, *J. Chem. Phys.*, 86, **1987**, 2483-2499

[298] T. Suzuki, N. Mikami, M. Ito, Two-color stimulated emission spectroscopy of *trans*-stilbene: large amplitude torsional motion in the ground state and its role in intramolecular vibrational redistribution, *J. Phys. Chem.*, 90, **1986**, 6431-6440

[299] A. B. Myers, M. O. Trulson, R. A. Mathies, Quantitation of homogeneous and inhomogeneous broadening mechanisms in *trans*-stilbene using absolute resonance Raman intensities, *J. Chem. Phys.*, 83, **1985**, 5000-5006

[300] P. Rademacher, A. L. Marzinzik, K. Kowski, M. E. Weiß, Photoelectron spectra, electronic structures, and conformational properties of (*E*)-stilbene, styrylthiophenes, and (thienylethenyl)pyridines, *Eur. J. Org. Chem.*, **2001**, 121-130

[301] J. A. Syage, P. M. Felker, A. H. Zewail, Picosecond dynamics and photoisomerization of stilbene in supersonic beams. I. Spectra and mode assignments, *J. Chem. Phys.*, 81, **1984**, 4685-6440

[302] T. Kobayashi, H. Suzuki, K. Ogawa, Conformational analysis of stilbenes by photoelectron spectroscopy, *Bull. Chem. Soc. Jpn.*, 55, **1982**, 1734-1738

[303] M. Traetteberg, E. B. Frantsen, F. C. Mijlhoff, A. Hoekstra, A gas electron diffraction study of the molecular structure of *trans*-stilbene, *J. Mol. Struct.*, 26, **1975**, 57-68

[304] P. D. Chowdary, T. J. Martinez, M. Gruebele, The vibrationally adiabatic torsional potential energy surface of *trans*-stilbene, *Chem. Phys. Lett.*, 440, **2007**, 7-11

[305] J. Catalán, On the non-planarity of *trans*-stilbene, *Chem. Phys. Lett.*, 421, **2006**, 134-137

[306] M. L. Freile, S. Risso, A. Curaqueso, M. A. Zamora, R. D. Enriz, *Ab initio* conformational study of vinylogues. 2-Butene, stilbene and their conjugated polyenes, *J. Mol. Struct.: Theochem.*, 731, **2005**, 107-114

[307] R. Vendrame, V. R. Coluci, D. S. Galvão, Comparative parametric method 5 (PM5) study of *trans*-stilbene, *J. Mol. Struct.: Theochem.*, 686, **2004**, 103-108

[308] N. Arul Murugan, S. Yashonath, Structure, energetics, and dynamics of pedal-like motion in stilbene from molecular simulation and *ab initio* calculations, *J. Phys. Chem. B*, 108, **2004**, 17403-17411

[309] J. Quenneville, T. J. Martínez, *Ab initio* study of *cis - trans* photoisomerization in stilbene and ethylene, *J. Chem. Phys. A*, 107, **2003**, 829-837

[310] S. P. Kwasniewski, L. Claes, J.-P. François, M. S. Deleuze, High level theoretical study of the structure and rotational barriers of *trans*-stilbene, *J. Chem. Phys.*, 118, **2003**, 7823-7836

[311] P. C. Chen, Y. C. Chieh, Azobenzene and stilbene: a computational study, *J. Mol. Struct.: Theochem.*, 624, **2003**, 191-200

[312] G. Baranović, Z. Meić, A. H. Maulitz, Vibrational analysis of stilbene and its isotopomers on the ground state potential energy surface, *Spectrochim. Acta A*, 54, **1998**, 1017-1039

[313] V. Molina, M. Merchan, B. O. Roos, Theoretical study of the electronic spectrum of *trans*-stilbene, *J. Phys. Chem. A*, 101, **1997**, 3478-3487

[314] F. W. Langkilde, R. Wilbrandt, A. M. Brouwer, F. Negri, F. Zerbetto, G. Orlandi, Molecular structure of stilbene in the T1 state. Transient resonance Raman spectra of stilbene isotopomers and quantum chemical calculations, *J. Phys. Chem.*, 98, **1994**, 2254-2265

[315] D. S. Galvão, Z. G. Soos, S. Ramasesha, S. Etemad, A parametric method 3 (PM3) study of *trans*-stilbene, *J. Chem. Phys.*, 98, **1993**, 3016-3021

[316] J. Troe, K. M. Weitzel, MNDO calculations of stilbene potential energy properties relevant for the photoisomerization dynamics, *J. Chem. Phys.*, 88, **1988**, 7030-7039

[317] K. Furuya, K. Kawato, H. Yokoyama, A. Sakamoto, M. Tasumi, Molecular distortion of *trans*-stilbene and the Raman intensity of the in-phase CH out-of-plane wag of the central CH=CH group, *J. Phys. Chem. A*, 107, **2003**, 8251-8258

[318] A. Bree, M. Edelson, An investigation of the low-frequency torsional modes of *trans*-stilbene using Raman spectroscopy, *Chem. Phys.*, 51, **1980**, 77-88

[319] M. Edelson, A. Bree, The geometry of *trans*-stilbene in the liquid phase, *Chem. Phys. Lett.*, 41, **1976**, 562-564

[320] C. H. Choi, M. Kertesz, Conformational information from vibrational spectra of styrene, *trans*-stilbene, and *cis*-stilbene, *J. Phys. Chem. A*, 101, **1997**, 3823-3831

[321] P. Novak, Z. Meić, H. Sterk, Conformational dependence of deuterium-induced isotope effects on the olefinic one-bond ^{13}C-^{1}H and three-bond ^{1}H-^{2}H coupling constants in *cis*- and *trans*-stilbene, *J. Chem. Soc. Perkin Trans. 2*, 11, **1996**, 2531-2536

[322] Á. Kvaran, B. I. Ásgeirsson, J. K. F. Geirsson, ^{1}H NMR and UV-vis spectroscopy of fluorine and chlorine substituted stilbenes: conformational studies, *J. Mol. Struct.*, 563-564, **2001**, 513-516

[323] E. J. Seus, C. V. Wilson, New synthesis of stilbene and heterocyclic stilbene analogs, *J. Org. Chem.*, 26, **1961**, 5243

[324] G. Celebre, M. Concistré, G. De Luca, M. Longeri, G. Pileio, Intrinsic information content of NMR dipolar couplings: a conformational investigation of 1,3-butadiene in a nematic phase, *Chem. Phys. Chem.*, 7, **2006**, 1930-1943

[325] J. W. Emsley, G. De Luca, A. Lesage, D. Merlet, G. Pileio, The structure and conformation of a mesogenic compound between almost zero and almost complete orientational order, *Liq. Cryst.*, 34, **2007**, 1071-1093

[326] O. Lhost, J. L. Brédas, Theoretical study of torsion potentials in *trans*-stilbene and substituted *trans*-stilbenes: modeling torsions in poly(paraphenylene vinylene) and derivatives, *J. Chem. Phys.*, 96, **1992**, 5279-5288

[327] L. Claes, S. Kwasniewski, M. S. Deleuze, J. P. François, Comparative study of the molecular structure of stilbene using molecular mechanics, Hartree-Fock and density functional theories, *J. Mol. Struct.: Theochem.*, 549, **2001**, 63-67

[328] S. P. Kwasniewski, M. S. Deleuze, J. P. François, Optical properties of *trans*-stilbene using semiempirical and time-dependent density functional theory: a comparative study, *Int. J. Quantum Chem.*, 80, **2000**, 672-680

GENERAL CONCLUSION

Aim of this Ph.D. project – in cotutorship between Università della Calabria and Université Paris Sud - was to explore orientational and positional order, structure and conformational distribution of small rigid and flexible organic molecules in solution, starting from experimental dipolar couplings that can be extracted from their NMR spectra when dissolved in partially ordered media. As discussed in the first chapter, these observables D_{ij}^{obs} can give direct access to such valuable information - structure, order and, for flexible molecules, conformational equilibrium - through respectively the internuclear vector r_{ij}, the Saupe order parameters $S_{\alpha\beta}$ and the orientational distribution function $P_{LC}(\Omega, \{\phi\})$.

In the second chapter, the highly symmetric molecule of tetramethylallene (TMA) was chosen as example of solutes experiencing very weak orientational ordering conditions and investigated by ^{1}H and ^{13}C NMR spectroscopy when dissolved in the uniaxial nematic I52 solvent. A peculiar ^{1}H spectral behavior was observed on cooling, that is the spectral width initially decreases until it reaches its minimum value, before increasing again at lower temperatures. Some considerations individuated the most reasonable explanation for the observed data in the presence of a minimum of magnitude for S_{aa}. Following this hypothesis, a series of approximations led us to estimate the different contributions playing a role in the direct C-H coupling. A predominant effect of the non-rigid term emerged. Indeed, this contribution is typically very small compared to other terms and then difficult to appreciate and estimate in non-symmetric solutes, but it becomes relevant in a *quasi*-spherical methane-like molecule as TMA. Therefore, an approximate assessment of the non-rigid contribution to the direct ^{13}C-^{1}H dipolar coupling was derived.

In the second part of chapter 2 the orientational analysis of small rigid solutes dissolved in smectic solvents was demonstrated to be a promising route to probe the latter's positional order. The basic idea is to exploit the fine changes that the orientational order parameters of certain solutes may undergo upon the onset of layering to get information on the positional order of the smectic liquid crystalline solutions. The strategy bases on the treatment by a statistical thermodynamic density-functional theory (ST-DFT) of a series of NMR experimental data, that is the solvent orientational order parameter η (obtained from ^{2}H spectra of the deuterated solvent) and the Saupe ordering matrices $\left[S_{\alpha\beta}\right]_\sigma^{exp}$ of a number of rigid solutes dissolved therein (obtained from their ^{1}H spectra). Realistic results for both the solute's and the solvent's positional order parameters were obtained after application of this methodology to the apolar SmA phase of 4,4'-di-*n*-heptylazoxybenzene (HAB) and the interdigitated SmA$_d$ phase of 4-*n*-octyloxy-4'-cyanobyphenyl (8OCB), by using 1,4-dichlorobenzene, naphthalene, biphenylene and pyrene as probes. This strategy may

represent thus a complementary or alternative tool with respect to standard methods, all relying on diffraction experiments, and it would be of interest to extend it to a smectic C phase or even speculate on how it could contribute to study the partitioning of small solutes in lipid bilayers, an issue of basic importance in biochemistry and pharmacology.

In chapter 3 conformational distribution as well as structure and order of various flexible molecules were investigated when dissolved in highly or weakly ordering liquid crystals. The achievement of such amount of information requires, however, proper theoretical models in order to give to D_{ij}^{obs} a physical meaning. In all studies we used the Additive Potential model combined with the Direct Probability Description of the torsional distributions in terms of Gaussian functions. This AP-DPD approach is recognized to be reliable and effective for highly ordered solutes, but to date there are no many evidences of its robustness for weakly orienting phases, too.

The first case discussed in chapter 3 is the single-rotor 10-spin system of biphenyl, dissolved in the thermotropic 4-*n*-octyl-4'-cyanobiphenyl (8CB) liquid crystal. The molecule was chosen as test for a joint experimental and MD-simulated ^{1}H NMR study at different temperatures, aimed at evaluating if molecular dynamics simulations can be exploited as tool for estimating a set of dipolar couplings to be used in a "line-assignment" operator-mediated analysis of the ^{1}H NMR spectrum of a solute in a thermotropic solvent. Indeed, the availability of a good set of input parameters, and in particular of dipolar couplings, is probably the main obstacle in the iterative analysis of proton spectra of solutes dissolved in highly ordering media and, even if several strategies have been proposed in the past, none of them has proven to be resolutive. Despite not negligible differences in terms of transitions temperatures emerged from the comparison on the biphenyl/8CB system, the set of simulated D_{ij} was rather in agreement with the experimental one and allowed a standard operator-mediated spectral analysis when used as starting set of parameters. The strategy applied here to the relatively simple molecule of biphenyl may represent in the future a viable solution in the NMR spectral analysis of more complex compounds dissolved in anisotropic media when no other information is available.

The conformational problem becomes crucial when dealing with flexible molecules endowed with biological or pharmacological activity. This is the reason why we tackled the conformational study by liquid crystal NMR of some nonsteroidal anti-inflammatory drugs (NSAIDs) belonging to the families of salicylates (diflunisal and its non-fluorinated analogue, phenylsalicylic acid) and profens (naproxen, flurbiprofen and ibuprofen). Being the NMR spectra of these asymmetrical flexible compounds in thermotropics difficult to be recorded at

high resolution and almost impossible to analyse without a very good set of starting parameters, we chose to dissolve them in PBLG phases, where spectra retain only weak second-order features and extraction of residual dipolar couplings (RDCs) appears simpler. This is not properly true and in the case of diflunisal the absence of simple and time-saving experiments for the edition of proton-fluorine couplings prompted us to develop the new GET-SERF pulse sequence. Combining selective refocusing and frequency spatial encoding approaches, this experiment allows the trivial edition of all long and short range ^{1}H-^{19}F scalar or dipolar couplings in one single NMR experiment, for a given fluorine atom. If its application appears relatively easy in the case of a difluorinated molecule as diflunisal, it may represent a relevant tool when dealing with more complex systems containing n and m non-equivalent proton and fluorine sites, since only m experiments are needed to selectively extract all ^{1}H-^{19}F couplings in the whole molecule, and it might be extended to other high-abundance heteronuclei. With a large set of 40 D_{ij}^{obs} (among which 10 inter-ring RDCs) the probability distribution of diflunisal in PBLG/THF could be quite accurately described, obtaining a couple of *trans* conformers (global minima, with ^{19}F in *ortho* position opposite to the carboxylic group), with φ_1^{max} = ±45.5° and relative percentage of 56%, and a couple of *cis* conformers (relative minima, with ^{19}F in *ortho* position on the same side relative to the carboxylic group), with φ_2^{max} = ±41.1° and a relative percentage of 44%, in very good agreement with the theoretical results obtained at DFT level. Moreover, the similar experimental outcomes in both chiral (PBLG/THF) and achiral (PBG/THF) phases proves there are no effects on the conformational equilibrium resulting from the chirality of the medium. In order to probe the influence the fluorine nuclei have on the conformational equilibrium of the diflunisal, its non-fluorinated analogue, phenylsalicylic acid, was studied under similar conditions. Results seem to suggest no significant effects on the torsion angle values and a smoothing in the rotational barriers. Encouraged by the results obtained for these salicylic acid derivates, displaying only one degree of flexibility, the same strategy was applied to the naproxen molecule, whose torsional description implies two non-cooperative rotations to be taken into account. In agreement with DFT theoretical calculations, four minimum energy structures have been successfully individuated by treating the experimental D_{ij}^{obs} with the AP-DPD approach: a couples of more stable conformers (I and II, with relative percentages of 57.4% and 29.6%, respectively) with the methoxy group in the *cis* arrangement and α-hydrogen atom *quasi*-planar relative to the aromatic ring, and a couple of less stable conformers (III and IV, relative percentages of 8.6% and 4.4%, respectively) involving the *trans* geometry of the methoxy group and the same geometry of the chiral side chain. Despite a better or even similar reproduction of the

observed dipolar couplings cannot be achieved considering a different conformational equilibrium, it is to admit that, due to the relatively small number of independent inter-fragment D_{ij}^{obs} collected, it is not possible to unambiguously individuate precise values of torsional angles for the major conformers but rather small ranges where molecule is more likely to be confined. These first studies prove then that NMR spectroscopy in weakly orienting PBLG phases, combined with the AP-DPD model, is a promising approach in the study of conformational equilibria of anti-inflammatory drugs displaying one or two torsional degrees, encouraging the extension towards more complex flexible molecules, otherwise impossible to treat using thermotropic solvents. To proceed further, preliminary studies have been already carried out on two other profen derivatives, flurbiprofen and ibuprofen. The former displays two non-coupled torsions and was mainly chosen for investigating the effect on the torsional potential of the fluorine atom in *ortho* position relative to the inter-ring C-C single bond, with the final purpose of comparing the inter-ring torsional distribution obtained for this mono-fluorinated molecule with those already obtained for the non-fluorinated biphenyl and the bifluorinated diflunisal. However, the overlap of several lines along with second order effects prevented so far from collecting an experimental data set that is large enough to accurately describe the torsional potential of the biphenyl fragment. Alternative solutions to test in the near future include more sophisticated NMR experiments on the same sample and/or a change in the organic co-solvent. The conformational study of ibuprofen, displaying two coupled rotations in the methylpropyl substituent, together with an additional torsion of the propionic fragment with respect to the central phenyl ring, is theoretically more challenging. From the experimental viewpoint, the double substitution on the phenyl ring allows for ^{1}H and ^{13}C signals that are sufficiently far apart in the anisotropic NMR spectra to precisely measure an acceptable number of RDCs. Next task is to treat such data set by the AP-DPD approach to perform a conformational analysis that takes into account all the degrees of flexibility in the molecule.

The last study presented in the third chapter was intended to provide a comprehensive orientational, structural and conformational investigation of the same molecule, *trans*-stilbene, in both a highly and weakly orienting medium. *trans*-Stilbene is indeed a 12-spin system possessing two cooperative rotations. Therefore, even considering its symmetry, neither the ^{1}H spectral analysis nor the conformational description *via* the AP-DPD approach are trivial. In order to have a good set of starting parameter for the analysis of its ^{1}H spectrum in the thermotropic ZLI1132 liquid crystal, we synthesised the *trans*-4,4'-dichlorostilbene. Twelve independent D_{ij}^{obs} were extracted from the ^{1}H spectrum of this 10-spin system

dissolved in ZLI1132 by guessing a trial set of order parameters corresponding to a non-planar C_2 structure. This D_{ij}^{obs} set was subsequently used for estimating a good trial set of D_{ij} for the analysis of the more complex spectrum of *trans*-stilbene. The AP-DPD treatment of the accurate sets of D_{ij}^{obs} obtained for both molecules gave detailed $P_{iso}(\phi_1, \phi_2)$ distributions characterized by four more stable symmetry related conformations, that is a couple of global minima, where the molecule exhibits a propeller-like C_2 symmetry ($\phi_1^{max} = \phi_2^{max}$), and a couple of C_i local minima, where the rings are conrotated of the same angle ($\phi_1^{max} = -\phi_2^{max}$). The four minima energy conformers were found to be located at ϕ_1^{max} = 16.8° with relative percentages of 59% and 41% for *t*-St, and at ϕ_1^{max} = 18.7° with relative percentages of 63% and 37% for DCS. Overall, this indicates very limited effects of the 4,4' Cl-substitutions on the positions of the conformational minima, even if the sharper and higher peaks with respect to *trans*-stilbene seem to suggest a preference for the chlorinated molecule to be confined in proximity of its conformational minima. Note, moreover, that the *trans*-4,4'-dichlorostilbene can be considered as a prototype molecule of 4,4'-substituted *trans*-stilbene derivatives, such as the *trans*-4,4'-dihydroxystilbene that is known to possess innumerable interesting healthy properties. Hence, a rigorous investigation of the conformational equilibrium of DCS may help in shedding more light on the mechanisms by which *para*-disubstituted *trans*-stilbene analogs play their role and contribute then to a better understanding of useful structure-property relationships. Once obtained a reliable conformational and structural description of *t*-St in the highly orienting liquid crystal, it was dissolved in a PBLG/THF-d$_8$ phase, in order to compare results from both phases and especially collecting evidence about the accuracy and reliability of the data extracted by NMR spectroscopy in weakly ordering phases. In the PBLG medium, a reduced number of small residual dipolar couplings allowed to define limited ranges where conformers are more probably confined, $0 \leq \phi_1^{max} = \pm\phi_2^{max} \leq 20°$ and $0.4 \leq A_{C_2} \leq 0.6$. Despite the evident loss of precision when compared to thermotropic data, the intervals determined are perfectly consistent with the more precise location of the minima found in the thermotropic LC. The agreement between outcomes from the two phases testifies that there is no perceptible influence of the phase on the conformational equilibrium and represents a proof that conformational information derived from a weakly ordered sample is maybe less accurate than from the corresponding thermotropic one, but it is reliable in individuating restricted intervals that contain the "real" minimum energy conformers. This encourages the application of NMR in PBLG phases for the conformational study of flexible more complex asymmetric molecules, whose spectra in a thermotropic phase are too difficult to be recorded at high resolution and/or to be analysed by standard techniques. A last remark on the

comparison between the highly and weakly oriented sample was derived about the orientational order. When *t*-St is dissolved in the PBLG phase, an increase of S_{bb} at the expense of S_{aa} and S_{cc} is recorded. This would indicate that in the weakly ordering phase the molecule has a more marked preference to orient with its *b* axis perpendicular with respect to the director, while its *a* axis is basically oriented parallel to the director but undergoes more fluctuations than in ZLI1132.

To conclude, the work carried out during this thesis project covered different issues having the same common starting point, *i.e.* (residual) dipolar couplings extracted from NMR spectra of small organic molecules dissolved in thermotropic or PBLG phases. These experimental data were then used to investigate both orienting behaviours of rigid molecules and conformational equilibria of flexible molecules. Outcomes demonstrated that NMR in liquid crystals is effectively a flexible and meaningful tool for studying order, structure and conformation and can greatly benefit from the availability of several aligning media inducing a different degree of order.

APPENDICES

Appendix A1. *Rotation of reference frames*

NMR investigations focus on molecular properties, expressed in the MOL frame, but the observable quantities are typically measured in the LAB frame. This needs a continuous change of reference frame to be performed. In order to switch among frames, rotation around axes is needed. The angles of rotation for switching from the $\{x, y, z\}$ frame F' to the $\{X, Y, Z\}$ frame F are the well-known Euler angles (Figure A1.1), defined as $\Omega_{FF'} = \{\alpha_{FF'}, \beta_{FF'}, \gamma_{FF'}\}$, with α being the angle of rotation around the $\vec{z}$ axis of F'; β being the angle between the $\vec{z}$ axis of F' and the $\vec{Z}$ axis of F spanned by the rotation around a chosen axis and, finally, γ being the angle of rotation around the $\vec{Z}$ axis of F. The line of nodes (N), shown in green, is defined as the intersection of the xy and the XY coordinate planes. It can be observed that it corresponds to the orientation of X after the first elemental rotation.

Figure A1.1. Euler angles describing the rotation from the $\{x, y, z\}$ frame F' to the $\{X, Y, Z\}$ frame F

Rotations in Cartesian representation are carried out using conventional rotational matrices of director cosine. Wigner matrices are the analogues in the irreducible spherical representation [1]. In general, it is always possible to express the $T_\lambda^{(l,m)}$ irreducible spherical components of the tensor representing the λ-th interaction as:

$$\left[T_\lambda^{(l,m)}\right]^F = \sum_{m'=-l}^{+l} \left[T_\lambda^{(l,m')}\right]^{F'} D_{m'm}^l (\Omega_{FF'})$$

where $D_{mm'}^l$ is the m-th, m'-th component of a rank l Wigner matrix which transform the frame F' into F.
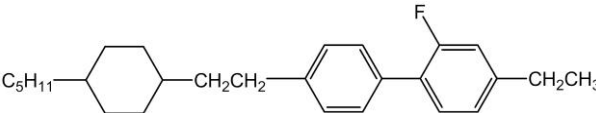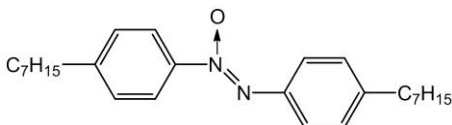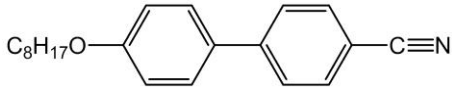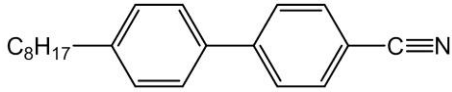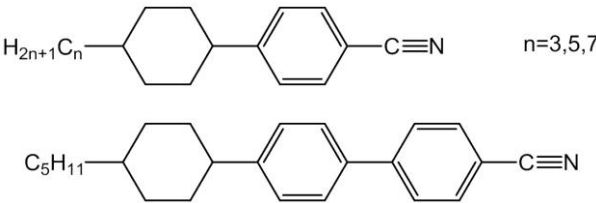
References
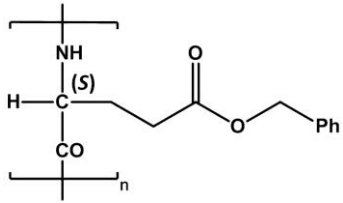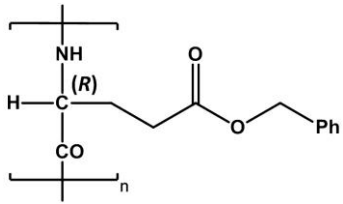
[1] M. E. Rose, *Elementary Theory of Angular Momentum*, Dover Publication, Inc., New York, **1995**, ISBN: 9780486684802

Appendix A2. *Structure and main properties of the used liquid crystals*

We report here a list of the liquid crystals used in this Ph.D. thesis, including structure, magnetic anisotropy $\Delta\chi$, transition temperatures (for thermotropics) and liquid-crystal concentration range (for lyotropics). Double-headed arrows indicate bidirectional transition phases, while single-headed arrows represent phase transition after supercooling. All transition temperatures are given in °C.

Thermotropic LCs	*acronym*	*magnetic anisotropy*	*transition temperatures*
4-ethyl-2-fluoro-4'-[2-(trans-4-*n*-pentylcyclohexyl)-ethyl]biphenyl	I52	$\Delta\chi > 0$	$C \overset{24}{\underset{}{\xleftarrow{}}} S_B \overset{13}{\xleftarrow{}} N \overset{103.4}{\underset{}{\xleftrightarrow{}}} I$ [1]
4,4'-di-*n*-heptyl-azoxybenzene	HAB	$\Delta\chi > 0$	$C \overset{29}{\xleftrightarrow{}} S_A \overset{53}{\xleftrightarrow{}} N \overset{70}{\xleftrightarrow{}} I$ [2]
4-*n*-octyloxy-4'-cyanobyphenyl	8OCB	$\Delta\chi > 0$	$C \overset{55}{\xleftrightarrow{}} S_A \overset{67}{\xleftrightarrow{}} N \overset{75}{\xleftrightarrow{}} I$ [3]
4-*n*-octyl-4'-cyanobiphenyl	8CB	$\Delta\chi > 0$	$C \overset{21.5}{\xleftrightarrow{}} S_A \overset{33.5}{\xleftrightarrow{}} N \overset{40.5}{\xleftrightarrow{}} I$ [4]
mixture of *trans*-4-*n*-propyl-(4-cyanophenyl)-cyclohexane (24%), *trans*-4-*n*-pentyl-(4-cyanophenyl)-cyclohexane (36%), *trans*-4-*n*-heptyl-(4-cyanophenyl)-cyclohexane (25%), *trans*-4-*n*-pentyl-(4'-cyanobiphenyl-4)-cyclohexane (15%)	ZLI1132	$\Delta\chi > 0$	$C \overset{<-40}{\xleftrightarrow{}} N \overset{72}{\xleftrightarrow{}} I$ [5]

Structure labels within the table:

I52: C$_5$H$_{11}$—cyclohexane—CH$_2$CH$_2$—biphenyl(2-F)—CH$_2$CH$_3$

HAB: C$_7$H$_{15}$—azoxybenzene—C$_7$H$_{15}$

8OCB: C$_8$H$_{17}$O—biphenyl—C≡N

8CB: C$_8$H$_{17}$—biphenyl—C≡N

ZLI1132: H$_{2n+1}$C$_n$—cyclohexane—phenyl—C≡N (n=3,5,7); C$_5$H$_{11}$—cyclohexane—biphenyl—C≡N

Lyotropic LCs				
polymer	**organic co-solvent**	**acronym**	**magnetic anisotropy**	**LC concentration range**
 poly-γ-benzyl-L-glutamate (DP = 743)	THF CHCl$_3$	PBLG	$\Delta\chi > 0$	12-15 wt% [6]
 poly-γ-benzyl-D-glutamate (DP = 685)	THF	PBDG	$\Delta\chi > 0$	12-15 wt% [6]

References

[1] U. Finkenzeller, T. Geelhaar, G. Weber, L. Pohl, Liquid-crystalline reference compounds, *Liq. Cryst.*, 5, **1989**, 313-321

[2] Data sheet, Sigma-Aldrich, **2006**

[3] D. Demus, J. W. Goodby, G. W. Gray, H. W. Spiess, V. Vill, *Handbook of Liquid Crystals, vol.1: Fundamentals*, Wiley-VCH, Verlag, **1998**, ISBN: 978352792707

[4] P. Collings, M. Hird, *Introduction to Liquid Crystals: Chemistry and Physics*, Taylor&Francis Ltd., **1997**, ISBN: 0748406433

[5] Data sheet, Merck KGaA, Darmstadt, **1996**

[6] M. Sarfati, P. Lesot, D. Merlet, J. Courtieu, Theoretical and experimental aspects of enantiomeric differentiation using natural abundance multinuclear nmr spectroscopy in chiral polypeptide liquid crystals, *Chem. Commun.*, **2000**, 2069-2081

Appendix A3. *Samples preparation*

Details about the preparation of the different samples studied in this Ph.D. thesis are reported here, including concentration of various components and standard preparation procedures.

Highly ordered samples

Sample are heated several times up to their clearing point, strongly shaken to give a very homogeneous solution and left to cool slowly in the magnetic field of the NMR spectrometer

solute	solvent
10 mg TMA [1]	433 mg I52 [2]
10 mg BIF [1]	550 mg mixture HAB [1] / HAB-d_4 [3] at 9.3 wt%
12 mg PYR [1]	570 mg mixture HAB [1] / HAB-d_4 [3] at 9.3 wt%
15.3 mg DCB [1]	499 mg 8OCB [1]
14.4 mg BIF [1]	468 mg mixture 8OCB [1] / 8OCB-d_8 [4] at 8.0 wt%
14.9 mg PYR [1]	502 mg mixture 8OCB [1] / 8OCB-d_8 [4] at 8.0 wt%
16.0 mg 2P [1] + 1.5 mg 1,3,5-trichlorobenzene [1, 5]	550 mg 8CB [1]
14.4 mg DCS [6]	540 mg ZLI1132 [2]
20.6 mg *t*-St [1]	550 mg ZLI1132 [2]

Weakly ordered samples

Samples were prepared using standard procedure described in ref. [2] and the resulting 5 mm NMR tubes were centrifuged back and forth until an optically homogeneous birefringent phase was obtained

solute	solvent
33 mg DFL [1]	82 mg PBLG [1, 7] + 474 mg THF

33.5 mg DFL [1]	87 mg PBG [8] + 471.5 mg THF
27 mg APS [1]	84 mg PBLG [1, 7] + 484.5 mg THF
41.0 mg NAP [1]	76.4 mg PBLG [1, 7] + 393.0 mg THF-d_8 [9]
40.6 mg NAP [1]	76.0 mg PBLG [1, 7] + 392.6 mg THF
47.2 mg t-St [1]	92.5 mg PBLG [1, 7] + 483.6 mg THF-d_8 [9]

Isotropic samples

solute	*solvent*
30 mg DFL [1]	483 mg THF-d_8 [9]
23 mg APS [1]	490 mg THF-d_8 [9]
39.5 mg NAP [1]	519 mg THF-d_8 [9]
36.2 mg t-St [1]	665.5 mg THF-d_8 [9]

[1] purchased from Sigma Aldrich

[2] purchased from Merck Ltd

[3] deuterated in the *ortho* positions with respect to the two alkyl chains, provided by C. A. Veracini (Dipartimento di Chimica, Università di Pisa)

[4] deuterated in the biphenyl fragment, prepared according to the procedure described in ref. [1]

[5] added as orientational probe

[6] synthesised as described in section 3.4.1.1

[7] DP= 743

[8] racemic mixture composed of equimolar amounts of PBLG [1, 7] and PBDG (DP = 685, purchased from Sigma Aldrich)

[9] purchased from Eurisotop

References

[1] H. Zimmermann, Specifically deuteriated intermediates for the synthesis of liquid crystals and liquid-crystalline polymers, *Liq. Cryst.,* 4, **1989**, 591-618

[2] M. Sarfati, P. Lesot, D. Merlet, J. Courtieu, Theoretical and experimental aspects of enantiomeric differentiation using natural abundance multinuclear nmr spectroscopy in chiral polypeptide liquid crystals, *Chem. Commun.*, **2000**, 2069-2081

Appendix A4.   *Optimised geometries of minimum energy conformers of DFL and APS*

This appendix reports the optimised geometries obtained by the Gaussian09 software package (B3LYP/6-31++G**) for a *trans* and a *cis* minimum energy conformers of diflunisal and for one of the four equally probable minimum energy conformers of phenylsalicylic acid (structure and atomic labelling are reported in Figure A4.1). Bond lengths (R) are given in Å; valence angles (A) and dihedral angles (D) are expressed in degrees.
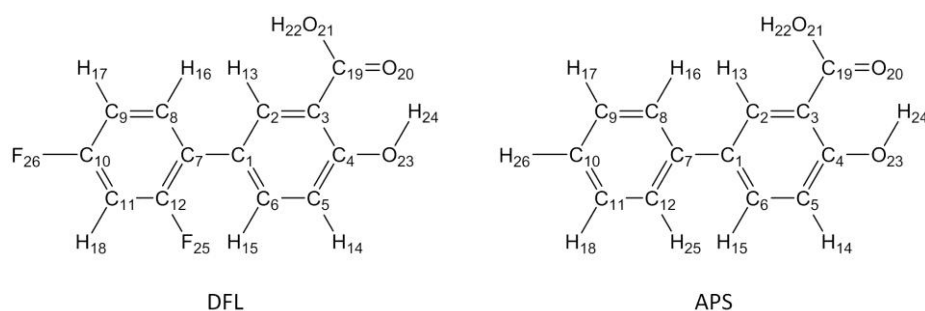
Figure A4.1. Topological structure and atomic labelling of diflunisal (DFL) and phenylsalicylic acid (APS).

	DFL *trans* conformer	DFL *cis* conformer	APS
R(1,2)	1,3932	1,3943	1,3940
R(1,6)	1,4145	1,4133	1,4142
R(1,7)	1,4857	1,4856	1,4862
R(2,3)	1,4086	1,4074	1,4088
R(2,13)	1,0841	1,0828	1,0839
R(3,4)	1,4186	1,4193	1,4188
R(3,19)	1,4649	1,4665	1,4650
R(4,5)	1,4047	1,4038	1,4040
R(4,23)	1,3435	1,3438	1,3448
R(5,6)	1,3851	1,3861	1,3860
R(5,14)	1,0847	1,0846	1,0848
R(6,15)	1,0847	1,0863	1,0861
R(7,8)	1,4075	1,4075	1,4063
R(7,12)	1,4019	1,4022	1,4063
R(8,9)	1,3949	1,3950	1,3958
R(8,16)	1,0853	1,0855	1,0862
R(9,10)	1,3893	1,3892	1,3976
R(9,17)	1,0840	1,0840	1,0863

R(10,11)	1,3886	1,3886	1,3974
R(10,26)	1,3565	1,3565	1,0860
R(11,12)	1,3895	1,3895	1,3959
R(11,18)	1,0833	1,0833	1,0863
R(12,25)	1,3591	1,3585	1,0863
R(19,20)	1,2334	1,2334	1,2339
R(19,21)	1,3500	1,3485	1,3499
R(20,24)	1,7510	1,7504	1,7500
R(21,22)	0,9719	0,9719	0,9719
R(23,24)	0,9858	0,9857	0,9856
A(2,1,6)	117,7633	117,7233	117,4574
A(2,1,7)	120,3735	122,0226	121,3723
A(6,1,7)	121,8509	120,2424	121,1699
A(1,2,3)	121,7113	121,5391	121,8013
A(1,2,13)	120,0726	120,2326	119,9877
A(3,2,13)	118,2077	118,2262	118,1967
A(2,3,4)	119,4950	119,7007	119,5782
A(2,3,19)	121,6630	121,5141	121,6510
A(4,3,19)	118,8405	118,7847	118,7687
A(3,4,5)	118,9014	118,8784	118,8442
A(3,4,23)	123,0706	123,1030	123,1035
A(5,4,23)	118,0279	118,0183	118,0522
A(4,5,6)	120,4694	120,2737	120,3393
A(4,5,14)	118,3141	118,3983	118,3297
A(6,5,14)	121,2159	121,3239	121,3268
A(1,6,5)	121,6583	121,8838	121,9792
A(1,6,15)	119,4330	119,2546	119,1857
A(5,6,15)	118,9061	118,8524	118,8226
A(1,7,8)	121,2821	121,1832	120,9982
A(1,7,12)	122,8170	122,9384	120,8713
A(8,7,12)	115,8970	115,8744	118,1305
A(7,8,9)	122,4667	122,5048	120,9435
A(7,8,16)	118,4961	118,5633	119,5019
A(9,8,16)	119,0274	118,9213	119,5396
A(8,9,10)	118,2029	118,1918	120,2847
A(8,9,17)	121,6768	121,6723	119,6251
A(10,9,17)	120,1159	120,1319	120,0867

A(9,10,11)	122,3204	122,3020	119,4136
A(9,10,26)	119,2129	119,2211	120,2879
A(11,10,26)	118,4664	118,4768	120,2984
A(10,11,12)	117,3244	117,3664	120,2675
A(10,11,18)	121,6712	121,6592	120,1085
A(12,11,18)	121,0014	120,9721	119,6209
A(7,12,11)	123,7880	123,7603	120,9596
A(7,12,25)	119,2800	119,3538	119,5754
A(11,12,25)	116,9239	116,8787	119,4479
A(3,19,20)	124,2811	124,2197	124,3161
A(3,19,21)	115,0586	115,0466	115,1043
A(20,19,21)	120,6602	120,7337	120,5795
A(19,21,22)	106,8873	106,9621	106,8398
A(4,23,24)	107,9586	107,9452	107,8825
D(6,1,2,3)	0,4314	0,3096	0,0920
D(6,1,2,13)	-178,4930	179,7637	-178,5030
D(7,1,2,3)	-178,3200	-178,4487	179,8744
D(7,1,2,13)	2,7556	1,0054	1,2798
D(2,1,6,5)	-0,3620	-0,3906	0,0744
D(2,1,6,15)	-179,7763	178,4906	-178,6240
D(7,1,6,5)	178,3698	178,3908	-179,7090
D(7,1,6,15)	-1,0445	-2,7280	1,5929
D(2,1,7,8)	43,2010	135,9499	39,4107
D(2,1,7,12)	-136,0481	-44,8090	-140,4800
D(6,1,7,8)	-135,4983	-42,7777	-140,8150
D(6,1,7,12)	45,2526	136,4634	39,2948
D(1,2,3,4)	-0,2704	-0,0648	-0,2152
D(1,2,3,19)	-179,8162	179,6733	-179,6790
D(13,2,3,4)	178,6733	-179,5295	178,4036
D(13,2,3,19)	-0,8725	0,2086	-1,0598
D(2,3,4,5)	0,0242	-0,1141	0,1710
D(2,3,4,23)	-179,9137	-179,9277	-179,9150
D(19,3,4,5)	179,5829	-179,8593	179,6498
D(19,3,4,23)	-0,3551	0,3270	-0,4361
D(2,3,19,20)	179,7094	179,8358	179,7693
D(2,3,19,21)	-0,3842	-0,2066	-0,3275
D(4,3,19,20)	0,1607	-0,4237	0,3018

D(4,3,19,21)	-179,9328	179,5338	-179,7950
D(3,4,5,6)	0,0431	0,0371	-0,0106
D(3,4,5,14)	179,7687	-179,2457	179,2595
D(23,4,5,6)	179,9841	179,8602	-179,9290
D(23,4,5,14)	-0,2902	0,5775	-0,6590
D(3,4,23,24)	0,2708	-0,0146	0,1941
D(5,4,23,24)	-179,6677	-179,8297	-179,8910
D(4,5,6,1)	0,1296	0,2210	-0,1149
D(4,5,6,15)	179,5469	-178,6646	178,5884
D(14,5,6,1)	-179,5880	179,4824	-179,3630
D(14,5,6,15)	-0,1707	0,5969	-0,6595
D(1,7,8,9)	-179,0985	179,1670	-179,7140
D(1,7,8,16)	2,0512	-2,0356	1,7013
D(12,7,8,9)	0,2000	-0,1252	0,1797
D(12,7,8,16)	-178,6503	178,6723	-178,4060
D(1,7,12,11)	179,2734	-179,2715	179,9637
D(1,7,12,25)	0,3406	-0,2768	1,4788
D(8,7,12,11)	-0,0132	0,0069	0,0704
D(8,7,12,25)	-178,9461	179,0017	-178,4150
D(7,8,9,10)	-0,2817	0,1970	-0,2860
D(7,8,9,17)	-179,5210	179,4726	-179,6090
D(16,8,9,10)	178,5628	-178,5964	178,2986
D(16,8,9,17)	-0,6766	0,6793	-1,0239
D(8,9,10,11)	0,1777	-0,1527	0,1379
D(8,9,10,26)	-179,6597	179,7334	-179,8210
D(17,9,10,11)	179,4293	-179,4399	179,4573
D(17,9,10,26)	-0,4081	0,4462	-0,5018
D(9,10,11,12)	-0,0025	0,0416	0,1104
D(9,10,11,18)	179,3665	-179,4090	179,4616
D(26,10,11,12)	179,8361	-179,8453	-179,9310
D(26,10,11,18)	-0,7950	0,7041	-0,5792
D(10,11,12,7)	-0,0823	0,0335	-0,2159
D(10,11,12,25)	178,8738	-178,9842	178,2710
D(18,11,12,7)	-179,4557	179,4880	-179,5700
D(18,11,12,25)	-0,4996	0,4704	-1,0835
D(3,19,21,22)	179,7747	179,7921	179,9010
D(20,19,21,22)	-0,3152	-0,2487	-0,1919

Appendix A5.   *Optimised geometry for NAP used in the conformational analysis*

The averaged geometry used for the conformational analysis of *S*-(+)-naproxen (structure and atomic labelling reported in Figure A5.1) and derived from theoretical calculations by the Gaussian09 software package (B3LYP/6-31++G**) is given here in the Z-matrix format. Bond lengths are given in Å, while valence angles and dihedral angles in degrees.
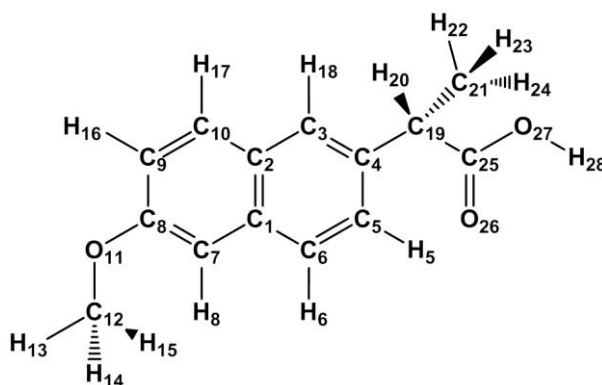
Figure A5.1. Topological structure and atomic labelling of *S*-(+)-naproxen (NAP).

atom number	atom type	1st connection	bond length	2nd connection	valence angle	3rd connection	dihedral angle
1	C						
2	C	1	1.432				
3	C	2	1.420	1	119.370		
4	C	3	1.382	2	121.540	1	0.000
5	C	4	1.423	3	118.780	2	0.000
6	C	5	1.377	4	121.120	3	0.000
7	C	1	1.420	6	122.269	5	180.000
8	C	7	1.383	1	120.444	6	180.000
9	C	8	1.422	7	120.233	1	0.000
10	C	9	1.376	8	120.072	7	0.000
11	O	8	1.367	7	125.762	1	-179.965
12	C	11	1.422	8	118.732	7	variable φ
13	H	12	1.095	11	109.532	8	179.860
14	H	12	1.095	11	109.532	8	298.569
15	H	12	1.095	11	109.532	8	61.149
16	H	9	1.084	8	120.072	7	180.000
17	H	10	1.087	9	119.710	8	180.000
18	H	3	1.088	2	118.472	10	0.000
19	C	4	1.529	3	121.033	2	180.000
20	H	19	1.094	4	107.579	3	variable ϑ
21	C	19	1.539	4	112.620	20	-120.743
22	H	21	1.094	19	110.521	4	56.790
23	H	21	1.094	19	110.521	4	176.799
24	H	21	1.094	19	110.521	4	-63.282
25	C	19	1.523	4	109.389	20	115.780
26	O	25	1.214	19	125.779	4	91.293
27	O	25	1.357	19	112.026	4	-87.619
28	H	27	0.973	25	107.084	19	177.136
29	H	5	1.087	6	119.663	1	180.000
30	H	6	1.087	1	118.946	7	0.000
31	H	7	1.085	8	120.203	9	180.000

1D, 2D, 3D: one-, two-, three-dimensional

2P: biphenyl

5CB: 4-*n*-pentyl-4'-cyanobiphenyl

8CB: 4-*n*-octyl-4'-cyanobiphenyl

8OCB: 4-*n*-octyloxy-4'-cyanobyphenyl

AM1: Austin Model n°1

AP: Additive Potential

APME: Additive Potential Maximum Entropy

APS: phenylsalicylic acid

B3LYP: Becke, 3-parameter, Lee-Yang-Parr functional

BBI: BroadBand Inverse

BHT: butylated hydroxytoluene, 2,6-bis(1,1-dimethylethyl)-4-methylphenol

BIF: biphenylene

BLYP: Becke-Lee-Yang-Parr functional

BVWN Becke-Vosko-Wilk-Nusair functional

COSY: COrrelation SpectroscopY

COX: enzyme cyclooxygenase

CPCl: cetylpyridinium chloride

CPBr: cetylpyridinium bromide

CPU: Central Processing Unit

D_h: hexagonal columnar

D_r: rectangular columnar

DCB: 1,4-dichlorobenzene

DCS: *trans*-4,4'-dichlorostilbene

DFL: diflunisal

DFT: Density Functional Theory

DHPC: dihexanoylphosphatidylcholine

DIR: DIRector frame

DMF: dimethylformamide

DMPC: dimyristoylphosphatidylcholine

DMSO: dimethylsulfoxide

DOE: Differential Ordering Effect

DP: Degree of Polymerization

DPD: Direct Probability Description

EBBA: 4-butyl-N-(4-ethoxybenzylidene)aniline

E-BURP: Excitation Band-selective Uniform Response Pure-phase

E.COSY: Exclusive COrrelation SpectroscopY

FDA: Food and Drug Administration

FF: Force Field

FWHM: Full-Width-at-Half-Maximum

GET-SERF: Gradient Encoded heTeronuclear ^{1}H-^{19}F SElective ReFocusing

G-SERF: Gradient encoded homonuclear SElective ReFocusing

HAB: 4,4'-di-*n*-heptylazoxybenzene

HETSERF: HETeronuclear ^{13}C-^{1}H SElective ReFocusing

HF: Hartree-Fock

HF-SERF: heteronuclear ^{1}H-^{19}F SElective ReFocusing

HFA: High Field Approximation

HMBC: Heteronuclear Multiple Bond Correlation

HSQC: Heteronuclear Single-Quantum Coherence

I52: 4-ethyl-2-fluoro-4'-[2-(trans-4-n-pentylcyclohexyl)ethyl]biphenyl

INEPT: Insensitive Nuclei Enhanced by Polarization Transfer

LAB: LABoratory frame

LB: Line Broadening

LC: Liquid Crystal

MD: Molecular Dynamics

ME: Maximum Entropy

MOL: MOLecular frame

MM: Magic Mixture (55wt% ZLI1132/EBBA)

MP2: Second-order Møller-Plesset

MQ: Multiple Quantum

N: nematic

N*: calamitic nematic or cholesteric

N_{col}: columnar

N_D: discotic nematic

N_D*: chiral discotic nematic

NAD: Natural Abundance Deuterium

NAP: naproxen

NFT: naphthalene

NMR: Nuclear Magnetic Resonance

nOe: nuclear Overhauser effect

NOESY: Nuclear Overhauser Effect SpectroscopY

NSAIDs: NonSteroidal Anti-Inflammatory Drugs

OMAS: Off Magic Angle Spinning

PAA: poly(acrylamide)

PAN: poly(acrylonitrile)

PAS: Principal Axis System

PBG: racemic mixture of PBLG and PBDG

PBDG: poly-γ-benzyl-D-glutamate

PBLG: poly-γ-benzyl-L-glutamate

PCBLL: poly-ε-carbobenzyloxy-L-lysin

PCM: Polarizable Continuum Model

PDLF: Proton-Detected Local Field

PDMS: poly(dimethylsiloxane)

PELG: poly-γ-ethyl-L-glutamate

PEO: poly(ethyleneoxide)

PEOMMA: poly(ethyleneoxide)-methylmethacrylate

PES: Potential Energy Surface

PFG: Pulsed-Field Gradient

PH-PDMAA: poly(dimethylacrylamide) copolymer

PM3: Parametric Model n°3

PM5: Parametric Model n°5

PMMA: poly(methylmethacrylate)

PS: polystyrene

PU: polyurethane

PVAc: poly(vinylacetate)

PYR: pyrene

Q-COSY: Quadrupolar COrrelation SpectroscopY

QUOSY: QUadrupole Ordered SpectroscopY

QXO: Quadruple resonance X-Observed

RDCs: Residual Dipolar Couplings

RE-BURP: REfocusing Band-selective Uniform Response Pure-phase

RF: RadioFrequency

RHF: Restricted Hartree-Fock

RIS: Rotamer Isomeric State

RMS: Root Mean Square

RTE: Relative Torsional Energy

SAG: Strain induced Alignment in a Gel

SERF: SElective ReFocusing

SLF: Separated-Local Field

SmA: smectic A

SmA*: chiral smectic A

SmA$_2$: bilayer smectic A

SmA$_d$: interdigitated bilayer smectic A

SmB: smectic B

SmC: smectic C

SmC*: chiral smectic C

SmF: smectic F

SmI: smectic I

SQ: Single-Quantum

ST-DFT: Statistical Thermodynamic Density Functional Theory

T$_c$: clearing point

T$_m$: melting point

t-St: *trans*-stilbene

TBO: Triple resonance Broadband Observe

TCB: 1,3,5-trichlorobenzene

THF: tetrahydrofuran

TFE: trifluoroethanol

TMA: tetramethylallene

VASS: Variable Angle Sample Spinning

ZLI1132: mixture of alkylcyclohexylcyanobenzenes and alkylcyclohexylcyanobiphenyl

La spettroscopia NMR in mezzi fortemente e debolmente orientanti è stata la tecnica utilizzata efficacemente per trattare problemi orientazionali, posizionali, strutturali e conformazionali di una varietà di piccole molecole organiche rigide e flessibili in soluzione.

Inizialmente, per una molecola di forma globulare disciolta in una fase nematica, l'ordine orientazionale molto basso è stato sfruttato per esplorare il ruolo dei diversi contributi agli accoppiamenti dipolari osservati. In tale situazione limite, è emerso un effetto predominante del termine di accoppiamento riorientazione-vibrazione. In seguito, dati NMR, ottenuti a partire da piccole molecole usate come sonde all'interno di solventi smettici, sono stati combinati con metodologie di termodinamica statistica e teoria del funzionale densità, con l'obiettivo di misurare i parametri di ordine posizionale sia del solvente che dei soluti. La metodologia ha dato risultati incoraggianti per cristalli liquidi formanti sia la comune fase smettica A che la fase smettica interdigitata A_d.

La strategia è stata estesa successivamente all'indagine di struttura, ordine ed equilibrio conformazionale di molecole flessibili bioattive o biomimetiche disciolte in vari solventi NMR parzialmente ordinati. Dapprima è stato affrontato uno studio sperimentale e teorico sulla molecola simmetrica del bifenile, caratterizzata da una singola rotazione tra i due anelli benzenici (singolo rotore), disciolta in un cristallo liquido termotropico. Questo caso esemplificativo dimostra che le simulazioni di dinamica molecolare rappresentano uno strumento promettente per stimare un set di accoppiamenti dipolari di un soluto in un solvente nematico termotropico. Il set di D_{ij} ottenuto dalla dinamica molecolare è stato infatti usato come set di parametri di partenza in un'analisi spettrale standard. In seguito è stato preso in esame l'equilibrio conformazionale di alcuni farmaci anti-infiammatori non steroidei a singolo e doppio rotore, appartenenti alle famiglie dei salicilati e dei profeni, disciolti in fasi nematiche chirali debolmente orientanti a base di PBLG. È stata sviluppata in questo contesto una nuova sequenza di impulsi che consente, per un dato atomo di fluoro, l'estrazione di tutti gli accoppiamenti [1]H-^{19}F in un singolo esperimento NMR. Partendo dagli accoppiamenti dipolari omo- ed eteronucleari, difficili da estrarre in cristalli liquidi termotropici per via della complessità spettrale, le distribuzioni torsionali di tali molecole sono state adeguatamente descritte attraverso il modello AP-DPD. Infine, l'equilibrio conformazionale e l'ordine orientazionale di due stilbenoidi aventi torsioni cooperative sono stati indagati in una fase liquido cristallina sia fortemente che debolmente orientante. Questo studio comparativo ha permesso di trarre alcune interessanti conclusioni circa affidabilità, accuratezza e accessibilità dei dati desiderati estratti nelle due diverse fasi.

La spectroscopie RMN alliée à l'utilisation de solvants cristal-liquide fortement et faiblement orientants est une stratégie efficace pour élucider les structures et distributions conformationnelles de petites molécules organiques rigides et flexibles en solution, et déterminer les ordres orientationnel et positionnel des solutés comme des solvants orientés.

Dans une première partie, afin d'explorer les différentes contributions aux couplages dipolaires d'un soluté donné, la très faible amplitude de l'ordre orientationnel d'une molécule quasi-sphérique, le tetramethylallène, dissoute dans un nématique thermotrope est exploitée. Dans cette situation limite, le caractère prédominant des mécanismes de réorientation et de vibration moléculaire est mis en évidence, et estimé. Dans une seconde partie, les données RMN obtenues à partir de solutés de petites tailles dissous dans des solvants smectiques sont combinées aux résultats de calculs reposant sur des concepts de thermodynamique statistique et de la théorie de la fonctionnelle de densité. L'efficacité de cette méthode dans la détermination des paramètres d'ordres positionnel du solvant et orientationnel des molécules-sondes est démontrée aussi bien dans le cas de phases conventionnelles smectiques A que celui plus délicat de smectiques interdigitées A_d.

La stratégie d'analyse proposée est ensuite étendue à l'investigation des structures tridimensionnelles et équilibres conformationnels de molécules flexibles bioactives ou biomimétiques. Dans une perspective méthodologique, à l'aide d'études expérimentale et théorique portant sur le biphényle, molécule symétrique constituée d'un unique rotor, il est tout d'abord démontré l'intérêt des méthodes de simulations par dynamique moléculaire pour évaluer l'ensemble des couplages dipolaires d'un soluté donné dans une phase thermotrope, ultérieurement utilisés comme paramètres initiaux dans une analyse spectrale itérative, et *in fine* déterminées précisément. L'analyse spectrale chronophage et dont l'aboutissement est incertain si les paramètres initiaux sont difficiles à estimer, en est ainsi facilitée. Puis, les distributions conformationnelles d'anti-inflammatoires non stéroïdiens de dérivés salicylés et profènes, fluorés ou non, constitués d'un ou deux rotors indépendants sont présentées. *Via* l'utilisation inédite du modèle AP-DPD dans les solvants nématiques (chiraux) lyotropes faiblement orientants, et à partir des couplages dipolaires homo- et hétéronucléaires notamment obtenus grâce à l'expérience RMN GET-SERF, créée à propos pour permettre l'extraction simple et rapide des couplages ^{1}H-^{19}F, les surfaces d'énergie potentielle de ces biomolécules sont décrites de façon satisfaisante. Enfin, les équilibres conformationnels de deux stilbénoïdes constitués de deux rotors coopératifs sont déterminés dans deux solvants cristal-liquide, l'un fortement, l'autre faiblement orientant. Ces études comparatives permettent de discuter la fiabilité, la précision et l'accessibilité des observables RMN extraites dans les phases, et d'établir la complémentarité des analyses RMN réalisées dans ces solvants.

Publications

G. Celebre, G. De Luca, M. E. Di Pietro, Experimental assessment of the vibration-reorientation contribution to liquid crystal NMR dipolar couplings: the case of tetramethylallene dissolved in a nematic mesophase, *J. Phys. Chem. B*, 115 (**2011**) 11119-11126, DOI: dx.doi.org/10.1021/jp2021598

M. E. Di Pietro, G. Celebre, G. De Luca, G. Cinacchi, Rigid probe solutes in a smectic-A liquid crystal: an unconventional route to the latter's positional order parameters, *Phys. Rev. E*, 84 (**2011**) 061703.1-7, DOI: 10.1103/PhysRevE.84.061703

G. Celebre, G. De Luca, M. E. Di Pietro, Conformational distribution of *trans*-stilbene in solution investigated by liquid crystal NMR spectroscopy and compared with *in vacuo* theoretical predictions, *J. Phys. Chem. B*, 116 (**2012**) 2876-2885, DOI: dx.doi.org/10.1021/jp211962w

M. E. Di Pietro, G. Celebre, G. De Luca, H. Zimmermann, G. Cinacchi, Smectic order parameters *via* liquid crystal NMR spectroscopy: application to a partial bilayer smectic A phase, *Eur. Phys. J. E*, 35 (**2012**) 112.1-10, DOI: 10.1140/epje/i2012-12112-0

G. Celebre, G. De Luca, M. E. Di Pietro, The stable conformations of 4,4'-dichloro-*trans*-stilbene in solution by liquid crystal NMR spectroscopy, *J. Mol. Struct.*, 1034 (**2013**) 283-288, DOI: dx.doi.org/10.1016/j.molstruc.2012.10.057

M. E. Di Pietro, C. Aroulanda, D. Merlet, GET-SERF, a new gradient encoded SERF experiment for the trivial edition of ^{1}H-^{19}F couplings, *J. Magn. Reson.*, 234 (**2013**) 101-105, DOI: dx.doi.org/10.1016/j.jmr.2013.06.011

A. Pizzirusso, L. Muccioli, C. Zannoni, M. Longeri, G. Celebre, G. De Luca, M. E. Di Pietro, Alignment of biphenyl in nematic and smectic liquid crystals. Comparing atomistic simulations and proton NMR experiments for 5CB and 8CB solutions, *in preparation*

M. E. Di Pietro, C. Aroulanda, D. Merlet, G. De Luca, G. Celebre, Conformational investigation in solution of an anti-inflammatory drug by NMR spectroscopy in weakly ordering media, *in preparation*

Oral Communications

M. E. Di Pietro, D. Merlet, C. Aroulanda, G. De Luca, G. Celebre, NMR in weakly ordering liquid crystals as a tool for the conformational analysis of bioactive molecules, *NMR in Oriented Phases*, Tropea (VV), Italy, 28th September – 2nd October 2013

Posters

- M. E. Di Pietro, G. De Luca, G. Celebre, M. Longeri, Structural and conformational investigation of stilbene derivatives as solutes in nematic liquid crystalline solvents, *International School of Liquid Crystals 18th Course*, Erice (TP), Italy, 3rd-10th July 2011

- M. E. Di Pietro, D. Merlet, C. Aroulanda, G. De Luca, G. Celebre, Contribution de la RMN dans les solvants cristaux liquides à l'étude de molécules bioactives, *Conférence Thématique du GERM*, Val de Loire, France, 29th May – 1st June 2012

- M. E. Di Pietro, D. Merlet, C. Aroulanda, G. De Luca, G. Celebre, Contribution of NMR spectroscopy in weakly orienting liquid crystals to the study of biologically active molecules, *10° Congresso Nazionale Società Italiana Cristalli Liquidi* - Sapienza Università di Roma, Roma, Italy, 21th-23th June 2013

- M. E. Di Pietro, C. Aroulanda, D. Merlet, G. De Luca, G. Celebre, M. Longeri, Conformational distribution of antiinflammatory drugs investigated by NMR in weakly ordering liquid crystals, *XL Congresso Nazionale di Chimica Fisica* - Università del Piemonte Orientale "A. Avogadro", Alessandria, Italy, 23th-27th June 2013

PUBLISHED PAPER

Experimental Assessment of the Vibration-Reorientation Contribution to Liquid Crystal NMR Dipolar Couplings: The Case of Tetramethylallene Dissolved in a Nematic Mesophase

Giorgio Celebre,* Giuseppina De Luca, and Maria Enrica Di Pietro

Dipartimento di Chimica, Università della Calabria, v. P. Bucci, I-87036 Rende (CS), Italy

ABSTRACT: In the present paper, the peculiar orientational behavior, studied by liquid crystal NMR (LXNMR) spectroscopy, of the D_{2d} symmetry quasi-spherical molecule of tetramethylallene (TMA) dissolved in the nematic solvent I52 is exploited to attempt a quantitative experimental assessment of the correlation between molecular vibrations and overall rotations in weakly oriented molecules. The analysis of the very small D_{HH} and $^1D_{^{13}C-H}$ dipolar couplings, available from the natural abundance LXNMR spectra of TMA at different temperatures, allows for a derivation leading (by making a few approximations) to the quantification of the vibration–reorientation (also called *nonrigid*) contribution affecting the observed direct $^1D_{^{13}C-H}$ dipolar coupling. The obtained results show that, under the particular conditions of the studied system (very weak orientational ordering of a highly symmetric molecule), this contribution is particularly important, in order to reproduce the whole value of the "observed" dipolar coupling. This issue is discussed and commented on at length in the work, also, by making reference to the analogy with perfectly symmetric molecules (such as methane and analogues) dissolved in liquid crystalline phases.
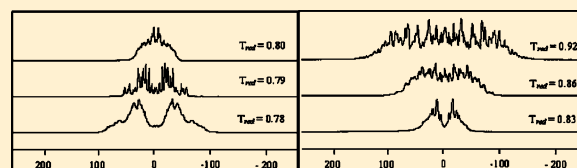
1. INTRODUCTION

Since the seminal work of Saupe and Englert[1] (the ^{1}H NMR spectrum of benzene in a nematic solution), the liquid crystal NMR (LXNMR) spectroscopy of molecules dissolved in uniaxial liquid crystalline solvents (typically nematics, but also smectic A mesophases) has been recognized as a very powerful tool to investigate molecular interactions in condensed phases. In particular, the observed dipolar couplings D_{ij}^{obs} between the *i*-th and *j*-th magnetically active nuclei present in the probe molecule potentially bring a significant amount of invaluable information. In a uniaxial anisotropic medium where the mesophase director $\hat{n}$ aligns along the external *Z*-applied magnetic field (i.e., $\hat{n}\|Z$, as for the nematic solvent I52 used in this work; see below), the expression giving the D_{ij}^{obs} has to be strictly written in the following way:[2]

$$\forall\ i,j,\ D_{ij}^{obs} = -\mu_0\gamma_i\gamma_j\frac{\hbar}{16\pi^2}\sum_{(a,b)\ \in\ \{x,y,z\}^2}\langle s_{ab}d_{ij}^{ab}\rangle \qquad (1)$$

where $\hbar = h/2\pi$ (being, of course, *h* the Planck's constant), γ is the nuclear magnetogyric ratio, and μ_0 is the vacuum magnetic permeability. Moreover,

$$d_{ij}^{ab} = \frac{\cos\theta_{ij}^a\cos\theta_{ij}^b}{r_{ij}^3} \qquad (2)$$

with r_{ij} as the *i*−*j* internuclear distance and θ_{ij}^a as the angle between the *a*-axis of the molecular frame and the *ij* direction. Finally,

$$s_{ab} = \frac{3\cos\omega_n^a\cos\omega_n^b - \delta_{ab}}{2} \qquad (3)$$

where δ_{ab} is the Kronecker delta function and ω_n^a represents the instantaneous angle between $\hat{n}$ and the *a*-axis of a Cartesian coordinate system (*a*, *b*, *c*) fixed on the solute molecule. The angular brackets of eq 1 denote averaging over all the relevant molecular motions, namely, the vibrational and reorientational motions (the latter are also called "overall rotations" or "molecular tumbling") of the molecule. The calculations of the dipolar couplings are, of course, made easier by assuming the internal and reorientational motions of the molecule are independent. So, for convenience, the average of eq 1 is often "conventionally"[3h] decoupled to give

$$\forall\ i,j,\ D_{ij}^{obs} \equiv -\mu_0\gamma_i\gamma_j\frac{\hbar}{16\pi^2}\sum_{(a,b)\ \in\ \{x,y,z\}^2}\langle d_{ij}^{ab}\rangle_{vibrations}\langle s_{ab}\rangle_{overall rotations}$$

$$(4)$$

where $\langle s_{ab}\rangle_{overall rotations} = S_{ab}$ represents the familiar Saupe matrix, made up of the solute order parameters (the symbol "$\equiv$" stands for "assumed equal to"). The assumption of eq 4 would be strictly valid only in the very particular case where the ordering process is completely independent of the internal state of the molecule;[3a,c,g] if this is not so (as in the overwhelming majority of cases), the correlation between molecular vibrations and reorientational motions should be, in principle, taken into account (for a wide selection of works treating the problem, see the long list reported in ref 3). In our opinion, a very effective way to express the approximated D_{ij}^{obs}
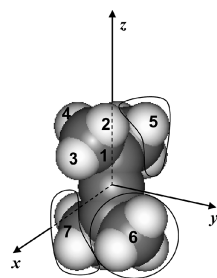
Figure 1. Structure of the D_{2d} symmetry tetramethylallene (TMA), numbering of atoms ($^{13}C1$, H2, H3, and H4), groups of equivalent methyl protons (5, 6, and 7), and the molecular frame.

term is that suggested by a formulation developed in the past within a perturbation approach, taking as zero-order wave functions the products of electronic, harmonic vibrational, and rigid rotor rotational wave functions (for more theoretical details, see refs 3a–3g and 3m–3o):

$$D_{ij}^{obs} \approx D_{ij}^{eq} + D_{ij}^{a} + D_{ij}^{h} + D_{ij}^{nonrigid} \tag{5}$$

where D_{ij}^{w} (with w = eq, a, or h) represents the "equilibrium", "anharmonic", and "harmonic" contributions, whereas the last $D_{ij}^{nonrigid}$ is a correction term accounting for the coupling between vibrational and reorientational motions. An important feature of eq 5 is that the first three terms all scale with the usual Saupe solute orientation parameters S_{ab}, according to the following generalized formula:

$$D_{ij}^{w} = -K_{ij} \sum_{a,b} S_{ab} (^{w}\Phi_{ij}^{ab}); w = eq, a, h \tag{6}$$

where, as usual, $K_{ij} = \mu_0 \gamma_i \gamma_j (\hbar/16\pi^2)$ and the generic $^{w}\Phi_{ij}^{ab}$ terms (whose form is dependent on the chosen model) can be, in principle, determined following the existing and widely used methods.[2c,3b–3o,4] On the contrary, the nonrigid contribution shows a different, more complex orientational dependence of the kind $\langle s_{ab}s_{kl}\rangle_{overallrotations}$, where the k and l subscripts run over the components of some second-rank tensorial property β_{kl} of the solute molecule.[3m] The assessment of the relative weights of the different contributions D_{ij}^{w} (and, in particular, of $D_{ij}^{nonrigid}$) in reproducing the sum D_{ij}^{obs} is a debated question.[3n] As a matter of fact, D_{ij}^{eq}, D_{ij}^{a}, and D_{ij}^{h} could be estimated, as said above (at least in principle), by theoretical calculations and/or experimental procedures,[2c,3b–o,4] whereas the term $D_{ij}^{nonrigid}$ is rather subtle and elusive and it is usually considered as an adjustable parameter[3n,o] or its value is taken from that (calculated by least-squares fits) of similar groups in different, simpler molecules,[3l] claiming a certain degree of transferability.[3m] It is indeed very difficult to assess experimentally the single nonrigid contribution because, of course, only the whole sum giving the observed D_{ij}^{obs} is known from the experiment. Anyway, there are cases (in particular, when the orientational ordering of the molecule is very small and some of the other D_{ij}^{w} contributions can be safely neglected) where we will show it is possible to appreciate the "experimental" value of the $D_{ij}^{nonrigid}$ term; this is the case of the quasi-spherical D_{2d} symmetry tetramethylallene molecule (TMA; see Figure 1 for structure, molecular frame, and atom numbering) dissolved in the nematic solvent I52, whose chemical structure is reported in ref 5. Of course, the symmetry of the molecule is such that only one order parameter (namely, S_{zz}) is required to describe the orientational ordering of the solute.
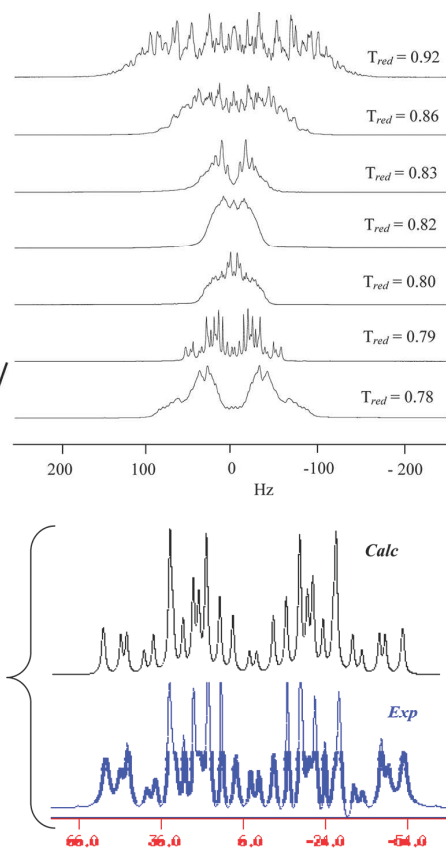
Figure 2. 500 MHz experimental ^1H spectra of TMA dissolved in I52 at different values of T_{red} (top). The comparison between the experimental spectrum and the fitted spectrum for the best case ($T_{red} = 0.79$) is also shown. The dipolar couplings used to obtain the calculated spectrum are those reported in Table 1; moreover, only J_{25} has been set slightly different from 0 ($J_{25} = -0.2$ Hz) to reproduce some fine features of the spectrum.

2. NMR EXPERIMENTS

A dilute solution ($\sim$3 wt %) was prepared by dissolving the TMA (commercially available from Aldrich) in the nematic liquid crystal solvent I52 (purchased from Merck Ltd.). The sample was heated a few times up to its nematic–isotropic transition temperature (T_{NI}); then, it was strongly shaken to give a very homogeneous solution; and finally, it was left to cool slowly in the magnetic field of the NMR spectrometer. The ^1H and ^{13}C (^1H coupled) spectra were recorded at various temperatures on a Bruker Avance 500 MHz instrument (11.74 T) within 40–50 min intervals of thermostatization for each T value. The proton spectra were recorded upon cooling from the isotropic phase, ranging from 363 to 260 K (so covering, in practice, the whole range of the nematic phase; in terms of reduced temperature $T_{red} = T/T_{NI}$; this corresponds to the range 0.70–0.99). In Figure 2, the experimental ^1H spectra at different values of T_{red} are shown. Unfortunately, as a result of the low ordering of the solute and the high number of lines, we were not able to obtain always "very good" spectra with well separated and sharp lines. Some spectra appear crowded with quite broad lines due to the many transitions of the twelve-spin system, so that an extremely thorough analysis is not always possible. The best case (shown at

the bottom of Figure 2) is at $T_{red} = 0.79$, where the D_{26} is zero (see below) and the proton NMR spectrum is simply described by two coupled methyl groups (i.e. it is the same six-spin system as that of acetone); this explains the relatively simple spectrum obtained. On the other hand, the quality of the spectra is good enough to appreciate the following two main features, which deserve to be immediately emphasized: (1) all the spectra are characterized by a whole spectral width of only a few tens of hertz (which is indicative, as said above, of a very weak orientational order of the molecule); (2) it is possible to observe the peculiar phenomenon that, on cooling, the spectral width initially decreases until it reaches its minimum value at $T_{red} = 0.82$ (where the narrowest spectrum is recorded), then it starts to increase again on going to lower temperatures. The just mentioned points were revealed to be crucial in this work. The second point, in particular, suggested to us intuitively the possibility that S_{zz} changes its sign along T_{red} (in this case, the molecular order parameter should cross through 0 at about $T_{red} = 0.82$, as said above). As we will explain, even though the hypothesis of the change of sign is immediate and, probably, the more physically sensible, it is not fully satisfactory because it conflicts with other reasonable considerations that can be made about our system. Thanks to the small orientational ordering of the molecule in I52, it was possible to record also the natural abundance ^{13}C spectra. Each ^{13}C NMR spectrum, recorded averaging over 5000 free induction decays, resulted to be basically composed by the lines resulting from the C1 carbon coupled with the three equivalent protons H2, H3, and H4 (see Figure 1), so producing a quadruplet from which the D_{12} dipolar coupling constant was extracted by fixing $J_{12} = 127$ Hz (value obtained from the isotropic spectrum of TMA in CDCl$_3$). Unfortunately, the ^{13}C spectra showed a satisfactory signal-to-noise ratio only at the following three reduced temperatures, in common with the ^{1}H spectra: $T_{red} = 0.79$; $T_{red} = 0.83$; and $T_{red} = 0.86$. Nonetheless, the information from the carbon LXNMR resulted to be of fundamental importance for the whole development of this study; as a matter of fact, it is the only D_{ij}^{obs} for which the magnitude and absolute sign can be attributed unambiguously.

3. RESULTS AND DISCUSSION

The ^{1}H and ^{13}C (^{1}H coupled) NMR spectra of TMA in I52 at different temperatures were analyzed by the homemade iterative computer program ARCANA.[6] About the ^{1}H spectra, a perfect analysis was not always possible because of the already explained "physiological" low resolution of the spectra. The values reported below for the D_{ij}^{obs} are, anyway, the only ones able to reproduce, at best, our experimental spectra; as a consequence, in this work, we considered these values sufficiently reliable to carry out our study at a semiquantitative level. Moreover, only the magnitudes and relative signs of the three D_{HH} couplings can be determined from the proton spectra, whereas the magnitude and absolute sign of $^1D_{^{13}C-H}$ (corresponding to D_{12}^{obs}) can be unequivocally assigned, as said in the previous section, from the ^{13}C spectra. The D_{12}^{obs} and the magnitude and relative signs of the remaining three D_{HH} couplings obtained from the analysis (D_{23}^{obs}, D_{25}^{obs}, and D_{26}^{obs}) are reported in Table 1. The just described limitations affecting our observed dipolar couplings hinder a possible unambiguous interpretation of the phenomena; on the contrary, they generate at least a couple of possible scenarios for the explanation of the experimental observations. Even though neither of the two scenarios is fully satisfactory in explaining all the observations, both converge in

Table 1. Observed Dipolar Couplings D_{ij}^{obs} (Hz) of TMA Dissolved in I52^{a,b}

T/K (T_{red})	283 (0.77)	290 (0.79)	305 (0.83)	315 (0.86)
D_{12}		9.92 ± 0.10	4.82 ± 0.17	2.92 ± 0.47
D_{23}	14.87 ± 0.30	9.70 ± 0.20	9.13 ± 0.11	12.26 ± 0.20
D_{25}	-14.89 ± 0.25	-8.11 ± 0.10	-7.61 ± 0.11	-10.07 ± 0.18
D_{26}	2.61 ± 0.60	0.04 ± 0.15	2.18 ± 0.50	4.29 ± 0.60

^{a} About the J_{HH} indirect couplings, only J_{25} has been set slightly different from 0 ($J_{25} = -0.2$ Hz) in order to reproduce some fine features of the spectra. ^{b} Concerning the three D_{HH} couplings, only the magnitudes and relative signs can be obtained from the spectra (see text).

indicating that the contribution to the dipolar couplings accounting for the vibrational–reorientational correlation plays a very important role. In the following, we will try to emphasize the pros and cons of the proposed different interpretations of the experimental observations, and then, we will draw the conclusions.

As already said above, in the NMR Experiments section, our first intuition was that the three D_{HH} couplings change sign at some T_{red} between 0.79 and 0.83 as a consequence of the fact that S_{zz} crosses through 0. According to the literature, the nonrigid contribution for the "long-range" D_{26} and the anharmonic and harmonic contributions for all three interproton couplings are usually considered to be very small or even negligible[7,4,3m] (less than 1%). Following these assumptions, we can simply write from eq 5

$$\left.\begin{aligned} D_{23}^{obs} &\approx D_{23}^{eq} + D_{23}^{nonrigid} \\ D_{25}^{obs} &\approx D_{25}^{eq} + D_{25}^{nonrigid} \\ D_{26}^{obs} &\approx D_{26}^{eq} \end{aligned}\right\} \qquad (7)$$

The surviving term D_{26}^{eq} is seen to vanish at T_{red} about 0.79 (see Table 1), and this could be read as a symptom that, at that T_{red}, S_{zz} is ~0. As a consequence of this, also, the contributions D_{23}^{eq}, D_{25}^{eq}, and D_{12}^{eq} should vanish at that temperature, so that, at least for the interproton couplings, the observed values of Table 1 at $T_{red} = 0.79$ should be due exclusively to the nonrigid contributions (in other words $D_{23}^{obs} \approx D_{23}^{nonrigid}$ and $D_{25}^{obs} \approx D_{25}^{nonrigid}$ at $T_{red} = 0.79$). About D_{12}^{obs}, a vibrational contribution (even though probably very small, as a result of the low order of the solute) besides the nonrigid one could be hypothetized. There are, however, a couple of considerations that bring into question this very simple, straightforward, and physically sensible interpretation (which we will call "scenario α") of the data. First of all, the values reported in Table 1 are, in our opinion, too large (in particular for the two interproton couplings D_{23}^{obs} and D_{25}^{obs}) to be due exclusively to the nonrigid term. This prompted us to test indirectly the influence of the nonrigid contributions on D_{23}^{obs} and D_{25}^{obs} by plotting the ratio D_{23}/D_{25} vs T_{red}. As a matter of fact, because our D_{2d} molecule requires that all except nonrigid contributions to the D_{ij} to an excellent approximation, be proportional to the sole S_{zz} order parameter, the ratios between the experimental dipolar couplings are expected to be essentially independent of T when the nonrigid contributions are negligible. The ratio D_{23}/D_{25} for the temperatures where the ^{13}C spectra are available is shown in Figure 3.

Immediately, an almost perfect T independence of the D_{23}/D_{25} ratio is observed. Of course, this result could be a coincidence; however, it might be also read as a significant clue that D_{23} and D_{25} both are devoid of nonrigid effects. In this case (because, as said above, the harmonic and anharmonic terms,
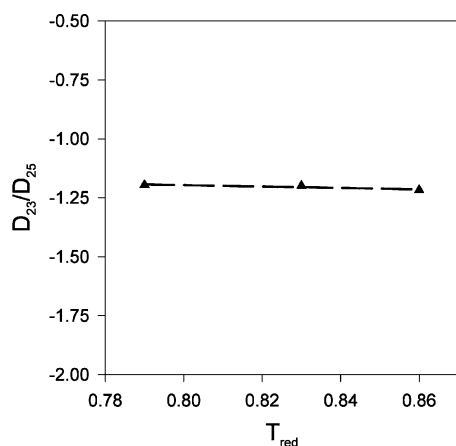
Figure 3. Ratio D_{23}/D_{25} for the temperatures where the ^{13}C NMR spectra are available.

scaling as S_{zz}, typically entail very small corrections to the already small couplings) we should reject what was said above, and on the contrary, we would be allowed to write

$$\left. \begin{array}{l} D_{23}^{obs} \approx D_{23}^{eq} \\ D_{25}^{obs} \approx D_{25}^{eq} \end{array} \right\} \tag{8}$$

Another criticism, based on common physical sense and intuition, can be raised to the hypothesis α. The D_{12}^{obs} is observed to decrease as T_{red} increases, so that the decreased value of this coupling at $T_{red} = 0.83$ ($D_{12}^{obs} = 4.82$) with respect to $D_{12}^{obs} = 9.92$ at $T_{red} = 0.79$ should be due to an additional contribution opposite in sign to the nonrigid one. Now, if we reasonably admit that $D_{12}^{eq} \gg D_{12}^{a}, D_{12}^{h}$, in order to have a negative additional contribution to $D_{12}^{nonrigid}$ at $T_{red} = 0.83$, we should have an order parameter that, from being ~ 0 at $T_{red} = 0.79$, becomes positive at $T_{red} = 0.83$ (this is because D_{12}^{eq} is negative when S_{zz} is positive). This is in principle possible, of course, but if we consider this situation within our scenario α, where S_{zz} changes its sign crossing through 0 at $T_{red} \approx 0.79$, this means that the order parameter is negative at temperatures lower than $T_{red} = 0.79$ and becomes positive for higher temperatures. This result is, in our opinion, quite counterintuitive, because the solute seems to prefer the parallel alignment for higher temperatures (where the orientational thermal disorder is higher) whereas it "opts" for the more hampered perpendicular orientation when the temperature is lower and the thermal disorder is less important. If we invert the sequence of the signs of S_{zz}, assuming the more reasonable one (positive for $T_{red} < 0.79$, 0 for $T_{red} = 0.79$, and negative for $T_{red} > 0.79$), the behavior of D_{12} vs T_{red} becomes inexplicable, because after $T_{red} = 0.79$ the significant additional term to $D_{12}^{nonrigid}$ (i.e., D_{12}^{eq}) is positive, so that an increase of D_{12} with the increase in temperature should be expected, contrary to what we observe. In the light of the arguments expounded above, the scenario α (i.e., the immediate and intuitive qualitative explanation that the observed phenomenon is due to the change of sign of the order parameter) is, in our opinion, not completely satisfactory because it conflicts with the reasonable considerations carried out above about our system. If the change of sign of S_{zz} does not occur, the order parameter has to be necessarily negative (as a result of the D_{12} couplings trend), and the dipolar
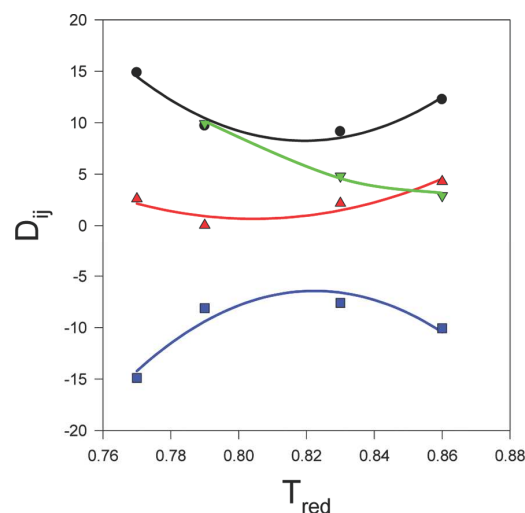
Figure 4. Behaviors of interproton dipolar couplings (D_{23}, black circle; D_{26}, red triangle; and D_{25}, blue square) and of the $^{13}C-H$ coupling (D_{12}, green inverted triangle) as a function of T_{red} when $S_{zz} < 0$ is assumed (see text for explanation). The local quadratic fittings of the curves are drawn just as eye-guides.

couplings pass through a minimum (maximum) when S_{zz} reaches its smallest possible magnitude (see Figure 4). This originates another possible scenario (called β), which is undoubtedly less intuitive. Looking at Figure 4, it is immediately realized that the three interproton dipolar couplings share their minimum magnitude at the same $(T_{red})_{min}$ of about 0.82 (that is, of course, exactly the temperature where the experimental ^1H-LXNMR spectra show their narrowest whole spectral width); on the contrary, the extrapolated minimum of the $^{13}C-H$ dipolar coupling D_{12} falls at $T_{red} > 0.86$. Now, keeping the approximation of neglecting the vibrational contributions and accepting eq 8, as suggested by Figure 3, we are allowed to write $D_{23}^{obs} \approx D_{23}^{eq}$; $D_{25}^{obs} \approx D_{25}^{eq}$; and $D_{26}^{obs} \approx D_{26}^{eq}$. Following this assumption, it is very simple, by adopting standard regular geometries for the molecule,[8] to calculate the values of S_{zz} (reported in Table 2 and shown in Figure 5) from the interproton dipolar couplings D_{23} and D_{25} at the different temperatures.

Note that the observed D_{26} couplings have been excluded in this case from the calculation of the order parameter because they are too small and affected by large relative errors. If we include it, the results concerning S_{zz} are in practice the same (even though affected by quite high relative errors) but the D_{26} observed values at the different temperatures are very badly reproduced.

In Figure 5, it is evident, as expected, that the minimum of magnitude of the S_{zz} order parameter falls at $(T_{red})_{min} = 0.82$, the temperature where the interproton dipolar couplings are simultaneously the smallest ones in magnitude and the proton LXNMR spectra are, of course, the narrowest ones (see Figure 2). At this point, we tried to evaluate quantitatively the different contributions playing a role in the remaining $^{13}C-H$ coupling D_{12}^{obs}. From eq 5, we can write

$$\Delta_{12} \equiv (D_{12}^{obs} - D_{12}^{eq}) \approx (D_{12}^{a} + D_{12}^{h} + D_{12}^{nonrigid}) \tag{9}$$

where the D_{12}^{eq} are calculated by using the S_{zz} values of Table 2. In Table 3, the so obtained D_{12}^{eq} and Δ_{12} are reported.

Table 2. Values of the S_{zz} Order Parameter of TMA Dissolved in I52 at Different Temperatures[a]

T/K (T_{red})	283 (0.77)	290 (0.79)	305 (0.83)	315 (0.86)
D_{23}(calcd)	14.29	8.52	8.01	10.68
D_{25}(calcd)	−15.42	−9.20	−8.65	−11.53
rms	0.55	1.13	1.08	1.52
S_{zz}	− 0.0119 ± 0.0005	− 0.007 ± 0.0009	− 0.007 ± 0.0009	− 0.009 ± 0.0013

[a] Obtained from the interproton dipolar couplings D_{23} and D_{25} (see text for more explanations). Moreover, the root mean square (rms) between observed and calculated dipolar couplings is also reported (the relative errors affecting the obtained S_{zz} values have been estimated to be proportional, on average, to the ratio between the rms and the calculated D_{ij} at the different temperatures).
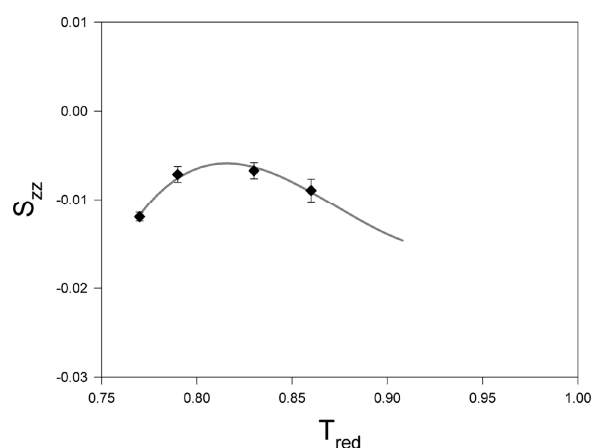
Figure 5. Behavior of the S_{zz} order parameter vs T_{red}. The cubic fitting of the curve is also shown in gray.

Figure 6. Behavior of the Δ_{12} values of Table 3 vs T_{red}. The quadratic fitting of the curve is also shown in gray (the value $\Delta_{12} = 0$ at $T_{red} = 1$ has been added as a boundary condition).

Table 3. Values of D_{12}^{eq} and Δ_{12}[a]

T/K (T_{red})	290 (0.79)	305 (0.83)	315 (0.86)
D_{12}^{eq}	6.36 ± 0.25	5.98 ± 0.48	7.97 ± 1.11
Δ_{12}	3.56 ± 0.35	− 1.16 ± 0.68	− 5.05 ± 1.58

[a] See eq 9. Obtained by using the S_{zz} values of Table 2. The errors affecting the D_{12}^{eq} values have been estimated, by error propagation, from the corresponding errors on the order parameter (see Table 2).

By following eq 6, the sum of the harmonic and anharmonic contributions can be collected as

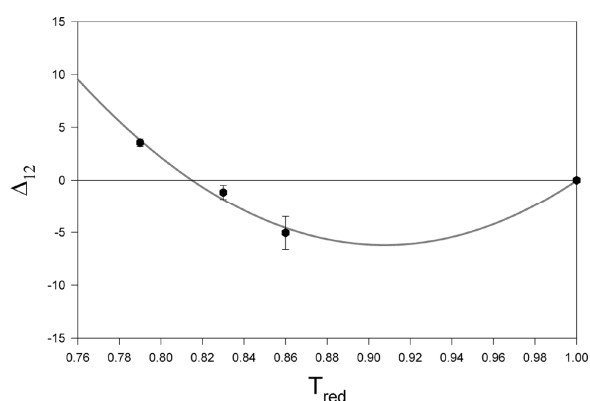$$(D_{12}^{a} + D_{12}^{h}) = - S_{zz}\Gamma_{12} \quad (10)$$

where

$$\Gamma_{12} = [K_{12}(^{a}\Phi_{12}^{zz} + {}^{h}\Phi_{12}^{zz})] \quad (11)$$

so that eq 9 becomes

$$\Delta_{12} \approx - S_{zz}\Gamma_{12} + D_{12}^{nonrigid} \quad (12)$$

Because S_{zz} vs T_{red} is known from the interproton dipolar couplings (its behavior has been extrapolated to the whole range of T_{red} by a cubic fitting, as shown in Figure 5), if we are able to determine the Γ_{12} term of eq 11, we have all the ingredients to quantitatively assess (of course within the approximations used in the derivation) the $D_{12}^{nonrigid}$ contribution from eq 12. To evaluate Γ_{12} without force fields and theoretical calculations about harmonic and anharmonic vibrational corrections affecting

D_{12}, it can be useful to plot the different Δ_{12} (Table 3) as a function of T_{red} (Figure 6).

We observe that Δ_{12} crosses through 0, changing its sign, exactly at $T_{red} = 0.82$, which, as we already said, is the $(T_{red})_{min}$ of the three interproton dipolar couplings (see Figure 4). We do not know if this is a coincidence or not (this is an interesting point, deserving additional investigations, but it is, at the moment, out of the scope of the work; further studies are planned to shed more light on this observation); however, we can exploit this fact to proceed with our derivation. Because when $\Delta_{12} = 0$ then $D_{12}^{obs} = D_{12}^{eq}$, this result seems to suggest, intriguingly, that at least at $T_{red} = 0.82$, only the equilibrium contributions survive for all the dipolar couplings, including D_{12}. Of course, this can occur when the single D_{12}^{a}, D_{12}^{h}, and $D_{12}^{nonrigid}$ are negligibly small (as it is, according to our crude assumptions, for interproton couplings in the whole temperature range), or as we suspect, it is the case for the $^{13}C-H$ coupling D_{12}, when there is a particular temperature (in this case, exactly $T_{red} = 0.82$), where (possibly by chance) a perfect balance of the effects exists, such that from eq 12

$$(D_{12}^{nonrigid})_{T_{red} = 0.82} = \Gamma_{12}(S_{zz})_{T_{red} = 0.82} \quad (13)$$

Coming back to our first aim of determining Γ_{12} in order to calculate $D_{12}^{nonrigid}$, we cannot directly exploit eq 13 for this purpose, because the nonrigid contribution itself is involved. On the other hand, if we consider Γ_{12} to be independent of T_{red} (which is a reasonable approximation), we can exploit the fact that the function $\Delta_{12}(T_{red})$ reaches its minimum at $T_{red} = 0.91$ (see Figure 6); so, its derivative calculated there has to vanish. In light of

what was said above, from eq 12, the following relation holds:

$$\left(\frac{\partial \Delta_{12}}{\partial T_{\mathrm{red}}}\right)_{T_{\mathrm{red}}=0.91} = -\Gamma_{12}\left(\frac{\partial S_{zz}}{\partial T_{\mathrm{red}}}\right)_{T_{\mathrm{red}}=0.91}$$

$$+ \left(\frac{\partial D_{12}^{\mathrm{nonrigid}}}{\partial T_{\mathrm{red}}}\right)_{T_{\mathrm{red}}=0.91} = 0 \qquad (14)$$

so that Γ_{12} is given by

$$\Gamma_{12} = \left(\frac{\partial D_{12}^{\mathrm{nonrigid}}}{\partial T_{\mathrm{red}}}\right)_{T_{\mathrm{red}}=0.91} \bigg/ \left(\frac{\partial S_{zz}}{\partial T_{\mathrm{red}}}\right)_{T_{\mathrm{red}}=0.91} \qquad (15)$$

By introducing eq 15 in eq 12 we obtain the following explicit general equation giving the $D_{12}^{\mathrm{nonrigid}}$ contribution as a function of T_{red} (in other words, the magnitude of the vibrational–reorientational correlation at a chosen T_{red}):

$$D_{12}^{\mathrm{nonrigid}}(T_{\mathrm{red}}) \approx \Delta_{12}(T_{\mathrm{red}}) + S_{zz}(T_{\mathrm{red}})\Gamma_{12}$$

$$= \Delta_{12}(T_{\mathrm{red}}) + S_{zz}(T_{\mathrm{red}})\left(\frac{B}{A}\right) \qquad (16)$$

where $A = \partial S_{zz}/(\partial T_{\mathrm{red}})_{T_{\mathrm{red}}=0.91}$ and $B = \partial D_{12}^{\mathrm{nonrigid}}/(\partial T_{\mathrm{red}})_{T_{\mathrm{red}}=0.91}$. Of course, in order to use eq 16, we should be able to evaluate the terms A and B. The term A can be easily calculated by the cubic fitting

$$S_{zz}(T_{\mathrm{red}}) = -8.5765$$

$$+ 29.702 T_{\mathrm{red}} - 34.1819(T_{\mathrm{red}})^2$$

$$+ 13.0565(T_{\mathrm{red}})^3 \qquad (17)$$

shown in gray in Figure 5. As a consequence, we have

$$A = \left(\frac{\partial S_{zz}}{\partial T_{\mathrm{red}}}\right)_{T_{\mathrm{red}}=0.91}$$

$$= 29.7020 - 68.3638(0.91) + 39.1695(0.91)^2$$

$$= -0.0728 \qquad (18)$$

The calculation of the term B is a little bit more complicated. Assuming B is constant within a very narrow range of T_{red} in the proximity of the minimum of Δ_{12} ($T_{\mathrm{red}} = 0.91$), we will consider the following limit expressions:

$$D_{12}^{\mathrm{nonrigid}}(T_{\mathrm{red}} = 0.91) \approx \Delta_{12}(0.91) + S_{zz}(0.91)\left(\frac{B}{A}\right) \qquad (19a)$$

$$\lim_{T_{\mathrm{red}} \to 0.91^+} D_{12}^{\mathrm{nonrigid}}(T_{\mathrm{red}}) \equiv D_{12}^{\mathrm{nonrigid}}(0.91) \qquad (19b)$$

$$\lim_{T_{\mathrm{red}} \to 0.91^-} D_{12}^{\mathrm{nonrigid}}(T_{\mathrm{red}}) \equiv D_{12}^{\mathrm{nonrigid}}(0.91) \qquad (19c)$$

The limits reported above for eqs 19b and 19c (approaching 0.91 from the left and right but, of course, never reaching exactly 0.91) have been calculated numerically from eq 16, by exploiting eq 17 for the evaluation of the function $S_{zz}(T_{\mathrm{red}})$ and the following quadratic (eq 20):

$$\Delta_{12}(T_{\mathrm{red}}) = 590.0644 - 1313.9702 T_{\mathrm{red}}$$

$$+ 723.8776(T_{\mathrm{red}})^2 \qquad (20)$$

Table 4. Values of the $D_{12}^{\mathrm{nonrigid}}$ Contributions Referred to the Temperatures Where Observed Data D_{12}^{obs} are Available[a]

T/K (T_{red})	290 (0.79)	305 (0.83)	315 (0.86)
$D_{12}^{\mathrm{nonrigid}}$	3.44 ± 0.39	-2.15 ± 0.72	-5.00 ± 1.64

[a] The errors affecting the values have been estimated by error propagation, starting from those affecting the Δ_{12} and the order parameters (of course, the errors, even though quite large, cannot quantify the degree of approximation used in the derivation).
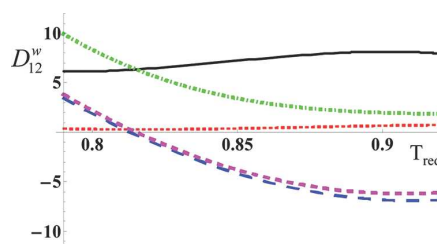
Figure 7. Different D_{12} contributions as a function of T_{red}: $D_{12}^{\mathrm{nonrigid}}$ (blue large-dashed line); $D_{12}^{\mathrm{a}} + D_{12}^{\mathrm{h}}$ (red dotted line); and D_{12}^{eq} (black solid line). For comparison, $D_{12}^{\mathrm{obs}} = D_{12}^{\mathrm{eq}} + D_{12}^{\mathrm{a}} + D_{12}^{\mathrm{h}} + D_{12}^{\mathrm{nonrigid}}$ (green dotted-dashed line) and $\Delta_{12} \equiv D_{12}^{\mathrm{obs}} - D_{12}^{\mathrm{eq}} = D_{12}^{\mathrm{a}} + D_{12}^{\mathrm{h}} + D_{12}^{\mathrm{nonrigid}}$ (pink small-dashed line) have been plotted. It is worthwhile to remember that the large errors affecting the curves are not shown in the figure.

(shown in gray in Figure 6) for the evaluation of the function $\Delta_{12}(T_{\mathrm{red}})$. By using the A value of eq 18, we verified that eqs 19b and 19c converge to eq 19a for $B = \partial D_{12}^{\mathrm{nonrigid}}/(\partial T_{\mathrm{red}})_{T_{\mathrm{red}}0.91} = -3.487$. Finally, by introducing the A and B values in eq 16 we obtain

$$D_{12}^{\mathrm{nonrigid}}(T_{\mathrm{red}}) \approx \Delta_{12}(T_{\mathrm{red}}) + 47.9 S_{zz}(T_{\mathrm{red}}) \qquad (21)$$

By calculating the nonrigid contributions for D_{12}^{obs} at the three experimental temperatures, we obtained the following results (reported in Table 4). Of course, knowing $D_{12}^{\mathrm{nonrigid}}$, D_{12}^{obs}, and D_{12}^{eq} as functions of T_{red}, we can also obtain, by difference, the contribution $(D_{ij}^{\mathrm{a}} + D_{ij}^{\mathrm{h}})$ vs T_{red}. It is interesting to observe the behavior of the different contributions plotted in Figure 7, even though it is worthwhile to emphasize that the information emerging from the figure should be considered just at a semiquantitative level (as a matter of fact, the figure could be rather deceptive because the large errors affecting the curves are not explicitly shown).

At a first glance, it is manifest that, in our just described scenario β, the nonrigid contribution (blue large-dashed line) basically represents the whole Δ_{12} (pink small-dashed line). In other words, the difference between "observed" and "equilibrium" dipolar coupling terms seems to be essentially due to the reorientational–vibration correlation, whereas, on the contrary, the sum of the harmonic and anharmonic contributions (red dotted line) plays a very minor role. This predominance is reasonably due to the fact that our solute is a very symmetric and quasi-spherical molecule, so that a very low orientational ordering (linearly affecting D_{12}^{a} and D_{12}^{h}) has to be expected. It is interesting at this point to emphasize that, from both our α and β descriptions, a kind of "methane-like" behavior can probably be invoked for our solute. In other words, we could be in the presence of a phenomenon similar to that observed for methane[9a–e,3b,d,e,g,k] and other very symmetric (about spherical)

molecules[9c,f−i] dissolved in uniaxial orienting mesophases, where the dipolar couplings should vanish because of the high molecular symmetry. On the contrary, non-null (even though very small) dipolar couplings are observed. The origin of the phenomenon cannot lie on the orientational order parameters that, as said above, are predicted to be null as a result of the structural symmetry of the undistorted molecule. On the other hand, structural deformations of the solute exerted by the liquid crystal medium, representing the first "historical" explanations of the phenomenon,[9f−h,2] have been subsequently discarded and finally basically rejected (even though this hypothesis has been aired again[10]). At present, the more reliable explanation for the existence of dipolar couplings seems to consist in the correlation between molecular vibrations and overall reorientational rotations (the so-called "tumbling") of the solute.[3m,j] As said above, we suspect we are in a similar situation (as a matter of fact, the D_{12}^{obs} value is very low, much smaller than the J_{12} indirect coupling), so that the behavior of TMA in I52 can be probably associated with that of methane and similar molecules in nematic solutions. Of course, we cannot exclude that our results and conclusions are biased by the imperfect reliability of our observed dipolar couplings and/or by the adopted assumptions and approximations. In particular, the β explanation describes a situation where the order parameter would have a minimum of magnitude at $(T_{red})_{min} = 0.82$, and no intuitive reasons why this would occur are immediately available (possible suggestions include competition between opposite ordering/disordering mechanisms and collective phase order effects due to the TMA doping). At the same time, we are quite convinced that the significant values of $D_{12}^{nonrigid}$, predicted by both α and β scenarios, are physically sensible, thus representing a very important contribution to the experimental D_{12}^{obs}.

4. CONCLUSIONS

The intriguing behavior of the very weak orientational ordering of TMA in I52, studied by LXNMR spectroscopy at different T_{red} values, allowed for a quantitative assessment, within a certain number of approximations, of the nonrigid contribution (as a result of the reorientational−vibrational correlation) affecting the observed direct $^1D_{^{13}C−H}$ dipolar coupling. Two possible scenarios (α and β) for the interpretation of the observations have been presented and discussed with their pros and cons. In any case, the obtained issue is that the reorientational−vibrational interaction represents a fundamental contribution to the value of the observed experimental dipolar coupling. This result recalls the importance of the nonrigid contributions shown in the past for perfectly symmetric molecules (such as methane and analogues) dissolved in liquid crystalline phases. Obviously, this result lends itself to a series of considerations about the reliability of the derivation and, of course, of the consequent outcome. Anyway, apart from the more or less important consequences of the approximations (discussed at length in the Results and Discussion section), we think that our final results are to be considered quite plausible in indicating the magnitude of the $D_{12}^{nonrigid}$ term. Important points remain to be explained about both α and β, namely, the reasons and the mechanisms of the unexpected and intriguing behavior of the whole spectral width vs T, clearly shown in Figure 2 and, as a consequence, the possibility to decide unambiguously between α and β (or other possible solutions we were unable to see). Anyway, this is another story; the mentioned problems will be addressed in our future works in addition to trying to obtain more reliable dipolar couplings from a more careful spectral analysis (which probably

needs to be performed by fitting to the overall line shape and not only to peak frequencies).

■ AUTHOR INFORMATION

Corresponding Author
*E-mail: giorgio.celebre@unical.it. Phone: +39-0984493321. Fax: +39-0984493301.

■ REFERENCES

(1) Saupe, A.; Englert, G. *Phys. Rev. Lett.* **1963**, *11*, 462.
(2) (a) Emsley, J. W.; Lindon, J. C. In *NMR Spectroscopy Using Liquid Crystal Solvents*; Pergamon: Oxford, 1975. (b) *NMR of Ordered Liquids*; Burnell, E. E., de Lange, C. A., Eds.; Kluwer: Dordrecht, Netherlands, 2003. (c) Diehl, P. In *Nuclear Magnetic Resonance of Liquid Crystals*; Emsley, J. W., Ed.; Reidel: Dordrecht, Netherlands, 1985; p 147 (and the references therein).
(3) (a) Emsley, J. W.; Luckhurst, G. R. *Mol. Phys.* **1980**, *41*, 19. (b) de Lange, C. A.; Burnell, E. E. *J. Chem. Phys.* **1982**, *76*, 3474. (c) Burnell, E. E.; de Lange, C. A.; Mouritsen, O. G. *J. Magn. Reson.* **1982**, *50*, 188. (d) Snijders, J. G.; de Lange, C. A.; Burnell, E. E. *J. Chem. Phys.* **1982**, *77*, 5386. (e) Snijders, J. G.; de Lange, C. A.; Burnell, E. E. *J. Chem. Phys.* **1983**, *79*, 2964. (f) Snijders, J. G.; de Lange, C. A.; Burnell, E. E. *Isr. J. Chem.* **1983**, *23*, 269. (g) Burnell, E. E.; de Lange, C. A. *J. Magn. Reson.* **1980**, *39*, 461. (h) Lounila, J.; Diehl, P. *Mol. Phys.* **1984**, *52*, 827. (i) Lounila, J.; Diehl, P. *J. Magn. Reson.* **1984**, *56*, 254. (j) Lounila, J. *Mol. Phys.* **1986**, *58*, 897. (k) de Lange, C. A.; Snijders, J. G.; Burnell, E. E. In *Nuclear Magnetic Resonance of Liquid Crystals*; Emsley, J. W., Eds.; Reidel: Dordrecht, 1985; p 181 (and the references therein). (l) Barnhoorn, J. B. S.; de Lange, C. A. *Mol. Phys.* **1996**, *88*, 1. (m) Burnell, E. E.; de Lange, C. A.; Barnhoorn, J. B. S.; Aben, I.; Levelt, P. F. *J. Phys. Chem. A* **2005**, *109*, 11027. (n) de Lange, C. A.; Meerts, W. L.; Weber, A. C. J.; Burnell, E. E. *J. Phys. Chem. A* **2010**, *114*, 5878. (o) Burnell, E. E.; de Lange, C. A.; Capitani, D.; Angelini, C.; Ursini, O. *Chem. Phys. Lett.* **2010**, *486*, 21.
(4) (a) Kaski, J.; Vaara, J.; Jokisaari, J. *J. Am. Chem. Soc.* **1996**, *118*, 8879. (b) Kaski, J.; Lantto, P.; Vaara, J.; Jokisaari, J. *J. Am. Chem. Soc.* **1998**, *120*, 3993. (c) Vaara, J.; Kaski, J.; Jokisaari, J. *J. Phys. Chem. A* **1999**, *103*, 5675. (d) Aroulanda, C.; Celebre, G.; De Luca, G.; Longeri, M. *J. Phys. Chem. B* **2006**, *110*, 10485. (e) Celebre, G.; De Luca, G.; Longeri, M.; Pileio, G. *Mol. Cryst. Liq. Cryst.* **2007**, *465*, 289.
(5) Celebre, G.; De Luca, G.; Longeri, M. *Liq. Cryst.* **2010**, *37*, 923.
(6) Celebre, G.; De Luca, G.; Longeri, M.; Sicilia, E. *J. Chem. Inf. Comput. Sci.* **1994**, *34*, 539.
(7) (a) Diehl, P. In *Encyclopedia of NMR*; Grant, D. M., Harris, M. K., Eds.; Wiley: New York, 1996; p 4591 (and the references therein). (b) De Luca, G.; Longeri, M.; Pileio, G.; Lantto, P. *ChemPhysChem* **2005**, *6*, 2086.
(8) The used geometries are the following: C═C = 1.31 Å, C—C$_{Me}$ = 1.50 Å, C—H = 1.11 Å, C$_{Me}\hat{C}$C$_{Me}$ = 120°, and regular tetrahedral structures. Moreover, about the description of the rotation of methyl groups when calculating intermethyl couplings, we used the usual "120° three site" model, exploiting the 3-fold symmetry of the methyl groups and "freezing" them in their sterically less hindered conformations.
(9) (a) Snyder, L. C.; Meiboom, S. *J. Chem. Phys.* **1966**, *44*, 4057. (b) Ader, R.; Loewenstein, A. *Mol. Phys.* **1972**, *24*, 455. (c) Ader, R.; Loewenstein, A. *Mol. Phys.* **1975**, *30*, 199. (d) Loewenstein, A. *Chem.*

11125

dx.doi.org/10.1021/jp2021598 |*J. Phys. Chem. B* 2011, 115, 11119–11126

Phys. Lett. **1976**, *38*, 543. (e) Van der Est, A. J.; Barker, P. B.; Burnell, E. E.; de Lange, C. A.; Snijders, J. G. *Mol. Phys.* **1985**, *56*, 161. (f) Bailey, D.; Buckingham, A. D.; Fujiwara, F.; Reeves, L. W. *J. Magn. Reson.* **1975**, *18*, 344. (g) Diehl, P.; Kunwar, A. C.; Zimmermann, H. *J. Magn. Reson.* **1978**, *30*, 621. (h) Wei, I. Y.; Johnson, C. S. *J. Magn. Reson.* **1976**, *23*, 259. (i) Montana, A. J.; Dailey, B. P. *J. Magn. Reson.* **1976**, *22*, 117.

(10) Shahkhatuni, A. G.; Shahkhatuni, A. A.; Panosyan, H. A.; Park, G. H. J.; Martin, R. W.; Pines, A. *J. Phys. Chem. A* **2004**, *108*, 6809.

Rigid probe solutes in a smectic-*A* liquid crystal: An unconventional route to the latter's positional order parameters

Maria Enrica Di Pietro, Giorgio Celebre, and Giuseppina De Luca

Dipartimento di Chimica, Università della Calabria, Campus di Arcavacata, Via Pietro Bucci Cubo 12C, I-87036 Rende (Cosenza), Italy

Giorgio Cinacchi[*]

Departamento de Física Teórica de la Materia Condensada, Universidad Autónoma de Madrid, Campus de Cantoblanco, E-28049 Madrid, Spain

(Received 10 August 2011; published 13 December 2011; corrected 22 December 2011)

Biphenylene and pyrene were dissolved in the nematic and smectic-*A* phases of the liquid crystal 4,4'-di-*n*-heptyl-azoxybenzene and the orientational order parameters of both solutes and solvent measured via proton and deuteron nuclear-magnetic-resonance spectroscopy. This new data set was then merged with the one previously obtained, formed by 4,4'-di-chloro-benzene and naphthalene as solutes in the same solvent, and the resulting overall data set analyzed with a statistical thermodynamic density-functional theory to provide positional-orientational distribution functions of the various solutes along with the smectic solvent's positional order parameters.

I. INTRODUCTION

Smectic liquid crystals are interesting phases of matter. Their constituent particles both have an orientational order, as in the more common nematic (*N*) phase, and a *quasi*-long-range one-dimensional positional order. Smectics indeed consist of layers, stacked one above the other. In the simplest case, the smectic-*A* (S_A) phase, particles within a layer have a liquidlike short-range order and preferentially orient along the layer normal ($\hat{\boldsymbol{n}}$) [1].

Perhaps surprisingly, there is no straightforward experimental method to quantitatively assess the extent of layering. Positional order can be readily quantified through a series of parameters τ_k, defined as [1]

$$\tau_k = \frac{1}{\delta} \int_0^{\delta} dz \, \cos\left(2\pi k \frac{z}{\delta}\right) \rho(z), \tag{1}$$

with $\rho(z)$ the distribution function of z, the particle displacement from the midlayer position resolved along $\hat{\boldsymbol{n}}$, δ the layer spacing, and k a positive integer. Yet the very value borne by these parameters is experimentally hard to know for a molecular smectic liquid crystal.

Diffraction techniques would appear as the most suited to investigate positional order in smectics. Indeed, they provide accurate values of the layer spacing. For a S_A phase, δ turns out of the order of the molecular length. Unfortunately, they cannot provide as straightforwardly also the values of the parameters τ_k. In fact, the measured quantities, the relative scattering intensities of the first, second,..., *k*th peak, I_{00k}, do turn out proportional to τ_k^2, but the proportionality constant is unknown. Thus just ratios of the type $\tau_{k'}/\tau_{k''}$ can, in principle, be confidently obtained, though, in practice, only the ratio τ_2/τ_1 is most often achievable as usually peaks up to the second only can be detected.

To proceed further and eventually arrive at values of the parameters τ_k, a Gaussian shape for $\rho(z)$ was assumed in Ref. [2]. While there has been also an attempt to link τ_1 with the coherence length of the smectic layers, the latter accessible in a diffraction experiment [3], the procedure of Ref. [2] was the one applied most in the past [4,5]. More recently, two methods have been proposed trying to overcome its inherent difficulties.

In the first, the unknown proportionality constant has been determined by assuming a "Haller-like" extrapolation of the temperature dependence of the measured relative intensity to the absolute zero temperature [6]. This way, values of the parameter τ_1 for a range of smectogenic materials were obtained. In the second, small-angle neutron scattering has been used to measure the absolute intensity of the first peak, while relying upon an atomistic model for the calculation of the molecular form factor [7]. This way, values of the parameter τ_1 for the bilayered S_A mesogen usually labeled 8CB were obtained.

In recent years, the problem of determining positional order parameters in smectics was also being addressed from viewpoints other than the traditional one based on diffraction techniques. Nuclear-magnetic-resonance (NMR) spectroscopy is at the heart of these new attempts.

In one case, proton NMR was used to determine the diffusion coefficients in the *N* and S_A phases and then these data were related to the τ_k's via a theoretical model validated by computer simulation [8].

In the other cases, rigid and relatively small molecules were dissolved in a smectogenic solvent and their Saupe ordering matrices, *S* [1], determined via liquid-crystal NMR (LX-NMR) spectroscopy [9]. The aim of these studies is to exploit the changes that the orientational order parameters of certain solutes may undergo upon the onset of layering to get informaton on the positional order of the smectic liquid-crystalline solutions. These studies can be further subdivided in two groups depending on how they analyze solutes' *S*'s. This analysis has important consequences on what can be

unveiled about the structure of the smectic liquid-crystalline solutions.

One series of these studies [10] makes use of mean-field models, developed from the classic Maier-Saupe and McMillan theories [1], and their outputs are the positional order parameters of the solutes.

In the other two studies instead [11,12], a statistical thermodynamic density-functional theory (ST-DFT), developed from the classic Onsager theory [1], is used that expresses solutes' positional-orientational distribution function in terms of the solvent's positional-orientational distribution. Importantly, this allows for the determination of the positional order parameters of the solvent too. As the solutions are sufficiently dilute, these parameters should not differ from those characterizing the pure smectic solvent. The method developed in Refs. [11,12] thus offers another way to determine the positional order parameters of a smectic liquid crystal.

The present work belongs to the above-mentioned second group. New experimental data for the Saupe ordering matrices of the solutes biphenylene (BIF) and pyrene (PYR) dissolved in the N and S_A phases of the liquid crystal 4,4'-di-n-heptyl-azoxybenzene (HAB) were determined. These new experimental data were then merged with those previously determined for the solutes 1,4-di-chloro-benzene (DCB) and naphthalene (NFT) dissolved in the same solvent [12] to form a larger set, with which potentialities and limits of the ST-DFT-based methodology can be better assessed. In the next section, the latter is briefly recalled, while Sec. III contains a concise description of the new LX-NMR experiments and presentation of the data acquired from them. Section IV thoroughly discusses the ST-DFT based analysis of the overall experimental data set. Conclusions are drawn and future perspective outlined in Sec. V.

II. RECALL OF THE METHODOLOGY

In this section, the ST-DFT based methodology is succinctly recalled. For all details, the reader is referred to Refs. [11,12]. The basic equation coming out from the ST-DFT is

$$\ln \rho_\sigma(z,\Omega) = -2\Psi \int_{-\infty}^{+\infty} dz' d\Omega' \rho_\Sigma(z',\Omega')$$
$$\times A_{\sigma\Sigma}(z-z',\Omega,\Omega') - \ln \Xi. \quad (2)$$

The meaning of the terms entering this equation is explained here below.

(i) $\rho_\sigma(z,\Omega)$ is the probability density to find a solute molecule σ in the state defined by the position of its center of mass along $\hat{n}$, z, and its orientation, specified by the usual set of Euler angles [13] collected under the symbol Ω.

(ii) In close analogy with what is written above, $\rho_\Sigma(z',\Omega')$ is the probability density to find a solvent molecule Σ in the positional-orientational state defined by z' and Ω'.

(iii) The quantity $A_{\sigma\Sigma}(z-z',\Omega,\Omega')$ measures solute-solvent interactions. More specifically, it is given by minus the integral of the Mayer function $M_{\sigma\Sigma}(\boldsymbol{R},z-z',\Omega,\Omega')$ over $\boldsymbol{R}$, the vector of the distance between the two molecules' centers of mass resolved perpendicularly to $\hat{n}$; $M_{\sigma\Sigma}(\boldsymbol{R},z-z',\Omega,\Omega') = \exp[-\frac{u_{\sigma\Sigma}(\boldsymbol{R},z-z',\Omega,\Omega')}{k_B T}] - 1$, with k_B the Boltzmann constant, T the temperature, and $u_{\sigma\Sigma}(\boldsymbol{R},z-z',\Omega,\Omega')$ the

intermolecular solute-solvent interaction potential energy function [14].

(iv) The factor Ψ helps correct in an effective way for the neglect of higher-order (virial) terms involving ever more complicated integrals.

(v) Ξ is the normalization constant, ensuring that $\int dz\, d\Omega\, \rho_\sigma(z,\Omega) = 1$.

Equation (2) is valid for very dilute solutions. Under these conditions, the positional-orientational distribution function of a solute is linked to the positional-orientational distribution function of the solvent via the function $A_{\sigma\Sigma}$.

Once an approximation for solute-solvent interactions has been set out and $\rho_\Sigma(z,\Omega)$ suitably parametrized, these parameters can be determined by fitting the experimental Saupe ordering matrices, obtained by means of LX-NMR, to those calculated by the ST-DFT.

If $[S_{ab}]_\sigma^{expt}$ is the ab element of the experimental Saupe ordering matrix of the solute σ, the corresponding calculated quantity, $[S_{ab}]_\sigma^{calc}$, is

$$[S_{ab}]_\sigma^{calc} = \int dz\, d\Omega\, \rho_\sigma(z,\Omega) \left[\frac{3}{2}(\hat{\boldsymbol{a}} \cdot \hat{\boldsymbol{n}})(\hat{\boldsymbol{b}} \cdot \hat{\boldsymbol{n}}) - \frac{\delta_{ab}}{2} \right], \quad (3)$$

with $\hat{\boldsymbol{a}}$ the ath axis of the molecular reference frame and δ_{ab} the Krönecker symbol. What one is required to minimize is then a sum of the following kind:

$$\tilde{\chi}^2 = \frac{1}{\nu} \sum_\sigma \sum_{ab} \left\{ [S_{ab}]_\sigma^{expt} - [S_{ab}]_\sigma^{calc} \right\}^2, \quad (4)$$

with ν the number of data minus the number of parameters.

III. EXPERIMENTS

Two dilute solutions, approximately 3% by mole fraction, were prepared dissolving the rigid solutes BIF and PYR in a mixture of HAB and HAB-d_4, the latter being the version deuterated in the positions *ortho* with respect to the two alkyl chains. The solutes BIF and PYR and the solvent HAB were purchased from Aldrich, while the deuterated sample of HAB-d_4 was provided by C. A. Veracini (Dipartimento di Chimica, Università di Pisa). In Fig. 1, the structures of the solvent and all solute molecules considered in this work are reported together with the molecular reference frame chosen for these solute molecules.
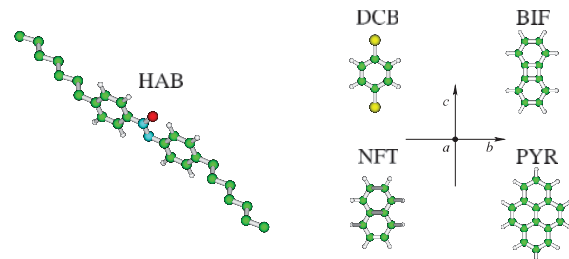

FIG. 1. (Color online) "Ball-and-stick" structures of the solvent and solute molecules, referred to with their respective label defined in the text. Shown are also the axes, a, b and c, of the molecular reference frame adopted for the solute molecules.
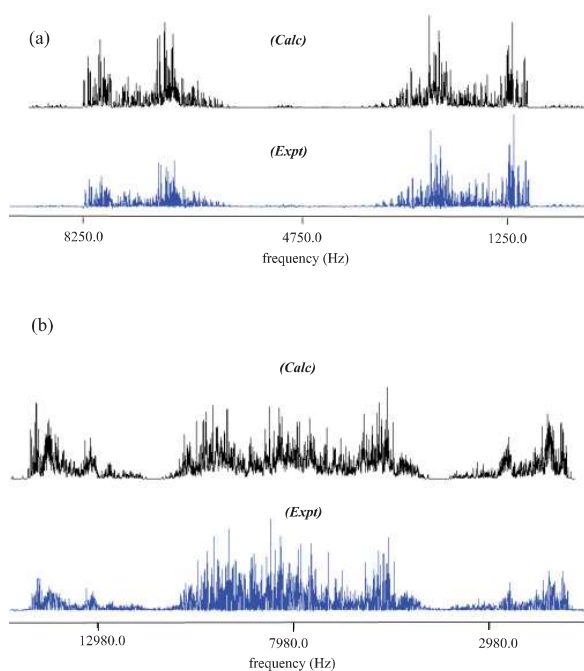
FIG. 2. (Color online) Calculated and experimental ^{1}H-NMR spectra of (a) BIF and (b) PYR in HAB at $T^* = 0.93$.

On both samples, ^{1}H spectra of the solutes and ^{2}H spectra of the solvent were recorded at different common reduced temperatures $T^* = T/T_{NI}$, with T_{NI} the nematic-isotropic phase-transition temperature. The temperature range spanned both N and S_A liquid-crystal phases. All anisotropic spectra were recorded on a Bruker Avance 500 MHz spectrometer working at a field strength of 11.74 T and equipped with a temperature control unit. All proton spectra were analyzed using the iterative computer program ARCANA [15]. Figure 2 reports, as an example, the calculated and the experimental ^{1}H spectra in HAB at $T^* = 0.93$ for BIF and PYR, respectively.

The final experimental data, that is the hydrogen atom i-hydrogen atom j residual dipolar couplings, D_{ij}'s, are given, for each temperature, in Table I for BIF and in Table II for PYR. Tables III and IV report the **S** matrices obtained from the residual dipolar coupling data for the two solutes. Following the procedure already described in Ref. [12], the deuterium spectra of the solvent were used to obtain the numerical values of the solvent's second-rank orientational order parameter η. These are listed in Table V. For the sake of completeness, we need to mention an interesting approach, recently proposed, to determine the orientational order of the pure HAB [16]. This involves the simultaneous analysis of several NMR observables (^{13}C chemical shift anisotropies, ^{1}H-^{2}H and ^{13}C-^{2}H dipolar couplings, and ^{2}H quadrupolar splittings) supplemented by quantum chemical density-functional theory calculations, in order to derive HAB orientational order parameters supposedly more reliable than

TABLE I. Experimental residual dipolar couplings (Hz) of BIF in HAB at different reduced temperatures. The transition between the nematic and smectic-*A* phases is recorded at about $T^* = 0.94$. The chemical structure provides the hydrogen atom numbering.

T^*	D_{12}	D_{13}	D_{14}	D_{15}	D_{16}	D_{17}	D_{18}
0.97	-1349.93 ± 0.08	-75.07 ± 0.11	13.24 ± 0.31	-39.94 ± 0.33	-60.57 ± 0.10	-125.54 ± 0.09	-529.65 ± 0.25
0.96	-1444.93 ± 0.08	-78.38 ± 0.12	17.11 ± 0.36	-40.76 ± 0.35	-65.06 ± 0.12	-135.06 ± 0.10	-568.15 ± 0.25
0.95	-1512.69 ± 0.06	-80.26 ± 0.08	19.47 ± 0.24	-43.02 ± 0.24	-68.11 ± 0.08	-141.27 ± 0.07	-595.34 ± 0.17
0.94	-1572.97 ± 0.05	-83.03 ± 0.06	19.83 ± 0.19	-45.46 ± 0.22	-70.62 ± 0.06	-147.15 ± 0.05	-620.20 ± 0.14
0.93	-1634.03 ± 0.04	-88.10 ± 0.05	20.25 ± 0.15	-46.78 ± 0.15	-73.46 ± 0.05	-152.51 ± 0.05	-642.55 ± 0.11
0.92	-1661.51 ± 0.04	-90.88 ± 0.04	18.68 ± 0.16	-48.01 ± 0.13	-74.73 ± 0.04	-154.93 ± 0.04	-652.48 ± 0.10
0.91	-1679.02 ± 0.04	-93.08 ± 0.05	17.46 ± 0.16	-48.67 ± 0.17	-75.38 ± 0.05	-156.39 ± 0.04	-658.69 ± 0.11

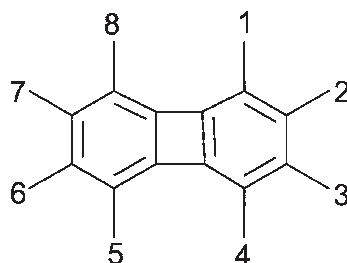| T^*	D_{23}	D_{26}	D_{27}
0.97	124.17 ± 0.31	-44.91 ± 0.31	-56.90 ± 0.25
0.96	151.58 ± 0.34	-49.29 ± 0.33	-60.69 ± 0.26
0.95	171.23 ± 0.25	-51.48 ± 0.24	-63.94 ± 0.18
0.94	183.44 ± 0.18	-52.78 ± 0.20	-66.58 ± 0.16
0.93	175.21 ± 0.15	-55.44 ± 0.15	-69.26 ± 0.11
0.92	167.01 ± 0.13	-56.02 ± 0.13	-70.24 ± 0.10
0.91	158.09 ± 0.15	-56.78 ± 0.15	-70.53 ± 0.11

TABLE II. Experimental residual dipolar couplings (Hz) of PYR in HAB at different reduced temperatures. The transition between nematic and smectic-A phase is recorded at about $T^* = 0.94$. The chemical structure provides the hydrogen atom numbering.

T^*	D_{12}	D_{13}	D_{14}	D_{15}	D_{16}		
0.97	-56.82 ± 0.10	-84.65 ± 0.14	-154.98 ± 0.14	-554.17 ± 0.09	-43.02 ± 0.16		
0.96	-60.24 ± 0.09	-86.89 ± 0.12	-161.67 ± 0.12	-569.45 ± 0.08	-46.20 ± 0.15		
0.95	-60.71 ± 0.08	-91.04 ± 0.12	-166.66 ± 0.11	-578.34 ± 0.07	-46.87 ± 0.13		
0.94	-64.21 ± 0.07	-94.70 ± 0.09	-171.01 ± 0.10	-586.90 ± 0.06	-49.80 ± 0.10		
0.93	-65.42 ± 0.07	-96.13 ± 0.09	-175.54 ± 0.09	-592.99 ± 0.05	-51.36 ± 0.09		
0.92	-68.87 ± 0.07	-99.92 ± 0.11	-178.06 ± 0.11	-597.84 ± 0.07	-53.65 ± 0.11		
0.91	-69.39 ± 0.08	-102.03 ± 0.11	-183.01 ± 0.12	-601.79 ± 0.07	-54.57 ± 0.11		
T^*	D_{23}	D_{24}	D_{25}	D_{27}	D_{28}	D_{29}	D_{210}
0.97	-1654.15 ± 0.09	-554.17 ± 0.09	-115.05 ± 0.12	-48.67 ± 0.16	-37.78 ± 0.14	-24.12 ± 0.15	-4.46 ± 0.16
0.96	-1733.40 ± 0.07	-569.45 ± 0.08	-118.41 ± 0.10	-51.07 ± 0.14	-39.46 ± 0.11	-22.40 ± 0.11	0.27 ± 0.14
0.95	-1798.50 ± 0.06	-578.34 ± 0.07	-123.35 ± 0.09	-53.88 ± 0.12	-39.58 ± 0.10	-22.31 ± 0.10	1.70 ± 0.12
0.94	-1864.45 ± 0.06	-586.90 ± 0.06	-127.18 ± 0.08	-54.04 ± 0.10	-42.46 ± 0.09	-22.20 ± 0.09	4.88 ± 0.11
0.93	-1911.60 ± 0.05	-592.99 ± 0.05	-131.37 ± 0.07	-54.44 ± 0.10	-43.42 ± 0.09	-22.02 ± 0.08	10.58 ± 0.10
0.92	-1974.15 ± 0.06	-352.22 ± 0.07	-135.20 ± 0.08	-55.30 ± 0.12	-43.58 ± 0.11	-21.12 ± 0.10	12.30 ± 0.12
0.91	-2015.29 ± 0.06	-359.85 ± 0.07	-139.14 ± 0.08	-58.66 ± 0.13	-44.41 ± 0.10	-20.44 ± 0.10	15.41 ± 0.12
T^*	D_{34}	D_{38}	D_{39}				
0.97	-2269.34 ± 0.12	-12.84 ± 0.19	-1.23 ± 0.20				
0.96	-2383.02 ± 0.09	-12.40 ± 0.16	-0.82 ± 0.17				
0.95	-2474.10 ± 0.08	-12.06 ± 0.14	0.37 ± 0.13				
0.94	-2572.08 ± 0.07	-11.05 ± 0.12	0.76 ± 0.12				
0.93	-2642.06 ± 0.07	-10.79 ± 0.11	1.88 ± 0.11				
0.92	-2734.75 ± 0.08	-10.49 ± 0.15	4.03 ± 0.16				
0.91	-2796.91 ± 0.09	-10.35 ± 0.15	4.25 ± 0.15				

the ones obtained by the traditional approach, based on the simpler analysis of ^{2}H spectra. That more elaborated approach could not be applied in the present case, though, as solutions of HAB, and not the pure HAB, are dealt with here: this implies that, in principle, the aromatic signals of ^{13}C NMR spectra of the solutes may interfere with those of HAB. Therefore, it was decided to pursue with the traditional approach. It is anyway nice to see that the data of Table V are consistent with those of Fig. 6 of Ref. [16].

IV. DATA ANALYSIS AND DISCUSSION

The analysis of the whole set of experimental data, composed of the S's of DCB, NFT, BIF, and PYR as a function of temperature, started with a choice of a model for solute-solvent interactions. In analogy with what was done in the previous work [12], both solute and solvent molecules were described at the atomistic, chemically detailed level (Fig. 1). Yet atom-atom interactions were taken of the hard sphere type, with each sphere radius equal to the corresponding atom (or group: the united atom approximation was used for methylene and methyl groups in the alkyl chains of HAB) van der Waals radius [17]. The model chosen was thought of as a compromise between: on one hand, the desire of preserving the individuality of each molecule together with the knowledge that fluid structure is primarily determined by short-range interactions (e.g. Ref. [18]) and, among these, the ones of the shape-and-size type are usually dominating; on

TABLE III. Elements of the Saupe ordering matrix for BIF in HAB as a function of reduced temperature.

T^*	S_{cc}	$S_{bb}-S_{aa}$
0.97	0.2560 ± 0.0003	0.2261 ± 0.0004
0.96	0.2767 ± 0.0003	0.2382 ± 0.0002
0.95	0.2882 ± 0.0003	0.2469 ± 0.0003
0.94	0.3002 ± 0.0003	0.2561 ± 0.0004
0.93	0.3111 ± 0.0003	0.2689 ± 0.0004
0.92	0.3158 ± 0.0003	0.2757 ± 0.0003
0.91	0.3210 ± 0.0003	0.2855 ± 0.0003

TABLE V. Temperature dependence of η, the solvent's orientational order parameter.

T^*	η
0.97	0.65
0.96	0.68
0.95	0.71
0.94	0.72
0.93	0.75
0.92	0.78
0.91	0.80

the other hand, the need to keep calculations as simple as possible. For the same reason, the solvent was allowed to adopt a single conformation, the one shown in Fig. 1, having the central core planar, the dihedral angles defined by the first two methylene groups of the chains and the corresponding phenyl ring set, respectively, at $\pm 90°$ and the two chains in an *all trans* conformation.

The second step was the parametrization of the solvent distribution function. In analogy with what was done in the previous work, $\rho_\Sigma(z',\Omega')$ was written as the product of positional and orientational terms:

$$\rho_\Sigma(z',\Omega') = \frac{\exp\left[\lambda \cos\left(2\pi \frac{z'}{\delta}\right)\right]}{\Upsilon_\lambda} \frac{\exp[\gamma P_2(\cos\theta')]}{\Upsilon_\gamma}. \quad (5)$$

In the equation above, λ is the parameter regulating the steepness of the positional distribution function, while γ is that one regulating the steepness of the orientational distribution function and bearing a one-to-one correspondence with the solvent's orientational order parameter η; θ' is the angle formed by a solvent molecule's main axis with $\hat{n}$; Υ_λ and Υ_γ are the two respective normalization constants. Since η is known from the ^{2}H-NMR measurements, the solvent's orientational distribution function is completely determined under this approximation. It can thus be used to orientationally average the above-mentioned function $A_{\sigma\Sigma}(z-z',\Omega,\Omega')$ leading to the function $\alpha(z,\Omega|\eta)$, parametrically depending on the solvent's orientational order parameter.

To this point, solute's distribution functions depend, in general, on three parameters: Ψ, λ, and δ. These are determined by fitting the predicted elements of solute Saupe ordering matrices with those obtained experimentally.

Two series of fittings were carried out. In the first, the phase was assumed N throughout the temperature range explored.

In this case, λ was set equal to 0 and δ thus left undefined, so that Ψ was the sole parameter left to vary. In the second, the phase was assumed S_A throughout the temperature range explored. In this case, λ was varied together with Ψ, while δ was fixed at the value of 28.9 Å as reported in a past diffraction experiment [19]. As the experimental data set was large enough, there was no need to make any extrapolation of the result for Ψ in the N phase down to the S_A phase, as done in the previous work [12]. There, the values of Ψ obtained in the N phase were linearly extrapolated into the S_A phase and only the parameter λ was varied in the layered phase. The few experimental data available at that time compelled the assumption of an extrapolation, which was made linear for the sake of simplicity.

Table VI gives the values of the parameters resulting from the two series of fittings. It can be noticed how the trend of the $\tilde{\chi}^2$'s is in good agreement with the known phase sequence. While $\tilde{\chi}^2{}_N$ increases with decreasing temperature, $\tilde{\chi}^2{}_{S_A}$ has in general the opposite behavior. This means that, as expected, the addition of the parameter λ leads to progressively better fittings. Nonetheless, $\tilde{\chi}^2{}_N$ remains smaller for the first two highest temperatures, while at $T^* = 0.95$ the two values of $\tilde{\chi}^2$ are essentially equivalent. This means that, for the three highest temperatures, the extra parameter added does not improve the quality of the fitting obtained by varying the sole parameter Ψ. This is consistent with the N character of the liquid-crystalline solutions for $T^* \geqslant 0.95$. The addition of λ leads to fittings of a substantially better quality for $T^* \leqslant 0.94$, where the liquid-crystalline solutions are indeed in the S_A phase. While $\tilde{\chi}^2{}_{S_A}$ does decrease in general with temperature, it does not do so at the lowest temperature considered, at which its value is comparable to the one obtained at $T^* = 0.95$. There is no evident reason for that at the moment.

TABLE IV. Elements of the Saupe ordering matrix for PYR in HAB as a function of reduced temperature.

T^*	S_{cc}	$S_{bb} - S_{aa}$
0.97	0.2876 ± 0.0016	0.2903 ± 0.0028
0.96	0.3038 ± 0.0027	0.2998 ± 0.0023
0.95	0.3150 ± 0.0029	0.3080 ± 0.0023
0.94	0.3271 ± 0.0028	0.3152 ± 0.0022
0.93	0.3375 ± 0.0025	0.3196 ± 0.0019
0.92	0.3477 ± 0.0028	0.3262 ± 0.0024
0.91	0.3561 ± 0.0027	0.3300 ± 0.0020

TABLE VI. Parameters of the two series of fitting as a function of reduced temperature.

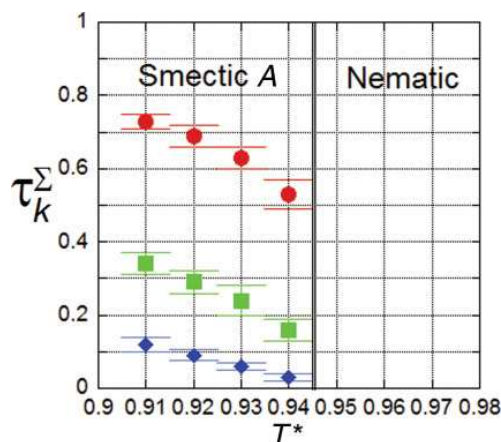| T^*	$10^4\tilde{\chi}^2{}_N$	$10^4\Psi_N$	$10^4\tilde{\chi}^2{}_{S_A}$	$10^4\Psi_{S_A}$	λ
0.97	5.73	3.62	6.66	3.82	0.35
0.96	5.90	3.15	6.52	3.74	0.67
0.95	6.11	2.71	5.93	3.67	0.94
0.94	6.60	2.12	4.92	3.34	1.27
0.93	7.94	1.66	3.77	3.13	1.66
0.92	9.65	1.39	3.56	2.93	1.95
0.91	12.11	1.13	5.88	2.52	2.24

FIG. 3. (Color online) Solvent's positional order parameters τ_k as a function of reduced temperature: $k = 1$ (red circles), $k = 2$ (green squares), and $k = 3$ (blue diamonds).
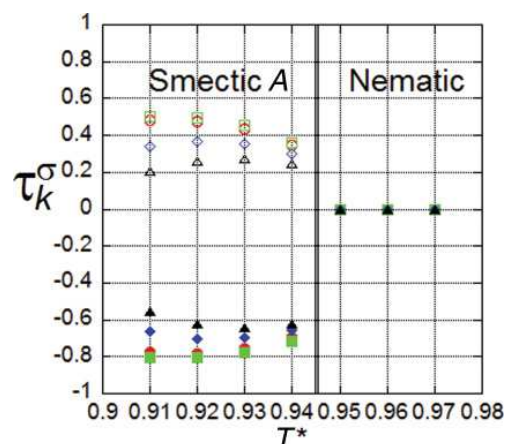

FIG. 4. (Color online) Solutes' positional order parameters as a function of reduced temperature: DCB (red circles), NFT (green squares), BIF (blue diamonds), and PYR (black triangles). Full symbols correspond to $k = 1$, while empty symbols to $k = 2$.

The main result of the analysis of the experimental *S*'s are the solvent's τ_k's. Figure 3 shows them for $k = 1,2,3$ as a function of temperature. The error in these parameters was estimated assuming a 10% error in the value of η. Uncertainty in this quantity was indeed observed to be the main contribution to the uncertainty affecting the final results.

By-products of the analysis are the solutes' positional-orientational distribution functions Eq. (2). From these functions, positional order parameters of the solutes are calculated. Figure 4 shows them. Noteworthy is the negative value of τ_1, indicating that the solutes prefer to reside in the interlayer regions. This confirms what was previously found elsewhere [10–12]. The positive value of τ_2 is just a further reflection of the layered nature of the S_A phase.

V. CONCLUSIONS

This work exploits the LX-NMR experimental technique coupled with a statistical thermodynamic density-functional theory to get values of the positional order parameters of a typical molecular smectic-*A* liquid crystal. These parameters

are the key quantities characterizing this type of layered mesophase. To devise a procedure to obtain them is a goal of basic importance for all liquid-crystal science. The methodology used in this work is intimately different from the ones used in past and recent years, all relying on diffraction experiments. Thus, it offers a complementary tool to achieve the above-mentioned goal. It would be interesting to compare the outcomes of the present methodology with those of any diffraction-based one. This piece of research would be a significant step forward for all liquid-crystal science.

[1] *Introduction to Liquid Crystals*, edited by E. B. Priestley, P. J. Wojtowicz, and P. Sheng (Plenum Press, New York, 1974); *The Molecular Physics of Liquid Crystals*, edited by G. R. Luckhurst and G. W. Gray (Academic Press, London, 1979).

[2] A. J. Leadbetter and E. K. Norris, Mol. Phys. **38**, 669 (1979).

[3] Z. X. Fan and W. Haase, J. Chem. Phys. **95**, 6066 (1991).

[4] J. Watanabe and M. Hayashi, Macromolecules **22**, 4083 (1989).

[5] Y. Takanishi, A. Ikeda, H. Takezoe, and A. Fukuda, Phys. Rev. E **51**, 400 (1995).

[6] N. Kapernaum and F. Giesselmann, Phys. Rev. E **78**, 062701 (2008).

[7] G. G. Alexander, S. M. King, R. M. Richardson, and H. Zimmermann, Liq. Cryst. **37**, 961 (2010).

[8] M. Cifelli, G. Cinacchi, and L. De Gaetani, J. Chem. Phys. **125**, 164912 (2006).

[9] *NMR of Ordered Liquids*, edited by E. E. Burnell and C. A. de Lange (Kluwer, Dordrecht, 2003).

[10] A. Yethiraj, Z. Sun, R. Y. Dong, and E. E. Burnell, Chem. Phys. Lett. **398**, 517 (2004); A. Yethiraj, A. C. J. Weber, R. Y. Dong, and E. E. Burnell, J. Phys. Chem. B **111**, 1632 (2007); A. Yethiraj, R. Y. Dong, and E. E. Burnell, Chem. Phys. Lett. **441**, 245 (2007); A. C. J. Weber, X. Yang, R. Y. Dong, W. L. Meerts, and E. E. Burnell, *ibid.* **476**, 116 (2009); A. C. J. Weber, X. Yang, R. Y. Dong, and E. E. Burnell, J. Chem. Phys. **132**, 034503 (2010).

[11] G. Cinacchi, Chem. Phys. Lett. **416**, 238 (2005).

[12] G. Celebre, G. Cinacchi, and G. De Luca, J. Chem. Phys. **129**, 094509 (2008).

[13] M. E. Rose, *Elementary Theory of Angular Momentum* (John Wiley & Sons, New York, 1957).

[14] T. L. Hill, *Statistical Thermodynamics* (Addison-Wesley, Reading, MA, 1960).

[15] G. Celebre, G. De Luca, M. Longeri, and E. Sicilia, J. Chem. Inf. Comput. Sci. **34**, 539 (1994).

[16] L. Calucci, M. Geppi, A. Marini, and C. A. Veracini, Phys. Rev. E **82**, 041702 (2010).

[17] A. Bondi, J. Phys. Chem. **68**, 441 (1964).

[18] I. Nezbeda, Mol. Phys. **103**, 59 (2005).

[19] E. H. Pape, Mol. Cryst. Liq. Cryst. **102**, 271 (1984).

Conformational Distribution of *trans*-Stilbene in Solution Investigated by Liquid Crystal NMR Spectroscopy and Compared with *in Vacuo* Theoretical Predictions

Giorgio Celebre,* Giuseppina De Luca, and Maria Enrica Di Pietro

Dipartimento di Chimica, Università della Calabria, v. P. Bucci, I-87036 Rende (CS), Italy

ABSTRACT: The basic question about the structure and the conformational distribution of a π-conjugated, flexible organic molecule (interesting in itself, in relation to the balance of forces determining its torsional equilibrium) becomes a really intriguing problem in the case of *trans*-stilbene (*t*-St), a "fundamental" molecule from a chemical point of view, as well as the prototype fragment of a series of derivatives endowed with several important biological and technological properties. As a matter of fact, the problem of *t*-St planarity when the molecule is isolated or in solution is a particularly debated question. In the present paper we studied the conformational distribution of *t*-St in solution, by resorting to the powerful technique of liquid crystal NMR spectroscopy (LXNMR), and we compared the obtained experimental results with accurate theoretical calculations carried out *in vacuo*, by using the MP2/6-31G** method (allowing for bond lengths and angles relaxation every 3° torsional steps). Our theoretical and experimental outcomes agree in indicating the nonplanarity of the molecule which, on the contrary, exhibits the coexistence of four stable rotamers, two by two symmetry related. In particular, we have found a couple of global minima corresponding to propeller-like C_2 symmetry conformations, where both the rings are "disrotated", with respect to the vinyl group, of about 17° in solution and of 27° *in vacuo* (theoretical value). Besides this, the presence of a couple of C_i local minima, with both the rings "conrotated" of 17° (fluid phase) or of 27° (MP2/6-31G** calculations for the isolated molecule) has been determined.
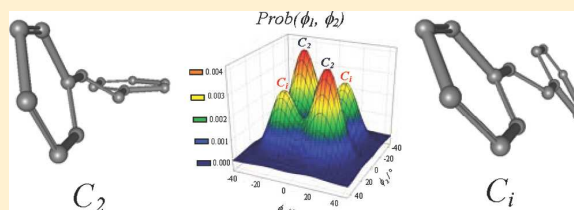
1. INTRODUCTION

The structure and conformational distribution of *trans*-diphenylethene, better known as *trans*-stilbene (*t*-St) and representing the shortest oligomer of the poly(*p*-phenylenevinylene) family, has attracted much interest over the last decades. The structures and the point groups of those that, presumably, represent the three most probable candidates to be stable conformations for *t*-St are described in Figure 1 (where also the sign convention for internal rotations is shown): C_{2h} (full planar molecule), C_2 (disrotatory, propeller-like conformation, where the rings are tilted at the same angle with respect to the *ene* plane, i.e. $\phi_1 = \phi_2$) and C_i (conrotatory conformation, where the rings are parallel to each other, i.e. tilted at angles equal in magnitude but opposite in sign: $\phi_1 = -\phi_2$). The question about the planarity of a π-conjugated organic molecule is interesting in itself, in relation to the balance of forces determining its conformational equilibrium. In the particular case of *t*-St, the torsional distribution is, of course, the result of the balance between the steric repulsions of the phenyl groups and the vinyl system and the loss in conjugation energy stabilization of the just cited π systems. Anyway, besides the fundamental interest for structural and conformational determinations, there is also another reason why, in our opinion, the *t*-St conformational equilibrium deserves to be studied. As a matter of fact, this molecule and its derivatives show several interesting biological and technological properties

that could be affected, to a certain extent, by the rotameric distribution of the molecule.

About the biochemistry of the molecule, many naturally occurring stilbenic compounds, namely resveratrol (3,4′,5-trihydroxy-*trans*-stilbene), piceatannol (3,3′,4′,5-tetrahydroxy-*trans*-stilbene) or rhapontigenin (3,3′,5-trihydroxy-4′-methoxy-*trans*-stilbene), have been reported to possess multiple healthy biological activities.[1] As a consequence, the last decades have witnessed intense research devoted to these natural compounds and their analogues, that can play an important role in the prevention of a wide variety of human pathological processes.[1a,b,2−6] Moreover, green plants of various taxonomic groups naturally biosynthesize stilbenoic compounds acting as protective agents against adverse conditions, such as microbial attacks or environmental stress.[7] If, on the contrary, we consider the technological point of view, it is well know that *t*-St is the building block of several commercially available liquid crystals and it has been included in many macromolecular backbones, such as polymers or dendrimers, for inducing liquid-crystalline behavior.[8] More, conjugated polymers, such as poly(*p*-phenylenevinylene), present semiconducting characteristics, are optically active in the visible region, and
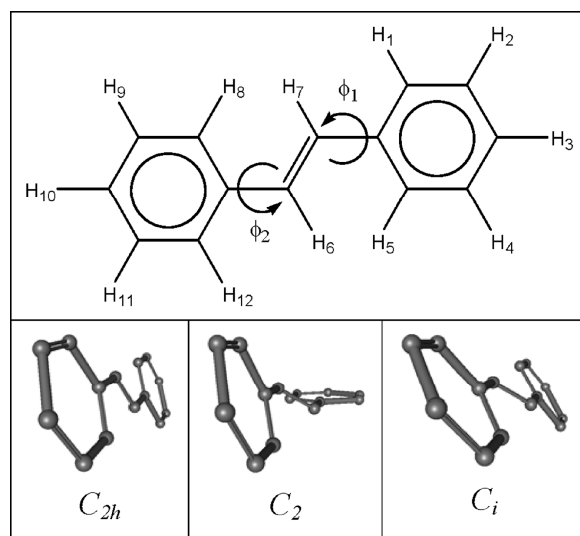
Figure 1. *trans*-Stilbene: hydrogen numbering, torsional angles ϕ_1 and ϕ_2 and possible stable structures (with corresponding *point groups*).

at the same time promise mechanical flexibility, ease and, consequently, low cost of fabrication through wet chemistry, motivating thus intensive research worldwide.[9] Stilbene and its related substituted analogues are also associated with photochemical and photophysical phenomena and are among the most widely investigated organic chromophores.[10] Photosystems including stilbenic molecules are used in LEDs, photoresistors, photoconductive devices, imaging and optical switching techniques, materials for nonlinear optics (NLO) and laser dyes.[11] Finally, stilbene moieties have been used as photoresponsive groups to functionalize different kinds of devices such as hydrogels or polymeric vescicles, making them susceptible to light stimuli for a photochemical control of drug release.[12] As said above, all these properties could depend (totally or, at least, in part) on the molecular conformations, and in fact the problem of *t*-St planarity is a particularly debated question.[13−38] It is worth emphasizing that the conformational equilibrium of *t*-St is, in principle, affected by the material's phase. This means that the molecule could show different torsional distributions depending on its physical state and, as a matter of fact, it has been found to be basically planar in solid phase[13,14] (the greatest deviation from planarity being a twist angle of 5° of the phenyl from the vinyl group[13]). The *t*-St rotameric equilibrium has been also investigated in polycrystalline *n*-alkane lattices at very low temperatures, by the so-called Shpolskii spectroscopy (see 15 and references therein). The resolved absorption, fluorescence excitation and fluorescence spectra of *t*-St in *n*-C$_6$ and *n*-C$_8$ matrices at 5 K led the authors to assess that the *t*-St molecule tends to be, at most, just slightly twisted, so that its symmetry is either C_{2h} or C_i, as in the pure crystal.[15] When, on the contrary, we pass to consider the results in vapor phase, we discover that they are quite controversial. Optical absorption,[16] two-color stimulated emission spectroscopy,[17] pure rotational coherence effects on picosecond fluorescence polarization experiments[18] and

several other fluorescence studies[19−23] seem to lead to a C_i or a C_{2h} planar structure for the isolated molecule. Anyway, other fluorescence works disagree with these outcomes, suggesting that the structure for the molecule is basically C_2.[24] This is in agreement with gas electron diffraction results, that gives a C_2 structure where the rings are rotated of 32.5°.[25] Photoelectron spectroscopy also has yielded conflicting results: a quite old study found a planar structure,[26] whereas a more recent work concludes that the phenyl groups are twisted of about 15−20°.[27] From a theoretical point of view, calculations for the isolated molecule (*in vacuo*) give different results depending on the used methods and basis sets: B3LYP/6-31G, and B3LYP/6-31G** found that the molecule is planar; on the contrary, the studies carried out by using HF/6-31G, HF/6-31G** and MP2/6-31G** gave the *t*-St to be nonplanar.[28] About this, an high level theoretical study of the structure and rotational barriers of *t*-St[29] emphasizes that the controversy is still unresolved. As a matter of fact, DFT functionals (producing the planar result, as said above) are believed to fail in correctly describing long-range nonbonding interactions, whereas several other methods (widely tested and illustrated in that paper,[29] by investigating also the basis set dependence of the results) contrast with the benchmark calculations there presented (MP2 geometry optimization using the aug-cc-pVDZ basis set). This leads the authors to the conclusion that, in the non relativistic limit and within the frozen core approximation, *t*-St *in vacuo* is a strictly planar molecule in its absolute energy minimum form. Other authors obtain that the ground-state equilibrium geometry of Stilbene in its trans conformation, optimized at the SA-2-CAS(2/2) level, is a nonplanar, approximately C_{2v} symmetry structure,[30] whereas fully relaxed ab initio RHF/3-21G calculations (preliminary to the introduction of correlation effects, included by using B3LYP functional and 6-31G(d) basis set)[31] interestingly show four (two global and two local) symmetry related torsional minima. In the two absolute minima, the planes of the phenyl groups are tilted in a **n**on-parallel, C_2 symmetry way (so that the authors call them **np**), with the dihedral angles between the rings and the ethylenic group of 27° (or 23°, depending on the used basis set); on the contrary, in the relative minima (C_i structures called **p**) the phenyls are parallel and tilted of the same angle of 27° (or 23°) magnitude. Semiempirical methods PM5 and AM1 predict a nonplanar ground state for *t*-St, while PM3 predicts the planar one.[32] Intriguingly, there is also a study suggesting that *t*-St is planar at low temperature in gas phase, but departs from planarity as the temperature is raised.[33] Another theoretical study suggests possible important effects of the zero point vibrational energy (ZPVE) correction, in the adiabatic approximation, on the torsional barrier of *t*-St: ZPVE corrections could play a significant role in the experimentally observed planar structure of the molecule.[34] A predominant C_2 structure for the molecule is also found by Raman spectroscopy in fluid phases (in the melt and in solution).[35] NMR techniques in isotropic phase confirm the twisted nature of *t*-St in solution, by studying the conformational dependence of deuterium-induced isotopic effects.[36] Contrary to what just said, another study, aimed to obtain conformational information on *t*-St in solution from vibrational spectra, leads to the result that the molecule is planar in solution,[37] implying

that this preferred molecular conformation is mainly determined by intermolecular rather than intramolecular forces. Finally, other authors[38] observe that the Raman spectrum of t-St in solution shows a weak band at about 960 cm^{-1} (due to the in-phase ethylenic CH wag), which is not present in the solid state. Now, the in-phase ethylenic CH wag is Raman-inactive for the planar structure and acquires higher Raman intensities with increasing degree of molecular distortion. From these premises, the conclusions of the paper are that the probable range of torsional distortion around the C=C bond is 2.5−4.0° while the tilt angle from the planar structure is 8.0−12.0° around the C−Ph bond.[38] About the reasons why the molecule in solution is distorted from the planar structure, the authors say that no simple answers to this question are available: solvation, dimerization, clustering, etc., occurring in solution or in the liquid state may account for the stabilization of the system accompanied by molecular distortion, but no evidence for any of such possibilities has been obtained. In this work, we will present the results obtained about the t-St conformational distribution in solution, studied by the powerful technique of liquid crystal NMR spectroscopy (LXNMR),[39−46] (there is also an Appendix at the end of the paper) and we will compare the obtained experimental results with accurate theoretical calculations for the isolated molecule.

2. THEORETICAL BACKGROUND OF THE LXNMR APPROACH

The target of our LXNMR spectral analysis (described in the next section) is represented by the observed D_{ij}^{obs} dipolar (or direct) couplings between the ith and jth magnetically active nuclei present in the studied molecule (in this case, the protons of t-St). The observed dipolar couplings are partially averaged quantities, where the average is over all the relevant motions of the molecule (namely, internal vibrations and rotations and whole reorientational motions, often called "overall rotations" or "molecular tumbling") with respect to the external applied magnetic field B_0, conventionally aligned along the Z direction of the Laboratory reference system (so that, in practice, $D_{ij}^{obs} \equiv \tilde{D}_{ijZZ}$, where the tilde symbol "∼" represents the process of average). Given the aim and the nature of the present work, involving only interproton dipolar couplings, the approximation of neglecting the effects of high-frequency, small-amplitude molecular vibrations can be quite safely adopted (for detailed information about vibrational corrections in LXNMR and their importance in structural-conformational determinations, the reader is referred to refs 43−48 and references therein). Moreover, for small flexible molecules with two internal rotational degrees of freedom ϕ_1 and ϕ_2 (as is the case of t-St; see Figure 1) undergoing large-amplitude motions which are fast compared with the changes produced in the couplings, the internal motion can be explicitly taken into account by its torsional probability distribution $p(\phi_1,\phi_2)$. In the light of the above considerations, it can be shown that the

observed dipolar couplings can be quite properly approximated by the following formula:[44a]

$$
\begin{aligned}
D_{ij}^{obs} \equiv \tilde{D}_{ijZZ} &\approx \left(\frac{3\cos^2\alpha - 1}{2} \right) \\
&\times \frac{2}{3} \int_{\phi_2} \int_{\phi_1} \int_{\gamma} \int_{\beta} p_{LC}(\beta, \gamma, \phi_1, \phi_2) \\
&\times \sum_{\rho\sigma} ((3[\cos\omega_\rho]_{(\beta,\gamma)}[\cos\omega_\sigma]_{(\beta,\gamma)} - \delta_{\rho\sigma})/2) \\
&\times D_{ij}^{\rho\sigma}(\phi_1, \phi_2)\sin\beta\, d\beta\, d\gamma\, d\phi_1\, d\phi_2 \\
&= \left(\frac{3\cos^2\alpha - 1}{2} \right) \left[\frac{2Z_{iso}}{3Z} \int_{\phi_2} \int_{\phi_1} p_{iso}(\phi_1, \phi_2) \right. \\
&\times \left. W(\phi_1, \phi_2) \sum_{\rho\sigma} S_{\rho\sigma}(\phi_1, \phi_2) \times D_{ij}^{\rho\sigma}(\phi_1, \phi_2)\, d\phi_1\, d\phi_2 \right]
\end{aligned}
$$

(1)

where α is the angle between B_0, defining the Z direction in the laboratory frame, and $\hat{n}$, the director of the mesophase;[44b] the Euler angles $\{\beta, \gamma\}$ characterize the orientation of $\hat{n}$ in the molecule-fixed frame and ω_ρ (which is a function of β and γ) is the instantaneous angle between $\hat{n}$ and the ρ axis of a Cartesian coordinate system fixed on the solute molecule; $\delta_{\rho\sigma}$, finally, is the Kronecker delta function. The terms (a) $S_{\rho\sigma}(\phi_1, \phi_2)$ (called "order parameters") and (b) $D_{ij}^{\rho\sigma}(\phi_1, \phi_2)$ are, respectively: (a) the Cartesian components, given in the molecular frame, of the Saupe matrix S (describing the orientational ordering of the solute, i.e., the degree of statistical alignment of the molecular axes to the director) and (b) the Cartesian components, given in the molecular frame, of the D_{ij} tensor of the dipolar coupling between the ith and jth nucleus. Both depend on the molecular conformation, defined by the torsional angles ϕ_1 and ϕ_2. About the D_{ij} tensor, the following relation holds:

$$
\begin{aligned}
D_{ij}^{\rho\sigma}(\phi_1, \phi_2) = &-\frac{K_{ij}}{r_{ij}^3(\phi_1, \phi_2)} \times [3\cos\vartheta_{ij}^\rho(\phi_1, \phi_2) \\
&\times \cos\vartheta_{ij}^\sigma(\phi_1, \phi_2) - \delta_{\rho\sigma}]
\end{aligned}
$$

(2)

with

$$
K_{ij} = \frac{\mu_0 \hbar \gamma_i \gamma_j}{16\pi^2}
$$

(3)

γ_i and μ_0 being respectively the ith nuclear magnetogyric ratio and the vacuum magnetic permeability, and ϑ_{ij}^ρ the angle between the distance vector r_{ij} and the ρ molecular axis. With regard to the order parameters, they can be written as:

$$
\begin{aligned}
S_{\rho\sigma}(\phi_1, \phi_2) = &\left[\int ((3[\cos\omega_\rho]_{(\beta,\gamma)}[\cos\omega_\sigma]_{(\beta,\gamma)} - \delta_{\rho\sigma})/2) \right. \\
&\times p_\Omega(\beta, \gamma, \phi_1, \phi_2)\sin\beta\, d\beta\, d\gamma] \\
&/[\int p_\Omega(\beta, \gamma, \phi_1, \phi_2)\, d\beta\, d\gamma]
\end{aligned}
$$

(4)

A thorough examination of eq 1 leads to conclude that the term $p_{LC}(\beta,\gamma,\phi_1,\phi_2)$ (giving the probability of finding the mesophase director (β, γ)-oriented in the solute-fixed frame,

when the probe-molecule is in its $\{\phi_1, \phi_2\}$ conformation in the liquid crystalline solution) is necessarily the following:

$$p_{LC}(\beta, \gamma, \phi_1, \phi_2)$$
$$= \frac{p_\Omega(\beta, \gamma, \phi_1, \phi_2)p_{iso}(\phi_1, \phi_2)W(\phi_1, \phi_2)Z_{iso}}{Z} \quad (5)$$

being the following relations verified in eqs 1 and 4:

$$Z_{iso} = \int p_{iso}(\phi_1, \phi_2)\, d\phi_1\, d\phi_2 \quad (6)$$

$$Z = \int W(\phi_1, \phi_2)p_{iso}(\phi_1, \phi_2)\, d\phi_1\, d\phi_2 \quad (7)$$

$$W(\phi_1, \phi_2) = \int \exp[-U_{ext}(\beta, \gamma, \phi_1, \phi_2)/k_BT]$$
$$\times \sin\beta\, d\beta\, d\gamma \quad (8)$$

$$p_\Omega(\beta, \gamma, \phi_1, \phi_2) = \frac{\exp[-U_{ext}(\beta, \gamma, \phi_1, \phi_2)/k_BT]}{Q} \quad (9)$$

with

$$Q = \int \exp[-U_{ext}(\beta, \gamma, \phi_1, \phi_2)/k_BT]$$
$$\times \sin\beta\, d\beta\, d\gamma\, d\phi_1\, d\phi_2 \quad (10)$$

where k_B is the Boltzmann constant and $U_{ext}(\beta,\gamma,\phi_1, \phi_2)$ is a solute−solvent purely anisotropic external orientational potential. Very importantly, $p_{iso}(\phi_1, \phi_2)$ of eqs 1 and 5 represents the probability distribution of the solute in a "virtual" isotropic phase of the nematic solvent at the experiment temperature: it is, after all, the basic target of conformational studies in liquids.[44a] In order to calculate the order parameters $S_{\rho\sigma}(\phi_1, \phi_2)$ of eqs 1 and 4, it is necessary to adopt a theoretical model describing the interdependent conformational-orientational problem. Here, we used the AP-DPD approach (additive potential[45,46] for the treatment of the ordering interactions, combined with the direct probability description of the torsional distribution $p_{iso}(\phi_1, \phi_2)$).[41,47−54] In the particular case of t-St, the $p_{iso}(\phi_1, \phi_2)$ has been modeled directly as a sum of bidimensional Gaussian functions:

$$p_{iso}(\phi_1, \phi_2)$$
$$\propto \frac{w(C_2)}{4}(e^{-[(\sin^2(\phi_1-\phi_1^M)/2h_1^2)+(\sin^2(\phi_2-\phi_2^M)/2h_2^2)]}$$
$$+ e^{-[(\sin^2(\phi_1-(\pi-\phi_1^M))/2h_1^2)+(\sin^2(\phi_2-(\pi-\phi_2^M))/2h_2^2)]}$$
$$+ e^{-[(\sin^2(\phi_1-(\pi-\phi_1^M))/2h_1^2)+(\sin^2(\phi_2+\phi_2^M)/2h_2^2)]}$$
$$+ e^{-[(\sin^2(\phi_1-\phi_1^M)/2h_1^2)+(\sin^2(\phi_2+(\pi-\phi_2^M))/2h_2^2)]})$$
$$+ \frac{w(C_i)}{4}(e^{-[(\sin^2(\phi_1-\phi_1^M)/2h_1^2)+(\sin^2(\phi_2+\phi_2^M)/2h_2^2)]}$$
$$+ e^{-[(\sin^2(\phi_1-(\pi-\phi_1^M))/2h_1^2)+(\sin^2(\phi_2+(\pi-\phi_2^M))/2h_2^2)]}$$
$$+ e^{-[(\sin^2(\phi_1-(\pi-\phi_1^M))/2h_1^2)+(\sin^2(\phi_2-\phi_2^M)/2h_2^2)]}$$
$$+ e^{-[(\sin^2(\phi_1-\phi_1^M)/2h_1^2)+(\sin^2(\phi_2-(\pi-\phi_2^M))/2h_2^2)]}) \quad (11)$$

where ϕ_1^M and ϕ_2^M represent the most probable values of the twist angles shown in Figure 1; $w_{(C_2)}$ and $w_{(C_i)}$ are the relative weights of the C_2 and C_i structures (we also fixed the constraint that $w_{(C_2)} + w_{(C_i)} = 1$) and, finally, h_1 and h_2 give the width at

half-maximum height along each dimension of the bidimensional Gaussians (note that the use of sinusoidal functions in the exponent of the Gaussians, introduced by us for the first time with this work, assures the right periodicity of the p_{iso} probability distribution simplifying its analytical expression with respect to those used in the past papers).[41,47−54] About the term $U_{ext}(\beta,\gamma,\phi_1, \phi_2)$ of eqs 8−10, it is described as follows:

$$U_{ext}(\beta, \gamma, \phi_1, \phi_2)$$
$$= -\varepsilon_{2,0}(\phi_1, \phi_2)C_{2,0}(\beta)$$
$$- 2\, \mathrm{Re}(\varepsilon_{2,2}(\phi_1, \phi_2))\, \mathrm{Re}(C_{2,2}(\beta, \gamma)) \quad (12)$$

Here the $C_{2,m}(\beta, \gamma)$ are modified spherical harmonics,[55] and the $\varepsilon_{2,m}(\phi_1,\phi_2)$ are the elements of suitable conformation-dependent solute−solvent interaction tensors. The peculiar feature of the AP method is that the general $\varepsilon_{2,m}(\{\varphi\})$ elements are constructed as a sum of conformationally independent terms $\varepsilon_{2,p}(l)$ representing the single contributions of each rigid fragment l in the molecule to the whole interaction tensors:

$$\varepsilon_{2,m}(\{\varphi\}) = \sum_l \sum_p \varepsilon_{2,p}(l)D^2_{p,m}(\Lambda^l_\phi) \quad (13)$$

(in eq 13, the second-rank Wigner rotation matrix $D^2_{p,m}(\Lambda^l_\varphi)$[55] relates the conformation-dependent Λ^l_φ orientation of the lth molecular subunit to the molecule-fixed reference frame). Essentially, the $\varepsilon_{2,p}(l)$ are unknown quantities whose values are adjusted to produce the best agreement with the experimental data. Once they are known, following the equations given above, it is possible to predict the behavior of the order parameters as a function of the molecular conformation. The use of all this theoretical apparatus will be described "in action" in the section 4 (Conformational Analysis by LXNMR).

## 3. PREPARATION OF THE SAMPLE, NMR EXPERIMENT, AND ANALYSIS OF ^{1}H-LXNMR SPECTRUM

In order to obtain the experimental data set of interproton observed dipolar couplings D^{obs}_{ij}, a dilute solution (approximately 5 wt %) was prepared by dissolving the t-St molecule (available from Aldrich) in a commercial nematic solvent (from Merck), known as ZLI1132 (a mixture of three phenyl cyclohexanes and one biphenyl cyclohexane; more information about the chemical nature of ZLI1132 can be found, for example, in ref 41). The sample was heated a few times up to its nematic−isotropic transition temperature T_{NI} and strongly shaken to homogenize the solution; then, it has been left to cool slowly in the magnetic field of the NMR spectrometer. The ^{1}H-LXNMR spectrum was recorded at room temperature (298 K) on a Bruker Avance 500 MHz (11.74 T) instrument. The extremely complex proton spectrum, shown in Figure 2 (being the molecule, from a NMR point of view, a 12-spin system, the spectrum is affected by a good 19 independent dipolar coupling constants D^{ob}_{ij}), was analyzed by using a homemade, user-assisted iterative computer program called ARCANA.[42]

The first step of the analysis of such a crowded spectrum requires a quite reliable estimation of the spectral parameters, in order to calculate a sufficiently good starting trial spectrum. The starting values of chemical shifts δ_{ij} and scalar couplings J_{ij} were taken from the *routine* analysis of the proton NMR spectrum of a isotropic solution of t-St dissolved in CDCl$_3$; moreover, looking for a starting set of dipolar couplings good enough to reproduce at

(Calc)

(Exp)

|28220.0 | 19220.0 | 10220.0 | 1220.0 |
| | | Hz | |
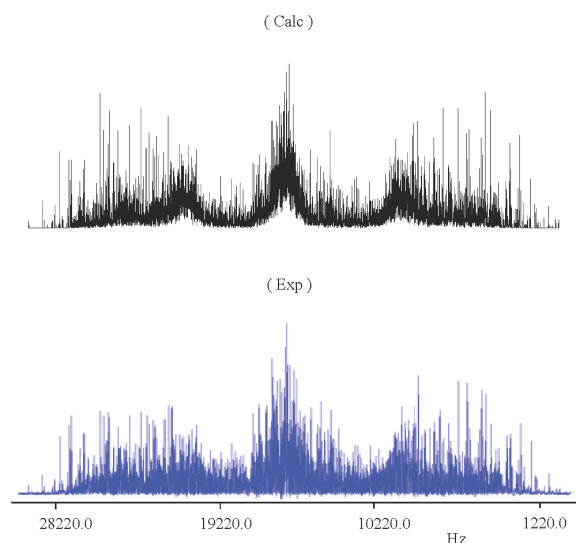
Figure 2. The 500 MHz ^{1}H-LXNMR experimental spectrum (bottom, in blue) of *trans*-stilbene dissolved in the liquid crystalline nematic mesophase ZLI1132 at 298 K. For comparison, the spectrum calculated by using the D_{ij}^{obs} spectral parameters (obtained from the analysis and reported in Table 1) is also shown, in black, at the top of the figure.

best (or, at least, in a acceptable way) the basic features of the spectrum, two different trial sets of D_{ij}^{trial} were produced by fixing the geometry of the molecule in both planar, C_{2h} symmetry, and nonplanar, C_2 symmetry, structure (see Figure 1). The D_{ij}^{trial} obtained by fixing the molecule in the planar conformation and adjusting, by trial and error, the longitudinal order parameter S_{cc} and the biaxiality order parameter $S_{aa} - S_{bb}$ (see Figure 3 for the
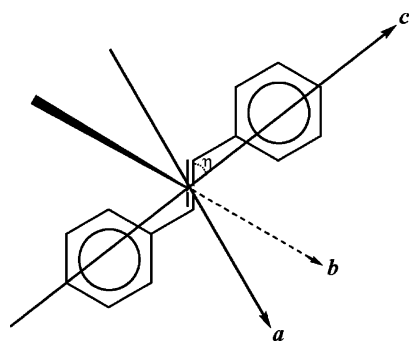
Figure 3. Definition of the $\{a, b, c\}$ molecular frame for *trans*-stilbene (the b axis is perpendicular to the (ac) plane, where the vinyl group lies). Moreover, in the figure is also shown the η angle (describing an integral rotation of the $\{a, b, c\}$ system about the b axis) which locates the Principal axis system (PAS) of the S matrix for the C_2 structure (see the section 4 for details).

definition of the $\{a, b, c\}$ molecular frame) were rejected because we immediately realized that the simulated trial spectra (corresponding to different sets of D_{ij}^{trial} obtained as functions of the S_{ij} variables) invariably showed a distribution of lines completely incompatible with the experimental one.

This was the first significant, "model-free" symptom we recorded where the molecule is not planar in solution (this point will be taken up in the discussion of section 6). On the contrary, a reasonable set of starting dipolar couplings was predicted by guessing from literature[27] a nonplanar conformation with a torsion angle $\phi_1 = \phi_2$ of about 15° and two trial order parameters having the values $S_{cc} = 0.590$ and $S_{aa} - S_{bb} = 0.134$. In this case, the trial spectrum was sufficiently close, in terms of total width and line distribution, to the observed one and this led us to the successful analysis. The whole set of final spectral parameters is reported in Table 1.

Table 1. Chemical Shifts $\delta_{ij} = \nu_i - \nu_j$, Scalar Couplings J_{ij}, and Observed Dipolar Couplings D_{ij}^{obs} (i and j Hydrogen Labels from Figure 1) Determined by the Analysis of ^{1}H-LXNMR Spectrum of *trans*-Stilbene Dissolved in ZLI1132^a

i,j	J_{ij}/Hz	D_{ij}^{obs}/Hz	D_{ij}^{AP-DPD}/Hz
1,2	8.00	−4004.33 ± 0.03	−4004.85
1,3	2.00	−507.48 ± 0.06	−507.37
1,4		−1.48 ± 0.04	−0.69
1,5	2.00	247.46 ± 0.08	246.73
1,6		−2462.52 ± 0.08	−2462.51
1,7		−1732.91 ± 0.07	−1732.84
1,8		−397.17 ± 0.05	−399.16
1,9		−140.41 ± 0.04	−138.98
1,10		−104.60 ± 0.06	−103.64
2,3	6.00	−20.45 ± 0.06	−19.85
2,4	2.00	246.98 ± 0.08	248.33
2,6		−380.11 ± 0.09	−376.75
2,7		−364.85 ± 0.09	−364.74
2,9		−64.74 ± 0.06	−63.36
2,10		−50.75 ± 0.06	−49.68
3,6		−254.36 ± 0.14	−256.08
3,7		−271.60 ± 0.14	−270.23
3,10		−39.58 ± 0.08	−39.82
6,7	17.50	681.36 ± 0.10	676.55
i,j		δ_{ij}/Hz	
15,17		−459.39 ± 0.06	
16,17		−444.85 ± 0.07	
25,17		−666.61 ± 0.07	
		rms = 1.67 Hz	

^{a}In the last column, the D_{ij}^{AP-DPD} values, obtained from the so-called AP-DPD method (see Sections 2 and 4, for the description of the model and its application), are also reported for comparison. Finally, in order to emphasize the good performance of the used approach, the resulting value of *RMS* (the root mean square target function) between AP-DPD-calculated and observed dipolar coupling values is reported in the last row.

4. CONFORMATIONAL ANALYSIS BY LXNMR

Following the theoretical background and the approximations described in section 2, it is possible to realize immediately that, for the case studied in the present work, the observed dipolar couplings of eq 1 can be effectively rewritten as:

$$D_{ij}^{obs} = \frac{2Z_{iso}}{3Z} \int_{\phi_2} \int_{\phi_1} p_{iso}(\phi_1, \phi_2) W(\phi_1, \phi_2)$$
$$\times \sum_{\rho\sigma} S_{\rho\sigma}(\phi_1, \phi_2) D_{ij}^{\rho\sigma}(\phi_1, \phi_2) \, d\phi_1 \, d\phi_2 \qquad (15)$$

As said above, the distinctive feature of eq 15, making the LXNMR technique so useful for studying the conformations of flexible molecules in solution, is the presence in the formula of the p_{iso} function: this can allow for the determination of the conformational probability from the experimental dipolar

couplings. It is worthwhile to emphasize that p_{iso} should be considered, in principle, as the "real" conformational distribution of our solute in a "conventional" isotropic liquid sharing, at the studied temperature, the same physical properties (determining the thermodynamics of the solution, as, for example, polarity, density etc.) of the used liquid crystalline solvent, with the exception of its ordering power (in other words, unlike the $p_{LC}(\phi_1, \phi_2)$ of eqs 1 and 5, $p_{iso}(\phi_1, \phi_2)$ is in principle free from possible conformational effects induced by the orientational ordering of the mesophase). In the light of sections 2 and 3, we think it can now be useful to quickly summarize the basic steps leading to the LXNMR determination of the conformational distribution of the studied molecule as well as of its orientational behavior: **1**) the direct couplings D_{ij}^{obs} are obtained from the analysis of the ^{1}H-LXNMR spectrum; **2**) the dipolar coupling tensor $D_{ij}^{\rho\sigma}(\phi_1, \phi_2)$, for each (ϕ_1,ϕ_2) conformation and for each i-j pair of hydrogens, is obtainable on the basis of the molecular geometry; the interdependent **3**) conformation-dependent Saupe matrix $S_{\rho\sigma}(\phi_1, \phi_2)$ and **4**) torsional distribution $p_{iso}(\phi_1, \phi_2)$, are derived from a fit of the experimental data set of point 1), by assuming a model (in our case, the AP-DPD) for their dependence upon the $\{\phi_1,\phi_2\}$ angles. In treating the t-St molecule we assumed, as usually done in literature,[44a,48] that the phenyl rings and the vinyl "rigid" fragments maintain a fixed structure as they rotate relative to each other. Each ring was assumed to have C_{2v} symmetry, and it therefore requires a couple of interaction parameters $\varepsilon_{2,0}^R$ and $\varepsilon_{2,2}^R$, whereas the vinyl group, assumed as effectively represented by an axially symmetric interaction tensor, needs just one independent element $\varepsilon_{2,0}^{(H_6-C=C-H_7)}$, the component along the C=C bond direction. Then, we tried to reproduce the whole set of D_{ij}^{obs} (Table 1 of the paper), starting with the geometries of the fragments given in the Appendix and simultaneously adjusting (in a iterative way, by a nonlinear fitting program based on the gradients method),[56] the following parameters: the $\varepsilon_{2,0}^R$, $\varepsilon_{2,2}^R$ and $\varepsilon_{2,0}^{(H_6-C=C-H_7)}$ interaction tensor parameters of eq 13; the $\phi_1^M = \pm \phi_2^M$ angle, the $h_1 = h_2$ value and the $w_{(C_2)} = 1 - w_{(C_i)}$ weight of eq 11. This has been made in order to minimize the rms (root-mean-square) target function:

$$\text{rms} = \left\{ M^{-1} \sum_{i<j} \left[D_{ij}(observed) - D_{ij}(calculated) \right]^2 \right\}^{1/2}$$

(16)

being M the number of independent couplings. It is worth emphasizing that ϕ_1^M, h_1, and $w_{(C_2)}$ can be varied independently, but with the constraint that $p_{iso}(\phi_1, \phi_2)$ of eq 11 is normalized (in particular, because of the molecular symmetry, we normalized the distribution function for $-45° \leq \phi_1 \leq 45°$ and $-45° \leq \phi_2 \leq 45°$). By the optimized values of iteration parameters (reported in Table 2) and by a slight refining of the vinyl geometries (see Table 3 in the Appendix) we were finally successful in reproducing the observed direct couplings with a low, very satisfactory *rms* of 1.67 Hz (the single dipolar couplings D_{ij}^{AP-DPD} calculated by this approach are reported, for comparison, in the last column of Table 1).

The surface $p_{iso}(\phi_1,\phi_2)$, resulting from the procedure described above, and the corresponding contour plot are shown in Figure 4. The main feature of the obtained $p_{iso}(\phi_1,\phi_2)$ function is certainly represented by the existence of four symmetry related maxima of the probability function, corresponding to the C_2 (absolute maxima) and C_i (relative maxima)

Table 2. Optimized Values of the Iteration Parameters Required by the AP-DPD Approach

	t-St in ZLI1132
$\phi_1{}^M = \pm \phi_2^M/\text{deg}$	16.80 ± 0.02
$h_1 = h_2/\text{deg}$	10 (after parametrization)
$w_{(C_2)}$	0.59 ± 0.01
$\varepsilon_{2,0}^R/\text{kJ mol}^{-1}$	0.473 ± 0.002
$\varepsilon_{2,2}^R/\text{kJ mol}^{-1}$	1.349 ± 0.001
$\varepsilon_{2,0}^{(H_6-C=C-H_7)}/\text{kJ mol}^{-1}$	1.593 ± 0.006
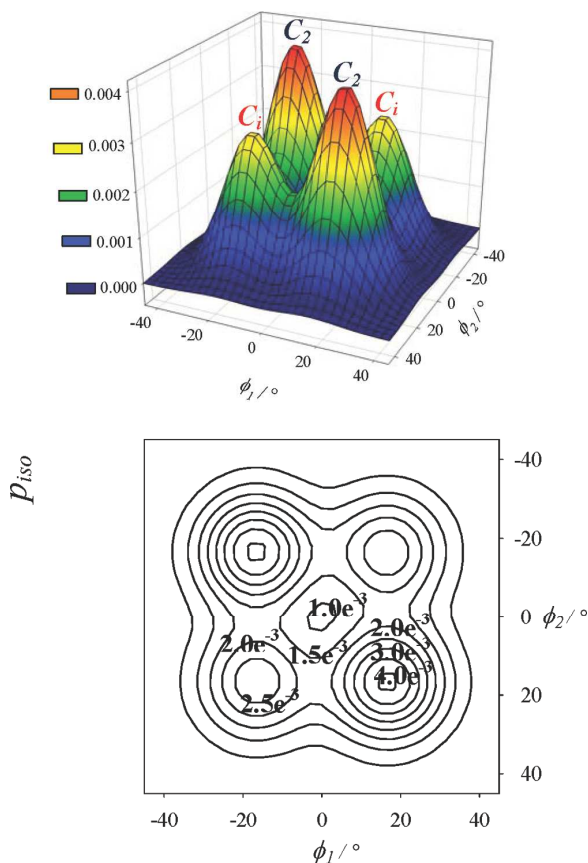
Figure 4. Experimental probability distribution $p_{iso}(\phi_1,\phi_2)$ for *t*-St dissolved in the nematic solvent ZLI1132 at 298 K, obtained by the LXNMR conformational analysis (both, the 3D surface and its contour plot, are shown for the sake of clarity).

structures characterized by having, respectively, $\phi_1^M = \phi_2^M$ and $\phi_1^M = -\phi_2^M$, with $\phi_1^M = 16.8°$ (see Table 2).

Finally, even though this paper is not aimed at determining the orientational ordering of *t*-St in liquid crystals, for the interested readers we report the **S** matrices of the stable rotamers of the molecule dissolved in ZLI1132 at 298 K. For the C_2 conformation, the order parameters given in the Principal Axis System (PAS) of the Saupe matrix are the following (see Figure 3 for the definition of the molecular axes and of the η angle, giving the location of the PAS): $S_{cc} = 0.525$ and $S_{aa} - S_{bb} = 0.174$, with $\eta = 44.92°$. In the same molecular frame (the **S** PAS of C_2) we also give the C_i order parameters: $S_{cc} = 0.506$, $S_{aa}-S_{bb} = 0.176$, $S_{ab} = \pm 0.055$, $S_{ac} \sim 0.0$ and $S_{bc} = \mp 0.029$ (the $\pm$ and $\mp$ signs are of course referred to the two possible forms of C_i, namely $\{\phi_1^M = +16.8° ; \phi_2^M = -16.8°\}$

and $\{\phi_1^M = -16.8°\,;\,\phi_2^M = +16.8°\}$). *A posteriori*, it is interesting to observe that the final values of S_{cc} and $S_{aa}-S_{bb}$ are really very similar to the trial ones $S_{cc} = 0.590$ and $S_{aa}-S_{bb} = 0.134$ "guessed" by us (by trial and error) to analyze the experimental spectrum (see section 3 above).

5. QUANTUM CHEMICAL CALCULATIONS

In order to shed more light on the problem widely described above, we decided to carry out rather accurate theoretical calculations *in vacuo*, by using the MP2/6-31G** method (fairly reliable for this kind of conformational problems)[34] to determine the minima on the conformational potential energy surface (PES) for *t*-St (we also allowed for bond lengths and angles relaxation of the structure every 3° torsional steps). The calculations were performed using the Gaussian 03 (rev. C.02) software package[57] and required 17 days, 17 h and 15 min of CPU time on a server IBM e326, equipped with two processors AMD Opteron 2.6 GHz and 2GB of RAM (O.S.: SUSE Linux Enterprise Server 9 for AMD64). The obtained conformational PES is shown in Figure 5,
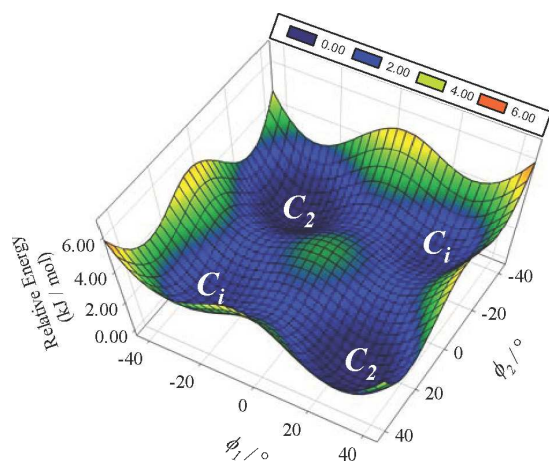
Figure 5. The conformational potential energy surface (PES) obtained for *trans*-stilbene from MP2/6-31G** calculations. The locations of absolute and relative minima are labeled by means of their point group symbols (see text for more details).

where the presence of two global and two local minima is clearly evident (the significant geometrical parameters for the molecule in its more stable conformation are given in Table 3 of the Appendix).

The resulting absolute minima (C_2 structures, where the relative torsional energy (RTE) is, of course, fixed to be 0 kJ/mol) and the relative minima (C_i structures corresponding to a RTE ~ 1.2 kJ/mol) are characterized by having, respectively, $\phi_1^m = \phi_2^m$ and $\phi_1^m = -\phi_2^m$, with $\phi_1^m = 27°$. The C_{2h} planar conformation ($\phi_1 = \phi_2 = 0°$) is neither a minimum nor a saddle point, but rather a local maximum corresponding to a RTE of about 3 kJ/mol (anyway, it is worthwhile to emphasize that the just quoted values of energy could be more or less affected by the ZPVE corrections).[34] Even though, as said in the Introduction, the past literature witnesses that different theoretical approaches can give quite different results, it should be noticed that something very similar to what we have found here has been already obtained by another method;[31] this increases, in our opinion, the reliability of our findings. In order to make more effective and immediate the comparison between the just described theoretical results, referred to the isolated molecule, and the experimental LXNMR results in solution, we decided to

plot the probability resulting from the *ab initio* calculations as a function of ϕ_1 and ϕ_2. The theoretical probability distribution p_{theo} (normalized for $-45° \leq \phi_1 \leq 45°$ and $-45° \leq \phi_2 \leq 45°$) is shown in Figure 6, where both the 3D and the contour plots of the function are given for more clarity.
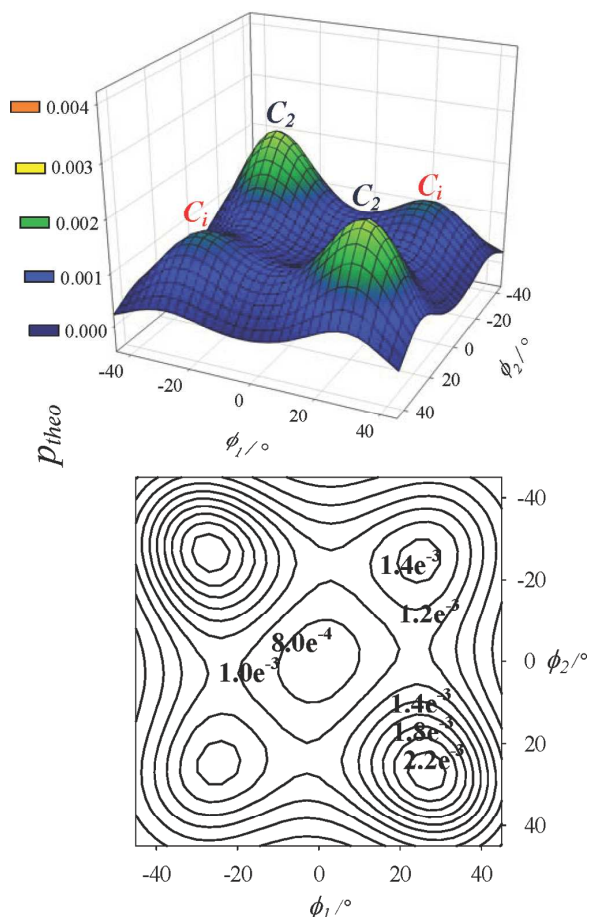
Figure 6. Normalized probability distribution p_{theo} for *trans*-stilbene, obtained from the theoretical PES of Figure 5.

6. COMPARISON BETWEEN *IN VACUO* THEORETICAL CALCULATIONS AND EXPERIMENTAL RESULTS IN SOLUTION

As interestingly anticipated in section 3, the basic non planarity of the molecule in solution had been qualitatively guessed, in a "model-free" way, from the simple appearance of the experimental LXNMR spectrum. Now, in the light of our final results, we observe that both the investigations carried out in this work manifestly agree in indicating non planar structures as the more stable conformations for the molecule. More in detail, a glance at Figure 4 and Figure 6 immediately reveals significant similarities, but also important differences, between the conformational probability distributions obtained from the two different treatments applied in this work. The similarities consist, of course, in the presence of the peculiar four "peaks" of probability belonging to the same symmetries (the two C_2 global and the two C_i local maxima). The differences are in the

precise locations of the maxima and in their different heights. It is not possible to discern with certainty to which extent the differences are physically sensible or, on the contrary, whether the obtained results are deeply biased by the adopted methods of investigation of the torsional equilibrium. Reasoning within the more interesting hypothesis of real physical effects, we think that, all things considered, the fact that in solution the twist angles are smaller than those theoretically predicted *in vacuo* should not surprise us. As a matter of fact, in the above cited gas phase experimental study of ref 25 (whose issues can be quite safely compared with our theoretical results, both concerning the isolated *t*-St), the molecule was recognized to be basically a C_2 structure with a twist angle of about 32.5°, not very dissimilar from our calculated 27°. Then, it seems that the intermolecular interactions, absent for the isolated molecule, contribute to force the molecule toward a less twisted arrangement (following this argument, it can be useful to recall here that the *t*-St is practically planar in its solid phase). This behavior is quite usual in conjugated systems as, for example, biphenyl (see ref 41 and references therein). Finally, our calculations say that the isolated molecule is "less confined" in the C_2 and C_i high probability conformations with respect to the liquid state, where the probability peaks are higher and, of course, sharper. Nonetheless, a crude ratio between the probabilities exactly corresponding to C_2 and C_i structures (given in the contour plots of Figures 4 and 6) roughly indicates relative percentages to be about 62% of C_2 against 38% of C_i both in liquid and in gas phase.

7. CONCLUSIONS

A basically non planar arrangement of *trans*-stilbene quite clearly emerges from our theoretical results *in vacuo* and from experimental outcomes in solution. This evidently means that the differences between the conformational behavior of the molecule in solution (where inter- and intramolecular forces act), with respect to the calculations on the isolated molecule (where, on the contrary, only intramolecular interactions are considered), are not enough to cancel the main features of the torsional probability distribution. As a matter of fact, four more stable conformations, two by two symmetry related (represented by a couple of global minima, where the molecule exhibits a propeller-like C_2 symmetry, and a couple of C_i local minima, where the rings are "conrotated" of the same angle) have been found both for the molecule *in vacuo* (via the reliable MP2/6-31G** theoretical calculations) and in solution (by the well tested experimental method of LXNMR conformational analysis). Of course, the probability distributions in the two phases are not identical, but the differences can be quite reasonably rationalized and explained. On the other hand, the calculated torsional potential of *t*-St (Figure 5) shows low barriers, comparable with $k_B T$ at room temperature. This has at least a couple of relevant consequences: (1) since the preference for one or the other conformation is relatively weak, the system needs to be described in terms of the full torsional distribution (in other words: at room temperature C_2 and C_i conformations are simultaneously present, and also the planar conformations are not totally absent); (2) the small energy differences may be one reason for the discrepancies between the results of different experiments (small changes of the experimental conditions, as the temperature and/or the solvent, might significantly affect the torsional distribution) and for the discrepancies between theoretical calculations performed at different levels (standard quantum chemical

calculations are not able to provide very reliable estimates of such small energy differences between minima). Given the great importance of *t*-St as a prototype molecule of many different compounds with innumerable properties (see the Introduction), we hope that our results, interesting, in our opinion, from a fundamental research point of view, can also contribute to a better understanding of useful structure–property relationships.

■ APPENDIX

Molecular Geometry of *trans*-Stilbene

Assuming, as usually done in literature,[44a,48] that the structures of the sub-units making up the flexible molecule (and rotating relative to each other) are "rigid", we can determine the fragment structures (independently from each other) from the whole set of observed interproton dipolar couplings obtained from the ^{1}H-LXNMR spectrum of *t*-St dissolved in ZLI1132 (Table 1 of the work). It is worth recalling here that, from the proton NMR spectrum, we cannot of course have direct information about the carbon geometries of the molecule; so, only a "virtual" skeleton of the molecule can be hypothesized and assumed, compatible with the proton coordinates able to reproduce the observed D_{ij}^{obs}.
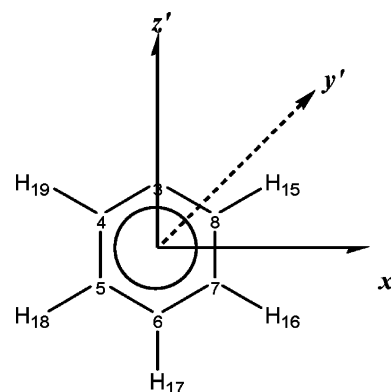

Phenyl Rings Structure

We have a total set of 6 intraring $D_{ij}^{Ring}(obs)$ values (of course, the two ring sub-units in the molecule have been assumed to be structurally identical). First of all, we fixed the proton coordinates correspondingly to an "all-120°" virtual (about what we mean with this word, see above) regular hexagon with $\overline{CC}$ =1.40 Å and $\overline{CH}$=1.09 Å: this implies for the rings a C_{2v} local symmetry (consistent with the nuclear spin symmetry). Then, we adjusted the local order parameters $S_{z'z'}^{Ring}$, $(S_{x'x'} - S_{y'y'})^{Ring}$, and the $C_7\hat{C}_8H_{15}$ angle (of course also the $C_5\hat{C}_4H_{19}$ angle, equal to $C_7\hat{C}_8H_{15}$, has been correspondingly changed to keep the C_{2v} symmetry of the rings) in order to reproduce the 6 intraring dipolar couplings (3 degrees of freedom *versus* 6 experimental data mathematically represent a good over-determination of the system). The final results were the following: $C_7\hat{C}_8H_{15}$ = 119.25°; $S_{z'z'}^{Ring}$ = 0.5068 and $(S_{x'x'} - S_{y'y'})^{Ring}$ = 0.1754. These ring geometries were then kept fixed in all subsequent calculations.

Structure of the Vinyl Fragment

Since only one local direct coupling is experimentally available for the *ene* fragment (the $D_{25,26}^{obs}$ coupling constant), we were forced to start by borrowing the virtual geometries of this sub-unit from the theoretical calculations carried out by the

MP2/6-31G** method (see text); then, during the LXNMR calculations, we slightly refined the initial geometries in order
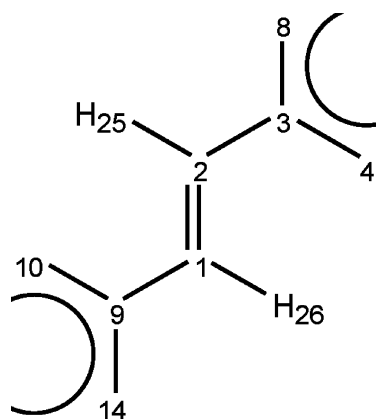
to better reproduce the whole set of the observed couplings. As reported below (Table 3), the starting and refined values are fortunately very similar, so that, in our opinion, the used geometries can be considered reliable.

Table 3. Starting and Refined Geometries of the *Ene* Group

geometrical parameter	initial value (from MP2/6-31G** theoretical calculations)	refined value
$r_{1,2}$ /Å	1.352	1.337
$r_{2,3}$ /Å	1.466	1.477
$C_1\hat{C}_2C_3$/deg	124.83	125.54
$C_2\hat{C}_3C_4$/deg	120.80	122.49
$C_1\hat{C}_2H_{25}$/deg = $C_2\hat{C}_1H_{26}$/deg	118.78	120.24

■ AUTHOR INFORMATION

Corresponding Author
*E-mail: giorgio.celebre@unical.it. Telephone: +39-0984493321. Fax: +39-0984493301.

Notes
The authors declare no competing financial interest.

■ ACKNOWLEDGMENTS

■ REFERENCES

(1) (a) Belluti, F.; Fontana, G.; Dal Bo, L.; Carenini, N.; Giommarelli, C.; Zunino, F. *Bioorgan. Med. Chem.* **2010**, *18*, 3543–3550. and refs therein (b) Frémont, L. *Life Sci.* **2000**, *66*, 663–673. (c) Matsuda, H.; Tomohiro, N.; Hiraba, K.; Harima, S.; Ko, S.; Matsuo, K.; Yoshikawa, M.; Kubo, M. *Biol. Pharm. Bull.* **2001**, *24*, 264–267.

(2) (a) Savio, M.; Coppa, T.; Bianchi, L.; Vannini, V.; Maga, G.; Forti, L.; Cazzalini, O.; Lazzè, M. C.; Perucca, P.; Prosperi, E.; Stivala, L. A. *Int. J. Biochem. Cell B.* **2009**, *41*, 2493–2502. (b) Queiroz, A. N.;

Gomes, B. A. Q.; Moraes, W. M. Jr.; Borges, R. S. *Eur. J. Med. Chem.* **2009**, *44*, 1644–1649.

(3) (a) Heynekamp, J. J.; Weber, W. M.; Hunsaker, L. A.; Gonzales, A. M.; Orlando, R. A.; Deck, L. M.; Van der Jagt, D. L. *J. Med. Chem.* **2006**, *49*, 7182–7189. and refs therein (b) Kim, S.; Min, S. Y.; Lee, S. K.; Cho, W. *J. Chem. Pharm. Bull.* **2003**, *51*, 516–521.

(4) (a) Bhat, K. P. L.; Lantvit, D.; Christov, K.; Mehta, R. G.; Moon, R. C.; Pezzuto, J. M. *Cancer Res.* **2001**, *61*, 7456–7463. (b) Korach, K. S.; Metzler, M.; McLachlan, J. A. *Proc. Natl. Acad. Sci. U.S.A.* **1978**, *75*, 468–471.

(5) Ko, S. K.; Lee, S. M.; Whang, W. K. *Arch. Pharm. Res.* **1999**, *22*, 401–403.

(6) (a) Hong, M. C.; Kim, Y. K.; Choi, J. Y.; Yang, S. Q.; Rhee, H.; Ryu, Y. H.; Choi, T. H.; Cheon, G. J.; An, G. I.; Kim, H. Y.; Kim, Y.; Kim, D. J.; Lee, J.-S.; Chang, Y.-T.; Lee, K. C. *Bioorgan. Med. Chem.* **2010**, *18*, 7724–7730. (b) Chen, X. *J. Mol. Struct.—THEOCHEM.* **2006**, *763*, 83–89.

(7) (a) Rotta, R.; Neto, Á. C.; de Lima, D. P.; Beatriz, A.; da Silva, G. V. J. *J. Mol. Struct.* **2010**, *975*, 59–62. (b) Aslam, S. N.; Stevenson, P. C.; Kokubun, T.; Hall, D. R. *Microbiol. Res.* **2009**, *164*, 191–195.

(8) (a) Ravikrishnan, A.; Sudhakara, P.; Kannan, P. *J. Mater. Sci.* **2010**, *45*, 435–442. (b) Buathong, S.; Gehringer, L.; Donnio, B.; Guillon, D. *C. R. Chim.* **2009**, *12*, 138–162.

(9) Zoppi, L.; Calzolari, A.; Ruini, A.; Ferretti, A.; Caldas, M. J. *Phys. Rev. B* **2008**, *78*, 165204.

(10) Papper, V.; Likhtenshtein, G. I. *J. Photochem. Photobiol. A* **2001**, *140*, 39–52 and refs. therein.

(11) Buruiana, E. C.; Zamfir, M.; Buruiana, T. *Eur. Polym. J.* **2007**, *43*, 4316–4324.

(12) (a) Tomatsu, I.; Peng, K.; Kros, A. *Adv. Drug Delivery Rev.* **2011**, *63*, 1257–1266. (b) Meng, F.; Zhong, Z.; Feijen, J. *Biomacromolecules* **2009**, *10*, 197–209.

(13) Finder, C. J.; Newton, M. G.; Allinger, N. L. *Acta Crystallogr.* **1974**, *B30*, 411–415.

(14) Bernstein, J. *Acta Crystallogr.* **1975**, *B31*, 1268–1271.

(15) Tachon, M.; Davies, E.; Lamotte, M.; Muszkat, K. A.; Wismontski-Knittel, T. *J. Phys. Chem.* **1994**, *98*, 11870–11877.

(16) Myers, A. B.; Trulson, M. O.; Mathies, R. A. *J. Chem. Phys.* **1985**, *83*, 5000–5006.

(17) Suzuki, T.; Mikami, N.; Ito, M. *J. Phys. Chem.* **1986**, *90*, 6431–6440.

(18) Baskin, J. S.; Felker, P. M.; Zewail, A. H. *J. Chem. Phys.* **1987**, *86*, 2483–2499.

(19) Spangler, L. H.; v. Zee, R.; Zwier, T. S. *J. Phys. Chem.* **1987**, *91*, 2782–2786.

(20) Spangler, L. H.; v. Zee, R.; Blankespoor, S. C.; Zwier, T. S. *J. Phys. Chem.* **1987**, *91*, 6077–6079.

(21) Baskin, J. S.; Zewail, A. H. *J. Phys. Chem.* **1989**, *93*, 5701–5717.

(22) Champagne, B. B.; Pfanstiel, J. F.; Plusquellic, D. F.; Pratt, D. W.; van Herpen, W. M.; Meerts, W. L. *J. Phys. Chem.* **1990**, *94*, 6–8.

(23) Chiang, W.-Y.; Laane, J. *J. Chem. Phys.* **1994**, *100*, 8755–8767.

(24) Syage, J. A.; Felker, P. M.; Zewail, A. H. *J. Chem. Phys.* **1984**, *81*, 4685–6440.

(25) Traetteberg, M.; Frantsen, E. B.; Mijlhoff, F. C.; Hoekstra, A. *J. Mol. Struct.* **1975**, *26*, 57–68.

(26) Maier, J. P.; Turner, D. W. *J. Chem. Soc., Faraday Trans. 2* **1973**, *54*, 196–206.

(27) Rademacher, P.; Marzinzik, A. L.; Kowski, K.; Weiß, M. E. *Eur. J. Org. Chem.* **2001**, 121–130.

(28) Chen, P. C.; Chieh, Y. C. *J. Mol. Struct.—THEOCHEM.* **2003**, *624*, 191–200 and references therein.

(29) Kwasniewski, S. P.; Claes, L.; François, J.-P.; Deleuze, M. S. *J. Chem. Phys.* **2003**, *118*, 7823–7836 and references therein.

(30) Quenneville, J.; Martínez, T. J. *J. Chem. Phys. A* **2003**, *107*, 829–837.

(31) Freile, M. L.; Risso, S.; Curaqueso, A.; Zamora, M. A.; Enriz, R. D. *J. Mol. Struct.—THEOCHEM.* **2005**, *731*, 107–114.

(32) Vendrame, R.; Coluci, V. R.; Galvão, D. S. *J. Mol. Struct.—THEOCHEM.* **2004**, *686*, 103–108.

(33) Catalán, J. *Chem. Phys. Lett.* **2006**, *421*, 134−137.

(34) Chowdary, P. D.; Martinez, T. J.; Gruebele, M. *Chem. Phys. Lett.* **2007**, *440*, 7−11.

(35) Bree, A.; Edelson, M. *Chem. Phys.* **1980**, *51*, 77−88.

(36) Novak, P.; Meić, Z.; Sterk, H. *J. Chem. Soc., Perkin Trans. 2* **1996**, *11*, 2531−2536.

(37) Choi, C. H.; Kertesz, M. *J. Phys. Chem. A* **1997**, *101*, 3823−3831.

(38) Furuya, K.; Kawato, K.; Yokoyama, H.; Sakamoto, A.; Tasumi, M. *J. Phys. Chem. A* **2003**, *107*, 8251−8258.

(39) Celebre, G.; De Luca, G.; Longeri, M.; Emsley, J. W. *Mol. Phys.* **1989**, *67*, 239−248 and references therein.

(40) Celebre, G.; De Luca, G.; Longeri, M.; Ferrarini, A. *Mol. Phys.* **1994**, *83*, 309−326 and references therein.

(41) Celebre, G.; De Luca, G.; Longeri, M. *Liq. Cryst.* **2010**, *37*, 923−933.

(42) Celebre, G.; De Luca, G.; Longeri, M.; Sicilia, E. *J. Chem. Inf. Comput. Sci.* **1994**, *34*, 539−545.

(43) Diehl, P. in *Nuclear Magnetic Resonance of Liquid Crystals*; Emsley, J. W., Ed.; Reidel: Dordrecht, The Netherlands, 1985; pp 147−180 and references therein.

(44) (a) Celebre, G.; Longeri, M. In *NMR of Ordered Liquids*; Burnell, E. E., de Lange, C. A., Eds.; Kluwer: Dordrecht, The Netherlands, 2003; pp 305−324. (b) The director aligns parallel or perpendicular to B_0, depending on the sign of solvent diamagnetic susceptibility anisotropy $\Delta\chi = \chi_{\parallel} - \chi_{\perp}$ (in particular, $\Delta\chi > 0$, parallel arrangement; $\Delta\chi < 0$, perpendicular arrangement): de Gennes, P. G.; Prost, J. *The Physics of Liquid Crystals*; Oxford Science: London, 1993.

(45) Emsley, J. W.; Luckhurst, G. R.; Stockley, C. P. *Proc. R. Soc. London, Ser. A* **1982**, *381*, 117−138.

(46) Emsley, J. W. in *Encylopedia of NMR*, Eds. Grant, D. M. Harris, R. K., J. Wiley & Sons Ltd: Chichester, 1996; pp 2781−2787.

(47) Celebre, G.; De Luca, G.; Emsley, J. W.; Foord, E. K.; Longeri, M.; Lucchesini, F.; Pileio, G. *J. Chem. Phys.* **2003**, *118*, 6417−6426.

(48) Celebre, G.; De Luca, G.; Longeri, M.; Pileio, G.; Emsley, J. W. *J. Chem. Phys.* **2004**, *120*, 7075−7084.

(49) Celebre, G.; Concistrè, M.; De Luca, G.; Longeri, M.; Pileio, G.; Emsley, J. W. *Chem.—Eur. J.* **2005**, *11*, 3599−3608.

(50) Concistrè, M.; De Lorenzo, L.; De Luca, G.; Longeri, M.; Pileio, G.; Raos, G. *J. Phys. Chem. A* **2005**, *109*, 9953−9963.

(51) Celebre, G.; Cinacchi, G. *J. Chem. Phys.* **2006**, *124*, 176101 and references therein.

(52) Celebre, G.; Concistrè, M.; De Luca, G.; Longeri, M.; Pileio, G. *Chem. Phys. Chem.* **2006**, *7*, 1930−1943.

(53) Emsley, J. W.; De Luca, G.; Lesage, A.; Merlet, D.; Pileio, G. *Liq. Cryst.* **2007**, *34*, 1071−1093.

(54) Emsley, J. W.; Lesot, P.; De Luca, G.; Lesage, A.; Merlet, D.; Pileio, G. *Liq. Cryst.* **2008**, *35*, 443−464.

(55) Brink, D. M.; Satchler, G. R., *Angular Momentum*, 3rd ed., Clarendon Press: Oxford, U.K., 1993.

(56) Schlegel, H. B. *J. Comput. Chem.* **1982**, *3*, 214−218.

(57) Gaussian 03, Revision C.02, Frisch, M. J.; Trucks, G. W.; Schlegel, H. B.; Scuseria, G. E.; Robb, M. A.; Cheeseman, J. R.; Montgomery, J. A., Jr.; Vreven, T.; Kudin, K. N.; Burant, J. C.; Millam, J. M.; Iyengar, S. S.; Tomasi, J.; Barone, V.; Mennucci, B.; Cossi, M.; Scalmani, G.; Rega, N.; Petersson, G. A.; Nakatsuji, H.; Hada, M.; Ehara, M.; Toyota, K.; Fukuda, R.; Hasegawa, J.; Ishida, M.; Nakajima, T.; Honda, Y.; Kitao, O.; Nakai, H.; Klene, M.; Li, X.; Knox, J. E.; Hratchian, H. P.; Cross, J. B.; Adamo, C.; Jaramillo, J.; Gomperts, R.; Stratmann, R. E.; Yazyev, O.; Austin, A. J.; Cammi, R.; Pomelli, C.; Ochterski, J. W.; Ayala, P. Y.; Morokuma, K.; Voth, G. A.; Salvador, P.; Dannenberg, J. J.; Zakrzewski, V. G.; Dapprich, S.; Daniels, A. D.; Strain, M. C.; Farkas, O.; Malick, D. K.; Rabuck, A. D.; Raghavachari, K.; Foresman, J. B.; Ortiz, J. V.; Cui, Q.; Baboul, A. G.; Clifford, S.; Cioslowski, J.; Stefanov, B. B.; Liu, G.; Liashenko, A.; Piskorz, P.; Komaromi, I.; Martin, R. L.; Fox, D. J.; Keith, T.; Al-Laham, M. A.; Peng, C. Y.; Nanayakkara, A.; Challacombe, M.; Gill, P. M. W.; Johnson, B.; Chen, W.; Wong, M. W.; Gonzalez, C.; Pople, J. A.; Gaussian, Inc.: Pittsburgh PA, 2003.

2885

dx.doi.org/10.1021/jp211962w | *J. Phys. Chem. B* 2012, 116, 2876−2885

**THE EUROPEAN
PHYSICAL JOURNAL E**

Regular Article

Smectic order parameters via liquid crystal NMR spectroscopy: Application to a partial bilayer smectic A phase

Maria Enrica Di Pietro[1], Giorgio Celebre[1], Giuseppina De Luca[1], Herbert Zimmermann[2], and Giorgio Cinacchi[3,a]

[1] Dipartimento di Chimica, Università della Calabria, Campus di Arcavacata, Via Pietro Bucci Cubo 12C, I-87036 Rende (Cosenza), Italy
[2] Max-Planck-Institut für Medizinische Forschung, Jahnstrasse 29, D-69120 Heidelberg, Germany
[3] Departamento de Física Teórica de la Materia Condensada, Universidad Autónoma de Madrid, Campus de Cantoblanco, E-28049 Madrid, Spain

Abstract. Solute molecules were dissolved in the liquid crystal 4-cyano-4'-n-octyloxybiphenyl (8OCB), known to form a partial bilayer smectic-A phase. Through measurement of solutes' and solvent's orientational order parameters via nuclear magnetic resonance spectroscopy, and their analysis via a statistical thermodynamic density functional theory, values of the solvent's positional order parameters and solutes' positional-orientational distribution functions were obtained. Near to the transition to the nematic phase, the main positional order parameter of the smectic liquid crystal turned out to be comprised in the interval 0.4–0.6, though the quality of the fittings assuming the phase as nematic all across the temperature range investigated was only slightly worse. This may be ascribed to the looseness of the partial bilayer smectic structure. Solutes were found to preferentially lie in those regions where liquid crystal molecule terminal chains are located.

1 Introduction

The distinctive feature of a smectic liquid crystal phase is its layered structure [1]. In general, the relative stability of this phase organisation is primarily due to the overall elongated shape of the constituent particles, be they molecules or colloids [2–4]. For thermotropic low-molecular-weight liquid crystals in particular, formed as they are by molecules having a rigid central core and flexible peripheral chains, the decisive additional role of the latter has been long recognized [5, 6] and very recently confirmed again [7]. To these two major factors, both of entropic nature, anisotropic energetic terms, such as attractive dispersion and/or electrostatic interactions, may add. Computer simulation studies have shown how suitable anisotropic attractive dispersion interactions may stabilise further or induce a smectic phase [8,9] and what may be the role of dipolar and quadrupolar electrostatic interactions in determining the relative stability and structure of these mesophases [10–19].

Whatever is the microscopic mechanism leading to the formation of layers, smectics further differentiate among themselves on the basis of the orientation that molecule long axes preferentially take with respect to the layer normal ($\hat{n}$) and of the degree of positional order within a

given layer. The simplest smectic phase is the smectic-A (S_A), formed by molecules that tend to orient along $\hat{n}$ and have just a short-range, liquid-like in-layer positional order. This state of affairs readily complicates as soon as (binary) mixtures, instead of single-component systems, are considered or, even in a single-component system, when molecules do not preferentially arrange side-by-side but in some shifted configuration.

This is, for example, the case of the members of the well-known n-alkyl and n-alkoxy cyano-biphenyl series of liquid crystal molecules (nCB and nOCB). These series of compounds were first reported in ref. [20] and they have been the object of a wealth of studies ever since. Provided n is large enough, a nematic (N) phase and, for $n \geq 8$, also a S_A phase form. Soon after their synthesis, X-ray diffraction studies were carried out that revealed that the wavelength of the smectic-like fluctuations in the N phase of 5CB and 7CB as well as the layer spacing (δ) in the S_A phase of the higher alkyl and alkoxy homologues were between once and twice a molecular length [21–23]. It was readily recognized that this had to be due to some sort of dimerisation, induced by the strong dipole moment borne by the terminal cyano groups, these interacting between them and with the phenyl groups of the biphenyl moiety: as a result, a partial bilayer S_A phase, labelled S_{A_d}, turns out; its structure is schematically given in fig. 1.

[a] e-mail: giorgio.cinacchi@uam.es
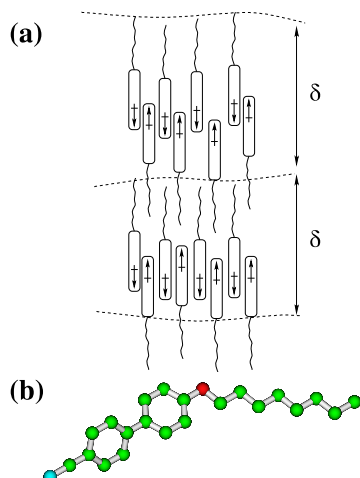
Fig. 1. (a) Schematic illustration of a partial bilayer smectic A phase, with molecules tending to pair up in a slipped-parallel configuration, as it occurs in 8OCB, whose "ball-and-stick" united-atom model molecular structure is also given (b).

The picture deducted from the diffraction experiments later received several confirmations (see, *e.g.*, ref. [24]), more recently also from a few computer simulation studies conducted on atomistic models of 8CB [25–27]. These computational studies also confirmed how the layered structure of the S_{A_d} of this compound is somewhat loose, with density waves (ρ) along $\hat{\boldsymbol{n}}$ of small amplitude. This is consistent with the well-known very weak, second-order character of the nematic-smectic phase transition in these compounds (see, *e.g.*, refs. [28,29] for a calorimetric and a volumetric study, respectively). Though we are unaware of analoguous simulation studies conducted on 8OCB, it is very likely that what found for 8CB applies also to its alkoxy counterpart, given the many similarities shared by the two compounds.

The aim of the present work is to use a recently proposed methodology, combining a statistical thermodynamic density functional theory (ST-DFT) with liquid crystal nuclear magnetic resonance (LX-NMR) spectroscopy, to obtain values of the positional order parameters of the S_{A_d} of 8OCB.

These parameters are defined as [5]

$$\tau_k = \frac{1}{\delta} \int_0^\delta \mathrm{d}z \cos\left(2\pi k \frac{z}{\delta}\right) \rho(z), \qquad (1)$$

with k a positive integer and z the molecular centre displacement from the mid-layer position resolved along $\hat{\boldsymbol{n}}$. These parameters quantify the extent of layering, with $\tau_k = 0$ meaning absence of a layered structure and $\tau_k = 1$ corresponding to molecules locked in the mid-layer positions. Yet, they are not amenable to a straightforward experimental assessment. This is unlike what happens for the orientational order parameters, the ones of lowest rank being readily available from NMR [5,30,31] or Raman [5,32] spectroscopies.

While past and a couple of more recent attempts at getting positional order parameters all rely on diffraction measurements [33–40], several studies have been published in these years that addressed this problem from a different standpoint. They all use NMR spectroscopy [41–50]. Most of them exploit the reliability of the NMR spectroscopy in providing very accurate orientational order parameters of solute molecules dissolved in a liquid crystal solvent [51–59] and then attempt to relate the (fine) changes that these parameters may undergo upon entering a smectic phase to get information on the extent of layering [42–50]. The ST-DFT–LX-NMR methodology [48–50] in particular allows for the determination of not only solutes' positional-orientational distribution functions but also of the smectic solvent's positional order parameters.

This methodology was previously applied to the typical S_A phase formed by the compound 4,4'-di-*n*-heptylaxoxybenzene (HAB) with encouraging results [49,50]. Here we wish to test its performances further by applying it to what is looking as a more delicate case, namely the S_{A_d} phase formed by 8OCB. The loose, partial bilayer character of its structure, linked to the very weak, second-order character of the nematic-smectic phase transition in compounds of this sort, would seem to play against a smooth extension of the previous results to this case. It is in fact not warranted that solutes' orientational order parameters do show any detectable sign of entering a smectic phase.

The plan of this work is as follows. In the next section we summarize the ST-DFT, recalling its basis and the approximations made in its implementation. Section 3 describes the LX-NMR experiments carried out. The analysis of the experimental data by means of the ST-DFT is reported in sect. 4, followed by a discussion of the results. Conclusions are drawn and perspectives briefly outlined in sect. 5.

2 Recall of theory and its implementation in the present case

In this section the ST-DFT is recalled. For full details on its derivation the reader is referred to refs. [48,49]. The main equation coming out from the ST-DFT is

$$\rho_\sigma(z, \Omega) = \frac{1}{\Xi} e^{-2\Psi \int_{-\infty}^{+\infty} \mathrm{d}z' \mathrm{d}\Omega' \rho_\Sigma(z', \Omega') A_{\sigma\Sigma}(z-z', \Omega, \Omega')}. \qquad (2)$$

The meaning of the terms entering this equation is the following:

- $\rho_\sigma(z, \Omega)$ is the probability density to find a solute molecule σ in the state defined by the position z of its centre of mass along $\hat{\boldsymbol{n}}$ and its orientation, specified by the usual set of Euler angles [60] collected under the symbol Ω.
- $\rho_\Sigma(z', \Omega')$ is the probablity density to find a solvent molecule Σ in the positional-orientational state defined by z' and Ω'. Here, the centre of a 8OCB molecule was taken coincident with the position of its oxygen atom.

The latter, the carbon atom bonded to it, the two carbon atoms joining the two phenyl groups, the carbon atom bonded to the cyano group and the carbon and nitrogen atoms of the latter all lie on the same line. The unit vector along this line and directed from the O to the N atoms, $\hat{\boldsymbol{u}}$, serves to indicate the molecule main axis direction.

- The quantity $A_{\sigma\Sigma}(z - z', \Omega, \Omega')$ measures solute-solvent interactions. More specifically, it reads

$$A_{\sigma\Sigma}(z - z', \Omega, \Omega') = -\int \mathrm{d}\boldsymbol{R} \mathsf{f}_{\sigma\Sigma}(\boldsymbol{R}, z - z', \Omega, \Omega'),$$
(3)

with $\mathsf{f}_{\sigma\Sigma}$ the solute-solvent Mayer function and $\boldsymbol{R}$ the vector of the distance between the two molecules' centres resolved perpendicularly to $\hat{\boldsymbol{n}}$. The Mayer function reads

$$\mathsf{f}_{\sigma\Sigma}(\boldsymbol{R}, z - z', \Omega, \Omega') = e^{-\frac{u_{\sigma\Sigma}(\boldsymbol{R}, z-z', \Omega, \Omega')}{k_B T}} - 1, \quad (4)$$

with $u_{\sigma\Sigma}$ the intermolecular solute-solvent interaction potential energy function, k_B the Boltzmann constant and T the temperature.

- The factor Ψ helps correct in an effective way for the neglect of higher-order (virial) terms involving ever more complicated integrals. It depends on the solvent's number density, ρ_Σ^0, and it reduces to it in the limit $\rho_\Sigma^0 \to 0$. It is worthwhile emphasizing that Ψ is a solvent property only that can be interpreted as the solvent's effective density.

- Ξ is the normalization constant, ensuring that

$$\int \mathrm{d}z \mathrm{d}\Omega \rho_\sigma(z, \Omega) = 1.$$
(5)

Equation (2) originates from classic Onsager second-virial DFT [61], the basic theory to understand liquid crystal thermodynamics and structure. Originally devised in the forties to explain the occurrence of an isotropic-nematic phase transition in some colloidal suspensions of inorganic and organic elongated particles, it would be a too long digression to summarize its success and its numerous applications and extensions to mixtures and positional heterogeneous phases such as smectic and columnar, and to thermotropics as well, which have appeared in the literature over the years. More in particular, eq. (2) originates from a development of Onsager theory proposed by Parsons [62]. This amounts to introducing a density-dependent prefactor, which effectively takes into account higher-order virial terms. Parsons theory is applicable to denser liquid crystal phases, predicts isotropic-nematic and nematic-smectic-A thermodynamic quantities in good agreement with computer simulations and has been more recently extended to mixtures [63]. Equation (2) is derivable from this recent extension once very dilute solutions are considered [48, 49]. Under these conditions, the positional-orientational distribution function of a solute is linked to the positional-orientational distribution function of the solvent via the function $A_{\sigma\Sigma}$. Yet, these are the very conditions under which we would like
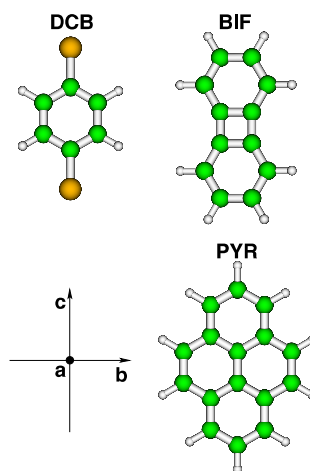
Fig. 2. "Ball-and-stick" molecular structure of the solutes employed, with their labels and the axes of their molecular reference frame.

to operate. Indeed, our main objective is to obtain values of the positional order parameters of the smectic liquid crystal solvent. If the solutions are dilute, it is reasonable to expect that these parameters are, at most, only slightly different from those of the neat smectic liquid crystal.

Once an approximation for solute-solvent interactions has been set out and $\rho_\Sigma(z', \Omega')$ suitably parameterized, these latter parameters can be determined by fitting suitable quantities predicted by the ST-DFT to the corresponding quantities measured experimentally.

In our case, these quantities are the Saupe ordering matrices, $\boldsymbol{S}$'s [5], of solute molecules dissolved in the liquid crystal solvent, whose measurement is possible via NMR spectroscopy. If $[S_{ab}]_\sigma^{\mathrm{expt}}$ is the ab element of the experimental Saupe ordering matrix of the solute σ, the corresponding calculated quantity, $[S_{ab}]_\sigma^{\mathrm{calc}}$, reads

$$[S_{ab}]_\sigma^{\mathrm{calc}} = \int \mathrm{d}z \mathrm{d}\Omega \rho_\sigma(z, \Omega) \left[\frac{3}{2}(\hat{\boldsymbol{a}} \cdot \hat{\boldsymbol{n}})(\hat{\boldsymbol{b}} \cdot \hat{\boldsymbol{n}}) - \frac{\delta_{ab}}{2} \right],$$
(6)

with $\hat{\boldsymbol{a}}$ the a-th axis of the molecular reference frame and δ_{ab} the Krönecker symbol. What one is required to minimise is then a sum of the following kind:

$$\tilde{\chi}^2 = \frac{1}{\nu} \sum_\sigma \sum_{ab} \left\{ [S_{ab}]_\sigma^{\mathrm{expt}} - [S_{ab}]_\sigma^{\mathrm{calc}} \right\}^2,$$
(7)

with ν the number of data minus the number of parameters and the two sums running, respectively, over the solute molecules dissolved and the independent elements of their respective Saupe ordering matrices. The solute molecules employed in the present work were: 1,4-di-chlorobenzene (DCB), biphenylene (BIF) and pyrene (PYR). Their "ball-and-stick" model molecular structure is given in fig. 2 along with the axes of their molecular reference frame.

With regards to solute-solvent interactions, we decided to make a compromise between the desire of preserving the

chemical identity of the molecules under consideration and the one of keeping the calculations as simple as possible. On sorting amid the various models put forward over the years to describe, at many levels of idealization/realism, interactions between molecules as complex as those giving rise to liquid crystalline phases, an intermediate choice involves modelling these interactions at an atomistic, chemically detailed level yet retaining only the repulsive part of the atom-atom interactions and assuming the latter of the hard-sphere type, with the radius of the various spheres taken from literature [64]. To reduce computational burden further, the following semplifications were made: i) the alkyl chain was kept in its fully extended, *all-trans*, conformation; ii) the hydrogen atoms of the liquid crystal molecule were grouped together with the carbon atom they are bonded to and each "united atom" group so formed was described by a single hard sphere, whose centre coincides with the position of the carbon atom and the radius is taken from ref. [64]; iii) on the basis of previous quantum chemical calculations [65], the chemical bond joining the first two methylene groups of the chain was constrained to lie on the plane of the oxygen atom and nearby phenyl group; iv) the dihedral angle between the two phenyl groups was set at the value of 42°, in accordance with previous quantum chemical calculations [66].

Within a hard-body model, the quantity $A_{\sigma\Sigma}$ is interpreted as the area that a solute and a solvent molecules exclude one another. The atomistic-hard-body models employed can certainly get more complicated by adding dispersion and/or electrostatic interactions and by allowing the alkyl chain to explore more of its conformational space. None the less, ref. [48] showed that the basic phenomenon at the origin of a change in the trend of solutes' orientational order parameters on entering a smectic phase, namely the partitioning of a solute in the intra- and inter-layer regions, can be understood resorting to excluded area arguments only. Within an atomistic-hard-body model, the most basic, chemical identity of a molecule ultimately amounts to its size and shape. This may appear simplistic. Yet, while there should be no need to stress the long recognized importance of molecular size and shape in the liquid crystal chemical physics, it might be pertinent to notice here that their importance is increasingly being appreciated nowadays even in the field of medicinal chemistry [67].

It may be worthwhile pointing out that these considerations are not in contradiction with the long recognized crucial role that electrostatic interactions have in the formation of a partial bilayer structure in higher homologues of the nCB and nOCB series of compounds. That is because what is required in the implementation of our method is a knowledge of solute-solvent interactions (and not of solvent-solvent interactions) together with an assumption on the solvent's positional-orientational distribution function. It is the latter that has to be in keeping with what already known about the solvent's smectic structure.

In this respect, solvent's positional and orientational variables were assumed decoupled. Detailed computer simulations on a idealized model for thermotropic liquid crys-

tal [9] come in support of this decision, (though it may be fair to mention that, in certain other cases, this approximation could not be that accurate (see, *e.g.*, ref. [68])). We took

$$\rho_\Sigma\left(z',\Omega'\right) = \rho_{\Sigma,\lambda}\left(z'\right)\rho_{\Sigma,\gamma}\left(\Omega'\right), \tag{8}$$

with $\rho_{\Sigma,\lambda}\left(z'\right)$ the positional and $\rho_{\Sigma,\gamma}\left(\Omega'\right)$ the orientational distribution functions. The partial bilayer nature of the 8OCB smectic liquid crystal implies the presence of two classes of solvent molecules, having, respectively, the cyano group parallel or anti-parallel to the arbitrarily chosen direction of the layer normal. We can therefore identify the former molecules with those having θ', the angle formed by $\hat{\boldsymbol{u}}$ with $\hat{\boldsymbol{n}}$ comprised between $[0;\pi/2]$ and the latter molecules with those such that $\theta' \in [\pi/2;\pi]$. We were therefore allowed to write the single-particle solvent density as a sum of two contributions:

$$\rho_\Sigma\left(z',\Omega'\right) = \rho_{\Sigma,\lambda}^\uparrow\left(z'\right)\rho_{\Sigma,\gamma}^\uparrow\left(\Omega'\right) + \rho_{\Sigma,\lambda}^\downarrow\left(z'\right)\rho_{\Sigma,\gamma}^\downarrow\left(\Omega'\right). \tag{9}$$

With the support of, among others, the computer simulations of ref. [9] again, we confidently took the positional distribution function of the molecules "↑" of the form below:

$$\rho_{\Sigma,\lambda}^\uparrow\left(z'\right) = \frac{e^{\lambda\cos\left(2\pi\frac{z'}{\delta}\right)}}{\varUpsilon_\lambda}, \tag{10}$$

with λ the parameter regulating the extent of its waviness and $\varUpsilon_\lambda$ the normalisation constant ensuring that

$$\frac{1}{\delta}\int_0^\delta \mathrm{d}z' \rho_{\Sigma,\lambda}^\uparrow\left(z'\right) = 1. \tag{11}$$

The orientational distribution function of the molecules "↑" has to comply with the uniaxial character of the liquid crystal phases of interest here. It was thus taken as

$$\rho_{\Sigma,\gamma}^\uparrow\left(\Omega'\right) = \frac{e^{\gamma P_2\left(\cos\theta'\right)}}{\varUpsilon_\gamma}, \tag{12}$$

with γ the parameter regulating its shape, having a one-to-one correspondence with the solvent's nematic order parameter (η), being $P_2(\ )$ the second Legendre polynomial and $\varUpsilon_\gamma$ the normalization constant such that

$$\begin{aligned}\varUpsilon_\gamma &= 2\pi\int_0^{\pi/2}\mathrm{d}\theta'\sin\theta' e^{P_2\left(\cos\theta'\right)}\\ &= 2\pi\int_{\pi/2}^\pi\mathrm{d}\theta'\sin\theta' e^{P_2\left(\cos\theta'\right)}.\end{aligned} \tag{13}$$

This choice for the orientational distribution function too is supported by the computer simulations of ref. [9]. The molecules of the two classes preferentially dwell in one of the two interdigitating sub-layers. We therefore wrote the positional distribution function of the molecules "↓" as

$$\rho_{\Sigma,\lambda}^\downarrow\left(z'\right) = \frac{e^{-\lambda\cos\left(2\pi\frac{z'}{\delta}\right)}}{\varUpsilon_\lambda}, \tag{14}$$
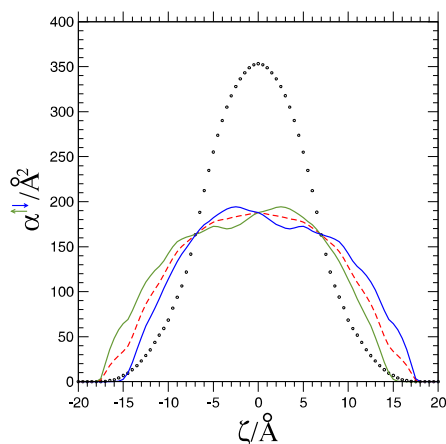
Fig. 3. The quantity α as a function of ζ, the distance between solute DCB and solvent 8OCB centres resolved along $\hat{n}$ for the cases: $\eta = 0$, *i.e.* fully orientationally averaged (black circles); $\eta = 0.95$ and solvent molecule $\uparrow$ (green solid line); $\eta = 0.95$ and solvent molecule $\downarrow$ (blue solid line); the average of the previous two curves (red dashed line). In all cases the DCB molecule Euler angles were all equal to 0 in the laboratory reference frame, that has its z-axis coincident with $\hat{n}$.

while their orientational distribution function, $\rho^{\downarrow}_{\Sigma,\gamma}(\Omega')$, was naturally taken coincident with $\rho^{\uparrow}_{\Sigma,\gamma}(\Omega')$, the only difference being that now $\theta' \in [\pi/2; \pi]$. To this point, we observe that η can be determined via deuterium LX-NMR spectroscopy. Under the approximation of eq. (12), once η is known, γ is also known, thus the solvent's orientational distribution function is fully determined. It can therefore be used to make an orientational average of the functions $A_{\sigma\Sigma}(z - z', \Omega, \Omega')$, thus leading to the functions $\alpha^{\uparrow}_{\sigma\Sigma}(z - z', \Omega|\eta)$ and $\alpha^{\downarrow}_{\sigma\Sigma}(z - z', \Omega|\eta)$, depending parametrically on η

$$\alpha^{\uparrow(\downarrow)}_{\sigma\Sigma}(z - z', \Omega|\eta) = \int d\Omega' \rho^{\uparrow(\downarrow)}_{\Sigma,\gamma}(\Omega') A_{\sigma\Sigma}(z - z', \Omega, \Omega'). \quad (15)$$

One example of these functions is given in fig. 3.

In terms of the functions $\alpha^{\uparrow(\downarrow)}_{\sigma\Sigma}(z - z', \Omega|\eta)$ the solute positional-orientational distribution function becomes

$$\rho_\sigma(z, \Omega|\eta) =$$

$$\frac{1}{\Xi} e^{-2\Psi \int_{-\infty}^{+\infty} dz' \left[\rho^{\uparrow}_{\Sigma,\lambda}(z') \alpha^{\uparrow}_{\sigma\Sigma}(z-z',\Omega|\eta) + \rho^{\downarrow}_{\Sigma,\lambda}(z') \alpha^{\downarrow}_{\sigma\Sigma}(z-z',\Omega|\eta) \right]}. \quad (16)$$

Unlike the solvent case, the solutes' distribution functions do show a coupling between positional and orientational variables. It is indeed this coupling that is to be exploited to get pieces of information on positional order from measured orientational observables. Equation (16), which can be seen as a generalisation to a S_{A_d} solvent of the expression used in refs. [69–71] to analyse the ordering of solutes in a nematic solvent, was used in the analysis of the experimentally determined Saupe ordering matrices of DCB,
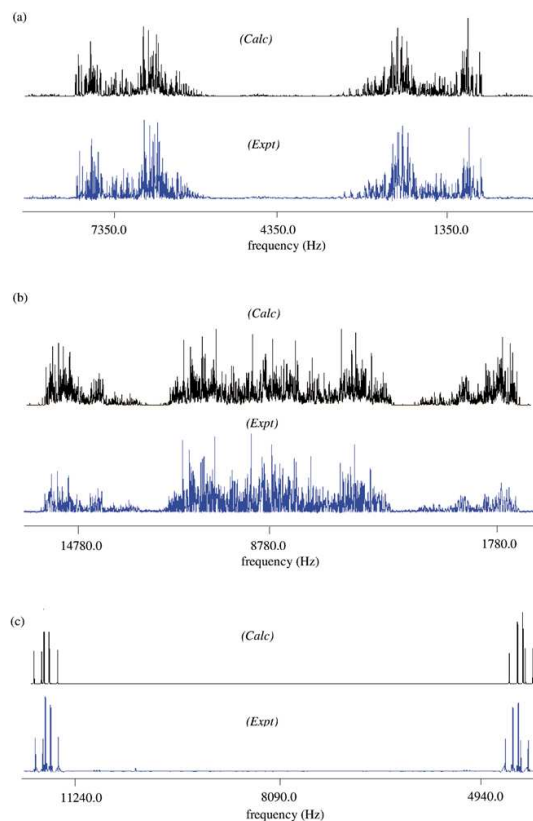
Fig. 4. Calculated and experimental ^{1}H-NMR spectra of (a) BIF, (b) PYR and (c) DCB in 8OCB at $T^* = 0.93$.

Table 1. Experimental residual dipolar couplings (Hz) of DCB in 8OCB at different reduced temperatures. The chemical structure provides hydrogen atom numbering.
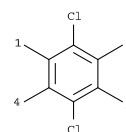
T^*	D_{12}	D_{13}	D_{23}
0.99	59.35 ± 0.07	-29.10 ± 0.08	-1797.19 ± 0.07
0.98	65.48 ± 0.10	-33.04 ± 0.11	-2020.42 ± 0.10
0.97	68.17 ± 0.09	-35.02 ± 0.09	-2125.43 ± 0.08
0.95	72.03 ± 0.09	-36.91 ± 0.09	-2244.50 ± 0.07
0.94	74.22 ± 0.06	-37.81 ± 0.07	-2303.16 ± 0.05
0.93	77.01 ± 0.03	-38.91 ± 0.03	-2396.70 ± 0.03
0.92	78.88 ± 0.06	-39.03 ± 0.06	-2412.36 ± 0.06

BIF and PYR dissolved in 8OCB. Prior to presenting and discussing this analysis, the experiments carried out are described and the data acquired from them listed in the next section.
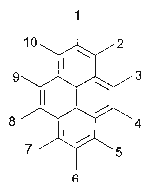
Table 2. Experimental residual dipolar couplings (Hz) of BIF in 8OCB/8OCB-d_8 at different reduced temperatures. The chemical structure provides hydrogen atom numbering.
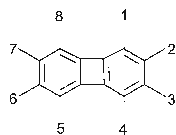
T^*	D_{12}	D_{13}	D_{14}	D_{15}	D_{16}	D_{17}	D_{18}
0.99	−1292.98±0.08	−75.27±0.10	−11.29±0.35	−38.65±0.38	−58.32±0.11	−113.98±0.09	−487.16±0.23
0.98	−1387.49±0.11	−80.34±0.14	4.17±0.51	−43.39±0.46	−63.14±0.16	−125.38±0.11	−539.56±0.35
0.97	−1482.65±0.07	−86.53±0.10	12.06±0.34	−44.34±0.33	−66.97±0.10	−137.73±0.08	−579.29±0.21
0.95	−1597.19±0.07	−91.65±0.11	12.36±0.32	−46.74±0.34	−72.20±0.11	−148.39±0.09	−625.75±0.22
0.94	−1662.52±0.06	−93.79±0.09	16.24±0.23	−48.35±0.25	−75.38±0.08	−154.70±0.07	−652.01±0.19
0.93	−1739.29±0.06	−96.17±0.07	18.53±0.25	−50.56±0.25	−78.29±0.08	−162.57±0.07	−683.95±0.16
0.92	−1801.83±0.05	−96.21±0.06	21.92±0.21	−51.89±0.22	−81.41±0.07	−168.91±0.06	−709.50±0.22

T^*	D_{23}	D_{26}	D_{27}
0.99	85.45 ± 0.32	−41.00 ± 0.35	−54.12 ± 0.25
0.98	100.16 ± 0.50	−44.52 ± 0.46	−60.12 ± 0.35
0.97	109.45 ± 0.33	−49.33 ± 0.31	−62.73 ± 0.20
0.95	133.55 ± 0.30	−53.87 ± 0.31	−66.83 ± 0.22
0.94	150.34 ± 0.24	−56.60 ± 0.24	−69.58 ± 0.21
0.93	178.22 ± 0.23	−59.15 ± 0.23	−73.39 ± 0.17
0.92	206.85 ± 0.19	−61.46 ± 0.22	−77.15 ± 0.15

Table 3. Experimental residual dipolar couplings (Hz) of PYR in 8OCB/8OCB-d_8 at different reduced temperatures. The chemical structure provides hydrogen atom numbering.

T^*	D_{12}	D_{13}	D_{14}	D_{15}	D_{16}
0.95	−695.22 ± 0.38	−180.66 ± 0.64	−93.79 ± 0.58	−59.87 ± 0.49	−47.19 ± 0.58
0.94	−717.25 ± 0.06	−188.03 ± 0.10	−99.06 ± 0.10	−66.21 ± 0.08	−52.08 ± 0.12
0.93	−728.17 ± 0.07	−192.80 ± 0.11	−102.05 ± 0.11	−67.99 ± 0.08	−53.60 ± 0.12
0.92	−731.32 ± 0.07	−194.81 ± 0.10	−103.60 ± 0.10	−69.77 ± 0.08	−53.99 ± 0.12

T^*	D_{23}	D_{24}	D_{25}	D_{27}	D_{28}	D_{29}	D_{210}
0.95	−1862.04±0.38	−326.75±0.41	−128.89±0.49	−55.27±0.78	−46.38±0.71	−32.71±0.63	−24.65±0.82
0.94	−1961.02±0.06	−344.87±0.07	−131.78±0.09	−57.01±0.11	−46.92±0.09	−32.50±0.09	−23.12±0.12
0.93	−2019.41±0.07	−354.93±0.07	−136.01±0.09	−59.95±0.13	−47.82±0.10	−32.05±0.10	−21.25±0.13
0.92	−2043.68±0.07	−359.40±0.07	−137.88±0.09	−60.64±0.12	−49.00±0.10	−31.93±0.10	−18.98±0.12

T^*	D_{34}	D_{38}	D_{39}
0.95	−2517.23 ± 0.57	−17.46 ± 0.86	−6.96 ± 0.14
0.94	−2657.81 ± 0.08	−16.56 ± 0.13	−6.45 ± 0.17
0.93	−2740.09 ± 0.09	−16.40 ± 0.13	−6.08 ± 0.14
0.92	−2774.83 ± 0.09	−16.32 ± 0.14	−5.47 ± 0.15

3 Experiments

Dilute solutions, approximately 3% by mole fraction, were prepared by dissolving solute DCB in 8OCB and solutes BIF and PYR in a mixture of 8OCB and 8OCB-d_8. The solvent 8OCB as well as the three solutes were purchased from Sigma-Aldrich while the deuterated sample 8OCB-d_8, with deuterons in the biphenyl fragment, was prepared according to the procedure described in ref. [72]. Samples were heated several times up to their clearing point, shaken to homogenize the solutions and then left to cool in the magnet. For all samples, ^{1}H spectra of the solutes were recorded at different common reduced temperatures $T^* = T/T_{NI}$, with T_{NI} the nematic-isotropic phase transition temperature, while, for the samples containing BIF and PYR, ^{2}H spectra of the solvent were also recorded at each T^*. The temperature range spanned both N and S_{A_d} phases. All spectra were recorded on a Bruker Avance 500 MHz spectrometer working at a field strength of 11.74 T and equipped with a temperature control unit. The home-made iterative computer program ARCANA [73] was used to analyze the ^{1}H spectra of the solutes. For the samples containing PYR, it was possible to analyze the proton spectra only at low temperatures in the S_{A_d} phase; due to their low quality, in terms of signal-to-noise ratio and line width, it proved impossible to analyze such complex spectra (10 spins) at higher temperatures in the N phase. In fig. 4 the calculated and experimental ^{1}H spectra of DCB, BIF and PYR in the liquid crystal solvent at $T^* = 0.93$ are reported.

The final hydrogen-atom-i–hydrogen-atom-j residual dipolar couplings, D_{ij}'s, are given, for each reduced temperature, in table 1 for DCB, in table 2 for BIF and in table 3 for PYR. The Saupe ordering matrices were obtained from the corresponding set of residual dipolar coupling data upon the adoption of standard molecular geometries for the three solutes. Table 4 reports the numerical value of η as obtained from the deuterium spectra of the solvent following a standard procedure [30,31].

4 Experimental data analysis and discussion

The analysis of the solute $\boldsymbol{S}$'s begun by considering the data in the N phase. For the three highest temperatures, data were available for DCB and BIF only. For each of these temperatures, S_{cc} and $S_{bb} - S_{aa}$ of the two compounds were fitted with eqs. (6) and (16), using the corresponding value of η in table 4, constraining $\lambda = 0$ and letting Ψ be the sole parameter to vary. The merit function considered is that of eq. (7). Table 5 reports the value of Ψ and $\tilde{\chi}^2$. The optimal values of Ψ, around 0.0018 Å^{-3} match well the value of the number density of 8OCB at temperatures in the proximity of the N-S_{A_d} phase transition. Past accurate measurements [29] reported a value for the density of 8OCB of $\cong 1$ g/cm^3, that corresponds to a number density of 0.001960 Å^{-3} [74]. One can none the less notice that the the value of $\tilde{\chi}^2$ increases with decreasing temperature. This trend remains if also the data

Table 4. Solvent's orientational order parameter, η, as a function of reduced temperature. The error estimated for them is 10%.

T^*	η
0.99	0.44
0.98	0.47
0.97	0.50
0.96	0.56
0.95	0.61
0.94	0.62
0.93	0.64
0.92	0.67

Table 5. Parameters of the fittings in the N phase, as a function of reduced temperature.

T^*	$10^3\tilde{\chi}^2$	$10^3\Psi$ (Å^{-3})
0.99	0.36	1.73±0.2
0.98	0.57	1.80±0.2
0.97	1.17	1.88±0.2

Table 6. Parameters of the fittings in the S_{A_d} phase, assumed as a N phase, as a function of reduced temperature.

| T^*	$10^3\tilde{\chi}^2$	$10^3\Psi$ (Å^{-3})
0.95	1.52	1.73±0.15
0.94	1.98	1.78±0.15
0.93	2.38	1.79±0.15
0.92	2.54	1.75±0.14

Table 7. Parameters of the fittings in the S_{A_d} phase as a function of reduced temperature.

T^*	$10^3\tilde{\chi}^2$	λ
0.95	1.40	1.0±0.5
0.94	1.80	1.1±0.5
0.93	2.00	1.2±0.5
0.92	2.00	1.5±0.6

in the smectic phase, this time including PYR, are analysed assuming that the solutes remain in a N phase, *i.e.* constraining $\lambda = 0$ and varying Ψ only. Table 6 gives the results of such fittings.

One alternative strategy attempted consisted in fitting the values of Ψ obtained in the N phase to a straight line and extrapolating it into the S_{A_d} phase, taking advantage of it being slightly dependent on temperature, and assuming as a value of δ the one experimentally determined, 32 Å [23], and then varying the sole λ. Table 7 gives the results of these fittings.

One can observe that the two series of fittings of tables 6 and 7 are essentially of the same quality, with the fittings assuming the phase as smectic just slightly bet-
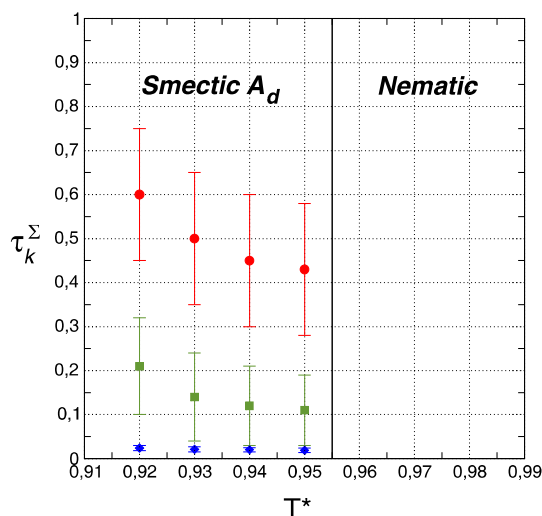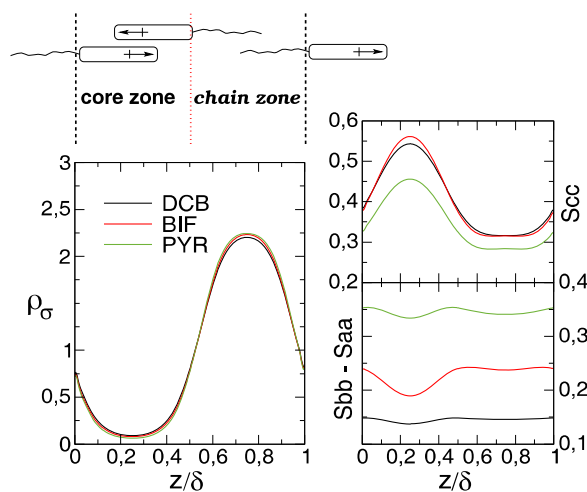
Fig. 5. Positional order parameters of solvent ↑ and solvent ↓ as a function of reduced temperature: $k = 1$ (red circles), $k = 2$ (green squares), $k = 3$ (blue diamonds).

Fig. 6. Solutes' positional distribution functions (left); $S_{cc}(z)$ (top right); $S_{bb} - S_{aa}(z)$ (bottom right).

ter, as measured by the values of $\tilde{\chi}^2$. This result can be thought of as consistent with the loose character of the layered structure in the smectic phase of 8OCB. From $\rho_{\Sigma,\lambda}^{\uparrow,\downarrow}(z)$, the solvent's positional order parameters τ_k can be calculated. The first three are shown in fig. 5. They are smaller and affected by a larger uncertainty than the ones previously determined for HAB at the same reduced temperatures [49,50].

In the past as well as in more recent times there have been other few attempts at determining τ_1 for either 8CB and/or 8OCB. In all these cases, a diffraction based method was employed. In ref. [33] a value of 0.44 was reported for 8CB. The "Haller-like" extrapolation method of ref. [39] led instead to larger values, 0.65–0.75 for both 8CB and 8OCB, with the values for the latter around 0.05 smaller than those for 8CB. In ref. [40] values comprised between 0.4 and 0.6 were reported for 8CB in the proximity of the transition to the N phase. The values of τ_1 found in this work for 8OCB are consistent with the old value of 0.44 in ref. [33] and also with the more recent values of ref. [40] for 8CB. The methods of refs. [33,40], based on diffraction measurements, share with ours, based on NMR spectroscopic measurements, the need for some microscopic assumptions, on the form of $\rho_\Sigma(z)$ and/or on molecular conformations and/or interactions in order to extract a value of the liquid crystal positional order parameter. Such assumptions are not required in the procedure of ref. [39].

Turning to the behaviour of the solutes, fig. 6 indicates that they prefer, as usual, to lie in the regions where the terminal chains of the liquid crystal molecule are more likely located. The extent of the partitioning is considerable; a solute has nearly 90% probability to be found dwelling in the chain region. Dwelling in the core or in the chain regions is associated to a different degree of ori-

entational ordering for the three solutes. It is of interest to see that for DCB and BIF S_{cc} is always larger than $S_{bb} - S_{aa}$, be a solute in the core or in the chain regions, whereas for PYR $S_{cc} \simeq S_{bb} - S_{aa}$ all across the layers. This would mean that, while DCB and BIF behave as ordinary "rod-like" particles, tending to be more aligned to the layer normal when they are in the core rather than in the chain regions, the orientational order of PYR changes little across a layer, its c- and a-axes always tending to be parallel and perpendicular to $\hat{n}$, respectively, and its b-axis more isotropically distributed.

5 Conclusion

In this work, the recently proposed ST-DFT–LX-NMR methodology has been applied to determine the positional order parameter of a partial bilayer smectic A liquid crystal. Its value has turned out to be in the range 0.4–0.6, that is smaller than that previously obtained for a normal smectic A liquid crystal at the same reduced temperatures. This may be traced back to the less well-defined layered structure that characterizes a partial bilayer smectic A phase. In perspective, it would be of interest to extend the ST-DFT–LX-NMR methodology to a smectic C phase.

This methodology rests upon the partitioning of small solute molecules in intra- and inter-layer regions of a smectic liquid crystal and their experiencing different orientational torques in the different regions. Understanding partitioning behavior of small solute molecules in lipid bilayers is of basic importance in biochemistry, and thus pharmacology (see, *e.g.* [75–77]). It is tempting to speculate on how the present methodology and the broader LX-NMR spectroscopy could be adapted to contribute to this.

References

1. P.G. de Gennes, J. Prost, *The Physics of Liquid Crystals* (Clarendon Press, Oxford, 1995).
2. M. Hosino, H. Nakano, H. Kimura, J. Phys. Soc. Jpn. **46**, 1709 (1979)
3. M. Hosino, H. Nakano, H. Kimura, J. Phys. Soc. Jpn. **47**, 740 (1979).
4. D. Frenkel, H.N.W. Lekkerkerker, A. Stroobants, Nature **332**, 822 (1988).
5. G.R. Luckhurst, G.W. Gray (Editors), *The Molecular Physics of Liquid Crystals* (Academic Press, London, 1979.
6. J.S. van Duijneveldt, M.P. Allen, Mol. Phys. **92**, 855 (1997).
7. Y. Yamaoka, Y. Taniguchi, S. Yasuzuka, Y. Yamamura, K. Saito, J. Chem. Phys. **135**, 044705 (2011).
8. E. de Miguel, E.M. del Rio, J.T. Brown, M.P. Allen, J. Chem. Phys. **105**, 4234 (1996).
9. M.A. Bates, G.R. Luckhurst, J. Chem. Phys. **110**, 7087 (1999).
10. D. Levesque, J.J. Weis, G.J. Zarragoicoechea, Phys. Rev. E **47**, 496 (1993).
11. K. Satoh, S. Mita, S. Kondo, Liq. Cryst. **20**, 757 (1996).
12. K. Satoh, S. Mita, S. Kondo, Chem. Phys. Lett. **255**, 99 (1996).
13. R. Berardi, S. Orlandi, C. Zannoni, Chem. Phys. Lett. **261**, 357 (1996).
14. S.C. McGrother, A. Gil-Villegas, G. Jackson, J. Phys.: Condens. Matter **8**, 9649 (1996).
15. A. Gil-Villegas, S.C. McGrother, G. Jackson, Chem. Phys. Lett. **269**, 441 (1997).
16. S.C. McGrother, A. Gil-Villegas, G. Jackson, Mol. Phys. **95**, 657 (1998).
17. M.P. Neal, A.J. Parker, Chem. Phys. Lett. **294**, 277 (1998).
18. M.P. Neal, A.J. Parker, Phys. Rev. E **63**, 011706 (2001).
19. I.M. Withers, J. Chem. Phys. **119**, 10209 (2003).
20. G.W. Gray, K.J. Harrison, J.A. Nash, Electron. Lett. **9**, 130 (1973).
21. A.J. Leadbetter, R.M. Richardson, C.N. Colling, J. Phys. (Paris) Colloq. **36**, C1-37 (1975).
22. J.E. Lydon, C.J. Coakley, J. Phys. (Paris) Colloq. **36**, C1-45 (1975).
23. A.J. Leadbetter, J.C. Frost, J.P. Gaughan, G.W. Gray, A. Mosley, J. Phys. (Paris) Colloq. **40**, 375 (1979).
24. P.E. Cladis, D. Guillon, F. R. Bouchet, P.L. Finn, Phys. Rev. A **23**, 2594 (1981).
25. Y. Lansac, M.A. Glaser, N.A. Clark, Phys. Rev. E **64**, 051703 (2001).
26. L. De Gaetani, G. Prampolini, Soft Matter **5**, 3517 (2009).
27. J. Zhang, J. Su, H. Guo, J. Phys. Chem. B **115**, 2214 (2011).
28. J. Thoen, H. Marynissen, W. Van Dael, Phys. Rev. A **26**, 2886 (1982).
29. A. Żywociński, S.A. Wieczorek, J. Stecki, Phys. Rev. A **36**, 1901 (1987).
30. J.W. Emsley (Editor), *Nuclear Magnetic Resonance of Liquid Crystals* (Reidel, Dordrecht, 1985).
31. R.Y. Dong, *NMR of Liquid Crystals* (Springer, New York, 1994).
32. C.D. Southern, H.F. Gleeson, Eur. Phys. J. E **24**, 119 (2007).
33. A.J. Leadbetter, J.L.A. Durrant, M. Rugman, Mol. Cryst. Liq. Cryst. **34**, 231 (1977).
34. A.J. Leadbetter, E.K. Norris, Mol. Phys. **38**, 669 (1979).
35. E.F. Gramsbergen, W.H. De Jeu, Liq. Cryst. **4**, 449 (1989).
36. J. Watanabe, M. Hayashi, Macromolecules **22**, 4083 (1989).
37. Z.X. Fan, W. Haase, J. Chem. Phys. **95**, 6066 (1991).
38. Y. Takanishi, A. Ikeda, H. Takezoe, A. Fukuda, Phys. Rev. E **51**, 400 (1995).
39. N. Kapernaum, F. Giesselmann, Phys. Rev. E **78**, 062701 (2008).
40. G.G. Alexander, S.M. King, R.M. Richardson, H. Zimmermann, Liq. Cryst. **37**, 961 (2010).
41. M. Cifelli, G. Cinacchi, L. De Gaetani, J. Chem. Phys. **125**, 164912 (2006).
42. A. Yethiraj, Z. Sun, R.Y. Dong, E.E. Burnell, Chem. Phys. Lett. **398**, 517 (2004).
43. A. Yethiraj, A.C.J. Weber, R.Y. Dong, E.E. Burnell, J. Phys. Chem. B **111**, 1632 (2007).
44. A. Yethiraj, R.Y. Dong, E.E. Burnell, Chem. Phys. Lett. **441**, 245 (2007).
45. A.C.J. Weber, X. Yang, R.Y. Dong, W.L. Meerts, E.E. Burnell, Chem. Phys. Lett. **476**, 116 (2009).
46. A.C.J. Weber, X. Yang, R.Y. Dong, E.E. Burnell, J. Chem. Phys. **132**, 034503 (2010).
47. E.E. Burnell, R.Y. Dong, A.C.J. Weber, X.Yang, A. Yethiraj, Can. J. Chem. **89**, 900 (2011).
48. G. Cinacchi, Chem. Phys. Lett. **416**, 238 (2005).
49. G. Celebre, G. Cinacchi, G. De Luca, J. Chem. Phys. **129**, 094509 (2008).
50. M.E. Di Pietro, G. Celebre, G. De Luca, G. Cinacchi, Phys. Rev. E **84**, 061703 (2011).
51. A. Saupe, G. Englert, Phys. Rev. Lett. **11**, 462 (1963).
52. J.W. Emsley, J.C. Lindon, *NMR Spectroscopy using Liquid Crystal solvents* (Pergamon Press, Oxford, 1975).
53. E.E. Burnell, C.A. de Lange, Chem. Rev. **98**, 2359 (1998).
54. E.E. Burnell, C.A. de Lange (Editors), *NMR of Ordered Liquids* (Kluwer, Dordrecht, 2003).
55. For more specific examples of LX-NMR studies see: G. Celebre, G. De Luca, M. Longeri, J.W. Emsley, J. Phys. Chem. **96**, 2466 (1992).
56. G. Celebre, G. De Luca, M. Longeri, A. Ferrarini, Mol. Phys. **83**, 309 (1994).
57. J.W. Emsley, G. De Luca, G. Celebre, M. Longeri, Liq. Cryst. **20**, 569 (1996).
58. G. Celebre, J. Chem. Phys. **115**, 9552 (2001).
59. G. Celebre, G. De Luca, Chem. Phys. Lett. **368**, 359 (2003).
60. M.E. Rose, *Elementary Theory of Angular Momentum* (John Wiley & Sons, New York, 1957).
61. L. Onsager, Ann. N. Y. Acad. Sci. **51**, 627 (1949).
62. J.D. Parsons, Phys. Rev. A **19**, 1225 (1979).
63. G. Cinacchi, L. Mederos, E. Velasco, J. Chem. Phys. **121**, 3854 (2004).
64. A. Bondi, J. Phys. Chem. **68**, 441 (1964).

65. G. Cinacchi, G. Prampolini, J. Phys. Chem. A **107**, 5228 (2003).
66. S. Tsuzuki, T. Uchimaru, K. Matsumura, M. Mikami, K. Tanabe, J. Chem. Phys. **110**, 2858 (1999).
67. A. Nicholls, G.B. McGaughey, R.P. Sheridan, A.C. Good, G. Warren, M. Mathieu, S.W. Muchmore, S.P. Brown, J.A. Grant, J.A. Haigh, N. Nevins, A.N. Jain, Brian Kelley, J. Med. Chem. **53**, 3862 (2010).
68. M.V. Gorkunov, M.A. Osipov, N. Kapernaum, D. Nonnenmacher, F. Giesselmann, Phys. Rev. E **84**, 051704 (2011).
69. A.F. Terzis, D.J. Photinos, Mol. Phys. **83**, 847 (1994).
70. A.F. Terzis, C.D. Poon, E.T. Samulski, Z. Luz, R. Poupko, H. Zimmermann, K. Müller, H. Toriumi, D.J. Photinos, J. Am. Chem. Soc. **118**, 2226 (1996).
71. T. Dingemans, D.J. Photinos, E.T. Samulski, A.F. Terzis, C. Wutz, J. Chem. Phys. **118**, 7046 (2003).
72. H. Zimmermann, Liq. Cryst. **4**, 591 (1989).
73. G. Celebre, G. De Luca, M. Longeri, E. Sicilia, J. Chem. Inf. Comput. Sci., **34**, 539 (1994).
74. Note that in the previous articles the order of magnitude of the values of the parameter Ψ turned out one smaller than the order of magnitude of the liquid crystal solvent's number density because they erroneously included a factor $\frac{2}{\Upsilon_\gamma}$. This did not affect the values of the other quantities and the final results on solvent's and solutes' positional order.
75. S.H. White, G.I. King, J.E. Cain, Nature **290**, 161 (1981).
76. T. Hessa *et al.*, Nature **433**, 377 (2005).
77. J.L. MacCallum, D.P. Tieleman, J. Am. Chem. Soc. **128**, 125 (2005).
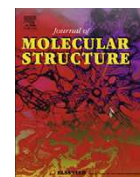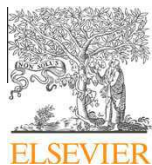
The stable conformations of 4,4′-dichloro-*trans*-stilbene in solution by liquid crystal NMR spectroscopy

Giorgio Celebre *, Giuseppina De Luca, Maria Enrica Di Pietro

Dipartimento di Chimica, Università della Calabria, v. P. Bucci, I-87036 Rende, CS, Italy

HIGHLIGHTS

▶ 4,4′-Dichloro-*trans*-stilbene is the prototype of biologically important stilbenes.
▶ Conformations of 4,4′-dichloro-*trans*-stilbene in solution were studied by LXNMR.
▶ Stable structures: C_2 (rings *disrotated* of ~19°) and C_i (rings *conrotated* of ~19°).

ABSTRACT

The mechanisms conferring to the *trans*-stilbene derivatives their well known important biological properties are not yet completely clear; then, it is reasonable to suppose that their conformational equilibrium could play some kind of role (as found for many other molecules of pharmacological interest). In this scenario, the 4,4′-dichloro-*trans*-stilbene (DCS) can be considered as the prototype of a series of stilbenes substituted in 4,4′ positions in order to enhance their properties. Following this starting idea, we decided to study the conformational distribution of DCS in solution by Liquid Crystal NMR Spectroscopy (LXNMR), one of the best techniques to obtain this kind of information in the liquid state of matter. Our results show that the molecule is basically not planar: the most populated conformations we found are (a) the couple of symmetry-related, propeller-like structures, belonging to the C_2 point group and characterized by the phenyl rings *disrotated* of about 18.7° with respect to the vinyl plane and (b) the couple of symmetry-related C_i structures (where the rings are parallel, like the pedals of a cycle) having this time the two rings *conrotated* of an angle of ~18.7° with respect to the vinyl fragment.

© 2012 Elsevier B.V. All rights reserved.

## 1. Introduction

Stilbene derivatives are a class of very interesting molecules, including natural compounds (first of all, the well known 3,5,4′-trihydroxy-trans-stilbene, called resveratrol) exhibiting a plethora of beneficial effects (an ample survey of which is given, for example, in [1] and in the references cited therein). In particular, a resveratrol analog, the 4,4′-dihydroxy-*trans*-stilbene (DHS), showed recently to have important antioxidant and antiestrogenic activities as well as other very interesting biological properties ([1–3] and references therein). Despite their recognized healthy properties, the mechanisms by which these compounds are effective are not yet completely clear [1]. A rigorous investigation aiming at collecting all the useful elements to shed more light on the nature of these effects cannot leave out of consideration the role of the conformational equilibrium of these derivatives. In order to address

the general problem of stable conformations of 4,4′-disubstituted analogs of *trans*-stilbene in liquid phase, we decided to undertake the study of the prototype molecule 4,4′-dichloro-*trans*-stilbene (DCS) by resorting to the very powerful techniques of Liquid Crystal NMR Spectroscopy (LXNMR), recently used to investigate the conformational distribution of *trans*-stilbene [4] (for a general survey of LXNMR fundamentals and examples of application, the reader is referred to Refs. [5–13]). The DCS molecule is shown in Fig. 1, where also three possible stable structures, with their point groups, are represented: C_{2h} (full planar molecule), C_2 (disrotatory, propeller-like conformation, where the rings are tilted at the same angle with respect to the vinyl plane, i.e. $\phi_1 = \phi_2$,) and C_i (conrotatory conformation, where the rings are parallel to each other, i.e. tilted at angles equal in magnitude but opposite in sign: $\phi_1 = -\phi_2$). The DCS has been on purpose synthesized, as described in the following Section 3, then dissolved in the nematic solvent ZLI1132 [4], where its anisotropic ^{1}H NMR spectrum has been recorded at room temperature. The successful analysis of the NMR spectrum led us to the knowledge of the direct dipolar coupling constants D_{ij} between the i–j pairs of hydrogen nuclei present in

* Corresponding author. Tel.: +39 0984493321; fax: +39 0984493301.
 E-mail addresses: giorgio.celebre@unical.it (G. Celebre), g.deluca@unical.it (G. De Luca), mariaenrica.dipietro@unical.it (M.E. Di Pietro).
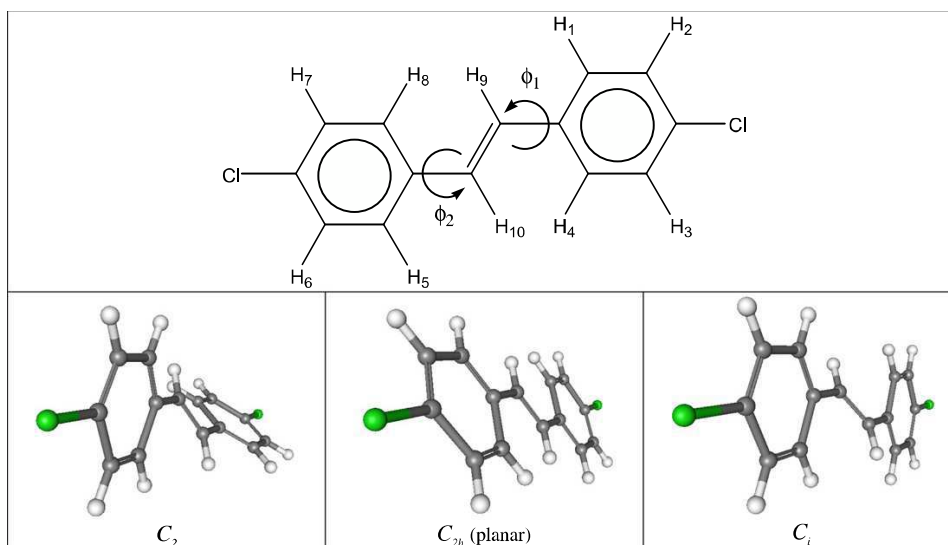
Fig. 1. Structure, torsional angles and hydrogen numbering of 4,4'-dichloro-*trans*-stilbene. Below, the possible stable rotamers (with the corresponding *point groups*) are also shown.

the molecule; then the obtained D_{ij} values were interpreted by means of the AP-DPD model ([4] and references therein) in order to obtain the sought conformational distribution.

In the following, all these phases of the work will be described in detail, till the conclusions and considerations on the treated case.

2. Theory

As said in Section 1, a successful LXNMR spectral analysis allows to obtain the invaluable experimental data represented by the observed D_{ij}^{obs} dipolar (or direct) couplings between the *i*th and *j*th magnetically active nuclei of the studied molecule (in this case, the protons of DCS). The observed dipolar couplings result from partial averages over all the relevant motions of the molecule (internal vibrations and rotations as well as the whole molecular tumbling) with respect to the external magnetic field B_0, conventionally aligned along the Z direction of the Laboratory reference system. When interproton dipolar couplings only are considered (as in the presently studied case) the approximation of neglecting the effects of high-frequency, small-amplitude molecular vibrations is quite safe [4,6]. Moreover, small flexible molecules undergoing large-amplitude internal rotations (characterized, for DCS, by the ϕ_1 and ϕ_2 torsional degrees of freedom) can be described by explicitly taking into account the torsional probability distribution $p(\phi_1, \phi_2)$. Following what said above, the observed dipolar couplings can be given, with a good approximation, by the following formula ([4] and references therein):

$$D_{ij}^{obs} \approx \left(\frac{3\cos^2\alpha - 1}{2}\right)$$
$$\cdot \left[\frac{2Z_{iso}}{3Z}\int_{\phi_2}\int_{\phi_1} p_{iso}(\phi_1, \phi_2)W(\phi_1, \phi_2)\sum_{\rho\sigma}S_{\rho\sigma}(\phi_1, \phi_2)D_{ij}^{\rho\sigma}(\phi_1, \phi_2)d\phi_1\,d\phi_2\right] \quad (1)$$

It is the presence, in this expression, of the function $p_{iso}(\phi_1, \phi_2)$ (i.e., the conformational probability distribution of the solute in a "virtual" isotropic solution at the experiment temperature; see below for more details) that makes the content of information of the observed dipolar couplings so appealing for conformational studies. Anyway, in order to fully understand the meaning of Eq. (1),

it needs to describe all its ingredients. The angle α is that between B_0, along the Z LAB direction, and $\hat{\mathbf{n}}$, the director of the mesophase located by the Euler angles $\{\beta, \gamma\}$ in the molecule-fixed frame; the terms $S_{\rho\sigma}(\phi_1, \phi_2)$ (named "order parameters" and constituting the so-called Saupe matrix [5]) describe the degree of statistical alignment of the solute molecular axes to the director, and can be written as follows:

$$S_{\rho\sigma}(\phi_1, \phi_2) = \frac{\int \left((3[\cos\omega_\rho]_{(\beta,\gamma)}[\cos\omega_\sigma]_{(\beta,\gamma)} - \delta_{\rho\sigma})/2\right)p_\Omega(\beta, \gamma, \phi_1, \phi_2)\sin\beta\,d\beta\,d\gamma}{\int p_\Omega(\beta, \gamma, \phi_1, \phi_2)d\beta\,d\gamma}$$
$$(2)$$

where ω_ρ (a function of β and γ) is the instantaneous angle between $\hat{\mathbf{n}}$ and the ρ axis of the solute reference system, and $\delta_{\rho\sigma}$ is the Kronecker delta function. The probability function $p_\Omega(\beta, \gamma, \phi_1, \phi_2)$ of Eq. (2) is given by:

$$p_\Omega(\beta, \gamma, \phi_1, \phi_2) = \frac{\exp[-U_{ext}(\beta, \gamma, \phi_1, \phi_2)/k_BT]}{Q} \quad (3)$$

with

$$Q = \int \exp[-U_{ext}(\beta, \gamma, \phi_1, \phi_2)/k_BT]\sin\beta\,d\beta\,d\gamma\,d\phi_1\,d\phi_2 \quad (4)$$

where k_B is the Boltzmann constant and $U_{ext}(\beta, \gamma, \phi_1, \phi_2)$ is a solute–solvent purely anisotropic external orientational potential. It is essential to emphasize that $p_\Omega(\beta, \gamma, \phi_1, \phi_2)$ is related to $p_{LC}(\beta, \gamma, \phi_1, \phi_2)$ (the probability of finding the mesophase director (β, γ)-oriented in the solute-fixed frame, when the probe-molecule is in its $\{\phi_1, \phi_2\}$ conformation in the liquid crystalline solution) and to $p_{iso}(\phi_1, \phi_2)$ by the following formula:

$$p_{LC}(\beta, \gamma, \phi_1, \phi_2) = \frac{p_\Omega(\beta, \gamma, \phi_1, \phi_2)p_{iso}(\phi_1, \phi_2)W(\phi_1, \phi_2)Z_{iso}}{Z} \quad (5)$$

where the partition functions Z_{iso} and Z and W of Eqs. (1) and (5) are the following:

$$Z_{iso} = \int p_{iso}(\phi_1, \phi_2)d\phi_1\,d\phi_2 \quad (6)$$

$$Z = \int W(\phi_1, \phi_2)\cdot p_{iso}(\phi_1, \phi_2)d\phi_1\,d\phi_2 \quad (7)$$

$$W(\phi_1, \phi_2) = \int \exp[-U_{ext}(\beta, \gamma, \phi_1, \phi_2)/k_B T] \sin \beta \, d\beta \, d\gamma \qquad (8)$$

Finally, in Eq. (1), $D_{ij}^{\rho\sigma}(\phi_1, \phi_2)$ are the cartesian components, given in the molecular frame, of the D_{ij} tensor of the dipolar coupling between the ith and jth nucleus:

$$D_{ij}^{\rho\sigma}(\phi_1, \phi_2) = -\frac{K_{ij}}{r_{ij}^3(\phi_1, \phi_2)}$$
$$\cdot \left[3\cos\vartheta_{ij}^{\rho}(\phi_1, \phi_2)\cos\vartheta_{ij}^{\sigma}(\phi_1, \phi_2) - \delta_{\rho\sigma} \right] \qquad (9)$$

with

$$K_{ij} = \frac{\mu_0 \hbar \gamma_i \gamma_j}{16\pi^2} \qquad (10)$$

γ_i and μ_0 being respectively the ith nuclear magnetogyric ratio and the vacuum magnetic permeability, and ϑ_{ij}^{ρ} the angle between the distance vector r_{ij} and the ρ molecular axis. In order to calculate the above mentioned order parameters $S_{\rho\sigma}(\phi_1, \phi_2)$, it is necessary to adopt a theoretical model describing the interdependent conformational–orientational problem. Here, we used the approximation called AP-DPD approach (Additive Potential [14,15] for the treatment of the ordering interactions, combined with the Direct Probability Description of the torsional distribution $p_{iso}(\phi_1, \phi_2)$) [16–24]. According to the DPD method, the $p_{iso}(\phi_1, \phi_2)$ of DCS was modeled directly as a sum of bidimensional Gaussian functions [4], by using the following general form:

$$p_{iso}(\phi_1, \phi_2) \propto \sum_{\text{(over the different } C_X \text{ -symmetry structures)}} \frac{w_{(C_X)}}{n_{(C_X)}}$$
$$\cdot \sum_{k=1}^{n_{(C_X)}} e^{-\left(\frac{\sin^2\left(\phi_1 - (\phi_1^M)_{C_X}^k\right)}{2h_1^2} + \frac{\sin^2\left(\phi_2 - (\phi_2^M)_{C_X}^k\right)}{2h_2^2} \right)} \qquad (11)$$

where $n_{(C_X)}$ is the number of rotamers belonging to the C_X point group; $w_{(C_X)}$ is the global relative weight of the C_X structures (so that $\sum_{\text{(over all the } C_X)} w_{(C_X)} = 1$); $(\phi_i^M)_{C_X}^k$ represents, for the ith torsion, the twist angle corresponding to the kth of the $n_{(C_X)}$ most probable conformations with C_X symmetry; and, finally, h_1 and h_2 give the width at half maximum height along each dimension of the bidimensional Gaussians (the recently introduced [4] use of sinusoidal functions in the exponent of the Gaussians assures the right periodicity of the p_{iso} probability distribution, simplifying its analytical expression with respect to those used in the past papers [16–24]). The term $U_{ext}(\beta, \gamma, \phi_1, \phi_2)$ of Eqs. (3), (4), and (8) represents, as said above, the purely anisotropic external orientational potential that, within the AP model approach [14,15], is approximated as follows:

$$U_{ext}(\beta, \gamma, \phi_1, \phi_2) = -\varepsilon_{2,0}(\phi_1, \phi_2)C_{2,0}(\beta)$$
$$- 2\text{Re}(\varepsilon_{2,2}(\phi_1, \phi_2))\text{Re}(C_{2,2}(\beta, \gamma)) \qquad (12)$$

where the $C_{2,m}(\beta, \gamma)$ are modified spherical harmonics [25], and the $\varepsilon_{2,m}(\phi_1, \phi_2)$ are the elements of suitable conformation-dependent solute–solvent interaction tensors. Following the AP philosophy, the $\varepsilon_{2,m}(\{\varphi\})$ elements (where $\{\varphi\}$ represents the proper n-uple of torsional variables) are constructed as sums of conformationally-independent terms $\varepsilon_{2,p}(l)$ representing the single contributions of each rigid fragment l in the molecule to the whole interaction tensors:

$$\varepsilon_{2,m}(\{\varphi\}) = \sum_l \sum_p \varepsilon_{2,p}(l) D_{p,m}^2(\Lambda_\varphi^l) \qquad (13)$$

(the second-rank Wigner rotation matrix $D_{p,m}^2(\Lambda_\varphi^l)$ [25] relates the conformation-dependent Λ_φ^l orientation of the lth molecular sub-unit to the molecule-fixed reference frame). The unknown $\varepsilon_{2,p}(l)$ values are adjusted to reproduce at best the experimental data.

Once they are known, following the equations given above, it is possible to predict the behavior of the order parameters as a function of the molecular conformation. This theoretical background will be operatively described in Section 4.

3. Experimental

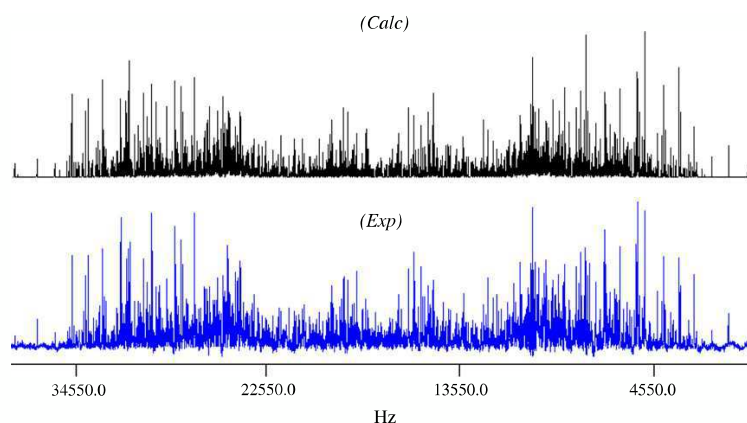### 3.1. Synthesis of 4,4'-dichloro-trans-stilbene

The DCS has been prepared following the procedure described in [26]. The 4-chlorobenzyl-phosphonate (1.19 g, 4.53 mmol) and sodium methoxide (270 mg, 4.99 mmol, 10% excess) were dissolved in dry dimethylformamide (25 ml) in a 250 ml RB flask fitted with a thermometer, calcium chloride guard tube, dropping funnel and magnetic stirrer. A solution of 4-chlorobenzaldehyde (640 mg, 4.57 mmol) in dry dimethylformamide (10 ml) was added dropwise, with stirring and cooling in an ice-bath (the temperature of the reaction was maintained between 30 °C and 40 °C). The reaction mixture was left stirring at room temperature for ~20 h, then hydrolyzed with water (25 ml). The precipitated product was collected on a filter, washed with water and freed of the solvent at reduced pressure. Then, the 4,4'-dichloro-trans-stilbene obtained was further purified by column chromatography with Merk 60 silica gel (70–230 mesh) and with hexane as eluent. Finally, the solid DCS weighed 0.81 g (3.25 mmol, 42%).

3.2. Preparation of the sample, NMR experiment and analysis of ^{1}H LXNMR spectrum

A dilute solution (approximately 5 wt.%) was prepared by dissolving the DCS (previously synthesized as described above) in the commercial nematic solvent ZLI1132 (from Merk). The sample was heated a few times up to its nematic–isotropic transition temperature T_{NI} and strongly shaken to homogenize the solution; then, it has been left to cool slowly in the magnetic field of the NMR spectrometer. The experimental ^{1}H LXNMR spectrum, shown in Fig. 2, was recorded at room temperature (298 K) on a Bruker Avance 500 MHz (11.74 T) instrument. The first step of the analysis of such a complex spectrum requires a quite good estimation of the spectral parameters, which must be close enough to the correct set so that the trial parameters can be used in a successful iterative analysis. The starting values of chemical shifts δ_{ij} were taken from the routine analysis of the proton NMR spectrum of an isotropic solution of DCS dissolved in CDCl$_3$; the scalar couplings J_{ij} were assumed to have the usual values [4], while two different sets of dipolar couplings were produced by tentatively fixing the geometry of the molecule in both planar, C_{2h} symmetry, and slightly non-planar, C_2 symmetry, conformation. As already observed for the case of trans-stilbene [4], the sets of D_{ij} obtained by fixing DCS in its planar conformation gave simulated trial spectra (corresponding to different sets of D_{ij}^{trial} obtained as functions of the S_{ij} variables) invariably showing a distribution of lines completely incompatible with the experimental one; so they were necessarily rejected, together with the hypothesis of the full planarity of the molecule.

On the contrary, the spectrum simulated with the set of dipolar couplings obtained by assuming a C_2 conformation with a torsion angle $\phi_1 = \phi_2$ of about 17° (similar to what previously found for trans-stilbene [4]) and the longitudinal and biaxiality order parameters having, respectively, the trial values of $S_{long} = 0.6$ and $S_{biax} = 0.12$ showed a certain similarity, in terms of total width and line distribution, with the experimental one. Starting from this set of dipolar couplings, the analysis of the spectrum was successfully carried out by using a home-made iterative computer program called ARCANA [27]: the resulting observed dipolar

(Calc)

(Exp)

| | 34550.0 | 22550.0 | 13550.0 | 4550.0 |

Hz

Fig. 2. The 500 MHz ^{1}H LXNMR experimental spectrum (bottom, in blue) of 4,4′-dichloro-*trans*-stilbene dissolved in the liquid crystalline nematic mesophase ZLI1132 at 298 K. For comparison, the spectrum calculated by using the D_{ij}^{obs} spectral parameters (obtained from the analysis and reported in Table 1) is also shown, in black, at the top of the figure.

couplings are reported in Table 1 (third column, where the errors affecting the D_{ij}^{obs} report on the accuracy with which ARCANA extracts the dipolar coupling values from the peak positions of the experimental spectrum), whereas the calculated spectrum is shown in Fig. 2 (top).

4. Conformational analysis: results and discussion

We think at this point it can be useful, for sake of clarity, to spend few words once more emphasizing the distinctive feature of Eq. (1), making the LXNMR technique so useful for studying the conformations of flexible molecules in solution. As said above, the p_{iso} function in the formula allows for the determination of the conformational probability from the experimental dipolar couplings. This distribution should be considered, in principle, as the "real" conformational distribution of our solute in a "conventional" isotropic liquid, sharing with the used liquid crystalline solvent (at the work temperature, of course) the same physical properties determining the thermodynamics of the solution (as, for example,

Table 1

Chemical shifts $\delta_{ij} = v_i - v_j$, scalar couplings J_{ij} (assumed as in [4]) and observed dipolar couplings D_{ij}^{obs} (i and j labels as in Fig. 1) from the analysis of ^{1}H LXNMR spectrum of 4,4′-dichloro-*trans*-stilbene dissolved in ZLI1132. In the last column, the $D_{ij}^{AP\text{-}DPD}$ obtained by AP-DPD method (see Section 2), are reported for comparison. Finally, the whole agreement is given by the RMS (the root mean square target function) between AP-DPD-calculated and observed dipolar couplings.

| i, j	J_{ij} (Hz)	D_{ij}^{obs} (Hz)	$D_{ij}^{AP\text{-}DPD}$ (Hz)
1, 2	8.00	−4860.10 ± 0.02	−4860.20
1, 3		31.86 ± 0.03	31.90
1, 4	2.00	371.32 ± 0.06	370.09
1, 5		−458.92 ± 0.03	−459.33
1, 6		−165.66 ± 0.02	−164.26
1, 9		−1881.08 ± 0.04	−1881.07
1, 10		−2965.13 ± 0.05	−2965.13
2, 3	2.00	373.17 ± 0.05	374.87
2, 6		−76.77 ± 0.04	−75.50
2, 9		−440.17 ± 0.05	−439.78
2, 10		−442.16 ± 0.05	−442.32
9, 10	17.50	1020.72 ± 0.07	1020.22
		δ_{ij} (Hz)	
1, 2		−115.23 ± 0.04	
9, 2		−206.54 ± 0.04	

RMS = 0.85 Hz.

polarity, density, etc.), with the exception of its ordering power (in other words, unlike the $p_{LC}(\phi_1, \phi_2)$ of Eq. (5), $p_{iso}(\phi_1, \phi_2)$ is in principle free from possible conformational effects induced by the orientational ordering of the mesophase). In the light of the previous sections, the basic steps leading to the LXNMR determination of the rotameric distribution of the molecule, as well as of its conformational-dependent ordering (very useful to investigate orientational mechanisms [28–32], to which we are however not interested in this work) can be quickly recalled: the dipolar coupling tensor $D_{ij}^{\rho\sigma}(\phi_1, \phi_2)$ (for each (ϕ_1, ϕ_2) conformation and for each i–j pair of hydrogens) is obtainable on the basis of a chosen molecular geometry, whereas the interdependent Saupe matrices $S_{\rho\sigma}(\phi_1, \phi_2)$ and torsional distribution $p_{iso}(\phi_1, \phi_2)$ are derived from a fit of the experimental data set (represented by the observed direct couplings D_{ij}^{obs} obtained from the analysis of the ^{1}H LXNMR spectrum) by assuming a model (in our case, the above mentioned AP-DPD) for their dependence upon the (ϕ_1, ϕ_2) angles. For DCS, as usually done in literature [4,7,17], the phenyl rings and the vinyl "rigid" fragments were assumed to keep a fixed structure as they rotate relative to each other. Moreover, each ring was assumed to have a C_{2v} symmetry, so requiring a couple of interaction parameters $\varepsilon_{2,0}^R$ and $\varepsilon_{2,2}^R$; on the contrary, the *ene* group, assumed as effectively described by an axially-symmetric interaction tensor, needs a single independent element $\varepsilon_{2,0}^{(H_6-C=C-H_7)}$, the component along the C=C bond direction. Then, we tried to reproduce the whole set of D_{ij}^{obs} (Table 1), assuming the same geometries of the fragments adopted for *trans*-stilbene and given in [4] and adjusting (in a iterative way, by a non-linear fitting program based on the gradients method [33]), the following parameters: the $\varepsilon_{2,0}^R, \varepsilon_{2,2}^R$ and $\varepsilon_{2,0}^{(H_6-C=C-H_7)}$ interaction tensor parameters of Eq. (13); the $\phi_1^M = \pm \phi_2^M$ angle, the $h_1 = h_2$ value and the $w_{(C_2)} = 1 - w_{(C_i)}$ weight of Eq. (11). This has been made in order to minimize the RMS (root mean square) target function:

$$\text{RMS} = \left\{ M^{-1} \sum_{i<j} \left[D_{ij}^{obs} - D_{ij}^{(\text{calc\_by\_AP-DPD})} \right]^2 \right\}^{\frac{1}{2}} \tag{14}$$

being $M = 12$ the number of independent couplings. It is worth emphasizing that ϕ_1^M, h_1 and $w_{(C2)}$ can be varied independently, but with the constraint that $p_{iso}(\phi_1, \phi_2)$, sampled in this case every 3° torsional steps, is normalized (in particular, because of the molecular symmetry, we normalized the distribution function for $-45° \leqslant \phi_1 \leqslant 45°$ and $-45° \leqslant \phi_2 \leqslant 45°$). By the optimized values of iteration parameters, reported in Table 2 (more details are given

Table 2
Adjusted values of the iteration parameters required by the AP-DPD approach.

	DCS in ZLI1132
$\phi_1^M = \pm\phi_2^M$ (°)	18.69 ± 0.17
$h_1 = h_2$ (°)	4.66 ± 2.64
$w_{(C_2)}$ (°)	0.63 ± 0.01
$\varepsilon_{2,0}^R$ (RT)	1.702 ± 0.002
$\varepsilon_{2,2}^R$ (RT)	0.720 ± 0.004
$\varepsilon_{2,0}^{(H_5-C=C-H_7)}$ (RT)	0.291 ± 0.015
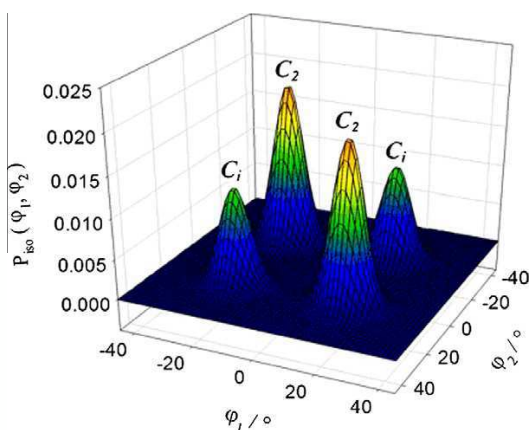
Fig. 3. Experimental probability distribution $p_{iso}(\phi_1, \phi_2)$ for DCS dissolved in the nematic solvent ZLI1132 at 298 K, obtained by the LXNMR conformational analysis.

in [34]) we were finally successful in reproducing the observed direct couplings with a very low, highly satisfactory RMS of just 0.85 Hz (the single dipolar couplings D_{ij}^{AP-DPD} calculated by this approach are reported, for comparison, in the last column of Table 1).

The surface $p_{iso}(\phi_1, \phi_2)$, resulting from the procedure described above, is shown in Fig. 3. The main feature of the obtained $p_{iso}(\phi_1, \phi_2)$ function is certainly represented by the existence of four symmetry related maxima of the probability function, corresponding to the C_2 (absolute maxima) and C_i (relative maxima) structures characterized by having, respectively, $\phi_1^M = \phi_2^M$ and $\phi_1^M = -\phi_2^M$, with $\phi_1^M = 18.69°$ (see Table 2).

The result obtained about the locations of the stable rotamers of DCS is very close to that of *trans*-stilbene [4], the magnitude of torsional angles being ~18.7° for DCS *vs* ~17° for *trans*-stilbene. This basically indicates very limited effects of the 4,4′ Cl-substitutions on the positions of the conformational minima, as reasonably expected. Also the relative weights $w_{(C_x)}$ of the two structures C_2 and C_i in DCS (related to the heights of the peaks of Fig. 3 and amounting to $w_{(C_2)} = 63\%$ and $w_{(C_i)} = 37\%$) are not far from what found for *trans*-stilbene (where the ratio $w_{(C_2)}$: $w_{(C_i)}$ was 59:41 in percentage [4]). Continuing with the comparison, the $p_{iso}(\phi_1, \phi_2)$ distribution we obtained for DCS is characterized by sharper peaks with respect to that of *trans*-stilbene (as shown by comparing Fig. 3 of this work with Fig. 4 of [4]). From a physical point of view, this would seem to suggest that DCS is more confined in the vicinity of its conformational minima with respect to the *trans*-stilbene molecule; anyway, in our opinion, this simple deduction should be more carefully and critically evaluated. As a matter of fact, the sharpness of the peaks is related to the magnitude of the h_i parameters of Eq. (11), determining the width at half-maximum height along each dimension of the bidimensional Gaussian. The value $h_1 = h_2 = 10°$ for *trans*-stilbene (Table 2 of [4]) has been obtained

by a parametrical ("trial and error") adjustment process; then, it is difficult to estimate the possible error affecting it. On the contrary, the smaller value $h_1 = h_2 = 4.7°$ for DCS (Table 2) resulted from a fitting of the experimental data where the h parameter has been used as a variable by a computer iteration process; so we can assess it is affected by a quite high error of ±2.64°, leading to a window of possible h values ranging from ~2° to ~7.5°. This indeterminacy on the "real" value of h makes the results for DCS and *trans*-stilbene more similar than it seems apparently. Finally, for sake of completeness, the $p_{LC}(\phi_1, \phi_2)$ too has been determined and compared to the $p_{iso}(\phi_1, \phi_2)$. The two distributions resulted to be basically very similar; being anyway the peaks of the $p_{LC}(\phi_1, \phi_2)$ slightly sharper than those of $p_{iso}(\phi_1, \phi_2)$. From the comparison, one could be induced to think that this is probably due to the "orienting power" exerted by the liquid crystal on the solute molecule (and absent in the $p_{iso}(\phi_1, \phi_2)$ distribution). Anyway this is just a possible intuitive explanation, not necessarily "the right one"; in particular, it cannot be generalized (in our experience, for other solutes and other solvents this kind of effect is not always observed; see, for example, [22]).

5. Conclusions

Four stable conformations, two by two symmetry related (represented by a couple of global minima, where the molecule exhibits a propeller-like C_2 symmetry, and a couple of C_i local minima, where the rings are "conrotated" of the same angle) have been found for the DCS molecule in a nematic solution, by the well tested experimental method of LXNMR conformational analysis. Given that DCS can be reasonably considered as the prototype molecule of many different compounds with innumerable properties (see Section 1), we think that the results of this work could contribute to a better understanding of useful structure–property relationships.

Acknowledgments

References

[1] M. Savio, T. Coppa, L. Bianchi, V. Vannini, G. Maga, L. Forti, O. Cazzalini, M.C. Lazzè, P. Perucca, E. Prosperi, L.A. Stivala, Int. J. Biochem. Cell B 41 (2009) 2493–2502 and references therein.
[2] Y.J. Cai, J.G. Fang, L.P. Ma, L. Yang, Z.L. Liu, Biochim. Biophys. Acta 1637 (2003) 31–38.
[3] K.V. Balan, Y. Wang, S.W. Chen, J.C. Chen, L.F. Zheng, L. Yang, et al., Biochem. Pharmacol. 72 (2006) 573–581.
[4] G. Celebre, G. De Luca, M.E. Di Pietro, J. Phys. Chem. B 116 (2012) 2876–2885.
[5] J.W. Emsley, J.C. Lindon, NMR Spectroscopy Using Liquid Crystal Solvents, Pergamon, Oxford, 1975.
[6] J.W. Emsley (Ed.), Nuclear Magnetic Resonance of Liquid Crystals, Reidel, Dordrecht, 1985.
[7] E.E. Burnell, C.A. de Lange (Eds.), NMR of Ordered Liquids, Kluwer, Dordrecht, 2003.
[8] G. Celebre, M. Longeri, J.W. Emsley, Liq. Cryst. 6 (1989) 689–700.
[9] G. Celebre, G. De Luca, M. Longeri, J.W. Emsley, J. Phys. Chem. 96 (1992) 2466–2470.
[10] J.W. Emsley, I.D. Wallington, D. Catalano, C.A. Veracini, G. Celebre, M. Longeri, J. Phys. Chem. 97 (1993) 6518–6523.
[11] J.W. Emsley, G. Celebre, G. De Luca, M. Longeri, F. Lucchesini, Liq. Cryst. 16 (1994) 1037–1049.
[12] G. Celebre, G. De Luca, M. Longeri, A. Ferrarini, Mol. Phys. 83 (1994) 309–326.
[13] J.W. Emsley, G. De Luca, G. Celebre, M. Longeri, Liq. Cryst. 20 (1996) 569–575.

[14] J.W. Emsley, G.R. Luckhurst, C.P. Stockley, Proc. R. Soc. London, Ser. A 381 (1982) 117–138.
[15] J.W. Emsley, in: D.M. Grant, R.K. Harris (Eds.), Encylopedia of NMR, J. Wiley & Sons Ltd., Chichester, 1996, pp. 2781–2787.
[16] G. Celebre, G. De Luca, J.W. Emsley, E.K. Foord, M. Longeri, F. Lucchesini, G. Pileio, J. Chem. Phys. 118 (2003) 6417–6426.
[17] G. Celebre, G. De Luca, M. Longeri, G. Pileio, J.W. Emsley, J. Chem. Phys. 120 (2004) 7075–7084.
[18] G. Celebre, M. Concistrè, G. De Luca, M. Longeri, G. Pileio, J.W. Emsley, Chem. Eur. J. 11 (2005) 3599–3608.
[19] M. Concistrè, L. De Lorenzo, G. De Luca, M. Longeri, G. Pileio, G. Raos, J. Phys. Chem. A 109 (2005) 9953–9963.
[20] G. Celebre, G. Cinacchi, J. Chem. Phys. 124 (2006) 176101. and references therein.
[21] G. Celebre, M. Concistrè, G. De Luca, M. Longeri, G. Pileio, Chem. Phys. Chem. 7 (2006) 1930–1943.
[22] J.W. Emsley, G. De Luca, A. Lesage, D. Merlet, G. Pileio, Liq. Cryst. 34 (2007) 1071–1093.
[23] J.W. Emsley, P. Lesot, G. De Luca, A. Lesage, D. Merlet, G. Pileio, Liq. Cryst. 35 (2008) 443–464.
[24] G. Celebre, G. De Luca, M. Longeri, Liq. Cryst. 37 (2010) 923–933.
[25] D.M. Brink, G.R. Satchler, Angular Momentum, third ed., Clarendon Press, Oxford, 1993.
[26] E.J. Seus, C.V. Wilson, J. Org. Chem. 26 (1961) 5243.
[27] G. Celebre, G. De Luca, M. Longeri, E. Sicilia, J. Chem. Inf. Comput. Sci. 37 (1994) 539–545.
[28] W.E. Palke, D. Catalano, G. Celebre, J.W. Emsley, J. Chem. Phys. 105 (1996) 7026–7033.
[29] G. Celebre, Chem. Phys. Lett. 342 (2001) 375–381.
[30] G. Celebre, J. Chem. Phys. 115 (2001) 9552–9556.
[31] G. Celebre, G. De Luca, J. Phys. Chem. B 107 (2003) 3243–3250.
[32] G. Celebre, G. De Luca, Chem. Phys. Lett. 368 (2003) 359–364.
[33] H.B. Schlegel, J. Comput. Chem. 3 (1982) 214–218.
[34] The values in Table 2 are given with a degree of precision and a number of decimal digits that are probably overestimated for a 3° torsional sampling grid; anyway, this is a usual, almost "physiological" effect, due to the process of interpolation carried out by basically all the non-linear fitting programs during minimization calculations.
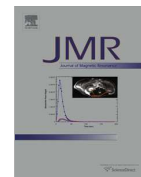
GET-SERF, a new gradient encoded SERF experiment for the trivial edition of ^{1}H–^{19}F couplings

Maria Enrica Di Pietro [a,b], Christie Aroulanda [a], Denis Merlet [a,*]

[a] *Equipe de RMN en milieu orienté, ICMMO, UMR 8182, Université Paris-Sud. 15, Georges Clemenceau, Orsay, France*
[b] *LXNMRSCAn, Dipartimento di Chimica, University of Calabria, via P. Bucci, Arcavacata di Rende (CS), Italy*

ARTICLE INFO

ABSTRACT

A new spatially encoded heteronuclear ^{1}H–^{19}F selective refocusing NMR experiment (GET-SERF) is proposed. This sequence allows editing in one single 2D experiment all couplings between a selected fluorine site and all the proton nuclei of the molecule. Its efficiency is illustrated in the case of diflunisal, a difluorinated anti-inflammatory drug, in isotropic and anisotropic media.

© 2013 Elsevier Inc. All rights reserved.

1. Introduction

In the last decades fluorocompounds have gained an impressive interest in medicinal chemistry [1]. Whereas organo-fluorine compounds are virtually absent as natural products, more than 150 pharmaceuticals in the world are fluorinated molecules [2]. Indeed, the introduction of a fluorine nucleus may cause deep modifications on the pharmacokinetic and pharmacodynamic properties of a bioactive molecule, enhancing its bioavailability and resistance to metabolic degradation, influencing its drug–ligand interactions and improving its bioactivity [3].

Due to the crucial role played by three-dimensional structure and conformational distribution in the biochemical reactivity of fluorinated compounds, the availability of analytical techniques aiming to provide their detailed structural and conformational elucidation becomes of utmost importance. In this optic ^{19}F NMR represents a very efficient tool. Indeed ^{19}F is a 100% naturally abundant ½-nuclear spin and it possesses a high gyromagnetic ratio, providing 83% of the proton NMR sensitivity for a given magnetic field. Moreover, the ^{19}F chemical shift is exquisitely sensitive to changes in the local environment, making it a very attractive nucleus for NMR studies of various complex molecules [4]. As generally recognized, scalar couplings (J_{ij}) and residual dipolar couplings (D_{ij}) are two of the most informative spin interactions. In particular, it has been demonstrated that J_{HF} can provide insights for structural elucidation and conformational design of organic compounds. Indeed Karplus-type relationships have been described for $^3J_{HF}$ [5] allowing their exploitation for conformational analysis [6] and many studies show how much long-range scalar $^nJ_{HF}$ couplings ($n > 3$) could report on local bond geometries [7]. Additional valuable information for structural refinement can be obtained in anisotropic media by ^{1}H–^{19}F residual dipolar couplings, since they provide through-space distances and angular restraints, typically absent in *J*-coupling measurements and not always available through nOe effect observations [8].

Unfortunately, the routine use of J_{HF} and especially D_{HF} couplings is often hindered by the inherent difficulties in their measurement, since the size of the investigated spin systems is often challenging and the overlap of NMR resonances as well as the complexity of the multiplicity overwhelms the resolution of the spectra. In order to simplify such spectral patterns a judicious choice of ^{1}H or ^{19}F decoupling techniques as well as more sophisticated methods has been employed [8a,9].

As ^{1}H and ^{19}F have similar NMR properties, NMR methodological strategies already developed for simplifying ^{1}H-^{1}H spectral patterns may provide a valuable starting point in order to design a new NMR tool aiming to simply edit spectral ^{1}H–^{19}F couplings. In the case of the homonuclear proton–proton couplings, an appealing approach is based on the use of semi-selective pulses. In particular, an efficient 2D NMR method for the measurement of a single specific J_{HH} coupling in isotropic media, the SElective ReFocusing (SERF) experiment, was developed in 1995 by Fäcke and Berger: by replacing the two hard pulses of a standard ^{1}H–^{1}H *J*-resolved method by selective and doubly selective RF pulses, this sequence simplifies the proton NMR spectra by selecting a coupling between

---

a pair of nuclei and allows the detection of the desired information [10]. The SERF experiment was then successfully improved and applied on a variety of compounds [11].

One of the main drawbacks of the SERF-type experiments is however that in each spectrum only the couplings between the nuclei covered by the selective pulses are edited on the 2D map. As a consequence several spectra should be acquired in order to gather the measurements of all couplings within the molecule, thus multiplying the experiments to be performed and therefore requiring a significant experimental time. To overcome this limitation, as previously proposed by Giraud et al., the frequency encoding approach could be used. Indeed the simultaneous application of a pulsed field gradient along the sample allows surmounting the problem by effectively applying the pulse on a broad range of chemical shifts according to their spatial position in the NMR tube [12]. In other words, in a Gradient encoded homonuclear SERF experiment (G-SERF) it becomes possible, thanks to the creation of a spatial frequency encoding along the sample, to run different selective experiments on different parts of the NMR tube and thus to individually assign and measure, in a single 2D spectrum, all the homonuclear couplings experienced by a given proton site in the molecule. In order to trivially edit in one single NMR experiment all ^{1}H–^{19}F couplings, we combine the frequency encoding approach to an *ad hoc* designed heteronuclear ^{1}H–^{19}F SERF experiment (denoted HF-SERF). The efficiency of the new Gradient Encoded heTeronuclear ^{1}H–^{19}F SElective ReFocusing NMR experiment (GET-SERF) is demonstrated and successfully applied to diflunisal, a difluorinated anti-inflammatory drug, to extract all scalar and residual dipolar couplings between each selected fluorine site and all the protons of the molecule.

2. Results and discussion

With the purpose to extract the ^{1}H–^{19}F couplings we adapted the SERF standard sequence replacing the doubly semi-selective π pulse on proton nuclei at the center of the t_1 evolution time by a doubly semi-selective π pulse on proton and fluorine. Consider how the heteronuclear ^{1}H–^{19}F SERF (HF-SERF) pulse sequence (Fig. 1a) acts in the simplest case of two nuclei, proton A and fluorine X: the first semi-selective $\pi/2$ pulse is applied at ν_A, the proton resonance frequency, which is the nucleus to be detected in the t_2 acquisition time. After an evolution time $t_1/2$ two semi-selective π pulses on A and X nuclei are applied sequentially permitting a
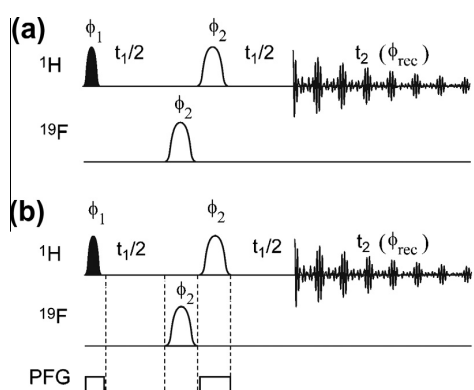

Fig. 1. Pulse sequences for the (a) HF-SERF and (b) GET-SERF experiments. Black and white ellipse shapes correspond to $\pi/2$- and π-shaped pulses, respectively. In this work the $\pi/2$ and π pulses used are the EBURP and REBURP shape pulses [13]. On the pulsed-field gradient (PFG) channel white rectangular bars refer to the application of a rectangular-shaped z-field gradient. The phase cycle is: $\phi_1 = \phi_{rec} = x$, $-x$, x, $-x$; $\phi_2 = x$, x, $-x$, $-x$.

future encoding. Then only the desired coupling evolves during the t_1 delay, whereas all the other couplings and the chemical shifts are refocused. In other words, one gets on the 2D map the signal corresponding to A with the full coupling multiplicity in the F_2 dimension and only the coupling between A and X in the F_1 domain. After tilt of the 2D spectrum the selected couplings are removed from the direct dimension allowing a simplification of the spectral pattern. The phase of the signal is modulated by the coupling during t_1 and thus the resulting lines are 'phase-twisted', so that the 2D spectrum is generally processed in magnitude mode. Note that in the latest years, heteronuclear ^{1}H–^{13}C selective refocusing experiments have been developed to benefit from the chemical shift dispersion of the ^{13}C nucleus [14]. Unlike ^{19}F, ^{13}C is a rare and poor sensitive spin. Therefore, even if only selective pulse on proton nucleus is necessary, such sequences often require NMR methods for enhancing signal intensity before acquisition (i.e. INEPT transfer) and a filter for eliminating ^{1}H–^{12}C coherences. The high sensitivity and abundance of ^{19}F explain why the ^{1}H–^{13}C selective refocusing experiments are not an adapted solution to resolve ^{1}H–^{19}F couplings. An alternative approach for the extraction of ^{1}H–^{19}F couplings could be the homonuclear *J*-resolved experiments where the heteronuclear couplings are read on the F_2-trace. Though commonly used [15], this method is not always efficient because (i) due to the numerous J_{HF} the spectrum is not always resolved enough to edit the couplings; (ii) even well resolved, the assignment of couplings could remain difficult. The HF-SERF experiment approach proposed here permits to disregard these difficulties.

In the absence of spatial encoding the HF-SERF results in a spectrum where only the coupling between the selected proton and fluorine sites is present. By applying a pulsed field gradient to the HF-SERF experiment we developed the Gradient Encoded heTeronuclear SERF (GET-SERF) pulse sequence reported in Fig. 1b. The application of two weak field gradients in correspondence of the proton selective pulses allows to carry out this selective experiment on each proton in separate "slices", editing all the ^{1}H–^{19}F couplings between a given fluorine site X and every others protons of the compound, within one single 2D spectrum.

To exemplify its efficiency, we applied the sequence to the extraction of the whole set of both J_{HF} and overall T_{HF} couplings ($T_{ij} = J_{ij} + 2D_{ij}$) of the model compound 2′,4′-difluoro-4-hydroxybiphenyl-3-carboxylic acid, commonly known as diflunisal, a nonsteroidal anti-inflammatory agent (NSAIA) member of the salicylate derivatives.

As first illustration, Fig. 2 shows the GET-SERF spectrum recorded on diflunisal dissolved in THF-d_8, together with the corresponding proton and fluorine 1D NMR spectra. In the refocusing block, the offset of the non-encoded semi-selective pulse was set at the F_4 resonance frequency, so as to edit every coupling involving this selected fluorine. In order to optimize the spatial encoding, the spectral width was limited to the aromatic region. The first frequency encoded $\pi/2$ pulse excites the proton spins having different chemical shifts in different cross sections of the sample and subsequently the selective refocusing block allows every interaction undergone by these protons to be refocused, except their couplings with F_4. The resulting spectrum is thus the sum of four sub-spectra originating from every slice in the sample. All the three cross sections corresponding to ν_1, ν_3, ν_8 (with ν_i the resonance frequency of the *i*th nucleus) have a doublet structure in the indirect domain, with splittings J_{H1F4}, J_{H3F4}, and J_{H8F4}, respectively. The last cross section corresponds to the three different protons, H$_2$, H$_5$ and H$_7$. In this case, the chemical shift difference is lower than the excitation band frequency then interactions among them will not be refocused and will appear in the F_1 dimension together with their couplings with F_4. For this reason, a doublet of doublet with splittings J_{H5H7} and J_{H5F4} and a doublet with the same splitting J_{H5H7} are
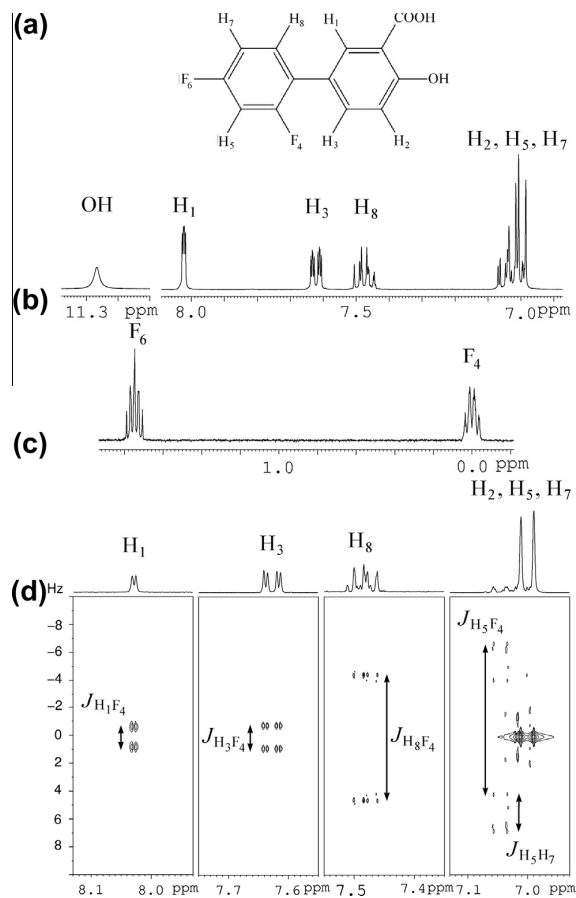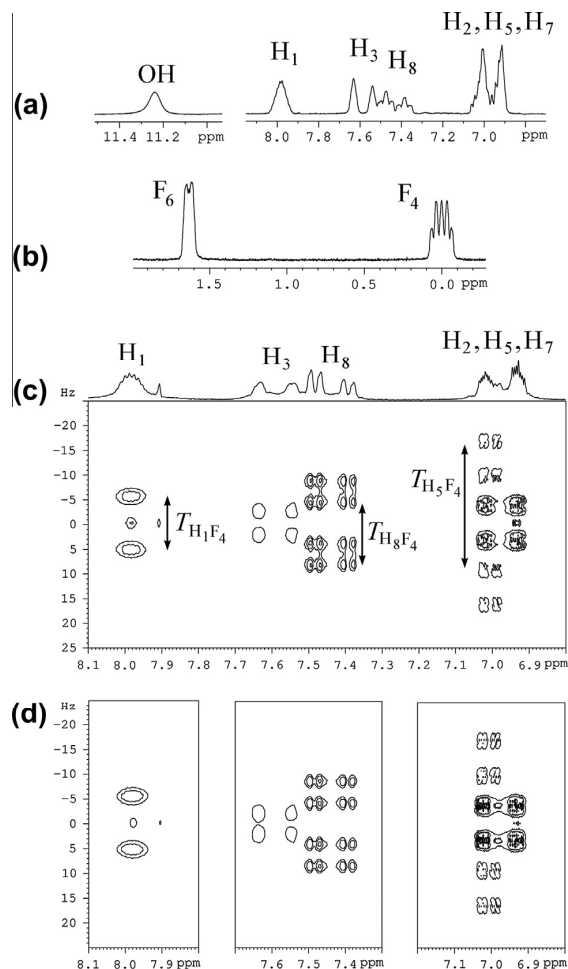
Fig. 2. (a) Diflunisal labeling, (b) 1D ^{1}H and (c) ^{19}F broadband excitation spectra of diflunisal in THF-d_8. F_4 signal was arbitrary set at 0 ppm. (d) 2D GET-SERF tilted spectrum of the same sample where the offset of the non-encoded inversion pulse is set at ν_4. Each F_1-trace obtained for a given proton H_i (at ν_i) is modulated by the heteronuclear coupling H_i–F_4 selectively edited as well as by all homonuclear couplings H_i–H_j it is submitted to.

Fig. 3. (a) 1D ^{1}H and (b) ^{19}F NMR spectra recorded on diflunisal in PBLG/THF at 300 K. (c) 2D GET-SERF tilted spectrum of the same sample where the offset of the non-encoded inversion pulse is set at ν_4. This spectrum was recorded in 13 min. (d) Set of three HF-SERF tilted spectra recorded under same experimental conditions. The offset of the selective pulses were set at ν_4 on the fluorine channel for all experiments, and at ν_1, $\nu_{3,8}$ or $\nu_{2,5,7}$ on the proton channel, respectively. Each 2D spectrum was recorded in 13 min, i.e. 39 min for the whole set of HF-SERF experiments.

observed at ν_5 and ν_7, respectively. H_2 is not coupled to H_5, H_7 or F_4 and it gives a singlet signal. Note how the separation of the information in different dimensions makes it trivial to assign the different couplings to each proton. Their magnitude has been confirmed by spectral iteration using Arcana software [16]. Artifacts visible in this cross section can be attributed to second-order coupling effects which for strongly coupled spin systems contribute to the creation of coherences that follow the same coherence transfer pathway as the desired signals and cannot be removed by standard phase cycling and gradient selection procedures. Analysis as well as individuation of methods for their suppression is out of the scope of this work. This experiment has also been successfully applied on the F_6 resonance and is presented in Fig. S1.

One can argues that ^{1}H–^{19}F J-couplings in such a system composed of only two fluorine nuclei could be extracted from simpler classical experiments as selective decoupling. However, in this case as 1D proton spectra would record the resolution is depending of the linewidth which will be decreased in the GET-SERF experiments due to the inhomogeneity refocusing.

Encouraged by these results obtained on a relatively complex isotropic spectrum, we checked the practical possibility to exploit the GET-SERF experiment for determining the T_{HF} couplings in an anisotropic medium, where the additional very large number of

long and short-range residual dipolar couplings makes the spectra even more complicated and often impossible to analyse. Fig. 3 shows the standard ^{1}H and ^{19}F NMR spectra and the GET-SERF spectrum recorded at 300 K on a sample prepared dissolving diflunisal in a liquid crystalline phase composed of poly-γ-benzyl-L-glutamate (PBLG) and THF. In this case, the 1D proton and fluorine spectra are too complex to unambiguously edit the whole set of heteronuclear couplings using simpler classical experiments supporting our effort to develop the GET-SERF experiment. Again, it is clear the GET-SERF experiment represents a simple and effective tool for the edition of the desired proton–fluorine couplings, otherwise impossible with standard procedures. The 2D map is the sum of three sub-spectra originating from different slices of the sample. The cross section corresponding to ν_1 shows clearly a doublet in the indirect domain with splitting T_{H1F4}. Unlike the isotropic sample, the signals at ν_3 and ν_8 are not far enough to allow the individual extraction in different slices of the NMR tube and they are collected together so that both T_{H3H8} and their couplings with F_4

will appear in the indirect dimension. In particular a doublet with splitting T_{H3H8} and a doublet of doublet with T_{H3H8} and T_{H8F4} splittings are visible at ν_3 and ν_8, respectively. Similar considerations on the cross section containing signals from H_2, H_5 and H_7 lead to the extraction of the coupling constants T_{H5F4}, T_{H5H7}, T_{H2H5} and T_{H2H7}. This experiment has also been successfully applied on the F_6 resonance and is presented in Fig. S2.

To stress the advantages derived by the use of spatial frequency encoding we compared the GET-SERF experiment with the series of three HF-SERF experiments, run under the same experimental conditions on the anisotropic sample, which allows to gather the same collection of data (Fig. 3d). Despite the same correlation pattern can be observed in both kinds of spectra, it has to be mentioned that the gradient encoding approach is intrinsically less sensitive than the non-encoded experiment, because only a spatially restricted cross section of the sample is responsible for the signal at a given resonance frequency. In the case of diflunisal, a 4-fold difference in intensity is observed between the broadband and the encoded spectra recorded under same experimental condition. Note that the loss in sensibility is in this case lower than previously reported [12b], due to the small spectral width to be encoded. As a consequence a greater number of scans and a longer experimental time are in principle required to obtain the same sensitivity for a single map. In the case of diflunisal however we can observe that the result of the gradient encoded experiment is still sensitive enough to be valuably exploited. Moreover, to collect every coupling involving F_4 spin at least three HF-SERF experiments are necessary leading finally to a total protocol that is longer than the spatial encoding approach (see Fig. 3). It is important to note that the experimental time is not constrained by the sensitivity but by the number of experiments in F_1 which depends of the long life time of coherence in t_1 due the inhomogeneity refocusing. More generally, for a spin system composed of n non-equivalent proton nuclei coupled to m fluorine sites, $n \times m$ HF-SERF spectra have to be recorded to measure every ^1H–^{19}F coupling constant. The design of the GET-SERF pulse sequence, which allows n spins to be individually probed, and their coupling to the mth nucleus to be selected, reduces the number of experiments required for the same coupling network to m. This constitutes a further proof of the potentiality of gradient encoded selective refocusing spectroscopy as a tool for acquiring more rapidly all the information about large spin networks.

2.1. Conclusion

Starting from the standard homonuclear SERF experiment and exploiting the spatial encoding approach, we developed the new GET-SERF pulse sequence. The application on a difluorinated anti-inflammatory drug illustrates the experiment allows the trivial edition of all long and short range ^1H–^{19}F scalar and residual dipolar couplings in one single NMR experiment. By comparison to the non-encoded corresponding sequence we demonstrated the GET-SERF experiment represents a valuable alternative to obtain the same analytical content in a less extended experimental time.

3. Experimental section

The isotropic NMR sample was obtained by diluting 30 mg of diflunisal in 483 mg of totally deuterated THF, while the anisotropic one was prepared dissolving 33 mg of diflunisal in a liquid–crystalline phase composed of 82 mg of poly-γ-benzyl-L-glutamate (PBLG, purchased from Sigma and used without further purification, DP = 793) and 474 mg of THF, using standard procedure described elsewhere [17]. The resulting 5 mm NMR tubes

were centrifuged back and forth until an optically homogeneous birefringent phase was obtained.

All the spectra were recorded on a classical high-resolution Bruker Avance 400 spectrometer (9.4 T) equipped with a QXO probe with a z field-gradient coil. The ^{19}F lock channel is used for the fluorine pulses. The temperature was controlled at 300 K by a standard variable-temperature unit (BVT 3000).

In this work the $\pi/2$ and π pulses used are the EBURP and RE-BURP shape pulse [13].

The GET-SERF spectrum of diflunisal in THF-d_8 was recorded using a data matrix of $4096(t_2) \times 512$ (t_1) with four scans per t_1 increment. The relaxation delays were 1 s. A zero filling to 1024 data points was applied in t_1 and sine functions in both dimensions were applied prior to double Fourier transform. The duration of the encoded RE-BURP refocusing and the E-BURP excitation pulses on the proton channel was 49.5 ms corresponding to a frequency width of 100 Hz. The sample was spatially encoded by a rectangular z pulsed field gradient of strength 0.3 G/cm. The duration of the RE-BURP refocusing pulse on the fluorine channel was 16.5 ms corresponding to a frequency width of 300 Hz. This spectrum was recorded in 4.5 h.

The GET-SERF and the three HF-SERF tilted spectra of diflunisal in PBLG/THF were recorded using a data matrix of $2048(t_2) \times 64(t_1)$ with four scans per t_1 increment. The relaxation delays were 1.5 s. Data were processed using zero-filling up to 256 points and a sine filter in t_1. On the proton channel the duration of the soft pulses was 27.5 ms corresponding to a frequency width of 180 Hz, while on the fluorine channel the duration of the RE-BURP pulse was 12.4 ms corresponding to a frequency width of 400 Hz. In the GET-SERF spectrum the sample was spatially encoded by a rectangular z pulsed field gradient of strength 0.2 G/cm. Each 2D spectrum was recorded in 13 min.

Appendix A. Supplementary material

Supplementary data associated with this article can be found, in the online version, at http://dx.doi.org/10.1016/j.jmr.2013.06.011.

References

[1] (a) J.T. Welch, S. Eswarakrishnan, Fluorine in Bioorganic Chemistry, John Wiley & Sons, New York, 1991;
(b) R. Filler, Y. Kobayashi, L.M. Yagupolskii, Organofluorine Compounds in Medicinal Chemistry and Biomedical Applications, Elsevier, Amsterdam, 1993;
(c) T. Hiyama, Organofluorine Compounds: Chemistry and Applications, Springer, Berlin, 2000;
(d) P. Maienfisch, R.G. Hall, The importance of fluorine in the life science industry, Chimia 58 (2004) 93–99.
[2] (a) C. Isanbor, D. O'Hagan, Fluorine in medicinal chemistry: a review of anti-cancer agents, J. Fluorine Chem. 127 (2006) 303–319;
(b) J.P. Bégué, D. Bonnet-Delpon, Recent advances (1995–2005) in fluorinated pharmaceuticals based on natural products, J. Fluorine Chem. 127 (2006) 992–1012;
(c) K.L. Kirk, Fluorine in medicinal chemistry: recent therapeutic applications of fluorinated small molecules, J. Fluorine Chem. 127 (2006) 1013–1029.
[3] (a) K.L. Kirk, Selective fluorination in drug design and development, an overview of biochemical rationales, Curr. Top. Med. Chem. 6 (2006) 1447–1456;
(b) K. Müller, C. Faeh, F. Diederich, Fluorine in pharmaceuticals: looking beyond intuition, Science 317 (2007) 1881–1886.
[4] (a) J.T. Gerig, Fluorine NMR of proteins, Prog. Nucl. Magn. Reson. Spectrosc. 26 (1994) 293–370;
(b) F. Rastinejad, C. Evilia, P. Lu, Studies of nucleic acids and their protein interactions by ^{19}F NMR, Methods Enzymol. 261 (1995) 560–575;
(c) M.A. Danielson, J.J. Falke, Use of ^{19}F NMR to probe protein structure and conformational changes, Annu. Rev. Biomol. Struct. 25 (1996) 163–195.

[5] (a) K.L. Williamson, Y.-F. Li, F.H. Hall, S. Swager, Dihedral angle and bond angle dependence of vicinal proton–fluorine spin–spin coupling, J. Am. Chem. Soc. 88 (1966) 5678–5680;
(b) C. Thibaudeau, J. Plavec, J. Chattopadhyaya, A new generalized Karplus-type equation relating vicinal proton–fluorine coupling constants to H–C–C–F torsion angles, J. Org. Chem. 63 (1998) 4967–4984.

[6] (a) Y.G. Gakh, A.A. Gakh, A.M. Gronenborn, Fluorine as an NMR probe for structural studies of chemical and biological systems, Magn. Reson. Chem. 38 (2000) 551–558;
(b) A. Solladié-Cavallo, L. Jierry, L. Bouérat, M. Schmitt, Conformation of tri- and tetra-substituted 2-fluoro cyclohexanones: proton non-equivalence, F–H and F–C coupling constants, conformational dependence of $3J_{FH}$ and $^4J_{FH}$, Tetrahedron 58 (2002) 4195–4199.

[7] (a) S. Jaime-Figueroa, L.J. Kurz, Y. Liu, R. Cruz, Synthesis and experimental study of through-space hydrogen–fluorine and carbon–fluorine spin–spin coupling in 4,5-substituted 1-acetyl-8-fluoronaphthalenes, Spectrochim. Acta Part A 56 (2000) 1167–1178;
(b) M. Hennig, M.L. Munzarová, W. Bermel, L.G. Scott, V. Sklenář, J.R. Williamson, Measurement of long-range ^1H–^{19}F scalar coupling constants and their glycosidic torsion dependence in 5-fluoropyrimidine-substituted RNA, J. Am. Chem. Soc. 128 (2006) 5851–5858;
(c) A.V. Afonin, Through space spin–spin coupling ^{19}F–^1H As the base for comparative analysis of conformational equilibrium in fluorine-substituted aryl vinyl selenides and sulfides, Russ. J. Org. Chem. 46 (2010) 1313–1316.

[8] (a) B. Luy, J.-P. Marino, Measurement and application of ^1H–^{19}F dipolar couplings in the structure determination of 2′-fluorolabeled RNA, J. Biomol. NMR 20 (2001) 39–47;
(b) J. Yan, F. Delaglio, A. Kaerner, A.D. Kline, H. Mo, M.J. Shapiro, T.A. Smitka, G.A. Stephenson, E.R. Zartler, Complete relative stereochemistry of multiple stereocenters using only residual dipolar couplings, J. Am. Chem. Soc. 126 (2004) 5008–5017.

[9] (a) B. Luy, J.J. Barchi, J.P. Marino, S^3E-E.COSY methods for the measurement of ^{19}F associated scalar and dipolar coupling constants, J. Magn. Reson. 152 (2001) 179–184;
(b) A. Foris, ^{19}F and ^1H NMR spectra of halocarbons, Magn. Reson. Chem. 42 (2004) 534–555.

[10] T. Facke, S. Berger, SERF, a new method for H,H spin-coupling measurement in organic chemistry, J. Magn. Reson. Ser. A 113 (1995) 114–116.

[11] (a) J. Farjon, D. Merlet, P. Lesot, J. Courtieu, Enantiomeric excess measurements in weakly oriented chiral liquid crystal solvents through 2D ^1H selective refocusing experiments, J. Magn. Reson. 158 (2002) 169–172;
(b) P. Nolis, A. Roglans, T. Parella, IFSERF, an isotope-filtered SERF experiment for the precise measurement of proton–proton coupling constants between chemically equivalent protons, J. Magn. Reson. 173 (2005) 305–309;
(c) L. Beguin, J. Courtieu, L. Ziani, D. Merlet, Simplification of the ^1H NMR spectra of enantiomers dissolved in chiral liquid crystals, combining variable angle sample spinning and selective refocusing experiments, Magn. Reson. Chem. 44 (2006) 1096–1101;
(d) J. Farjon, L. Ziani, L. Beguin, D. Merlet, J. Courtieu, Selective NMR excitations in chiral analysis, Annu. Rep. NMR 61 (2007) 283–293;
(e) J.M. Nuzillard, Biselective refocusing pulses and the SERF experiment, J. Magn. Reson. 187 (2007) 193–198;
(f) B. Baishya, U.R. Prabhu, N. Suryaprakash, Enantiomeric discrimination by double quantum excited selective refocusing (DQ-SERF) experiment, J. Phys. Chem. B 111 (2007) 12403–12410;

[12] (a) K. Zangger, H. Sterk, Observation of coupling across the ice–water interface by 2D time domain NMR, J. Magn. Reson. 124 (1997) 486–489;
(b) N. Giraud, L. Beguin, J. Courtieu, D. Merlet, Nuclear magnetic resonance using a spatial frequency encoding: application to J-edited spectroscopy along the sample, Angew. Chem., Int. Ed. 49 (2010) 3481–3484;
(c) A. Aguilar, S. Faulkner, M. Nilsson, G.A. Morris, Pure shift ^1H NMR: a resolution of the resolution problem?, Angew Chem., Int. Ed. 49 (2010) 3901–3903;
(d) D. Merlet, L. Beguin, J. Courtieu, N. Giraud, Spin–spin coupling edition in chiral liquid crystal NMR solvent, J. Magn. Reson. 209 (2011) 315–322;
(e) J.A. Aguilar, A.A. Colbourne, J. Cassani, M. Nilsson, G.A. Morris, Decoupling two-dimensional NMR spectroscopy in both dimensions: pure shift NOESY and COSY, Angew. Chem., Int. Ed. 51 (2012) 6460–6463.

[13] (a) H. Geen, R. Freeman, Band-selective radiofrequency pulses, J. Magn. Reson. 93 (1991) 93–141;
(b) R. Freeman, Shaped radiofrequency pulses in high resolution NMR, Prog. Nucl. Magn. Res. 32 (1998) 59–106.

[14] (a) J. Farjon, J.P. Baltaze, P. Lesot, D. Merlet, J. Courtieu, Heteronuclear selective refocusing 2D NMR experiments for the spectral analysis of enantiomers in chiral oriented solvents, Magn. Reson. Chem. 42 (2004) 594–599;
(b) N. Nath, B. Baishya, N. Suryaprakash, Visualization of enantiomers using natural abundant ^{13}C-filtered single and double quantum selective refocusing experiments: application to small chiral molecules, J. Magn. Reson. 200 (2009) 101–108;
(c) N. Nath, N. Suryaprakash, Enantiodiscrimination and extraction of short and long range homo- and hetero-nuclear residual dipolar couplings by a spin selective correlation experiment, Chem. Phys. Lett. 496 (2010) 175–182;
(d) N. Nath, N. Suryaprakash, Spin-selective correlation experiment for measurement of long-range J couplings and for assignment of (R/S) enantiomers from the residual dipolar couplings and DFT, J. Phys. Chem. B 115 (2011) 6868–6875.

[15] (a) L.D. Hall, S. Sukumar, Applications of homonuclear two-dimensional J spectroscopy: an alternative to broad band heteronuclear and homonuclear decoupling, J. Am. Chem. Soc. 101 (1979) 3120–3121;
(b) M. Barfield, E.W. Della, P.E. Pigou, S.R. Walter, Nuclear spin–spin coupling via nonbonded interactions. Importance of bridgehead interactions on vicinal carbon-13–fluorine-19 and long-range proton–fluorine-19 coupling constants in 1-fluorobicycloalkanes, J. Am. Chem. Soc. 104 (1982) 3549–3552;
(c) A. Jegorov, P. Sedmera, V. Havlicek, M. Husak, S. Pakhomova, B. Kratochvil, M. Kuchar, P. Bulej, Spectroscopic and structural study of flobufen, J. Fluorine Chem. 73 (1995) 213–219.

[16] G. Celebre, G. De Luca, M. Longeri, E.J. Sicilia, Graphical interactive strategy for the analysis of NMR spectra in liquid crystalline phases, J. Chem. Inf. Comput. Sci. 34 (1994) 539.

[17] M. Sarfati, P. Lesot, D. Merlet, J. Courtieu, Theoretical and experimental aspects of enantiomeric differentiation using natural abundance multinuclear NMR spectroscopy in chiral polypeptide liquid crystals, Chem. Commun. 21 (2000) 2069–2081.